Comptes Rendus
de l'Académie des sciences

Physique

Thematic issue / ***Numéro thématique***
Open questions in the quantum many-body problem
Questions ouvertes dans le problème quantique à N corps

Editors-in-chief / ***Rédacteurs en chef***
Yvan Castin, Carlos Sá de Melo

ACADÉMIE DES SCIENCES
INSTITUT DE FRANCE

Académie des sciences — Paris
ISSN : 1878-1535 (electronic)

CENTRE MERSENNE

Comptes Rendus
Physique

Objective of the journal

Comptes Rendus Physique is an international peer-reviewed electronic journal, covering all areas of physics and astrophysics.

It publishes thematic issues, original research articles, review articles, historical perspectives, pedagogical texts or conference proceedings, of unlimited length, in English or in French and in as flexible a format as necessary (figures, associated data, etc.).

Comptes Rendus Physique has been published since 2020 with the centre Mersenne pour l'édition scientifique ouverte (Mersenne Center for open scientific publishing), according to a virtuous Diamond Open Access policy, free for authors (no author processing charges nor publishing fees) as well as for readers (immediate and permanent open access).

About the journal

Comptes Rendus Physique is published exclusively in electronic format.

All information on the journal, as well as the full text of all articles, is available on its website at: https://comptes-rendus.academie-sciences.fr/physique.

Author enquiries

For any inquiries about submitting a manuscript, please refer to the journal's website: https://comptes-rendus.academie-sciences.fr/physique.

Contact

Académie des sciences
23 quai de Conti
75006 Paris (France)
cr-physique@academie-sciences.fr

ACADÉMIE DES SCIENCES
INSTITUT DE FRANCE

Comptes Rendus. Physique
https://doi.org/10.5802/crphys.sp.3

Contents / *Sommaire*

ACADÉMIE
DES SCIENCES
INSTITUT DE FRANCE

Comptes Rendus. Physique

Open questions in the quantum many-body problem / *Questions ouvertes dans le problème quantique à* N *corps*

Rédacteurs en chef invités

Guest editors

Yvan Castin

Carlos Sá de Melo

Yvan Castin est directeur de recherche au CNRS. Théoricien, il mène ses travaux au Laboratoire Kastler Brossel de l'École normale supérieure à Paris, depuis sa thèse de doctorat sur le refroidissement d'atomes par laser effectuée sous la direction de Jean Dalibard et Claude Cohen-Tannoudji de 1988 à 1992. Il contribue, avec Klaus Mølmer et Jean Dalibard, au développement de la méthode des fonctions d'onde Monte-Carlo. Depuis 1995, il travaille sur les condensats de Bose-Einstein atomiques gazeux dans l'équipe «atomes froids» créée par Claude Cohen-Tannoudji, avant d'ajouter les superfluides de fermions en interaction forte comme deuxième corde à son arc en 2004, en suivant Christophe Salomon dans l'équipe « gaz de fermions froids », dont il assure la direction de la partie théorique. On lui doit plusieurs résultats originaux sur l'effet Efimov à quatre corps et le développement en amas pour le gaz unitaire de fermions, les limites de la compression de spin et le temps de cohérence d'un condensat dans un gaz de bosons isolé, l'amortissement du son faiblement collisionnel dans les superfluides, en collaboration avec Alice Sinatra, Ludovic Pricoupenko, Felix Werner, Shimpei Endo et d'autres. Il a reçu (avec Laurent Lafforgue) le prix Jacques Herbrand de l'Académie des sciences en 2001, et en 2012 le prix d'équipe de la Fondation Louis D., décerné au responsable d'équipe Christophe Salomon.

Yvan Castin is Senior Researcher at the CNRS. A theoretician, he has been working at the Laboratoire Kastler Brossel, École normale supérieure, Paris, since his doctoral thesis on laser cooling of atoms, carried out under the supervision of Jean Dalibard and Claude Cohen-Tannoudji from 1988 to 1992. Together with Klaus Mølmer and Jean Dalibard, he contributed to the development of the Monte Carlo wave

function method. Since 1995, he has been working on gaseous atomic Bose-Einstein condensates in the «cold atom» group set up by Claude Cohen-Tannoudji, before adding strongly interacting fermion superfluids as a second string to his bow in 2004, following Christophe Salomon in the «ultracold Fermi gases» group, of which he is responsible for the theoretical part. He is responsible for several original results on the four-body Efimov effect and cluster expansion for the unitary fermion gas, spin squeezing limits and coherence time of a condensate in an isolated Bose gas, and collisionless sound damping in superfluids, in collaboration with Alice Sinatra, Ludovic Pricoupenko, Felix Werner, Shimpei Endo, and others. He received (with Laurent Lafforgue) the Jacques Herbrand prize from the Académie des Sciences in 2001, and in 2012 the Louis D. Foundation team prize, awarded to group leader Christophe Salomon.

Carlos A. R. Sá de Melo a obtenu un doctorat en physique théorique à l'Université de Stanford en 1991, avec une spécialisation en physique quantique à N corps, sous la direction du professeur Sebastian Doniach (prix Bardeen 2018), et a été chercheur postdoctoral au Science and Technology Center for Superconductivity dans l'Illinois, avec pour mentor feu le Dr Alexei Abrikosov (prix Nobel 2003). Il a ensuite rejoint l'Institut de technologie de Géorgie, où il est aujourd'hui professeur en sciences physiques. Le professeur Sá de Melo est surtout connu pour ses contributions théoriques à l'étude du raccordement entre la superfluidité de Bardeen-Cooper-Schrieffer (BCS) et la condensation de Bose-Einstein (CBE) dans les systèmes à une et deux bandes dans les années 1990 et 2000, un phénomène exploré expérimentalement depuis le milieu des années 2000. Pour ses travaux sur les atomes froids fermioniques et les superfluides de fermions, il a obtenu un poste de chercheur invité de deux ans au Joint Quantum Institute (UMD-NIST) de 2006 à 2008, a été élu membre de l'American Physical Society en 2012, a reçu une bourse Simons en 2017 pour une visite prolongée à l'Institut de physique théorique Galileo Galilei (Florence, Italie), a reçu le prix Fibonacci en 2018 lors de la conférence Quantum Complex Matter (Frascati, Italie), a été élu membre de l'American Association for the Advancement of Science en 2021 et a bénéficié d'une bourse Mercator de la Fondation allemande pour la recherche en 2024. Ses recherches sur les raccordements et transitions de phase quantiques entre régime BCS et régime CBE dans les superfluides ont influencé les travaux expérimentaux et théoriques non seulement en physique atomique, mais aussi en physique nucléaire et en physique de la matière condensée.

Prof. Carlos A. R. Sá de Melo earned a PhD in theoretical physics at Stanford University (1991), specializing in quantum many-body physics, under the supervision of Prof. Sebastian Doniach (Bardeen Prize 2018), and was a postdoctoral fellow at the Science and Technology Center for Superconductivity in Illinois, mentored by Dr. Alexei Abrikosov (Nobel Prize 2003, deceased). After that he moved to the Georgia Institute of the Technology, where he is a professor of physics today. Prof. Sá de Melo is best known for his theoretical contributions to the evolution from Bardeen-Cooper-Schrieffer (BCS) to Bose-Einstein condensation (BEC) superfluidity in single- and two-band systems during the 1990's and 2000's, a phenomenon explored experimentally since the mid-2000's. For his work on ultracold Fermi atoms and superfluids, he was awarded a two-year Visiting Fellow position at the Joint Quantum Institute (UMD-NIST) from 2006-2008, was elected Fellow of the American Physical Society in 2012, was granted a Simons Fellowship in 2017 for an extended visit to the Galileo Galilei Institute of Theoretical Physics (Florence, Italy), was presented the Fibonacci Prize in 2018 at the Quantum Complex Matter conference (Frascati, Italy), was elected Fellow of the American Association for the Advancement of Science in 2021, and was honored with a Mercator Fellowship by the German Research Foundation in 2024. His research on the crossover and quantum phase transitions from the BCS to the BEC regime in superfluids has influenced experimental and theoretical work not only in atomic, but also in nuclear and condensed matter physics.

ACADÉMIE
DES SCIENCES
INSTITUT DE FRANCE

Comptes Rendus. Physique

Open questions in the quantum many-body problem / *Questions ouvertes dans le problème quantique à* N *corps*

Avant-Propos

Foreword

Yvan Castin[a], **Carlos Sá de Melo**[b]

[a] Laboratoire Kastler Brossel, ENS-Université PSL, CNRS, Université Sorbonne et Collège de France, 24 rue Lhomond, 75231 Paris, France

[b] School of Physics, Georgia Institute of Technology, Atlanta, GA 30332, USA

English version follows French version

En physique, le problème quantique à N corps est une thématique de recherche actuelle très fédératrice, car il concerne un grand nombre de domaines, de la physique mathématique à la matière condensée en passant par la physique atomique et l'optique quantique, et met en jeu de nombreux systèmes, des supraconducteurs aux gaz quantiques en passant par les systèmes de spins, la matière topologique, les systèmes désordonnés et les systèmes photoniques dissipatifs, en dimension trois ou en dimensionalité réduite, avec des interactions à courte ou à longue portée, etc. Il soulève des questions particulièrement ardues, qui obligent à croiser plusieurs méthodes d'étude, mathématiques, analytiques, macroscopiques ou effectives de basse énergie, diagrammatiques, numériques, expérimentales, de simulation quantique, etc.

Il y a certes de nombreux congrès dans ce domaine, mais ils se limitent généralement à des présentations brèves de résultats déjà obtenus et se spécialisent dans l'un des aspects mentionnés. À notre connaissance, très peu d'entre eux cherchent à faire un bilan global des questions ouvertes et des grandes directions à explorer, dans l'esprit des fameux congrès Solvay d'autrefois, en réunissant les chercheurs des différents domaines ayant suffisamment de vision et de maturité pour faire des exposés de prospective longs (90 minutes) au tableau noir et à la craie (pas de projection), vec beaucoup de temps de discussion. C'est ce que nous avons fait en juillet 2024, à travers une quinzaine d'exposés sur cinq jours de colloque, ouverts à tous, dans le grand amphithéâtre Hermite de l'Institut Henri Poincaré (IHP) à Paris. Les exposés ont été enregistrés et mis en ligne sur la chaîne Carmin de l'IHP (cliquer ici).

Pour que l'exercice prenne toute sa valeur, nous avons souhaité que le colloque laisse une trace écrite – verba volant –, d'où le présent dossier thématique publié en accès libre aux Comptes Rendus Physique, qui regroupe les différentes contributions sous forme d'« Interventions en colloque ». Nous espérons que ceci incitera la communauté des chercheurs, doctorants et post-doctorants à se concentrer sur les grandes questions et à construire des ponts entre les différentes disciplines de la physique quantique à N corps.

Nous remercions chaleureusement les orateurs qui ont accepté le surcroît de travail qu'exige la rédaction d'actes de colloque, ainsi que la direction de l'IHP, qui a mis gracieusement à notre disposition son infrastructure et son équipe technique, en nous exemptant des frais de location de l'amphithéâtre. Enfin, nous sommes reconnaissants à Stephan Fauve d'avoir accepté notre dossier thématique avec enthousiasme, et à Isabelle Vallet d'en avoir accompagné la mise en œuvre avec efficacité.

English version

In physics, the quantum many-body problem is a highly unifying current research topic, since it touches a large number of fields, from mathematical physics to condensed matter, atomic physics and quantum optics, and involves numerous systems, from superconductors to quantum gases, spin systems, topological matter, disordered systems and dissipative photonic systems, in dimension three or reduced dimensions, with short- or long-range interactions, etc. It raises particularly challenging questions, requiring the cross-fertilization of a wide range of study methods: mathematical, analytical, macroscopic or effective low-energy, diagrammatic, numerical, experimental, quantum simulation, and more.

Although there are many congresses in this field, they are generally limited to brief presentations of the results already obtained, and specialize in one of the aspects mentioned. As far as we know, very few of them try to take stock of the open questions and the main directions to be explored, in the spirit of the famous Solvay congresses of yesteryear, by bringing together researchers from different fields with sufficient vision and maturity to give long (90-minute) foresight presentations on the blackboard (no projection), with plenty of time for discussion. This is what we did in July 2024, with about fifteen presentations over five days of a symposium open to all in the large Hermite amphitheatre at the Institut Henri Poincaré (IHP) in Paris. The presentations were recorded and posted online on the IHP's Carmin channel (click here).

To make the exercise as valuable as possible, we wanted the colloquium to leave a written trace – verba volant –, hence the present special issue published in open access in Comptes Rendus Physique, which brings together the various contributions in the form of conference proceedings. We hope this will encourage the community of researchers, PhD students and postdocs to focus on the big questions and to build bridges between the different disciplines of quantum many-body physics.

We would like to express our sincere gratitude to the speakers who accepted the extra work involved in writing the proceedings, and to the management of the IHP, who graciously made their infrastructure and technical team available to us, waiving the cost of renting the amphitheatre. Last but not least, we are grateful to Stephan Fauve for enthusiastically accepting our special issue, and to Isabelle Vallet for efficiently guiding its implementation.

ACADÉMIE DES SCIENCES
INSTITUT DE FRANCE

Comptes Rendus. Physique
2025, Vol. 26, p. 369-380
https://doi.org/10.5802/crphys.249

Intervention in a conference / *Intervention en colloque*

Some open mathematical problems concerning charged quantum particles

Quelques problèmes mathématiques ouverts sur les particules quantiques chargées

Mathieu Lewin [a]

[a] CEREMADE, CNRS and Université Paris Dauphine - PSL, Place de Lattre de Tassigny, 75 016 PARIS, France

E-mail: mathieu.lewin@math.cnrs.fr

Abstract. I present some open mathematical problems concerning electrons in quantum mechanics and charged particles in general. After discussing the Schrödinger Hamiltonian describing atoms and molecules with classical nuclei, I turn to infinite systems and in particular to the homogeneous electron gas.

Résumé. Je présente quelques problèmes mathématiques ouverts concernant les électrons en mécanique quantique et les particules chargées en général. Après avoir discuté de l'hamiltonien de Schrödinger décrivant les atomes et les molécules avec des noyaux classiques, je considère les systèmes infinis et en particulier le gaz homogène d'électrons.

Keywords. Schrödinger equation, Coulomb systems, Homogeneous electron gas.

Mots-clés. Équation de Schrödinger, Systèmes coulombiens, Gaz d'électrons homogène.

Manuscript received 6 November 2024, revised 28 March 2025, accepted 31 March 2025.

1. Introduction

In my talk at the Institut Henri Poincaré in July 2024 [1], I have discussed some open mathematical problems concerning charged quantum systems. I should first mention that an open mathematical problem need not be considered an open problem from the point of view of physics. Many questions that are extremely difficult to solve rigorously are considered to be fully understood by physicists, whether because of physical intuition, the existence of exact results on simpler models, or with the help of powerful numerical simulations.

So why should we care about proving things with full mathematical rigor? A first obvious reason is that a mathematical proof provides a kind of "seal of quality", that is, a stronger truth about the model under consideration. However, most mathematical physicists feel that adding epsilons and function spaces to an existing convincing physical argument is not the most exciting part of their work. It is much more interesting when the mathematical proof brings a new perspective and thus teaches us new physics. This must be the case in situations where the physical arguments are too vague and do not lead to a clear path for a rigorous proof.

What kinds of physical questions can be answered rigorously? Mathematics is sometimes not very good at dealing with quantitative properties of very particular systems (the chemical properties of a given molecule, for example). It is much better at explaining general (universal)

phenomena for a whole class of models, and at showing connections between situations that look different but are governed by the same mathematical laws.

Let us now turn to the systems of interest for this note, that is, charged particles interacting via the Coulomb interaction

$$\frac{qq'}{|x-x'|}$$

in atomic units. Here q, $q' \in \mathbb{Z}$ are the two charges and x, $x' \in \mathbb{R}^3$ are the positions of the two particles in consideration. The important mathematical properties of this potential are the singularity at the origin (two particles repel or attract each other strongly when $|x-x'| \ll 1$, depending on the sign of their charges) and the slow decay at infinity (the function $x \mapsto 1/|x|$ is not integrable at infinity in 3D). The singularity at the origin generates an instability for all classical Coulomb systems with opposite charges, leading to a collapse of the system. This is easily resolved by the quantum uncertainty principle. The slow decay of $1/|x|$ at infinity is of a different nature and only causes difficulties for large, macroscopic systems. In fact, every particle in the system feels the Coulomb potential induced by many other particles, even far away, and not just its nearest neighbors. This induces large-scale correlations that could cause the macroscopic object to become unstable. In fact, the existence of matter as we know it has been shown to be a consequence of both screening effects (the charges tend to balance out so that the system is essentially neutral locally, making the potential locally finite) and the fermionic nature of electrons [2]. We will discuss this in more detail below.

The paper is organized as follows. We first discuss open problems concerning the molecular Born–Oppenheimer Schrödinger Hamiltonian describing a finite set of N quantum electrons and M classical nuclei. In Section 3 we turn to infinite systems and, in particular, the homogeneous electron gas.

2. Atoms and molecules

Let us start by mentioning some famous open mathematical problems concerning the Schrödinger Hamiltonian of N electrons submitted to an external potential $V : \mathbb{R}^3 \to \mathbb{R}$,

$$H(V,N) = \sum_{j=1}^{N} \frac{-\Delta_{x_j}}{2} + \sum_{j=1}^{N} V(x_j) + \sum_{1 \le j < k \le N} \frac{1}{|x_j - x_k|}, \tag{1}$$

in atomic units. The operator acts on wavefunctions $\Psi(x_1,\sigma_1,\dots,x_N,\sigma_N)$ that are antisymmetric with respect to the exchanges of the position and spin variables $(x_j,\sigma_j) \in \mathbb{R}^3 \times \{\uparrow,\downarrow\}$ of the electrons. We are particularly interested in the case that V describes the potential induced by a finite number M of classical nuclei

$$V(x) = -\sum_{m=1}^{M} \frac{z_m}{|x - R_m|}, \tag{2}$$

where $z_m \in \mathbb{N}$ and $R_m \in \mathbb{R}^3$ are the nuclear charges and positions.

The Hamiltonian (1) has been the subject of much mathematical work, too much to mention with full details. Kato proved in the 50s [3] that for reasonable external potentials V, including the one in (2), the above Hamiltonian is well defined on the domain

$$\mathscr{D}(H(V,N)) = \left\{ \Psi : \int |\Psi|^2 + \sum_{j=1}^{N} \int |\Delta_{x_j}\Psi|^2 < \infty \right\}. \tag{3}$$

The integral is here understood in the sense of Lebesgue [4, Chapter 1]. More precisely, this is an integral for the space variables but a sum over the spin variables:

$$\int |\Psi|^2 := \sum_{\sigma_1,\dots\sigma_N \in \{\uparrow,\downarrow\}} \int_{\mathbb{R}^3} \cdots \int_{\mathbb{R}^3} |\Psi(x_1,\sigma_1,\dots,x_N,\sigma_N)|^2 \,\mathrm{d}x_1 \cdots \mathrm{d}x_N.$$

On the other hand, the Laplacian $\Delta_{x_j}\Psi$ is understood in the sense of distributions [4, Chapter 6]. The operator $H(V,N)$ cannot be defined on a smaller space (in particular it cannot be restricted to smooth functions only), otherwise its spectrum is the whole complex plane [5, Chapter 6]. The domain (3) is is the only one for which $H(V,N)$ is self-adjoint and has a real spectrum. It is nice but somewhat annoying that the abstract theories of Lebesgue integration and weak derivatives are unavoidable in quantum mechanics!

After the pioneering work of Kato, many have worked on establishing spectral properties of $H(V,N)$. Zhislin and his collaborators studied the eigenvalues (bound states energies) and the form of the continuous spectrum in the 60–70s. It was proved in particular that for an atom or a molecule, i.e., V of the form in (2), $H(V,N)$ admits infinitely many bound states below its continuous spectrum whenever $N \leq Z$, where

$$Z := \sum_{m=1}^{M} z_m$$

is the total nuclear charge [6]. In other words, the electrons can be bound to the nuclei as soon as the nuclear charge is greater than or equal to the number of electrons. This is due to the long range of the Coulomb potential, which ensures that any electron escaping to infinity is subject to an attractive force that brings it back to the neighborhood of the nuclei, where the charge is $Z-(N-1)>0$ or more. Later it was proved [7–11] that, on the contrary, there can be only finitely many bound states if $N > Z$, and in fact none at all if N is too large. This confirms the obvious intuition that a finite set of nuclei can bind only a finite number of electrons.

Mathematical physicists then turned to the more precise study of the continuous spectrum and of scattering theory. The latter is not so obvious due to the long range of the Coulomb potential [12,13]. Finally, the quantized photon field was included and its influence on the spectrum studied at length [14,15] (in this case only the ground state remains and the higher excited states become resonances). Below we discuss in Section 3 the limit of a large number of electrons and nuclei, $N, M \to \infty$.

2.1. *Ionization conjectures*

If we plot the experimental ground state energy of an arbitrary atom of the periodic table as a function of the number of electrons N, we obtain a curve that looks like the ones shown in Figure 1 for the particular cases of oxygen ($Z = 8$) and zinc ($Z = 30$). Let us discuss some general properties of these curves and ask what was rigorously proved for the (non-relativistic) Schrödinger Hamiltonian (1).

2.1.1. *Monotonicity*

A first remark is that the curves are decreasing (more precisely they are non-increasing since they can be constant). This is because adding an electron can only make the ground state energy smaller. In the worse case the additional electron escapes to infinity where it can have an arbitrary small energy. The monotonicity of the curve is not difficult to prove for the Hamiltonian $H(V,N)$. To make things more explicit, let us denote by

$$E(V,N) = \inf_{\Psi} \langle \Psi | H(V,N) | \Psi \rangle = \min \sigma(H(V,N))$$

the ground state energy of the system, which equals the minimum of the spectrum of the operator $H(V,N)$. When the infimum is attained, $E(V,N)$ is an eigenvalue (if N electrons can be bound by V). If this is not the case, $E(V,N)$ is part of the continuous spectrum. In fact, the HVZ theorem [6,17,18] states that the continuous spectrum of $H(V,N)$ equals a half interval and starts when one electron is sent to infinity:

$$\sigma_{\text{cont}}(H(V,N)) = [E(V,N-1), \infty). \tag{4}$$

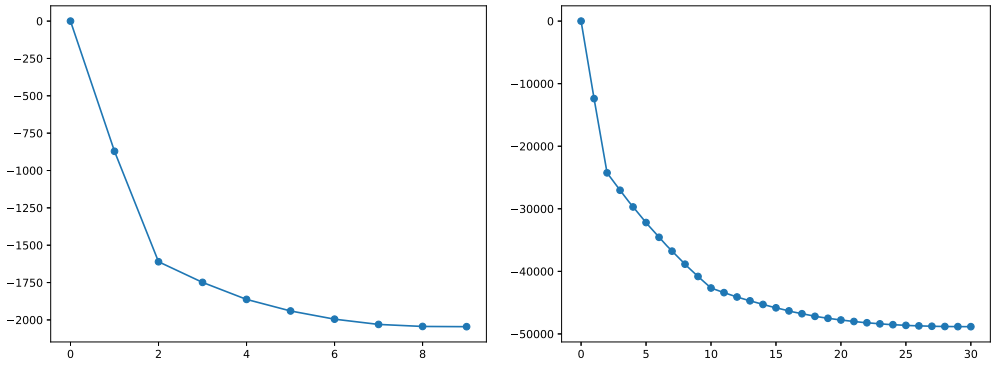

Figure 1. Experimental ground state energy (eV) of oxygen (left) and zinc (right) as a function of the number N of bound electrons, according to the NIST database [16]. The curve is constant on the right of the last value of N appearing in the graph, that is, the mentioned atoms do not seem to be able to bind more electrons.

This property is valid for any potential V that tends to 0 at infinity [5, Chapter 6], hence for any Coulomb potential of the form (2). Of course, the latter implies $E(V,N) \leq E(V,N-1)$ for all $N \in \mathbb{N}$ (with the convention $E(V,0) = 0$), which is the observed monotonicity.

2.1.2. *Maximum ionization*

When N exceeds Z by a few units, the ionization curves become flat, meaning that a given nucleus can only accept a few electrons more than its charge. For example, oxygen seems to be able to bind 9 electrons, but not 10. This is of course specific to Coulomb, since a potential V decaying slower than $-1/|x|$ can bind an arbitrarily large number of electrons. That the function $N \mapsto E(V,N)$ becomes constant at some point is quite difficult to prove. This was done in the papers [7–11] mentioned above. But proving that this happens starting from $Z + C$ with a reasonable constant C turned out to be extremely hard and is still open today.

Open Problem 1 (Maximal ionization). *Prove that the maximal number of electrons that a molecule can bind satisfies*

$$N_{\max} \leq Z + CM \tag{5}$$

where M is the number of (classical) nuclei, $Z = \sum_{m=1}^{M} z_m$ is the total nuclear charge, and C is a universal reasonable constant (ideally $C = 1$ or $C = 2$).

Of course, for heavy nuclei we should take relativistic effects into account, which we completely neglect here. If we let Z and N be arbitrarily large and look at the non-relativistic Hamiltonian $H(V,N)$, then no proof of (5) has been provided yet, even with a crazy constant like $C = 10^{100}$. The conjecture is due to Lieb in the 80s and is discussed in detail in the recent chapter [19]. It is also *Problem 10C* in a famous list by Simon [20] published exactly 40 years ago.

Why should we be interested in this conjecture? The main interest of this problem is that it must follow from a *complicated interplay between the Coulomb forces and the fermionic nature of the electrons*. In fact, as we will see below, the conjecture is known to be wrong if the electrons are replaced by charged bosons! A classical nucleus of charge Z can bind $N_{\max} \approx 1.21\,Z$ bosonic electrons for $Z \gg 1$ [21,22]. Consequently, any proof of the conjecture would require a deep understanding of how the Pauli principle is interrelated with the Coulomb forces. Any progress in this direction would tell us more about the nature of quantum matter.

Let us briefly discuss some important partial results concerning $N_{\max}$. The best bound currently known is due to Lieb in [11] and states that $N_{\max} < 2Z + M$. This nice proof uses

some special properties of the Coulomb potential, but no particle statistics (it works the same for bosons). Better bounds are known for atoms ($M = 1$). Taking into account the Pauli principle, Nam [23] obtained $N_{\max} < 1.22\ Z + 3Z^{1/3}$. If we restrict ourselves to $Z \leq 118$ as in the current periodic table, we get the somewhat unreasonable estimate

$$N_{\max} \leq Z + 40, \quad \text{for } Z \leq 118.$$

Still for $M = 1$ it was proved that $N_{\max} = Z + o(Z)$ in [24,25], which was later improved to $N_{\max} = Z + O(Z^{5/7})$ in [26,27]. Finally, Solovej managed to prove the conjecture in Hartree–Fock theory in a very delicate work [28,29], but with a huge constant C. The proof seems very difficult to generalize to the many-body problem.

2.1.3. *Convexity*

Let us return to the experimental ionization energies in Figure 1. Another property that stands out is that the curves are convex. This corresponds to the rather obvious fact that if we start from the right (say at $N = Z$) and remove the electrons one by one, we will first catch the one that is least bound to the nuclei, i.e., for which the ionization energy is the smallest in absolute value. As we remove more electrons, the energy we need pay should increase, because the core electrons are harder to remove than the valence electrons. The monotonicity of the ionization energy $N \mapsto |E(V,N) - E(V,N-1)|$ is exactly the observed convexity.

The obvious caveat to this intuitive argument is that, due to interactions, when we remove an electron, the remaining electrons will change their state to accommodate the missing electron. The new ionization energies, in principle, have nothing to do with those with an extra electron. A little argument shows that the ground state energy is always convex in N for a non-interacting system, so here we try to *understand how correlation affects ionization energies*.

Open Problem 2 (Convexity). *Find the class of external potentials V's for which the energy $N \mapsto E(V,N)$ is convex, that is, satisfies*

$$E(V,N) - E(V,N-1) \leq E(V,N+1) - E(V,N), \quad \forall N \in \mathbb{N}. \tag{6}$$

The importance of this problem was first mentioned in the context of Density Functional Theory by Perdew et al. [30] in 1982. In [31, Chapter 4], Parr and Yang stated the conjecture explicitly for all atoms and molecules, that is, for all V of the form (2). Lieb stated it for all possible potential V in [32, *Question 7*]. Simon mentions it only for atoms, as *Problem 10A* in his famous list of open questions [20] already mentioned above.

Despite the convexity of all experimental curves for atoms, we only have counterexamples for simpler systems. Lieb gave a counterexample to the inequality (6) for $N = 2$ when the Coulomb repulsion is replaced by a hard core. Ayers recently generalized this argument to the Riesz interaction $1/|x-y|^s$ with $s > 2\log 2/\log 3 \approx 1.26$ [33]. Other negative results concern particles interacting with a repulsive harmonic interaction in a harmonic trap [34,35], the 1D Hubbard model [36], or a system in nuclear physics [37].

While preparing the talk last July, I realized that a counterexample for the Coulomb interaction can be provided based on results I obtained earlier in a collaboration [38] with Simone Di Marino and Luca Nenna. This is now described in detail in the new article [39]. Our counterexample to the convexity (6) is for $N = 3$ and it has $M = 6$ nuclei placed very far apart but of very small charges $z_m \ll 1$. This shows that the convexity in N cannot be true for arbitrary potentials V, as Lieb suggested in [32]. However, the problem remains completely open for physical nuclei of integer charge. This recent work tells us that the situation is even more complicated than expected, and a mathematical explanation of why convexity is universally observed in experiments remains to be found. Note that the particle statistics does not play an important role, here. The counterexample of [39] also works for charged bosons.

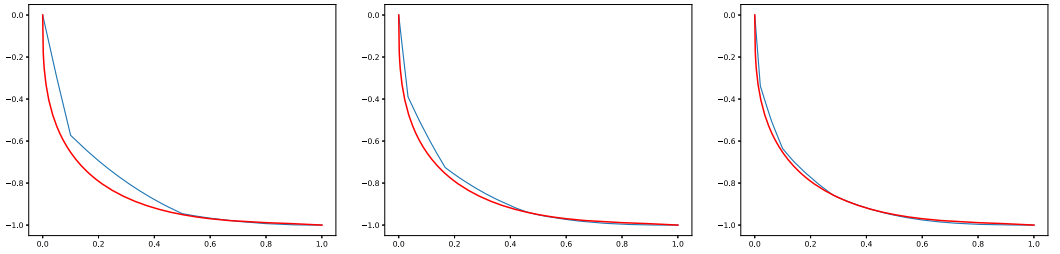

Figure 2. Experimental atomic ground state energies for $Z = 20$ (left), $Z = 60$ (center) and $Z = 100$ (right) according to the NIST database [16], plotted together with the Thomas–Fermi energy curve in red, all as functions of N/Z for $N \leq Z$. The energies are renormalized in the manner $E(-Z/|x|, N)/|E(-Z/|x|, Z)|$ and $e_{\mathrm{TF}}(\kappa)/|e_{\mathrm{TF}}(1)|$, that is, divided by the last energy so that the curves all end up at -1.

2.1.4. *The large-Z limit for fermions and bosons*

Next, we briefly discuss the limit of large nuclear charge Z. For simplicity we assume $M = 1$ (atoms) and we place the nucleus at the origin of space. Looking again at the curves in Figure 1, a natural question arises: do these curves converge in the limit $Z \to \infty$ if we properly renormalize them? The answer is yes, and a proof has been given by Lieb and Simon in [40–42]. If we take $Z \to \infty$ and at the same time $N \to \infty$ while fixing $\kappa = N/Z$, we end up with Thomas–Fermi theory. The formal statement is

$$E(-Z/|x|, N) \underset{\substack{N,Z\to\infty \\ \frac{N}{Z}\to\kappa}}{\sim} E_{\mathrm{TF}}(-Z/|x|, N), \tag{7}$$

where

$$\begin{aligned} E_{\mathrm{TF}}(-Z/|x|, N) &= \inf_{\substack{\rho\geq 0 \\ \int_{\mathbb{R}^3}\rho = N}} \left\{ c_{\mathrm{TF}} \int_{\mathbb{R}^3} \rho(x)^{\frac{5}{3}}\,\mathrm{d}x - Z\int_{\mathbb{R}^3} \frac{\rho(x)}{|x|}\,\mathrm{d}x + \frac{1}{2}\iint_{\mathbb{R}^6} \frac{\rho(x)\rho(y)}{|x-y|}\,\mathrm{d}x\,\mathrm{d}y \right\} \\ &= Z^{\frac{7}{3}} e_{\mathrm{TF}}\left(\frac{N}{Z}\right), \end{aligned} \tag{8}$$

and $c_{\mathrm{TF}} = (3/10)(6\pi^2)^{2/3}$. Here ρ is the total density of the system and

$$e_{\mathrm{TF}}(\kappa) = \inf_{\substack{\nu\geq 0 \\ \int_{\mathbb{R}^3}\nu = \kappa}} \left\{ c_{\mathrm{TF}} \int_{\mathbb{R}^3} \nu(x)^{\frac{5}{3}}\,\mathrm{d}x - \int_{\mathbb{R}^3} \frac{\nu(x)}{|x|}\,\mathrm{d}x + \frac{1}{2}\iint_{\mathbb{R}^6} \frac{\nu(x)\nu(y)}{|x-y|}\,\mathrm{d}x\,\mathrm{d}y \right\}. \tag{9}$$

To go from the first to the second line in (8), we have introduced the rescaled density $\nu(x) = Z^{-2}\rho(Z^{-1/3}x)$. In this limit the kinetic energy dominates and the system is paramagnetic (spins up and down are occupied with density $\rho/2$). To illustrate the convergence (7) on real data, we have plotted the experimental energy curves for $Z = 20, 60, 100$ together with the Thomas–Fermi curve $\kappa \mapsto e_{\mathrm{TF}}(\kappa)$ in Figure 2.

The Thomas–Fermi energy curve satisfies all the previously observed properties. Namely, it is convex decreasing and constant for $\kappa = N/Z \geq 1$. The convexity comes from the facts that the functional in the curly brackets in (9) is convex in the rescaled density ν and that κ appears as a linear constraint. That it admits no ground state for $N/Z > 1$ is not easy and was proved in [41,42]. Since all the desired properties are known to be valid in the limit $Z \to \infty$, it is natural to try to bring this information back to finite Z and get some results for the Schrödinger Hamiltonian, by a kind of perturbative argument. This turned out to be very difficult and so far was only achieved in Hartree–Fock theory [29].

Many more questions inspired by Thomas–Fermi theory can be posed concerning the Schrödinger Hamiltonian. We refer to [43] for a discussion of the radius of atoms and to [44] concerning the periodicity properties of the periodic table.

As a final comment, we mention that for bosonic electrons, the limit is the Hartree energy [22,45–47], given by

$$\inf_{\int_{\mathbb{R}^3}|\phi|^2=N}\left\{\frac{1}{2}\int_{\mathbb{R}^3}|\nabla\phi(x)|^2\,\mathrm{d}x - Z\int_{\mathbb{R}^3}\frac{|\phi(x)|^2}{|x|}\,\mathrm{d}x + \frac{1}{2}\iint_{\mathbb{R}^6}\frac{|\phi(x)|^2|\phi(y)|^2}{|x-y|}\,\mathrm{d}x\,\mathrm{d}y\right\} = Z^3\,e_{\mathrm{H}}\left(\frac{N}{Z}\right)$$

with ϕ the macroscopic condensate wavefunction and

$$e_{\mathrm{H}}(\kappa) = \inf_{\int_{\mathbb{R}^3}|\chi|^2=\kappa}\left\{\frac{1}{2}\int_{\mathbb{R}^3}|\nabla\chi(x)|^2\,\mathrm{d}x - \int_{\mathbb{R}^3}\frac{|\chi(x)|^2}{|x|}\,\mathrm{d}x + \frac{1}{2}\iint_{\mathbb{R}^6}\frac{|\chi(x)|^2|\chi(y)|^2}{|x-y|}\,\mathrm{d}x\,\mathrm{d}y\right\}. \tag{10}$$

This time we used $\phi(x) = Z^2\chi(Zx)$. The previous minimization admits ground states for $\kappa \le \kappa_c$ and none for $\kappa > \kappa_c$, where $\kappa_c \approx 1.21$. A perturbative argument proved that $N_{\max}/Z \to \kappa_c$ in the limit $Z \to \infty$, so bosonic atoms can bind many more electrons than real atoms [21,22]. Note that the limiting energy curve is still convex, suggesting that the convexity is not so closely related to the particle statistics.

2.2. *Chemical reactions*

Now let us look at another question that is closer to quantum chemistry. Lieb and Thirring proved in [48] that *all neutral molecules can bind*, at zero temperature. To state the result correctly, we include the nuclear energy and define the total energy of a molecule by

$$E_{\mathrm{mol}}(z_m, R_m, N) := E(V, N) + \sum_{1\le k<m\le M}\frac{z_k z_m}{|R_k - R_m|} \tag{11}$$

where, of course, V is given by (2). The statement is that when $N = Z = \sum_{m=1}^M z_m$, the function $(R_1,\dots,R_M) \mapsto E_{\mathrm{mol}}(z_m, R_m, N)$ reaches its minimum. More precisely, the lowest energy of a molecule is always strictly lower than when it is broken into pieces:

$$\min_{R_1,\dots,R_M\in\mathbb{R}^3} E_{\mathrm{mol}}(z_m, R_m, N) < \liminf_{\max_{1\le k<m\le M}|R_k-R_m|\to\infty} E_{\mathrm{mol}}(z_m, R_m, N). \tag{12}$$

The result is very intuitive when the molecule breaks into two charged pieces, because those have different signs and therefore must attract each other at infinity. The result of [48] concerns the situation where the molecule breaks into neutral clusters. It is proved that those attract with a van der Waals force, which results from an *interplay between correlation and the long range of the Coulomb potential*.

In [49–51] we studied the situation of a molecule that admits two local minima with respect to the nuclear positions $R_1,\dots,R_M$ and asked whether there exists a transition state between them (also called a *mountain pass* and corresponding to a saddle point of the energy functional). This was proved in many situations of physical interest by studying the critical points of the multipole interactions, but not yet in the general case.

Open Problem 3 (Chemical reactions). *Prove that for a molecule possessing two local stable configurations (that is, local minima of* $(R_1,\dots,R_M) \in (\mathbb{R}^3)^M \mapsto E_{\mathrm{mol}}(z_m, R_m, N)$*), the isomerization between them happens without breaking the molecule into pieces.*

3. Infinite systems, the homogeneous electron gas

Finally, we discuss some open problems for macroscopic Coulomb systems. Although these have been the subject of many studies in the last decades, several fundamental questions are still completely open on the mathematical side.

We should mention the beautiful theory of "stability of matter" by Dyson and Lieb [2,52–55], which led to both deep mathematical results and new physical insights. This concerns the situation where the number of electron diverges, $N \to \infty$, as well as the number of nuclei, $M \to \infty$ but the charges z_m remain bounded. One can choose the positions and charges of the nuclei, for instance place them on a lattice to describe a given material [56,57]. It is also possible to randomly perturb a given lattice (Anderson model) [58]. Finally, one can as well optimize over the number and positions of the nuclei [59] (assuming for instance that they all have the same charge $z_m = z$). In short, it was understood that such systems are always stable, which means that the ground state energy behaves linearly with particle number or volume. This is what is needed to ensure that a macroscopic system does not collapse. Note that for bosonic electrons, the energy behaves like $N^{5/3}$ [60] if the nuclei can be arbitrarily close to each other but it stays of order N if the nuclei have a finite distance to each other [57]. The Pauli principle therefore plays again a crucial role here.

Because of its importance in applications (in particular in Density Functional Theory [31]), the *Homogeneous Electron Gas* (HEG) has also been extensively studied. In this system, the classical nuclei are replaced by a uniform background of fixed positive charge (taken first in a finite domain and then extended to the whole space). Although screening effects still play an essential role, it is less important that the electrons are fermions. The HEG is also stable for charged bosons and even for classical electrons [61,62].

Stability is only the first step in the study of large quantum systems. The next step is to understand the properties of equilibrium states and, in particular, the sudden changes that can happen when varying the temperature or the density. Of particular interest is the lack of uniqueness due to the breaking of translational symmetry, that is expected to arise in the solid phase. Not much is known rigorously about the existence of such phase transitions.

Open Problem 4 (Phase transitions). *Prove that translational symmetry is broken for the Homogeneous Electron Gas or with classical point nuclei, at low density and/or low temperature.*

In the case of classical nuclei we can assume, for example, that we have only one kind of nuclei (all of the same charge z) and, at $T = 0$, that we are optimizing over the nuclear positions. Remember that they can all bind, as we saw in Section 2.2. It is also possible to take a finite number of charges $z_1, \dots, z_M$. We can then fix the average density of each species or just optimize over the charges as well.

Showing that translational symmetry is broken seems very hard. This requires first defining what it means to be an *infinite equilibrium state*, since the Gibbs state is always unique at $T > 0$ and non-uniqueness can only occur for an infinite system. Defining such infinite states is a hard problem because the equilibrium equations usually include the interaction potential between each electron and the rest of the system, which is typically a divergent integral or series due to the long range of the Coulomb interaction. Delicate compensations are expected due to screening effects, but proving that they actually occur is very difficult. For the 3D Coulomb potential, infinite equilibrium states have so far only been constructed for classical electrons at $T = 0$ in [62, Theorem 28] and for $T \gg 1$ in [63].

Even for short-range interactions we know very little concerning the existence of phase transitions. All existing rigorous results in this direction (e.g., [64,65]) are for very special systems and rely on specific methods that cannot be easily adapted to Coulomb systems. So the situation

is rather embarrassing! We have no mathematical intuition as to why translation invariance should be broken, nor even a strategy as to how to prove it. This is one of the most important open problems in mathematical physics.

Showing the breaking of translations is of course only a first step. We expect that the system will be a proper solid, that is, periodic with a non-trivial period. This is often referred to as *Wigner's crystallization conjecture* [66,67].

Open Problem 5 (Wigner crystallization). *Prove that at low temperature and/or low density, infinite equilibrium states are periodic. For the HEG, it must be the Body-Centered-Cubic lattice.*

For classical electrons, the conjectured periodic arrangement should arise from the fact that they repel each other and thus seek to minimize the repulsion energy by maximizing their relative distances, while at the same time being attracted to the uniform positive background. In the quantum case, this picture should remain true at low density, since the kinetic energy $1/a^2$ of an electron localized in a periodic cell of side length a remains small compared to the repulsion energy $1/a$ between neighboring electrons. Unfortunately, this intuitive image has never been rigorously justified for either classical or quantum electrons. The only system that is well understood is the one-dimensional HEG (with the interaction $-|x-y|$), for which crystallization was proved at all densities and temperatures [68–72].

For classical electrons, the crystallization conjecture has interesting links with number theory. This is because if we take an infinite lattice $\mathscr{L}$ of particles interacting with the Riesz potential $1/|x-y|^s$ with $s > d$ (the space dimension), the interaction energy of each particle with the rest of the system equals

$$\zeta_{\mathscr{L}}(s) = \frac{1}{2} \sum_{z \in \mathscr{L} \setminus \{0\}} \frac{1}{|z|^s}.$$

This is called the *Epstein Zeta function* and it is a generalization of the Riemann Zeta to higher dimensions. The series converges only for $s > d$ but the function admits a meromorphic continuation to the whole complex plane with a unique pole at $s = d$. This continuation is still denoted by $\zeta_{\mathscr{L}}(s)$. For $s < d$ it is known that $\zeta_{\mathscr{L}}(s)$ is nothing but the energy obtained by inserting a uniform background to compensate the divergence of the series [62, Section IV]. The analytic continuation allows us to place the long and short range cases into the same theory.

In this direction, we would like to mention the recent result [73] that gave the 2022 Fields medal to Maryna Viazovska, where Wigner crystallization was proved in dimensions $d = 8$ and $d = 24$, for all $s \geq d - 2$ [74], hence including the "Coulomb" potential of those dimensions. Dimensions 8 and 24 are special because there exists a specific lattice $\mathscr{L}$, called "universally optimal", that works for all s. The same phenomenon is expected in 2D with the triangular lattice, but not proved yet. In 3D there exists no universally optimal lattice and one expects either BCC or FCC depending on the value of s [67]. Apart from 1D, nothing is known in the quantum case.

It seems reasonable to expect that freezing is a universal phenomenon, in dimension 3, but it can still occur in many different ways. The phase diagram of the HEG is still being carefully studied numerically. For a long time it was thought that the system could be a ferromagnetic Wigner crystal, a ferromagnetic liquid, and a paramagnetic liquid. However, recent simulations indicate that the ferromagnetic fluid phase may not exist [75,76]. More transitions could also occur in the solid phase (e.g., an antiferromagnetic crystal). In the case of Hartree–Fock, thorough numerical studies [77–79] predicted many transitions in the solid region, including exotic "incommensurate" phases.

Open Problem 6 (Phase diagram). *Develop mathematical tools to study the phase diagram of the HEG and other materials.*

4. Conclusion

We have discussed some open mathematical problems concerning charged quantum particles. For atoms and molecules, we focused on the ionization curves obtained when electrons are added or removed from the system in its ground state. Many other open problems could have been mentioned, in particular concerning the inclusion of relativistic effects or the description of time-dependent phenomena. In another direction, we insisted on the poor rigorous understanding we have of macroscopic Coulomb systems. Phase transitions such as freezing occur experimentally for many Coulomb systems, but there is currently no mathematical tool to rigorously prove this happens. A simple question is why table salt has the structure we know and this must follow from Schrödinger's equation.

Declaration of interests

The authors do not work for, advise, own shares in, or receive funds from any organization that could benefit from this article, and have declared no affiliations other than their research organizations.

Acknowledgement

I thank the anonymous referee for useful comments.

References

[1] M. Lewin, *Some open mathematical problems concerning charged quantum particles*, 2024. Online at https://www.carmin.tv/en/collections/symposium-open-questions-in-the-quantum-many-body-problem/video/some-open-mathematical-problems-concerning-charged-quantum-particles (accessed on April 1, 2025). Talk delivered at the institut Henri Poincaré in the symposium "*Open Questions in the Quantum Many-body Problem*".

[2] E. H. Lieb and R. Seiringer, *The Stability of Matter in Quantum Mechanics*, Cambridge University Press: Cambridge, 2010.

[3] T. Kato, "Fundamental properties of Hamiltonian operators of Schrödinger type", *Trans. Am. Math. Soc.* **70** (1951), pp. 195–221.

[4] E. H. Lieb and M. Loss, *Analysis*, 2nd edition, Graduate Studies in Mathematics, vol. 14, American Mathematical Society: Providence, RI, 2001, pp. xxii+346.

[5] M. Lewin, *Spectral Theory and Quantum Mechanics*, Universitext, Springer International Publishing: Cham, 2024.

[6] G. M. Zhislin, "A study of the spectrum of the Schrödinger operator for a system of several particles", *Trudy Moskov. Mat. Obšč.* **9** (1960), pp. 81–120.

[7] G. M. Zhislin, "On the finiteness of the discrete spectrum of the energy operator of negative atomic and molecular ions", *Teoret. Mat. Fiz.* **21** (1971), pp. 332–341.

[8] D. R. Yafaev, "On the point spectrum in the quantum-mechanical many-body problem", *Math. USSR Izv.* **40** (1976), pp. 861–896. English translation.

[9] I. M. Sigal, "Geometric methods in the quantum many-body problem. Non existence of very negative ions", *Commun. Math. Phys.* **85** (1982), pp. 309–324.

[10] M. B. Ruskai, "Absence of discrete spectrum in highly negative ions: II. Extension to fermions", *Commun. Math. Phys.* **85** (1982), pp. 325–327.

[11] E. H. Lieb, "Bound on the maximum negative ionization of atoms and molecules", *Phys. Rev. A* **29** (1984), no. 6, pp. 3018–3028.

[12] I. M. Sigal and A. Soffer, "Long-range many-body scattering. Asymptotic clustering for Coulomb-type potentials", *Invent. Math.* **99** (1990), no. 1, pp. 115–143.

[13] J. Dereziński, "Asymptotic completeness of long-range N-body quantum systems", *Ann. of Math. (2)* **138** (1993), no. 2, pp. 427–476.

[14] V. Bach, J. Fröhlich and I. M. Sigal, "Spectral analysis for systems of atoms and molecules coupled to the quantized radiation field", *Commun. Math. Phys.* **207** (1999), no. 2, pp. 249–290.

[15] M. Griesemer, E. H. Lieb and M. Loss, "Ground states in non-relativistic quantum electrodynamics", *Invent. Math.* **145** (2001), no. 3, pp. 557–595.

[16] A. Kramida and Y. Ralchenko, *NIST Atomic Spectra Database, NIST Standard Reference Database 78*, 1999.

[17] W. Hunziker, "On the spectra of Schrödinger multiparticle Hamiltonians", *Helv. Phys. Acta* **39** (1966), pp. 451–462.

[18] C. Van Winter, "Theory of finite systems of particles. I. The Green function", *Mat.-Fys. Skr. Danske Vid. Selsk.* **2** (1964), no. 8, pp. 1–60.

[19] P. T. Nam, "The ionization problem in quantum mechanics", in *The Physics and Mathematics of Elliott Lieb. The 90th Anniversary Volume II* (R. L. Frank, A. Laptev, M. Lewin and R. Seiringer, eds.), EMS Press: Berlin, 2022, pp. 93–120.

[20] B. Simon, "Fifteen problems in mathematical physics", in *Perspectives in Mathematics: Anniversary of Oberwolfach 1984* (W. Jäger, J. Moser and R. Remmert, eds.), Birkhäuser: Basel, 1984, pp. 423–454.

[21] R. Benguria and E. H. Lieb, "Proof of the stability of highly negative ions in the absence of the Pauli principle", *Phys. Rev. Lett.* **50** (1983), pp. 1771–1774.

[22] J. P. Solovej, "Asymptotics for bosonic atoms", *Lett. Math. Phys.* **20** (1990), no. 2, pp. 165–172.

[23] P. T. Nam, "New bounds on the maximum ionization of atoms", *Commun. Math. Phys.* **312** (2012), no. 2, pp. 427–445.

[24] E. H. Lieb, I. M. Sigal, B. Simon and W. Thirring, "Asymptotic neutrality of large-Z ions", *Phys. Rev. Lett.* **52** (1984), pp. 994–996.

[25] E. H. Lieb, I. M. Sigal, B. Simon and W. Thirring, "Approximate neutrality of large-Z ions", *Commun. Math. Phys.* **116** (1988), no. 4, pp. 635–644.

[26] C. L. Fefferman and L. A. Seco, "On the energy of a large atom", *Bull. Amer. Math. Soc. (N.S.)* **23** (1990), no. 2, pp. 525–530.

[27] L. A. Seco, I. M. Sigal and J. P. Solovej, "Bound on the ionization energy of large atoms", *Commun. Math. Phys.* **131** (1990), no. 2, pp. 307–315.

[28] J. P. Solovej, "Proof of the ionization conjecture in a reduced Hartree–Fock model", *Invent. Math.* **104** (1991), no. 2, pp. 291–311.

[29] J. P. Solovej, "The ionization conjecture in Hartree–Fock theory", *Ann. of Math. (2)* **158** (2003), no. 2, pp. 509–576.

[30] J. P. Perdew, R. G. Parr, M. Levy and J. L. Balduz, "Density-functional theory for fractional particle number: Derivative discontinuities of the energy", *Phys. Rev. Lett.* **49** (1982), pp. 1691–1694.

[31] R. Parr and W. Yang, *Density-Functional Theory of Atoms and Molecules*, International Series of Monographs on Chemistry, Oxford University Press: USA, 1994.

[32] E. H. Lieb, "Density functionals for Coulomb systems", *Int. J. Quantum Chem.* **24** (1983), pp. 243–277.

[33] P. W. Ayers, "Energy is not a convex function of particle number for r^{-k} interparticle potentials with $k > \log_3 4$", *J. Chem. Phys.* **160** (2024), no. 4, article no. 044110.

[34] J. Lévy-Leblond, "Generalized uncertainty relations for many-fermion system", *Phys. Lett. A* **26** (1968), no. 11, pp. 540–541.

[35] P. Phillips and E. R. Davidson, "Chemical potential for harmonically interacting particles in a harmonic potential", *Int. J. Quantum Chem.* **23** (1983), no. 1, pp. 185–194.

[36] R. M. Fye, M. J. Martins and R. T. Scalettar, "Binding of holes in one-dimensional Hubbard chains", *Phys. Rev. B* **42** (1990), no. 10, pp. 6809–6812.

[37] J.-P. Blaizot and G. Ripka, *Quantum Theory of Finite Systems*, MIT Press: Cambridge, MA, 1985.

[38] S. Di Marino, M. Lewin and L. Nenna, "Grand-canonical optimal transport", *Arch. Ration. Mech. Anal.* **249** (2025), article no. 12.

[39] S. Di Marino, M. Lewin and L. Nenna, "Ground state energy is not always convex in the number of electrons", *J. Phys. Chem. A* **128** (2024), no. 49, pp. 10697–10706.

[40] E. H. Lieb and B. Simon, "Thomas–Fermi theory revisited", *Phys. Rev. Lett.* **31** (1973), pp. 681–683.

[41] E. H. Lieb and B. Simon, "The Hartree–Fock theory for Coulomb systems", *Commun. Math. Phys.* **53** (1977), no. 3, pp. 185–194.

[42] E. H. Lieb, "Thomas–Fermi and related theories of atoms and molecules", *Rev. Mod. Phys.* **53** (1981), pp. 603–641.

[43] J. P. Solovej, "A new look at Thomas–Fermi theory", *Mol. Phys.* **114** (2016), no. 7–8, pp. 1036–1040.

[44] A. Bjerg and J. P. Solovej, "Periodicity of atomic structure in a Thomas–Fermi mean-field model", preprint, 2024, 2406.19839.

[45] H. Brezis and E. H. Lieb, "A relation between pointwise convergence of functions and convergence of functionals", *Proc. Am. Math. Soc.* **88** (1983), no. 3, pp. 486–490.

[46] V. Bach, "Ionization energies of bosonic Coulomb systems", *Lett. Math. Phys.* **21** (1991), no. 2, pp. 139–149.

[47] V. Bach, R. Lewis, E. H. Lieb and H. Siedentop, "On the number of bound states of a bosonic N-particle Coulomb system", *Math. Z.* **214** (1993), no. 3, pp. 441–459.

[48] E. H. Lieb and W. E. Thirring, "Universal nature of Van Der Waals forces for Coulomb systems", *Phys. Rev. A* **34** (1986), pp. 40–46.

[49] M. Lewin, "A mountain pass for reacting molecules", *Ann. Henri Poincaré* **5** (2004), no. 3, pp. 477–521.

[50] M. Lewin, "Solution of a mountain pass problem for the isomerization of a molecule with one free atom", *Ann. Henri Poincaré* **7** (2006), no. 2, pp. 365–379.

[51] I. Anapolitanos and M. Lewin, "Compactness of molecular reaction paths in quantum mechanics", *Arch. Ration. Mech. Anal.* **236** (2020), no. 2, pp. 505–576.

[52] F. J. Dyson and A. Lenard, "Stability of matter. I", *J. Math. Phys.* **8** (1967), no. 3, pp. 423–434.

[53] E. H. Lieb, "The stability of matter", *Rev. Mod. Phys.* **48** (1976), no. 4, pp. 553–569.

[54] E. H. Lieb, "The stability of matter: from atoms to stars", *Bull. Amer. Math. Soc. (N.S.)* **22** (1990), no. 1, pp. 1–49.

[55] M. Loss, *Elliott Lieb's Work on Stability of Matter*, EMS Press: Berlin, 2022, pp. 31–45.

[56] C. Fefferman, "The thermodynamic limit for a crystal", *Commun. Math. Phys.* **98** (1985), no. 3, pp. 289–311.

[57] C. Hainzl, M. Lewin and J. P. Solovej, "The thermodynamic limit of quantum Coulomb systems. Part II. Applications", *Adv. Math.* **221** (2009), pp. 488–546.

[58] X. Blanc and M. Lewin, "Existence of the thermodynamic limit for disordered quantum Coulomb systems", *J. Math. Phys.* **53** (2012), article no. 095209. Special issue in honor of E. H. Lieb's 80th birthday.

[59] E. H. Lieb and J. L. Lebowitz, "The constitution of matter: Existence of thermodynamics for systems composed of electrons and nuclei", *Adv. Math.* **9** (1972), pp. 316–398.

[60] E. H. Lieb, "The $N^{5/3}$ law for bosons", *Phys. Lett. A* **70** (1979), no. 2, pp. 71–73.

[61] E. H. Lieb and H. Narnhofer, "The thermodynamic limit for jellium", *J. Stat. Phys.* **12** (1975), no. 4, pp. 291–310.

[62] M. Lewin, "Coulomb and Riesz gases: The known and the unknown", *J. Math. Phys.* **63** (2022), article no. 061101. Special collection in honor of Freeman Dyson.

[63] J. Z. Imbrie, "Debye screening for jellium and other Coulomb systems", *Commun. Math. Phys.* **87** (1982), no. 4, pp. 515–565.

[64] J. Fröhlich, B. Simon and T. Spencer, "Infrared bounds, phase transitions and continuous symmetry breaking", *Commun. Math. Phys.* **50** (1976), no. 1, pp. 79–95.

[65] F. J. Dyson, E. H. Lieb and B. Simon, "Phase transitions in quantum spin systems with isotropic and nonisotropic interactions", *J. Stat. Phys.* **18** (1978), no. 4, pp. 335–383.

[66] E. P. Wigner, "On the interaction of electrons in metals", *Phys. Rev.* **46** (1934), pp. 1002–1011.

[67] X. Blanc and M. Lewin, "The crystallization conjecture: A review", *EMS Surv. Math. Sci.* **2** (2015), no. 2, pp. 255–306.

[68] R. J. Baxter, "Statistical mechanics of a one-dimensional Coulomb system with a uniform charge background", *Proc. Camb. Philos. Soc.* **59** (1963), pp. 779–787.

[69] H. Kunz, "The one-dimensional classical electron gas", *Ann. Phys. (NY)* **85** (1974), no. 2, pp. 303–335.

[70] H. J. Brascamp and E. H. Lieb, "Some inequalities for Gaussian measures and the long-range order of the one-dimensional plasma", in *Functional Integration and its Applications* (A. Arthurs, ed.), Clarendon Press: Oxford, 1975.

[71] M. Aizenman and P. A. Martin, "Structure of Gibbs states of one dimensional Coulomb systems", *Commun. Math. Phys.* **78** (1980), no. 1, pp. 99–116.

[72] S. Jansen and P. Jung, "Wigner crystallization in the quantum 1D jellium at all densities", *Commun. Math. Phys.* **331** (2014), pp. 1133–1154.

[73] H. Cohn, A. Kumar, S. D. Miller, D. Radchenko and M. Viazovska, "Universal optimality of the E_8 and Leech lattices and interpolation formulas", *Ann. of Math. (2)* **196** (2022), no. 3, pp. 983–1082.

[74] M. Petrache and S. Serfaty, "Crystallization for Coulomb and Riesz interactions as a consequence of the Cohn–Kumar conjecture", *Proc. Am. Math. Soc.* **148** (2020), no. 7, pp. 3047–3057.

[75] M. Holzmann and S. Moroni, "Itinerant-electron magnetism: The importance of many-body correlations", *Phys. Rev. Lett.* **124** (2020), article no. 206404.

[76] S. Azadi and N. D. Drummond, "Low-density phase diagram of the three-dimensional electron gas", *Phys. Rev. B* **105** (2022), article no. 245135.

[77] L. Baguet, F. Delyon, B. Bernu and M. Holzmann, "Hartree–Fock ground state phase diagram of jellium", *Phys. Rev. Lett.* **111** (2013), article no. 166402.

[78] L. Baguet, F. Delyon, B. Bernu and M. Holzmann, "Properties of Hartree–Fock solutions of the three-dimensional electron gas", *Phys. Rev. B* **90** (2014), article no. 165131.

[79] F. Delyon, B. Bernu, L. Baguet and M. Holzmann, "Upper bounds of spin-density wave energies in the homogeneous electron gas", *Phys. Rev. B* **92** (2015), article no. 235124.

ACADÉMIE DES SCIENCES
INSTITUT DE FRANCE

Comptes Rendus. Physique
2025, Vol. 26, p. 113-124
https://doi.org/10.5802/crphys.232

Intervention in a conference / *Intervention en colloque*

Interlayer phase coherence and composite fermions

Cohérence de phase entre bicouche et fermions composites

Thierry Jolicoeur [a]

[a] Paris-Saclay University, CNRS, CEA, IPhT, France
E-mail: thierry.jolicoeur@ipht.fr

Abstract. The fractional quantum Hall effect (FQHE) realized in two-dimensional electron systems is explained by the emergent composite fermions (CF) out of ordinary electrons. It is possible to write down explicit wavefunctions explaining many if not all FQHE states. In bilayer systems there is a regime at integer filling of the lowest Landau level that displays a spontaneous breakdown of the $U(1)$ relative phase between the two layers. This can be seen as interlayer phase coherence (ILC) in terms of *electrons*. Recent experiments in double layer samples of graphene have revealed the appearance of many FQHE states unique to the bilayer case. We discuss extensions of the CF idea in this situation as well as the possible existence of ILC of CFs.

Résumé. L'effet Hall quantique fractionnaire (FQHE) réalisé dans les systèmes électroniques bidimensionnels s'explique par l'émergence de fermions composites (CF) à partir d'électrons ordinaires. Il est possible d'écrire des fonctions d'onde explicites expliquant de nombreux, voire tous les états de l'effet Hall quantique fractionnaire. Dans les systèmes formés de bicouches, il existe un régime de remplissage entier du niveau de Landau le plus bas qui présente une brisure spontanée de la phase relative $U(1)$ entre les deux couches. Cela peut être considéré comme une cohérence de phase entre les couches (ILC) en termes d'*électrons*. Des expériences récentes dans des échantillons à double couche de graphène ont révélé l'apparition de nombreux états FQHE propres au cas bicouche. Nous discutons des extensions de l'idée de CF dans cette situation ainsi que de l'existence possible d'ILC de CFs.

Keywords. Quantum Hall effect, Composite fermions, Interlayer phase coherence, Bilayer graphene.

Mots-clés. Effet Hall quantique, Fermions composites, Coherence entre couches, Bicouche de graphene.

Manuscript received 18 October 2024, revised 10 January 2025, accepted 13 January 2025.

1. Introduction

In the low-temperature regime quantum fluids may display physical properties governed by spontaneous symmetry breaking. This is the case of superfluids with the symmetry associated to the number of neutral particles. This also happens in superconductors with breakdown of the gauge symmetry of electrodynamics due to the condensation of Cooper pairs. Another set of phenomenon is due to the development of strong topological order known to happen in two-dimensional electrons gases in a magnetic field. This is the realm of the fractional quantum Hall effect (FQHE) [1, 2]. In this short review we will discuss the interplay of both phenomena in the context of graphene bilayers. Indeed it has been possible recently to fabricate devices

by stacking monolayers of graphene separated by a barrier of hexagonal boron nitride leading to an atomic scale physical separation between the layers and essentially no tunneling. Such devices have revealed a complex pattern of FQHE states and some of them may be described by spontaneous interlayer phase coherence of emerging entities [3] called "composite fermions". These composite fermions are in this case even more complex objects [4] than the ones appearing in single layer devices.

We will focus only on the approaches based on explicit wavefunctions written in terms of electron coordinates that have been shown to be extremely useful [3, 5, 6].

2. Fractional quantum Hall effect

To set the stage for the wavefunctions describing FQHE we first give a short introduction to Landau level physics and the integer quantum Hall effect which does not involve in a crucial way electron–electron interactions. The emerging dressed electrons called "composite fermions" that describe the FQHE will essentially be ruled by this regime. Numerous books are available, giving all necessary details [3, 7–9].

2.1. *Integer quantum Hall effect*

We consider a system of N_e electrons confined to two-dimensional plane under a perpendicular uniform magnetic field. This is a physical situation describing some electron gases in semiconductors, heterostructures or quantum wells. A simple description of this situation is given by the following Hamiltonian:

$$\mathscr{H} = \frac{1}{2m^*}(p + e\mathscr{A})^2, \tag{1}$$

where the vector potential can be taken in the so-called symmetric gauge $\mathscr{A} = (\mathscr{B} \times r)/2$. The effective mass m^* is a material dependent parameter. Solving for eigenvalues of the one-body Hamiltonian Equation (1) gives the Landau levels that have energies $E_N = (N + 1/2)\hbar\omega_\mathrm{c}$ with N a positive integer and $\omega_\mathrm{c} = eB/m^*$ the cyclotron frequency. There a macroscopic degeneracy in this situation: for each value of N there are exactly N_ϕ states that have this peculiar energy where N_ϕ is the number of flux quanta through the system $N_\phi = B \times A/(h/e)$. The FQHE is strongest when all electrons lie in the lowest Landau level (LLL) whose one-body eigenstates are given by the following formula:

$$\phi_M(r) = z^M \exp(-|z|^2/4\ell^2), \tag{2}$$

where we use the complex coordinate in the plane $z = x - \mathrm{i}y$ and we have defined the magnetic length $\ell = \sqrt{\hbar/(eB)}$. The power M is a positive or zero integer (we omit the normalization). With the special Landau level spectrum it is clear that even without considering interactions there are special cases when one has exact filling of an *integer* number of Landau levels, say p. With the formula for the degeneracy this happens when:

$$\nu = \frac{N_\mathrm{e}}{N_\phi} = \frac{nh}{eB} = p, \tag{3}$$

where we have defined the filling factor ν which is the fraction of occupied states, and n is the areal density of electrons. A naive thought is that in this integer case one has a magnetic-field induced insulator due to the presence of cyclotron gap $\hbar\omega_\mathrm{c}$. This gap lies between the highest occupied pth Landau level and the lowest empty $p+1$th level at zero temperature. This is the physical picture for the bulk sample. In a real finite-size sample the Landau levels are bent when approaching the boundaries and as a consequence the Landau levels will cross the Fermi

energy at some points that we may call "Fermi points" at the real-space edges of the system. As a consequence there is electric conduction with appearance of a Hall voltage V_{H} perpendicular to an imposed current I and its value is given by:

$$V_{\mathrm{H}} = \frac{1}{p}\frac{h}{e^2} I = \frac{1}{\nu}\frac{h}{e^2} I, \tag{4}$$

so that the Hall resistance defined by $R_{\mathrm{H}} = V_{\mathrm{H}}/I$ is quantized in units of h/e^2 and I is the current intensity in the sample. The presence of disorder in the sample leads to the appearance of plateaus as as a function of the magnetic field where the Hall resistance stays constant at the value Equation (4). This phenomenon, the so-called integer quantum Hall effect [10], does not involve in any crucial way the electron–electron interactions.

The closed-shell argument above suggests that for fractional filling no similar quantization should develop since partial filling of a flat band enlarged by disorder may host a Fermi liquid albeit with a large density of states. But striking experiments found evidence for the existence of a fractional quantum Hall effect when the filling factor ν is some rational fraction and the phenomenology of current transport is the same as in the integer case. The original discovery involved a plateau in the Hall resistance $R_{\mathrm{H}} = 3h/e^2$ corresponding to filling factor $\nu = 1/3$ in the LLL. To understand the fractional case one has to dig deep into the many-body problem of interacting electrons in the LLL. A generic many-body wavefunction is a sum of products of one-body states Equation (2) and thus can be written as a polynomial $\mathscr{P}$ in complex coordinates z_i times a universal (state-independent) Gaussian factor:

$$\Psi(z_1,\ldots,z_N) = \mathscr{P}(z_1,\ldots,z_N)\exp\left(-\sum_i |z_i|^2/4\ell^2\right). \tag{5}$$

In the spin-polarized case the polynomial $\mathscr{P}$ is antisymmetric to comply with the Pauli principle. In the general case it is hard to guess what are the relevant polynomials $\mathscr{P}$ but in the realm of the FQHE the successfull approach leads to explicit guess of the polynomials, the most famous case being the Laughlin wavefunction. We conclude this section by the giving the expression of $\mathscr{P}$ for the completely filled LLL. We first observe that the one-body states Equation (2) has a probability distribution which is a ring centered at $z = 0$ (because of the choice of gauge) whose radius grows with the exponent M. So fully filled LLL means that we occupy all one-body states from $M = 0$ up to a maximal value given by $M = N-1$ without any vacancy $z^0, z^1, z^2, \ldots, z^{N-1}$. This state is exactly a Slater determinant:

$$\Psi_{\nu=1} = \det(z_i^{j-1}) = \prod_{i<j}(z_i - z_j), \quad i,j = 1,\ldots,N, \tag{6}$$

where we have used the fact that the determinant is the so-called Vandermonde determinant. From now on we will omit the Gaussian factor from the one-body states since it is independent of the state under consideration. If we draw the charge density of state $\Psi_{\nu=1}$ in real space we find that it has the shape of a very flat pancake with uniform density in its interior and going to zero very quickly at the edge with a characteristic length ℓ.

2.2. *Laughlin wavefunction*

To explain the properties of the quantum state of electrons at $\nu = 1/3$ Laughlin proposed the following candidate wavefunction:

$$\Psi^{(3)} = \prod_{i<j}(z_i - z_j)^3 \exp\left(-\sum_i |z_i|^2/4\ell^2\right). \tag{7}$$

If we compute the charge density by some means we find also a very flat pancake as in state Equation (6) but with a mean density three times lower, corresponding to a uniform electronic

state with filling factor 1/3 (this would be $1/m$ if we were to put power m to the Vandermonde factor). This wavefunction has very good trial energy but is not an exact eigenstate of the Coulomb interacting electrons. So its theoretical status is not immediately clear. Another ansatz was the idea of starting from the Slater determinant of $\nu = 1$ and fill only one out of three orbitals: $z^0, z^3, z^6, \ldots$. Since this is still a determinant it can be easily computed giving $\prod_{i<j}(z_i^3 - z_j^3)$. This is not a good candidate for the FQHE state at $\nu = 1/3$. While it has the correct filling factor by construction it has higher energy than the Laughlin state because it lacks the big correlation hole around each electron due to the $(z_i - z_j)^3$ factor in the Laughlin wavefunction. Also this state called the Tao-Thouless state does not have a uniform density in real space and does not lead to the correct phenomenology of the FQHE at $\nu = 1/3$, contrary to the Laughlin state.

To clarify the status of the Laughlin state we now show to solve by elementary means any two-body problem in the LLL. The interacting Hamiltonian is:

$$\mathscr{H}_2 = \frac{1}{2m^*}(p_1 + e\mathscr{A}_{r_1})^2 + \frac{1}{2m^*}(p_2 + e\mathscr{A}_{r_2})^2 + V(r_1 - r_2), \tag{8}$$

where the positions of the electrons are r_1, r_2 and V is the interaction potential. In the context of the FQHE it is given by the Coulomb interaction $V(r) = e^2/r$. We now introduce the center of mass and relative coordinates $R = (r_1 + r_2)/2$, $r = r_1 - r_2$. The fact that the vector potential is linear in the coordinates leads to a simplification:

$$\mathscr{H}_2 = \frac{1}{2M}(\mathscr{P} + 2e\mathscr{A}_R)^2 + \frac{1}{2\mu}(p_r + (e/2)\mathscr{A}_r)^2 + V(r), \tag{9}$$

so the center of mass as well as the relative particle will live in their own separate Landau levels. If we focus on the relative particle we can take as a basis the one-body states of Equation (2) that are eigenstates of the angular momentum. If we consider a potential $V(r)$ which is rotationally invariant it will be automatically diagonal in such a basis. The eigenenergies are thus given by $V_m = \langle \phi_m | V(r) | \phi_m \rangle$. The numbers V_m are often called pseudopotentials and are given by a simple integral. In the Coulomb case the pseudopotentials decrease as $1/\sqrt{m}$. For spinless electrons only the odd values of m matter due to wavefunction antisymmetry. As a consequence, the full many-body interacting Hamiltonian can be written as:

$$\mathscr{H} = \sum_{i<j} \sum_{m=0}^{\infty} V_m \mathscr{P}_{ij}^{(m)} \tag{10}$$

where we have defined $\mathscr{P}_{ij}^{(m)}$ the projector onto the state of relative angular momentum m for the pair i, j of particles.

If now we retain only the $m = 1$ projector in the Hamiltonian Equation (10) then we note that the Laughlin state is an exact zero-energy eigenstate. Indeed since for all pairs of particles there is an overall factor z^3 with z the relative particle of pair i, j it means that it has no weight onto $m = 1$. For the experimentally relevant case of Coulomb interaction the $V_{m=1}$ pseudopotential is indeed the strongest which gives some weight to the relevance of the Laughlin state beyond the fact of having a good energy. The parametrization of Equation (10) suggests a way to interpolate between the Coulomb case and the hard-core limit involving only the projector $\mathscr{P}_1$ by varying the set of discrete pseudopotentials V_m. This idea was successfully implemented by F. D. M. Haldane (see his contribution in book [9]) showing that the Laughlin state is smoothly connected to the Coulomb ground state and thus these two states share the same physics.

As a polynomial in the electronic coordinates the Laughlin ansatz gives us a state which is already fully factorized. This is a mathematical statement concerning the polynomial appearing in the many-body wavefunction. It does not mean that the quantum state is factorizable, the Laughlin state is *not* a Slater determinant. Indeed it is known to be a case of strong entanglement, a property which does not exist in Slater determinant states. The zeros of this polynomial are

located exactly at the positions of the electrons, a very special feature which is not true in general. Let us rewrite the Laughlin polynomial in the following way:

$$\prod_{i<j}(z_i-z_j)^3=\prod_{i<j}(z_i-z_j)\times\prod_{i<j}(z_i-z_j)^2=\det(z_i^{j-1})\times\prod_{i<j}(z_i-z_j)^2. \tag{11}$$

Here we have explcitly factored out one power of the Vandermonde determinant Equation (6). We observe that if we pick one electron and drag it around the closest neighbor we see that the phase of the wavefunction changes by 6π while antisymmetry due to the Pauli principle requires only a 2π turn. We interpret this property by saying that there are exactly two vortices bound to each electron in this state of matter. The vortex attachment is directly due to the extra factor $\prod_{i<j}(z_i-z_j)^2$. While this reveals a fundamental property of the FQHE state, it does not lead immediately to a recipe to construct other candidate wavefunctions for filling factors beyond $\nu=1/3$. We now show in the next section how another rewriting of the Laughlin polynomial leads naturally to the so-called composite fermion construction.

2.3. *Composite fermion wavefunctions*

Experiments revealed also the appearance of the FQHE for fractions other than 1/3. The most prominent set of such states appears for filling factors $\nu=p/(2p\pm1)$ with p integer, asking for an explanation in terms of wavefunctions beyond the Laughlin state. One such state is given by the so-called composite fermion construction that we describe now. Much of our intuition of electron systems is based on Slater determinants and occupied/empty orbitals so the first step is to rephrase the successfull Laughlin state in this language. We write the correlation factor of the Laughlin state in the following way:

$$\prod_{i<j}(z_i-z_j)^3=\prod_{i<j}(z_i-z_j)\times\prod_{i\neq j}(z_i-z_j)=\det(z_i^{j-1})\times\prod_{i\neq j}(z_i-z_j). \tag{12}$$

Distributing the last among the columns of the determinant we arrive at the following identity:

$$\prod_{i<j}(z_i-z_j)^3=\det\left(z_i^{j-1}\prod_{k\neq i}(z_i-z_k)\right). \tag{13}$$

This can be interpreted as a Slater determinant for a filled Landau level provided one replaces the one-body wavefunctions by correlated one-body wavefunctions:

$$z^m\to z^m\prod_j(z-z_j), \tag{14}$$

where the product over j is over all other particles. The extra correlation factor is called a Jastrow factor in many-body physics. If we decide to adopt such correlated orbitals instead of the one-body states we can view the Laughlin state at $\nu=1/3$ as a completely filled Landau level with $\nu^*=1$. We guess then that excited states may involve higher-lying Landau levels provided one uses modified orbitals including the correlation factor Equation (14). In Landau levels other than the lowest the one-body eigenstates involve the complex conjugate z^* in addition of the complex coordinate z. Let us call $\phi_{N,m}(z,z^*)$ such a state in the Nth Landau level. We add Laughlin-style correlations by making the product as above:

$$\phi_{N,m}(z,z^*)\to\phi_{N,m}(z,z^*)\prod_j(z-z_j). \tag{15}$$

Such a state however does not live in the LLL due to the appearance of z^* factors. Since there is overwhelming evidence for FQHE in the LLL only we want to project such states into the LLL and then play the game of making Slater determinants. The operation of projection onto the LLL amounts to putting all z^* to the left-hand side of the formula and next replacing them by the

operator $2\partial/\partial z$. The result is then entirely in the LLL. In the $N = 1$ Landau level this manipulation amounts to the substitution:

$$z^m \to z^m \frac{\partial}{\partial z} \prod_j (z - z_j), \tag{16}$$

and going to even higher Landau levels simply add more derivatives acting onto the correlation factor. Since the correlation factors map $\nu = 1/3$ onto $\nu^* = 1$ one can say that the composite fermions feel a reduced magnetic field $B^* = B - 2n\phi_0$ by using the definition Equation (3) of the filling factor. This immediately suggests that there will be an IQHE for the composite fermions when $\nu^* = p$ with p filled Landau levels of the CFs. This translates in filling factors for electrons as $\nu = p/(2p+1)$. One can then write down Slater determinants made of correlated orbitals to describe such states. This procedure gives us explicit trial wavefunctions whose energies can be computed by a simple Metropolis sampling. Many if not all properties extracted from these CF wavefunctions are in excellent agreement with the known experimental data and also in agreement with numbers obtained from exact diagonalization of systems with a (very) small number of electrons. The series of FQHE states at $\nu = p/(2p+1)$ is prominent in high-quality samples and is called the Jain series of states. It is observed from $p = 1$ (the Laughlin state) up to at least $p = 10$. It is important to note that these states have *no* variational parameters and nevertheless offer a very accurate description of FQHE states (for detailed comparisons see e.g. [3]). The heuristic mapping $B \to B^*$ also correctly predict that when $B^* = 0$ the CFs form some kind of Fermi sea which is gapless as is observed in electron gases at $\nu = 1/2$.

With the notion of effective magnetic field B^* we note that it may be negative, leading to states with $\nu^* = -p$ hence $\nu = p/(2p-1)$ as observed in experiments. It is also easy to generalize the CF construction to fractions descending from the parent state $\nu = 1/5$. Indeed the Laughlin state can accommodate any odd power of the Jastrow factor for spin polarized fermions (even power for bosons). The same line of reasoning leads to series of states with $\nu = p/(4p+1)$ and $\nu = p/(4p-1)$, again many of such states are observed in nature. When the filling factors becomes low the FQHE are competing with a crystal state made out of electrons, called the Wigner crystal which does not have the same striking properties as the FQHE states.

The CF construction also gives a very simple picture of excited states. Since the CF are filling an integer of pseudo LLs a first type of excitations consists of promoting a CF from the topmost filled pseudo LL to the lowest empty pseudo LL. This is a neutral excitation with no change of the number of electrons or the number of flux quanta. One may expect that such an excited state has an energy cost given by the effective cyclotron energy for the CFs. There are also charged excited states obtained by making a hole in the topmost filled pseudo LL: such a state is called a quasihole. By reducing the applied magnetic flux one can also create a situation with only one electron promoted to the next pseudo LL. This is then the quasielectron state.

In the CF picture one still has to explain why the Hall resistance is quantized as $R_{xy} = (1/\nu)(h/e^2)$ with the ν the *electron* filling while there are p filled pseudo Landau levels of CF in the series $\nu = p/(2p+1)$. The explanation is that while the CF contains a charged electron it also binds two vortices. Indeed in the construction of the CF states the Jastrow factor squared is always present and in line with the case of the Laughlin state we interpret this factor by saying that there are two vortices bound to each eletron. The CF vortex carries two units of flux ϕ_0 and if such a vortex crosses a Hall bar it will induce a voltage drop $e = -\mathrm{d}\Phi/\mathrm{d}t = 2(h/e)(I/e)$ where I/e is the number of CF per unit time crossing the Hall bar. So there is an additional contribution to the Hall voltage: $V_{\mathrm{H}} = (1/p+2)h/e^2 I$. This completes the explanation of transport phenomenology in the FQHE regime which is mapped onto that of the IQHE.

Finally we mention that the composite fermions may undergo a pairing instability. This was proposed by Moore and Read [11] who introduced yet another intriguing explicit wavefunction called the Pfaffian:

$$\Psi_{\rm Pf} = {\rm Pf}\left(\frac{1}{z_i - z_j}\right)\prod_{i<j}(z_i - z_j)^2, \tag{17}$$

where the symbol Pf stands for the Pfaffian of the square matrix $1/(z_i - z_j)$. If we compute the determinant of an antisymmetric matrix we find that it is the square of a polynomial of the matrix elements. This polynomial is called the Pfaffian of the matrix. It appears when one projects a paired state like the BCS wavefunction onto a state with fixed number of particles. So the appearance of this peculiar factor is indicative of the paired nature of the Pfaffian state. Indeed the Pfaffian state is a p-wave paired state of composite fermions. The filling factor of the state can be easily computed and is $\nu = 1/2$. This state is not an exact eigenstate of the Coulomb interaction and is a trial state competing with the Fermi sea of composite fermions that exists at the same filling factor. In the LLL in semiconductors the Fermi sea has lower energy and the $\nu = 1/2$ state is compressible but it may be that this state becomes the ground state in the next Landau level where the effective Coulomb interaction is different from the LLL so it is a candidate for the FQHE state observed for $\nu = 2 + 1/2 = 5/2$ in some very clean devices. This state supports excitations with non-Abelian statistics which are very interesting quasiparticles. We will not discuss in more details this important FQHE topic.

3. Interlayer phase coherence

3.1. *The role of spin*

We now discuss the modifications of previous ideas when we consider the spin degree of freedom of charge carriers. The first remark is that the $\nu = 1$ state should be written as:

$$\Psi^{(1)} = \prod_{i<j}(z_i - z_j)|\uparrow\cdots\uparrow\rangle \tag{18}$$

since by construction it is fully polarized. More general states will not be a simple product of a spin part times an orbital part. If we consider the many-body problem of electrons interacting by the Coulomb potential we note that it has full $SU(2)$ spin rotation symmetry. This rotation symmetry will be broken down to $U(1)$ by the Zeeman coupling of the external field to the total spin. The state (18) has a spin projection onto the z axis equal to $S^z_{\rm tot} = +N/2$ and by rotational symmetry of the Hamiltonian it is also member of a multiplet of total spin $S_{\rm tot} = S^z_{\rm tot}$. This multiplet is exactly degenerate without Zeeman effect.

$$\Psi^{(1)} = \prod_k c^\dagger_{k\uparrow}|0\rangle \tag{19}$$

The $S^z_{\rm tot} = 0$ member of this spin multiplet is obtained by acting repeatedly with the spin lowering operator:

$$|S^z = 0\rangle = (S^-_{\rm tot})^{N/2}\prod_k c^\dagger_{k\uparrow}|0\rangle\,. \tag{20}$$

In this formula the spin operator acts only on the spin degrees of freedom but does not change the orbital part of the state. If we write the state in first quantization we decide to call z_i the coordinates of $\uparrow$ spins and w_k of $\downarrow$ spins and the orbital part of the $S^z_{\rm tot} = 0$ state is then:

$$\Psi^{(1)} = \prod_{i<j}(z_i - z_j)\prod_{k<l}(w_k - w_l)\prod_{i,k}(z_i - w_k). \tag{21}$$

The full wavefunction with the spin part is the antisymmetrized product of this orbital factor and of the zero spin state $|\uparrow\cdots\uparrow\downarrow\cdots\downarrow\rangle$. Halperin has proposed a generalization of the Laughlin wavefunction appropriate to states involving spin:

$$\Psi^{(mmn)} = \prod_{i<j}(z_i - z_j)^m \prod_{k<l}(w_k - w_l)^m \prod_{i,k}(z_i - w_k)^n. \tag{22}$$

Again this only the orbital part—it has to be supplemented by the spin part and antisymmetrized. Evaluation of spin-independent observables like the Coulomb energy only involve the orbital part so we simply omit the spin part for clarity. The filling factor of the trial state mmn has to be computed and is found to be $\nu = 2/(m+n)$ where the filling factor refers to the total filling including both species. In general it is not an eigenstate of total spin. Special cases include $m = n+1$ which is a singlet $S_{\rm tot} = 0$ and $m = n$ states that are ferromagnetic states as the state Equation (18). For example the (332) Halperin state describes the singlet state $\nu = 2/5$ that is a FQHE state appearing in samples with small Zeeman effect.

We note that at a given filling factor there are several Halperin state that are competing. For example at $\nu_{\rm tot} = 1/3$ one may construct the (333) state which has Laughlin correlations irrespective of the particle index and one can also build the (551) state which may become relevant when repulsion is weaker between the two components.

3.2. *Quantum Hall bilayers*

There are several physical situations where the electrons have a pseudospin index. This happens notably in many-valleys semiconductors. Monolayer graphene has two valleys and thus an extra pseudospin with two values in addition to the real spin. Some semiconductors like Si have up to six valleys. It may happens that the Coulomb interaction is independent of these extra degrees of freedom. This is approximately the case of monolayer graphene. We discuss now the case of engineered systems where two spatially separated layers of two-dimensional electron gases are close enough so that there are sizable Coulomb interactions. The layer index is then a pseudospin and the Coulomb interaction is different inside a given layer and between layers:

$$V_{\uparrow\uparrow} = V_{\downarrow\downarrow} = e^2/r, \quad V_{\uparrow\downarrow} = e^2/\sqrt{r^2+d^2}, \tag{23}$$

where d is the distance between layers. With this interaction the problem does not have the full $SU(2)$ rotation symmetry in pseudospin space but only the $U(1)$ rotation around the z axis which is the conservation law of the difference of particle numbers in the two layers. Let us concentrate on the case $\nu = 1$ first. In the limit $d \to 0$ we are back to the symmetric situation discusses in the previous section and the ground state is a ferromagnetic spin multiplet. If we now tune d small the members of the multiplet will no longer be degenerate. Since electron–electron interactions are weaker when they are in separate layers it means that the $S^z_{\rm tot} = 0$ state will have lower energy than all other states in the multiplet.

3.3. *Symmetry breaking and the phase*

If we increase the number of electrons at fixed interlayer distance d we discover that the multiplet of states $S^z_{\rm tot} = -N/2,\ldots,+N/2$ becomes degenerate as $N \to \infty$. This emergent degeneracy is the hallmark of broken symmetry. Since these states differ by the transfer of electron between layer it is the XY symmetry associated to the relative phase between layers which is broken. As in situations involving broken symmetry the physics become transparent once we use a function which breaks explicitly the symmetry. A simple choice is:

$$\Psi_x = \prod_k c^\dagger_{k,x}|0\rangle = \prod_k (c^\dagger_{k,\uparrow} + c^\dagger_{k,\downarrow})|0\rangle, \tag{24}$$

where k labels the one-body states of the LLL. This state has $\langle S^z_{\rm tot}\rangle = 0$ even though it is not an eigenstate of $S^z_{\rm tot}$. Expansion of the second formula reveals that it has weight over all members of the multiplet. This state is the analog of the BCS wavefunction for broken particle number. Its generalization to an arbitrary relative phase ϕ between layers is then:

$$\Psi(\phi) = \prod_k (c^\dagger_{k,\uparrow} + {\rm e}^{{\rm i}\phi} c^\dagger_{k,\downarrow})|0\rangle \tag{25}$$

This state gives equal weight to the two layers and this broken symmetry is aptly called interlayer phase coherence. In the magnetic language we are dealing with XY symmetry breaking and the relative phase ϕ is the XY order parameter. This phenomenon has been observed in semiconductor devices [12] for total filling factor unity and $d \lesssim \ell$. If the layer separation is too large then we have two essentially decoupled layers each hosting a $\nu = 1/2$ CF Fermi sea. There is at least one transition between the fully decoupled regime at large separation and the ILC phase at small separation. As expected in a system with a phase associated with symmetry breaking there should supercurrents in states with a gradient in space of this phase. However since the phase corresponds to the relative phase between the layers it implies that the supercurrent consists of opposite flows of charge carriers in opposite layers so with zero total current.

Let us now perform a particle-hole transformation on only one spin species of the state Equation (25) and call $d_{k,\uparrow}, d^\dagger_{k,\uparrow}$ the associated creation/annihilation operators. Then the state with definite phase Equation (25) can be written as:

$$\Psi(\phi) = \prod_k (1 + {\rm e}^{{\rm i}\phi} c^\dagger_{k,\downarrow} d_{k,\uparrow})|\bar{0}\rangle \tag{26}$$

where we have defined the new vacuum $|\bar{0}\rangle = \prod_k c^\dagger_{k,\uparrow}|0\rangle$. This new writing show that the ILC state at total filling factor $\nu = 1$ can be aptly called an exciton condensate where the two members of the exciton pairs reside in different layers.

There are two configurations of currents that can be used to reveal the ILC. The first one is the drag configuration in which a current is imposed only one layer (the "drive" layer) and may then measure the Hall voltage across the drive layer giving then a measurement of $R^{\rm drive}_{xy}$ and measure the Hall voltage across the other layer with no drive current (the "drag" layer) giving access to $R^{\rm drag}_{xy}$. If we consider the Halperin (111) wavefunction we note that driving an electron in one layer is accompanied by one vortex in the other layer so ILC has the special value:

$$R^{\rm drive}_{xy} = R^{\rm drag}_{xy} = \frac{h}{e^2} \tag{27}$$

The other configuration is the counterflow set-up in which the current of the drive layer is injected at the end of the Hall bar backwards in the top layer inducing a regime in which the currents flow in opposite directions in the two layers. If now we tune the magnetic field to reach $\nu_{\rm tot} = 1$ electrons and holes are locked together as in Equation (25) and thus form a neutral entity that does not feel the Lorenz force. So the Hall voltage in both layers goes to zero right at $\nu_{\rm tot} = 1$ a striking evidence of ILC [12].

4. Graphene bilayers in the modern era

It has been feasible recently to build devices with stacking of two atomically thin monolayers of graphene. Such systems can reach a regime where $d/\ell \approx 0.1$ which was out of reach of previous set-ups. Combined with high electronic mobility experiments have revealed numerous FQHE states [13, 14] that do not match the fillings of one-component states discussed in Section 2.3. One can first ask whether there is an extension of the CF wavefunctions giving trial wavefunctions for these states. Another more intriguing question is whether one can observe ILC involving as basic building blocks CF instead of electrons.

4.1. ${}^{2}_{1}CF$ *wavefunctions*

The Halperin family of states Equation (22) suggests a simple way to construct CF states [5]. We take a CF state in each layer, make a product and add a correlation factor between the two layers:

$$\Psi = \Psi_{\tilde{\nu}}(z_i) \times \Psi_{\tilde{\nu}}(w_k) \times \prod_{i,k}(z_i - w_k)^m. \tag{28}$$

Now the exponent m can be even or odd since there is no restriction from Fermi statistics. One may expect that the relevant values of m are smaller for larger separations between layers. This state has filling factors $\nu_{1,2}$ for each layer:

$$\frac{1}{\nu_{1,2}} = \frac{1}{\tilde{\nu}} + m = \frac{1}{\nu^*} + 2p + m \tag{29}$$

The CF that are formed in such states are called ${}^{2p}_{m}CF$ where there are $2p$ vortices attached to the electron in the same layer and m interlayer vortices, according to the interpretation of Jastrow factor in the CF language.

By increasing the distance d between the layers we expect a weakening of correlations and transitions [5] between competing states at fixed filling factor. For example at $\nu_{\rm tot} = 1/3$ one may have a ground state described by the (333) state at small separations which is a state of ${}^{2}_{3}CF$. For larger separation we construct the (551) at the same filling which is now a state of ${}^{4}_{1}CF$. For very large separations there should should no interlayer repulsion and so each layer should form a Fermi sea of ${}^{6}CF$ (note that at such a low filling factor $\nu = 1/6$ a Wigner crystal may form instead of a FQHE state). By considering compressible states one may enlarge the familty of trial states. For example there is the Fermi sea of ${}^{4}_{2}CF$ which is also competing at $\nu_{\rm tot} = 1/3$ that would lead to a compressible intermediate phase sandwiched between (333) and (551) states if we guess that the ordering of phase follow the power of the interlayer repulsion factor. At filling factor $\nu_{\rm tot} = 1/2$ one may consider the Halperin state (331) which may be realized in GaAs/GaAlAs devices [15, 16].

By similar reasoning we expect that for $\nu_{\rm tot} = 2/5$ by increasing the separation we find the (332) state which is a ${}^{2}_{2}CF$, then a Fermi sea of ${}^{4}_{1}CF$, then the state (550) which is a product of two Laughlin states at filling $1/5$, an incompressible state of ${}^{4}CF$.

It is also plausible [17] that other non-FQHE state enter the competition like crystal states of electrons or of composite fermions. Only partial theoretical analysis of this complicated situtation is available.

4.2. *Observed states*

By analogy with monolayer electronic gases one expects to find a prominent series of FQHE states involving ${}^{2}_{1}CF$ [5] which means $p = 1$ and $m = 1$ hence $\nu_{1,2} = n/(3n+1)$ where n is the number of filled pseudo-Landau levels of CFs. Indeed the states $\nu_{1,2} = 1/4$ ($n = 1$), $2/7$ ($n = 2$), $3/10$ ($n = 3$) are observed as incompressible states. The negative-flux series is also observed for $\nu_{1,2} = 1/2$ ($n = -1$), $2/5$ ($n = -2$), $3/8$ ($n = -3$). These two series of states should converge to a compressible state for $\nu_{1,2} = 1/3$. Some of these fractions have simple wavefunctions: this is the case of the $1/4$ state which involves two Laughlin states with one Jastrow power between the layers. The wavefunction is the (331) state in the Halperin family Equation (22). But these series of states do not exhaust the observations made in graphene bilayers.

Some additional fractions beyond the principal $n/(3n \pm 1)$ series include states with fractional n and odd denominator such as $\nu_{1,2} = 3/14$ corresponding to $n = 3/5$ or $\nu_{1,2} = 2/9$ with $n = 2/3$. It may be that such corresponds to FQHE states of composite fermions as observed in one-component systems for fractions like $\nu = 4/11$. They may fall in the general hierarchical scheme of FQHE.

Another set of states appear for $\nu_{1,2} = 1/3$ and $2/3$. These states do not manifest any drag Hall resistance so they are decoupled FQHE states likely (330) for $1/3$ and its particle-hole partner for $2/3$. The state observed at $\nu_{1,2} = 1/6$ may be a Halperin state (333) provided interlayer correlations are strong enough which is not completely consistent with uncorrelated states nearby at $1/3$. As we observed in the case of multicomponent states at a given filling factor there are several competing states when we vary the strength of interlayer coupling.

Finally there is evidence for states with half-integer filling of ${}^2_1CF$. This includes $\nu_{1,2} = 1/5\,(n = 1/2), 3/11$ $(n = 3/2), 5/17$ $(n = 5/2)$ and with negative flux $\nu_{1,2} = 3/7$ $(n = -3/2), 5/3$ $(n = -5/2)$. If we take into account the ILC phenomenology as well as the CF construction it is natural to conjecture that these states may display ILC of ${}^2_1CF$.

It is now a theoretical challenge to write down explicit wavefunctions capturing these states that combine the formation of emerging quasiparticles (the CFs) and their condensation in a broken symmetry state.

5. Conclusions

Recent experiments have given evidence for a fascinating interplay of topological order with the creation of a new type of composite fermions, the ${}^2_1CF$ entities. These CF quasiparticles may form Landau levels leading to incompressible states that are a generalization of the series of FQHE states already observed in single-layer one-component systems. However these experiments also revealed the appearence of other FQHE states whose description may involve interlayer phase coherence of composite fermions. Such states await detailed theoretical explanation. The technological advances in the manipulation of layered structures has opened a whole new field of investigation of correlated quantum states and the transitions between them.

Of course there are many more examples of multicomponent quantum Hall systems that we have not addressed in this short review. The experiments we have briefly discussed in this review [13, 14] have a thin insulating barrier of hexagonal boron nitride between two graphene monolayers. The barrier is thin enough to allow strong Coulomb interactions between the two electron gases but nevertheless thick enough to suppress tunneling. It is feasible to fabricate samples with nonzero tunneling. This leads a new set of physical properties. Notably the spin texture of charge excitations is changed and can be manipulated by tilting the applied magnetic field away from the direction perpendicular to the layers. The physics of this situation has been investigated in samples involving two semiconductor quantum wells coupled by tunnel effect. Each one-body quantum state in a well is then combined with its partner in the opposite well giving rise to eigenstates that are symmetric–antisymmetric (SAS) doublets with tunnel energy splitting $\Delta_{\rm SAS}$. It is thus feasible to investigate such a system as a function of the applied magnetic field and $\Delta_{\rm SAS}$. Such experiments have revealed the competition between one-component and two-component quantum Hall states as well as between single-layer and bilayer Wigner crystals [18, 19].

In the graphene world one can also study pure graphene bilayers where there is chemical bonding between two monolayers. The case of Bernal stacking (AB) has been investigated in detail in the quantum Hall regime. This is a very special case since the central Landau level has an orbital degeneracy between levels with $N = 0$ and $N = 1$ character where N is the Landau level index. This is in addition to the spin and valley degeneracies which are also present as in the case of monolayer graphene. The central level orbital degeneracy can be adjusted by applying an electric bias between the two layers leading to a tunable quantum Hall system which can interpolate between $N = 0$ and $N = 1$ FQHE physics. One expects that some if not all FQHE states can be described by appropriately generalized CF wavefunctions. Recent investigations [20] have revealed many FQHE states with *even* denominators that are outside the

scope of CF wavefunctions but likely to belong to the Pfaffian family of FQHE states or its particle-hole partner dubbed the "AntiPfaffian".

It is likely that progress in sample creation or fabrication will lead to more insights into these remarkable states of matter and more guidance for in-depth theoretical studies.

Declaration of interests

The authors do not work for, advise, own shares in, or receive funds from any organization that could benefit from this article, and have declared no affiliations other than their research organizations.

Acknowledgments

I thank Carlos Sá de Melo and Yvan Castin for giving me the opportunity to present this review at the workshop "Open questions in the quantum many-body problem" held in Paris in July 2024 at Institut Henri Poincaré.

References

[1] D. C. Tsui, H. L. Stormer and A. C. Gossard, "Two-dimensional magnetotransport in the extreme quantum limit", *Phys. Rev. Lett.* **48** (1982), no. 22, article no. 1559.

[2] R. B. Laughlin, "Anomalous quantum Hall effect: an incompressible quantum fluid with fractionally charged excitations", *Phys. Rev. Lett.* **50** (1983), no. 18, article no. 1395.

[3] J. K. Jain, *Composite Fermions*, Cambridge University Press: Cambridge, 2007.

[4] G. A. Csathy and J. K. Jain, "Next-level composite fermions", *Nat. Phys.* **15** (2019), pp. 883–884.

[5] V. W. Scarola and J. K. Jain, "Phase diagram of bilayer composite fermion states", *Phys. Rev. B* **64** (2001), article no. 085313.

[6] J. K. Jain and R. K. Kamilla, "Quantitative study of large composite-fermion systems", *Phys. Rev. B* **55** (1997), R4895–R4898.

[7] S. Das Sarma and A. Pinczuk, *Perspectives in Quantum Hall Effects: Novel Quantum Liquids in Low-Dimensional Semiconductor Structures*, Wiley: New Jersey, 2008.

[8] O. Heinonen, *Composite Fermions: A Unified View of the Quantum Hall Regime*, World Scientific: Singapore, 1998.

[9] R. E. Prange and S. M. Girvin, *The Quantum Hall Effect*, Springer New York: New York, 1989.

[10] B. I. Halperin, "Theory of the quantized Hall conductance", *Helv. Phys. Acta* **56** (1983), no. 1–3, pp. 75–102.

[11] G. Moore and N. Read, "NonAbelions in the fractional quantum Hall effect", *Nucl. Phys. B* **360** (1991), pp. 362–396.

[12] J. P. Eisenstein, "Exciton condensation in bilayer quantum Hall systems", *Annu. Rev. Condens. Matter Phys.* **5** (2014), pp. 159–181.

[13] X. Liu, Z. Hao, K. Watanabe, T. Taniguchi, B. I. Halperin and P. Kim, "Interlayer fractional quantum Hall effect in a coupled graphene double layer", *Nat. Phys.* **15** (2019), pp. 893–897.

[14] J. I. A. Li, Q. Shi, Y. Zeng, K. Watanabe, T. Taniguchi, J. Hone and C. R. Dean, "Pairing states of composite fermions in double-layer graphene", *Nat. Phys.* **15** (2019), pp. 898–903.

[15] Y. W. Suen, L. W. Engel, M. B. Santos, M. Shayegan and D. C. Tsui, "Observation of a $\nu = 1/2$ fractional quantum Hall state in a double-layer electron system", *Phys. Rev. Lett.* **68** (1992), pp. 1379–1382.

[16] J. P. Eisenstein, G. S. Boebinger, L. N. Pfeiffer, K. W. West and S. He, "New fractional quantum Hall state in double-layer two-dimensional electron systems", *Phys. Rev. Lett.* **68** (1992), pp. 1383–1386.

[17] W. N. Faugno, A. C. Balram, A. Wójs and J. K. Jain, "Theoretical phase diagram of two-component composite fermions in double-layer graphene", *Phys. Rev. B* **101** (2020), article no. 085412.

[18] H. C. Manoharan, Y. W. Suen, M. B. Santos and M. Shayegan, "Evidence for a bilayer quantum Wigner solid", *Phys. Rev. Lett.* **77** (1996), pp. 1813–1816.

[19] M. Shayegan, H. C. Manoharan, Y. W. Suen, T. S. Lay and M. B. Santos, "Correlated bilayer electron states", *Semicond. Sci. Technol.* **11** (1996), pp. 1539–1545.

[20] K. Huang, H. Fu, D. R. Hickey, N. Alem, X. Lin, K. Watanabe, T. Taniguchi and J. Zhu, "Valley isospin controlled fractional quantum Hall states in bilayer graphene", *Phys. Rev. X* **12** (2022), article no. 031019.

ACADÉMIE DES SCIENCES
INSTITUT DE FRANCE

Comptes Rendus. Physique
2025, Vol. 26, p. 533-569
https://doi.org/10.5802/crphys.258

Intervention in a conference / *Intervention en colloque*

How to exploit driving and dissipation to stabilize and manipulate quantum many-body states

Comment tirer parti du pompage et de la dissipation pour stabiliser et manipuler des états quantiques à N corps

Iacopo Carusotto[a]

[a] Pitaevskii BEC Center, INO-CNR and Dipartimento di Fisica, University of Trento, Italy
E-mail: iacopo.carusotto@ino.cnr.it

Abstract. We give a pedagogical introduction to the basic concepts of quantum fluids of light and to the different techniques that are being developed to exploit driving and dissipation to stabilize and manipulate interesting many-body states in quantum fluids of light in cavity configurations. In the weakly interacting regime, this approach has allowed to study, among others, superfluid light, nonequilibrium Bose–Einstein condensation, photonic analogs of Hall effects, and is opening the way towards the realization of a new family of analog models of gravity. In the strongly interacting regime, the recent observations of Mott insulators and baby Laughlin fluids of light are opening promising avenues towards the study of novel strongly correlated many-body states.

Résumé. Nous donnons une introduction pédagogique aux concepts de base des fluides quantiques de lumière et aux différentes techniques qui ont été développées pour exploiter le pompage et la dissipation afin de stabiliser et de manipuler des états à N corps intéressants dans des fluides quantiques de lumière en cavité. Dans le régime d'interaction faible, cette approche a permis d'étudier, entre autres, la lumière superfluide, la condensation de Bose–Einstein hors d'équilibre, les analogues photoniques des effets Hall, et ouvre la voie à la réalisation d'une nouvelle famille de modèles analogiques de la gravité. Dans le régime d'interaction forte, les observations récentes d'isolants de Mott et de tout petits fluides de Laughlin faits de lumière ouvrent des voies prometteuses pour l'étude de nouveaux états à N corps fortement corrélés.

Keywords. Driven-dissipative systems, many-body problem, nonequilibrium statistical mechanics, strongly correlated quantum fluids, quantum fluids of light.

Mots-clés. Systèmes dissipatifs pompés, problème à N corps, mécanique statistique hors d'équilibre, fluides quantiques fortement corrélés, fluides quantiques de lumière.

Funding. We acknowledge financial support by: Provincia Autonoma di Trento (PAT); from Q@TN, the joint lab between University of Trento, FBK-Fondazione Bruno Kessler, INFN-National Institute for Nuclear Physics and CNR-National Research Council; the National Quantum Science and Technology Institute through the PNRR MUR Project under grant PE0000023-NQSTI, co-funded by the European Union — NextGeneration EU; the Deutsche Forschungsgemeinschaft (DFG, German Research Foundation) via the Research Unit FOR 5688 "Driven-dissipative many-body systems of ultracold atoms", project number 521530974.

Manuscript received 18 March 2025, revised 3 July 2025, accepted 16 July 2025.

1. Introduction

In the last decades, a most promising platform for many-body physics has emerged thanks to the dramatic advances in the laser cooling techniques for dilute atomic gases. This has allowed to reach unprecedented temperatures in the sub-nanokelvin range and has allowed the clean observation of textbook many-body phenomena such as Bose–Einstein condensation (BEC), the crossover from BEC to a Bardeen–Cooper–Schrieffer (BCS) superconductive state of Fermi gases, and first realizations of strongly interacting states of matter such as Mott insulators and fractional quantum Hall fluids [1–4]. As compared to traditional condensed matter systems which are subject to sizable fabrication disorder and spurious additional effects, atomic gases enjoy an extraordinary level of cleanness and control at the microscopic level, which permits a quantitative comparison with ab initio theoretical calculations. Still, the available values of the temperature are typically still too high to observe the most exciting strongly correlated states of matter.

More or less in the same years, the merging of ideas from quantum optics and many-body physics has led to the development of the concept of fluid of light, namely an assembly of photons confined in suitable cavity devices where they display a finite effective mass and sizable interactions mediated by the optical nonlinearity of the medium [5]. As a result of these features, the photon gas starts displaying the typical collective properties of a standard quantum fluid such as superfluidity and condensation and, by now, an active research is being devoted to the quest for strongly correlated states of the fluid of light [6,7]. As a key difference compared to atomic gases, fluids of light in cavity configurations are typically characterized by a driven-dissipative nature, where the state of the fluid is not determined by a thermal equilibrium condition, but rather by a dynamical balance of pumping and losses [8,9].

This was initially considered as a serious drawback, as it made it difficult to realize the most celebrated textbook models of many-body physics. But over the years it has become clear that the nonequilibrium nature of the fluid opens the way to new physical phenomena and offers a wide variety of novel experimental tools for the stabilization, the manipulation and the diagnostics of the fluid. In particular, very different states of matter can be realized by simply tuning the properties of the laser beams used to generate the fluid of light. As the open nature of the fluid of light naturally provides a way to exchange energy and particles with the external world, it can be exploited to reduce the level of thermal-like excitation of the fluid. Rather than trying to cool the system towards lower and lower temperatures, the idea is then to design driving and loss mechanisms that autonomously stabilize the system into the desired quantum many-body state.

Quite interestingly, these efforts in the nonequilibrium stabilization of fluids of light go on par with analogous developments in the context of cold atoms aiming at exploiting driving and dissipation to stabilize interesting many-body states of atomic matter [10–12], also coupled to optical cavities [13–15]. As a key difference, however, the typical dissipation schemes considered for atoms do not involve a net flux of atoms through the system from/to external reservoirs. Stimulated by recent pioneering experiments [16–18], it will be an exciting new frontier to explore the new nonequilibrium physics of driven-dissipative cold atomic gases that can exchange particles with one or more external reservoirs.

The goal of this article is to summarize the main ideas in the physics of fluids of light in cavity configurations and introduce the reader to the different strategies that have been developed in this context for the driven-dissipative stabilization of different quantum many-body states. As several reviews are already available on this topic [5–9], our focus will be on a pedagogical presentation of the main theoretical tools that can be used to describe the system under different pumping conditions and to design schemes to exploit the driven-dissipative nature for novel investigations of many-body physics. A brief discussion of some specific experiments will also

be given, yet without the ambition of providing a complete bibliography on this wide and active field of research. In particular, we will not dwell into the active research that is going on in fluids of light in propagating geometries [19] and which has already led to a number of recent landmark experiments, ranging from superfluidity features [20,21], quantized vortices [22–24], turbulent [25,26] and condensation phenomena [27–29], to the quantum dynamics past quenches [30] and pioneering work on strongly interacting gases [31,32]. As the quantum dynamics of the propagating fluid of light is an essentially conservative one, this area of research is somehow disconnected from the driven-dissipative dynamics of cavity configurations that is the focus of the present article.

In spite of these limitations, we hope that our presentation will be useful to those researchers that wish to export ideas of quantum fluids of light into the field of cold atoms, so as to realize driven-dissipative schemes that autonomously stabilize strongly correlated states of matter in ultracold atomic gases. The structure of the article is the following. In Section 2 we give the basic concepts in the field of fluids of light and we summarize the basic blocks of their theoretical description. Section 3 is focussed to the regime of weakly interacting fluids where a mean-field theory provides an accurate description of the system: after a brief summary of the theoretical description, we will outline a few specific configurations where the driven-dissipative nature of the fluid of light opens new exciting possibilities of stabilizing and manipulating many-body states and gives rise to interesting new effects. In Section 4, we turn to strongly interacting systems, with a special attention being paid to the stabilization and the manipulation of driven-dissipative fractional quantum Hall states. In Section 5 we give our conclusions and we sketch our vision of the perspectives of this field, with a special emphasis on transferring ideas of quantum fluids of light back to atomic gases in novel driven-dissipative regimes.

2. Basic concepts of quantum fluids of light

In our intuitive picture, we are used to associate light to propagating electromagnetic waves or, in a quantum description, to a stream of corpuscular photons that travel across space at a very fast speed. The concept of *Quantum Fluid of Light (QFL)* defies this picture. Merging ideas from condensed matter physics and optics, it deals with the collective behaviours that assemblies of photons display when they are endowed of an effective mass and sizable inter-particle interactions [5] and are then manipulated as a standard fluid of many interacting particles.

This section starts with a brief review of these basic concepts and, then, elaborates on the intrinsically driven-dissipative nature of the fluid of light in cavity configurations and on the tools that are needed for its theoretical description.

2.1. *Conservative dynamics*

2.1.1. *Photon mass in cavity configurations*

Within special relativity, massless particles travel at a constant speed c and a finite mass is required to put particles at rest. In vacuo, the photons that constitute light beams are massless particles. The situation can dramatically change in spatially confined geometries, where photons acquire a finite effective mass for their motion along some dimensions thanks to the spatial confinement along the other dimensions.

The simplest case is the one sketched in the top panel of Figure 1, namely a cavity enclosed by a pair of plane-parallel metallic mirrors located along the xy plane and separated by a distance L_z along z. As the tangential component of the electric field has to vanish at the metallic mirrors, the z component of the wavevector is quantized as $k_z^{(q)} = \pi q / L_z$ according to the positive integer

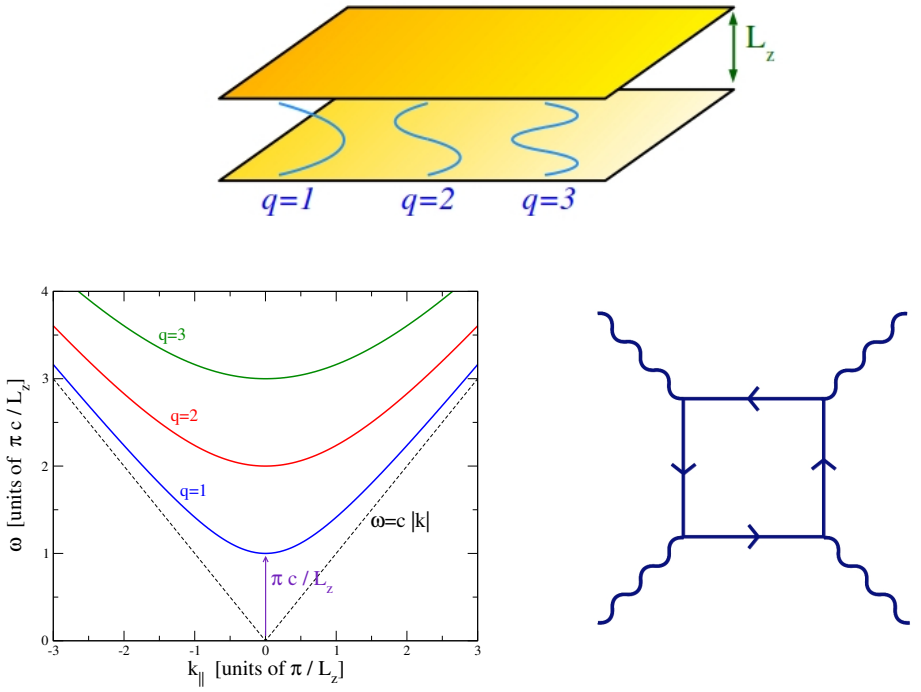

Figure 1. Light confinement in a planar microcavity (top) results in a relativistic dispersion for the in-plane motion of photons (bottom left). Feynman diagram describing the Heisenberg–Euler photon-photon interaction processes mediated by virtual electron-positron pairs in Quantum Electrodynamics (bottom right).

number $q > 0$ characterizing the number of field nodes along the z direction. On the other hand, given the translational symmetry along the xy plane, the motion along these directions is free and the corresponding component $\mathbf{k}_\parallel$ of the wavevector can have arbitrary values.

As a result, forgetting for simplicity the polarization degrees of freedom, electromagnetic waves in a planar cavity filled of a material of refractive index n can be described in terms of a massive relativistic-like dispersion,

$$\left(\hbar\omega^{(q)}(\mathbf{k}_\parallel)\right)^2 = (m^{(q)}c^2)^2 + \frac{\hbar^2 c^2}{n^2}\mathbf{k}_\parallel^2, \tag{1}$$

where the finite effective mass of each q branch

$$m^{(q)}c^2 = \frac{\hbar c k_z^{(q)}}{n} = \hbar\omega_o^{(q)} \tag{2}$$

arises from the zero-point confinement along z and grows with the quantum number q. As usual in special relativity, the mass parameter $m^{(q)}$ encodes both a *rest mass* related to the energy $\hbar\omega_o^{(q)}$ of a photon at rest in the zero-momentum $\mathbf{k}_\parallel = 0$ state and a *kinetic mass* related to growth of the energy of a photon when this is set into motion at a non-zero $\mathbf{k}_\parallel$. In the bottom left panel of Figure 1, the former can be read out as the energy gap below the dispersion, while the latter gives the curvature of the dispersion around its bottom.

Under a non-relativistic approximation, a parabolic form of the dispersion is obtained for each q branch at small in-plane momenta,

$$\omega^{(q)}(\mathbf{k}_\parallel) \simeq \omega_o^{(q)} + \frac{\hbar}{2m^{(q)}}\,\mathbf{k}_\parallel^2. \tag{3}$$

Upon quantization, the electric field in the cavity can be expanded as

$$\widehat{E}(\mathbf{r}_\parallel, z) = \sum_{q=1}^{\infty} \mathscr{E}_q(z)\,\widehat{\Psi}_q(\mathbf{r}_\parallel) + \mathscr{E}_q^*(z)\,\widehat{\Psi}_q^\dagger(\mathbf{r}_\parallel) \tag{4}$$

in terms of a set of quantum field operators $\widehat{\Psi}_q(\mathbf{r}_\parallel)$ describing each q branch and satisfying bosonic commutation rules,

$$\left[\widehat{\Psi}_q(\mathbf{r}_\parallel), \widehat{\Psi}_{q'}^\dagger(\mathbf{r}'_\parallel)\right] = \delta_{q,q'}\,\delta^{(2)}(\mathbf{r}_\parallel, \mathbf{r}'_\parallel). \tag{5}$$

The wavefunction of mode q around the bottom of the branch

$$\mathscr{E}_q(z) = \sqrt{\frac{4\pi\hbar\omega_o^{(q)}}{n^2 L}}\,\sin\!\left(\frac{\pi\, q\, z}{L}\right) \tag{6}$$

displays nodes at $z = 0, L$ and gives an energy $\hbar\omega_o^{(q)}$ per photon.

The form (3) of the dispersion suggests a straightforward way to generate an external potential for photons. Replacing in (3) the explicit dependence of $\omega_o^{(q)}$ on the cavity parameters (2), it is in fact immediate to see how a slow lateral dependence of the refractive index $n(\mathbf{r}_\parallel)$ and/or of the cavity thickness $L(\mathbf{r}_\parallel)$ can be exploited to generate an effective in-plane potential profile

$$V^{(q)}(\mathbf{r}_\parallel) = \omega_o^{(q)}(\mathbf{r}_\parallel) = \frac{c\pi q}{n(\mathbf{r}_\parallel)\,L(\mathbf{r}_\parallel)}. \tag{7}$$

Such a potential can be used, e.g., to exert uniform forces in the case of a uniform gradient or to localize the photons in suitably defined potential wells. Of course, in order to avoid introducing undesired losses due to the abrupt in-plane variation of the field mode, the $\mathbf{r}_\parallel$-dependence of L and n has to be sufficiently smooth to avoid non-adiabatic inter-branch transitions.

Even though these simple formulas have been obtained for the simplest case of metallic cavities, qualitatively similar results hold for other kinds of planar microcavities with translational symmetry along the xy plane, in particular semiconductor DBR microcavities enclosed by distributed Bragg reflectors [5,33].

2.1.2. *Photon-photon interactions*

A superposition principle for light fields directly follows from the linearity of the classical Maxwell equations in vacuo [34]: two light beams propagate independently of each other, and a light beam cannot be used to modify the propagation of another beam. Quite remarkably, this cornerstone of classical electrodynamics ceases to be true in quantum electrodynamics where photons can be converted into electron-positron pairs and back.

Among a plethora of other effects, this interaction vertex results into the effective photon-photon interaction process first pointed out by Heisenberg and Euler in the 1930's [35] and illustrated in the bottom right panel of Figure 1. As this process is mediated by the creation of virtual electron-positron pairs, the effective scattering cross section is only significant for high energy photons of energies comparable to the electron/positron rest mass of around 0.5 MeV, while it is dramatically suppressed at lower energies according to

$$\sigma \propto \alpha^4 \left(\frac{h}{m_{el}c}\right)^2 \left(\frac{\hbar\omega}{m_{el}c^2}\right)^6. \tag{8}$$

In addition to the squared electron Compton wavelength $h/(m_e c) \simeq 2.4$ pm and the four fine-structure $\alpha = e^2/\hbar c \sim 1/137$ factors corresponding to the four interaction vertices, the main suppression comes from the detuning of the virtual intermediate states due to the large rest mass of the virtual electron-positron pairs compared to the incident photon energy. For visible light in the eV range, this suppression factor can be as huge as 10^{-36} making the observation of Heisenberg–Euler photon-photon scattering processes in table-top experiments very difficult. Efforts are in progress to observe photon-photon scattering in vacuo using strong laser beams [36] or γ-rays [37–39] and experimental results have been reported for a related effect of photons scattering off the strong electrostatic field surrounding a heavy-ion [40].

The microscopic mechanism of photon-photon scattering in vacuo suggests that a huge reinforcement of the effect would be obtained if lighter particles were available as intermediate states of the scattering process. This naturally occurs in solid-state insulating materials, whose ground state consists of a filled valence band and an empty conduction band. Promoting an electron from the valence to the conduction band can be reinterpreted as the creation of an electron in the conduction band and a hole in the valence band [41]. The energy cost of this process is roughly determined by the electronic energy gap of the material, typically in the eV range. A naive translation of this result into the formula (8) predicts a dramatic reinforcement of the photon-photon scattering cross section by a factor of the order 10^{36} and suggests the actual observability of photon-photon collision processes in material media.

This intuitive picture of photon-photon collisions can be put on solid grounds in the framework of nonlinear optics [42,43]: here, binary photon-photon interactions are encoded in the $\chi^{(3)}$ optical nonlinearity of the medium, which describes a dielectric polarization proportional to the cube of the applied electric field. Such nonlinear optical processes occur in generic optical media and strong efforts are presently being paid to realize materials where the strength of the optical nonlinearities is reinforced well beyond the prediction of a naive extension of (8). Among the most promising platforms for this purpose, we can mention superconductor-based circuit-QED devices operating in the microwave range [7,44] or optically dressed atomic gases in the so-called Rydberg-EIT configurations [6,31,32]: such exceptional media are at the heart of the recent developments towards the realization of strongly interacting photon fluids that we are going to present later on in Section 4.

For the sake of simplicity, we will restrict our quantitative discussion of the photon-photon interaction Hamiltonian to a simplest case that can be worked out in analytical terms. We model photon-photon interactions as a normally-ordered, spatially local quartic term of the form

$$H_{\rm int} = \frac{\hbar g_{\rm 3d}}{2} \int {\rm d}^3\mathbf{r} : \widehat{E}(\mathbf{r})^4 : \tag{9}$$

By equating[1] the nonlinear frequency shift predicted by the Hamiltonian (9) for a given plane-wave mode at $\mathbf{k}$ in a spatially uniform geometry when only this mode is coherently occupied with amplitude $\overline{\alpha}$,

$$\delta\omega = 6 g_{\rm 3d} \, |\mathscr{E}|^4 \, |\overline{\alpha}|^2 \tag{10}$$

with the amplitude of the nonlinear polarization at the frequency of the mode predicted by the nonlinear optics formalism,

$$P_{\rm nl} = 3\chi^{(3)} \, |\mathscr{E}|^2 \mathscr{E} \, |\overline{\alpha}|^2 \, \overline{\alpha}, \tag{11}$$

we obtain that

$$g_{\rm 3d} = -\frac{\chi^{(3)}}{2\hbar}. \tag{12}$$

[1] We have assumed a spatio-temporally local nonlinearity, so the total nonlinear polarization is $P_{\rm nl}^{\rm (tot)}(\mathbf{r},t) = \chi^{(3)} E^3(\mathbf{r},t)$. The uniform-space mode normalization is $\mathscr{E} = (2\pi\hbar\omega/n^2)^{1/2}$. The amplitude of the coherent state is normalized as $\langle \hat{a}_{\mathbf{k}} \rangle = (2\pi)^3 \delta(\mathbf{k}-\mathbf{k}') \, \overline{\alpha}$.

Moving to a planar cavity geometry completely filled by the nonlinear medium and restricting our attention to the lowest $q = 1$ mode, we can insert the explicit expression for the cavity mode profile (6) into (9) and integrate over z, so that we obtain a nonlinear interaction term of the usual form

$$H_{\rm int} = \frac{\hbar g_{\rm nl}}{2} \int {\rm d}^2\mathbf{r}_\parallel \, \widehat{\Psi}^\dagger(\mathbf{r}_\parallel)\, \widehat{\Psi}^\dagger(\mathbf{r}_\parallel)\, \widehat{\Psi}(\mathbf{r}_\parallel)\, \widehat{\Psi}(\mathbf{r}_\parallel) \tag{13}$$

with an interaction strength $g_{\rm nl}$ that is related to the third-order nonlinear susceptibility $\chi^{(3)}$ of the medium by [45]

$$g_{\rm nl} = -\frac{18\pi^2(\hbar\omega_o)^2}{n^4 L}\,\chi^{(3)}. \tag{14}$$

2.1.3. *The Hamiltonian*

Putting all these effects together, the dynamics of the quantum fluid of light in the lowest energy states around the bottom of the $q = 1$ branch can be summarized by the following bosonic Hamiltonian [5]:

$$H = \int {\rm d}^2\mathbf{r}_\parallel \left[\hbar\omega_o \widehat{\Psi}^\dagger(\mathbf{r}_\parallel)\, \widehat{\Psi}(\mathbf{r}_\parallel) + \frac{\hbar^2}{2m^*} \nabla_\parallel \widehat{\Psi}^\dagger(\mathbf{r}_\parallel)\, \nabla_\parallel \widehat{\Psi}(\mathbf{r}_\parallel) + \hbar V(\mathbf{r}_\parallel)\, \widehat{\Psi}^\dagger(\mathbf{r}_\parallel)\, \widehat{\Psi}(\mathbf{r}_\parallel) + \right.$$
$$\left. + \frac{\hbar g_{\rm nl}}{2} \widehat{\Psi}^\dagger(\mathbf{r}_\parallel)\, \widehat{\Psi}^\dagger(\mathbf{r}_\parallel)\, \widehat{\Psi}(\mathbf{r}_\parallel)\, \widehat{\Psi}(\mathbf{r}_\parallel) \right]. \tag{15}$$

Here, the first and second terms respectively describe the rest energy of the photons and their (nom-relativistic) in-plane kinetic energy, as defined in (1)–(2). The third term models the external potential (7) acting on the photons and the fourth one accounts for the (contact) photon-photon interactions mediated by the optical nonlinearity (14). All together, it is immediate to recognize this Hamiltonian exactly corresponds to the one of a bosonic gas of material particles, in particular of ultracold atoms [1].

2.2. *Driving and dissipation*

In contrast to fluids of material particles where the lifetime of the microscopic constituents is typically very long compared to the many-body dynamics of interest, photons in the typical cavity devices used for experiments on quantum fluids of light experience a significant decay rate, due to a combination of non-radiative losses by absorption processes in the cavity material and radiative ones through the cavity mirrors.

Two philosophies are then available to deal with these processes. On one hand, a part of the community is making strong efforts to improve the cavity design to maximize the lifetime and, in this way, the time-window available for the conservative many-body dynamics. In addition to the optimized planar microcavity devices used to study quasi-equilibrium Bose–Einstein condensation effects in polariton fluids [46,47], such a strategy is implicitly undertaken in many experiments addressing the many-body physics of microwave photons in superconductor-based circuit-QED platforms [48–50].

On the other hand, one can try to *turn a bug into a feature* and exploit the driven-dissipative nature of the fluid of light to explore the new physics that arises from the interplay of driving and dissipation with the conservative many-body dynamics. Some external pump is in fact needed to overcome the effect of losses that would normally tend to dissipate the fluid: rather than considering it just as an experimental complication, the presence of the pump opens a range of new possibilities to manipulate the many-body state of the fluid. On top of this, one must not forget that radiative losses transfer all properties of the in-cavity field to the emitted light [51], so that the quantum state of the fluid of light can be reconstructed in real time just by looking at the quantum optical properties of the emitted radiation. As we are going to see in what follows,

these are crucial advantages of fluids of light as compared to, e.g., ultracold atomic systems where experiments often require destructive imaging techniques.

Before dwelling into this rich physics, it is important to complete the theoretical framework by discussing how the driving and dissipation processes can be included into the theoretical model. This will be the subject of the next subsections.

2.2.1. *Losses*

Losses in usual devices are linear in the field amplitude and have an approximately frequency- and wavevector-independent rate, so that they can be described at the level of the master equation for the density operator

$$\frac{\mathrm{d}\widehat{\rho}}{\mathrm{d}t} = -\frac{i}{\hbar}[H,\widehat{\rho}] + \mathscr{L}[\widehat{\rho}] \tag{16}$$

by Markovian Lindblad terms of the form

$$\mathscr{L}_{\rm loss}[\widehat{\rho}] = \frac{\gamma_{\rm loss}}{2}\int \mathrm{d}^2\mathbf{r}_\parallel \left[2\widehat{\Psi}(\mathbf{r}_\parallel)\,\widehat{\rho}\,\widehat{\Psi}^\dagger(\mathbf{r}_\parallel) - \widehat{\Psi}^\dagger(\mathbf{r}_\parallel)\,\widehat{\Psi}(\mathbf{r}_\parallel)\,\widehat{\rho} - \widehat{\rho}\,\widehat{\Psi}^\dagger(\mathbf{r}_\parallel)\,\widehat{\Psi}(\mathbf{r}_\parallel)\right]. \tag{17}$$

While this theory is sufficient to deal with typical experimental configurations with moderate to long photon lifetimes, one must not forget that some extra care has to be paid if the loss rate is comparable to the frequency of the cavity mode and/or one is operating in the so-called ultrastrong light-matter coupling regime where the quantum vacuum state of the cavity is strongly distorted from the usual QED vacuum: in this case, non-Markovian terms are often needed to avoid unphysical *perpetuum mobile* behaviours in the theory [52–54]. As the cavities that are typically used for quantum fluid of light experiments are far from this regime, in what follows we will safely stick to the form (17) of the loss term.

2.2.2. *Coherent pump*

The coherent pumping associated to the injection of photons by a coherent field incident on the cavity mirror can be described within the input-output formalism [51,55] by additional terms in the conservative Hamiltonian. In the simplest case where the transmission amplitude η of the cavity mirror is flat in both frequency and wavevector, these have the simple form

$$H_{\rm coh} = \int \mathrm{d}^2\mathbf{r}_\parallel \left[\hbar\eta\,\mathscr{E}_{\rm inc}(\mathbf{r}_\parallel,t)\,\widehat{\Psi}^\dagger(\mathbf{r}_\parallel) + \hbar\eta^*\,\mathscr{E}^*_{\rm inc}(\mathbf{r}_\parallel,t)\,\widehat{\Psi}(\mathbf{r}_\parallel)\right] \tag{18}$$

in terms of the (fully arbitrary) space- and time-dependent amplitude of the incident field $\mathscr{E}_{\rm inc}(\mathbf{r}_\parallel,t)$ at the cavity mirror location.

While this formulation is sufficient to deal with the typical microcavity devices used in quantum fluid of light experiments, more complicated situations can be described by replacing the constant mirror transmission amplitude η with a convolution with a spatio-temporal kernel $\eta(\mathbf{r}_\parallel,t)$ to account for the frequency- and wavevector-dependence of the mirror transmission amplitude. As usual in the input-output theory, such a generalized form of the transmission amplitude must be associated to a corresponding frequency and wavevector dependence of the radiative loss rate [53].

2.2.3. *Incoherent pump*

Incoherent pumping terms originate from an incident thermal radiation or from spontaneous emission processes by some suitably excited medium embedded in the cavity. This can consist, e.g., of population-inverted two-level systems or of an electrically-injected electron-hole gas. In contrast to the coherent pumping described in (18), such incoherent processes are totally phase-insensitive and do not inherit any coherence from the electric/optical mechanism used to excite the two-level systems or inject the electron-hole gas. While coherent pumping processes may

induce reversible oscillatory Rabi-flopping dynamics, incoherent pumping is characterized by an intrinsic irreversible push towards the excited states.

At a simplest level of approximation, one may be tempted to describe the effect of incoherent pumping within a Born and Markov approximation by including a Lindblad term of the form

$$\mathscr{L}_{\rm pump}[\widehat{\rho}] = \frac{\gamma_{\rm pump}}{2}\int \mathrm{d}^2\mathbf{r}_\parallel \left[2\widehat{\Psi}^\dagger(\mathbf{r}_\parallel)\,\widehat{\rho}\,\widehat{\Psi}(\mathbf{r}_\parallel) - \widehat{\Psi}(\mathbf{r}_\parallel)\,\widehat{\Psi}^\dagger(\mathbf{r}_\parallel)\,\widehat{\rho} - \widehat{\rho}\,\widehat{\Psi}(\mathbf{r}_\parallel)\,\widehat{\Psi}^\dagger(\mathbf{r}_\parallel)\right] \tag{19}$$

into the master equation (16). This is a good approximation as long as the gain has a broad-band nature and, more importantly, the pump rate remains below the loss rate $\gamma_{\rm pump} < \gamma_{\rm loss}$. In this regime, the effect of incoherent pumping is to sporadically inject some extra photon into the cavity, which is then rapidly lost: in addition to spontaneous processes injecting photons (almost) uniformly into all modes of the cavity, incoherent emission processes may also enjoy bosonic stimulation so the emission will be reinforced into those cavity modes that already contain photons.

On the other hand, a most interesting physics occurs when incoherent pumping overcomes losses and a coherent fluid of light is spontaneously generated in the cavity via a nonequilibrium condensation mechanism analogous to lasing [8]: in this case, a naive use of (19) would lead to a divergence of the in-cavity field amplitude so an accurate description of the steady-state of the in-plane cavity field requires including gain saturation effects.

2.2.4. *Gain saturation & frequency selectivity*

A common strategy to account for gain saturation is to explicitly include the microscopic dynamics of the emission process into the quantum theoretical description. Such an approach dates back to early works in laser theory [56,57], where the emitters are described as two-level systems driven in a population-inverted state by some external incoherent pumping.

In a simplest geometry where the field is discretized in a lattice of cavities each supporting a single optical mode and embedding a single two-level emitter, the local Hamiltonian of each site (to be supplemented by hopping terms in a full lattice model) has the form

$$H_{\rm site} = \hbar\omega_0\,\widehat{a}^\dagger\widehat{a} + \hbar\omega_{\rm em}\,\widehat{\sigma}_z + \hbar\Omega_R\left[\widehat{a}^\dagger\widehat{\sigma}^- + \widehat{a}\widehat{\sigma}^+\right] \tag{20}$$

where the bosonic $\widehat{a}$ and the spin $\sigma^{z,\pm}$ operators respectively describe the photonic field (of natural frequency ω_0) and the two-level emitter (of natural frequency $\omega_{\rm em}$). The population inversion is enforced by an incoherent pumping acting on the emitter, as described by a Lindblad term of the form

$$\mathscr{L}_{\text{pump-em}}[\widehat{\rho}] = \frac{\Gamma_{\rm P}}{2}\left[2\widehat{\sigma}^+\widehat{\rho}\widehat{\sigma}^- - \widehat{\sigma}^-\widehat{\sigma}^+\widehat{\rho} - \widehat{\rho}\widehat{\sigma}^-\widehat{\sigma}^+\right]. \tag{21}$$

which pushes the population towards the excited state.

Effective incoherent pumping rate. Emission by the emitters into the cavity occurs via the light-matter coupling term in (20). If the pump rate $\Gamma_{\rm P}$ well exceeds the Rabi frequency Ω_R, the dynamics of the emitter can be adiabatically eliminated and the coherent Rabi oscillations typical of the Jaynes–Cummings model of cavity-QED [51,57] are replaced by an irreversible emission into the cavity mode.

If we further assume that the in-cavity field is weak enough not to affect the population inversion, gain saturation is not significant and we obtain an effective incoherent pumping of the form (19) with a rate

$$\gamma^{\rm eff,0}_{\rm pump} = \frac{4\Omega_R^2}{\Gamma_{\rm P}}. \tag{22}$$

Of course, such a rate is only obtained when the emitter is exactly on resonance with the photon mode, otherwise the pumping rate is reduced according to a Lorentzian lineshape of width $\Gamma_{\rm P}$ around the resonant point $\omega = \omega_{\rm em}$,

$$\gamma^{\rm eff}_{\rm pump}(\omega) = \gamma^{\rm eff,0}_{\rm pump}\,\frac{\Gamma_{\rm P}^2/4}{(\omega-\omega_{\rm em})^2+\Gamma_{\rm P}^2/4}. \tag{23}$$

Including this ω dependence is straightforwardly done in a linear system: for each mode at frequency $\overline{\omega}$, one can write an incoherent pumping term of the form (19) with an effective $\gamma^{\rm eff}_{\rm pump}(\omega)$ evaluated at the mode frequency $\omega = \overline{\omega}$.

Things get more complex in interacting many-mode models, where different frequencies ω have to be considered for the different transitions between many-body eigenstates. At a simplest level of approximation [58], the standard Lindblad term (19) can be replaced by a generalized term in the form [59]

$$\mathscr{L}_{\rm em}(\rho) = \frac{\gamma^{\rm eff,0}_{\rm pump}}{2}\sum_j \big[\widetilde{a}^\dagger_i \rho \widehat{a}_i + \widehat{a}^\dagger_i \rho \widetilde{a}_i - \widehat{a}_i \widetilde{a}^\dagger_i \rho - \rho \widetilde{a}_i \widehat{a}^\dagger_i\big], \tag{24}$$

where the sum runs over the lattice sites j and the frequency dependence of the pumping process is encoded by the modified jump operator $\widetilde{a}^\dagger_j$ such that

$$\langle f'|\widetilde{a}^\dagger_j|f\rangle = \frac{\Gamma_{\rm P}/2}{i(\omega_{f,f'}-\omega_{\rm em})+\Gamma_{\rm P}/2}\langle f'|\widehat{a}^\dagger_j|f\rangle \tag{25}$$

for each pair of many-body states f, f' with respectively N and $N+1$ photons. Physically, this means that the effective jump amplitude from the many-body state f with N photons to the many-body state f' with $N+1$ photons under the creation of a photon in the j cavity mode depends on the frequency difference $\omega_{f,f'} = \omega_{f'} - \omega_f$ of the many-body states.

Inserting the explicit expression (25) into the Lindblad term (24) leads to a Lorentzian dependence of the $f \to f'$ transition rate on the frequency difference $\omega_{f,f'}$,

$$\mathscr{T}_{\rm pump}(f\to f') = \gamma^{\rm eff}_{\rm pump}(\omega_{f,f'})\sum_j \big|\langle f'|\widehat{a}^\dagger_j|f\rangle\big|^2, \tag{26}$$

to be compared with the frequency-independent transition rate due to the loss processes discussed in Section 2.2.1,

$$\mathscr{T}_{\rm loss}(f'\to f) = \gamma_{\rm loss}\sum_j \big|\langle f|\widehat{a}_j|f'\rangle\big|^2. \tag{27}$$

On top of this, the imaginary part of the resonance factor in (25) leads, upon substitution into the Lindblad term (24), to an additional conservative Hamiltonian term giving a (typically small) energy shift of the energy levels of the photonic system, which can be physically understood as a consequence of the effective refractive index of the population-inverted emitters. In the simplest case of a linear single-mode cavity, an explicit calculation leads to a frequency-shift of the cavity mode by

$$\delta\omega_0 = \frac{\Gamma_P\,\gamma^{\rm eff,0}_{\rm pump}/4}{(\omega_{\rm em}-\omega_0)^2+\Gamma_P^2/4}\,(\omega_{\rm em}-\omega_0); \tag{28}$$

note how this effect has an opposite sign compared to the usual refractive index of ground-state atoms so, in contrast to the usual polariton splitting [5], it leads to the attraction of the cavity mode towards the emitter in a sort of *frequency pulling* effect.

It is important to note that the generalized master equation (24) is only valid under a sort of perturbative expansion in the strength of the driving/dissipation processes: the jump amplitudes in (25) are in fact evaluated in terms of the energies of the conservative eigenstates. Writing master equations that go beyond this approximation and allow to deal with stronger driving/dissipation regimes is a topic of present-day research [58,60,61].

Gain saturation. As mentioned above, the effective description based on (24) also assumes that the emission into the photon mode is weak enough not to deplete the population inversion in the emitters. Of course, bosonic stimulation of the emission processes makes this constraint more severe when there is a sizable population in the photonic modes, $\gamma_{\rm pump}^{\rm eff}\, n_{\rm ph} \ll \Gamma_{\rm P}$.

In order to go beyond this assumption and account for those gain-saturation effects that play a major role in many physical phenomena, one needs to fully include the back-reaction effect of the emission onto the emitter dynamics. At the quantum level, this requires a complete description of the emitter and field dynamics: this is a challenging many-body task and typically has to be carried out under some other simplifying hypothesis, e.g. mimicking gain saturation by means of two-photon loss processes or performing some Gutzwiller site-decoupling approximation [62]. At the semiclassical level, instead, calculations can be performed in terms of generalized mean-field equations inspired by the semiclassical theory of lasers as we are going to see in the next section.

Alternative configurations. To conclude this section, it is important to also mention that different configurations to obtain a frequency-dependent pumping were proposed in [63] using parametric emission processes. The key element of such schemes is to replace the two-level emitter used in (20) with an additional ancilla cavity displaying strong losses $\Gamma_{\rm anc}$ described by a standard Lindblad master equation. Parametric processes then generate pairs of photons in the photonic mode and in the ancilla cavity according to

$$H = \hbar\omega_0 \widehat{a}^\dagger \widehat{a} + \hbar\omega_{\rm anc}\, \widehat{b}^\dagger \widehat{b} + \left[\hbar\Omega_{\rm par} e^{-i\omega_{\rm par} t}\, \widehat{a}^\dagger \widehat{b}^\dagger + \hbar\Omega_{\rm par}^* e^{i\omega_{\rm par} t}\, \widehat{a}\widehat{b}\right]; \tag{29}$$

an effective irreversibility naturally arises if the ancilla decay rate $\Gamma_{\rm anc}$ well exceeds the parametric emission rate $\Omega_{\rm par}$. Right at the parametric resonance point, this gives an effective pumping rate,

$$\gamma_{\rm pump}^{\rm eff,0} = \frac{4|\Omega_{\rm par}|^2}{\Gamma_{\rm anc}}. \tag{30}$$

Such a value, together with the parametric resonance condition $\omega_{\rm par} - \omega_{\rm anc} = \omega_0$ can be directly inserted in the theory of equation (24) and leads to closely analogous results up to the many-body level. Such a strategy was experimentally put into practice in [64] to generate a Mott insulator state of impenetrable photons.

Alternative photon-number-conserving schemes to force microwave photons to scatter from high- to low-momentum states and eventually accumulate into a condensate were proposed in [65]. Interesting connections between nonequilibrium condensation and quantum transport and non-Hermitian topology were then highlighted in [66]. The subtle interplay of dissipative stabilization techniques with Floquet engineering was investigated in [67] with the goal of stabilizing interesting states of a strongly interacting Bose gas in the presence of a synthetic magnetic field. More generally, note how related techniques for autonomous dissipative stabilization of desired quantum states are of widespread use beyond quantum fluids of light for various tasks in quantum science and technology [68–72].

3. Weakly interacting fluid

The new possibilities opened for quantum fluids of light by the presence of the driving and dissipation processes were first addressed in the context of weakly interacting fluids for which a mean-field approximation is legitimate. Such regimes have been long studied in the context of nonlinear optics and laser physics and, more recently, in the context of polariton fluids and polariton condensates. The literature on this physics is immense and we refer the interested reader to recent review articles [5,73]. With no hope of completeness, in what follows we will focus on a few cases where the physics is—to our eyes—most clear and illustrative of the general principles.

3.1. *Mean-field approximation*

The key idea of the mean-field approximation is to write an approximate equation of motion for the expectation value of the field operator $\psi(\mathbf{r}_\parallel, t) = \langle \widehat{\Psi}(\mathbf{r}_\parallel, t) \rangle$. Such an equation of motion can be derived by taking the Heisenberg equation for the field operator and then factorizing all operator products. Usually, this factorization assumption is accurate as long as the fluctuations around the mean-field are small, which is generally the case if interactions between the particles are weak.

Application of this procedure to the conservative Hamiltonian (15) leads to the Heisenberg equation

$$i\hbar \frac{\mathrm{d}\widehat{\Psi}(\mathbf{r}_\parallel, t)}{\mathrm{d}t} = [\widehat{\Psi}, H] = \hbar\omega_o \widehat{\Psi}(\mathbf{r}_\parallel) - \frac{\hbar^2}{2m}\nabla_\parallel^2 \widehat{\Psi}(\mathbf{r}_\parallel) + \hbar V(\mathbf{r}_\parallel)\,\widehat{\Psi}(\mathbf{r}_\parallel) + \hbar g_{\mathrm{nl}} \widehat{\Psi}^\dagger(\mathbf{r}_\parallel)\,\widehat{\Psi}(\mathbf{r}_\parallel)\,\widehat{\Psi}(\mathbf{r}_\parallel), \tag{31}$$

on which the factorization approximation

$$\langle \widehat{\Psi}^\dagger(\mathbf{r}_\parallel)\,\widehat{\Psi}(\mathbf{r}_\parallel)\,\widehat{\Psi}(\mathbf{r}_\parallel) \rangle \approx \left|\psi(\mathbf{r}_\parallel, t)\right|^2 \psi(\mathbf{r}_\parallel, t) \tag{32}$$

gives the usual Gross–Pitaevskii equation for an interacting Bose–Einstein condensate,

$$i\frac{\partial \psi}{\partial t} = \left[\omega_o - \frac{\hbar\nabla^2}{2m^*}\right]\psi + V\psi + g_{\mathrm{nl}}|\psi|^2\psi. \tag{33}$$

Necessary conditions for the validity of this mean-field approach can be obtained from the general many-body theory of dilute Bose–Einstein condensates at equilibrium [1,74]. For instance, for three-dimensional gases, the condition can be expressed in terms of a diluteness condition $n_{3d}\, a_{\mathrm{sc}}^3 \ll 1$, where n_{3d} is the three-dimensional density and a_{sc} is the atom-atom collisional scattering length, related to the interaction parameter by $g_{\mathrm{nl}} = 4\pi\hbar^2 a_{\mathrm{sc}}/m$. More subtle conditions have to be imposed in low-dimensional geometries, but a quite general formulation involves the characteristic kinetic and interaction energies, $\varepsilon_{\mathrm{kin}} = \hbar^2 n^{2/d}/2m \gg \varepsilon_{\mathrm{int}} = g_{\mathrm{nl}} n$ or, equivalently, the number of particles per healing length, $n\xi^d \gg 1$ where n is the d-dimensional density and $\xi = \sqrt{\hbar^2/m g_{\mathrm{nl}} n}$ is the healing length characterizing the microscopic structure of the weakly interacting fluid.

The same factorization procedure can be performed on the pumping and loss terms introduced in Section 2.2. The coherent pump is straightforwardly included at the level of the Heisenberg equation. As the corresponding Hamiltonian term (18) is linear in $\widehat{\Psi}$, no additional factorization approximation has to be made. As a result, one obtains a forcing term in the equation of motion for ψ of the form:

$$\ldots + \eta\,\mathscr{E}(\mathbf{r}_\parallel, t). \tag{34}$$

The linear loss and incoherent pumping terms (17) and (19) give linear, phase-insensitive gain and loss terms of the form

$$\ldots - \frac{\gamma_{\mathrm{loss}}}{2}\psi + \frac{\gamma_{\mathrm{pump}}}{2}\psi, \tag{35}$$

from which it is immediate to see how an unlimited exponential growth may arise if $\gamma_{\mathrm{pump}} > \gamma_{\mathrm{loss}}$ and no gain saturation mechanism is included in the model.

3.1.1. *Gain saturation & frequency selectivity*

Gain saturation can be included starting from the model of Section 2.2.4. In analogy to the semiclassical equations of lasers [56,57], we have to write the equations of motions for the single-mode field amplitude $\alpha = \langle \widehat{a} \rangle$,

$$\frac{\mathrm{d}\alpha}{\mathrm{d}t} = -i\omega_0\alpha - i\Omega_R\sigma^- - \frac{\gamma_{\mathrm{loss}}}{2}\alpha, \tag{36}$$

as well as for the expectation values of the emitter operators $\sigma^{\pm,z} = \langle \hat{\sigma}^{\pm,z} \rangle$. Performing all the factorization approximations of mean-field theory, we obtain

$$\frac{\mathrm{d}\sigma^z}{\mathrm{d}t} = \Gamma_\mathrm{P}(1-\sigma^z) - 2i\Omega_R(\sigma^+\alpha - \sigma^-\alpha^*), \tag{37}$$

$$\frac{\mathrm{d}\sigma^-}{\mathrm{d}t} = -i\omega_\mathrm{em}\sigma^- - \frac{\Gamma_\mathrm{P}}{2}\sigma^- + i\Omega_R\sigma^z a. \tag{38}$$

These equations for the single-mode configuration can be straightforwardly extended to spatially continuous geometries with many uniformly distributed emitters of in-plane density n_em. For this, we introduce space-dependent emitter spin variables $\sigma^{\pm,z}(\mathbf{r}_\parallel)$ and we replace the localized field amplitude α with the continuous field $\psi(\mathbf{r}_\parallel)$.

In the so-called good-cavity limit where the emitter pump rate Γ_P is much faster than the field dynamics and of the light-matter coupling Ω_R, one can eliminate the emitter degrees of freedom and write an effective equation of motion for the field only,

$$i\frac{\partial\psi}{\partial t} = \left[\omega_o - \frac{\hbar\nabla^2}{2m^*}\right]\psi + V\psi + g_\mathrm{nl}|\psi|^2\psi + \frac{i}{2}\left[\frac{P - 2i\,\delta\omega_0}{1+|\psi|^2/n_s} - \gamma_\mathrm{loss}\right]\psi + \eta\,E_\mathrm{inc}(\mathbf{r},t) \tag{39}$$

where the cavity mode experiences an effective pumping

$$P = \frac{n_\mathrm{em}\,\Omega_R^2\Gamma_P}{(\omega_\mathrm{em}-\omega_0)^2 + \Gamma_P^2/4} \tag{40}$$

with a saturation density

$$n_s = \frac{(\omega_\mathrm{em}-\omega_0)^2 + \Gamma_P^2/4}{2\Omega_R^2} \tag{41}$$

and a Lorentzian frequency-dependence of linewidth Γ_P analogous to the one of (26). In analogy to what was found in (42), the presence of the emitters also leads to a frequency-pulling effect towards the emitter of magnitude

$$\delta\omega_0 = \frac{n_\mathrm{em}\,\Omega_R^2}{(\omega_\mathrm{em}-\omega_0)^2 + \Gamma_P^2/4}\,(\omega_\mathrm{em}-\omega_0). \tag{42}$$

The formulas starting (39)–(42) implicitly assume that the cavity field dynamics takes place in a very narrow frequency band around ω_0. At a slightly more sophisticated level, we can Taylor-expand the frequency-dependence of the different quantities around ω_0. For instance, the frequency-dependence of the pumping rate P can be effectively modeled [75] by replacing

$$P \to P\left[1 - \frac{2(\omega_0-\omega_\mathrm{em})}{(\omega_\mathrm{em}-\omega_0)^2+\Gamma_P^2/4}\left(i\frac{\partial}{\partial t} - \omega_0\right)\right] \tag{43}$$

and letting the last time-derivative to only act on the field ψ. In some physical models of lasing, such a frequency-dependence of gain is crucial to theoretically recover a stable laser operation at the bottom of the photon band as observed in the experiment.

As a final point, it is important to highlight that equations analogous to (39) have been derived in several other contexts from different points of view. The approach of this article is inspired from the many-body theory of dilute Bose gases: in this framework, it is then natural to call this equation *generalized nonequilibrium Gross–Pitaevskii equation*. The very similar equations that are considered in the context of nonlinear dynamics typically go under the name of complex Ginzburg–Landau equations [76,77]. In the nonlinear optics literature, they go under the name of *Lugiato–Lefever equation*: originally formulated in [78], this equation is still now a powerful workhorse for the description of optical devices based on Kerr cavity solitons and frequency combs [73].

3.1.2. *Quantum fluctuations beyond mean-field*

Within a semiclassical approach, effects beyond the mean-field can be described within the so-called truncated Wigner approximation [55,79] by adding a stochastic white noise term $\xi(\mathbf{r}_\parallel, t)$ on the right-hand side of the motion equation (39) so as to account, at least at a lowest order, for quantum fluctuations. In the case of coherent pumping, the complex-valued noise term must have a random phase and its variance is to be set to

$$\left\langle \xi^*(\mathbf{r}_\parallel, t)\, \xi(\mathbf{r}'_\parallel, t') \right\rangle = \frac{\gamma_{\rm loss}}{2}\, \delta^{(2)}(\mathbf{r}_\parallel - \mathbf{r}'_\parallel)\, \delta(t-t'); \tag{44}$$

this is the minimum noise level as determined by the quantum fluctuations associated to the discreteness of the photon in the loss process. Of course, a higher noise level is found in incoherent pumping configurations [80] where additional fluctuations are given by spontaneous events in the pumping process,

$$\left\langle \xi^*(\mathbf{r}_\parallel, t)\, \xi(\mathbf{r}'_\parallel, t') \right\rangle = \frac{1}{2}\left(\gamma_{\rm loss} + \frac{\gamma_{\rm pump}}{1+|\psi|^2/n_S}\right) \delta^{(2)}(\mathbf{r}_\parallel - \mathbf{r}'_\parallel)\, \delta(t-t'). \tag{45}$$

Further sources of quantum noise may stem from the interaction of the Bogoliubov modes of the photon fluid with phonon modes in the solid-state crystal hosting the fluid of light [81]. Generalization of truncated Wigner methods to systems involving emitters as described e.g. in the Hamiltonian model of (20) are under way [82].

As typical of Wigner representations [55], for any product of fields $\psi(\mathbf{r}_\parallel)$ and $\psi^*(\mathbf{r}'_\parallel)$, the statistical average over the noise provides information on the corresponding *symmetrized* product of quantum operators $\widehat{\Psi}(\mathbf{r}_\parallel)$ and $\widehat{\Psi}^\dagger(\mathbf{r}'_\parallel)$, so commutators have to be subtracted to obtain the more standard normal-ordered quantities. While this is a quite trivial step for single-time operator products, it poses serious challenges for calculation multi-time quantities [83].

Interestingly, the driven-dissipative condition makes the truncated Wigner approach much more stable than in the conservative case, as the field fluctuations get to a driven-dissipative steady-state determined by the interplay of stochastic noise and dissipation well before approaching an inaccurate classical field thermal equilibrium state [84]. While this is often sufficient to get physically reliable predictions for the field correlation functions [79], it is important to note that the approximation of truncating higher-order noise terms [85] that underlies (45) typically loses accuracy when strong interactions and/or very non-perturbative processes in the quantum fluctuations are considered, such as quantum tunneling in bistable systems [86,87]. Quantitative studies of the limitations of the truncated Wigner approach [88] and of possible avenues to include the higher-order derivative terms [89] are the topic of current research.

3.2. *Coherent pumping*

The configuration where the new possibilities opened by driving and dissipations are clearest is the coherent pumping one. This configuration was exploited in the first experiments demonstrating superfluid light, as the flow speed and the density of the fluid can be directly controlled by the incidence angle (i.e. the in-plane wavevector), the frequency and the intensity of the incident field [90,91]. As a key difference from equilibrium condensates, the oscillation frequency of the field is not bound to the chemical potential but is freely determined by the one of the incident coherent field. As a result, the equation of state becomes richer and new phenomena can be observed.

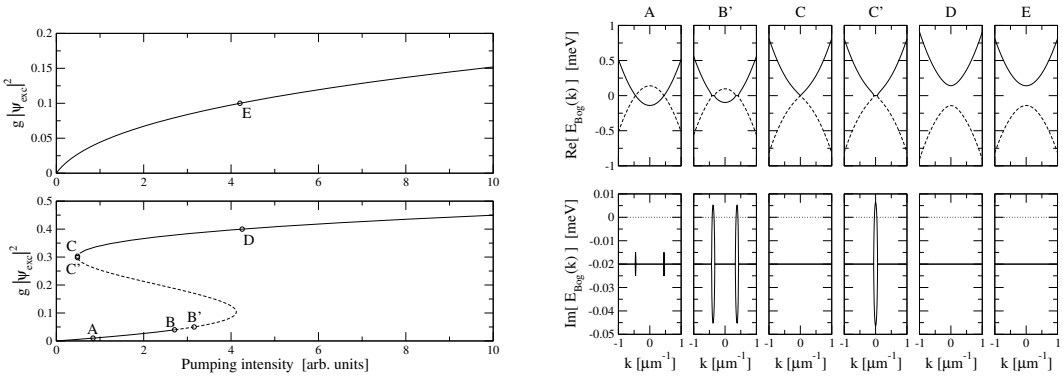

Figure 2. Left panels: plot of the equation of state of the fluid of light, expressed as fluid density as a function of pump intensity for two different incident frequencies in respectively the optical limiter regime (top) and the bistable regime (bottom). The dashed line indicates the dynamically unstable regions. Right panel: real part (top) and imaginary part (bottom) of the excitation frequencies for the nonequilibrium Bogoliubov modes corresponding to the points indicated as A, B', C, C', D, E in the left panel.

3.2.1. *Homogeneous fluid*

In the simplest case of a monochromatic incident field at $\omega_{\rm inc}$ with a spatially homogeneous profile, the fluid is at rest and the equation of state

$$\left[\left(\omega_0 + g_{\rm nl}|\psi|^2 - \omega_{\rm inc}\right)^2 + \frac{\gamma_{\rm loss}^2}{4}\right]|\psi|^2 = |\eta\, E_{\rm inc}|^2, \tag{46}$$

gives a complex nonlinear dependence of the density $|\psi|^2$ on the different parameters of the incident field. Some of the peculiar features of these nonequilibrium fluids are visually illustrated in Figure 2: the prediction of the equation of state (46) is displayed in the two left panels for the two cases of a pump frequency respectively below $\omega_{\rm inc} < \omega_0$ (top) and above $\omega_{\rm inc} > \omega_0$ (bottom) the bare resonance frequency (we are assuming $g_{\rm nl} > 0$): in the former case, the in-cavity intensity (proxied by $g|\psi_{\rm exc}|^2$ in the figure) grows monotonically but sublinearly with the pump intensity $|E_{\rm inc}|^2$; in the latter case, bistability effects are apparent, with two values of the density $|\psi|^2$ being available for the same value of the pump intensity $|E_{\rm inc}|^2$ (the intermediate branch is dynamically unstable).

Further consequences of the nonequilibrium condition are visible in the right panels, where the dispersion of the Bogoliubov modes on top of the homogeneous fluid [5,90] are plotted for the different operating points indicated by the capital letters in the left panels. As the oscillation frequency of the field ψ is not bound to $\omega_0 + g_{\rm nl}|\psi|^2$ as in the equilibrium case but is freely tunable via the incident frequency $\omega_{\rm inc}$, a wider range of behaviours can be observed depending on the pumping conditions. In particular, the Bogoliubov modes display a sonic long-wavelength behaviour $\omega = c_s|\mathbf{k}|$ only for a very specific operating point (C) at the end of the upper branch of the bistability loop. Away from this point, the dispersion may display finite gaps (D, E) and, even, precursors (A) or fully fledged (B, C') dynamical instabilities. Detailed experimental studies of the Bogoliubov dispersion in the different pumping regimes have been carried out by pump-probe spectroscopy in [92].

Going beyond mean-field, the consequences of the driven-dissipative condition are also visible in the steady-state fluctuations of the field ψ, which are well larger than the zero-point fluctuations of the Bogoliubov ground state of the corresponding equilibrium system. Within

a Bogoliubov picture, the loss process for a particle at momentum $\mathbf{k}$ involves in fact either the destruction of a quasi-particle at $\mathbf{k}$ or the creation of a quasi-particle at $-\mathbf{k}$. The overall magnitude of these fluctuations roughly corresponds to a temperature of the order of the interaction energy $g_{\rm nl}|\psi|^2$ and also display interesting correlation properties [93].

3.2.2. *Acoustic horizons and analog Hawking radiation*

This tunability of the Bogoliubov modes can be exploited to observe exciting new behaviours in spatially inhomogeneous configurations when the spatial profile of the coherent pump is suitably structured. In this perspective, a variety of configurations have been investigated in the literature, for instance vortices and vortex lattices that appear under a coherent pump carrying orbital angular momentum [94].

As a specific most exciting example, we focus here on configurations featuring a sonic horizon separating an upstream region of sub-sonic flow $c_u > v_u$ from a downstream region of super-sonic flow $v_d > c_d$ where $c_{u,d}$ and $v_{u,d}$ are respectively the sound and flow speeds in the two u,d regions. From the point of view of sound propagation, this configuration displays strong analogies with light propagation in the neighborhood of a black hole in gravitational physics and, upon quantization, sonic analogs of Hawking radiation have been anticipated to be emitted by the acoustic horizon [95].

With a careful design of the coherent pump, such analog black holes naturally arise as the driven-dissipative steady-state of a photon fluid. A natural possibility to achieve this [96] is to use a monochromatic pump and to design its phase profile so as to have a small in-plane wavevector in the upstream region and a larger one in the downstream region. Alternatively, the downstream region can be left unpumped so that the photon fluid is able to ballistically expand into this region. This latter configuration was experimentally realized in [97]. A spatially-resolved experimental characterization of the Bogoliubov modes on the two sides of the horizon has been performed in [98], explicitly showing the transition from a sub- to a super-sonic flow as the horizon is crossed: in the experiment, a super-sonic flow is signalled by the positive-norm branch of the Bogoliubov dispersion being pushed down to negative frequencies.

The on-going challenge is then to obtain experimental evidence of the analog Hawking emission by the acoustic horizon: to this purpose, numerical studies based on the Wigner formalism have shown that a clear signature of the Hawking radiation is present in the correlation function of density fluctuations on opposite sides of the horizon [96,97]. Physically, this correlation feature reflects the correlations between the Hawking phonon emitted outside the horizon into the sub-sonic region and its partner that propagates inside the horizon into the super-sonic region. Most interestingly, in contrast to atomic fluids where destructive measurements of atomic density profile are typically needed [99], intensity fluctuations are a quantity of direct and real-time experimental access in driven-dissipative photon fluids: radiative losses directly transfer the correlation functions of the in-cavity field into the ones of the emitted light, where the Hawking signal can be observed as peculiar intensity correlations of the emitted light.

Note that the extra fluctuations induced by the driven-dissipative nature [93] lead to a stimulation of the Hawking processes and, then, a reinforcement of the overall magnitude of the correlation signal. While this makes the correlations easier to detect, the resulting stimulated rather than spontaneous nature of the process may wash out the peculiar quantum entanglement features of Hawking radiation predicted in [100] in the context of analog models based on atomic condensates.

3.2.3. *Integer quantum Hall effect*

One of the most intriguing family of phenomena of quantum condensed matter physics is the quantum Hall effect [101]. This effect was originally discovered in two-dimensional electron

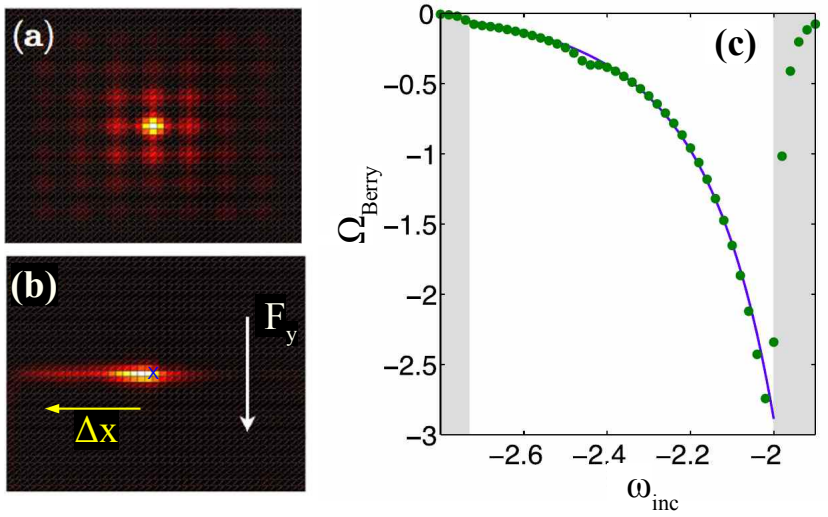

Figure 3. Left (a)–(b) panels: color plots of the numerically calculated steady-state intensity distribution in a coherently pumped $q = 5$ photonic Harper–Hofstadter model. The pump is localized on the central site and is resonant with the lowest photonic band. The loss rate is taken to be larger than the bandwidth $\gamma_{\rm loss}/\Delta\omega_{\rm band} = 2$, so as to be in the integer quantum Hall (IQH) regime. In the upper (a) panel, no external force is present and the distribution has a $\pi/2$ rotational symmetry. In the lower (b) panel, a force along the negative y direction is applied, so the intensity distribution moves leftwards along the transverse x direction. The magnitude of this displacement agrees with the prediction of the driven-dissipative IQH formula (48). Right panel: for a loss rate smaller than the bandwidth $\gamma_{\rm loss}/\Delta\omega_{\rm band} \simeq 1/30$ of the lowest band of a $q = 3$ Harper–Hofstadter, we are in the anomalous quantum Hall regime and the displacement is determined by the average of the Berry curvature over all states resonant with the pump frequency $\omega_{\rm inc}$. Within a photonic band (white region), the value of the Berry curvature extracted from the numerically calculated transverse shift (green points) are in good agreement with the value of the Berry curvature extracted from the Harper–Hofstadter band structure. Panels adapted from [102].

gases subject to strong magnetic fields and cooled to ultralow temperatures. While in room-temperature metals the transverse Hall resistivity ρ_{xy} shows a structureless linear dependence on the applied magnetic field B, the *quantum* Hall effect is visible as a series of plateaux in ρ_{xy} when the so-called filling factor

$$\nu = \frac{2\pi\hbar n_{2D}}{eB} \tag{47}$$

is in the neighborhood of integer (the so-called *integer quantum Hall (IQH)* effect) or fractional (*fractional quantum Hall (FQH)* effect) values. In this section, we are going to focus on the IQH effect, while a brief discussion of the FQH in an optical context will be given later on in Section 4.

Physically, the origin of the IQH can be traced to the complete and homogeneous filling of all states in the ν lowest Landau levels in the magnetic field B. In electronic systems where the number of electrons is conserved, the value of ν can be fixed by tuning the externally applied magnetic field B or the electronic density n_{2D} with suitable gates, so as to fix the Fermi energy between two Landau levels. While this simple argument explains the quantized value of the conductivity, the finite width of the plateaux results instead from a more subtle interplay

between localized and delocalized electronic states in the unavoidable disorder of any realistic system [101].

In analogy to these advances in quantum condensed matter systems, a strong interest is being devoted to the so-called topological photonic systems where new phenomena stemming from the non-trivial band topology of the photonic states have been observed, e.g. unidirectionally propagating chiral edge states [103]. In this context, a basic ingredient is the so-called synthetic magnetic field acting on photons: in the presence of a strong and uniform synthetic magnetic field, photonic modes closely resemble Landau levels and skipping orbits appear on the edges.

Even though in driven-dissipative photonic systems particles are continuously lost and replenished and no Fermi–Dirac statistics is available to impose a uniform population, a recent work [102] has pointed out that a spatially very localized coherent pump can be used to uniformly drive all states within a given Landau level. Even though the occupation is not pinned to 1 as it happens in the electronic case, the uniformity of the population is sufficient to observe a quantized response under the effect of a uniform force. In our photonic case, such a force—a sort of synthetic electric field—is obtained with a uniform spatial gradient of the cavity resonance frequency as described by a linearly varying potential term $V(\mathbf{r}_\parallel) = -\mathbf{F}\cdot\mathbf{r}_\parallel$ in (39).

Focusing for concreteness on the square-lattice Harper–Hofstadter model at $1/q$ flux per plaquette with a large q, the lateral spatial shift of the center of mass of the photon intensity distribution was in fact predicted [102] to be

$$\Delta x = \frac{q\mathscr{C}F}{\pi\gamma_{\rm loss}} \tag{48}$$

where a force of magnitude F is applied along the direction y and $\mathscr{C} = 1$ is the Chern number of the photonic band under examination: the driven-dissipative nature results in the transverse susceptibility being proportional to the lifetime $\gamma_{\rm loss}^{-1}$ times a quantized value.

While Landau levels in continuous space are perfectly flat in energy, the energy bands of discrete topological models on a lattice (e.g. the Harper–Hofstadter or the Haldane models) may display a significant bandwidth $\Delta\omega_{\rm band}$ in energy. In our driven-dissipative systems, this offers a further knob to stabilize and manipulate different states of the quantum fluid: depending on the relative value of the energy bandwidth $\Delta\omega_{\rm band}$ and of the loss rate $\gamma_{\rm loss}$, one can in fact transition from a IQH regime where $\gamma_{\rm loss} \gg \Delta\omega_{\rm band}$ and the coherent pumping uniformly drives all states within the band, to an anomalous Hall regime where $\gamma_{\rm loss} < \Delta\omega_{\rm band}$ and the frequency of the coherent drive specifically selects a set of resonant states. In this latter case, the lateral shift is no longer quantized and is determined by the averaged value of the Berry curvature over the set of resonant states. This provides a further example where the driven-dissipative nature of the photon fluid can be exploited to stabilize interesting many-body states and probe their physical properties.

An experiment that exploits driving and dissipation for a comprehensive study of anomalous and integer quantum Hall effect in a photonic Haldane model using a frequency-encoded synthetic dimension platform based on an optical fiber loop was recently reported in [104].

3.3. *Incoherent pumping*

In the previous subsection we have discussed coherent pumping schemes, where the phase of the in-cavity field is locked to the one of the incident field. A different range of physical phenomena are observed when an incoherent pump is used to inject photons in the system in a phase-insensitive way: as a most significant example, we will focus on the spontaneous generation of coherence via a nonequilibrium phase transition, a phenomenon that opens the way towards the study of critical phenomena in a novel nonequilibrium setting. While the

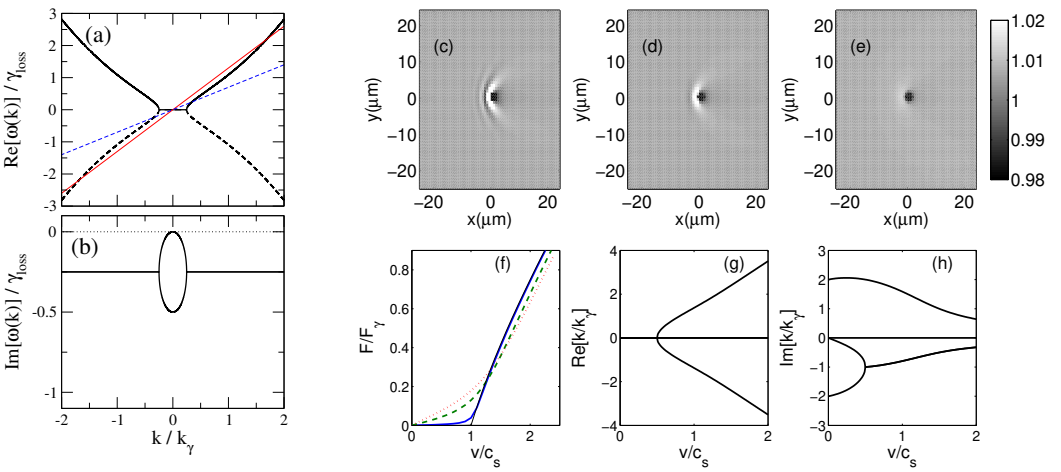

Figure 4. Left panels: plot of the real (a) and imaginary (b) parts of the dispersion of the collective excitations of a nonequilibrium condensate under incoherent pumping at $P/\gamma_{\rm loss} = 2$ with $\gamma_{\rm loss}/g_{\rm nl}|\psi|^2 = 1$. For small k values, the dispersion displays a diffusive plateau with a zero real part and a quadratically growing imaginary part. The oblique straight lines correspond to the Landau–Cherenkov $\omega = kv$ condition for a particle moving at $v/c_s = 0.7$ (blue dashed) or $v/c_s = 1.3$ (red solid). Wavevector is measured in units of k_γ such that $\hbar k_\gamma^2/2m = \gamma_{\rm loss}$. Right (c)–(h) panels: generalized Landau criterion for nonequilibrium condensates. Panels (c)–(e) show the density perturbation induced in a fluid moving in the positive x direction by an impurity at rest. The different panels refer to different values of the condensate velocity $v/c_s = 1.5$, 1, 0.4 across the (equilibrium) speed of sound $c_s = \sqrt{g_{\rm nl}|\psi|^2/m}$. Panel (f) shows the (normalized) force exerted by the fluid on the defect as a function of the condensate velocity v/c_s for different values of the nonequilibrium parameter $\gamma_{\rm loss}/g_{\rm nl}|\psi|^2 = 0$, 0.1, 1, 2. For the smallest $\gamma_{\rm loss}$ values, the sudden onset of friction that is visible in the vicinity of the critical speed $v/c_s = 1$ is a nonequilibrium counterpart of the Landau critical velocity of equilibrium superfluids [1,105]. Panels (g)–(h) show a cut of the real and the imaginary part of the wavevector of the collective excitations emitted in the negative x direction as a function of the speed for an intermediate loss case with $\gamma_{\rm loss}/g_{\rm nl}|\psi|^2 = 1$. The sudden onset of friction in (f) corresponds to the singular point that is visible in (g)–(h) slightly below $v/c_s = 1$. Panels (c)–(h) are adapted from [75].

underlying physics is very similar in the different systems, this phenomenon takes distinct names in distinct communities, e.g. laser oscillation in the optical literature or nonequilibrium Bose–Einstein condensation in the polaritonic one. An interdisciplinary review of this physics can be found in [8].

3.3.1. *Mean-field effects*

Restricting again to a weak interaction regime, a theoretical description of the field dynamics can be obtained at the mean-field level starting from the generalized Gross–Pitaevskii equation (39). In the absence of any coherent incident field $E_{\rm inc} = 0$, the system displays a marked threshold at $P_c = \gamma_{\rm loss}$ between a trivial $\psi = 0$ steady-state solution for a weak pump $P < \gamma_{\rm loss}$ to a condensed (or lasing) solution for a strong pump $P > \gamma_{\rm loss}$. In this latter regime, the steady-state

intensity is stabilized by nonlinear gain saturation effects to

$$|\psi|^2 = n_s\left(\frac{P}{\gamma_{\rm loss}} - 1\right) \tag{49}$$

but the phase of ψ remains free and is randomly chosen at every instance of the experiment. Under the $E_{\rm inc} = 0$ condition, the equation of motion (39) displays in fact a global $U(1)$ symmetry $\psi \to \psi\, e^{i\varphi}$ for arbitrary φ and this symmetry is spontaneously broken above threshold where the field ψ selects a specific and uniform phase across the whole system and its time-evolution displays a monochromatic oscillation at the intensity-dependent frequency $\omega = \omega_0 + g|\psi|^2$. The combination of a monochromatic oscillation in time and of a spatially uniform phase showcases the interest of this configuration as a source of spatio-temporally coherent light.

Diffusive Goldstone mode. Even though the driven-dissipative steady-state shares many properties with a standard Bose–Einstein condensate at equilibrium, one must not forget that the nonequilibrium condition is responsible for important deviations in the collective properties of the fluid, in particular for what concerns the Goldstone mode that is associated to the spontaneously broken $U(1)$ symmetry. As it is illustrated in Figure 4(a)–(b), the dispersion of the long-wavelength, low-frequency collective excitations does not show the usual sonic behaviour $\omega = c_s|\mathbf{k}|$ of equilibrium condensates with a speed of sound c_s, but rather displays a diffusive plateau in the form $\omega = -i\alpha k^2$ with a real and positive α. The usual behaviour with propagating collective excitations is only recovered at shorter wavelengths. The transition between the two regimes is typically associated to an exceptional point in the dispersion, whose position is determined by the strength of the departure from equilibrium, namely by the value of the loss rates: the larger $\gamma_{\rm loss}$, the wider the diffusive plateau. The theoretical prediction of a diffusive behaviour of the Goldstone mode of a nonequilibrium condensate has been recently confirmed in a pump-and-probe experimental measurement of the dispersion of the collective modes of an exciton-polariton condensate [106].

Generalized Landau criterion for superfluidity. This diffusive behaviour has been anticipated in [75] to impact the conceptual meaning of the Landau criterion for superfluidity in the driven-dissipative context. In stark contrast to the equilibrium case, it is shown in Figure 4(a) how the real part of the dispersion has an intersection with the Landau–Cherenkov $\omega = k\,v$ straight line for any non-zero value of v. A naive application of the Landau criterion for superfluidity [1,105] would then predict that an impurity moving across a fluid will experience a significant friction force for any value of the flow speed v, with no specific feature at the (equilibrium) speed of sound $c_s = \sqrt{g_{\rm nl}|\psi|^2/m}$.

This prediction is shown in Figure 4(f) to disagree with a full numerical solution of the generalized Gross–Pitaevskii equation (39): for small or moderate values of the nonequilibrium parameter $\gamma_{\rm loss}/g_{\rm nl}|\psi|^2$, the friction force exerted by an impurity at rest onto a moving fluid displays in fact a sudden upwards kink at a value of v/c_s close to the (equilibrium) critical velocity $v_{\rm cr} = c_s$. Such a change in behaviour can be associated to the singularity in the wavevector of the collective excitations emitted by the impurity shown in Figure 4(g)–(h): at low speed, this wavevector is purely imaginary, so the collective excitation generated by the impurity does not transport momentum; at large speeds, instead, this wavevector acquires a finite real part, which is directly associated to the momentum dissipated by the impurity into the fluid.

Spatial structure of the condensate and supersolid behaviours. While thermodynamical arguments impose that equilibrium condensates form in the lowest-energy single-particle orbital [1,107], exciting features are observed in the spatial structure of finite-size nonequilibrium condensates. For instance, restricting the incoherent pump to a limited region of space allows to control the shape of the condensate via the so-called volcano effect: condensation mostly occurs

at the center of the pump spot, and then the coherent particles get expelled by the repulsive interactions and form a macroscopic outward-expanding radial flow. Originally observed in [108], this effect was theoretically interpreted in [109] and fully confirmed experimentally in [110].

While this is the typical behaviour of spatially homogeneous systems, even more intriguing phenomena are observed in spatially periodic lattice geometries [111]. Here, condensation into an excited state at the top of a photonic band is favoured by the interplay of a positive interaction energy and a negative effective mass which result in effectively attractive interactions. These keep the condensate localized in space with a soliton-like shape [112,113] and, in this way, reduce the condensation threshold with respect to condensation into the expanding positive-mass states at the bottom of the band.

A presently very active direction of research concerns the realization of quantum fluids of light that simultaneously display a long-range coherence and a spontaneously formed spatially periodic density modulation. This physics has been recently investigated in both theory and experiments [114,115] using devices displaying several photonic bands in the same energy range. While the main condensation process occurs at the top of a photonic band, a spatial modulation of the condensate density spontaneously appears as the result of coherent parametric scattering processes into finite wavevector modes in the side photonic bands. Such configurations can be seen as photonic analogs of the so-called supersolid states of matter as recently observed in atomic condensates [116].

With a proper design of the device geometry, e.g. in ring resonators, related parametric processes can be induced into modes at different frequencies: in this case, the density modulation continuously moves in space and gives temporally periodic oscillations in the emitted light intensity, while preserving a long-time phase coherence of the emission. The importance of such *optical comb generators* for a number of opto-electronic applications [117,118] suggests that the new insight on the stabilization of complex states of matter offered by the use of many-body physics concepts in the novel driven-dissipative context will open interesting perspectives also for opto-electronic technologies.

3.3.2. *Fluctuation and quasi-condensation effects*

Going beyond the mean-field approximation, it is interesting to look at the process of condensation from the point of view of statistical mechanics and, in particular, highlight the role of quantum and thermal fluctuations. In this context, a natural question is to assess under which conditions the nonequilibrium steady state can recover a thermal equilibrium case: as a general trend, a quasi-equilibrium state is approached if the rate of thermalizing collisions between particles within the fluid is faster than their decay rate [8]. While early works have assessed thermality in terms of the momentum distribution approaching or not a Bose–Einstein distribution at a well defined temperature[2] and chemical potential [119,120], recent works have highlighted the need to establish thermalization in terms of rigorous fluctuation-dissipation relations and frequency-dependent observables [121]. As we have mentioned from the beginning of this article, this departure from equilibrium is a key asset rather than a hindrance and underlies the exciting developments that we are reviewing here.

In full generality, condensation in a spatially uniform geometry is typically associated [1,107] to the appearance of a sharp and macroscopic $\mathbf{k} = 0$ peak in the momentum distribution $n(\mathbf{k}) = \langle \widehat{\widetilde{\Psi}}^{\dagger}(\mathbf{k})\, \widehat{\widetilde{\Psi}}(\mathbf{k}) \rangle$ where $\widetilde{\Psi}(\mathbf{k})$ is the Fourier transform of the quantum field $\widehat{\Psi}(\mathbf{r})$. Equivalently, from a

[2] Note that the fluid of light may well thermalize at a temperature different from the one of the solid-state device that is hosting it.

real-space perspective, condensation is instead signalled by the onset of long-range order in the correlation function

$$G^{(1)}(\mathbf{r},\mathbf{r}') = \left\langle \hat{\Psi}^{\dagger}(\mathbf{r})\,\hat{\Psi}(\mathbf{r}') \right\rangle \tag{50}$$

which tends to a non-zero value at long distances $|\mathbf{r}-\mathbf{r}'| \to \infty$ [122].

This criterion for condensation can be physically understood in analogy with ferromagnetism where the ferromagnetic transition is characterized in terms of the magnetization correlation function

$$G^{(1)}(\mathbf{r},\mathbf{r}') = \left\langle \vec{M}(\mathbf{r})\,\vec{M}(\mathbf{r}') \right\rangle. \tag{51}$$

In the high-temperature disordered state, the correlation function only displays short-range correlations and quickly tends to zero at long distances. On the other hand, long-range order is visible in the low-temperature ferromagnetic state where the correlation function tends to a finite value at long distances signalling a uniform magnetization throughout the whole system[3].

More formally, the SO(2) rotational symmetry that is spontaneously broken by the ferromagnetic transition of the xy model is mathematically equivalent to the $U(1)$ group describing the $\Psi \to \Psi\, e^{i\phi}$ symmetry that is spontaneously broken at the condensation transition. As the specific direction of the magnetization is randomly selected at every instance of the experiment, the average value of the magnetization $\vec{M}$ is zero by symmetry unless some external magnetic field is present to pin its direction. In this case, the reduced symmetry makes a gap to open in the dispersion of the soft magnon branch associated to the spontaneous symmetry breaking [123].

A similar phenomenon is expected to take place for the condensation phase transition: in the absence of external fields, the $U(1)$ symmetry guarantees the presence of a soft Goldstone mode such that $\lim_{k\to 0}\omega(k) = 0$ in both its real and imaginary parts. On the other hand, when the $U(1)$ symmetry is explicitly broken by some external field, a gap opens in the Goldstone mode dispersion. While particle-number conservation makes it difficult to verify this prediction in atomic condensates at equilibrium [124], the phase of an optical condensate can be pinned by an additional incident coherent laser [125] and a clear gap in the Goldstone mode dispersion is clearly observed in experiments [106]. Differently from the equilibrium case, however, the gap may open in the imaginary and/or in the real parts of the Goldstone mode dispersion depending on the specific system parameters.

Quasi-condensation effects in low-dimensions. While three-dimensional geometries are the most natural ones in condensed matter systems, standard optical systems are typically limited to a maximum of two dimensions. In analogy to the bounds imposed on phase transitions by the Hohenberg–Mermin–Wagner theorem of equilibrium statistical mechanics [107], it is then natural to wonder whether the reduced dimensionality has a similar impact also on the nonequilibrium phase transition. Even though the general theorem cannot be directly applied to the nonequilibrium context, specific calculations have predicted [126] that in one dimension the long range order does not survive the long-wavelength fluctuations and is replaced by an exponential decay of the same-time coherence, yet on relatively long distance scales. As a rough estimate, the fluctuations in this one-dimensional quasi-condensate can be interpreted as a temperature on the order of the loss rate $k_B T \sim \hbar\gamma$ [127]. Even more subtle features have been pointed out for the intermediate two-dimensional case where the Berezinskii–Kosterlitz–Thouless transition typical of equilibrium systems [128,129] may be replaced by a Kardar–Parisi–Zhang (KPZ) physics [130–132].

[3] It is interesting to note that a three-dimensional easy-plane (in the xy plane) model of ferromagnetism subject to an orthogonal magnetic field (along z) is expected to display a steady rotation of the magnetization rotation along z. As a result, the x and y components of the magnetization display monochromatic oscillations as it happens to the field ψ of the optical model.

A common tool for the theoretical study of these phenomena is offered by the stochastic Gross–Pitaevskii equation discussed in Section 3.1.2. From an experimental standpoint, a very important asset for the study of the critical properties and of the spatio-temporal correlation function in the different regimes is provided by the radiative loss channel: as the coherence properties of the in-cavity field are imprinted into the one of the emitted radiation, their measurement can be straightforwardly performed with standard optical techniques. This feature has been exploited in experimental studies of the correlation properties across the phase transition and, in particular, for the recent observation of KPZ universal behaviours in a one-dimensional configuration [133].

While moving up to two-dimensional systems is not expected to pose additional conceptual challenges to optical experiments, three- and higher-dimensional configurations require the use of synthetic dimension schemes where extra spatial dimension are encoded in some other degrees of freedom of the photon, e.g. the different cavity modes of a ring resonator [134–136]. Pioneering experimental work on the collective dynamics arising from the combination of gain with one synthetic dimension in a ring laser was reported in [137,138]; an extension to a topological two-dimensional array of coupled ring resonators was presented in [139]. As next steps, we anticipate the possibility of extending this idea to study condensation in novel high-dimensional contexts and, in this way, unveil peculiar statistical behaviours resulting from the interplay of KPZ physics with the roughening transition [140–143].

4. Strongly correlated systems

In the previous sections we have discussed the physics of dilute driven-dissipative systems: for sufficiently weak interactions, a mean-field theory based on (stochastic) partial differential equations for classical fields provides an accurate description of the steady-state and of the dynamics of the system. In this last section, we briefly summarize the state-of-the-art and some future developments in the direction of realizing strongly correlated states of photonic matter that can be observed in systems with strong optical nonlinearities.

4.1. *Coherent drive*

4.1.1. *Photon blockade in a single-mode cavity*

The first proposal in this direction [144] was the so-called *photon blockade* effect. The dynamics of the quantum electromagnetic field in a nonlinear single-mode cavity can be described by a nonlinear oscillator Hamiltonian of the form

$$H = \hbar\omega_o \hat{a}^\dagger \hat{a} + \frac{\hbar\omega_{\rm nl}}{2} \hat{a}^\dagger \hat{a}^\dagger \hat{a}\hat{a} \tag{52}$$

where the anharmonicity is quantified by the parameter $\omega_{\rm nl}$ proportional to the $\chi^{(3)}$ optical nonlinearity of the nonlinear medium embedded in the cavity. In a planar geometry, we can make use of (15) to get

$$\omega_{\rm nl} = \frac{g_{\rm nl}}{\mathscr{S}} \tag{53}$$

where the effective mode area $\mathscr{S}$ is defined as

$$\mathscr{S} = \frac{\left(\int \mathrm{d}^2\mathbf{r}_\parallel \left|\mathscr{E}_\parallel(\mathbf{r}_\parallel)\right|^2\right)^2}{\int \mathrm{d}^2\mathbf{r}_\parallel \left|\mathscr{E}_\parallel(\mathbf{r}_\parallel)\right|^4} \tag{54}$$

in terms of the mode profile $\mathscr{E}_\parallel(\mathbf{r}_\parallel)$ along the cavity plane.

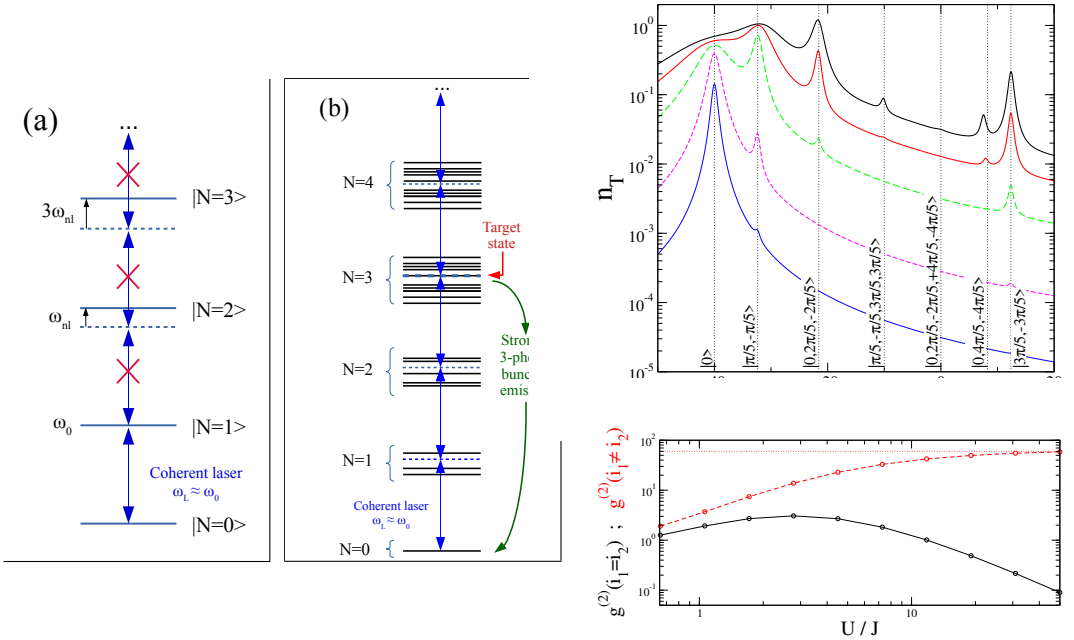

Figure 5. Left panel (a): sketch of the photon blockade mechanism for a single-mode cavity under a coherent pumping exactly on resonance with the bare cavity frequency, $\omega_{\rm inc} = \omega_o$. Because of the strong nonlinearity $\omega_{\rm nl} \gg \gamma_{\rm loss}$, transitions to all $N > 1$ states are non-resonant and the dynamics is confined to the $N = 0, 1$ states, giving effectively impenetrable photons. Central panel (b): sketch of the coherent pumping scheme to selectively excite a $N = 3$-photon state via a three-photon transition. Top-right panel: generation of a Tonks–Girardeau gas of fermionized photons under coherent pumping. Spectrum of total photon number n_T as a function of the incident frequency $\Delta\omega_p = \omega_{\rm inc} - \omega_o$ for different values of the pump intensity, $F/\gamma_{\rm loss} = 0.1, 0.3, 1, 2, 3$. Photons are assumed to be perfectly impenetrable $U/\gamma_{\rm loss} = \infty$ and losses small enough to resolve many-body states $J/\gamma_{\rm loss} = 20$. The vertical dotted lines indicate the theoretical prediction for the position of the N-photon resonance peak corresponding to each many-body state; the label indicates the orbitals filled in the corresponding fermionic wavefunction. Bottom-right panel: second order photon correlations in the emission from the same (black) and from different (red) sites as a function of the interaction constant $\omega_{\rm nl}/\gamma_{\rm loss}$. At each point, the coherent drive is set on resonance with the lowest two-photon state of a 3-sites chain. The right panels are adapted from [145].

Independently of the specific geometry, the eigenstates of (52) are labelled by the photon number and have an energy

$$E_n = n\hbar\omega_o + \hbar\omega_{\rm nl}\frac{n(n-1)}{2}. \tag{55}$$

As it is sketched in the left-most panel of Figure 5, the energy separation $E_{n+1} - E_n = \hbar\omega_o + n\hbar\omega_{\rm nl}$ is a growing function of n. As such, a coherent incident field resonant with the $0 \to 1$ transition will not be able to further excite the system to the $n \geq 2$ states as the corresponding transitions are no longer resonant. For instance, the $1 \to 2$ transition is detuned by an effective interaction energy $\omega_{\rm nl}$: as soon as this exceeds the cavity linewidth $\omega_{\rm nl} \gg \gamma_{\rm loss}$, the coherent field is not able to efficiently drive this second transition, so the cavity system ends up behaving as an effective

two-level system. In physical terms, this can be understood as photons becoming effectively impenetrable objects, a situation that is in stark contrast with the prediction of the linear Maxwell equations where photons are rigorously non-interacting particles.

4.1.2. *Many-body states*

A straightforward generalization of this pumping scheme can be exploited to generate strongly correlated many-photon states in spatially extended geometries such as cavity arrays. The key idea, sketched in the central panel of Figure 5, is to resonantly drive a N-photon transition to bring the system from its zero-photon vacuum state to the desired N-photon eigenstate of the conservative many-body Hamiltonian: the crucial requirement for an efficient selectivity of this preparation scheme is that the energy gap between the desired N-photon eigenstate and its neighbors exceeds the linewidth of the N-photon states, which typically grows as $N\gamma_{\rm loss}$.

As a first example, this idea was theoretically explored in view of realizing a Tonks–Girardeau gas of impenetrable photons in a one-dimensional chain of coupled cavities [145]. This is described by a Hamiltonian in the form

$$H = \sum_j \hbar\omega_o \hat{a}_j^\dagger \hat{a}_j + \frac{\hbar\omega_{\rm nl}}{2} \hat{a}_j^\dagger \hat{a}_j^\dagger \hat{a}_j \hat{a}_j - \hbar J \sum_{\langle j,j'\rangle} \hat{a}_j^\dagger \hat{a}_{j'} \tag{56}$$

where the indices j, j' run over the sites of the chain, assumed to have periodic boundary conditions, and the hopping terms of amplitude $J > 0$ are restricted to next-neighbor sites. The impenetrability condition is enforced by assuming $\omega_{\rm nl} \gg J$. A coherent pump is assumed to drive all sites according to the discrete version of (18),

$$H_{\rm coh} = \hbar \sum_j \left[F_j(t)\, \hat{a}_j^\dagger + \hbar F_j(t)^*\, \hat{a}_j \right]. \tag{57}$$

In what follows, we assume that all sites are driven in a monochromatic way with the same amplitude F and frequency $\omega_{\rm inc}$, that is $F_j(t) = F\, e^{-i\omega_{\rm inc} t}$. As the master equation is in the Lindblad form, the steady-state and the dynamics of the system can be calculated with standard numerical tools, e.g. by projecting the master equation on the basis of number states. Note that efficient high-level numerical libraries are nowadays available for these tasks [146].

Examples of spectra of the steady-state total population $n_T = \sum_j \langle \hat{a}_j^\dagger \hat{a}_j \rangle$ as a function of the incident frequency $\omega_{\rm inc}$ are shown in the upper-right panel of Figure 5 for growing values of the incident intensity $|F|^2$: at low intensity (blue line), the spectrum is characterized by a single main peak corresponding to the 1-photon transition to the $k = 0$ orbital. At growing intensities, additional peaks at frequencies corresponding to the higher $N = 2, 3, \ldots$ photon transitions appear. As expected, the position of each of these peaks matches the frequency of the N-photon resonance from the vacuum state (at zero energy) to some N-photon state of energy ω_N^α within the $k = 0$ sector,

$$\omega_{\rm inc} = \omega_N^\alpha / N. \tag{58}$$

In the specific Tonks–Girardeau case, the different excited states are labeled by the quasi-momenta of the (fermionized) particles and their energy can be analytically calculated [147]. The expected position of the resonances is indicated in the Figure by the vertical lines, which indeed match well with the position of the numerically calculated resonance peaks.

In order to be able to selectively drive the desired many-body state, the frequency separation from the neighboring states has to exceed the linewidth: as the separation is typically set by the hopping J and interaction $\omega_{\rm int}$ energies and the broadening grows as $N\gamma_{\rm loss}$, the requirement on the linewidth $\gamma_{\rm loss}$ becomes more and more stringent as larger N states are targeted. On top of this, one must not forget that for growing values of the drive amplitude F, each peak eventually displays a sizable power-broadening on top of its natural linewidth.

As it is well known from atomic physics [148], a coherent illumination leads to a reversible oscillatory dynamics between the different states, with absorption processes followed by stimulated emission ones until a steady-state is enforced via spontaneous emission processes. In particular, for very strong incident intensities, the steady-state tends to an equidistribution of the population among the different states. As such, a continuous-wave excitation can hardly be used to transfer all the population to a given excited state, but more complex pulsed schemes have to be adopted to generate, e.g., a state with a well-defined N.

Nonetheless, as the steady-state population of many-body states is typically a decreasing function of their photon number N, this difficulty can be circumvented by specifically looking at N-photon observables. Such observables are in fact strictly zero on all lower $N' < N$ photon states and, up to moderate values of the incident intensity, only receive a sub-dominant contribution from the higher $N' > N$ ones. A concrete example of application of this idea is illustrated in the bottom-right panel of Figure 5, where we specifically look at $N = 2$ observables such as the second-order correlation function of the emission

$$g^{(2)}(i_1, i_2) = \frac{\langle \widehat{a}^\dagger_{i_1} \widehat{a}^\dagger_{i_2} \widehat{a}_{i_2} \widehat{a}_{i_1} \rangle}{\langle \widehat{a}^\dagger_{i_1} \widehat{a}_{i_1} \rangle \langle \widehat{a}^\dagger_{i_2} \widehat{a}_{i_2} \rangle}. \tag{59}$$

Depending on the relative value of the interaction and hopping parameters $\omega_{\rm nl}/J$, the $N = 2$-photon eigenstates go from being delocalized, approximately non-interacting-photon states to fermionized, impenetrable-photon states. This key difference directly translate to the shape of $g^{(2)}(i_1, i_2)$: for non-interacting photons it has a position-independent value equal to 1; for impenetrable photons, its same-point value is much suppressed with respect to its different-point value, $g^{(2)}(i_1 = i_2) \ll g^{(2)}(i_1 \neq i_2)$. This illustrates how a coherent drive followed by a measurement of a N-photon correlation function allows to obtain interesting information on the many-body eigenstates of a strongly interacting system. A conceptually related experiment was reported using a superconducting circuit-QED platform in [149].

Further theoretical work [150] has extended this idea to a two-dimensional lattice geometry where impenetrable photons are also subject to a synthetic magnetic field. In this geometry, the optical transitions occur from the vacuum state to strongly correlated N-photon states analogous to the ones of fractional quantum Hall systems. An example of the peculiar physics of this regime is illustrated in the top-left panel (a) of Figure 6. Here, we show how tuning the coherent pump frequency on the lowest $N = 2$-photon resonance peak, one can extract information on the complex microscopic structure of the Laughlin states from the two-photon correlations of the emitted light: even in a small 4×4 lattice, we recognize in the wavefunction a clear antibunching feature between pairs of strongly interacting photons as well as a complex phase profile as a function of the relative position.

A closely related idea has been experimentally explored in a recent experiment [152]: strong interactions between photons are obtained by coupling light to optically dressed atoms in a Rydberg-EIT configuration [31,153]; a synthetic magnetic field in a cylindrically symmetric geometry is obtained by using a twisted optical ring-cavity [154]. Combining these elements, a two-photon Laughlin state is selectively created using a coherent laser pump with finite angular momentum and its microscopic structure is probed by looking at the correlation functions of the emitted light at different spatial positions and in different orbital angular momentum channels.

Scaling up the idea to larger photon numbers is naturally the next goal, but several challenges are still present along this way. As it was mentioned above, an obvious difficulty comes from the decreasing value of the spacing between many-body resonances which imposes stricter constraints on their linewidth. An even more serious challenge comes from the quickly decreasing value of the matrix element for driving a N-photon transition from the trivial vacuum state to a topologically non-trivial FQH state with a coherent light beam formed by uncorrelated photons.

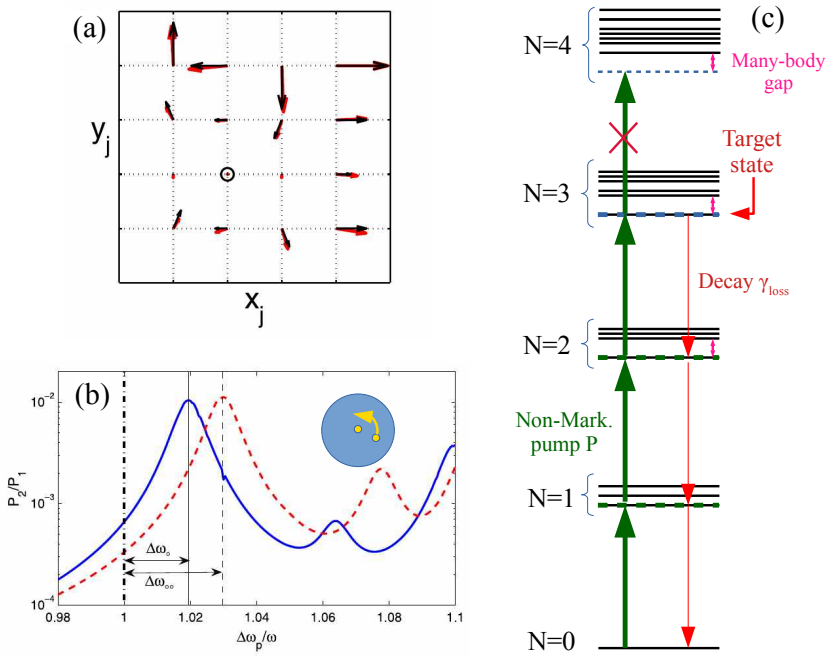

Figure 6. Top-left panel (a): reconstruction of the two-particle wavefunction of a Laughlin state from the two-photon correlations of the light emitted by the two-photon FQH state generated under coherent pumping. The marker indicates the position of one photon; the x_j, y_j coordinates on the plot correspond to the second photon's position: the red arrows indicate the two-photon emission amplitude, the black ones indicate the value of the complex-valued Laughlin wavefunction discretized in the lattice. Bottom-left panel (b): frequency-shift of the two-photon resonance peak under the effect of the braiding of a quasi-hole. The continuous blue line is the spectrum for a single quasi-hole braided around the cloud at a radius $r/\ell = 0.4$; the dashed red line spectrum includes also a stationary second hole located at $r = 0$, as indicated in the sketch in the inset. Right panel (c): sketch of the frequency-selective incoherent pumping scheme to stabilize a $N = 3$ FQH state. The non-Markovian nature of the pump prevents excitation across the many-body gap. The (Markovian) photon losses cannot lead to states above the many-body gap. All together, this restricts the dynamics to states with $N \leq 3$ photons below the many-body gap. Panel (a) is adapted from [150]. Panel (b) is adapted from [151].

4.1.3. *Signatures of the braiding phase*

In spite of these difficulties, an intriguing new possibility offered by the driven-dissipative condition is illustrated in the bottom-left panel (b) of Figure 6. One of the key feature of a topological state of matter is encoded in the so-called *braiding phase* that the many-body wavefunction acquires when two quasi-holes are made to adiabatically move through the fluid and encircle each other as sketched in the inset. While the braiding phase is a mathematically well defined concept [101,155], an experimental observation of the overall phase of a quantum wavefunction requires to design some interference process between different quantum states [156–158]. Quan-

tum superpositions of the vacuum state and the desired many-body state are naturally generated by a coherent pumping process, so any extra phase acquired by the many-body wavefunction may be observed as a shift in the resonance frequency of the corresponding transition.

A concrete implementation of this general idea to measure the braiding phase in driven-dissipative fractional quantum Hall fluids of light was proposed in [151]. In the presence of one or more localized repulsive potentials, the lowest energy two-photon eigenstate consists of a Laughlin state pierced by quasi-holes pinned at the position of the potentials. When a single quasi-hole is braided around the fluid at a radius r_o from the center with a constant angular velocity Ω, the many-body wavefunction acquires at each roundtrip a phase given by the flux of synthetic magnetic field enclosed by the trajectory. This phase, of geometric origin, is responsible for the shift $\Delta\omega_o$ of the main $N=2$-photon peak visible on the blue spectrum of Figure 6(b). When a second hole is present at the origin, the shift $\Delta\omega_{oo}$ acquires an additional contribution due to the braiding of one quasi-hole around the other,

$$\Delta\omega_{oo} - \Delta\omega_o = \varphi_{Br}\frac{\Omega}{2\pi}. \tag{60}$$

where φ_{Br} is the braiding phase accumulated at each round trip and $2\pi/\Omega$ is the time needed for a round-trip. The frequency shift observed in the numerical simulation in Figure 6(b) is in excellent agreement with the value theoretically extracted from a microscopic calculation of the many-body braiding phase for this configuration. As it is discussed in detail in [151], the value of the braiding phase tends to the topological value π as soon as the cloud has a macroscopic size and edge effects can be neglected. In principle this requires a number $N \gg 1$ of particles; interestingly in view of experiments, a qualitative effect is already visible for $N=3$ and the asymptotic value is closely approached for $N\sim 10$.

This theoretical prediction shows how the quantum superposition nature of the state that is naturally generated in a coherent pumping process is not only a limitation of the preparation process, but can be exploited as a new asset to observe the peculiar properties of the many-body wavefunction of topological states of matter.

4.2. *Incoherent pumping*

In the previous subsection we have seen how the reversible nature of the coherent pumping process makes the driven-dissipative steady-state to typically consist of a superposition of different number states. If one wishes to concentrate the population on a single excited state, many-photon generalizations of the π-pulses used in the coherent manipulation of the internal state of atoms [148] can be envisaged. As the many-body states are very close in energy, sophisticated quantum control techniques may be required to achieve a good selectivity, which furthermore rely on some preliminary theoretical knowledge of the system.

An alternative way, inspired to population inversion in laser physics, is to exploit an incoherent pumping scheme to irreversibly push the population upwards towards higher-N states. In its simplest formulation with a broad-band incoherent pump as described within the Markovian setting of (19), this incoherent pump scheme allows to efficiently push the population upwards but the absence of energy-selectivity makes the population spread among the different many-body states forming each N-photon manifold, typically in a uniform way [59]. As a result, the fluid ends up displaying an effectively infinite temperature which prevents observation of interesting quantum many-body effects.

A promising way-out is to introduce a frequency-selectivity of the pumping scheme which provides non-Markovian features in the irreversible coupling between the system and the external bath used for pumping. A simple implementation of this idea is sketched in the right panel

of Figure 6 in the context of generating a FQH fluid of light: provided the spectrum of the incoherent pump is narrower than the many-body gap protecting the target FQH state, the pumping cannot lead to states above the many-body gap. As states above the many-body gap cannot be reached by loss processes either[4], the population remains concentrated within the states below the many-body gap. If the geometry of the fluid has periodic boundary conditions, the incompressibility of the bulk puts an upper bound to the number of particles that can be accommodated in a non-interacting state before one has to cross the many-body energy gap, e.g. a maximum of $N = 3$ particles for the configuration illustrated in the sketch. If the incoherent pumping rate $\gamma_{\rm pump}$ exceeds the loss rate $\gamma_{\rm loss}$, the population is irreversibly pushed up along the ladder of N states and gets eventually concentrated in the upmost available state which is indeed our target FQH state.

The situation is slightly more complicate if the periodic boundary conditions are replaced by a finite geometry with physical edges, e.g., when the fluid is subject to a confining potential [159] or has open boundary conditions [160,161]. In these cases, the energy gap to the lowest edge excitation is typically much smaller than the many-body gap in the bulk and scales inversely to the cloud perimeter. This puts more and more severe constraints on the energy selectivity of the pumping process that is required to suppress spurious edge excitations. However, since these excitations are confined on the edge of the cloud, they do not create any harm to the topological properties of the bulk which remains well stabilized in a very pure fractional quantum Hall state.

In order to put these qualitative arguments onto solid and quantitative grounds one needs to develop a theoretical description that is able to account for the non-Markovian features associated to the frequency-dependence of the pumping process. In [62,162], this was done by explicitly introducing into the model two-level emitters that provide a frequency-dependent injection of photons as discussed at the beginning of Section 2.2.4. This allows to reformulate the frequency-dependent incoherent pumping in terms of a master equation in the Lindblad form, which can then be solved with standard methods, e.g. using one of the numerical libraries that are available for these tasks [146]. In the fast repumping regime where the emitters can be adiabatically eliminated, a simplified photon-only description based on generalized Lindblad master equation can be used, as presented in Section 2.2.4. This has provided interesting insight both in lattice and in continuum geometries [63,163]. On top of these numerical works, some analytical results have also been obtained in specific limiting cases [164], further confirming the promise of this framework for the autonomous stabilization of FQH states. On top of these feasibility studies, interesting consequences of the driven-dissipative nature of the fluid have also been pointed out in theoretical works. While isolated quasi-holes in the bulk of a standard equilibrium FQH fluid move along deterministic trajectories, typically with very low speeds, a recent work [165] has anticipated that repeated loss and repumping processes in the neighborhood of a quasi-hole give rise to an effectively stochastic motion of quasi-holes.

The conceptual facility of this mechanism for the *autonomous stabilization* of a fractional quantum Hall fluid of light is a consequence of the peculiar structure of the many-body spectrum and of the many-body eigenstates. Something similar occurs for the deep Mott insulator state,

[4] This is easy to see on the analytical form of the Laughlin wavefunctions of FQH states [101],

$$\psi(z_1,\dots,z_N) = P(z_1,\dots,z_N) \prod_{i>j} (z_i - z_j)^p \, e^{-\sum_i |z_i|^2},$$

where P is an arbitrary symmetric polynomial in the normalized complex $z_i = (x_i + i\, y_i)/\ell_B$ coordinates of the $i = 1,\dots,N$ particles and p is an integer (even for bosonic particles like photons and odd for fermionic particles like electrons) characterizing the specific FQH state under consideration. The non-interacting nature of this state is enforced by the presence of factors $(z_i - z_j)$ for any pair i, j of particles, which give zeros in the wavefunction for overlapping particles. This impenetrability condition is preserved when a particle is removed from the system.

whose stabilization was experimentally demonstrated [64] using a superconductor-based circuit-QED platform operating in the $\omega_{\rm nl} \gg J$ regime (in the notation of the lattice Hamiltonian (56)). In this limit, the thickness of the band of hole states (on the order of J) is much smaller than the energy separation (on the order of $\omega_{\rm nl}$) from excited states featuring some doubly occupied site: choosing a repumping rate $J \ll \Gamma_P \ll \omega_{\rm nl}$ then guarantees an effective replenishing of any hole, while suppressing the creation of unwanted doublons.

An even richer physics occurs when J and $\omega_{\rm nl}$ have comparable values, so that the driven-dissipative condition interplays with the superfluid-insulator quantum phase transition occurring at a finite critical value of $J/\omega_{\rm nl}$ [3]. In [166,167], a square-like form of the incoherent emission spectrum, arising e.g. from an inhomogeneously broadened distribution of emitters, was considered, that leads to an equilibrium-like superfluid-insulator transition. The case of a Lorentzian spectrum was instead considered in [162] and specific nonequilibrium features were pointed out for the superfluid-insulator transition. Beyond the steady-state, the spectrum of the collective excitations on top of the driven-dissipative steady state was studied across the different regimes in [62]: similarly to the equilibrium case, gapped particle-hole excitations are found in the insulating state and a gapless Goldstone mode in the superfluid state. As a typical feature of driven-dissipative systems, this latter was predicted to have the same diffusive properties as in the weakly-interacting case discussed in Section 3.3.

5. Conclusions and perspectives

In this article we have reviewed the basic concepts of the driven-dissipative many-body physics of quantum fluids of light and we have summarized the main theoretical tools used for their description. A special emphasis has been given to those new effects and those new tools that the driven-dissipative nature introduces for the stabilization and the manipulation of interesting states of photonic matter.

As illustrative examples, in the weakly interacting regime, a suitable coherent pump can be used to generate inhomogeneous flows displaying acoustic horizons; in topological photonic systems, the interplay between the bandwidth of energy bands and the loss rate can be exploited to smoothly transition from an anomalous Hall to a quantum integer Hall regime in the transverse drift under crossed synthetic magnetic and electric fields. In the strongly interacting regime, spectroscopical signatures of the anyonic braiding phase in fractional quantum Hall fluids of light have been anticipated under coherent pumping and promising incoherent pumping schemes to stabilize macroscopic strongly correlated fluids are being actively investigated.

These advances are opening exciting perspectives in a number of interdisciplinary directions, at the crossroad of many-body physics, nonlinear statistical mechanics, and quantum simulation of gravitational problems. As we have mentioned along the article, acoustic horizons in inhomogeneous flows have been predicted to give acoustic analogs of Hawking radiation, which could be experimentally detected in the intensity correlations of the emitted light. The flexibility in the generation and the manipulation of different flow geometries is of utmost interest in view of studying more complex phenomena where, e.g., Hawking radiation interplays with superradiance and localized quasi-normal modes [168] of the underlying space-time. The coherence properties of condensates and quasi-condensates display universality features that fall in the framework of the Kardar–Parisi–Zhang framework: going beyond the one-dimensional geometries considered so far in experiments, the combination of condensation with synthetic dimensions opens the way to studies of nonequilibrium statistical mechanics and many-body effects in high dimensional geometries beyond the three dimensions of our physical space [169]. Finally, application of the frequency-dependent incoherent pumping techniques to strongly interacting photons in

complex geometries and/or in the presence of non-trivial band topologies offers promising avenues towards the driven-dissipative stabilization of strongly correlated states of photonic matter and the observation of their peculiar collective excitations, including those Abelian and non-Abelian anyonic statistics that are of interest for topological quantum computing [170].

Beyond quantum fluids of light, driven-dissipative schemes are presently attracting a growing interest also in the context of ultracold atomic gases. A well-established direction is to design dissipation channels that tend to push the atomic gas towards a desired many-body state [10–15]. A more recent research avenue focuses on configurations where a net particle flux is established by letting the system exchange atoms with several suitably designed reservoirs, either in an incoherent way via inter-atomic collisions or in a coherent way via internal transitions driven by incident electromagnetic fields. Examples of this strategy are the engineered evaporation leading to condensation into a (topological) excited state observed in [171] and, even more directly, the continuously loaded Bose–Einstein condensate that was generated in the driven-dissipative steady-state of a complex atom cooling apparatus in [16]. Taking inspiration from fluids of light [106,133], a natural next question is to explore the consequences of the nonequilibrium nature on the coherence and on the collective modes of the driven-dissipative atomic condensate. On the coherent pumping side, macroscopic atomic reservoirs involving a condensate have been used to realize atomic analogs of the coherent pumping schemes: first experiments have demonstrated bistability effects in single mode geometries [17,18]; along the lines of the recent experiments demonstrating baby fractional quantum Hall fluids of light [152], analogous work is in progress in the direction of stabilizing strongly correlated states of atomic matter.

Declaration of interests

The author does not work for, advise, own shares in, or receive funds from any organization that could benefit from this article, and has declared no affiliations other than their research organizations.

References

[1] L. P. Pitaevskiĭ and S. Stringari, *Bose–Einstein condensation and superfluidity*, International Series of Monographs on Physics, Oxford University Press, 2016, 512 pages.

[2] C. Gross and I. Bloch, "Quantum simulations with ultracold atoms in optical lattices", *Science* **357** (2017), no. 6355, pp. 995–1001.

[3] I. Bloch, J. Dalibard and W. Zwerger, "Many-body physics with ultracold gases", *Rev. Mod. Phys.* **80** (2008), no. 3, pp. 885–964.

[4] N. R. Cooper, J. Dalibard and I. B. Spielman, "Topological bands for ultracold atoms", *Rev. Mod. Phys.* **91** (2019), no. 1, article no. 015005.

[5] I. Carusotto and C. Ciuti, "Quantum fluids of light", *Rev. Mod. Phys.* **85** (2013), no. 1, pp. 299–366.

[6] D. E. Chang, V. Vuletić and M. D. Lukin, "Quantum nonlinear optics – photon by photon", *Nature Photon.* **8** (2014), no. 9, pp. 685–694.

[7] I. Carusotto, A. A. Houck, A. J. Kollár, P. Roushan, D. I. Schuster and J. Simon, "Photonic materials in circuit quantum electrodynamics", *Nat. Phys.* **16** (2020), no. 3, pp. 268–279.

[8] J. Bloch, I. Carusotto and M. Wouters, "Non-equilibrium Bose–Einstein condensation in photonic systems", *Nat. Rev. Phys.* **4** (2022), no. 7, pp. 470–488.

[9] L. M. Sieberer, M. Buchhold and S. Diehl, "Keldysh field theory for driven open quantum systems", *Rep. Prog. Phys.* **79** (2016), no. 9, article no. 096001.

[10] S. Diehl, A. Micheli, A. Kantian, B. Kraus, H. P. Büchler and P. Zoller, "Quantum states and phases in driven open quantum systems with cold atoms", *Nat. Phys.* **4** (2008), no. 11, pp. 878–883.

[11] C.-E. Bardyn, M. A. Baranov, E. Rico, A. Imamoğlu, P. Zoller and S. Diehl, "Majorana modes in driven-dissipative atomic superfluids with a zero Chern number", *Phys. Rev. Lett.* **109** (2012), article no. 130402.

[12] J. C. Budich, P. Zoller and S. Diehl, "Dissipative preparation of Chern insulators", *Phys. Rev. A* **91** (2015), article no. 042117.

[13] F. Mivehvar, F. Piazza, T. Donner and H. Ritsch, "Cavity QED with quantum gases: new paradigms in many-body physics", *Adv. Phys.* **70** (2021), no. 1, pp. 1–153.

[14] F. Ferri, R. Rosa-Medina, F. Finger, N. Dogra, M. Soriente, O. Zilberberg, T. Donner and T. Esslinger, "Emerging dissipative phases in a superradiant quantum gas with tunable decay", *Phys. Rev. X* **11** (2021), article no. 041046.

[15] B. P. Marsh, R. M. Kroeze, S. Ganguli, S. Gopalakrishnan, J. Keeling and B. L. Lev, "Entanglement and replica symmetry breaking in a driven-dissipative quantum spin glass", *Phys. Rev. X* **14** (2024), no. 1, article no. 011026.

[16] C.-C. Chen, R. González Escudero, J. Minář, B. Pasquiou, S. Bennetts and F. Schreck, "Continuous Bose–Einstein condensation", *Nature* **606** (2022), no. 7915, pp. 683–687.

[17] R. Labouvie, B. Santra, S. Heun and H. Ott, "Bistability in a driven-dissipative superfluid", *Phys. Rev. Lett.* **116** (2016), article no. 235302.

[18] J. Benary, C. Baals, E. Bernhart, J. Jiang, M. Röhrle and H. Ott, "Experimental observation of a dissipative phase transition in a multi-mode many-body quantum system", *New J. Phys.* **24** (2022), no. 10, article no. 103034.

[19] Q. Glorieux, C. Piekarski, Q. Schibler, T. Aladjidi and M. Baker-Rasooli, "Paraxial fluids of light", preprint, 2025. Online at https://arxiv.org/abs/2504.06262.

[20] C. Michel, O. Boughdad, M. Albert, P.-É. Larré and M. Bellec, "Superfluid motion and drag-force cancellation in a fluid of light", *Nat. Commun.* **9** (2018), no. 1, pp. 1–6.

[21] Q. Fontaine, T. Bienaimé, S. Pigeon, É. Giacobino, A. Bramati and Q. Glorieux, "Observation of the Bogoliubov dispersion in a fluid of light", *Phys. Rev. Lett.* **121** (2018), no. 18, article no. 183604.

[22] P. Coullet, L. Gil and F. Rocca, "Optical vortices", *Opt. Commun.* **73** (1989), no. 5, pp. 403–408.

[23] M. Vaupel, K. Staliunas and C. O. Weiss, "Hydrodynamic phenomena in laser physics: modes with flow and vortices behind an obstacle in an optical channel", *Phys. Rev. A* **54** (1996), pp. 880–892.

[24] M. Baker-Rasooli, T. Aladjidi, N. A. Krause, A. S. Bradley and Q. Glorieux, "Observation of Jones–Roberts solitons in a paraxial quantum fluid of light", *Phys. Rev. Lett.* **134** (2025), article no. 233401.

[25] M. Baker-Rasooli, W. Liu, T. Aladjidi, A. Bramati and Q. Glorieux, "Turbulent dynamics in a two-dimensional paraxial fluid of light", *Phys. Rev. A* **108** (2023), article no. 063512.

[26] T. D. Ferreira, J. Garwoła and N. A. Silva, "Exploring the dynamics of the Kelvin–Helmholtz instability in paraxial fluids of light", *Phys. Rev. A* **109** (2024), no. 4, article no. 043704.

[27] K. Baudin, A. Fusaro, K. Krupa, J. Garnier, S. Rica, G. Millot and A. Picozzi, "Classical Rayleigh–Jeans condensation of light waves: observation and thermodynamic characterization", *Phys. Rev. Lett.* **125** (2020), article no. 244101.

[28] K. Krupa, A. Tonello, B. M. Shalaby, M. Fabert, A. Barthélémy, G. Millot, S. Wabnitz and V. Couderc, "Spatial beam self-cleaning in multimode fibres", *Nature Photon.* **11** (2017), no. 4, pp. 237–241.

[29] A. Chiocchetta, P.-É. Larré and I. Carusotto, "Thermalization and Bose–Einstein condensation of quantum light in bulk nonlinear media", *Eur. Phys. Lett.* **115** (2016), no. 2, article no. 24002.

[30] J. Steinhauer et al., "Analogue cosmological particle creation in an ultracold quantum fluid of light", *Nat. Commun.* **13** (2022), no. 1, pp. 1–7.

[31] T. Peyronel, O. Firstenberg, Q.-Y. Liang, S. Hofferberth, A. V. Gorshkov, T. Pohl, M. D. Lukin and V. Vuletić, "Quantum nonlinear optics with single photons enabled by strongly interacting atoms", *Nature* **488** (2012), no. 7409, pp. 57–60.

[32] O. Firstenberg, T. Peyronel, Q.-Y. Liang, A. V. Gorshkov, M. D. Lukin and V. Vuletić, "Attractive photons in a quantum nonlinear medium", *Nature* **502** (2013), no. 7469, pp. 71–75.

[33] A. V. Kavokin, J. J. Baumberg, G. Malpuech and F. P. Laussy, *Microcavities*, revised edition, Oxford Science Publications, Oxford University Press, 2011, 488 pages.

[34] J. D. Jackson, *Classical electrodynamics*, 3rd edition, John Wiley & Sons, 1999.

[35] W. Heisenberg and H. Euler, "Folgerungen aus der Diracschen Theorie des Positrons", *Z. Phys.* **98** (1936), no. 11, pp. 714–732.

[36] E. Lundström, G. Brodin, J. Lundin, M. Marklund, R. Bingham, J. Collier, J. T. Mendonça and P. Norreys, "Using high-power lasers for detection of elastic photon-photon scattering", *Phys. Rev. Lett.* **96** (2006), article no. 083602.

[37] D. Micieli et al., "Compton sources for the observation of elastic photon-photon scattering events", *Phys. Rev. Accel. Beams* **19** (2016), no. 9, article no. 093401.

[38] E. Milotti et al., "Exploring quantum vacuum with low-energy photons", *Int. J. Quantum Inf.* **10** (2012), no. 08, article no. 1241002.

[39] K. I. Beloborodov, T. A. Kharlamova and V. I. Telnov, "Problems of studying $\gamma\gamma \to \gamma\gamma$ scattering at e^+e^- and $\gamma\gamma$ colliders", preprint, 2023. Online at https://arxiv.org/abs/2301.07089.

[40] ATLAS Collaboration, "Evidence for light-by-light scattering in heavy-ion collisions with the ATLAS detector at the LHC", *Nat. Phys.* **13** (2017), no. 9, pp. 852–858.

[41] N. W. Ashcroft and N. D. Mermin, *Solid state physics*, Cengage Learning, Cengage, 2022.

[42] P. N. Butcher and D. Cotter, *The elements of nonlinear optics*, Cambridge Studies in Modern Optics, Cambridge University Press, 2008, xiv+344 pages.

[43] R. W. Boyd, *Nonlinear optics*, Academic Press Inc., 2008, xix+613 pages.

[44] A. Blais, A. L. Grimsmo, S. M. Girvin and A. Wallraff, "Circuit quantum electrodynamics", *Rev. Mod. Phys.* **93** (2021), article no. 025005.

[45] S. Ferretti and D. Gerace, "Single-photon nonlinear optics with Kerr-type nanostructured materials", *Phys. Rev. B* **85** (2012), article no. 033303.

[46] B. Nelsen, G. Liu, M. Steger, D. W. Snoke, R. Balili, K. West and L. N. Pfeiffer, "Dissipationless flow and sharp threshold of a polariton condensate with long lifetime", *Phys. Rev. X* **3** (2013), no. 4, article no. 041015.

[47] Y. Sun et al., "Bose–Einstein condensation of long-lifetime polaritons in thermal equilibrium", *Phys. Rev. Lett.* **118** (2017), no. 1, article no. 016602.

[48] P. Roushan et al., "Chiral ground-state currents of interacting photons in a synthetic magnetic field", *Nat. Phys.* **13** (2017), no. 2, pp. 146–151.

[49] P. Roushan et al., "Spectroscopic signatures of localization with interacting photons in superconducting qubits", *Science* **358** (2017), no. 6367, pp. 1175–1179.

[50] C. Wang et al., "Realization of fractional quantum Hall state with interacting photons", *Science* **384** (2024), no. 6695, pp. 579–584.

[51] D. F. Walls and G. J. Milburn, *Quantum optics*, Graduate Texts in Physics, Springer, 2008, 425 pages.

[52] C. Ciuti, G. Bastard and I. Carusotto, "Quantum vacuum properties of the intersubband cavity polariton field", *Phys. Rev. B* **72** (2005), article no. 115303.

[53] C. Ciuti and I. Carusotto, "Input-output theory of cavities in the ultrastrong coupling regime: the case of time-independent cavity parameters", *Phys. Rev. A* **74** (2006), article no. 033811.

[54] A. Frisk Kockum, A. Miranowicz, S. De Liberato, S. Savasta and F. Nori, "Ultrastrong coupling between light and matter", *Nat. Rev. Phys.* **1** (2019), no. 1, pp. 19–40.

[55] C. W. Gardiner and P. Zoller, *Quantum noise*, Springer Series in Synergetics, Springer, 2004, xxii+450 pages.

[56] W. E. Lamb, "Theory of an optical maser", *Phys. Rev.* **134** (1964), pp. A1429–A1450.

[57] M. O. Scully and M. S. Zubairy, *Quantum optics*, Cambridge University Press, 1997, xxii+630 pages.

[58] H.-P. Breuer and F. Petruccione, *The theory of open quantum systems*, Oxford University Press, 2002, 648 pages.

[59] J. Lebreuilly, M. Wouters and I. Carusotto, "Towards strongly correlated photons in arrays of dissipative nonlinear cavities under a frequency-dependent incoherent pumping", *C. R. Phys.* **17** (2016), no. 8, pp. 836–860.

[60] T. Becker, L.-N. Wu and A. Eckardt, "Lindbladian approximation beyond ultraweak coupling", *Phys. Rev. E* **104** (2021), article no. 014110.

[61] C. S. Tello Breuer, T. Becker and A. Eckardt, "Benchmarking quantum master equations beyond ultraweak coupling", *Phys. Rev. B* **110** (2024), article no. 064319.

[62] F. Caleffi, M. Capone and I. Carusotto, "Collective excitations of a strongly correlated nonequilibrium photon fluid across the insulator-superfluid phase transition", *Phys. Rev. Lett.* **131** (2023), no. 19, article no. 193604.

[63] E. Kapit, M. Hafezi and S. H. Simon, "Induced self-stabilization in fractional quantum Hall states of light", *Phys. Rev. X* **4** (2014), article no. 031039.

[64] R. Ma, B. Saxberg, C. Owens, N. Leung, Y. Lu, J. Simon and D. I. Schuster, "A dissipatively stabilized Mott insulator of photons", *Nature* **566** (2019), no. 7742, pp. 51–57.

[65] D. Marcos, A. Tomadin, S. Diehl and P. Rabl, "Photon condensation in circuit quantum electrodynamics by engineered dissipation", *New J. Phys.* **14** (2012), no. 5, article no. 055005.

[66] L. Garbe, Y. Minoguchi, J. Huber and P. Rabl, "The bosonic skin effect: boundary condensation in asymmetric transport", *SciPost Phys.* **16** (2024), article no. 029.

[67] F. Petiziol and A. Eckardt, "Cavity-based reservoir engineering for Floquet-engineered superconducting circuits", *Phys. Rev. Lett.* **129** (2022), article no. 233601.

[68] S. Hacohen-Gourgy, V. V. Ramasesh, C. De Grandi, I. Siddiqi and S. M. Girvin, "Cooling and autonomous feedback in a Bose–Hubbard chain with attractive interactions", *Phys. Rev. Lett.* **115** (2015), article no. 240501.

[69] M. Mamaev, L. C. G. Govia and A. A. Clerk, "Dissipative stabilization of entangled cat states using a driven Bose–Hubbard dimer", *Quantum* **2** (2018), article no. 58 (11 pages).

[70] P. M. Harrington, E. J. Mueller and K. W. Murch, "Engineered dissipation for quantum information science", *Nat. Rev. Phys.* **4** (2022), no. 10, pp. 660–671.

[71] Z. Li, T. Roy, Y. Lu, E. Kapit and D. I. Schuster, "Autonomous stabilization with programmable stabilized state", *Nat. Commun.* **15** (2024), article no. 6978 (6 pages).

[72] R. Lescanne et al., "Exponential suppression of bit-flips in a qubit encoded in an oscillator", *Nat. Phys.* **16** (2020), no. 5, pp. 509–513.

[73] L. A. Lugiato, F. Prati, E. Brambilla and A. Gatti, "The cavity Kerr medium model and the surprising history around it", in *Quantum fluids of light and matter*, Proceedings of the International School of Physics "Enrico Fermi", vol. 209, IOS Press, 2025, pp. 5–21.

[74] Y. Castin, "Bose–Einstein condensates in atomic gases: simple theoretical results", in *Coherent atomic matter waves* (R. Kaiser, C. Westbrook and F. David, eds.), EDP Sciences; Springer, 2001, pp. 1–136. Online at https://cel.hal.science/cel-00092947v1. Lecture notes of Les Houches summer school.

[75] M. Wouters and I. Carusotto, "Superfluidity and critical velocities in nonequilibrium Bose–Einstein condensates", *Phys. Rev. Lett.* **105** (2010), no. 2, article no. 020602.

[76] M. C. Cross and P. C. Hohenberg, "Pattern formation outside of equilibrium", *Rev. Mod. Phys.* **65** (1993), no. 3, pp. 851–1112.

[77] I. S. Aranson and L. Kramer, "The world of the complex Ginzburg–Landau equation", *Rev. Mod. Phys.* **74** (2002), no. 1, pp. 99–143.

[78] L. A. Lugiato and R. Lefever, "Spatial dissipative structures in passive optical systems", *Phys. Rev. Lett.* **58** (1987), no. 21, article no. 2209.

[79] I. Carusotto and C. Ciuti, "Spontaneous microcavity-polariton coherence across the parametric threshold: quantum Monte Carlo studies", *Phys. Rev. B* **72** (2005), no. 12, article no. 125335.

[80] M. Wouters and V. Savona, "Stochastic classical field model for polariton condensates", *Phys. Rev. B* **79** (2009), no. 16, article no. 165302.

[81] I. Frérot, A. Vashisht, M. Morassi, A. Lemaître, S. Ravets, J. Bloch, A. Minguzzi and M. Richard, "Bogoliubov excitations driven by thermal lattice phonons in a quantum fluid of light", *Phys. Rev. X* **13** (2023), no. 4, article no. 041058.

[82] M. H. Szymańska, "Stochastic and tensor network methods for open dissipative quantum lattice models", 2025. Talk at the "MEOQS2025 — Methods for many-body open quantum systems" workshop, Trento (2025).

[83] B. Berg, L. I. Plimak, A. Polkovnikov, M. K. Olsen, M. Fleischhauer and W. P. Schleich, "Commuting Heisenberg operators as the quantum response problem: time-normal averages in the truncated Wigner representation", *Phys. Rev. A* **80** (2009), article no. 033624.

[84] A. Sinatra, C. Lobo and Y. Castin, "The truncated Wigner method for Bose-condensed gases: limits of validity and applications", *J. Phys. B. At. Mol. Opt. Phys.* **35** (2002), no. 17, article no. 3599.

[85] M. J. Steel, M. K. Olsen, L. I. Plimak, P. D. Drummond, S. M. Tan, M. J. Collett, D. F. Walls and R. Graham, "Dynamical quantum noise in trapped Bose–Einstein condensates", *Phys. Rev. A* **58** (1998), pp. 4824–4835.

[86] P. D. Drummond, "Quantum optical tunneling: a representation-free theory valid near the state-equation turning points", *Phys. Rev. A* **33** (1986), pp. 4462–4464.

[87] K. Vogel and H. Risken, "Quantum-tunneling rates and stationary solutions in dispersive optical bistability", *Phys. Rev. A* **38** (1988), pp. 2409–2422.

[88] M. Van Regemortel, W. Casteels, I. Carusotto and M. Wouters, "Spontaneous Beliaev–Landau scattering out of equilibrium", *Phys. Rev. A* **96** (2017), no. 5, article no. 053854.

[89] A. Polkovnikov, "Quantum corrections to the dynamics of interacting bosons: beyond the truncated Wigner approximation", *Phys. Rev. A* **68** (2003), no. 5, article no. 053604.

[90] I. Carusotto and C. Ciuti, "Probing microcavity polariton superfluidity through resonant Rayleigh scattering", *Phys. Rev. Lett.* **93** (2004), article no. 166401.

[91] A. Amo et al., "Superfluidity of polaritons in semiconductor microcavities", *Nature Phys.* **5** (2009), no. 11, pp. 805–810.

[92] F. Claude, M. J. Jacquet, R. Usciati, I. Carusotto, É. Giacobino, A. Bramati and Q. Glorieux, "High-resolution coherent probe spectroscopy of a polariton quantum fluid", *Phys. Rev. Lett.* **129** (2022), no. 10, article no. 103601.

[93] X. Busch, I. Carusotto and R. Parentani, "Spectrum and entanglement of phonons in quantum fluids of light", *Phys. Rev. A* **89** (2014), no. 4, article no. 043819.

[94] T. Boulier, E. Cancellieri, N. D. Sangouard, R. Hivet, Q. Glorieux, É. Giacobino and A. Bramati, "Lattices of quantized vortices in polariton superfluids", *C. R. Phys.* **17** (2016), no. 8, pp. 893–907.

[95] C. Barcelo, S. Liberati and M. Visser, "Analogue gravity", *Living Rev. Relativ.* **14** (2011), pp. 1–159.

[96] D. Gerace and I. Carusotto, "Analog Hawking radiation from an acoustic black hole in a flowing polariton superfluid", *Phys. Rev. B* **86** (2012), no. 14, article no. 144505.

[97] H. S. Nguyen et al., "Acoustic black hole in a stationary hydrodynamic flow of microcavity polaritons", *Phys. Rev. Lett.* **114** (2015), no. 3, article no. 036402.

[98] K. Falque, A. Delhom, Q. Glorieux, É. Giacobino, A. Bramati and M. J. Jacquet, "Polariton fluids as quantum field theory simulators on tailored curved spacetimes", *Phys. Rev. Lett.* **135** (2025), article no. 023401 (7 pages).

[99] J. R. Muñoz de Nova, K. Golubkov, V. I. Kolobov and J. Steinhauer, "Observation of thermal Hawking radiation and its temperature in an analogue black hole", *Nature* **569** (2019), no. 7758, pp. 688–691.

[100] S. Finazzi and I. Carusotto, "Entangled phonons in atomic Bose–Einstein condensates", *Phys. Rev. A* **90** (2014), no. 3, article no. 033607.

[101] D. Tong, "Lectures on the quantum Hall effect", preprint, 2016. Online at https://arxiv.org/abs/1606.06687.

[102] T. Ozawa and I. Carusotto, "Anomalous and quantum Hall effects in lossy photonic lattices", *Phys. Rev. Lett.* **112** (2014), no. 13, article no. 133902.

[103] T. Ozawa et al., "Topological photonics", *Rev. Mod. Phys.* **91** (2019), no. 1, article no. 015006.
[104] A. Chénier, B. d'Aligny, F. Pellerin, P.-É. Blanchard, T. Ozawa, I. Carusotto and P. St-Jean, "Quantized Hall drift in a frequency-encoded photonic Chern insulator", preprint, 2024. Online at https://arxiv.org/abs/2412.04347.
[105] I. Carusotto and G. Rousseaux, "The Cerenkov effect revisited: from swimming ducks to zero modes in gravitational analogues", in *Analogue gravity phenomenology: analogue spacetimes and horizons, from theory to experiment*, Lecture Notes in Physics, vol. 870, Springer, 2013, pp. 109–144.
[106] F. Claude, M. J. Jacquet, Q. Glorieux, M. Wouters, É. Giacobino, I. Carusotto and A. Bramati, "Observation of the diffusive Nambu–Goldstone mode of a non-equilibrium phase transition", *Nat. Phys.* **21** (2025), pp. 924–930.
[107] K. Huang, *Statistical mechanics*, John Wiley & Sons, 1987, xiv+498 pages.
[108] M. Richard, J. Kasprzak, R. Romestain, R. Andre and L. S. Dang, "Spontaneous coherent phase transition of polaritons in CdTe microcavities", *Phys. Rev. Lett.* **94** (2005), no. 18, article no. 187401.
[109] M. Wouters, I. Carusotto and C. Ciuti, "Spatial and spectral shape of inhomogeneous nonequilibrium exciton-polariton condensates", *Phys. Rev. B* **77** (2008), article no. 115340.
[110] E. Wertz et al., "Spontaneous formation and optical manipulation of extended polariton condensates", *Nat. Phys.* **6** (2010), no. 11, pp. 860–864.
[111] A. Amo and J. Bloch, "Exciton-polaritons in lattices: a non-linear photonic simulator", *C. R. Phys.* **17** (2016), no. 8, pp. 934–945.
[112] D. Tanese et al., "Polariton condensation in solitonic gap states in a one-dimensional periodic potential", *Nat. Commun.* **4** (2013), no. 1, article no. 1749.
[113] F. Baboux et al., "Unstable and stable regimes of polariton condensation", *Optica* **5** (2018), no. 10, pp. 1163–1170.
[114] D. Nigro, D. Trypogeorgos, A. Gianfrate, D. Sanvitto, I. Carusotto and D. Gerace, "Supersolidity of polariton condensates in photonic crystal waveguides", *Phys. Rev. Lett.* **134** (2025), no. 5, article no. 056002.
[115] D. Trypogeorgos et al., "Emerging supersolidity in photonic-crystal polariton condensates", *Nature* **639** (2025), pp. 337–341.
[116] A. Recati and S. Stringari, "Supersolidity in ultracold dipolar gases", *Nat. Rev. Phys.* **5** (2023), no. 12, pp. 735–743.
[117] S. A. Diddams, K. Vahala and T. Udem, "Optical frequency combs: coherently uniting the electromagnetic spectrum", *Science* **369** (2020), article no. eaay3676 (12 pages).
[118] L. Chang, S. Liu and J. E. Bowers, "Integrated optical frequency comb technologies", *Nature Photon.* **16** (2022), no. 2, pp. 95–108.
[119] D. Bajoni, P. Senellart, A. Lemaître and J. Bloch, "Photon lasing in GaAs microcavity: similarities with a polariton condensate", *Phys. Rev. B* **76** (2007), article no. 201305.
[120] Y. Sun et al., "Bose–Einstein condensation of long-lifetime polaritons in thermal equilibrium", *Phys. Rev. Lett.* **118** (2017), no. 1, article no. 016602.
[121] A. Chiocchetta, A. Gambassi and I. Carusotto, "Laser operation and Bose–Einstein condensation: analogies and differences", in *Universal themes of Bose–Einstein condensation*, Cambridge University Press, 2017, pp. 409–423.
[122] C. Cohen-Tannoudji, "Lectures at Collège de France", 1999-2000. Online at https://www.phys.ens.fr/sites/default/files/2024-03/1999-00.pdf.
[123] S. M. Rezende, *Fundamentals of magnonics*, Lecture Notes in Physics, Springer, 2020, xvii+358 pages.
[124] J. D. Gunton and M. J. Buckingham, "Condensation of the ideal Bose gas as a cooperative transition", *Phys. Rev.* **166** (1968), pp. 152–158.
[125] M. Wouters and I. Carusotto, "Goldstone mode of optical parametric oscillators in planar semiconductor microcavities in the strong-coupling regime", *Phys. Rev. A* **76** (2007), article no. 043807.
[126] R. Graham and H. Haken, "Laserlight–first example of a second-order phase transition far away from thermal equilibrium", *Z. Phys. A, Hadrons Nuclei* **237** (1970), pp. 31–46.
[127] M. Wouters and I. Carusotto, "Absence of long-range coherence in the parametric emission of photonic wires", *Phys. Rev. B* **74** (2006), article no. 245316 (6 pages).
[128] P. Minnhagen, "The two-dimensional Coulomb gas, vortex unbinding, and superfluid-superconducting films", *Rev. Mod. Phys.* **59** (1987), pp. 1001–1066.
[129] Z. Hadzibabic and J. Dalibard, "Two-dimensional Bose fluids: an atomic physics perspective", *Riv. Nuovo Cim.* **34** (2011), no. 6, pp. 389–434.
[130] E. Altman, L. M. Sieberer, L. Chen, S. Diehl and J. Toner, "Two-dimensional superfluidity of exciton polaritons requires strong anisotropy", *Phys. Rev. X* **5** (2015), no. 1, article no. 011017.
[131] L. M. Sieberer, M. Buchhold and S. Diehl, "Keldysh field theory for driven open quantum systems", *Rep. Prog. Phys.* **79** (2016), no. 9, article no. 096001.
[132] A. Zamora, L. M. Sieberer, K. Dunnett, S. Diehl and M. H. Szymańska, "Tuning across universalities with a driven open condensate", *Phys. Rev. X* **7** (2017), no. 4, article no. 041006.
[133] Q. Fontaine et al., "Kardar–Parisi–Zhang universality in a one-dimensional polariton condensate", *Nature* **608** (2022), no. 7924, pp. 687–691.

[134] T. Ozawa, H. M. Price, N. Goldman, O. Zilberberg and I. Carusotto, "Synthetic dimensions in integrated photonics: from optical isolation to four-dimensional quantum Hall physics", *Phys. Rev. A* **93** (2016), no. 4, article no. 043827.
[135] M. Ehrhardt, S. Weidemann, L. J. Maczewsky, M. Heinrich and A. Szameit, "A perspective on synthetic dimensions in photonics", *Laser Photonics Rev.* **17** (2023), no. 7, article no. 2200518.
[136] L. Yuan, Q. Lin, M. Xiao and S. Fan, "Synthetic dimension in photonics", *Optica* **5** (2018), no. 11, pp. 1396–1405.
[137] I. Heckelmann, M. Bertrand, A. Dikopoltsev, M. Beck, G. Scalari and J. Faist, "Quantum walk comb in a fast gain laser", *Science* **382** (2023), no. 6669, pp. 434–438.
[138] A. Dikopoltsev, I. Heckelmann, M. Bertrand, M. Beck, G. Scalari, O. Zilberberg and J. Faist, "Collective quench dynamics of active photonic lattices in synthetic dimensions", *Nat. Phys.* **21** (2025), pp. 1134–1140.
[139] C. J. Flower et al., "Observation of topological frequency combs", *Science* **384** (2024), no. 6702, pp. 1356–1361.
[140] K. A. Takeuchi, "An appetizer to modern developments on the Kardar–Parisi–Zhang universality class", *Phys. A: Stat. Mech. Appl.* **504** (2018), pp. 77–105. Lecture Notes of the 14th International Summer School on Fundamental Problems in Statistical Physics.
[141] K. J. Wiese, "On the perturbation expansion of the KPZ equation", *J. Stat. Phys.* **93** (1998), no. 1, pp. 143–154.
[142] E. Marinari, A. Pagnani and G. Parisi, "Critical exponents of the KPZ equation via multi-surface coding numerical simulations", *J. Phys. A. Math. Gen.* **33** (2000), no. 46, article no. 8181.
[143] L. Canet, H. Chaté, B. Delamotte and N. Wschebor, "Nonperturbative renormalization group for the Kardar–Parisi–Zhang equation", *Phys. Rev. Lett.* **104** (2010), article no. 150601.
[144] A. Imamoğlu, H. Schmidt, G. Woods and M. Deutsch, "Strongly interacting photons in a nonlinear cavity", *Phys. Rev. Lett.* **79** (1997), no. 8, pp. 1467–1470.
[145] I. Carusotto, D. Gerace, H. E. Tureci, S. De Liberato, C. Ciuti and A. Imamoğlu, "Fermionized photons in an array of driven dissipative nonlinear cavities", *Phys. Rev. Lett.* **103** (2009), article no. 033601.
[146] J. R. Johansson, P. D. Nation and F. Nori, "QuTiP: an open-source Python framework for the dynamics of open quantum systems", *Comput. Phys. Commun.* **183** (2012), no. 8, pp. 1760–1772.
[147] Y. Castin, "Simple theoretical tools for low dimension Bose gases", *J. Phy. IV France* **116** (2004), pp. 89–132.
[148] C. Cohen-Tannoudji, J. Dupont-Roc and G. Grynberg, *Atom-photon interactions: basic processes and applications*, Physics Textbook, John Wiley & Sons, 1998, xxii+656 pages.
[149] G. P. Fedorov et al., "Photon transport in a Bose–Hubbard chain of superconducting artificial atoms", *Phys. Rev. Lett.* **126** (2021), article no. 180503.
[150] R. O. Umucalılar and I. Carusotto, "Fractional quantum Hall states of photons in an array of dissipative coupled cavities", *Phys. Rev. Lett.* **108** (2012), article no. 206809.
[151] R. O. Umucalılar and I. Carusotto, "Many-body braiding phases in a rotating strongly correlated photon gas", *Phys. Lett. A* **377** (2013), no. 34–36, pp. 2074–2078.
[152] L. W. Clark, N. Schine, C. Baum, N. Jia and J. Simon, "Observation of Laughlin states made of light", *Nature* **582** (2020), no. 7810, pp. 41–45.
[153] A. V. Gorshkov, J. Otterbach, M. Fleischhauer, T. Pohl and M. D. Lukin, "Photon-photon interactions via Rydberg blockade", *Phys. Rev. Lett.* **107** (2011), article no. 133602.
[154] N. Schine, A. Ryou, A. Gromov, A. Sommer and J. Simon, "Synthetic Landau levels for photons", *Nature* **534** (2016), no. 7609, pp. 671–675.
[155] A. Stern, "Anyons and the quantum Hall effect. A pedagogical review", *Ann. Phys.* **323** (2008), no. 1, pp. 204–249.
[156] B. Paredes, P. Fedichev, J. I. Cirac and P. Zoller, "$\frac{1}{2}$-anyons in small atomic Bose–Einstein condensates", *Phys. Rev. Lett.* **87** (2001), no. 1, article no. 010402.
[157] F. Grusdt, N. Y. Yao, D. Abanin, M. Fleischhauer and E. Demler, "Interferometric measurements of many-body topological invariants using mobile impurities", *Nat. Commun.* **7** (2016), no. 1, article no. 11994.
[158] A. Muñoz de las Heras, E. Macaluso and I. Carusotto, "Anyonic molecules in atomic fractional quantum Hall liquids: a quantitative probe of fractional charge and anyonic statistics", *Phys. Rev. X* **10** (2020), no. 4, article no. 041058.
[159] E. Macaluso and I. Carusotto, "Hard-wall confinement of a fractional quantum Hall liquid", *Phys. Rev. A* **96** (2017), no. 4, article no. 043607.
[160] A. Nardin, D. De Bernardis, R. O. Umucalılar, L. Mazza, M. Rizzi and I. Carusotto, "Quantum nonlinear optics on the edge of a few-particle fractional quantum Hall fluid in a small lattice", *Phys. Rev. Lett.* **133** (2024), no. 18, article no. 183401.
[161] F. Binanti, N. Goldman and C. Repellin, "Spectroscopy of edge and bulk collective modes in fractional Chern insulators", *Phys. Rev. Res.* **6** (2024), article no. L012054 (6 pages).
[162] A. Biella, F. Storme, J. Lebreuilly, D. Rossini, R. Fazio, I. Carusotto and C. Ciuti, "Phase diagram of incoherently driven strongly correlated photonic lattices", *Phys. Rev. A* **96** (2017), no. 2, article no. 023839.
[163] R. O. Umucalılar and I. Carusotto, "Generation and spectroscopic signatures of a fractional quantum Hall liquid of photons in an incoherently pumped optical cavity", *Phys. Rev. A* **96** (2017), no. 5, article no. 053808.

[164] R. O. Umucalılar, J. Simon and I. Carusotto, "Autonomous stabilization of photonic Laughlin states through angular momentum potentials", *Phys. Rev. A* **104** (2021), no. 2, article no. 023704.

[165] P. Kurilovich, V. D. Kurilovich, J. Lebreuilly and S. M. Girvin, "Stabilizing the Laughlin state of light: dynamics of hole fractionalization", *SciPost Phys.* **13** (2022), no. 5, article no. 107 (34 pages).

[166] M. Hafezi, P. Adhikari and J. M. Taylor, "Chemical potential for light by parametric coupling", *Phys. Rev. B* **92** (2015), article no. 174305.

[167] J. Lebreuilly, A. Biella, F. Storme, D. Rossini, R. Fazio, C. Ciuti and I. Carusotto, "Stabilizing strongly correlated photon fluids with non-Markovian reservoirs", *Phys. Rev. A* **96** (2017), no. 3, article no. 033828.

[168] M. J. Jacquet et al., "Quantum vacuum excitation of a quasinormal mode in an analog model of black hole spacetime", *Phys. Rev. Lett.* **130** (2023), no. 11, article no. 111501.

[169] T. Ozawa and H. M. Price, "Topological quantum matter in synthetic dimensions", *Nat. Rev. Phys.* **1** (2019), no. 5, pp. 349–357.

[170] C. Nayak, S. H. Simon, A. Stern, M. Freedman and S. Das Sarma, "Non-Abelian anyons and topological quantum computation", *Rev. Mod. Phys.* **80** (2008), pp. 1083–1159.

[171] T. Tsuno, S. Taie, Y. Takasu, K. Yamashita, T. Ozawa and Y. Takahashi, "Gain engineering and topological atom laser in synthetic dimensions", preprint, 2024. Online at https://arxiv.org/abs/2404.13769.

ACADÉMIE DES SCIENCES
INSTITUT DE FRANCE

Comptes Rendus. Physique
2025, Vol. 26, p. 339-348
https://doi.org/10.5802/crphys.247

Intervention in a conference / *Intervention en colloque*

Mathematical physics of dilute Bose gases

Physique mathématique des gaz de bosons dilués

Jan Philip Solovej [a]

[a] QMATH, Department of Mathematical Sciences, University of Copenhagen, Universitetsparken 5, DK-2100, Copenhagen, Denmark

E-mail: solovej@math.ku.dk

Abstract. We discuss recent progress in the mathematical analysis of dilute Bose gases. We review results in one to three dimensions, but the focus will be on three dimensions. In all dimensions we have a two term asymptotic expansion of the ground state energy density by an expression that depends only on the scattering length of the potential. In dimension three this is the celebrated Lee–Huang–Yang formula. In dimensions two and three the dilute limit is a weakly interacting regime whereas in dimension one it is rather strongly interacting. We sketch briefly the mathematical difficulties and review some remaining open problems in the field.

Résumé. Nous discutons des progrès récents dans l'analyse mathématique des gaz de bosons dilués. Nous passons en revue les résultats obtenus en une, deux et trois dimensions, mais l'accent sera mis sur le cas tridimensionnel. En chaque dimension, nous disposons d'un développement asymptotique à deux termes de la densité d'énergie de l'état fondamental, sous la forme d'expressions ne dépendant que de la longueur de diffusion du potentiel. En dimension trois, il s'agit de la célèbre formule de Lee–Huang–Yang. En dimension deux et en dimension trois, la limite diluée est dans le régime d'interaction faible, alors qu'en dimension un, elle est au contraire en interaction forte. Nous esquissons brièvement les difficultés mathématiques rencontrées et passons en revue quelques problèmes encore ouverts dans ce domaine.

Keywords. Ground states of Bose gases, Cold atomic gases, Bose–Einstein condensation, Bogolyubov approximation, Lee–Huang–Yang formula.

Mots-clés. États fondamentaux des gaz de bosons, Gaz atomiques froids, Condensation de Bose–Einstein, Approximation de Bogolioubov, Formule de Lee–Huang–Yang.

Funding. VILLUM Foundation (grant #10059).

Manuscript received 13 December 2024, revised 17 March 2025, accepted 18 March 2025.

1. Introduction

Our goal here is to discuss the mathematical analysis of dilute Bose gases and, in particular, the ground state energy density in this limit. We consider N bosons moving in a cube $[0,L]^d$ of length $L>0$ in dimension $d=1,2$ or 3. We use units in which $\hbar=1$ and the mass of the boson is $1/2$. The kinetic energy of a boson is thus represented by the Laplace operator $-\Delta=-\nabla^2$. The bosons will interact through a two-body potential v such that the system Hamiltonian is given by

$$H_N(v)=\sum_{i=1}^{N}-\Delta_i+\sum_{i<j}v(x_i-x_j) \tag{1}$$

acting on an appropriate subspace $\mathscr{D}$ of symmetric square integrable functions on $[0,L]^{Nd}$, i.e., of $L^2([0,L]^{Nd}) = \bigotimes^N L^2([0,L]^d)$. Symmetry refers to interchange of the N boson coordinates in $[0,L]^d$. The problem will not depend very much on the choice of the domain $\mathscr{D}$, i.e., boundary conditions (e.g., Dirichlet, Neumann or periodic) will, in general, not be important. We will nevertheless consider it to consist of functions that have two continuous partial derivatives and that satisfy periodic boundary conditions on $[0,L]^d$. This is of course equivalent to consider particles on a torus.

The assumptions on the two-body potential v are, however, important for the known mathematical results. These assumptions relate to some of the open problems we will highlight. We need to assume that $v \geq 0$ and that v is spherically symmetric. For simplicity here we will also assume that v vanishes outside a bounded region. This last assumption can certainly be relaxed to some sufficiently fast decay, but the assumption that v is non-negative is important and removing it is a challenge. The only known work, relating to what we discuss, allowing v to be slightly negative is [1]. The potential is allowed to be rather singular. The most important example is maybe the hard-core potential

$$v(x) = \begin{cases} \infty, & |x| < R \\ 0, & |x| > R. \end{cases} \tag{2}$$

We will here be concerned with the *ground state energy*, i.e., the case of zero temperature $T = 0$:

$$E_L(N,v) = \inf_{\Psi \in \mathscr{D}} \frac{\langle \Psi | H_N | \Psi \rangle}{\langle \Psi | \Psi \rangle}.$$

The inf here is not necessarily a min, because the normalized ground state Ψ_0 which satisfies

$$E_L(N,v) = \langle \Psi_0 | H_N | \Psi_0 \rangle$$

may not be in the domain $\mathscr{D}$ that we chose, but may only be approximated from $\mathscr{D}$. Moreover here it is not really important that $\mathscr{D}$ consists of symmetric functions. If we ignored this condition the infimum would be the same, i.e., the ground state Ψ_0 is automatically symmetric, i.e., bosonic.

We are really interested in the *thermodynamic limit* of the ground state energy density

$$e(\rho,v) = \lim_{\substack{L\to\infty \\ NL^{-d}\to\rho}} L^{-d} E_L(N)$$

for a particle number density $\rho \geq 0$. It is not difficult to prove that this limit exists and that $e(\rho)$ is a convex function of ρ.

While the energy $E_L(N,v)$ may depend on the boundary conditions we choose on the boundary of $[0,L]^d$ the thermodynamic energy density $e(\rho)$ will not.

The goal is to understand the structure of the ground state and of $e(\rho)$ in the dilute limit $\rho \to 0$. In particular we would like to prove Bose–Einstein Condensation (BEC) in $d = 2$ and 3 and to understand the asymptotic expansion of $e(\rho)$ in the dilute limit.

We should, however, first understand what we mean exactly by the dilute limit, i.e., what is the right parameter to compare ρ to. For that we need to introduce the *Scattering Length* of the potential v. We will do that in Section 2. In Section 3 we formulate the main mathematical results on the dilute limit of the ground state energy density. In Section 4 we review the Bogolubov approximation as a variational theory and explain what it gives in the dilute limit. In Section 5 we discuss Bose–Einstein condensation and what is known about it rigorously. In Section 6 we sketch some of the ideas involved in proving the energy asymptotics in three dimensions—the Lee–Huang–Yang formula. Finally, in Section 7 we make a few remarks about the one-dimensional case where we do not have BEC and compare the result on the dilute limit for general potentials with the exact results for the hard-core gas and the Lieb–Liniger gas. We conclude in Section 8 with a summary and open questions.

2. Scattering length

To introduce the scattering length we consider the zero energy scattering equation [2]

$$-\Delta u + \tfrac{1}{2} v u = 0, \quad \text{on } \mathbb{R}^d.$$

Here the factor $1/2$ may be seen as coming from the reduced mass of the two-body problem, i.e., that there is a factor 2 in front of the Laplacian in relative coordinates.

If v vanishes outside a ball of radius R there will in dimension $d = 1,2,3$ be a unique solution u satisfying that for $|x| > R$

$$d = 1\text{: } u(x) = |x| - a, \quad d = 2\text{: } u(x) = \ln(|x|/a), \quad d = 3\text{: } u(x) = 1 - \frac{a}{|x|}$$

for a unique length scale a called the *scattering length* of the potential v.

Note that we must have $a \le R$ otherwise the scattering function u changes sign and hence, by the Sturm oscillation principle, the potential v will have a two-body bound state. For the hard-core potential (2) we have $a = R$.

Under our assumption $v \ge 0$ this cannot happen and moreover in dimensions 2 and 3, $a \ge 0$. In dimension 1 we may have a negative even if v is positive, e.g., for the delta interaction, i.e., the Lieb–Liniger gas.

The free case $v = 0$ corresponds to $a = 0$ in dimensions $d = 2$ and 3, but in dimension $d = 1$ it corresponds to $a = -\infty$. Since $a = 0$ for the free gas in 2 and 3 dimensions the dilute limit can also be seen as the weakly interacting case. In dimension 1, however, the dilute gas corresponds rather to the strongly interacting case.

In dimension three we have $0 \le u \le 1$ and it will be convenient for us to write the scattering solution as $u(x) = 1 - \omega(x)$, with $0 \le \omega(x) \le 1$ and $\omega(x) = a/|x|$ for large $|x|$. It is also easy to see, in this case, that

$$8\pi a = \int v(x) u(x)\, \mathrm{d}x \le \int v(x)\, \mathrm{d}x. \tag{3}$$

Equivalently the scattering length could have been defined from the two particle ground state energy satisfying the following $L \to \infty$ asymptotics

$$E_L(N = 2, v) = \begin{cases} 2\pi^2 (L - a)^{-2} + o(aL^{-3}), & d = 1 \\ 4\pi L^{-2} \left| \ln \dfrac{a}{L} \right|^{-1} (1 + o(1)), & d = 2 \\ 8\pi a L^{-3} (1 + o(1)), & d = 3. \end{cases} \tag{4}$$

Here it is important that we consider wave functions satisfying periodic boundary conditions.

Having defined the scattering length we can make the condition of diluteness more precise. Indeed, it refers to the dimensionless parameter $\rho |a|^d$ being small.

3. Main result on energy density asymptotics

The main mathematical results on the ground state energy density of dilute gases is collected in the following theorem.

Theorem 1 (Ground state energy density asymptotics). *For $v \ge 0$ with finite range in the ball $|x| \le R$ we find in the limit $\rho |a|^d \to 0$ that*

$$d = 3\text{: } \; e(\rho) = 4\pi\rho^2 a \left(1 + \frac{128}{15\sqrt{\pi}} (\rho a^3)^{1/2} + o((\rho a^3)^{1/2}) \right)$$

$$d = 2\text{: } \; e(\rho) = 4\pi\rho^2 Y \left(1 + Y \log(Y\pi) + \left(2\Gamma + \frac{1}{2} \right) Y + o(Y) \right), \quad Y = |\log(\rho a^2)|^{-1}$$

$$d = 1\text{: } \; e(\rho) = \frac{\pi^2}{3} \rho^3 (1 + 2\rho a + o(\rho R)).$$

The result in dimension three requires $v \in L^3$, i.e., that the $|v|^3$ is integrable, but this is only required to prove the upper bound in the estimate. Above Γ is the Euler–Mascheroni constant.

The error in dimension one is not only in terms of ρa but involves the range R. In the one-dimensional case we may have $a = 0$ for a non-trivial potential and we can then not write the error solely in terms of ρa.

The leading term in the asymptotic formula in dimension 3 goes back to Lenz [3]. The full two-term asymptotics in $d = 3$, *the Lee–Huang–Yang formula*, goes back to the 1957 work of Lee–Huang–Yang [4] based on an analysis of the hard-core gas. They conjectured that the two terms should hold universally. The universality of the upper bound in the leading term was established by Dyson [5] in 1957 and the leading order lower bound by Lieb and Yngvason in 1998 [6]. The upper bound to the Lee–Huang–Yang precision was proved by Yau and Yin [7] and simplified in [8]. It requires, as explained in the theorem, the potential v to satisfy integrability conditions and does not include the hard-core case. The lower bound was proved in [9,10]. It holds also for the hard-core potential. It is curious that Lee, Huang, and Yang derived the formula from an analysis of the hard-core gas while this case is still a mathematical challenge. The recent paper [11] derives an upper bound on the ground state energy density for the hard-core gas with an error of the order of the Lee–Huang–Yang correction but with too large a constant. In [12] a version of the upper bound to the Lee–Huang–Yang precision was derived in a confined Gross–Pitaevskii regime. The Lee–Huang–Yang formula was observed experimentally in a cold dilute gas of ^{7}Li atoms in [13,14].

The two-dimensional leading-order case was studied by Schick in [15] and rigorously by Lieb and Yngvason in [16]. The higher corrections were studied in [17–20]. A complete proof including the hard-core case for both the upper and lower bounds was given in [21]. The one-dimensional case was proved in [22].

In dimension three corrections beyond the Lee–Huang–Yang order were predicted by Wu [23] to be of the form

$$e(\rho) = 4\pi\rho^2 a\left(1 + \frac{128}{15\pi^{1/2}}(\rho a^3)^{1/2} + 8\left(\frac{4\pi}{3} - \sqrt{3}\right)\rho a^3 \ln(\rho a^3) + \mathscr{E}\rho a^3 + o(\rho a^3)\right). \tag{5}$$

The constant $\mathscr{E}$ can be found more explicitly in [24] which claims

$$\mathscr{E} = \frac{D}{12\pi a^4} + \pi\frac{r_s}{a} + C,$$

where C is a universal constant, D is the three-body scattering hyper-volume, and r_s is the effective range (for the hard-core $r_s = 2a/3$, see [24]). From the rigorous point of view, all terms beyond Lee–Huang–Yang are a challenge for thermodynamic systems. In a confined setting progress on the third term above was achieved in [25].

In dimension two Mora and Castin [20] find[1]

$$e(\rho) = 4\pi\rho^2 Y\left(1 + Y(\log(Y\pi) + 2\Gamma + 1/2) + Y^2(\log(Y\pi) + 2\Gamma + 1)^2 - \frac{8I}{\pi}Y^2 + o(Y^2)\right), \tag{6}$$

where I is a universal constant.

4. Second quantization and Bogolyubov Theory

In this section we will briefly sketch how to understand the Lee–Huang–Yang formula from the Bogolyubov approximation [26]. We shall however proceed in a somewhat non-standard way. Usually the Bogolyubov approximation approximates the Hamiltonian by a quadratic Hamiltonian in bosonic creation and annihilation operators. Such a Hamiltonian will be minimized by a

[1] I thank the referee for suggesting to add the formula in this form which has not appeared previously.

Gaussian or quasi-free state. Rather than approximating the Hamiltonian we will introduce Bogolyubov theory as a variational approach where we leave the Hamiltonian unchanged but restrict to quasi-free states. For details see [27,28]. This has the advantage that the resulting approximation is actually an upper bond on the true energy density.

We write the Hamiltonian (1) on the 3-dimensional torus in second quantized form.

$$H_N(v) = \sum_{p\in(2\pi\mathbb{Z}/L)^3} p^2 a_p^\dagger a_p + \frac{1}{2L^3}\sum_{p,q,k} \widehat{v}(k) a_{p+k}^\dagger a_{q-k}^\dagger a_q a_p.$$

Here we use the convention $\widehat{v}(p) = \int v(x)\mathrm{e}^{-\mathrm{i}px}\,\mathrm{d}x$ for the Fourier transform, i.e., on the torus the interaction v between two particles is a function of the distance between them measured on the torus.

We perform a unitary transformation $a_0 \to a_0 + \sqrt{\rho_0 L^3}$ that rewrites the Hamiltonian in terms of variables expanding around the condensate with density ρ_0 in the zero momentum state.

After this we evaluate in a quasi-free translation invariant state where all expectation values can be expressed by Wick's Theorem in terms of the two quantities:

$$\gamma(p) = \langle a_p^\dagger a_p\rangle, \quad \alpha(p) = \langle a_p^\dagger a_{-p}^\dagger\rangle.$$

It is sufficient here to restrict to $\alpha(p)$ real. They satisfy that the matrix

$$\begin{pmatrix} \gamma(p) & \alpha(p) \\ \alpha(p) & 1+\gamma(p)\end{pmatrix}$$

is positive semi-definite and hence

$$\alpha(p)^2 \le \gamma(p)(1+\gamma(p)).$$

We find the energy density in the thermodynamic limit expressed as the functional

$$\begin{aligned}\mathscr{E}_{\mathrm{Bog}}(\rho_0,\gamma,\alpha) \;=\; & (2\pi)^{-3}\int p^2\gamma(p)\,\mathrm{d}p + \frac{1}{2}\widehat{v}(0)\left(\rho_0 + (2\pi)^{-3}\int \gamma(p)\,\mathrm{d}p\right)^2 \\ & + \rho_0(2\pi)^{-3}\int \widehat{v}(p)(\gamma(p)+\alpha(p))\,\mathrm{d}p \\ & + \frac{1}{2}(2\pi)^{-6}\iint \widehat{v}(p-q)(\gamma(p)\gamma(q)+\alpha(p)\alpha(q))\,\mathrm{d}p\,\mathrm{d}q. \end{aligned} \tag{7}$$

We will now sketch how to get the leading term in the $d=3$ expansion from this expression. The minimizer will have $\alpha(p) = -\sqrt{\gamma(p)(1+\gamma(p))}$. It can be shown that the minimizer of the Bogolyubov functional (7) has almost complete condensation, i.e.,

$$\rho := \rho_0 + (2\pi)^{-3}\int \gamma(p)\,\mathrm{d}p \approx \rho_0$$

and we will have $\gamma(p) \ll 1$. We can therefore approximate $\gamma(p) \approx \alpha(p)^2$. If we write the inverse Fourier transform of α as $\check{\alpha}(x)$, we see that

$$(2\pi)^{-3}\int p^2\gamma(p)\,\mathrm{d}p \approx \int |\nabla\check{\alpha}(x)|^2\,\mathrm{d}x.$$

The energy density is therefore approximated by

$$\int |\nabla\check{\alpha}(x)|^2\,\mathrm{d}x + \rho\int v(x)\check{\alpha}(x)\,\mathrm{d}x + \frac{1}{2}\int v(x)|\check{\alpha}(x)|^2\,\mathrm{d}x + \frac{1}{2}\widehat{v}(0)\rho^2. \tag{8}$$

With these approximations the variational equation for $\check{\alpha}$ is

$$-\Delta\check{\alpha} + \tfrac{1}{2}v\check{\alpha} + \tfrac{1}{2}\rho v = 0. \tag{9}$$

We can rewrite this equation as

$$-\Delta(1+\rho^{-1}\check{\alpha}) + \tfrac{1}{2}v(1+\rho^{-1}\check{\alpha}) = 0.$$

We recognize this as the scattering equation and conclude that $\check{\alpha}(x) \approx -\rho\omega(x)$. Multiplying Equation (9) by $\check{\alpha}$ and integrating we find that the approximation (8) to the energy density gives

$$\frac{1}{2}\rho\int v(x)\check{\alpha}(x)\,\mathrm{d}x + \frac{1}{2}\widehat{v}(0)\rho^2 = \frac{1}{2}\rho^2\int v(x)(1-\omega(x))\,\mathrm{d}x = 4\pi\rho^2 a,$$

i.e., exactly the leading term in the 3-dimensional energy asymptotics. Here we used that the scattering solution is $u(x) = 1-\omega(x)$ and the identity (3).

In the usual formulation of the Bogolyubov approximation a_0 is replaced by a number (c-number substitution) and the remaining Hamiltonian is approximated by an operator quadratic in the remaining creation and annihilation operators by ignoring cubic and quartic terms. Proceeding in such a fashion it is, actually not even possible to get the correct leading term in the energy density asymptotics. In fact, the scattering length will not appear but we will find the larger value $(8\pi)^{-1}\int v = (8\pi)^{-1}\,\widehat{v}(0)$ in its place. It should also be clear from the analysis above that we, indeed, did not ignore the quartic terms.

The approximations above can be controlled rigorously [28]. The argument originally goes back to the paper [29]. In [28] it was shown by a more detailed analysis that minimizing the Bogolyubov functional in (7) does not give the second correction in the Lee–Huang–Yang formula. It does give the formula if $\widehat{v}(0)$ is replaced everywhere by the smaller quantity $8\pi a$. In fact, the difficulty in the rigorous analysis is exactly to understand this replacement.

Restricting to quasi-free states, indeed, ignores the cubic terms of the form

$$\widehat{v}(k)a_k^\dagger a_{q-k}^\dagger a_q a_0 + \text{hermitian conjugates}$$

in the Hamiltonian just as in the usual Bogolyubov approximation. It was, however, understood both in [7] and in [9,10] that these terms cannot be ignored if the goal is to get the Lee–Huang–Yang order correctly.

5. Bose–Einstein condensation

In the previous section we saw that the optimal Bogolyubov trial state has almost complete condensation. It is, however, one of the major open problems in the mathematical analysis of Bose gases to show Bose–Einstein condensation (BEC) for the true ground state. The precise meaning of BEC is that in the thermodynamic limit we have for the true ground state Ψ_L (indicating explicitly that it of course depends on L) that

$$\lim_{\substack{L\to\infty\\ N/L^d\to\rho}} L^{-3}\langle\Psi_L, a_0^\dagger a_0\Psi_L\rangle = \rho_0 \neq 0$$

i.e., that we have macroscopic occupation in the zero momentum state.

It turns out, however, that to rigorously establish the Lee–Huang–Yang formula we do not need to prove BEC in the thermodynamic limit. It is enough to establish condensation for the gas confined to a finite size corresponding to the Gross–Pitaevskii regime. More precisely, in dimension 3 this means that the gas shows condensation if confined to a box of length scale L of order the *healing length* $\sim(\rho a)^{-1/2}$. On this scale condensation can be proved if the ground state energy can be approximated to sufficient accuracy. To understand this heuristically note that if $\rho_+ = \rho - \rho_0$ is the density of particles not in zero momentum then in a cube of length L these particles would have a kinetic energy density of at least $\rho_+\pi^2 L^{-2}$. If we control the energy to the Lee–Huang–Yang order this would imply that $\rho_+ L^{-2} \ll \rho^2 a\sqrt{\rho a^3}$, or

$$\frac{\rho_+}{\rho} \ll (L\sqrt{\rho a})^2\sqrt{\rho a^3}.$$

This was first seen rigorously for trapped potentials in [30] and improved in [31–35]. In the thermodynamic limit, however, condensation cannot be derived from controlling the energy

density. The only known cases in which BEC has been established in the thermodynamic limit is for the hard core Bose gas on a lattice at half filling [36,37].

It is an interesting question whether the experimental observations of BEC going back to the seminal works [38,39] can be said to be in a thermodynamic regime in the sense that the confinement is in a region large compared to the healing length, properly defined. The original works were in a harmonic trapping potential whereas more recent experiments [40] are closer to the uniform case. The experiment considers confinement of ^{87}Rb atoms in a cylindrical "box" with cross-sectional diameter $R = 35$ μm and length $L = 70$ μm. The experiment starts with 6×10^5 particles before evaporative cooling and ends with a condensate density of 2×10^{12} cm^{-3} = 2 μm^{-3} corresponding to approximately 5×10^5 condensate particles. It may not be entirely clear how to define the healing length in order to make a comparison. A reasonable comparison would be whether the leading order energy per particle, i.e. $4\pi\rho a$, corresponds to many transversal kinetic energy modes. The number of transversal energy modes up to level $\lambda = 4\pi\rho a$ may be estimated by the phase-space volume. With a scattering length of ^{87}Rb around 5×10^{-3} μm [41] and using for ρ the condensate density 2 μm^{-3} we find for this estimate on the number of transversal modes

$$(2\pi)^{-2}\iint_{p^2\leq\lambda, r<R} \mathrm{d}^2p\,\mathrm{d}^2r = \frac{1}{4}\lambda R^2 = \pi\rho a R^2 \approx 35^2\pi/100 \approx 38.$$

This is a reasonably large number of modes. It would still be interesting to increase the size of the sample to push our understanding of BEC further.

Likewise, it may be considered whether the experimental study of the Lee–Huang–Yang correction for ^{7}Li atoms in [13] is in a trapped (Gross–Pitaevskii regime) or closer to a thermodynamic regime. In this setup the healing length is approximately 1 μm whereas the cylindrical trap (in this case harmonic) has cross-sectional radius 5 μm and length 100 μm.

6. Ideas behind the proof of the Lee–Huang–Yang formula

We will give a very sketchy overview of how to prove the lower bound in the Lee–Huang–Yang formula. The long and technical details can be found in [9] and [10]. There are two main steps in the proof. The first step is to control condensation by localizing the gas to a box of size of the healing length $\ell \sim (\rho a)^{-1/2}$ without paying too high a localization prize.

In a box of that size we may conclude condensation as described above. In fact, if we only want to show $\rho_+ \ll \rho$ it is enough to control the energy to any order better than the leading order $\rho^2 a$.

In a box $B = [0,\ell]^3$ we consider the projection P onto constant functions, i.e.,

$$P = \ell^{-3}\,|1_B\rangle\langle 1_B|$$

and the orthogonal projection $Q = 1 - P$. Note that the operator $\sum_i P_i$ acting on the many-body space counts the number of particles in the condensate, i.e., $\sum_i P_i = a_0^\dagger a_0$ in second quantization, and $\sum_i Q_i$ counts the particles *not* in the condensate. Thus we know a-priori from the first step that $\sum_i Q_i$ is not too big.

We may write

$$\begin{aligned}\sum_{i<j} v(x_i - x_j) &= \sum_{i<j}(P_i+Q_i)(P_j+Q_j)v(x_i-x_j)(P_i+Q_i)(P_j+Q_j)\\ &= \sum_{i<j} P_iP_j v(x_i-x_j)P_iP_j + \cdots + Q_iQ_j v(x_i-x_j)Q_iQ_j,\end{aligned}$$

where in the last expression we have expanded in 16 terms. The usual Bogolyubov approximation corresponds to keeping terms with 2 or fewer Q operators and ignoring the terms with 3 and 4 Q's. We know however that this will not work.

A crucial idea in [9] was to recognize that the expression that we can afford to ignore in the lower bound is the positive expression (using that $v \geq 0$)

$$\sum_{i<j} (Q_iQ_j + (P_iP_j + P_iQ_j + P_jQ_i)\omega)\, v(Q_iQ_j + \omega(P_iP_j + P_iQ_j + P_jQ_i)) \geq 0.$$

Recall that $u = 1-\omega$ was the scattering solution. The dependence of ω and v on $x_i - x_j$ is omitted to lighten the notation. Put differently we subtract this term from the Hamiltonian to get a lower bound. This will have the effect to remove the 4-Q term and in the other terms replace v by either $v(1-\omega)$ or $v(1-\omega^2)$. Note that replacing v by $v(1-\omega) = vu$ gives us a potential (see (3)) with the property that $\int vu = 8\pi a$, which is the main point in this idea.

There are still the $(1-\omega^2)v = (1-\omega)v + \omega(1-\omega)v$ terms as well as the 3-Q terms. The 3-Q terms require a difficult analysis before a standard Bogolyubov diagonalization can be performed. It leads to a calculation where the additional terms with $\omega(1-\omega)v$ exactly cancel to arrive at the Lee–Huang–Yang formula.

7. Some reflections on the one-dimensional case

We will not discuss the one-dimensional case of Theorem 1 in details but will only make a few remarks about it. In the one-dimensional case there are two cases in which the ground state energy can, at least in principle, be determined explicitly.

The simplest case is that of a hard-core potential. In this case the ground state energy of the Bose gas is identical to the ground state energy of the free Fermi gas in the smaller length ("volume") $L - Na$ corresponding to the higher density $\rho(1-\rho a)^{-1}$. Recalling that the ground state energy of the free Fermi gas in one-dimension is $(\pi^2/3)N^3L^{-2}$ an easy calculation shows that the ground state energy of the hard-core Bose gas is $(\pi^2/3)N\rho^2(1-\rho a)^{-2}$. I.e., the ground state energy density is

$$e(\rho) = \frac{\pi^2}{3}\rho^3(1-\rho a)^{-2} = \frac{\pi^2}{3}\rho^3(1+2\rho a + o(\rho a)).$$

In agreement with Theorem 1.

The other case that can be treated exactly is the Lieb–Liniger gas [42] with delta interactions $v(x) = 2c\delta(x)$, $c > 0$. It was solved exactly in [42]. To be more precise calculating the ground state energy is reduced to solving an integral equation. This is not entirely trivial and a closed form expression does not exist. It is, however, known that in the dilute limit ρ small or equivalently c large (the strongly interacting case) we have

$$e(\rho) = \frac{\pi^2}{3}\rho^3((1+2\rho/c)^{-2} + o(\rho/c)).$$

Since the scattering length of v in this case is negative with $a = -2/c$ we again arrive at the formula in Theorem 1. The rigorous proof that this is universally true for all potentials is, at least, for the lower bound based on a comparison with the Lieb–Liniger model. The details of both the upper and lower bound are given in [22].

8. Conclusion and summary of open problems

We have briefly discussed the known mathematical results on the ground state energy density of Bose gases in the dilute limit. For positive (repulsive) potentials we know under fairly general circumstances a two-term asymptotic expansion for the ground state energy density. The most important unsolved case is the hard-core potential in three dimensions. In this case, we know that the Lee–Huang–Yang formula gives a correct lower bound on the ground-state energy density. For the upper bound, the best result [11] is an estimate with a coefficient on the term of

Lee–Huang–Yang order that is too large. Finally, it is still a major challenge to go beyond the Lee–Huang–Yang order and prove the Wu corrections in (5) and the corresponding two-dimensional Mora–Castin corrections in (6).

Another important open problem is generalizing to potentials that are allowed to be negative. The best result here is [1]. Of course, it must be a requirement that the potential has no k-body bound states for any finite particle number k. Thus, in particular, it rules out potentials with range smaller than the scattering length where there are two-body bound states. Thus, the situation studied in experiments with cold atomic gases where the scattering length is significantly larger than the range are at best meta-stable. Analyzing such systems mathematically would be a major challenge, as we would not have a true ground state.

The most challenging mathematical problem for dilute gases is to establish Bose–Einstein condensation. It has been done for confined gases, but, except for a few cases that are certainly not dilute, it is an open problem in the thermodynamic limit corresponding to gases confined to regions much larger than the healing length. It might also be interesting to consider experiments that probe condensation even further into this regime.

Declaration of interests

The authors do not work for, advise, own shares in, or receive funds from any organization that could benefit from this article, and have declared no affiliations other than their research organizations.

Funding

The work is supported by the VILLUM Foundation grant #10059.

References

[1] J. Yin, "The ground state energy of dilute Bose gas in potentials with positive scattering length", *Commun. Math. Phys.* **295** (2010), no. 1, pp. 1–27. (English).

[2] E. H. Lieb, R. Seiringer, J. P. Solovej and J. Yngvason, *The Mathematics of the Bose Gas and its Condensation*, Oberwolfach Seminars, Birkhäuser: Basel, 2005. (English).

[3] W. Lenz, "Die Wellenfunktion und Geschwindigkeitsverteilung des entarteten gases", *Z. Phys.* **56** (1929), no. 11–12, pp. 778–789.

[4] T. D. Lee, K. Huang and C. N. Yang, "Eigenvalues and eigenfunctions of a Bose system of hard spheres and its low-temperature properties", *Phys. Rev.* **106** (1957), no. 6, pp. 1135–1145.

[5] F. J. Dyson, "Ground-state energy of a hard-sphere gas", *Phys. Rev., II. Ser.* **106** (1957), pp. 20–26. (English).

[6] E. H. Lieb and J. Yngvason, "Ground state energy of the low density Bose gas", *Phys. Rev. Lett.* **80** (1998), no. 12, pp. 2504–2507.

[7] H.-T. Yau and J. Yin, "The second order upper bound for the ground energy of a Bose gas", *J. Stat. Phys.* **136** (2009), no. 3, pp. 453–503. (English).

[8] G. Basti, S. Cenatiempo and B. Schlein, "A new second-order upper bound for the ground state energy of dilute Bose gases", *Forum Math. Sigma* **9** (2021), article no. e74.

[9] S. Fournais and J. P. Solovej, "The energy of dilute Bose gases", *Ann. Math.* **192** (2020), no. 3, pp. 893–976.

[10] S. Fournais and J. P. Solovej, "The energy of dilute Bose gases. II: the general case", *Invent. Math.* **232** (2023), no. 2, pp. 863–994. (English).

[11] G. Basti, S. Cenatiempo, A. Giuliani, A. Olgiati, G. Pasqualetti and B. Schlein, "Upper bound for the ground state energy of a dilute Bose gas of hard spheres", *Arch. Ration. Mech. Anal.* **248** (2024), no. 6, article no. 100. (English).

[12] G. Basti, S. Cenatiempo, A. Olgiati, G. Pasqualetti and B. Schlein, "A second order upper bound for the ground state energy of a hard-sphere gas in the Gross–Pitaevskii regime", *Commun. Math. Phys.* **399** (2023), no. 1, pp. 1–55. (English).

[13] N. Navon, S. Piatecki, K. Günter, B. Rem, T. C. Nguyen, F. Chevy, W. Krauth and C. Salomon, "Dynamics and thermodynamics of the low-temperature strongly interacting Bose gas", *Phys. Rev. Lett.* **107** (2011), article no. 135301.

[14] N. Navon, S. Nascimbene, F. Chevy and C. Salomon, "The equation of state of a low-temperature Fermi gas with tunable interactions", *Science* **328** (2010), no. 5979, pp. 729–732.
[15] M. Schick, "Two-dimensional system of hard-core bosons", *Phys. Rev. A* **3** (1971), no. 3, pp. 1067–1073.
[16] E. H. Lieb and J. Yngvason, "The ground state energy of a dilute two-dimensional Bose gas", *J. Stat. Phys.* **103** (2001), no. 3–4, pp. 509–526.
[17] D. Hines, N. Frankel and D. Mitchell, "Hard-disc Bose gas", *Phys. Lett. A* **68** (1978), no. 1, pp. 12–14.
[18] A. Y. Cherny and A. A. Shanenko, "Dilute Bose gas in two dimensions: density expansions and the Gross–Pitaevskii equation", *Phys. Rev. E* **64** (2001), article no. 027105.
[19] C. N. Yang, "Pseudopotential method and dilute hard "sphere" Bose gas in dimensions 2, 4 and 5", *Europhys. Lett.* **84** (2008), no. 4, article no. 40001.
[20] C. Mora and Y. Castin, "Ground state energy of the two-dimensional weakly interacting Bose gas: first correction beyond Bogoliubov theory", *Phys. Rev. Lett.* **102** (2009), article no. 180404.
[21] S. Fournais, T. Girardot, L. Junge, L. Morin and M. Olivieri, "The ground state energy of a two-dimensional Bose gas", *Commun. Math. Phys.* **405** (2024), no. 3, article no. 59.
[22] J. Agerskov, R. Reuvers and J. P. Solovej, "Ground state energy of dilute Bose gases in 1D", *Commun. Math. Phys.* **406** (2025), no. 2, article no. 27.
[23] T. T. Wu, "Ground state of a Bose system of hard spheres", *Phys. Rev.* **115** (1959), no. 6, pp. 1390–1404.
[24] S. Tan, "Three-boson problem at low energy and implications for dilute Bose–Einstein condensates", *Phys. Rev. A* **78** (2008), article no. 013636.
[25] C. Caraci, A. Olgiati, D. S. Aubin and B. Schlein, "Third order corrections to the ground state energy of a Bose gas in the Gross–Pitaevskii regime", preprint, 2024, 2311.07433.
[26] N. N. Bogolyubov, "On the theory of superfluidity", *Proc. Inst. Math. Kiev* (1947), no. 9, pp. 89–103. Rus. Trans Izv. Akad. Nauk Ser. Fiz. 11, 77 (1947), Eng. Trans. J. Phys. (USSR), 11, 23 (1947).
[27] M. Napiórkowski, R. Reuvers and J. P. Solovej, "The Bogoliubov free energy functional. I: existence of minimizers and phase diagram", *Arch. Ration. Mech. Anal.* **229** (2018), no. 3, pp. 1037–1090. (English).
[28] M. Napiórkowski, R. Reuvers and J. P. Solovej, "The Bogoliubov free energy functional. II: the dilute limit", *Commun. Math. Phys.* **360** (2018), no. 1, pp. 347–403. (English).
[29] L. Erdös, B. Schlein and H.-T. Yau, "Ground-state energy of a low-density Bose gas: a second-order upper bound", *Phys. Rev. A* **78** (2008), article no. 053627.
[30] E. H. Lieb and R. Seiringer, "Proof of Bose–Einstein condensation for dilute trapped gases", *Phys. Rev. Lett.* **88** (2002), article no. 170409.
[31] C. Boccato, C. Brennecke, S. Cenatiempo and B. Schlein, "Complete Bose–Einstein condensation in the Gross–Pitaevskii regime", *Commun. Math. Phys.* **359** (2018), no. 3, pp. 975–1026. (English).
[32] C. Boccato, C. Brennecke, S. Cenatiempo and B. Schlein, "Bogoliubov theory in the Gross–Pitaevskii limit", *Acta Math.* **222** (2019), no. 2, pp. 219–335. (English).
[33] C. Boccato, C. Brennecke, S. Cenatiempo and B. Schlein, "Optimal rate for Bose–Einstein condensation in the Gross–Pitaevskii regime", *Commun. Math. Phys.* **376** (2020), no. 2, pp. 1311–1395.
[34] A. Adhikari, C. Brennecke and B. Schlein, "Bose–Einstein condensation beyond the Gross–Pitaevskii regime", *Ann. Henri Poincaré* **22** (2021), no. 4, pp. 1163–1233. (English).
[35] S. Fournais, "Length scales for BEC in the dilute Bose gas", *Partial Differential Equations, Spectral Theory, and Mathematical Physics*, EMS Press: Berlin, 2021, pp. 115–133.
[36] T. Kennedy, E. H. Lieb and B. S. Shastry, "The *XY* has long-range order for all spins and all dimensions greater than one", *Phys. Rev. Lett.* **61** (1988), no. 22, pp. 2582–2584.
[37] M. Aizenman, E. H. Lieb, R. Seiringer, J. P. Solovej and J. Yngvason, "Bose–Einstein quantum phase transition in an optical lattice model", *Phys. Rev. A* **70** (2004), article no. 023612.
[38] M. H. Anderson, J. R. Ensher, M. R. Matthews, C. E. Wieman and E. A. Cornell, "Observation of Bose–Einstein condensation in a dilute atomic vapor", *Science* **269** (1995), no. 5221, pp. 198–201.
[39] K. B. Davis, M.-O. Mewes, M. R. Andrews, N. J. van Druten, D. S. Durfee, D. M. Kurn and W. Ketterle, "Bose–Einstein condensation in a gas of sodium atoms", *Phys. Rev. Lett.* **75** (1995), no. 22, pp. 3969–3973.
[40] A. L. Gaunt, T. F. Schmidutz, I. Gotlibovych, R. P. Smith and Z. Hadzibabic, "Bose–Einstein condensation of atoms in a uniform potential", *Phys. Rev. Lett.* **110** (2013), article no. 200406.
[41] J. P. Burke and J. L. Bohn, "Ultracold scattering properties of the short-lived Rb isotopes", *Phys. Rev. A* **59** (1999), no. 2, pp. 1303–1308.
[42] E. H. Lieb and W. Liniger, "Exact analysis of an interacting bose gas. I. The general solution and the ground state", *Phys. Rev.* **130** (1963), no. 4, pp. 1605–1616.

ACADÉMIE DES SCIENCES
INSTITUT DE FRANCE

Comptes Rendus. Physique
2024, Vol. 25, p. 389-413
https://doi.org/10.5802/crphys.222

Intervention in a conference / *Intervention en colloque*

Reflections on dipolar quantum fluids

Réflexions sur les fluides quantiques dipolaires

Wilhelm Zwerger[a]

[a] Physik Department TU München, James Franck Strasse, 85748 Garching, Germany
E-mail: zwerger@tum.de

Abstract. We present a thermodynamic description of ultracold gases with dipolar interactions which properly accounts for the long-range nature and broken rotation invariance of the interactions. It involves an additional thermodynamic field conjugate to the linear extension of the gas along the direction of the dipoles. The associated uniaxial pressure shows up as a deviation from the Gibbs–Duhem relation in the density profile of a trapped gas. It has to vanish in self-bound droplets, a condition which determines the observed dependence of the aspect ratio on particle number. A tensorial generalization of the virial theorem and a number of further exact thermodynamic relations are derived. Finally, extending a model due to Nozières, a simple criterion for the freezing transition to a superfluid mass density wave is given.

Résumé. Nous donnons une description thermodynamique des gaz froids en interaction dipolaire qui tient compte de la longue portée de ces interactions et de leur absence d'invariance par rotation. Elle fait intervenir un champ thermodynamique supplémentaire conjugué à l'extension linéaire du gaz selon la direction des dipôles. La pression uniaxiale associée se manifeste par un écart à la relation de Gibbs–Duhem dans le profil de densité du gaz piégé. Elle doit s'annuler dans les gouttelettes (des états liés du système), une condition qui détermine la dépendance observée du rapport d'aspect avec le nombre de particules. Une généralisation tensorielle du théorème du viriel et un certain nombre d'autres relations thermodynamiques exactes sont obtenues. Enfin, en étendant un modèle dû à Nozières, on aboutit à un critère simple pour la transition de solidification vers une onde de densité de masse superfluide.

Keywords. Ultracold atoms, Dipolar fluids, Supersolids, Thermodynamic limit, Long-range interactions.

Mots-clés. Atomes froids, Fluides dipolaires, Supersolides, Limite thermodynamique, Interactions à longue portée.

Manuscript received 15 November 2024, accepted 18 November 2024.

1. Introduction

The realization of a Bose Einstein condensate with Chromium [1] has opened a new field of research in ultracold gases. It allows to explore a wide range of phenomena which are uniquely tied to the long-range and partially attractive nature of dipolar interactions. Following the extension to condensates with Erbium or Dysprosium where the strength of these interactions may exceed the short-range repulsion, the field has grown immensely in recent years. This is based, in particular, on the discovery of self-bound droplets [2] and of supersolid phases [3–5], where superfluidity coexists with broken translation invariance: see [6] for a recent review of magnetic dipolar gases and the Lectures [7, 8] for an introduction to the underlying concepts. On the theory side, a successful qualitative description of the observations is provided by an extended Gross–Pitaevskii equation, where a non-analytic contribution proportional to $|\psi|^5$ is added to the energy functional. As will be discussed below, a proper microscopic derivation of

this procedure in the relevant regime of strong dipolar interactions, where the chemical potential may assume negative values, is lacking. It is therefore of interest to develop a description which only relies on general thermodynamic relations, properly accounting for the long-range and anisotropic nature of the interactions. A step in this direction will be taken in the present contribution for quantum fluids in thermal equilibrium, extending concepts from classical polar fluids [9] and liquid crystals [10]. In particular, it is shown that the anisotropy and long-range nature of the interactions require the introduction of an additional contribution $h_1 dL_z$ in the differential of the free energy, with L_z the system length along the direction of the dipoles. It gives rise to the shape-dependence of thermodynamic properties and an anisotropy in the momentum current tensor $\underline{\Pi}(x)$ and thus effectively to pressure. The appearance of an additional extensive variable L_z in the free energy $F(T,V,L_z,N)$ beyond particle number and volume leads to a violation of the Gibbs–Duhem relation which is reflected in the density profile of harmonically trapped gases. Moreover, for the case of self-bound droplets where the internal forces have to balance locally, the vanishing of the uniaxial contribution implies a scale-dependent aspect ratio $\kappa(N) \sim N^{-1/4}$, approaching zero in the thermodynamic limit where the droplets evolve into a needle-like shape. Finally, we address the nature of the transition from a homogeneous superfluid to a supersolid and discuss a simple model due to Nozières [11] which provides a criterion for the associated critical value of the roton gap beyond mean-field.

In general, the aim of the present contribution is to clarify a number of conceptual points in the theory of dipolar gases, thus providing a better understanding of some fundamental issues and open problems.

2. Thermodynamics of uniaxial quantum fluids

In close analogy to the standard description of classical polar fluids [9], the two-body interaction

$$V(x_{12}) = V_{\rm sr}(r_{12}) - \frac{\mu_m^2}{4\pi}\frac{2P_2(\hat{z}\cdot\hat{x}_{12})}{r_{12}^3}\cdot\chi(r_{12}) \tag{1}$$

in Bose quantum fluids whose permanent dipoles μ_m are all oriented along the z-direction may be separated into a rotation invariant short-range plus the long-range, anisotropic dipolar contribution (we use magnetic dipoles in the following and units where $\mu_0 \equiv 1$ but our results also hold for electric ones with minor changes). Here, $P_2(x) = (3x^2-1)/2$ is the standard Legendre polynomial and $\hat{z}$, $\hat{x}_{12}$ are unit vectors along, respectively, the dipole orientation or the separation vector $x_{12} = x_1 - x_2$. In the ultracold limit, the two-body scattering amplitude associated with $V_{\rm sr}(r_{12})$ only involves s-wave scattering and thus is fully characterized by the scattering length a, which is assumed to be positive. The short-range interaction can therefore be replaced by a zero-range pseudopotential with strength parameter $g = 4\pi\hbar^2 a/m$. A similar simplification is possible for the dipolar interaction, whose strength defines an additional effective length $a_{\rm dd} > 0$ by $g_{\rm dd} = \mu_m^2/3 = 4\pi\hbar^2 a_{\rm dd}/m$. Indeed, dipolar scattering at low energies arises from large separations, where $V_{\rm dd}(x_{12}) \sim \mu_m^2/r_{12}^3$ is weak. Asymptotically, the two-body scattering amplitude

$$f_{\rm dd}(\hat{k}_i \to \hat{k}_f, |k|) \xrightarrow[|k|a_{\rm dd}\ll 1]{} f_{\rm dd}^{(B)}(\hat{k}_i \to \hat{k}_f) = -a_{\rm dd}\cdot 2P_2(\hat{z}\cdot\hat{q}) \quad \text{for } |q| = 2|k|\sin(\theta/2) \neq 0 \tag{2}$$

is therefore given by the Born approximation, proportional to the Fourier transform $V_{\rm dd}(q) = g_{\rm dd}\, 2P_2(\hat{z}\cdot\hat{q})$ of the bare dipolar interaction at the momentum transfer wave vector $q = k_f - k_i$. Note that $V_{\rm dd}(q)$ is independent of $|q|$ only for $|q|r_0 \ll 1$, where the short distance cutoff function $\chi(r)$ in Equation (1) may be replaced by unity and also that the forward scattering limit $\theta = 0$ is ill-defined. Moreover, since $V_{\rm dd}(x_{12})$ is not rotationally symmetric, the scattering amplitude cannot be decomposed into separate angular momenta and also depends on the initial direction $\hat{k}_i$ [1].

[1] A discussion of how this affects rethermalization in dipolar gases has been given by Bohn and Jin [12].

The validity of the result (2) has been tested by Bohn et al. [13] based on a numerical solution of the full dipolar two-body scattering problem. Using a pure power law dependence of $V_{\rm dd}(x_{12})$ with a sharp cutoff at a distance $r_0 \ll a_{\rm dd}$, the cross section $\bar{\sigma}(|k|)$ averaged over all incident directions $\hat{k}_i$ is found to essentially coincide with the Born approximation value obtained for $|k|a_{\rm dd} \to 0$ up to energies of order $\hbar^2/(m a_{\rm dd}^2)$. For typical values $a_{\rm dd} \approx a \simeq 100\, a_0$, dipolar scattering in ultracold gases is therefore fully described in terms of a single parameter $a_{\rm dd}$ and deviations of the actual dipolar interaction from a pure power law at short distances $r_{12} < r_0$ are not relevant. This standard assumption, where point-like dipoles are combinded with a zero-range pseudopotential has to be used with caution, however. Indeed, the cutoff scale r_0 explicitely enters the corrections beyond the Born approximation. Specifically, while both the real and the imaginary part $\mathrm{Im}\, f_{\rm dd}(0) = |k|\sigma_{\rm dd}(\hat{k}_i)/(4\pi) \sim |k| a_{\rm dd}^2$ of the forward scattering amplitude vanish at low energies and are independent of r_0, the real part $\mathrm{Re}\, f_{\rm dd}^{(2B)}(0) \sim a_{\rm dd}^2/r_0$ is finite in second order Born approximation and linearly sensitive to the short distance cutoff. A more serious problem arises at the many-body level where the expectation value of the dipolar interaction

$$\langle \hat{H}_{\rm dd} \rangle = \int_{x_1}\int_{x_2} \left[-\frac{\mu_m^2}{8\pi} \frac{2\, P_2(\hat{z}\cdot\hat{x}_{12})}{r_{12}^3} \right] \rho^{(2)}(x_1, x_2) \quad \text{with } \rho^{(2)}(x_1,x_2) = \rho^{(1)}(x_1)\rho^{(1)}(x_2)\cdot g^{(2)}(x_1,x_2) \quad (3)$$

depends on the exact two-particle density $\rho^{(2)}(x_1, x_2)$. It thus requires knowledge not only of the one-particle density $\rho^{(1)}(x)$ of the atomic cloud but also of the associated two-particle distribution function $g^{(2)}(x_1, x_2)$ (we consider a general inhomogeneous situation, following the notation for classical fluids in [9]). Expressed in terms of center-of-mass and relative coordinates X and x_{12}, the integral in (3) is well defined despite the short-distance singularity $1/r_{12}^3$ provided $\rho^{(2)}(X, x_{12})$ is regular in the limit $x_{12} \to 0$ (for a mathematically precise statement see e.g. [14]). The disappearance of the singularity due to the vanishing angular average of $P_2(\hat{z}\cdot\hat{x}_{12})$ is spoiled, however, if the effective range of $V_{\rm sr}(r_{12})$ is set to zero. Indeed, provided the actual interaction becomes isotropic at short distances, the two-particle density is asymptotically determined by the one obtained from a pseudopotential approach where

$$\rho^{(2)}(X, x_{12}) \xrightarrow[x_{12}\to 0]{} \frac{\mathscr{C}_2(X)}{(4\pi)^2}\left(\frac{1}{r_{12}^2} - \frac{2}{a r_{12}} + \cdots \right) \quad (4)$$

is singular at short distances [15, 16]. Here, $\mathscr{C}_2(X) \to [4\pi\rho^{(1)}(X)a]^2$ is the Tan contact density in the weak interaction limit, which replaces the ill-defined local pair distribution function $g^{(2)}(0)$ for zero-range interactions (see [7] for an introduction to the Tan relations and the associated singular behavior of short distance correlations for Bosons). In practice, this problem—which does not show up at the mean-field level where $g^{(2)}(x_1, x_2) \to 1$ is replaced by one—is avoided if the expectation value of the dipolar interaction energy is evaluated with a two-particle density $\rho^{(2)}(X, x_{12})$ which is averaged over separations large compared to the actual interaction range. In particular, for $r_{12} \gg a$, the most singular term in Equation (4) is negligible and the next-to-leading term only gives rise to a small correction $\delta\rho^{(2)}(X, x_{12}) = -[\rho^{(1)}(X)]^2\, 2a/r_{12}$ to the mean-field result. As will be shown below, a cutoff at short distances is also required to properly account for the angular dependence of the pair distribution function.

Beyond the issue of the singularity of the dipolar interaction at short distances for Bosons, which generically have a finite probability to be at the same point in space, a major problem that needs to be addressed in dipolar fluids concerns the long-range and anisotropic, partially attractive nature of the interaction. Indeed, the standard proofs by Ruelle [17] and Fisher [18] on the existence of a proper thermodynamic limit require interactions which decay faster than $1/r^3$ for large distances, leaving dipolar fluids as a marginal case. This problem has been discussed first by Griffiths [19] for dipoles on a lattice and then, more generally, also for continuum fluids

in [20, 21]. What has been shown by these authors is that—in the presence of a stabilizing short distance regularization e.g. via a lattice or a hard-sphere potential—the long-range and partially attractive dipolar interaction gives rise to an extensive free energy $F(T,V,N) = N\cdot\tilde{f}(T,v=V/N)$ with a free energy per particle $\tilde{f}$ which is finite and independent of the boundary conditions provided the expectation value $\mu_m\sum_j\langle\hat{d}_j\rangle \equiv 0$ of the total dipole moment vanishes. The proof thus covers standard polar fluids like water whose electric dipoles point in an arbitrary direction or magnetic systems in the absence of an ordering external field. The situation is fundamentally different, however, for dipolar gases where the dipole directions $\hat{d}_j$ are all identical and their sum $\sum_j \hat{d}_j = N\hat{z}$ is extensive. As a consequence, even if the issue of the existence of a well defined limit $N\to\infty$ is ignored for typical particle numbers $N\simeq 10^4$ [6], standard results like the Gibbs–Duhem relation $\mu = \tilde{f} + pv$ are not expected to hold and, moreover, thermodynamic quantities will become shape-dependent. These points will be addressed in some detail in the following.

2.1. *Magneto-chemical potential and demagnetization tensor*

A well known feature in the thermodynamics of particles with charge q is that the full chemical potential $\mu(x)+q\phi(x)$ whose gradient determines the current in an inhomogenous situation contains the interaction energy with the local electrostatic potential $\phi(x)$ in addition to the contribution $\mu(x)$ associated with other interactions. In a completely analogous manner, for particles with permanent magnetic dipole moments pointing along $\hat{z}$, the relevant magneto-chemical potential contains a contribution $\mu_m B_z(x)$, where $B_z(x)$ is the exact magnetic field at the position of the particle. In a formal manner, this can be derived by noting that the local chemical potential

$$\mu(x) = \frac{\delta F[\rho^{(1)}]}{\delta\rho^{(1)}(x)} = \mu_{\rm sr}(x) - \mu_m B_z(x) \quad \text{with } -\mu_m B_z(x) = \int_{x'} V_{\rm dd}(x-x')\,\rho^{(1)}(x')g^{(2)}(x,x') \qquad (5)$$

is obtained by a functional derivative of the free energy (or simply $\langle\hat{H}\rangle$ at $T=0$) with respect to the one-particle density [9]. Here, the explicit expression for the exact local magnetic field due to all other dipoles follows from differentiation of the associated interaction energy (3) while the contribution $\mu_{\rm sr}(x)$ arises from the short-range interactions, including the change in kinetic energy due to $\hat{H}_{\rm dd}$. As a consequence of the long-range nature of the dipolar interaction, $\mu(x)$ is not—as usual—fully determined by temperature and the local one-particle density $\rho^{(1)}(x)$ but depends on the overall shape of the sample. This is evident already at the mean-field level $g^{(2)}_{\rm mf}\equiv 1$ where the calculation of $B_z(x)$ reduces to a problem in classical magnetostatics with given magnetization $\mathbf{M}(x) = \mu_m\rho^{(1)}(x)\hat{z}$. The appearance of shape-dependent thermodynamics is well known in this context and it is a standard textbook problem to show e.g. that the internal magnetic field in a sphere with constant magnetization is $\mathbf{B}_{\rm in} = (2/3)\mathbf{M}$ [22]. An exact solution is available also for more general geometries provided the magnetization current density $\mathbf{j}_M(x) = \mathrm{rot}\,\mathbf{M}(x)$ may be approximated by a pure surface current. This applies naturally in solid ferromagnets with a sharp boundary and it carries over to the inner region of trapped or self-bound dipolar gases where the spatial dependence of $\mathbf{M}(x)$ is negligible. The relevant demagnetization field $\mathbf{H} = -\underline{\mathbf{N}}\mathbf{M}$ in $\mathbf{B} = \mathbf{H}+\mathbf{M}$ is then determined by a shape-dependent demagnetization tensor $\underline{\mathbf{N}}$ which obeys $\mathrm{Tr}\,\underline{\mathbf{N}} = 1$ [23]. Specifically, for a spheroid with aspect ratio $\kappa = R_x/R_z$ and $\mathbf{M}$ pointing along the z-axis, the tensor $\underline{\mathbf{N}}$ is diagonal. Symmetry fixes the relevant eigenvalue $n^{(z)}$ to be equal to $1/3$ in the case of a sphere while $n^{(z)}$ approaches zero for a long cylindrical spheroid with $\kappa\to 0$, where the demagnetization effect is negligible. Now, there is a subtle point which needs to be taken into account in an application of these results to the interaction induced field $B_z(x)$ that enters the local chemical potential (5). This has to do with the fact that the contribution $(2/3)\mathbf{M}$ to the inner field of a spherical configuration comes entirely from the singular self-interaction term due to an effective delta function in the magnetic field of a point dipole [22]. In contrast to the corresponding

zero-range contribution to the interaction between an electron and a nuclear magnetic moment which is the origin of hyperfine shifts in s-states [24], it is physically reasonable to assume that there is no direct overlap between the partially filled electronic shells in rare-earth atoms. The effective delta function contribution must therefore be subtracted, which leads to $\mathbf{B}_{\rm dd} = \mathbf{H} + \mathbf{M}/3$ for the inner field due to the dipolar interaction. Using $\mu_m^2 = 3g_{\rm dd}$, the resulting contribution to the chemical potential at the mean-field level

$$\mu_m B_z^{(\rm mf)}(x) = g_{\rm dd}(1-3\,n^{(z)})\rho^{(1)}(x) = g_{\rm dd}\, f(\kappa)\rho^{(1)}(x) \tag{6}$$

displays a simple shape-dependence via the demagnetization tensor element $n^{(z)}$. The explicit result for $n^{(z)}$ is derived e.g. in [23] in the context of the equivalent problem of depolarization fields of perfect conductors. For an oblate spheroid with excentricity $e = \sqrt{\kappa^2 - 1}$ it is given by

$$n^{(z)}(e) = (1+e^2)\,\frac{e - \arctan(e)}{e^3} \to (1-\tilde{e}^2)\,\frac{\operatorname{artanh}(\tilde{e}) - \tilde{e}}{\tilde{e}^3} = n^{(z)}(\tilde{e}) \in (0, 1/3] \tag{7}$$

which also determines the demagnetization factor $n^{(z)}(\tilde{e})$ in a prolate situation with excentricity $\tilde{e} = \sqrt{1-\kappa^2}$ by straightforward analytic continuation $e \to i\tilde{e}$. The expression (6) reproduces a result that has been derived early on in the field, based on a Gaussian Ansatz for the density profile of a dipolar gas in a harmonic trap [25, 26]. It has been shown to hold also in the exact solution of the Gross–Pitaevskii equation in the Thomas–Fermi limit [27] but—somewhat surprisingly—the simple connection $f(\kappa) = 1 - 3n^{(z)}$ of the shape function $f(\kappa)$ with the standard demagnetization tensor of magnetostatics does not seem to have been realized in the literature so far. Note that due to $n^{(z)}(\tilde{e}) < 1/3$ in a prolate configuration $\kappa < 1$, the internal magnetic field $B_z(x)$ in the bulk of the atomic cloud is pointing along the positive z-direction. This leads to a lowering of the chemical potential with respect to the value $\mu_{\rm sr}(x)$ determined by the short-range interactions, reflecting the dominance of attractively interacting dipoles in such a configuration.

An obvious question is to which extent corrections beyond mean-field which are contained in the deviation of the pair distribution function $g^{(2)}(x, x')$ in Equation (5) from the trivial limit one, do affect the result (6). It turns out that there is indeed an important qualitative change which arises from the anisotropy of the dipolar interaction. For a rotation invariant $V_{\rm sr}(r_{12})$, the two-particle density $\rho^{(2)}(X, x_{12})$ only depends on the magnitude $r_{12} = |x_{12}|$ of the separation vector. This is no longer true for anisotropic interactions, where also the orientation of x_{12} with respect to the dipole direction enters. The associated physics has been described in quantitative terms in a landmark paper by Wertheim on a classical fluid of hard spheres with point dipoles whose directions $\hat{d}_j$ fluctuate statistically [28]. Following his notation[2], the pair correlation function of a homogeneous dipolar fluid with rotation invariance around the z-axis can be decomposed in the form

$$h^{(2)}(x_{12}) = g^{(2)}(x_{12}) - 1 = h_S(r_{12}) + h_D(r_{12}) \cdot 2P_2(\hat{z}\cdot\hat{x}_{12}) + \cdots . \tag{8}$$

Here, the dots indicate terms involving Legendre polynomials of higher order which are neglected since their contribution to $\mu_m B_x(x)$ contains angular integrals $\int_\Omega P_2\, P_l$ which tend to cancel (only even l appear as long as $z \to -z$ is a symmetry). The two scalar functions $h_S(r_{12})$ and $h_D(r_{12})$ describe quite different physics and turn out to have opposite sign. Specifically, $h_S(r_{12}) < 0$ accounts for an effective short-range repulsion, reducing the probability to find two particles at separation r_{12} below that of an uncorrelated state. In turn, at fixed r_{12}, a positive $h_D(r_{12}) > 0$ favors attractive head-to-tail configurations with $(\hat{z}\cdot\hat{x}_{12})^2 > 1/3$. In explicit form, the different behavior of separation and angular orientation correlations with respect to the z-axis may be derived for a uniform Bose gas in the limit of weak dipolar interactions $\varepsilon_{\rm dd} = a_{\rm dd}/a \ll 1$ by

[2] In [28], an additional contribution $h_\Delta(r_{12})\hat{d}_1\cdot\hat{d}_2$ appears which couples to the relative orientation of the dipoles. In the present case with $\hat{d}_1\cdot\hat{d}_2 \equiv 1$, this contribution can be incorporated into the rotation invariant function $h_S(r_{12})$.

expanding the static structure factor within the Bogoliubov approximation in the regime of small momenta

$$S(q) = 1 + nh^{(2)}(q) \xrightarrow[\text{Bog.}]{} [1 + 2nV(q)/\varepsilon_q]^{-1/2} \xrightarrow[|q|\xi,\varepsilon_{\rm dd}\ll 1]{} \frac{|q|\xi}{\sqrt{2}}[1 - \varepsilon_{\rm dd} P_2(\hat{z}\cdot\hat{q}) + \cdots]. \tag{9}$$

Here, $V(q) = g + V_{\rm dd}(q)$ is the Fourier transform of the interaction, $\xi = 1/\sqrt{8\pi n a}$ the healing length associated with its short-range part and $\varepsilon_q = \hbar^2 q^2/(2m)$ the free particle dispersion. The expansion (9) of the static structure factor at low momenta precisely matches the corresponding one in real space of Equation (8). Moreover, the non-analytic behavior in q implies that the associated pair correlation functions $nh_S(r) \to -\xi/(\sqrt{2}\pi^2 r^4)$ and $nh_D(r) \to +\varepsilon_{\rm dd}\cdot\sqrt{2}\xi/(\pi^2 r^4)$ follow a power law decay at $T = 0$ and have opposite sign. A further point which distinguishes the correlations of the magnitude of separation vectors from those which describe their orientation with respect to the dipole direction shows up at finite temperature: while $h_S(r)$ decays to zero exponentially beyond the thermal wavelength λ_T, the angle dependent contribution

$$h_D(r)|_{T\neq 0} \to h_\infty/r^3 \quad \text{with } nh_\infty = \frac{3}{4\pi}\frac{(\varepsilon(0)-1)^2}{\varepsilon(0)}\frac{k_{\rm B}T}{g_{\rm dd}n} \tag{10}$$

retains a power law decay, following that of the dipolar interaction. The asymptotic behavior (10) is an exact result first derived by Wertheim [28] for classical fluids with randomly oriented electric dipoles and $\varepsilon(0)$ the associated static dielectric constant. It is consistent with a correlation inequality at finite temperature which implies that correlations cannot decay faster than the interactions. Using the connection $S(q) \to k_{\rm B}T/mc^2(\hat{q})$ between the static structure factor at low momenta and the angle dependent sound velocity $c(\hat{q})$ of dipolar gases [29], it is straightforward to show that—to linear order in $\varepsilon(0) - 1 \to \varepsilon_{\rm dd} \ll 1$, where the homogeneous system with average density n is stable—the result (10) continues to hold for quantum fluids of magnetic dipoles which are fully polarized.

An important consequence of the results above for the thermodynamics of dipolar gases shows up by considering nearly spherical configurations, where mean-field predicts that the dipolar interactions average to zero. Obviously, this result remains valid more generally for an arbitrary pair correlation function which is rotation invariant. Including the angular dependent contribution $h_D(r) \neq 0$, however, there is a non-vanishing magnetic field

$$\mu_m B_z(x)\big|_{\kappa=1} = (12/5) g_{\rm dd}\, \rho^{(1)}(x)\cdot K \quad \text{with } K = \int_0^\infty {\rm d}r\, \frac{h_D(r)}{r} > 0 \tag{11}$$

near the center which points along the positive z-direction. The dimensionless parameter K, which plays a central role in a microscopic theory of the dielectric constant in classical polar fluids[3], apparently requires a cutoff at short distances. As mentioned above, a description of dipolar gases beyond mean-field must therefore take into account the finite range of interactions which, in practice, is of the order of the short-range scattering length a. An experimental estimate of the parameter K may be obtained by observing the finite critical strength $\varepsilon_{\rm dd}^{(c)}(\kappa = 1) = 5/(12\,K)$ of the dipolar interaction where even a spherical cloud becomes unstable because the chemical potential $\mu(x) \approx g\rho^{(1)}(x) - \mu_m B_z(x)$ turns negative at leading order.

2.2. *Pressure and uniaxial tension from dilatations*

In the discussion so far, the consequences of the anisotropy and long-range nature of the dipolar interctions have been addressed by assuming a given shape, characterized e.g. by the

[3] Combining point dipoles with hard spheres, the dielectric constant is a function only of the volume fraction $\eta = (\pi/6)n\sigma^3$ and the ratio $y = g_{\rm dd}n/(3k_{\rm B}T)$. Remarkably, this extremely oversimplified model reproduces quite well the observed value $\varepsilon(0) = 78.4$ for water under normal conditions, where $\eta \simeq 0.42$ and $y \simeq 3.35$, see Figure 11.5 in [9].

aspect ratio κ. In reality, the specific shape of the atomic cloud is not an independent variable but is determined by the interaction strength and the external confinement, if present. In thermal equilibrium, it follows from the balance of forces which—in quite general form—may be expressed in terms of the associated momentum current tensor $\underline{\Pi}(x)$ by

$$\nabla \underline{\Pi}(x) \xrightarrow[\text{equ.}]{} \begin{pmatrix} \partial_x \Pi^{xx} \\ \partial_y \Pi^{yy} \\ \partial_z \Pi^{zz} \end{pmatrix} = \begin{cases} 0 & \text{self-bound} \\ -\rho_\phi^{(1)}(x)\, \mathrm{grad}\, \phi(x) & \text{trapped.} \end{cases} \tag{12}$$

Here, $\phi(x)$ is the external trap potential and $\rho_\phi^{(1)}(x)$ the resulting equilibrium value of the inhomogeneous one-particle density. Moreover, we have used the fact that in thermal equilibrium the tensor $\underline{\Pi}(x)$ has no off-diagonal elements as would appear e.g. in the presence of a finite Hall viscosity. Now, for rotation invariant interactions, all diagonal elements of $\underline{\Pi}(x)$ are equal and they define a local pressure $p(x)$. The left hand side of Equation (12) is then just the gradient of pressure in a standard hydrostatic equilibrium. For a harmonic confinement, where the external contribution to the total Hamiltonian

$$\hat{H}_\omega = \hat{H} + \frac{1}{2} \mathrm{Tr}\, (\underline{\omega}^2\, \underline{\hat{\theta}}) \quad \text{with } (\underline{\hat{\theta}})^{ij} = \int_x x^i x^j \hat{\rho}(x) \tag{13}$$

can be expressed in terms of a tensor $\underline{\omega}^2$ of the trap frequencies and the inertia tensor $\underline{\hat{\theta}}$ defined via the mass density operator $\hat{\rho}(x)$, the resulting cloud shape follows from the exact relation

$$\langle \underline{\hat{\theta}} \rangle_{\mathrm{eq}} = (\underline{\omega}^2)^{-1} \int_x p(x) = E_{\mathrm{rel}}\, (\underline{\omega}^2)^{-1} \quad \text{for rotation invariant } V(x_{12}) = V(r_{12}) \tag{14}$$

obtained by taking the scalar product of Equation (12) with $\mathbf{x}$ and integrating over all space. Note that the relation (14) provides only an implicit result for the cloud shape as characterized by its inertia tensor since the release energy $E_{\mathrm{rel}} = \int_x p(x)$ is itself shape-dependent. An exact consequence of Equation (14), however, is that the aspect ratio which—irrespective of the detailed density profile—is defined by $\kappa = [\theta^{xx}/\theta^{zz}]^{1/2}$ coincides with the ratio $\lambda = \omega_z/\omega_x$ of the trap frequencies (we assume $\omega_x = \omega_y \neq \omega_z$ in general, i.e. there is rotation invariance around the z-axis).

The anisotropy of the dipolar interaction invalidates the simple relation (14) and leads to shapes with $\kappa < \lambda$ which are elongated along the z-direction since the energy is lowered if the dipoles tend to arrange in a head-to-tail configuration. Dipolar gases are thus uniaxial quantum fluids which—in quite general terms—may be defined by $\Pi^{xx} = \Pi^{yy} \neq \Pi^{zz}$ in equilibrium. To characterize their size and shape one needs two instead of just a single scalar function. Specifically, we will use $\mathrm{Tr}\, \underline{\Pi}$ and the anisotropy $h = \Pi^{xx} - \Pi^{zz}$, which acts like a uniaxial tension tending to stretch the system along z. As will be discussed below, the system length L_z will then appear as an additional thermodynamic variable which is conjugate to the field h. On a microscopic level, an explicit expression for both $\mathrm{Tr}\, \underline{\Pi}(x)$ and $h(x)$ may be derived by extending the results of Martin and Schwinger [30] for the momentum current tensor in a non-relativistic quantum many-body problem with rotation invariant interactions. Quite generally, pressure—as the field conjugate to a local expansion—is defined by the change in energy density under a uniform isotropic dilatation $x \to bx$ with scale factor $b \to 1$. This only fixes $\mathrm{Tr}\, \underline{\Pi}(x)$, however. In order to specify the two independent components Π^{xx} and Π^{zz} it is necessary to consider, in addition, the volume preserving dilatation $x \to \theta[x]$ where the components $z \to \theta z$ and $(x, y) \to (x, y)/\sqrt{\theta}$ are scaled differently. The full momentum current tensor of uniaxial quantum fluids is thus obtained from the microscopic Hamiltonian density $\hat{\mathscr{H}}(x)$ in $\hat{H} = \int_x \hat{\mathscr{H}}(x)$ by evaluating the response to the two independent dilatations (note the different signs)

$$\mathrm{Tr}\, \underline{\Pi}(x) = 2\Pi^{xx}(x) + \Pi^{zz}(x) = -\left.\frac{\partial \langle \hat{\mathscr{H}}(bx) \rangle_{\mathrm{eq}}}{\partial b}\right|_{b=1} \quad \text{and} \quad h(x) = \left.\frac{\partial \langle \hat{\mathscr{H}}(\theta[x]) \rangle_{\mathrm{eq}}}{\partial \theta}\right|_{\theta=1}. \tag{15}$$

In explicit form, the anomalous field $h(x)$ receives contributions only from the kinetic energy and the dipolar interaction. They can be expressed in terms of the field operators $\hat{\psi}$ as

$$h(x) = \frac{\hbar^2}{m}\left[\frac{1}{2}\langle\nabla_\perp\hat{\psi}^\dagger\cdot\nabla_\perp\hat{\psi}\rangle_{\rm eq}(x) - \langle\partial_z\hat{\psi}^\dagger\partial_z\hat{\psi}\rangle_{\rm eq}(x)\right] + \partial_\theta\mathscr{D}(\theta[x])|_{\theta=1}\,. \tag{16}$$

Here, $\nabla_\perp$ denotes the gradient with respect to the radial coordinates (x,y) and $\mathscr{D}(x)$ is a dipolar analog of the contact density $\mathscr{C}_2(x)$ for zero-range interactions. It is defined by the expectation value of the dipolar interaction energy density

$$\mathscr{D}(x) = \langle\hat{\mathscr{H}}_{\rm dd}(x)\rangle_{\rm eq} = -\tfrac{1}{2}\langle\hat{M}_z(x)\hat{B}_z(x)\rangle_{\rm eq} \tag{17}$$

which involves the product of the operators for the magnetization $\hat{M}_z(x)$ and the field $\hat{B}_z(x)$ from all other dipoles at position x. Due to the long-range nature of the interaction, $\mathscr{D}(x)$ is in fact non-local and shape-dependent, a point which will be discussed further below. This is very different from the energy density $\varepsilon_{\rm sr}(x)$ and the associated contribution [7,31]

$$p_{\rm sr}(x) = \frac{2}{3}\varepsilon_{\rm sr}(x) + \frac{\hbar^2}{24\pi m a}\mathscr{C}_2(x) \underset{\rm mf}{\longrightarrow} \frac{g}{2}[\rho^{(1)}(x)]^2 + \cdots \tag{18}$$

to the pressure arising from short-range interactions which—at the mean-field level—is quadratic in the local one-particle density $\rho^{(1)}(x)$ and independent of the shape. Using the microscopic definition (15), the full momentum current tensor of dipolar gases in turn contains the shape-dependent contributions $\mathscr{D}(x)$ and $\partial_\theta\mathscr{D}(\theta[x])|_{\theta=1}$ according to

$$\Pi^{xx}(x) = p_{\rm sr}(x) + \mathscr{D}(x) + \tfrac{1}{3}h(x). \tag{19}$$

The formal relations above turn out to lead to observable and intuitively plausible consequences for the density profile of harmonically trapped dipolar gases. In a situation with $\omega_x = \omega_y$, where one has rotation invariance around the z-axis, a radial integration of the (x,y)-components of the equilibrium condition (12) shows that the integrated column density

$$\tilde{n}_\phi(z) = \int {\rm d}x\,{\rm d}y\,\rho^{(1)}_\phi(x,y,z) = \frac{2\pi}{m\omega_x^2}\,\Pi^{xx}(0,0,z) \tag{20}$$

at a given z is a direct measure of the xx-component of the momentum current tensor along the center of the atomic cloud. This relation is equivalent to one derived by Ho and Zhou for rotation invariant interactions in the context of imbalanced Fermi gases [32]. A different result appears, however, for the z-derivative of the density profile which follows from the third component of the momentum balance (12). The fact that Π^{xx} and Π^{zz} no longer coincide in the uniaxial case leads to a violation of the Gibbs–Duhem relation which shows up as a non-vanishing contribution on the right-hand side of the equation

$$\frac{{\rm d}\tilde{n}_\phi(z)}{{\rm d}z} + 2\pi\frac{\omega_z^2}{\omega_x^2}\,z\,\rho^{(1)}_\phi(0,0,z) = \frac{2\pi}{m\omega_x^2}\,\partial_z h(0,0,z) > 0. \tag{21}$$

Since the anomalous field $h(x)$ is negative and decays along the z-direction away from the center, the profile $\tilde{n}_\phi(z)$ falls off more slowly than what is expected for rotation invariant interactions. The uniaxial nature of dipolar gases and the associated field $h(x)$ can thus be inferred directly from in-situ density profiles.

2.3. *Thermodynamic relations and the tensor virial theorem*

The appearance of a finite uniaxial tension in dipolar gases leads to a fundamental change in thermodynamic relations. This turns out to provide an understanding of the shape-dependence mentioned above and also the peculiar form of self-bound droplets that will be discussed in the following subsection. In order to derive the extension to uniaxial fluids of the standard relation ${\rm d}F = -p\,{\rm d}V$ for the change in free energy associated with a shape deformation at a fixed value of

temperature and particle number it is convenient to introduce a local deformation tensor $\underline{u}(x)$ as in solids. Quite generally, $\underline{u}(x)$ is the conjugate field to the momentum current (or stress) tensor $\underline{\Pi}(x)$ [10] which, by the definition of an uniaxial fluid in thermal equilibrium, is diagonal with just two independent components. As a consequence, the associated differential of the free energy

$$\mathrm{d}F[\mathrm{Tr}\,\underline{u}, u_{zz}]\big|_{T,N} = -\int_x \mathrm{Tr}\,[\underline{\Pi}(x)\,\mathrm{d}\underline{u}(x)] \xrightarrow[\text{fluid}]{} \int_x [-\Pi^{xx}(x)\,\mathrm{d}\,\mathrm{Tr}\,\underline{u}(x) + h(x)\,\mathrm{d}u_{zz}(x)] \tag{22}$$

depends on the two dimensionless variables $\mathrm{Tr}\,\underline{u}$ and u_{zz}. In physical terms, they describe a local change $\mathrm{d}\,\mathrm{Tr}\,\underline{u}(x) = \mathrm{d}v(x)/v$ in volume per particle at a fixed extension along the z-direction or a change of length $\mathrm{d}u_{zz} = \mathrm{d}L_z/L_z$ at fixed volume[4]. The relation (22) shows that for a uniaxial fluid $\Pi^{xx} \to p$ can be identified with the pressure as the variable conjugate to volume at fixed length. In addition, the anomalous field $h(x)$ gives rise to a line tension contribution in the Gibbs relation

$$\mathrm{d}F(T,V,L_z,N) = -S\,\mathrm{d}T - p\,\mathrm{d}V + h_1\,\mathrm{d}L_z + \mu\,\mathrm{d}N \quad \text{with } h_1 L_z = \int_x h(x), \tag{23}$$

favoring an increase of length L_z at given volume to lower the free energy ($h_1 < 0$). As will be shown below, the fact that L_z appears as an additional extensive thermodynamic variable leads to a violation of the Gibbs–Duhem relation. Typically, such violations become negligible in the thermodynamic limit, which holds e.g. for a finite surface tension σ in a self-bound liquid state described by $\mathrm{d}F = \sigma\,\mathrm{d}A$ at fixed T,N,V. For short-range interactions, this contribution scales with the surface area $A \sim N^{2/3}$ and thus eventually becomes subdominant compared with the extensive terms. The situation is different here, however, due to the long-range nature of the dipolar interaction. Indeed, since the interaction contribution $\partial_\theta \mathscr{D}(\theta[x])\,|_{\theta=1}$ in Equation (16) to the underlying variable $h(x)$ is intensive, $\mathrm{d}F = h_1\,\mathrm{d}L_z \sim N$ remains extensive for an arbitrary large system. In physical terms, this can be understood from the fact that the dipolar contact density $\mathscr{D}(x)$ in Equation (17) arises from the magnetic field which, as discussed in Section 2.1, is effectively generated by surface currents. The demagnetization field $\mathbf{H}(x) = -\mathrm{grad}\,\phi_M(x)$ is thus non-local, arising from magnetic surface "charges" with density $\sigma_M = \mathbf{n}\cdot\mathbf{M}$ ($\mathbf{n}$ is the unit normal vector) [22]. As emphasized in [21], the $1/r^2$ decay of the field is precisely cancelled by the increase $\sim r^2$ of the surface area. Both the magnetic field and the associated energy density $\mathscr{D}(x) = \langle \hat{\mathscr{H}}_{\mathrm{dd}}(x)\rangle_{\mathrm{eq}}$ are therefore independent of the system size.

The extended Gibbs relation (23) implies that—at fixed temperature T—the pressure and chemical potential involve the strain tensor element u_{zz} as a further thermodynamic variable beyond the volume per particle v. The associated dependence is determined by the Maxwell relations

$$v\frac{\partial p}{\partial v} = \frac{\partial \mu}{\partial v} \quad \text{at fixed } u_{zz}, \quad \frac{\partial \mu}{\partial u_{zz}} = \frac{\partial h}{\partial (1/v)} \quad \text{and} \quad \frac{\partial p}{\partial u_{zz}} = v\frac{\partial h}{\partial v}. \tag{24}$$

In an inhomogeneous situation, where the density $\rho^{(1)}(x)$ and the field $h(x)$ are spatially varying, the standard Gibbs–Duhem relation $\mathrm{d}\mu|_T = v\,\mathrm{d}p|_T$ is therefore violated. This leads to an anomalous contribution to the axial derivative of the density profile of a harmonically trapped dipolar gas derived in Equation (21). A further consequence of the dependence of pressure $p(v,u_{zz},T)$ on the uniaxial strain u_{zz} is the angular dependence of the sound velocity in a uniform dipolar gas. In quite general terms, the difference $\Delta f = f - f_{\mathrm{eq}}$ in the free energy density with respect its value f_{eq} in a homogeneous situation with vanishing deformations $(\mathrm{Tr}\,\underline{u})_{\mathrm{eq}} = (u_{zz})_{\mathrm{eq}} \equiv 0$ can be written in the form of an elastic free energy of a uniaxial solid [10]

$$\Delta f[\mathrm{Tr}\,\underline{u}, u_{zz}] = \frac{1}{2}(u_{xx}+u_{yy}, u_{zz}) \begin{pmatrix} K_{11} & K_{13} \\ K_{13} & K_{33} \end{pmatrix} \begin{pmatrix} u_{xx}+u_{yy} \\ u_{zz} \end{pmatrix} = \frac{K_{11}}{2}[\mathrm{Tr}\,\underline{u} + \tilde{\gamma} u_{zz}]^2 + \frac{\tilde{B}}{2}u_{zz}^2 \tag{25}$$

[4] While a cloud of atoms has no sharp boundary beyond the Thomas–Fermi limit where the kinetic energy is negligible, the associated Thomas–Fermi radius R_z still provides an appropriate measure for the length $L_z \to 2R_z$.

which is rotation invariant in the x,y-plane. The condition that Equation (25) describes a fluid rather than a solid requires that the associated tensor of elastic constants has vanishing determinant $\tilde{B}K_{11} = K_{33}K_{11} - K_{13}^2 = 0$. The last term is then absent and there is only a single sound mode[5]. Its velocity depends on the direction with respect to the orientation of the dipoles according to $\bar{\rho}c^2(\hat{q}) = K_{11} + (K_{33} - K_{11})\cdot(\hat{z}\cdot\hat{q})^2$ [10,33]. This angular dependence is a result of the coupling between density and strain described by the dimensionless parameter $\tilde{\gamma}$ in

$$h = \left.\frac{\partial f}{\partial u_{zz}}\right|_{\mathrm{Tr}\,\underline{u}} \to \tilde{\gamma}K_{11}(\mathrm{Tr}\,\underline{u} + \tilde{\gamma}u_{zz}) \quad \text{with } \tilde{\gamma} = \frac{K_{13}}{K_{11}} - 1 \underset{\text{mf}}{\longrightarrow} \left(\frac{1+2\varepsilon_{\text{dd}}}{1-\varepsilon_{\text{dd}}}\right)^{1/2} - 1. \tag{26}$$

A physical understanding of this coupling is provided by the observation that—according to Equation (25)—the energy cost for a compression $\mathrm{Tr}\,\underline{u} < 0$ of a uniform dipolar gas can be exactly compensated by an expansion along z with $u_{zz} = -\mathrm{Tr}\,\underline{u}/\tilde{\gamma} > 0$. The mean-field result for $\tilde{\gamma}$ in terms of the dimensionless strength ε_{dd} of the dipolar interaction follows from the angular dependence $V(q) = g[1 + \varepsilon_{\text{dd}}\cdot 2P_2(\hat{z}\cdot\hat{q})]$ of the two-body interaction. It indicates that the uniform gas with a homogeneous mass density $\bar{\rho}$ is stable only as long as $\varepsilon_{\text{dd}} < 1$, a point which will be discussed in detail in the following subsection.

An exact relation that holds for many-body problems in both classical and quantum physics is the virial theorem. It is a scalar identity which follows by considering the change in energy under a uniform dilatation of the coordinates $(x_1 \ldots x_N) \to (bx_1 \ldots bx_N)$ [37]. Now, as discussed in Equation (15) above, uniform dilatations are not sufficient to characterize the thermodynamically relevant set of shape deformations in the case of interactions which are not invariant under rotation. To deal with this more general situation, it is necessary to extend the virial theorem to a tensorial form, as was first derived by Parker [38] for a classical system of point particles in an astrophysical context. The extension to the quantum many-body problem is straightforward in principle. Indeed, the virial theorem in its most general form simply states that the expectation value of the commutator

$$\langle i[\hat{H} + \hat{H}_{\text{ex}}, \underline{\hat{D}}]\rangle \equiv 0 \underset{\text{harm.}}{\longrightarrow} \langle i[\hat{H}, \underline{\hat{D}}]\rangle = \langle \underline{\omega}^2\underline{\hat{\theta}}\rangle \quad \text{with } (\underline{\hat{D}})^{ij} = \int_x x^i \hat{g}^j(x)/\hbar \tag{27}$$

of the total Hamiltonian with the dilatation tensor operator $\underline{\hat{D}}$ vanishes in eigenstates of $\hat{H} + \hat{H}_{\text{ex}}$. The dimensionless dilatation tensor involves the components $\hat{g}^j(x)$ of the momentum density operator and generates dilatations along the j-direction proportional to separate components x^i of the coordinates [39]. In the particular case of a harmonic confinement, the contribution of $\hat{H}_{\text{ex}}$ is reduced to the expectation value of the tensor contraction $\underline{\omega}^2\underline{\hat{\theta}}$. Its trace yields twice the trap energy E_{tr} according to Equation (13). For rotation invariant interactions, the equilibrium expectation value $\langle i[\hat{H}, \underline{\hat{D}}]\rangle_{\text{eq}} = \underline{1}\cdot\int_x p(x)$ is proportional to the unit tensor. The tensorial form of the virial theorem then reduces to the standard one obtained from a uniform dilatation $x \to bx$. In particular, the moment of inertia tensor is given by Equation (14). This is violated in the uniaxial situation, where the aspect ratio $\kappa = [\theta^{xx}/\theta^{zz}]^{1/2}$ no longer coincides with the ratio $\lambda = \omega_z/\omega_x$ of external trap frequencies. The difference is determined by the exact relation

$$-\int_x h(x) = \omega_z^2\theta^{zz} - \omega_x^2\theta^{xx} = 2E_{\text{tr}}\cdot\frac{\lambda^2 - \kappa^2}{\lambda^2 + 2\kappa^2} > 0 \tag{28}$$

which follows from the tensor virial theorem (27) in an equilibrium state by considering the volume preserving dilatation $x \to \theta[x]$ introduced in Equation (15). A detailed discussion of

[5] For finite values of the parameter $\tilde{B}$, the free energy (25) describes a smectic-A phase with broken translation invariance along the z-direction [10]. It exhibits two independent sound modes, both in the case of a classical fluid [33] and also—in the quite different form of a wave-like propagation of defects in supersolids predicted by Andreev and Lifshitz [34]—in the superfluid [35]. These two modes have very recently been observed in a 2D smectic phase of a Bose Einstein condensate in the presence of a periodic in time modulation of the scattering length [36], allowing to determine both the superfluid fraction f_s and the effective layer compression modulus $\tilde{B}$ in quantitative terms.

the connection between κ and λ as a function of the dipolar interaction strength $\varepsilon_{\rm dd}$ has been given by Eberlein et al. [27] within the Thomas–Fermi approximation, where the density profile $\rho^{(1)}_{\phi}(x)$ has a sharp boundary. In particular, they have shown that, in the presence of a strong external confinement $\lambda \gg 1$ along the z-direction, a dipolar gas remains stable even in the limit $\varepsilon_{\rm dd} \gg 1$ of negligible short-range repulsion. This has been verified experimentally by Koch et al. [40] for particle numbers $N \simeq 10^4$. Effects beyond mean-field, which are contained in Equation (28), therefore do not give rise to qualitative changes in a tightly confined situation. As will be shown below, the situation is quite different in self-bound droplets whose form is completely determined by such corrections. A second independent relation which follows from the tensorial virial theorem is connected with the uniform dilatation $x \to bx$ generated by the scalar operator $\hat{D} = {\rm Tr}\,\underline{\hat{D}}$. It can be written in terms of the local contact densities $\mathscr{C}_2(x)$ and $\mathscr{D}(x)$ associated with the short-range and dipolar interactions in the form

$$\langle i[\hat{H},\hat{D}]\rangle = \langle \hat{H}\rangle + E_{\rm tr} + \frac{\hbar^2}{16\pi m a}\int_x \mathscr{C}_2(x) + \frac{1}{2}\int_x \mathscr{D}(x) = 2E_{\rm tr}. \tag{29}$$

A similar relation was derived in [41] for dipolar gases in 2D, however there are two important differences: since the dipolar interaction in 2D also leads to s-wave scattering, the two-body contact density $\mathscr{C}_2(x)$ is defined by the adiabatic derivative of the energy with respect to the full scattering length of the combined interaction $V_{\rm sr} + V_{\rm dd}$. As a consequence, the exact expression for the dipolar contact density $\mathscr{D}(x)$ requires a subtraction in the pair distribution function at short distances associated with the contribution of $V_{\rm sr}(r_{12})$ [41]. A second point is that the angular independent dipolar interactions $\sim \mu_m^2/r_{12}^3$ in 2D are effectively of a short-range nature. In contrast to the situation here, the associated contact density $\mathscr{D}(x)$ is then shape-independent.

2.4. *Self-bound droplets and the LHY correction*

One of the major new developments associated with ultracold dipolar gases was the surprising observation of self-bound droplets by Ferrier-Barbut et al. [2]. These droplets are very different from what is expected for droplets of a standard liquid, whose equilibrium configuration is spherical due to the presence of a finite surface tension σ. Indeed, as will be shown below, the combination of anisotropy and the dominantly attractive nature of dipolar interactions in a non-confined situation leads to droplets whose aspect ratio $\kappa(N) \sim N^{-1/4}$ approaches zero for large particle numbers[6].

Based on the quite general hydrostatic equilibirium condition (12), the existence of stable self-bound droplets requires that the divergence $\nabla\underline{\Pi}(x) \equiv 0$ of the momentum current tensor vanishes. In a uniaxial fluid with long-range and angle-dependent attractive interactions, this condition is obeyed only if both ${\rm Tr}\,\underline{\Pi}(x)$ and $h(x)$ are zero. In contrast to the situation in stars, where a single scalar equation for the balance of the radial component of the internal and gravitational pressure is sufficient to determine the equilibrium shape (see e.g. [43] for an instructive discussion), two separate conditions need to be fulfilled here. In order to formulate these in a physically intuitive manner, it is convenient to rewrite the virial theorem (29) in a form where the external trap is eliminated

$$\langle i[\hat{H},\hat{D}]\rangle = \int_x \left[2\,\varepsilon_{\rm sr}(x) + \frac{\hbar^2}{8\pi m a}\mathscr{C}_2(x) + 3\mathscr{D}(x)\right] = 3\int_x [p_{\rm sr}(x) + \mathscr{D}(x)] = \int_x {\rm Tr}\,\underline{\Pi}(x). \tag{30}$$

[6] This scaling law has been seen originally in numerical simulations by Baillie et al. [42] and has recently been derived in analytical form by Dalibard [8], based on a different but physically equivalent line of arguments.

Here, following the Tan pressure relation in Equation (18), we have introduced the local pressure $p_{\rm sr}(x)$ which arises from the short-range interactions[7]. Beyond the associated energy density $\varepsilon_{\rm sr}(x)$, it involves the two-body contact density $\mathscr{C}_2(x)$ which is defined by the adiabatic derivative of $\langle\hat{\mathscr{H}}(x)\rangle_{\rm eq}$ with respect to the inverse scattering length $1/a$ [16,31]. Equation (30) shows that the condition of a vanishing $\mathrm{Tr}\,\underline{\Pi}(x)\equiv 0$ is equivalent to a local pressure balance $p_{\rm sr}(x)+\mathscr{D}(x)=0$, with $\mathscr{D}(x)$ playing the role of the pressure associated with the dipolar interactions. Prior to a detailed discussion of this exact and quite intuitive relation a number of comments should be added:

- The fact that the pressure arising from dipolar interactions is equal to the associated energy density $\mathscr{D}(x)$ is a consequence of the assumption that the interaction $V_{\rm dd}(x_{12})\sim \mu_m^2/r_{12}^3$ follows an inverse cube power law at all distances.
- Despite the formal notation, $\mathscr{D}(x)$ is not a local variable but depends on the overall shape of the droplet, as becomes evident in the mean-field result (31) below.
- The separation of pressure into a short-range and a dipolar contribution follows from the additivity $V=V_{\rm sr}+V_{\rm dd}$ of the interactions in the underlying Hamiltonian. It does not imply that pressure is simply additive, however, which is true only in mean-field. In general, the contributions $p_{\rm sr}(x)$ and $\mathscr{D}(x)$ will depend on both g and $g_{\rm dd}$.
- The identification of $\mathrm{Tr}\,\underline{\Pi}(x)$ with $3\,[p_{\rm sr}(x)+\mathscr{D}(x)]$ on a local level neglects a possible divergence which integrates to zero in the virial equation. Indeed, quite generally, the momentum current tensor is not unique and the equilibirium condition (12) remains unchanged under $(\underline{\Pi})^{ij}\to(\underline{\Pi})^{ij}+(\partial^i\partial^j-\delta^{ij}\nabla^2)\Phi$ with an arbitrary scalar function $\Phi(x)$ which vanishes at infinity [39]. This freedom is removed by the concrete choice (31) below for $\mathscr{D}(x)$ in the central region of the self-bound droplet.

Explicit results for both the dipolar contact density $\mathscr{D}(x)$ and the local anomalous field $h(x)$ are available at the mean-field level. Specifically, we use Equation (16) which connects the interaction contribution to $h(x)$ to the derivative of the dipolar contact density (17) with respect to the parameter θ. Within mean-field, this yields

$$\mathscr{D}^{(\rm mf)}(x)=-\tfrac{1}{2}\langle\hat{M}_z(x)\rangle\,B_z^{(\rm mf)}(x)=-\tfrac{1}{2}g_{\rm dd}\,[\rho^{(1)}(x)]^2 f(\kappa)\to h^{(\rm mf)}(x)=-\tfrac{3}{4}g_{\rm dd}\,[\rho^{(1)}(x)]^2 b(\kappa) \tag{31}$$

where we have used the result (6) for the magnetic field and the fact that the aspect ratio changes according to $\mathrm{d}\kappa=-(3/2)\kappa\,\mathrm{d}\theta$ under $x\to\theta[x]$. The positive function

$$b(\kappa)=-\kappa\frac{\mathrm{d}f(\kappa)}{\mathrm{d}\kappa}\to\begin{cases}6\kappa^2\ln(2/\kappa) & \text{for }\kappa\ll 1\\ 3\pi/(2\kappa) & \text{for }\kappa\gg 1\end{cases} \tag{32}$$

is determined by Equation (7) for the demagnetization tensor element $n^{(z)}$. It decays to zero for both strongly prolate or oblate configurations $\kappa\ll 1$ or $\kappa\gg 1$ and exhibits a broad maximum $b(\kappa=1.563\ldots)=0.852\ldots$ slightly above the value $b(\kappa=1)=4/5$ in the spherical limit. Now, the combination of Equation (31) with the leading order result (18) for the pressure due to short-range interactions shows that the two separate equilibrium conditions $p_{\rm sr}(x)+\mathscr{D}(x)=0$ and $h(x)=0$ for a self-bound droplet cannot be obeyed within mean-field where both $p_{\rm sr}(x)+\mathscr{D}(x)$ and $h(x)$ are negative for $\varepsilon_{\rm dd}f(\kappa)>1$ or arbitrary values of κ, respectively. A resolution of the first problem, already proposed in the original publication on self-bound droplets [2], is provided by adding a contribution to the short-range pressure which scales with a higher power in density than the quadratic behavior stated as the low-density limit of the exact expression in Equation (18). On a purely empirical level, a self-bound liquid can then be stabilized against

[7] In the application of the Tan relations to Bosons, we consistently neglect three-body correlations which are connected with the Efimov effect and the underlying dependence of $\langle\hat{\mathscr{H}}(x)\rangle_{\rm eq}$ on the short-range parameter κ_* [7, 16, 31].

collapse by extending the mean-field effective potential by a local term proportional to $|\psi(x)|^{2k}$ with $k > 2$ in the form

$$V_{\rm eff}[\psi] = -\mu|\psi(x)|^2 + \frac{g}{2}|\psi(x)|^4 + \frac{1}{2}|\psi(x)|^2\int_{x'} V_{\rm dd}(x-x')|\psi(x')|^2 + \frac{\lambda_k}{k}|\psi(x)|^{2k} \quad (?) \qquad (33)$$

where $\lambda_k > 0$ is assumed to be positive. From a microscopic point of view, the true effective potential must, of course, be derived from the underlying Hamiltonian. In fact, due to the anisotropy of the dipolar interaction, the simple form (33) where the stabilizing contribution is rotation invariant, is not expected to be valid. In principle, a microscopic derivation of $V_{\rm eff}[\psi]$ is possible by expressing the exact partition function in terms of a coherent state functional integral [44]. The first three terms in Equation (33) then arise from minimizing the bare associated action. At this mean-field (or tree-) level, only two-body interactions enter. It provides a proper description of the zero density limit near the vacuum state $\psi(x) \equiv 0$, where two-body scattering amplitudes are sufficient to deal with the many-body problem at finite density. For self-bound droplets, which arise from the vacuum via a first-order transition at a critical value $\mu_{\rm c} < 0$ of the chemical potential where the density jumps from zero to a finite value $\bar{n} \neq 0$, this is no longer valid. A formal procedure to extract the form of $V_{\rm eff}[\psi]$ near the vacuum-to-liquid transition requires to determine the generating functional $\Gamma[\psi_{\rm c}]$ for the vertex functions from the exact partition function $Z[J]$ in the presence of an external field J [45, 46]. In practice, this has been achieved in [47] for rotation invariant short-range interactions which become attractive beyond a zero crossing of the scattering length, where $g < 0$. The exact effective potential obtained from $\Gamma[\psi_{\rm c}]$ then indeed contains a cubic term $k = 3$ as in (33) whose strength $\lambda_3 = \hbar^2 D/(2m)$ is proportional the three-body scattering hypervolume D introduced by Tan [48]. It has dimension (length)^4 and may be determined for a given two-body interaction $V_{\rm sr}(r_{12})$ from a solution of the three-body scattering problem. Specifically, it is defined by the asymptotic behavior

$$\psi_{E=0}(x_1, x_2, x_3)|_{a=0} = 1 - \frac{\sqrt{3}\,D}{2\pi^3(r_{12}^2 + r_{13}^2 + r_{23}^2)^2} + \cdots \quad \text{if } V(x_{12}) = V(r_{12}) \qquad (34)$$

of the three-body wave function at zero energy and vanishing scattering length. The parameter $\lambda_3 \sim D$ characterizes the strength of effective three-body interactions which arise beyond mean-field even for a microscopic Hamiltonian which only contains two-body interactions. Explicit results for D are available for simple model interactions like hard spheres [48], an attractive square well [49] or a Lennard-Jones potential [50]. In the two latter cases, the existence of two-body bound states gives rise to a finite imaginary part of the hypervolume. It determines the three-body loss coeffcient $L_3 = -(\hbar/m)\,{\rm Im}\,D = (\hbar/m)\,L_{\rm rec}^4$ or the equivalent recombination length $L_{\rm rec}$ [51]. Now, for a possible stabilization of a liquid state due to three-body interactions in the regime where $g_{\rm eff}(\kappa) = g - g_{\rm dd} f(\kappa) < 0$ is negative, it is the real part of the hypervolume D which is relevant. In the realistic situation of finite three-body losses, the parameter which determines the liquid density $\bar{n} = 3|g_{\rm eff}|/(4\bar{\lambda}_3)$ from the condition $p_{\rm sr}(x) + \mathscr{D}(x) = 0$ in the presence of the additional pressure $\Delta p_{\text{3-body}}(x) = (2/3)\bar{\lambda}_3\,[\rho^{(1)}(x)]^3$ due to three-body interactions is therefore $\bar{\lambda}_3 = \hbar^2\,{\rm Re}\,D/(2m)$. Evidently, ${\rm Re}\,D$ must be positive for a stable liquid, a condition which can be verified only by a concrete solution of the three-body problem. In particular, ${\rm Re}\,D$ assumes both positive and negative values, depending on the position of three-body bound states which is determined by the poles of the hypervolume [49–51]. In [2] and the literature beyond, a stabilization of self-bound droplets by repulsive three-body interactions in the regime $g_{\rm eff} < 0$ has been excluded by the argument that the experimental value of the loss coefficient L_3 gives rise to an estimate for the magnitude of the complex parameter λ_3 which is far too small to be consistent with the observed central droplet densities $\bar{n} \simeq 10^{-14}$ cm^{-3}. Since the real part $\bar{\lambda}_3 \sim {\rm Re}\,D$ may be much larger than the estimate of λ_3 based on $|{\rm Im}\,D|$, this argument is not compelling, however. For the moment, we will postpone a further discussion of the origin of the

beyond mean-field contribution $\Delta p \sim [\rho^{(1)}(x)]^k$ to the short-range pressure in Equation (18) and proceed by assuming that such a term is present on purely empirical grounds.

The shape-dependence of the effective coupling constant $g_{\rm eff}(\kappa)$ that determines the position of the mean-field instability gives rise to a corresponding shape-dependence of the liquid density, e.g. via $\bar{n}(\kappa) = 3|g_{\rm eff}(\kappa)|/(4\bar{\lambda}_3)$ in the case of repulsive three-body interactions. For a homogeneous fluid, this is a rather strange conclusion and indeed it is immediately changed if one takes into account that equilibrium in a uniaxial dipolar fluid requires in addition to $p_{\rm sr}(x) + \mathscr{D}(x) = 0$ also that the anomalous field $h(x) = 0$ must vanish. Using the mean-field result (31), this can be obeyed only if $b(\kappa) = 0$ which implies that κ is fixed to be either zero or infinity. The second possibility of an extremely oblate configuration is excluded since the dipolar interactions are then repulsive and the zero pressure condition cannot be fulfilled. By contrast, the limit $\kappa \to 0$ of a strongly prolate droplet turns out to desribe the actual physical situation, consistent with the tendency of oriented dipoles to arrange in a head-to-tail configuration. More precisely, the condition $h(x) = 0$ gives rise to a finite value for the aspect ratio of a self-bound droplet rather than the singular result $\kappa^{(\rm mf)} \equiv 0$ within mean-field if one includes the contribution to $h(x)$ in Equation (16) which arises from the kinetic energy $\hat{H}_0$. This is a local term which—in contrast to the ill-defined kinetic contribution to $\mathrm{Tr}\,\underline{\Pi}(x)$—is finite even if the range of $V_{\rm sr}(r_{12})$ is taken to zero. Indeed, if the interactions become rotation invariant at very short distances, the contribution of large momenta in $h^{(0)} \sim \int_k (k_x^2 + k_y^2 - 2k_z^2)\, n(k)$ cancels since the asymptotic momentum distribution $n(k) \to \mathscr{C}_2/|k|^4$ is then independent of the direction $\hat{k}$. A concrete result for $h^{(0)}$ can be obtained by assuming an anisotropic Gaussian profile with central density $\rho^{(1)}(x=0) = \bar{n}$ [8]. In the relevant limit $\kappa \ll 1$, only the radial contribution in Equation (16) remains and the condition $h(x) = 0$ in the center of the droplet is reduced to

$$\bar{n}\frac{\hbar^2}{2m}\pi\left(\frac{\bar{n}}{N\kappa}\right)^{2/3} = \frac{3}{4}g_{\rm dd}\bar{n}^2\cdot 6\kappa^2\ln(2/\kappa) \quad \to \quad \kappa^{8/3}\ln(2/\kappa) = [36\,\bar{n}^{1/3}a_{\rm dd}\cdot N^{2/3}]^{-1} = \epsilon. \tag{35}$$

With typical particle numbers $N \simeq 10^4$ and central densities $\bar{n}^{1/3}a_{\rm dd} = \mathscr{O}(1)$, the smallness of the parameter $\epsilon \simeq 6\cdot 10^{-5}$ allows an asymptotically exact solution of the transcendental equation for $\kappa(\epsilon)$ in the form

$$\kappa(\epsilon) = \left[\frac{\epsilon}{\ln(2/\epsilon^{3/8})}\right]^{3/8} \quad \to \quad \kappa(N) = \frac{0.26}{[\bar{n}^{1/3}a_{\rm dd}\cdot\ln[2/\epsilon^{3/8}(N)]]^{3/8}}\cdot N^{-1/4}. \tag{36}$$

Apart from the logarithmic correction in the denominator which changes the result only by a numerical factor of order one, the aspect ratio thus approaches zero according to $\kappa(N) \sim N^{-1/4}$ for large particle numbers. In practice, with $N < 10^5$, typical aspect ratios are in the range $1/\kappa \simeq 5$–30 [42, 52]. An important point to note is that the result (36) holds irrespective of the specific mechanism which stabilizes the central density $\bar{n}$ at a finite value provided only that $\bar{n}^{1/3}a_{\rm dd}$ does not itself depend on N. The dependence on the deviation $\varepsilon_{\rm dd} - 1$ from the critical strength $\varepsilon_{\rm dd}^c = 1$ of the dipolar interactions, which is now shape-independent due to $\kappa \approx 0$, is sensitive to that, however. In particular, for a beyond mean-field contribution $\sim|\psi(x)|^{2k}$, the liquid density approaches zero like $\bar{n}(\varepsilon_{\rm dd}) \sim (\varepsilon_{\rm dd} - 1)^{1/(k-2)}$. On physical grounds, the fact that the equilibrium configuration of self-bound dipolar fluids corresponds to an increasingly prolate object for large particle numbers is a consequence of the anisotropy of the interactions. In contrast to the situation of attractive short-range interactions stabilized by a repulsive three-body force discussed in [47, 53], there is no homogeneous liquid state at all. This quite unusual behavior is elucidated by a few further comments:

[8] This assumption has been made in this context by Dalibard [8]. More precisely, an exact result due to Triay [14] shows that—within an extended Gross–Pitaevskii description and for a negative chemical potential—the density profile of a non-confined dipolar gas is smooth and falls off exponentially.

- The existence of a finite aspect ratio rather than the mean-field value zero relies on the kinetic energy contribution to the anomalous field. This must be carefully distinguished from a standard quantum pressure term, which may stabilize only self-bound droplets whose size vanishes as $N \gg 1$. Examples are the bright soliton in the Lieb-Liniger model with positive two-body scattering length $a_1 > 0$ or the droplets formed by attractive three-body interactions studied by Sekino and Nishida [54]. In both cases, the droplet extension approaches zero for large N according to $R_N \to a_1/N$ or $R_N \sim \exp[-(4/\sqrt{3}\pi)N^2]$ instead of increasing like $L_z(N) \sim \sqrt{N}$ in the case of 3D dipolar gases.
- There is a bound N_0 on the particle number below which the droplets evaporate. This has been investigated by Baillie et al. [52], where $N_0(\varepsilon_{\rm dd})$ has been determined from an extended Gross–Pitaevskii description by the condition of a finite binding energy despite the competing quantum pressure term. The analogous problem for a Bose droplet with short-range interactions has been studied in [47] and—with concrete predictions for the lifetime of metastable droplets in a finite window $N_1 < N < N_0$—by Son et al. [55]. As discussed in [47], the critical number $N_0 \sim \sqrt{D}/a^2$ in this context determines the scattering lengths at which N-body bound states detach from the continuum.
- Non-spherical self-bound objects have been studied a long time ago for stars with strong, frozen-in magnetic fields B by Chandrasekhar and Fermi [56]. The balance between the decrease of the attractive gravitational energy with a finite excentricity and the gain in magnetic energy due an expansion in the direction perpendicular to the field results in an oblate deformation with aspect ratio $\kappa - 1 \simeq (B/B_*)^2$, where B_* is the field beyond which the star is no longer bound since magnetic pressure overwhelms gravitation.

Following the suggestion in the original publication on self-bound droplets [2], the mechanism for stabilizing a non-confined dipolar gas beyond the critical interaction strength $\varepsilon_{\rm dd} = 1$ where the homogeneous fluid is unstable is commonly believed [6] to be a generalized form of the Lee, Huang and Yang (LHY) correction, originally calculated for a dilute, homogeneous hard-sphere Bose gas [57]. Including the effect of anisotropy in the presence of an additional dipolar interaction [58], it gives rise to a beyond mean-field contribution to the effective potential of the form introduced in Equation (33) with $k = 5/2$ and a positive (as long as $\varepsilon_{\rm dd} \le 1$) coefficient

$$\lambda_{5/2}(g,\varepsilon_{\rm dd}) = \frac{4g}{3\pi^2}(4\pi a)^{3/2}\cdot Q_5(\varepsilon_{\rm dd}) \quad \text{where } Q_5(\varepsilon_{\rm dd}) = \int_0^1 {\rm d}x[1+\varepsilon_{\rm dd}\cdot 2P_2(x)]^{5/2}. \tag{37}$$

For the standard case of repulsive short-range interactions, the LHY term provides the leading correction beyond mean-field in the equation of state, giving rise to an additional contribution of order $gn^2\sqrt{na^3}$ to the pressure. It is important here to carefully separate the dependence on density from that on the chemical potential as the thermodynamically conjugate variable. In particular, for a homogeneous fluid, there is an exact relation $-V_{\rm eff}[n(\mu)] = p(\mu)$ which allows to infer the effective potential evaluated at the equilibrium value $n(\mu) = \partial p(\mu)/\partial\mu$ of the density from the pressure at given μ [47]. The increase of pressure with density which results from the positive LHY contribution in $V_{\rm eff}[\psi]$ thus arises from a corresponding negative correction to $p(\mu)$. In explicit form, this emerges within a field-theoretic formulation where the beyond mean-field contribution determined by LHY is just the one-loop correction [45, 46]

$$p^{(1)}(\mu) = -\frac{1}{2}\,{\rm Tr}\ln\det[\delta^{(2)}S] \xrightarrow[\rm hom.]{} -\frac{1}{2}\int_q\int_\omega \ln[E_q^2+(\hbar\omega)^2] \xrightarrow[\rm reg.]{} -\frac{8}{15\pi^2}\,\mu\Big(\frac{m\mu}{\hbar^2}\Big)^{3/2} \tag{38}$$

to the tree-level result $p^{(0)}(\mu) = \mu^2/(2g)$ for the pressure of a dilute Bose gas[9]. In physical terms, it describes the contribution to pressure due to zero-point fluctuations of the Bogoliubov

[9] Note that $p^{(1)}(\mu)$ does not explicitely depend on the scattering length. The contact density $\mathscr{C}_2(\mu) \to (m\mu/\hbar^2)^2$ is therefore still given by its mean-field value and the LHY correction of relative order $(na^3)^{1/2}$, which contributes to a corresponding one in the pressure (18), only shows up as a function of density.

excitations. Similar to the analogous Casimir effect, it is negative and it comes entirely from the low-energy part of the spectrum [46, 59]. In particular, after regularization of the divergent integration over momenta q, the remaining expression involves an integral $\int_q E_q^2 \sim \int_0 q^2\, \mathrm{d}q\, c^2(\hat{q}) q^2$. Here—in an extension to anisotropic interactions—we include a possible dependence of the sound velocity $c(\hat{q})$ on direction. Now, it is a crucial point that the correction (38) to the pressure is fully determined by the excitations near $q = 0$. As a consequence, an anisotropic sound velocity $c^2(\hat{q}) = c^2[1 + \tilde{\varepsilon} f(\hat{q})]$ with strength $\tilde{\varepsilon}$ and an arbitrary function $f(\Omega)$ of direction changes the LHY contribution (38) just by a numerical factor $Q(\tilde{\varepsilon}) = \int (\mathrm{d}\Omega)/(4\pi)\, [1 + \tilde{\varepsilon} f(\Omega)]^{5/2}$. For the special case of dipolar interactions, this immediately explains the origin of the function $Q(\tilde{\varepsilon}) \to Q_5(\varepsilon_{\mathrm{dd}})$ derived by Lima and Pelster [58]. It is obvious, however, that the LHY correction is well defined only as long as $c^2(\hat{q}) > 0$ remains positive. This requirement is violated in dipolar gases if $\varepsilon_{\mathrm{dd}} > 1$, where the homogeneous fluid is unstable. Formally, this shows up as a finite imaginary part of the function $Q_5(\varepsilon_{\mathrm{dd}})$ which is, however, neglected in the extended Gross–Pitaevskii description of the inhomogeneous configurations that are considered in practice.

For a proper understanding of the mechanism which underlies the stabilization of self-bound droplets and which allows to fulfill the zero pressure condition $p_{\mathrm{sr}}(x) + \mathscr{D}(x) = 0$, it is of course necessary to provide a physical argument that justifies the addition of a contribution $\Delta p_{\mathrm{LHY}}(x) = (3/5)\lambda_{5/2}\, [\rho^{(1)}(x)]^{5/2}$ of the LHY-form to the short-range pressure in a regime where the chemical potential is negative and the microscopic derivation along the lines in Equation (38) evidently fails. On a rather qualitative level, the inclusion of an LHY term even in the regime $\varepsilon_{\mathrm{dd}} > 1$ may be justified by noting that the characteristic radial extension $R_\perp \sim N^{1/4}$ of self-bound droplets is only of the order of the healing length ξ [8]. As a result, there is no sound propagating in the (x, y)-plane in such a configuration and the fact that $c^2(\hat{q}) < 0$ for the associated wave vectors is irrelevant. The argument is not conclusive, however, because it does not address the problem that an exponent 5/2 in the relation between pressure and density requires a corresponding power law in $p(\mu)$, which is excluded for negative values of μ. To obtain some further insight, it is useful to investigate the microscopic origin of the LHY correction from a different point of view. The associated characteristic exponent $k = 5/2$ indicates that it can be attributed neither to two-body nor to three-body interactions which—as discussed above—lead to $k = 3$. Now, as noted already by Lee, Huang and Yang [57] and expanded in detail later by Lüscher [60] and by Tan [48], the LHY term can be understood to arise from a finite size correction in the two-body problem. More precisely, the repulsive contribution $\sim g n (n a^3)^{1/2}$ in the interaction energy per particle beyond mean-field emerges from a correction of order a/L beyond the leading term $E^{(0)}_{N=2}(L) = g/L^3$ in the two-particle problem in a box with periodic boundary conditions. At finite density, the relevant size $L \simeq \xi$ for this correction is set by the healing length beyond which the pair distribution is no longer determined by two-body physics. In the presence of the long-range and anisotropic dipolar interactions, both $E^{(0)}_{N=2}(L)$ and its finite size correction will depend on the aspect ratio κ and the dimensionless strength parameter $\varepsilon_{\mathrm{dd}}$. A microscopic derivation of the LHY correction for dipolar gases in a configuration which mimics the elongated droplets thus requires the solution of the two-body problem in an anisotropic box of size $L \times L \times L/\kappa$ with periodic boundary conditions. Specifically, the parameter $\lambda_{5/2}(\kappa, \varepsilon_{\mathrm{dd}})$ is determined by the coefficient of the a/L—contribution to the energy in a finite size expansion analogous to that derived by Lüscher for rotation invariant short-range interactions [60]. While straightforward in principle, proving that $\lambda_{5/2}$ is finite and positive along these lines is nontrivial. A fully microscopic derivation of either the LHY correction or a possible repulsive three-body force that might contribute to the stabilization of self-bound droplets thus remains an open problem. It should be emphasized, however, that this is essentially a conceptual challenge, not a practical one. Indeed, as demonstrated recently by Bombín et al. [61], numerical approaches to dipolar gases in the regime $\varepsilon_{\mathrm{dd}} > 1$ based on quantum Monte Carlo provide results which agree quite

well with experiment, e.g. for the critical number N_0 where droplets unbind or for the supersolid transition.

3. Effective theories for the transition to a supersolid

The prediction that dipolar gases in a pancake geometry with $\lambda \gg 1$ will exhibit a roton-maxon character in their excitation spectrum has been made even before the experimental realization of dipolar condensates [62, 63]. In contrast to the situation in ^{4}He, where the roton gap Δ_r is essentially independent of pressure up to the superfluid-to-solid transition at $p_c \simeq 25$ atm, the depth of the roton minimum is now tunable. In fact, within mean-field, the roton gap in dipolar gases is found to vanish beyond a critical value of the interaction strength where the spectrum of Bogoliubov excitations reaches zero [62, 63]. A simple model capturing the essential physics is based on assuming a uniform quasi-2D situation with a Gaussian density profile in the transverse direction with characteristic length ℓ_z. The resulting effective dipole–dipole interaction [63, 64]

$$V_{\rm dd}(q) = \frac{\hbar^2}{m}\tilde{g}_{\rm dd}\left[2 - 3\sqrt{\frac{\pi}{2}}(q\ell_z)\exp\left(q^2\ell_z^2/2\right)\mathrm{erfc}(q\ell_z/\sqrt{2})\right] \tag{39}$$

in momentum space $q = (q_x, q_y)$ approaches a positive constant $V_{\rm dd}(q) \to 2\hbar^2\tilde{g}_{\rm dd}/m$ in the limit $|q|\ell_z \ll 1$, where $\tilde{g}_{\rm dd} = \sqrt{8\pi}a_{\rm dd}/\ell_z$ is a dimensionless coupling constant. The fact that $V_{\rm dd}(q=0)$ is positive guarantees that—in contrast to the situation in 3D—the homogeneous fluid is now stable for an arbitrary strength of the dipolar interaction. This does not exclude an instability at finite wave vector, however. Indeed, the effective interaction $V_{\rm dd}(q)$ turns negative beyond $|q|\ell_z$ of order one and asymptotically approaches the constant value $-\hbar^2\tilde{g}_{\rm dd}/m$. In physical terms, this describes attractive head-to-tail collisions between aligned dipoles at distances less than ℓ_z with an effective scattering length $-a_{\rm dd}$. For strong dipolar interaction strengths, the negative contributions to the total interaction $V(q) = \hbar^2\tilde{g}_2/m + V_{\rm dd}(q)$ give rise to a roton minimum in the spectrum $E_q^2 = 2nV(q)\varepsilon_q + \varepsilon_q^2$ of Bogoliubov excitations which eventually touches zero at a characteristic wave vector q_0. A crucial point in this context is that the scale for q_0 is set by the inverse of the confinement length ℓ_z, which is unrelated to and much larger than the average interparticle spacing in the transverse direction.

The predicted appearance and subsequent softening of a roton has been observed in dipolar condensates of Dysprosium in a cigar-shaped trap by Petter et al. [65] using Bragg spectroscopy. By tuning $\varepsilon_{\rm dd} = a_{\rm dd}/a$ via a Feshbach resonance that allows to change the short-range scattering length at fixed $a_{\rm dd}$, the measured dynamic structure factor shows a sharp increase near a critical value $\varepsilon_{\rm dd}^c$ of order one, consistent with theoretical results based on a solution of the Bogoliubov equations [66]. This signals a macroscopic occupation of the roton mode associated with a spontaneous density modulation along the weakly confined direction in the trap, as seen directly from in-situ density profiles [67]. The formation of a static density wave at a coupling strength where the roton dip is still not very pronounced and the interpretation of this state in terms of a supersolid has been confirmed in a number of experiments [6] which will not be discussed here in detail. Instead, we will present an elementary approach which allows to understand the nature of the associated phase transition and the underlying physics independent of specific details. In particular, based on a simple model due to Nozières [11], we will show that the mean-field roton instability is preempted into a first-order transition by an amount which depends on the strength of the short-range repulsion. As a first step, it is necessary to properly define the notion of a supersolid which, in a rather broad sense, may be characterized by:

In a supersolid, superfluidity (defined by a finite superfluid fraction) **appears together with a non-vanishing modulation of the density due to spontaneously broken translation invariance**.

Now, according to this definition, any spatially modulated superfluid like the vortex lattice is also a supersolid. To exclude such well known cases, the notion of a genuine supersolid should therefore be restricted to phases where spontaneously broken translation invariance and superfluidity are present simultaneously as *two independent* order parameters. The modulation in density is then still present even after superfluidity is lost. An important result due to Leggett [68] states that in any superfluid with a non-uniform density, there is an upper bound on the superfluid fraction f_s strictly smaller than one. Specifically, the Leggett bound is of the form

$$f_s(T=0) \leq \left[\frac{\bar{n}}{d} \int_0^d \frac{\mathrm{d}x}{n_1(x)} \right]^{-1}, \quad \text{in mean-field } f_s^{(\mathrm{mf})}(T=0) = m/m_{\mathrm{B}} \tag{40}$$

where the inverse of the density $n_1(x)$ is integrated over a unit cell of the lattice whose length is denoted by d. Here, $n_1(x)$ is the average of the microscopic density $\langle \hat{\rho}^{(1)}(x) \rangle$ over the transverse directions of the unit cell and $\bar{n}$ its average value (without loss of generality, the x-direction has been singled out). Apparently, the bound is always finite unless the density vanishes identically in some region. Within mean-field, the ground state wave function factorizes into a product of single-particle ones. The Leggett bound then turns into an equality and relates the superfluid fraction to the ratio m/m_{B} of the bare and the band mass m_{B} in the given periodic potential. For a conventional solid, where the particle density is concentrated near a discrete set $\{\mathbf{R}\}$ of lattice sites with an exponentially suppressed value at interstitial positions, the upper bound on f_s is much smaller than one. In the limit of a fluid with uniform density, in turn, Equation (40) reduces to the trivial identity $f_s \leq 1$. Obviously, supersolids with an appreciable superfluid fraction can only be found in situations where the density modulation is weak. A few important points should be noted in this context: First, the bound (40) does not provide a sufficient criterion for superfluidity in a state with broken translation invariance: a finite value of the bound is still compatible with no superfluidity at all. A case in point is the solid phase of ^{4}He, where the microscopic density profile is known from path integral Monte Carlo and the Leggett bound gives $f_s \leq 0.16$ [69] while the true value vanishes[10]. A second point is that the bound (40) makes no assumption about the physical origin of the density modulation. It may arise from a spontaneous breaking of translation invariance but it also holds if the density modulation is externally imposed. In fact, the latter method has been used in a recent experimental test of the Leggett bound [72]. Finally, a quite subtle point is that the bound holds independent of whether the number of particles within a unit cell happens to be an integer or not. Now, as emphasized in the classic paper by Andreev and Lifshitz [34], the generic realization of supersolids requires an incommensurate situation with a finite concentration of defects in the ground state. A detailed argument which shows that delocalized vacancies or interstitial atoms are indeed a necessary condition for a supersolid has been given by Prokof'ev and Svistunov [73]. This suggests that supersolids are in general just superfluid mass-density waves, with the homogeneous part of the density playing the role of delocalized "defects". The ground state of generic solids like ^{4}He, in turn, has an integer number of particles per unit cell and vanishing defect concentration [70]. The finite energy necessary for the creation of either vacancies or interstitials identifies such a state as a Mott-insulator, which cannot have a finite superfluid fraction.

3.1. *Mean-field theory of freezing in classical and quantum systems*

It is a classic argument due to Landau [74] that the transition from a uniform fluid to a state with a periodic modulation of the density is of first order. The argument relies on an expansion of the

[10] For a discussion of why a supersolid phase of bulk ^{4}He can be ruled out, see [69, 70] and the review [71].

free energy in terms of the Fourier components $n_{\mathbf{G}} \neq 0$ of the density

$$\rho^{(1)}(x) = \langle \rho^{(1)}(x) \rangle + \sum_{\mathbf{G}\neq 0} n_{\mathbf{G}} e^{i\mathbf{G}\cdot\mathbf{x}} = n_{\rm sol} + \sum_{\mathbf{G}\neq 0} n_{\mathbf{G}} e^{i\mathbf{G}\cdot\mathbf{x}} \tag{41}$$

in the symmetry broken phase with average density $n_{\rm sol}$, where $\{\mathbf{G}\}$ denotes the set of associated reciprocal lattice vectors [10]. In the weak crystallization limit, the density jump $\Delta n = n_{\rm sol} - n_{\rm liq}$ is small and the instability is dominated by a single wave vector q_0 where the static structure factor of the homogeneous fluid exhibits a pronounced maximum $S(q_0)$. The magnitude $|\mathbf{G}| = q_0$ of the reciprocal lattice vectors is then fixed and the problem reduces to finding the lattice with the lowest free energy. Within Landau theory, this is of the generic form [10]

$$\Delta f_L(T) = f_{\rm sol} - f_{\rm liq} = \frac{r(T)}{2} n_G^2 - w n_G^3 + u n_G^4 \quad \text{with } r(T) = T - T^* \text{ and } u > 0. \tag{42}$$

Here, $n_G^2 \sim \sum_{\mathbf{G}}' |n_{\mathbf{G}}|^2$ is a sum of the magnitudes of the non-vanishing Fourier components with fixed $|\mathbf{G}| = q_0$, rescaled in such a way that makes it independent of their number in the specific lattice and dimensionless[11]. Now, the simplified form (42) hides the dependence on the specific lattice structure which is contained in the detailed values of w and u. For a finite $w \neq 0$, reciprocal lattices in which triads of different $\mathbf{G}'$s add up to zero are favored. At fixed $|\mathbf{G}| = q_0$, therefore, the planar hexagonal, the fcc and icosahedral lattices are the only possibilities [10], giving rise to a triangular lattice in real space as the unique option in 2D. Quite generally, the transition temperature $T_{\rm c}$ is determined by the condition $\Delta f_L(T_{\rm c}) = 0$ at a finite value $n_G(T_{\rm c}) = w/(2u) \neq 0$, where the fluid with $n_G \equiv 0$ is degenerate with a state where the density develops a non-vanishing spatial modulation. Due to the presence of the third-order term, the critical temperature $T_{\rm c} = T^* + w^2/(2u)$ lies above the temperature T^* introduced in the phenomenological Ansatz for $r(T)$. Physically, T^* is the lowest temperature down to which the fluid exists as a metastable configuration. Despite its purely phenomenological nature, the Landau theory of crystallization captures many aspects of real first-order fluid-to-solid transitions, like the preference for (real space) bcc lattices near the melting line [75] or the fact that a fluid can be undercooled by a far larger amount than solids can be overheated. Indeed, the temperature below which the solid exists at least as a metastable configuration is given by $T_1 = T^* + 9w^2/(16u)$ and the Ansatz in Equation (42) thus leads to $T_{\rm c} - T^* = 8(T_1 - T_{\rm c})$. A further consequence of Landau theory, not mentioned usually, is that the static structure factor in the uniform fluid right at the transition has a quasi-universal value $S(q_0)|_{T_{\rm c}} = T_{\rm c}/r(T_{\rm c}) = T_{\rm c}/(T_{\rm c} - T^*)$ of order one. A similar result was in fact found to hold for strong crystallization transitions e.g. of a Lennard-Jones fluid by Hansen and Verlet [76]. It has led to the empirical Hansen–Verlet criterion $S_{\rm HV}(q_0)|_{T_{\rm c}} = 2.85$ as a system-independent estimate for the position of the fluid-to-solid transition in classical systems with short-range interactions from properties within the fluid phase itself.

The Landau theory for the fluid-to-solid transition in a classical system can be extended into a quantum theory which describes the appearance of a mass-density wave in a superfluid. Based on an approach indicated already in the ground-breaking work of Gross on inhomogeneous Bose fluids [77], this has been developed by Pomeau et al. [78, 79]. Focussing again on density fluctuations with wave vectors of a fixed length $|\mathbf{G}| = q_0$, the leading order expansion $\sum_q |\delta n_q|^2/2\chi(q)$ in the change of energy through density fluctuations $\delta n_q \neq 0$ in any fluid gives rise to a contribution $\tilde{r} n_G^2/2$, where $\tilde{r} = 1/\chi(q_0)$ is the inverse of the static density response function. Now, within the Bogoliubov approximation, this response is determined by the ratio $\chi(q) = 2\varepsilon_q/E_q^2$ of the free particle energy ε_q and the dispersion E_q of the collective excitations of the superfluid [80]. In particular, for interactions that lead to a roton minimum with energy $\Delta_r = E_{|q|=q_0}$, the parameter $\tilde{r}$ near the corresponding wave vector is given by $\tilde{r} = \Delta_r^2/(2\varepsilon_r)$ with $\varepsilon_r = \varepsilon_{|q|=q_0}$. It is important

[11] Note that the sign of w, assumed to positive here, is irrelevant since it can be changed trivially by $n_G \to -n_G$.

to note that—within the Bogoliubov approximation—a roton minimum requires two-body interactions $V(q)$ which are negative in a certain range of wave vectors but not necessarily an attractive interaction in real space as in dipolar gases. As an example, a purely repulsive box potential $V(r_{12})$ of strength V_0 and size σ gives rise to a negative $V(q)$ in a range $4.5 < q\sigma < 7.7$. The energy of the resulting roton minimum and the associated parameter $\tilde{r}$ can then be tuned by changing the dimensionless coupling strength $n\sigma^3 \cdot V_0\, m\sigma^2/\hbar^2$. This leads to a roton instability at the point where $\tilde{r}$ vanishes and the uniform superfluid becomes unstable. The nontrivial question now is whether this instability can be cured by a nonlinear contribution to the energy analogous to the one which is introduced by hand in Landau's Ansatz (42). As shown by Pomeau and Rica [78] this is indeed the case and the resulting energy functional

$$\Delta f_{\rm GP} = f[n(x)] - f[\bar{n}] = \frac{\tilde{r}}{2} n_G^2 - \tilde{w} n_G^3 + \tilde{u} n_G^4 \quad \text{with } \tilde{r} = \Delta_r^2/(2\varepsilon_r) \tag{43}$$

is in fact of the same form. Moreover, in contrast to the case of classical fluid-to-solid transitions where the parameters $r(T), w, u$ are introduced in a purely phenomenological manner, the coefficients in Equation (43) can now be derived from a microscopic energy functional. In particular, the nonlinear terms involving $\tilde{w}$ and $\tilde{u}$ follow from the expansion of the denominator in the quantum pressure contribution $\hbar^2\,[\mathrm{grad}\, n(x)]^2/[8m\, n(x)]$ around the fluid state with uniform density $\bar{n}$. For a given characteristic wave vector q_0 of the emerging density wave, they are on the order of the associated recoil energy $\tilde{w}, \tilde{u} \simeq \varepsilon_r$, with detailed values again depending on the specific lattice. As in the standard Landau theory, the presence of a finite third-order term $\tilde{w} \neq 0$ implies that the uniform superfluid freezes with a jump in density determined by $n_G|_{\rm c} = \tilde{w}/(2\tilde{u})$ at a critical value $\tilde{r}_{\rm c} = \tilde{w}^2/2\tilde{u}$. The mean-field roton instability at $\tilde{r} = 0$, which characterizes the interaction strength up to which the homogeneous superfluid exists at least as a metastable configuration, is thus preempted by first-order transition at a finite critical value $\Delta_r/\varepsilon_r|_{\rm c} = \mathcal{O}(1)$ of the roton gap. For the specific case of a triangular lattice in 2D, this value turns out to be $\Delta_r/\varepsilon_r|_{\rm c} = 0.23$ [78].

3.2. *Effects beyond mean-field and a two-mode model*

The extension above of Landau's classical theory to the freezing of a uniform superfluid into a state with broken translation invariance describes a mean-field supersolid in the sense that its condensate fraction stays at the non-interacting value $f_0^{(\rm mf)} = 1$. By contrast—consistent with the Leggett bound (40)—the superfluid fraction is reduced below one depending on the magnitude of the density modulation. The model thus provides a qualitative description of the supersolid transition in dipolar gases where the emerging density wave is a phase-coherent superfluid. This is rather different from the situation in ^{4}He, where the solid phase beyond the critical pressure $p_{\rm c}$ is a commensurate Mott-insulator [70]. The result that the roton gap has a finite value Δ_r^c at the supersolid transition implies a quantum generalization of the Hansen–Verlet criterion. Indeed, the expression $\chi(q) = 2\varepsilon_q/E_q^2$ for the density response also holds for finite temperatures below the superfluid transition as long as the condensate fraction remains close to one [80]. As a result, the static structure factor of the homogeneous superfluid at finite temperature is related to its ground state value $S(q) = \varepsilon_q/E_q$ by a thermal enhancement factor $\coth(E_q/2T)$. Right at the supersolid transition, it has thus a quasi-universal value

$$S_{\rm c}(q_0) = \left(\frac{\varepsilon_r}{\Delta_r^c}\right) \coth\left(\frac{\Delta_r^c}{2T}\right) \xrightarrow[T \gg \Delta_r^c]{} \frac{T}{\tilde{r}_{\rm c}} \gg 1 \tag{44}$$

determined only by the ratios between the roton gap Δ_r^c and the recoil energy or temperature. As indicated, the value is large compared to one in the experimentally relevant limit $T \gg \Delta_r^c$. In particular, this applies to the measurements of the static structure factor in [67], where a pronounced peak in $S(q_0)$ near the ordering wave vector is found at the supersolid transition.

There are two major shortcomings of the approach sketched above: First of all, the description fails in cases where the emerging lattice does not give rise to a third-order invariant in the free energy. This applies e.g. to the situation realized in many experiments where the density modulation appears along a single direction preferred by the geometry in cigar-shaped traps. The functional (43) then leads to a continuous transition at the point where the roton gap vanishes which is not consistent with observation[12], see e.g. [67]. A second point is that, even at finite values of $\tilde{w}$, the shift of the roton instability away from its mean-field value zero to a finite $\tilde{r}_c = \tilde{w}^2/2\tilde{u}$ predicted by Equation (43) gives rise to a critical roton gap of order ε_r, independent of the strength of interactions. In the following, we will outline an approach in which both of these problems are absent. The crucial point to recognize is that beyond mean-field there is a fundamental difference between density fluctuations and the quasi-particles of the superfluid. It is only in the limit of weak interactions where they coincide and one may infer the density response $\chi(q) \to 2\varepsilon_q/E_q^2$ from the quasi-particle dispersion E_q. A simple model for dealing with the interplay of density modes and superfluid quasi-particles was suggested by Nozières [11], whose aim was to shed light on the complex question about the role of the roton minimum in superfluid ^{4}He for the transition to a solid. Based on a diagrammatic argument, Nozières showed that beyond the standard leading order term $\Sigma_q(\omega) \to n_0 V(q)$ of the self-energy, there is a contribution proportional to $V^2(q)\cdot\chi(q,\omega)$ which involves the dynamic density response function $\chi(q,\omega)$. Within a simple Ansatz $\chi(q,\omega) \simeq 2\varepsilon_q/(\Omega_q^2-\omega^2)$ for this response in the absence of the coupling to superfluid quasi-particles, a two-mode model emerges whose excitation energies $E_\pm^2(q)$ follow from a bi-quadratic equation [11]

$$E_\pm^2(q) = E_q^2 - f_0\frac{\Lambda_q}{\Omega_q^2 - E_\pm^2(q)} \quad \to \quad \tilde{r}^{\rm eff}(q) = \frac{E_-^2(q)}{2\varepsilon_q} \simeq \frac{E_q^2}{2\varepsilon_q} - f_0\frac{\Lambda_q}{2\varepsilon_q\cdot E_q^2} = \tilde{r}^{\rm mf}(q) - \frac{f_0\Lambda_q/(2\varepsilon_q)^2}{\tilde{r}^{\rm mf}(q)}. \tag{45}$$

The effective coupling contains the condensate fraction f_0 and the parameter Λ_q which is at least quadratic in the interactions. With increasing coupling, the two modes $E_\pm^2(q)$ shift in an opposite direction and it is the lower one $E_-(q)$ whose softening signals the onset of a density wave at given q. In particular, the associated effective stiffness $\tilde{r}^{\rm eff}(q)$ is renormalized down compared with the mean-field value by an amount which scales inversely with $\tilde{r}^{\rm mf}(q)$ itself[13]. The fact that a mean-field approximation overestimates the stiffness for density fluctuations is consistent with the exact inequality $m_p^2(q) \le m_{p+1}(q)\, m_{p-1}(q)$ for the pth moment of the dynamic structure factor [80]. In fact, in the special case $p=0$, this reduces to

$$S^2(q) \le \varepsilon_q\cdot\chi(q)/2 \quad \to \quad 1/\chi(q) \le \frac{\varepsilon_q}{2S^2(q)} \underset{\rm mf}{\longrightarrow} \frac{\Delta_r^2}{2\varepsilon_r} \tag{46}$$

in general, respectively evaluated at the roton minimum within mean-field. It is only in the limit where the dynamic structure factor has a single sharp peak that Equation (46) becomes an equality. A quantitative result for the renormalization of $\tilde{r}^{\rm mf}(q)$ requires to determine the parameter Λ_q. This may be estimated by assuming that the relevant wave vector is large enough that Λ_q can be inferred from the exact short-distance expansion

$$\frac{1}{\chi(q)} \to \frac{\varepsilon_q}{2}\left[1 - \frac{\pi\mathscr{C}_2}{8nq} + \cdots\right] \quad \to \quad \frac{\Lambda_q}{\varepsilon_q^4} = \frac{\pi\mathscr{C}_2}{8nq} \tag{47}$$

for Bose gases with repulsive short-range interactions derived in [83]. The requirement that this is consistent with Equation (45) then fixes $\Lambda_q \sim \varepsilon_q^4\mathscr{C}_2/q$ to be proportional to the two-body

[12] This problem may be eliminated by incorporating a further wave vector q_0' for the density wave, which breaks the symmetry $n_G \to -n_G$. The option comes, however, at the expense of introducing at least two additional free parameters.

[13] This is reminiscent of the Brazovskii equation in the beyond mean-field description of classical fluid-to-solid transitions [81, 82] but note that the sign here is opposite and the effect scales with the condensate fraction f_0.

contact density $\mathscr{C}_2$. Now, the characteristic wave vectors of the actually observed supersolids are considerably smaller than those where the expansion for high momenta in (47) is expected to apply and—moreover—effects of the long-range dipolar interactions have been ignored. The result is thus only of a rather qualitative nature. Nevertheless, it indicates how the problems of the mean-field approximation mentioned above can be resolved. Specifically, from the fact that the inverse static density response $\tilde{r}^{\rm eff}(q_0)$ of the homogeneous fluid at the freezing transition is expected to be finite but very small, the critical value

$$\left(\frac{\Delta_r}{\varepsilon_r}\right)_{\rm c}^4 \simeq f_0\,\frac{\pi\mathscr{C}_2}{8nq_0} \tag{48}$$

for the ratio between the roton gap Δ_r and the recoil energy ε_r at the transition into a supersolid state can be estimated. Independent of the existence of a third-order invariant, it is always finite. Moreover, it depends explicitely on the interaction strength via the two-body contact density $\mathscr{C}_2$. In particular, the simple mean-field roton instability with a vanishing $\Delta_r^{c}|^{(\rm mf)} \equiv 0$ is obtained in the limit of vanishing short-range repulsion, where $\mathscr{C}_2 \sim a^2 \to 0$. It is obvious that the rather crude arguments above need to be replaced by a proper microscopic theory for effects beyond mean-field in the transition to a supersolid. This is an open but clearly quite challenging problem.

4. Conclusion and open problems

The thermodynamic approach developed in this work provides a description of dipolar quantum fluids which fully accounts for the anisotropy and the long-range nature of the interactions. It allows to derive a number of exact results, e.g. for the effective magnetic field in the center of a spherical cloud (11) and the resulting instability beyond a critical value of the interaction strength, the violation of the Gibbs–Duhem relation in the density profile of trapped gases (21) or the number-dependence (36) of the aspect ratio in a self-bound droplet. An interesting perspective to obtain further exact results is provided by a possible extension into an effective field theory, similar to the one that has been developed by Son and Wingate for the unitary Fermi gas [84]. Concerning the transition into a supersolid phase, the discussion in this work has been of a rather qualitative nature and a better understanding of the effects beyond mean-field is an open problem.

It is obvious, that a number of basic problems in the theory of dipolar gases have only been raised but have not been answered. This is true, in particular, for a microscopic derivation of the exact effective potential which replaces the simple ad hoc Ansatz assumed in Equation (33). Specifically, both the detailed form of an LHY-like contribution $\sim|\psi|^5$ with a proper positive strength $\lambda_{5/2}(g,\varepsilon_{\rm dd},\kappa) > 0$ and a quantitative theory for a possible contribution of three-body forces are missing. In addition, the transition from the supersolid phase to a collection of separate, incoherent droplets [6] is still not well understood.

Finally, the approach to uniaxial quantum fluids presented here applies to a situation where the breaking of rotation invariance is imposed externally by the fixed orientation of the dipoles. It is a challenge to see whether it can be extended to cover a situation where the symmetry breaking is spontaneous, e.g. in a quantum version of a nematic liquid crystal[14].

Declaration of interests

The authors do not work for, advise, own shares in, or receive funds from any organization that could benefit from this article, and have declared no affiliations other than their research organizations.

[14] I am grateful to Alan Dorsey for pointing out such a possibility.

Acknowledgements

The present contribution is based on a Lecture on dipolar gases and supersolids given at the Institut Henri Poincaré in July 2024. I am very grateful to Yvan Castin for the invitation to this Lecture and for extensive discussions. It is also a pleasure to thank Jean Dalibard for a number of comments and a copy of the Notes for his Lectures on the subject at the Collège de France [8]. Finally, I am indebted to Markus Holzmann for clarifying some basic points about the freezing transition of quantum fluids.

References

[1] A. Griesmaier, J. Werner, S. Hensler, J. Stuhler, T. Pfau, "Bose–Einstein condensation of chromium", *Phys. Rev. Lett.* **94** (2005), article no. 160401.
[2] I. Ferrier-Barbut, H. Kadau, M. Schmitt, M. Wenzel, T. Pfau, "Observation of quantum droplets in a strongly dipolar Bose gas", *Phys. Rev. Lett.* **116** (2016), article no. 215301.
[3] F. Böttcher, J.-N. Schmidt, M. Wenzel, J. Hertkorn, M. Guo, T. Langen, T. Pfau, "Transient supersolid properties in an array of dipolar quantum droplets", *Phys. Rev. X* **9** (2019), article no. 011051.
[4] L. Tanzi, E. Lucioni, F. Famà *et al.*, "Observation of a dipolar quantum gas with metastable supersolid properties", *Phys. Rev. Lett.* **122** (2019), article no. 130405.
[5] L. Chomaz, D. Petter, P. Ilzhöfer *et al.*, "Long-lived and transient supersolid behaviors in dipolar quantum gases", *Phys. Rev. X* **9** (2019), article no. 021012.
[6] L. Chomaz, I. Ferrier-Barbut, F. Ferlaino, B. Laburthe-Tolra, B. L. Lev, T. Pfau, "Dipolar physics: a review of experiments with magnetic quantum gases", *Rep. Prog. Phys.* **86** (2023), article no. 026401.
[7] W. Zwerger, "Basic concepts and some current directions in ultracold gases", in *Lectures at the Collège de France*, 2021, https://pro.college-de-france.fr/jean.dalibard/CdF/2021.
[8] J. Dalibard, "Magnetic interactions between cold atoms: Quantum droplets and supersolid states", in *Lectures at the Collège de France*, 2024, https://pro.college-de-france.fr/jean.dalibard/CdF/2024.
[9] J.-P. Hansen, I. McDonald, *Theory of Simple Liquids*, 3rd ed., Elsevier, Academic Press, Amsterdam, 2006.
[10] P. M. Chaikin, T. C. Lubensky, *Principles of Condensed Matter Physics*, Cambridge University Press, Cambridge, 1995.
[11] P. Nozières, "Is the roton in superfluid helium 4 the ghost of a Bragg spot?", *J. Low Temp. Phys.* **137** (2004), p. 45-67.
[12] J. L. Bohn, D. S. Jin, "Differential scattering and rethermalization in ultracold dipolar gases", *Phys. Rev. A* **89** (2014), article no. 022702.
[13] J. L. Bohn, M. Cavagnero, D. Ticknor, "Quasi-universal dipolar scattering in cold and ultracold gases", *New J. Phys.* **11** (2009), article no. 055039.
[14] A. Triay, "Existence of minimizers in generalized Gross–Pitaevskii theory with the Lee–Huang–Yang correction", preprint, 2019, https://arxiv.org/abs/1904.10672.
[15] S. Tan, "Energetics of a strongly correlated Fermi gas", *Ann. Phys.* **323** (2008), p. 2952-2970.
[16] E. Braaten, D. Kang, L. Platter, "Universal relations for identical Bosons from three-body physics", *Phys. Rev. Lett.* **106** (2011), article no. 153005.
[17] D. Ruelle, "Classical statistical mechanics of a system af particles", *Helvetica Phys. Acta* **36** (1963), p. 183-197.
[18] M. E. Fisher, "The free energy of a macroscopic system", *Arch. Rat. Mech. Anal.* **17** (1964), p. 377-410.
[19] R. B. Griffiths, "Free energy of interacting magnetic dipoles", *Phys. Rev.* **176** (1968), p. 655-659.
[20] J. Fröhlich, Y.-M. Park, "Correlation inequalities and the thermodynamic limit for classical and quantum continuous systems", *Comm. Math. Phys.* **59** (1978), p. 235-266.
[21] S. Banerjee, R. B. Griffiths, M. Widom, "Thermodynamic limit for dipolar media", *J. Stat. Phys.* **93** (1998), p. 109-141.
[22] J. D. Jackson, *Classical Electrodynamics*, 3rd ed., John Wiley, New York, 1999.
[23] L. Landau, E. Lifshitz, *Electrodynamics of Continuous Media*, Pergamon Press, New York, 1984.
[24] D. J. Griffiths, "Hyperfine splitting in the ground state of hydrogen", *Am. J. Phys.* **50** (1982), p. 698-703.
[25] S. Yi, L. You, "Trapped condensates of atoms with dipole interactions", *Phys. Rev. A* **63** (2001), article no. 053607.
[26] S. Giovanazzi, A. Görlitz, T. Pfau, "Ballistic expansion of a dipolar condensate", *J. Opt. B: Quantum Semiclass. Opt.* **5** (2003), p. S208-S211.
[27] C. Eberlein, S. Giovanazzi, D. H. J. O'Dell, "Exact solution of the Thomas–Fermi equation for a trapped Bose–Einstein condensate with dipole–dipole interactions", *Phys. Rev. A* **71** (2005), article no. 033618.
[28] M. S. Wertheim, "Exact solution of the mean spherical model for fluids of hard spheres with permanent electric dipole moments", *J. Chem. Phys.* **55** (1971), p. 4291-4298.
[29] G. Bismut, B. Laburthe-Tolra, E. Maréchal, P. Pedri, O. Gorceix, L. Vernac, "Anisotropic excitation spectrum of a dipolar quantum Bose gas", *Phys. Rev. Lett.* **109** (2012), article no. 155302.

[30] P. C. Martin, J. Schwinger, "Theory of many-particle systems. I", *Phys. Rev.* **115** (1959), p. 1342-1373.
[31] F. Werner, Y. Castin, "General relations for quantum gases in two and three dimensions. II. Bosons and mixtures", *Phys. Rev. A* **86** (2012), article no. 053633.
[32] T.-L. Ho, Q. Zhou, "Obtaining the phase diagram and thermodynamic quantities of bulk systems from the densities of trapped gases", *Nat. Phys.* **6** (2010), p. 131-134.
[33] P. C. Martin, O. Parodi, P. S. Pershan, "Unified hydrodynamic theory for crystals, liquid crystals, and normal fluids", *Phys. Rev. A* **6** (1972), p. 2401-2420.
[34] A. Andreev, I. Lifshitz, "Quantum theory of defects in crystals", *Sov. Phys. JETP* **29** (1969), p. 1107-1113.
[35] J. Hofmann, W. Zwerger, "Hydrodynamics of a superfluid smectic", *J. Statist. Mech.: Theory Exp.* (2021), no. 3, article no. 033104.
[36] N. Liebster, M. Sparn, E. Kath, J. Duchene, H. Strobel, M. K. Oberthaler, "Observation of supersolid sound modes in a driven quantum gas", preprint, 2024, University of Heidelberg.
[37] F. Werner, "Virial theorems for trapped cold atoms", *Phys. Rev. A* **78** (2008), article no. 025601.
[38] E. N. Parker, "Tensor virial equations", *Phys. Rev.* **96** (1954), p. 1686-1689.
[39] Y. Nishida, D. T. Son, "Nonrelativistic conformal field theories", *Phys. Rev. D* **76** (2007), article no. 086004.
[40] T. Koch, T. Lahaye, J. Metz, B. Fröhlich, A. Griesmaier, T. Pfau, "Stabilization of a purely dipolar quantum gas against collapse", *Nat. Phys.* **4** (2008), p. 218-222.
[41] J. Hofmann, W. Zwerger, "Universal relations for dipolar quantum gases", *Phys. Rev. Res.* **3** (2021), article no. 013088.
[42] D. Baillie, R. M. Wilson, P. B. Blakie, "Collective excitations of self-bound droplets of a dipolar quantum fluid", *Phys. Rev. Lett.* **119** (2017), article no. 255302.
[43] R. Balian, J. Blaizot, "Stars and statistical physics: A teaching experience", *Am. J. Phys.* **67** (1999), p. 1189-1206.
[44] J. W. Negele, H. Orland, *Quantum Many-Particle Systems, Advanced Book Classics*, Westview Press, Boulder, CO, 1998.
[45] C. Itzykson, J.-M. Drouffe, *Statistical Field Theory*, Academic Press, Springer, New York, 1991.
[46] A. Zee, *Quantum Field Theory in a Nutshell*, 2nd ed., Princeton University Press, Princeton, NJ, 2010.
[47] W. Zwerger, "Quantum-unbinding near a zero temperature liquid–gas transition", *J. Statist. Mech.: Theory Exp.* (2019), no. 10, article no. 103104.
[48] S. Tan, "Three-boson problem at low energy and implications for dilute Bose–Einstein condensates", *Phys. Rev. A* **78** (2008), article no. 013636.
[49] P. M. A. Mestrom, V. E. Colussi, T. Secker, S. J. J. M. F. Kokkelmans, "Scattering hypervolume for ultracold bosons from weak to strong interactions", *Phys. Rev. A* **100** (2019), article no. 050702.
[50] P. M. A. Mestrom, V. E. Colussi, T. Secker, G. P. Groeneveld, S. J. J. M. F. Kokkelmans, "van der Waals Universality near a quantum tricritical point", *Phys. Rev. Lett.* **124** (2020), article no. 143401.
[51] S. Zhu, S. Tan, "Three-body scattering hypervolumes of particles with short-range interactions", preprint, 2017, https://arxiv.org/abs/1710.04147.
[52] D. Baillie, R. M. Wilson, R. N. Bisset, P. B. Blakie, "Self-bound dipolar droplet: A localized matter wave in free space", *Phys. Rev. A* **94** (2016), article no. 021602.
[53] D. T. Son, M. Stephanov, H.-U. Yee, "The phase diagram of ultra quantum liquids", *J. Statist. Mech.: Theory Exp.* (2021), no. 1, article no. 013105.
[54] Y. Sekino, Y. Nishida, "Quantum droplet of one-dimensional bosons with a three-body attraction", *Phys. Rev. A* **97** (2018), article no. 011602.
[55] D. T. Son, M. Stephanov, H.-U. Yee, "Fate of multiparticle resonances: From Q-balls to ^{3}He droplets", *Phys. Rev. A* **106** (2022), article no. L050801.
[56] S. Chandrasekhar, E. Fermi, "Problems of gravitational stability in the presence of a magnetic field", *Astrophys. J.* **118** (1953), p. 116-141.
[57] T. D. Lee, K. Huang, C. N. Yang, "Eigenvalues and eigenfunctions of a Bose system of hard spheres and its low-temperature properties", *Phys. Rev.* **106** (1957), p. 1135-1145.
[58] A. R. P. Lima, A. Pelster, "Quantum fluctuations in dipolar Bose gases", *Phys. Rev. A* **84** (2011), article no. 041604.
[59] M. D. Schwartz, *Quantum Field Theory and the Standard Model*, Cambridge University Press, Cambridge, 2014.
[60] M. Lüscher, "Volume dependence of the energy spectrum in massive quantum field theories", *Commun. Math. Phys.* **105** (1986), p. 153-188.
[61] R. Bombín, V. Cikojević, F. Mazzanti, J. Boronat, "Quantum-Monte-Carlo–based functional for dysprosium dipolar systems", *Phys. Rev. A* **109** (2024), article no. 033312.
[62] L. Santos, G. V. Shlyapnikov, M. Lewenstein, "Roton-maxon spectrum and stability of trapped dipolar Bose–Einstein condensates", *Phys. Rev. Lett.* **90** (2003), article no. 250403.
[63] D. H. J. O'Dell, S. Giovanazzi, G. Kurizki, "Rotons in gaseous Bose–Einstein condensates irradiated by a laser", *Phys. Rev. Lett.* **90** (2003), article no. 110402.
[64] U. R. Fischer, "Stability of quasi-two-dimensional Bose–Einstein condensates with dominant dipole-dipole interactions", *Phys. Rev. A* **73** (2006), article no. 031602.

[65] D. Petter, G. Natale, R. M. W. van Bijnen, A. Patscheider, M. J. Mark, L. Chomaz, F. Ferlaino, "Probing the roton excitation spectrum of a stable dipolar Bose gas", *Phys. Rev. Lett.* **122** (2019), article no. 183401.
[66] P. B. Blakie, D. Baillie, R. N. Bisset, "Roton spectroscopy in a harmonically trapped dipolar Bose–Einstein condensate", *Phys. Rev. A* **86** (2012), article no. 021604.
[67] J. Hertkorn, J.-N. Schmidt, F. Böttcher *et al.*, "Density fluctuations across the superfluid-supersolid phase transition in a dipolar quantum gas", *Phys. Rev. X* **11** (2021), article no. 011037.
[68] A. J. Leggett, "Can a Solid Be "Superfluid"?", *Phys. Rev. Lett.* **25** (1970), p. 1543-1546.
[69] D. M. Ceperley, B. Bernu, "Ring exchanges and the supersolid phase of ^{4}He", *Phys. Rev. Lett.* **93** (2004), article no. 155303.
[70] M. Boninsegni, A. B. Kuklov, L. Pollet, N. V. Prokof'ev, B. V. Svistunov, M. Troyer, "Fate of vacancy-induced supersolidity in ^{4}He", *Phys. Rev. Lett.* **97** (2006), article no. 080401.
[71] M. Boninsegni, N. V. Prokof'ev, "Colloquium: Supersolids: What and where are they?", *Rev. Mod. Phys.* **84** (2012), p. 759-776.
[72] G. Chauveau, C. Maury, F. Rabec *et al.*, "Superfluid fraction in an interacting spatially modulated Bose–Einstein condensate", *Phys. Rev. Lett.* **130** (2023), article no. 226003.
[73] N. Prokof'ev, B. Svistunov, "Supersolid state of matter", *Phys. Rev. Lett.* **94** (2005), article no. 155302.
[74] L. Landau, "Zur Theorie der Phasenumwandlungen II", *Phys. Z. Sowjetunion* **11** (1937), p. 26-35.
[75] S. Alexander, J. McTague, "Should all crystals be bcc? Landau theory of solidification and crystal nucleation", *Phys. Rev. Lett.* **41** (1978), no. 10, p. 702-705.
[76] J.-P. Hansen, L. Verlet, "Phase transitions of the Lennard-Jones system", *Phys. Rev.* **184** (1969), p. 151-161.
[77] E. P. Gross, "Classical theory of boson wave fields", *Ann. Phys.* **4** (1958), p. 57-74.
[78] Y. Pomeau, S. Rica, "Dynamics of a model of a supersolid", *Phys. Rev. Lett.* **72** (1994), no. 15, p. 2426-2429.
[79] C. Josserand, Y. Pomeau, S. Rica, "Coexistence of ordinary elasticity and superfluidity in a model of a defect-free supersolid", *Phys. Rev. Lett.* **98** (2007), article no. 195301.
[80] L. Pitaevskii, S. Stringari, *Bose–Einstein Condensation and Superfluidity*, Oxford University Press, Oxford, 2016.
[81] S. Brazovskii, "Phase transition of an isotropic system to a nonuniform state", *Sov. Phys. JETP* **41** (1975), p. 85-89.
[82] S. Brazovskii, I. Dzyaloshinskii, A. Muratov, "Theory of weak crystallization", *Sov. Phys. JETP* **66** (1987), p. 625-633.
[83] J. Hofmann, W. Zwerger, "Deep inelastic scattering on ultracold gases", *Phys. Rev. X* **7** (2017), article no. 011022.
[84] D. T. Son, M. Wingate, "General coordinate invariance and conformal invariance in nonrelativistic physics: Unitary Fermi gas", *Ann. Phys. (NY)* **321** (2006), p. 197-224.

ACADÉMIE DES SCIENCES
INSTITUT DE FRANCE

Comptes Rendus. Physique
2025, Vol. 26, p. 393-461
https://doi.org/10.5802/crphys.244

Intervention en colloque / *Intervention in a conference*

Questions ouvertes pour les gaz de fermions en interaction forte et de portée nulle

Open questions for strongly interacting Fermi gases with zero-range interactions

Yvan Castin [a]

[a] Laboratoire Kastler Brossel, ENS-Université PSL, CNRS, Université Sorbonne et Collège de France, 24 rue Lhomond, 75231 Paris, France

Courriel : yvan.castin@lkb.ens.fr

Résumé. Nous passons en revue quelques questions théoriques non résolues dans les gaz tridimensionnels de fermions à deux composantes, en nous inspirant des expériences réalisées récemment sur les atomes froids dans des pièges immatériels près d'une résonance de Feshbach magnétique. Nous distinguons successivement (i) les questions ouvertes apparaissant dans le problème à petit nombre de corps avec interactions de contact dites de Wigner–Bethe–Peierls — essentiellement la stabilité du gaz vis-à-vis de l'effet Efimov et le calcul des coefficients d'amas (ou du viriel), (ii) celles relevant de la théorie effective de basse énergie dite hydrodynamique quantique de Landau et Khalatnikov — essentiellement l'amortissement des modes de phonons et le temps de cohérence du condensat de paires liées, et enfin (iii) les questions nécessitant une résolution complète, microscopique, du problème à N corps, comme les propriétés précises de la branche d'excitation sonore (de Goldstone) du condensat de paires, ou de sa branche d'excitation collective (de Higgs) dans le continuum de paire brisée.

Abstract. We review some unresolved theoretical issues in three-dimensional two-component Fermi gases, drawing on recent experiments on cold atoms in immaterial traps close to a magnetic Feshbach resonance. We distinguish successively (i) the open questions arising in the few-body problem with Wigner–Bethe–Peierls contact interactions—essentially the stability of the gas with respect to the Efimov effect and the calculation of the cluster (or virial) coefficients, (ii) those arising in the effective low-energy theory of Landau and Khalatnikov quantum hydrodynamics—essentially the damping of phonon modes and the coherence time of the condensate of pairs, and finally (iii) questions requiring a complete, microscopic solution of the many-body problem, such as the specific properties of the acoustic excitation branch (Goldstone) of the condensate of pairs, or its collective excitation branch (Higgs) in the broken-pair continuum.

Mots-clés. Gaz de fermions, Hydrodynamique quantique, Effet Efimov, Limite unitaire, Interactions de contact, Développement en amas ou du viriel, Mode de Higgs.

Keywords. Fermi gases, Quantum hydrodynamics, Efimov effect, Unitary limit, Contact interactions, Cluster or virial expansion, Higgs mode.

Manuscrit reçu le 25 octobre 2024, révisé et accepté le 3 mars 2025.

Sommaire

Version française (English version starts on p 426)

1. Introduction et présentation générale

Ce texte est essentiellement la retranscription de notre exposé de 90 minutes au colloque de prospective « Questions ouvertes dans le problème quantique à N corps » qui s'est tenu à l'Institut Henri Poincaré à Paris, du 8 au 12 juillet 2024, d'où son style et son niveau de précision différents de ceux d'un article de recherche habituel. Il est plus complet que l'exposé sur la section 4 (traitée rapidement à l'oral) et sur la section 5 (omise à l'oral par manque de temps). Les notes en bas de page peuvent être ignorées en première lecture. L'exposé a été enregistré et est disponible en ligne sur la chaîne Carmin de l'IHP (cliquer ici).

Le système considéré est inspiré des expériences sur les atomes froids : il s'agit d'un gaz tridimensionnel de fermions à deux composantes (comprendre deux états internes $\uparrow$ et $\downarrow$) dans un piège immatériel — fait de lumière, à des températures très basses de l'ordre du microkelvin. C'est le digne descendant des gaz d'atomes refroidis par laser (dans les fameuses « mélasses optiques », voir le prix Nobel de physique 1997 décerné à Steven Chu, William Phillips et Claude Cohen-Tannoudji) puis des condensats de Bose–Einstein atomiques gazeux refroidis par évaporation (voir le prix Nobel de physique 2001 décerné à Eric Cornell, Carl Wieman et Wolfgang Ketterle).

Par rapport à leurs illustres prédécesseurs, les gaz d'atomes froids fermioniques ont l'avantage (i) d'être composés de fermions, ce qui permet de couvrir les deux statistiques possibles (on peut toujours « bosoniser » le gaz en formant des paires fortement liées $\uparrow\downarrow$) et de faire un lien direct avec les systèmes d'électrons (des fermions!) de la physique du solide, (ii) de rester collisionnellement stables (peu de pertes à trois corps par recombinaison vers des états moléculaires profonds) même dans le régime d'interaction forte comme dans la fameuse « limite unitaire » décrite plus bas (au contraire pour l'instant des gaz d'atomes froids bosoniques), et (iii) de constituer dans ledit régime des systèmes modèles, beaux, simples et universels, grâce à la portée négligeable des interactions de van der Waals entre $\uparrow$ et $\downarrow$ (plus précisément, la longueur de van der Waals associée est négligeable) ; comme nous le verrons, ceci autorise à remplacer l'interaction par des conditions de contact sur la fonction d'onde à N corps dépendant de la seule longueur de diffusion a dans l'onde s, longueur que les expérimentateurs ajustent à volonté au moyen d'une résonance de Feshbach, par simple application d'un champ magnétique uniforme bien choisi.

Notre système n'est pas sans rapport avec ceux d'autres exposés du colloque. Le lien est évident avec la contribution de Tilman Enss sur la viscosité des gaz de fermions en interaction forte [1], complémentaire de la nôtre. Mais si l'on place nos fermions dans un réseau optique, à raison d'environ une particule par site (près du demi-remplissage), on retombe sur les problèmes de fermions fortement corrélés et de supraconductivité à haute température critique discutés par Antoine Georges. Dans un régime qui plus est d'interaction sur site $U_{\uparrow\downarrow}$ forte devant le couplage tunnel t entre sites voisins, $U_{\uparrow\downarrow} \gg t$, le système est décrit par un hamiltonien modèle de spins de type Heisenberg, avec un couplage magnétique $J \propto t^2/U_{\uparrow\downarrow}$, ce qui fait le lien avec l'exposé de Sylvain Capponi [2]. En revenant à un système uniforme (sans réseau) mais en appliquant un champ de jauge artificiel (un champ magnétique fictif) à nos atomes froids fermioniques pourtant neutres, ce que les expérimentateurs savent faire, voir l'exposé de Sylvain Nascimbène [3], on tombe sur des problématiques proches des exposés de Thierry Jolicœur [4] (sur l'effet Hall quantique fractionnaire à 2D) et de Carlos Sá de Melo [5] (couplage spin–orbite à une dimension d'espace). Tous ces ponts vers la physique du solide ne sont cependant pas si faciles que cela à emprunter, à cause d'effets parasites non conservatifs, de la taille finie des échantillons et d'une difficulté à descendre à suffisamment basse température (en unités de la température de Fermi T_F ou de couplage magnétique J/k_B), voir les exposés de Wolfgang Ketterle, de Sylvain Nascimbène et d'Antoine Georges.

Terminons par le plan de notre contribution. Dans la section 2, nous partons du réel en esquissant le cheminement des expériences sur les atomes froids depuis les années 1980 et la situation atteinte dans le cas des fermions. Dans la section 3, nous adoptons un point de vue microscopique, d'interactions remplacées par des conditions de contact, et passons en revue quelques questions ouvertes dans le problème à petit nombre de fermions. Dans la section 4, nous adoptons au contraire un point de vue macroscopique, celui d'une théorie effective de basse énergie (l'hydrodynamique quantique), et passons en revue quelques questions ouvertes liées à l'interaction entre les phonons (les quanta des ondes sonores) dans la phase superfluide. Enfin, dans la courte section 5, nous croisons les points de vue, en listant quelques questions ouvertes requérant un traitement théorique microscopique du problème à N corps complet.

2. Un système physique assez récent

Commençons par une mise en contexte de nos gaz de fermions, au moyen d'un bref historique des atomes froids.

L'aventure commence au début des années 1980 par le refroidissement laser des alcalins. Les basses températures atteintes sont spectaculaires lorsqu'on les exprime en kelvins, $T \approx 1$ μK, mais les densités spatiales sont malheureusement très faibles, $\rho \lesssim 10^{10}$ at/cm^3, si bien que les gaz ont une très faible dégénérescence quantique, c'est-à-dire une très faible densité dans l'espace des phases, $\rho\lambda^3 \ll 1$, où λ est la longueur d'onde thermique de de Broglie des atomes de masse m :

$$\lambda = \left(\frac{2\pi\hbar^2}{m k_B T}\right)^{1/2} \tag{1}$$

Les effets de statistique quantique (bosoniques ou fermioniques) sont imperceptibles.

Tout change en 1995, lorsqu'Eric Cornell et Carl Wieman au JILA [6], suivis de peu par Wolfgang Ketterle au MIT [7], atteignent la condensation de Bose–Einstein (CBE), évidemment sur des isotopes bosoniques, grâce au refroidissement par évaporation dans des potentiels de piégeage non dissipatifs à fond harmonique[1]. Les températures de transition restent dans la gamme du refroidissement laser, $T_c^{\rm CBE} \simeq 0{,}1$ à 1 μK, mais les densités spatiales sont considérablement plus élevées, $\rho = 10^{12}$ à 10^{15} at/cm^3, ce qui permet l'atteinte de la dégénérescence quantique $\rho\lambda^3 \gtrsim 1$.

Enfin, en 2004, le refroidissement par évaporation est étendu avec succès aux isotopes fermioniques jusqu'à la température de transition [11,12] ; les gaz à deux états internes ↑ et ↓ ne forment plus des condensats de Bose–Einstein mais condensent par paires ↑↓ par le mécanisme BCS [13] : les interactions de van der Waals attractives entre ↑ et ↓ conduisent, en présence d'une mer de Fermi dans chaque état interne, à la formation de paires liées, les fameuses paires de Cooper, des « bosons composites », qui peuvent former un condensat à suffisamment basse température, $T < T_c^{\rm BCS}$. Les températures les plus basses accessibles expérimentalement sont de l'ordre de $0{,}1\,T_F$, où la température de Fermi T_F reste de l'ordre du microkelvin ; ceci suffit néanmoins à franchir $T_c^{\rm BCS}$ car les interactions entre ↑ et ↓ sont rendues très fortes au moyen d'une résonance de diffusion à deux corps (résonance de Feshbach magnétique) : la température de transition $T_c^{\rm BCS}$ est alors une fraction de T_F et l'on évite la situation extrême des supraconducteurs BCS, pour lesquels $T_c^{\rm BCS} \lll T_F$ par plusieurs ordres de grandeur.

Décrivons maintenant notre système d'atomes froids fermioniques dans ses grandes lignes, dans un début d'idéalisation de la réalité expérimentale. (i) Les fermions sont à deux états internes ↑ et ↓ ; comme nous n'envisageons pas ici de couplage de Rabi interconvertissant ↑ et ↓, nos considérations s'appliquent aussi au cas d'un mélange de deux espèces chimiques de fermions formellement sans spin ; pour cette raison, nous ne supposons pas que les masses m_σ des particules sont égales dans les deux états internes[2] et nous considérons le rapport $m_\uparrow/m_\downarrow$ comme un paramètre libre. (ii) Les fermions sont piégés, soit dans des potentiels harmoniques isotropes de même pulsation de piégeage ω pour les deux composantes σ,

$$U_\sigma(\mathbf{r}) = \tfrac{1}{2} m_\sigma \omega^2 r^2 \tag{2}$$

[1] La référence [8] a réussi plus tard, au moyen d'astuces bien trouvées, à obtenir un condensat de Bose–Einstein sans évaporation, par le seul refroidissement laser (voir aussi la référence [9]) ; pour cela, il a fallu en particulier (i) utiliser une raie atomique étroite à faible saturation pour rendre aussi basse que possible la température limite du refroidissement laser [10] et (ii) réussir à éviter que les photons d'émission spontanée, qui emportent une partie de l'énergie du mouvement des atomes, ne la redéposent par réabsorption dans le gaz.

[2] Dans le cas où ↑ et ↓ sont deux états de spin d'une même espèce chimique, on a naturellement $m_\uparrow = m_\downarrow$ dans l'expérience. On pourrait cependant, par application d'un réseau optique se couplant différemment aux deux états internes (dans une limite de faible taux de remplissage), produire des masses effectives m_σ différentes. Ceci reste à faire.

où **r** est le vecteur position à 3D, soit dans la boîte de quantification cubique $[0,L]^3$ commune aux deux composantes, avec les habituelles conditions aux limites périodiques[3]. (iii) L'interaction de van der Waals entre les deux états internes ↑ et ↓, représentée schématiquement sur la figure 1a, est rendue de manière effective très forte (résonnante) dans l'onde s (moment cinétique orbital relatif $l=0$) par application d'un champ magnétique idoine[4] si bien que la longueur de diffusion a entre deux atomes ↑ et ↓ (définie mathématiquement dans la section 3.1) est suffisamment grande en valeur absolue (elle peut être positive ou négative) pour que

$$\rho^{1/3}|a| \gtrsim 1 \tag{3}$$

On rappelle que la théorie des gaz de bosons en interaction faible fait usage du petit paramètre $(\rho a^3)^{1/2} \ll 1$, voir la contribution de Jan Solovej [17] aux actes du colloque; la condition (3) est donc au contraire la marque d'un gaz en interaction forte. La longueur du diffusion a est également beaucoup plus grande en valeur absolue que la portée b de l'interaction, définie sur la figure 1a,

$$|a| \gg b \tag{4}$$

ce qui est bien la marque d'une résonance de diffusion à deux corps. Comme b est de l'ordre de quelques nanomètres dans les expériences, on a aussi

$$b \ll \rho^{-1/3}, \lambda \tag{5}$$

ce qui donne l'idée de construction d'un système modèle, par passage à la limite $b \to 0$ à a fixé d'une interaction de portée nulle, caractérisée seulement par la longueur algébrique a. Cette idée sera mise en œuvre dans la section 3.1. (iv) En revanche, l'interaction n'est pas résonnante dans l'onde p (moment cinétique orbital relatif $l=1$) donc les interactions ↑↑ et ↓↓, qui se produisent de façon prédominante dans cette onde à basse énergie (antisymétrie fermionique oblige), sont négligeables.

Comme nous le verrons dans la section 3, l'existence d'un modèle bien défini (d'énergie bornée inférieurement lorsque $b \to 0$) constitue un problème mathématiquement non trivial. On peut déjà en proposer une condition nécessaire, inspirée de la réalité expérimentale. On l'aura en effet bien compris sur la figure 1a : puisque l'interaction de van der Waals admet (au moins) un état lié à deux corps de taille $\approx b$, la phase gazeuse considérée jusqu'à présent et vue dans les expériences n'est qu'une phase métastable, échappant temporairement à la solidification prédite par les lois de la physique à l'équilibre, solidification dont les pertes à trois corps sont les précurseurs (voir la figure 1b). Ces pertes se produisent avec un taux estimé comme suit dans la référence [18] pour des masses égales :

$$\Gamma^{3\text{ corps}}_{\text{pertes}} \propto \frac{\hbar}{mb^2}\,\text{Proba(3 fermions } \uparrow\uparrow\downarrow \text{ ou } \downarrow\downarrow\uparrow \text{ dans une même boule de rayon } b) \tag{6}$$

[3] Expérimentalement, on sait réaliser des boîtes de potentiel à fond plat au moyen de faisceaux de Laguerre–Gauss ou de Bessel–Gauss et de nappes de lumière laser, après compensation de la pesanteur (mise en lévitation des atomes) par un gradient de champ magnétique [14-16].

[4] Sans entrer dans les détails, signalons que, pour comprendre cette résonance, il faut tenir compte de la structure interne des atomes et décrire leur interaction binaire a minima par un modèle à deux voies, une voie ouverte de potentiel d'interaction $V_o(r_{12})$ et une voie fermée de potentiel d'interaction $V_f(r_{12})$ — on pourra penser aux potentiels d'interaction singulet et triplet de deux fermions de spin 1/2. Lors d'une collision, les atomes ↑ et ↓ entrent par la voie ouverte et, par conservation de l'énergie, sortent aussi par la voie ouverte car leur énergie cinétique relative incidente est inférieure à la différence des limites de dissociation $V_f(+\infty) - V_o(+\infty) > 0$. Comme il existe un couplage entre les deux voies, les atomes peuplent cependant virtuellement la voie fermée pendant la collision. Le champ magnétique B appliqué induit un déplacement Zeeman différent dans les deux voies. Il suffit alors de choisir B astucieusement pour que l'énergie d'un état lié dans $V_f(r_{12})$ — pas l'énergie nue mais l'énergie déplacée par le couplage — coïncide presque avec la limite de dissociation $V_o(+\infty)$, ce qui induit une résonance de diffusion (ou de collision) à deux corps dans la voie ouverte et fait diverger la longueur de diffusion a.

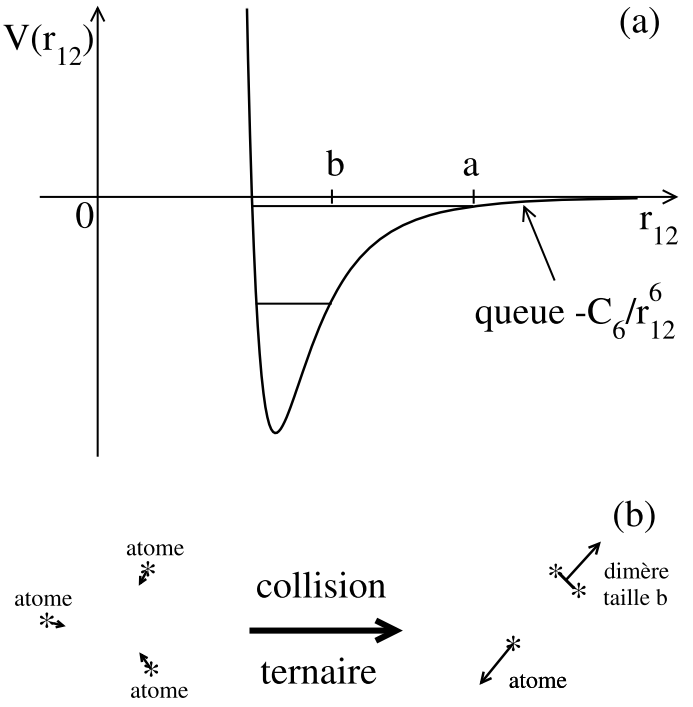

Figure 1. (a) Représentation schématique de l'interaction de van der Waals (plus précisément de Lennard-Jones) résonnante ($|a| \gg b$) entre les fermions $\uparrow$ et $\downarrow$ en fonction de leur distance relative. Le potentiel admet au moins un état fortement lié d'extension de l'ordre de la longueur de van der Waals $b \simeq (mC_6/\hbar^2)^{1/4}$ donc d'énergie de liaison $\approx \hbar^2/mb^2$ et, dans le cas d'une longueur de diffusion $a > 0$ comme sur la figure, un dernier niveau d'énergie d'extension a (d'énergie de liaison $\hbar^2/ma^2$) sur « le point de disparaître » (ici $m_\uparrow = m_\downarrow = m$ comme dans les expériences) ; si a était grande mais négative ($|a| \gg b, a < 0$), cet état faiblement lié serait sur « le point d'apparaître ». (b) L'état dimère fortement lié peut être peuplé par des collisions à trois corps, ce qui est à l'origine de pertes de particules dans le gaz de fermions, dites pertes à trois corps (les produits de la collision emportent l'énergie de liaison $\approx \hbar^2/mb^2$ considérable sous forme d'énergie cinétique et quittent le piège). Les flèches représentent les quantités de mouvement avant et après la collision.

Le premier facteur représente l'échelle d'énergie pertinente de ce processus de recombinaison : c'est l'énergie de liaison du dimère fortement lié formé, et l'échelle de longueur $|a| \gg b$ ne peut intervenir. Le second facteur tient compte du fait que le processus à trois fermions ne peut pas se produire si l'un des fermions est séparé des deux autres par une distance $\gg b$, par quasi-localité dans l'espace des positions : en effet, la portée des interactions et la taille du dimère fortement lié sont toutes deux de l'ordre de b. Le coefficient de proportionnalité dans l'équation (6) dépend des détails de la physique microscopique. Nous aboutissons ainsi à une condition de stabilité expérimentale du gaz de fermions dans la limite $b \to 0$ d'une interaction de contact :

$$\Gamma^{3\,\text{corps}}_{\text{pertes}} \underset{b\to 0}{\to} 0 \tag{7}$$

L'étude de ce système, pourtant gazeux, est rendue non triviale par la force des interactions. Par exemple, puisque $k_F|a| \approx 1$, où $k_F = (3\pi^2\rho)^{1/3}$ est le nombre d'onde de Fermi, la température de transition superfluide est a priori de l'ordre de la température de Fermi $T_F = E_F/k_B$ (il n'y a pas

d'autre échelle disponible que l'énergie de Fermi $E_F = \hbar^2 k_F^2/2m$) et sera difficile à calculer avec précision : la théorie BCS sera au mieux qualitative, et les méthodes de Monte-Carlo quantique sont difficiles à appliquer aux fermions ; le défi a cependant été relevé par la référence [19], il est vrai dans le cas symétrique de masses et de potentiels chimiques égaux dans les deux composantes, où existent des méthodes de Monte-Carlo exemptes du fameux « problème de signe ».

3. Questions ouvertes dans un point de vue microscopique

Dans cette section, les interactions entre fermions sont remplacées dans une limite de portée nulle par des conditions de contact sur la fonction d'onde à N corps, l'opérateur hamiltonien se réduisant alors à celui du gaz parfait (modèle de Wigner–Bethe–Peierls [20,21]).

3.1. *Définition du modèle de Wigner–Bethe–Peierls*

Pour construire le modèle, partons de la perception simple que nous en donnerait une photographie du gaz, c'est-à-dire une mesure des positions des N fermions comme les microscopes à gaz quantique permettent de le faire depuis peu dans le cas homogène [22]. Dans la limite où la portée b de l'interaction tend vers zéro, la photo typique ressemble à la figure 2a : les fermions sont séparés deux à deux par une distance $\gg b$ et le potentiel d'interaction $V(\mathbf{r}_i - \mathbf{r}_j)$ est négligeable. La fonction d'onde à N corps obéit dans ce cas à l'équation de Schrödinger stationnaire

$$E\psi = H_{\text{gaz parfait}}\psi \tag{8}$$

avec l'opérateur hamiltonien du gaz parfait, somme des termes d'énergie cinétique $\mathbf{p}^2/2m_\sigma$ et de piégeage $U_\sigma(\mathbf{r})$ dans chaque état interne σ :

$$H_{\text{gaz parfait}} = \sum_{i=1}^{N_\uparrow} \left(\frac{\mathbf{p}_i^2}{2m_\uparrow} + U_\uparrow(\mathbf{r}_i) \right) + \sum_{j=N_\uparrow+1}^{N} \left(\frac{\mathbf{p}_j^2}{2m_\downarrow} + U_\downarrow(\mathbf{r}_j) \right) \tag{9}$$

On convient ici de numéroter les particules de façon que les $N_\uparrow$ premières soient dans l'état interne $\uparrow$ et les $N_\downarrow$ dernières soient dans l'état interne $\downarrow$; la fonction d'onde $\psi(\mathbf{r}_1, \ldots, \mathbf{r}_N)$ est alors une fonction antisymétrique des $N_\uparrow$ premières positions et une fonction antisymétrique des $N_\downarrow$ dernières positions.

Certaines photos ressembleront cependant à la figure 2b : deux fermions i et j, d'états internes différents, respectivement $\uparrow$ et $\downarrow$, sont séparés des autres par une distance $\gg b$ mais sont séparés entre eux d'une distance $\approx b$ donc subissent l'effet du potentiel d'interaction $V(\mathbf{r}_i - \mathbf{r}_j)$. La bonne façon de voir est de dire que i et j sont en train de subir dans le gaz une diffusion à deux corps isolée, ce qui a deux conséquences, l'une qualitative, l'autre quantitative.

Qualitativement, on comprend qu'il vaut mieux, dans notre gaz très peu dense (au sens où $\rho b^3 \ll 1$), caractériser l'interaction entre $\uparrow$ et $\downarrow$ par son amplitude de diffusion à deux corps, plus généralement par un opérateur de transmission dit matrice T, que par la fonction $V(\mathbf{r})$ elle-même ; comme l'interaction se produit dans l'onde s, l'amplitude de diffusion f est isotrope et ne dépend que du nombre d'onde relatif k_{rel} des deux particules ; dans la limite $b \to 0$ à longueur de diffusion a fixée, on dispose alors du développement de basse énergie[5]

$$f_{k_{\text{rel}}} = \frac{-1}{a^{-1} + \mathrm{i}k_{\text{rel}} - (1/2)k_{\text{rel}}^2 r_e + O(k_{\text{rel}}^3 b^2)} \tag{10}$$

[5] Si $V(\mathbf{r})$ décroît plus vite que $1/r^7$ à l'infini, on peut mettre un $O(k_{\text{rel}}^4 b^3)$ au dénominateur.

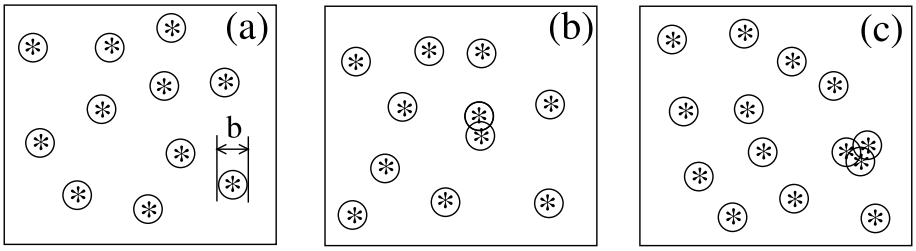

FIGURE 2. Photographie du gaz montrant les positions (étoiles) des N fermions, comme le ferait un microscope à gaz quantique, dans la limite d'une interaction de portée $b \to 0$ (à titre indicatif, nous avons entouré chaque étoile d'un cercle de diamètre b). (a) Cas typique : les particules sont séparées deux à deux par une distance $\gg b$ et n'interagissent pas. Ceci fixe l'opérateur hamiltonien (9) du modèle de Wigner–Bethe–Peierls. (b) Cas où deux particules $\uparrow$ et $\downarrow$, bien séparées des autres, subissent une collision binaire. Ceci fixe les conditions de contact (17) du modèle. (c) Cas d'une collision ternaire isolée. Ceci interroge sur la nécessité de conditions de contact à trois corps.

Nous supposons dans la suite que la portée effective de l'interaction r_e est un $O(b)$ donc devient négligeable lorsque $b \to 0$ [6]. Aussi l'amplitude de diffusion se réduit-elle à la forme universelle pour une interaction de contact

$$f_{k_{\rm rel}}^{\rm contact} = \frac{-1}{a^{-1} + {\rm i}k_{\rm rel}} \tag{11}$$

Quantitativement, on s'attend à ce que les deux fermions $\uparrow$ et $\downarrow$ proches se découplent des $N-2$ autres dans la fonction d'onde à N corps, au sens où

$$\psi(\mathbf{r}_1,\ldots,\mathbf{r}_N) \underset{r_{ij}=O(b)}{\simeq} \phi(\mathbf{r}_i-\mathbf{r}_j) A_{ij}(\mathbf{R}_{ij};(\mathbf{r}_k)_{k\neq i,j}) \tag{12}$$

où $\mathbf{R}_{ij} = (m_\uparrow \mathbf{r}_i + m_\downarrow \mathbf{r}_j)/(m_\uparrow + m_\downarrow)$ est la position du centre de masse des particules i et j, $\mathbf{r}_{ij} = \mathbf{r}_i - \mathbf{r}_j$ est leur position relative, $(\mathbf{r}_k)_{k\neq i,j}$ est le $(N-2)$-uplet des positions des autres particules, la fonction A_{ij} n'est en général pas connue mais $\phi(\mathbf{r})$ est un état de diffusion à deux corps, solution de l'équation de Schrödinger

$$\varepsilon\phi(\mathbf{r}) = -\frac{\hbar^2}{2m_{\rm rel}}\Delta\phi(\mathbf{r}) + V(\mathbf{r})\phi(\mathbf{r}) \tag{13}$$

pour le mouvement relatif de masse $m_{\rm rel} = m_\uparrow m_\downarrow/(m_\uparrow + m_\downarrow)$ à une énergie ε dont l'expression formelle est donnée dans la référence [24] (voir son équation (85)) mais dont nous retiendrons seulement qu'elle est $\approx \hbar^2 k_{\rm typ}^2/2m_{\rm rel}$, où le nombre d'onde typique $k_{\rm typ}$ dans le gaz est de l'ordre de $k_{\rm F}$ pour $T = O(T_{\rm F})$. Dans la limite $b \to 0$, il suffit en fait d'analyser l'équation (13) dans l'intervalle

$$b \ll r \ll k_{\rm typ}^{-1} \tag{14}$$

le cas $r \leq b$ n'apportant que des détails non universels sur l'interaction et le cas $r > k_{\rm typ}^{-1}$ invalidant la factorisation (12) (la paire ij n'est plus bien isolée comme sur la photo de la figure 2b). La première inégalité dans l'équation (14) permet de mettre $V(\mathbf{r})$ à zéro au second membre,

[6] Expérimentalement, il existe cependant des résonances de Feshbach magnétiques dites étroites, pour lesquelles r_e, négatif, est gigantesque à l'échelle atomique et peut être de l'ordre de $1/k_{\rm F}$, à cause d'un couplage anormalement faible entre les voies ouverte et fermée de notre note 4, voir la référence [23]. Ces résonances sont difficiles à utiliser car elles nécessitent un très bon contrôle du champ magnétique. L'existence d'une portée effective de limite non nulle lorsque $b \to 0$ a cependant l'avantage de stabiliser le gaz dans le régime instable de la section 3.2 (le spectre reste borné inférieurement et le taux de pertes à trois corps (6) tend vers zéro), et devrait permettre la préparation et l'observation d'états liés efimoviens de longue durée de vie, pour peu que le rapport de masse $m_\uparrow/m_\downarrow$ soit assez grand. L'expérience reste à faire.

la seconde permet d'assimiler l'énergie ε à zéro au premier membre de l'équation (13), d'où l'équation de Schrödinger simplifiée

$$0 = -\frac{\hbar^2}{2m_{\rm rel}}\Delta\phi(\mathbf{r}) \tag{15}$$

Sa solution générale dans l'onde s (invariante par rotation) est combinaison linéaire de la solution constante 1 (l'onde incidente d'énergie nulle) et de la solution de Coulomb (l'onde diffusée) avec une amplitude relative fixée par $V(\mathbf{r})$ aux courtes distances :

$$\phi(\mathbf{r}) = \mathcal{N}\left(1-\frac{a}{r}\right) = \frac{1}{a}-\frac{1}{r} \tag{16}$$

Par définition, voir la contribution de Jan Solovej [17], la quantité a est la longueur de diffusion du potentiel. Au troisième membre, nous avons choisi la normalisation commode (facteur $\mathcal{N}$ pris égal à $1/a$ au second membre) pour avoir un résultat fini à la résonance de diffusion $a^{-1}=0$.

Nous arrivons ainsi naturellement à la définition du modèle de Wigner–Bethe–Peierls pour notre système tridimensionnel de $(N_\uparrow, N_\downarrow)$ fermions à deux composantes en interaction de portée nulle et de longueur de diffusion $a\neq 0$ dans l'onde s :

(1) l'opérateur hamiltonien est le même que celui du gaz parfait, comme dans les équations (8), (9)

(2) il y a antisymétrie fermionique du vecteur d'état ψ pour les $N_\uparrow$ premières et pour les $N_\downarrow$ dernières positions

(3) l'interaction est décrite non pas par un potentiel V mais par les conditions de contact suivantes sur ψ : pour tout indice $i\in\{1,\dots,N_\uparrow\}$ et tout indice $j\in\{N_\uparrow+1,\dots,N=N_\uparrow+N_\downarrow\}$, il existe une fonction A_{ij} telle que[7]

$$\psi(\mathbf{r}_1,\dots,\mathbf{r}_N) \underset{r_{ij}\to 0}{=} A_{ij}(\mathbf{R}_{ij},(\mathbf{r}_k)_{k\neq i,j})\left(\frac{1}{r_{ij}}-\frac{1}{a}\right)+O(r_{ij}) \tag{17}$$

où l'on fait tendre vers zéro la distance r_{ij} entre les particules i et j à positions fixées de leur centre de masse $\mathbf{R}_{ij}$ et des autres particules $\mathbf{r}_k$, en imposant $\mathbf{R}_{ij}\neq\mathbf{r}_k\forall k\neq i,j$ et les $\mathbf{r}_k$ deux à deux distincts (comme sur la figure 2b).

Mathématiquement, le point 3 signifie que le domaine de l'opérateur hamiltonien n'est pas le même que celui du gaz parfait : en l'absence d'interaction ($a=0$), on élimine à juste titre les solutions qui divergent en $1/r_{ij}$, comme il est dit dans tout bon ouvrage de mécanique quantique. C'est la seule différence mais elle est de taille[8] !

La figure 2c, qui montre un trio d'atomes proches, bien séparés des autres et en train de subir une diffusion à trois corps, fait naître une interrogation légitime : faut-il compléter le modèle par des conditions de contact à trois corps ? à quatre corps ? etc. Réponse dans la section suivante.

3.2. *Questions d'existence*

Il n'est pas évident que le modèle de Wigner–Bethe–Peierls, tel que nous l'avons défini en page 401, conduise à un hamiltonien auto-adjoint (sans conditions de contact supplémentaires) et,

[7] Les fonctions A_{ij} ne sont pas indépendantes. L'antisymétrie fermionique impose que $A_{ij}(\mathbf{R}_{ij},(\mathbf{r}_k)_{k\neq i,j}) = (-1)^{i-1}(-1)^{j-(N_\uparrow+1)}A_{1,N_\uparrow+1}(\mathbf{R}_{ij},(\mathbf{r}_k)_{k\neq i,j})$ (pour les amener en première position dans leur état interne respectif et faire ainsi apparaître la fonction $A_{1,N_\uparrow+1}$, on a dû faire passer $\mathbf{r}_i$ à travers $i-1$ vecteurs positions de fermions $\uparrow$ et $\mathbf{r}_j$ à travers $j-(N_\uparrow+1)$ vecteurs positions de fermions $\downarrow$, d'où les signes).

[8] Un point clé est que l'état de diffusion $\phi(\mathbf{r})=1/r-1/a$ est bien de carré sommable sur un voisinage de l'origine, $\int_{r<r_{\max}} \mathrm{d}^3 r\,|\phi(\mathbf{r})|^2<\infty$: il n'y a donc pas de coupure à mettre à courte distance et a est la seule longueur associée à l'interaction. C'est différent dans les ondes de moment cinétique $l>0$: $\phi(\mathbf{r})=Y_l^{m_l}(\theta,\varphi)(r^l+a_{\rm gen}^{2l+1}/r^{l+1})$ (où le paramètre $a_{\rm gen}\neq 0$ généralisant a est une longueur et $Y_l^{m_l}$ est une harmonique sphérique) n'est alors plus de carré sommable, et il faut introduire une coupure donc une seconde longueur pour caractériser l'interaction [25].

surtout, à un spectre d'énergie borné inférieurement. En effet, nous avons quand même fait tendre une échelle d'énergie vers $-\infty$, celle $-\hbar^2/m_{\rm rel}b^2$ associée à la portée de l'interaction, en prenant la limite $b \to 0$ à longueur de diffusion a fixée donc sans faire tendre la force des interactions vers zéro, ce qui pourrait provoquer un effondrement du système sur lui-même, comme dans l'effet Thomas bien connu en physique nucléaire [26] !

La discussion s'éclaire dans le cas particulier $a^{-1} = 0$, dit de la limite unitaire (l'amplitude de diffusion (11) du modèle atteint en module la valeur maximale $k_{\rm rel}^{-1}$ autorisée dans l'onde s par l'unitarité de la matrice de collision S), car les conditions de contact (17) deviennent invariantes d'échelle (c'est aussi le régime le plus intéressant et le plus ouvert car d'interaction maximale en phase gazeuse). Pour simplifier encore, limitons-nous aux états propres d'énergie $E = 0$ dans l'espace libre, avec un centre de masse des N fermions au repos. Comme il n'y a alors ni énergie ni potentiel extérieur pour introduire une échelle de longueur, on s'attend à ce que l'état propre ψ lui-même soit invariant d'échelle, c'est-à-dire une fonction homogène des coordonnées (invariante à un facteur près par l'homothétie $\mathbf{r}_i \to \lambda \mathbf{r}_i$ de rapport λ sur les N positions), de la forme [27,28]

$$\psi(\mathbf{r}_1, \ldots, \mathbf{r}_N) = R^{s-\frac{3N-5}{2}} \Phi(\Omega) \tag{18}$$

où (i) R est l'hyperrayon interne, écart quadratique moyen des positions des N particules à leur centre de masse $\mathbf{C}$ pondérées par les masses,

$$MR^2 = \sum_{i=1}^{N} m_i (\mathbf{r}_i - \mathbf{C})^2 \tag{19}$$

avec $M = \sum_{i=1}^N m_i$ la masse totale et $M\mathbf{C} = \sum_{i=1}^N m_i \mathbf{r}_i$; (ii) l'exposant d'échelle (le degré d'homogénéité) est commodément repéré par la quantité s après translation de $(3N-5)/2$ — pour révéler une symétrie $s \leftrightarrow -s$; (iii) Φ est une fonction inconnue des $3N-4$ hyperangles complétant R dans le paramétrage des $\mathbf{r}_i - \mathbf{C}$ en coordonnées hypersphériques. Le report de l'ansatz (18) dans l'équation de Schrödinger (8) (avec $E = 0$ et $U_\sigma \equiv 0$ comme il a été dit) donne une équation aux valeurs propres sur Φ :

$$\left[-\Delta_\Omega + \left(\frac{3N-5}{2} \right)^2 \right] \Phi(\Omega) = s^2 \Phi(\Omega) \tag{20}$$

dont les valeurs propres ne sont autres que s^2 ! Comme le laplacien Δ_Ω est pris sur un compact, l'hypersphère unité S_{3N-4}, les valeurs possibles de s^2 forment un ensemble discret, dans $\mathbb{R}$ à supposer que l'hamiltonien soit hermitien ; on ne sait en général pas les calculer, à cause des difficiles conditions de contact (17) sur $\Phi(\Omega)$ [9].

Nous nous contenterons dans la suite d'écrire formellement que s est la racine d'une fonction transcendante paire, dite fonction d'Efimov,

$$\Lambda_{N_\uparrow, N_\downarrow}(s) = 0 \tag{21}$$

sans spécifier cette fonction (le plus direct pour l'obtenir est d'imposer les conditions de contact (17) sur un ansatz de Faddeev écrit dans l'espace réciproque[10], ce qui mène à une équation intégrale dite de Skorniakov–Ter-Martirosian — ici à la limite unitaire et à énergie nulle, dans

[9] Les conditions de contact (17) ne contraignent en revanche pas la dépendance de ψ en l'hyperrayon. C'est que, si ψ obéit aux conditions de contact, $f(R)\psi$ y obéit aussi, pourvu que le facteur $f(R)$ soit une fonction régulière de R. En effet, dans la limite $r_{ij} \to 0$ à $\mathbf{R}_{ij}$ et $(\mathbf{r}_k)_{k\neq i,j}$ fixés, on a $MR^2 = m_i(\mathbf{r}_i - \mathbf{C})^2 + m_j(\mathbf{r}_j - \mathbf{C})^2 + \text{cte} = m_i \mathbf{r}_i^2 + m_j \mathbf{r}_j^2 + \text{cte} = (m_i + m_j)\mathbf{R}_{ij}^2 + m_{\rm rel} r_{ij}^2 + \text{cte} = O(r_{ij}^2) + \text{cte}$. Or, $(1/r_{ij} - 1/a)O(r_{ij}^2)$ est un $O(r_{ij})$ négligeable.

[10] Rappelons brièvement la construction de l'ansatz. On écrit d'abord l'équation de Schrödinger à énergie nulle au sens des distributions, $H_{\text{gaz parfait}}\psi = \sum_{i=1}^{N_\uparrow} \sum_{j=N_\uparrow+1}^{N} (2\pi\hbar^2/m_{\rm rel}) \delta(\mathbf{r}_{ij}) A_{ij}(\mathbf{R}_{ij}, (\mathbf{r}_k)_{k\neq i,j})$ où les distributions de Dirac proviennent de l'action des opérateurs d'énergie cinétique sur les singularités en $1/r_{ij}$, en vertu de l'équation de Poisson $\Delta_{\mathbf{r}}(1/r) = -4\pi\delta(\mathbf{r})$, et $m_{\rm rel}$ est la masse réduite de deux fermions de spins opposés comme nous l'avons dit. On en prend ensuite la transformée de Fourier ($\psi \to \tilde{\psi}$, $\Delta_{\mathbf{r}} \to -k^2$). En tirant parti de l'antisymétrie fermionique comme dans la note 7 et de l'invariance par translation spatiale (le centre de masse est au repos), on se réduit à $\tilde{\psi}(\mathbf{k}_1, \ldots, \mathbf{k}_N) =$

laquelle on reporte l'équivalent de Fourier de l'ansatz (18) ; l'équation transcendante (21) qui en résulte admet une écriture explicite pour $N = 3$ [29], et s'écrit comme le déterminant d'un opérateur pour $N > 3$, cet opérateur étant donné explicitement pour $N = 4$ dans le secteur $(3,1)$ par la référence [30] et dans le secteur $(2,2)$ par la référence [31]). Il faut maintenant distinguer deux cas.

Premier cas : $s^2 > 0$**.** Il y a alors deux valeurs possibles correspondantes de l'exposant d'échelle, une valeur > 0 que nous convenons d'appeler s, et la valeur opposée $-s < 0$. Par un phénomène similaire à celui de l'équation (16), ψ est en général une combinaison linéaire de deux solutions, l'une contenant un facteur R^s, l'autre contenant un facteur R^{-s}, les amplitudes relatives étant fixées de manière univoque par une longueur ℓ (l'équivalent de a dans l'équation (16)) déterminée par les détails microscopiques de l'interaction à courte distance $O(b)$ [11,12] :

$$\psi = \left[(R/\ell)^s - (R/\ell)^{-s}\right] R^{-\frac{3N-5}{2}} \Psi(\Omega) \tag{22}$$

Cependant, en l'absence de résonance de diffusion à N corps, on s'attend à ce que $\ell = O(b)$, si bien que $\ell \to 0$ lorsque $b \to 0$: la solution en R^{-s} devient négligeable, la longueur ℓ disparaît du problème et l'on garde la condition de contact à N corps invariante d'échelle suivante dans la voie d'exposant d'échelle s [32] :

$$\psi \underset{R\to 0}{\approx} R^{s-\frac{3N-5}{2}} \tag{23}$$

La fonction d'onde ψ, considérée comme une fonction de R, est sans nœud donc l'énergie $E = 0$ correspond à l'état fondamental : il n'y a pas d'état lié, d'énergie $E < 0$ pouvant tendre vers $-\infty$ lorsque $b \to 0$ [13,14].

$(\delta(\mathbf{k}_1 + \cdots + \mathbf{k}_N)/\sum_{n=1}^N \hbar^2 k_n^2/2m_n) \sum_{i=1}^{N_\uparrow} \sum_{j=N_\uparrow+1}^{N} (-1)^{i+j} D((\mathbf{k}_n)_{n\neq i,j})$ où D est la seule fonction inconnue (chaque A_{ij} est une fonction des $(\mathbf{r}_k - \mathbf{R}_{ij})_{k\neq i,j}$ dont $D((\mathbf{k}_n)_{n\neq i,j})$ est la transformée de Fourier à un facteur près).

[11] L'état de diffusion (16) correspond au cas $N = 2$; alors $s = 1/2$ et $(3N-5)/2 = 1/2$, et ψ dans l'équation (22) est bien combinaison linéaire de R^0 et R^{-1} ; dans ce cas, $R \propto r_{12}$ et $\Phi(\Omega) =$ cte dans l'onde s. Le calcul explicite de l'expression (22) pour $N = 2$ donne en effet $\psi \propto (r_{12}/\bar{\ell})^{s-1/2} - (r_{12}/\bar{\ell})^{-s-1/2}$ avec $\bar{\ell} = (m_1 + m_2)\ell/(m_1 m_2)^{1/2}$, ce qui doit être proportionnel à (16), d'où la valeur annoncée de l'exposant $s = 1/2$; le paramètre à deux corps $\bar{\ell}$ n'est autre que la longueur de diffusion a.

[12] On a mis un signe moins entre les deux termes entre crochets dans l'équation (22) ; un signe plus serait aussi possible, suivant le modèle microscopique.

[13] Le cas spécial d'une résonance de diffusion à $(N_\uparrow, N_\downarrow)$ corps, où ℓ reste non infinitésimal dans la limite $b \to 0$, est traité en détail dans la référence [33], qui explique quelle condition de contact à N corps utiliser pour décrire correctement l'état faiblement lié qui en résulte. En effet, la condition (22) déjà proposée dans [27] n'est satisfaisante que pour s assez petit (pour $s > 1$, on voit bien que l'état (22) n'est plus de carré intégrable en $R = 0$ et qu'une deuxième longueur — une coupure — doit être introduite).

[14] Sur une résonance de Feshbach étroite, voir la note 6, la portée effective r_e est — pour $1/a = 0$ — la seule échelle de longueur pertinente lorsque la portée vraie b tend vers zéro, si bien que la longueur ℓ est de l'ordre de $|r_e| \gg b$. La fonction d'onde ψ dans l'équation (22) admet alors un nœud très « en dehors » du potentiel d'interaction : la solution à $E = 0$ ne serait pas d'énergie minimale, et le système admettrait un état lié à $(N_\uparrow, N_\downarrow)$ fermions (avec $N > 2$) ! Cependant, une étude spécifique du cas $(N_\uparrow = 2, N_\downarrow = 1)$ montre qu'il n'en est rien (tant que le rapport de masse $m_\uparrow/m_\downarrow$ reste assez faible pour que $s^2 \geq 0$ bien entendu) [29,34]. Fallait-il s'en étonner? Raisonnons par l'absurde. S'il y avait vraiment un état lié, il conduirait à un nombre d'onde relatif $k_{\rm rel} \approx 1/|r_e|$ entre les fermions, le terme de portée effective ne serait pas négligeable au dénominateur de l'amplitude de diffusion (10) et l'on perdrait l'invariance d'échelle donc la séparabilité en coordonnées hypersphériques. L'équation (22) serait inapplicable et la prédiction d'un état lié caduque. Plus généralement, pour pouvoir croire à (22) — c'est une condition nécessaire, il faut que l'hyperrayon R soit beaucoup plus grand que toute échelle de longueur apparaissant dans tout sous-système $(n_\uparrow, n_\downarrow)$ [avec $n_\uparrow \leq N_\uparrow$, $n_\downarrow \leq N_\downarrow$ et $n_\uparrow + n_\downarrow < N_\uparrow + N_\downarrow = N$], en particulier $R \gg b$ et $R \gg |r_e|$ pour $(n_\uparrow = 1, n_\downarrow = 1)$. Faut-il le préciser, la résonance à $(N_\uparrow, N_\downarrow)$ corps de la note 13 ne remet pas (22) et l'existence d'un nœud à l'hyperdistance ℓ en question puisque la longueur $\ell \gg b$ anormalement grande qui apparaît ne préexiste dans aucun sous-système.

Deuxième cas : $s^2 < 0$**.** Il y a là aussi deux valeurs possibles de l'exposant d'échelle, l'une $s = \mathrm{i}|s|$ dans $\mathrm{i}\mathbb{R}^+$ que nous convenons d'appeler s, et l'autre, son complexe conjugué $-\mathrm{i}|s|$, ou encore son opposé $-s$, dans $\mathrm{i}\mathbb{R}^-$. Comme dans le premier cas, on conclut qu'il existe une longueur ℓ, fonction des détails microscopiques de l'interaction, réglant l'amplitude relative des deux solutions :

$$\psi = [(R/\ell)^{\mathrm{i}|s|} - (R/\ell)^{-\mathrm{i}|s|}]R^{-\frac{3N-5}{2}}\Psi(\Omega) = 2\mathrm{i}\sin[|s|\ln(R/\ell)]R^{-\frac{3N-5}{2}}\Psi(\Omega) \tag{24}$$

Cette fois, les deux solutions sont de même module donc il faut les garder toutes les deux (aucune ne l'emporte sur l'autre dans la limite $b \to 0$) ! La longueur ℓ ne disparaît pas du problème mais définit dans la limite $b \to 0$ une condition de contact à N corps (24) qui brise explicitement l'invariance d'échelle continue de la limite unitaire. Comme ψ comporte un nombre infini de nœuds à une hyperdistance R arbitrairement grande — arbitrairement plus grande que la portée b de l'interaction — (voir l'écriture du troisième membre de l'équation (24)), il existe un nombre infini d'états liés à N corps sous la solution d'énergie $E = 0$; comme la condition aux limites (24) est invariante par changement de ℓ en $\exp(\pm\pi/|s|)\ell$, on passe d'un état N-mère à l'autre par une homothétie de rapport $\exp(\pi/|s|)$, le spectre correspondant formant une suite géométrique de limite nulle mais non bornée inférieurement dans la limite de portée nulle[15] :

$$E_n = -E_{\mathrm{glob}}\mathrm{e}^{-2\pi n/|s|}, \quad n \in \mathbb{N}^*, \quad \text{avec } E_{\mathrm{glob}} \approx \hbar^2/Mb^2 \tag{25}$$

Ces états liés à N corps, historiquement prédits par Efimov dans le cas $N = 3$, sont dits efimoviens. Il serait très intéressant de les stabiliser dans une expérience d'atomes froids (on vérifie malheureusement que, si $s \in \mathrm{i}\mathbb{R}^{+*}$ dans le problème à $(2,1)$ fermions, ce qui se produit pour $m_\uparrow/m_\downarrow > 13{,}6069\ldots$ comme nous le verrons, le taux de pertes à trois corps de l'équation (6) ne tend pas vers zéro lorsque $b \to 0$, mais plutôt vers une quantité proportionnelle à $\hbar k_{\mathrm{F}}^2/m$ dans le gaz homogène à $T = 0$, ce qui est considérable), par exemple en utilisant la note 6.

Mais revenons à notre problème mathématique : nous concluons que le gaz de $(N_\uparrow, N_\downarrow)$ fermions est stable pour une interaction $\uparrow\downarrow$ de portée nulle, et que l'hamiltonien du modèle de Wigner–Bethe–Peierls est auto-adjoint et borné inférieurement, si et seulement si les exposants d'échelle sont tous réels :

$$s \in \mathbb{R}^* \quad \forall s \text{ solution de } \Lambda_{N_\uparrow,N_\downarrow}(s) = 0 \tag{26}$$

Bien entendu, aucun sous-système $(n_\uparrow, n_\downarrow)$ du gaz ne doit non plus présenter d'effet Efimov, sinon (i) il faudrait introduire un paramètre à $n_\uparrow + n_\downarrow < N_\uparrow + N_\downarrow$ corps sur le modèle de l'équation (24) et l'invariance d'échelle à l'origine de la séparabilité (18), donc du résultat (26), serait brisée — on perdrait la séparabilité à toutes les distances, et (ii) le sous-système pourrait s'effondrer sur lui-même dans la limite $b \to 0$ d'une interaction de portée nulle et l'énergie ne serait pas bornée inférieurement. Sans le dire, nous avons effectué un raisonnement par récurrence et l'équivalent de la condition de stabilité (26) doit être satisfait pour tout nombre $n_\uparrow \le N_\uparrow$ et tout nombre $n_\downarrow \le N_\downarrow$.

Remarque 1. On pourrait ajouter $s = 0$ en troisième cas : c'est en fait précisément le seuil d'un effet Efimov. En développant l'équation (24) au premier ordre en $|s|$, on trouve que

$$\psi \propto \ln(R/\ell)R^{-\frac{3N-5}{2}}\Phi(\Omega) \tag{27}$$

c'est-à-dire que la longueur ℓ règle l'amplitude relative des solutions $R^{-(3N-5)/2}$ et $(\ln R)R^{-(3N-5)/2}$. Ceci ressemble furieusement à la définition de la longueur de diffusion de

[15] L'expression précise de E_{glob} en fonction de s et ℓ, et de l'ordre de $\hbar^2/Mb^2$ pour $\ell \approx b$, figure par exemple dans la référence [35]. Dans l'équation (25) nous prenons $n \ge 1$ (étant admis que $\exp(-2\pi/|s|) \ll 1$ — sinon le spectre ne serait pas entièrement géométrique [29]) car le modèle de Wigner–Bethe–Peierls ne peut s'appliquer qu'à un état lié de taille $\gg b$. On peut toutefois avoir $\ell \approx |r_{\mathrm{e}}| \gg b$ et $E_{\mathrm{glob}} \approx \hbar^2/Mr_{\mathrm{e}}^2 \ll \hbar^2/Mb^2$ sur une résonance de Feshbach étroite, voir notre note 6 ; même si ce n'est pas évident, l'exclusion de $n = 0$ dans (25) reste correcte dans ce cas [29,34]. Cette exclusion de $n = 0$ est cohérente avec l'absence d'état lié lorsque $s^2 \ge 0$, voir notre note 14 : du côté efimovien, l'ensemble du spectre discret doit tendre vers zéro lorsque $|s| \to 0$ sachant que E_{glob} a une limite finie et non nulle.

deux particules en dimension deux, voir par exemple la référence [36] et la contribution de Jan Solovej [17]. Cependant, dans le cas $\ell = O(b)$ où nous sommes, la longueur ℓ tend vers zéro lorsque $b \to 0$, la première solution — de coefficient $\ln(1/\ell) \to +\infty$ — l'emporte sur la deuxième et l'on garde la condition de contact à N corps dans la continuité de (23) :

$$\psi \underset{R\to 0}{\approx} R^{-(3N-5)/2} \tag{28}$$

Dans le modèle de portée nulle, il n'y a donc pas de brisure d'invariance d'échelle ni d'état lié au seuil efimovien[16,17].

Remarque 2. Nous avons pris ici $a = \infty$ pour simplifier mais si le système est instable pour $a = \infty$, il le restera pour a fini (toutes choses égales par ailleurs), car les N-mères efimoviens du gaz unitaire de taille $\ll |a|$ (il y en a autant qu'on veut pour $b \to 0$) ne font pas de différence entre une longueur de diffusion infinie et une longueur de diffusion finie a.

Complément. À la limite unitaire, la présente analyse se généralise à énergie E non nulle (toujours avec le centre de masse du système au repos). L'équation (18) devient

$$\psi = F(R) R^{-\frac{3N-5}{2}} \Phi(\Omega) \tag{29}$$

(elle satisfait aux conditions de contact de Wigner–Bethe–Peierls en vertu de la note 9) avec

$$EF(R) = -\frac{\hbar^2}{2M}\Delta_{2D}F(R) + \frac{\hbar^2 s^2}{2MR^2}F(R) \tag{30}$$

et Δ_{2D}, le laplacien à 2D pour la variable R, se réduit ici (en l'absence de dépendance angulaire) à $\mathrm{d}^2/\mathrm{d}R^2 + R^{-1}\mathrm{d}/\mathrm{d}R$. Le cas efimovien $s^2 < 0$ correspond donc simplement au problème connu de « chute sur le centre » dans un potentiel attractif en $1/R^2$ [38]. La séparabilité en coordonnées hypersphériques (29) s'étend même au cas piégé [27,28], il suffit d'ajouter le terme de piégeage $(1/2)M\omega^2 R^2 F(R)$ au second membre de l'équation (30), et de faire la substitution $E \to E - E_{\mathrm{cdm}}$, la valeur propre de l'équation sur $F(R)$ étant l'énergie interne par opposition à celle E_{cdm} du centre de masse. Pour $s^2 > 0$, ceci conduit au spectre

$$E - E_{\mathrm{cdm}} = (s + 1 + 2q)\hbar\omega, \quad q \in \mathbb{N} \tag{31}$$

3.3. *Ce qui est connu sur le domaine de stabilité*

Le problème de savoir si la condition de stabilité (26) est satisfaite peut être attaqué par deux extrémités opposées.

Par la première, on résout le problème à $(N_\uparrow, N_\downarrow)$ fermions à $E = 0$ dans le modèle de Wigner–Bethe–Peierls et on calcule les exposants d'échelle s (on procède analytiquement le plus loin possible mais il y a une dernière étape numérique, en tout cas pour $N > 3$). À notre connaissance, ce programme a été rempli dans le problème fermionique $(N_\uparrow > 1, N_\downarrow = 1)$ jusqu'à $N_\uparrow = 4$, voir la figure 3 : on trouve à chaque fois qu'un effet Efimov apparaît au-delà d'un rapport de masse critique $m_\uparrow/m_\downarrow$ (l'impureté $\downarrow$ doit être suffisamment légère), lui-même évidemment fonction

[16] Les considérations de la note 14 s'appliquent au seuil. En particulier, il ne faut pas croire à l'état lié d'énergie $\propto -\hbar^2/M\ell^2$ que l'équation (27) nous inciterait à prédire : il serait d'extension spatiale ℓ et ne pourrait être décrit par notre modèle de portée nulle lorsque $\ell \approx b$; il n'existerait pas non plus pour $(N_\uparrow = 2, N_\downarrow = 1)$ dans le cas — pourtant apparemment favorable — d'une résonance de Feshbach étroite où $\ell \approx |r_{\mathrm{e}}| \gg b$, voir la note 14 et les références [29,34].

[17] Le fait que $\ln(1/\ell)$ tende lentement vers l'infini lorsque $b \to 0$ n'est pas sans conséquence pratique : si l'on veut comparer aux expériences, il vaut mieux garder la contribution en $\ln R$ dans (27) [et le terme $(R/\ell)^{-s}$ dans (22) pour $s > 0$ assez proche de zéro] pour former la condition de contact à N corps. Ainsi, on trouve que le troisième coefficient d'amas $b_{2,1}$ défini dans la section 3.4 est en réalité une fonction régulière du rapport de masse $m_\uparrow/m_\downarrow$ donc de s^2, alors qu'il est de dérivée infinie en $s^2 = 0$ dans le modèle de portée nulle [35,37] donc dans l'équation (33).

FIGURE 3. Résultats connus sur la stabilité du système $(N_\uparrow, 1)$ de $N_\uparrow$ fermions de spin $\uparrow$ et un fermion de spin $\downarrow$, pour une interaction de portée nulle, en fonction du rapport de masse $m_\uparrow/m_\downarrow$ entre une particule $\uparrow$ et la particule $\downarrow$. Flèches verticales : valeurs critiques de $m_\uparrow/m_\downarrow$ (seuils) pour l'effet Efimov à $(N_\uparrow, 1)$ corps obtenues par résolution du problème correspondant, voir les références [39] pour $N_\uparrow = 2$, [30] pour $N_\uparrow = 3$, [40] pour $N_\uparrow = 4$; quand $m_\uparrow/m_\downarrow$ excède ces valeurs, l'énergie du système n'est plus bornée inférieurement. Barre verticale avec flèche horizontale : rapport de masse critique α_c, dont l'existence est établie par le théorème de Moser–Seiringer [41], en dessous duquel le système $(N_\uparrow, 1)$ est stable $\forall N_\uparrow$; le théorème ne donne pas la valeur exacte de α_c mais une minoration, $\alpha_c > 2{,}77$, plus contraignante que celle, $m_\uparrow/m_\downarrow = 1$, des expériences sur les atomes froids (une supériorité cependant de ces dernières est que le gaz unitaire de fermions semble y être stable, sans effondrement ni pertes à trois corps significatives, pour toutes les valeurs de $N_\uparrow$ et $N_\downarrow$).

décroissante de $N_\uparrow$ [18]. On remarque que les rapports de masse critiques successifs sont de plus en plus rapprochés; mathématiquement, on ne sait pas cependant si cette séquence continue (existe-t-il un effet Efimov à (5,1) corps? à (6,1) corps? etc.). Le cas $(N_\uparrow > 1, N_\downarrow = 2)$ a été étudié pour $N_\uparrow = 2$ par la référence [31] qui conclut à la stabilité, tant que les sous-systèmes (2,1) et (1,2) le sont.

Par la seconde extrémité, on cherche à contraindre (plutôt qu'à calculer) les rapports de masse critiques, par une minoration du spectre de l'hamiltonien. C'est ce qu'a fait la référence [41] pour le problème à $(N_\uparrow, N_\downarrow = 1)$ fermions : elle démontre le magnifique

Théorème. *Il existe un rapport de masse critique $m_\uparrow/m_\downarrow = \alpha_c$ en dessous duquel le système fermionique $(N_\uparrow, N_\downarrow = 1)$ est stable $\forall N_\uparrow$ pour une interaction de contact, et $\alpha_c > 1/0{,}36 = 2{,}77$.*

3.4. *Développement en amas ou du viriel*

Certains diront que c'est le problème macroscopique à N corps qui doit être en définitive l'objet de notre attention, plus que le problème à petit nombre de corps. Ce à quoi nous répondrons que le second peut dire quelque chose sur le premier au moyen du développement en amas, un développement de la pression P du gaz homogène à l'équilibre thermique grand-canonique en puissances des fugacités des composantes σ (la température $T = 1/k_B\beta$ est fixée mais les potentiels chimiques μ_σ tendent vers $-\infty$, ce qui correspond à une limite quantiquement non dégénérée) :

$$\frac{P\bar{\lambda}^3}{k_B T} = \sum_{(n_\uparrow, n_\downarrow) \in \mathbb{N}^{2*}} b_{n_\uparrow, n_\downarrow} \mathrm{e}^{\beta\mu_\uparrow n_\uparrow} \mathrm{e}^{\beta\mu_\downarrow n_\downarrow} \tag{32}$$

[18] Une fois qu'on a un effet Efimov dans le problème à $(N_\uparrow, N_\downarrow)$ fermions, comme nous l'avons dit après l'équation (26), on perd l'invariance d'échelle et on ne peut plus mettre en œuvre le raisonnement sous-tendu par les équations (18), (20) pour passer au problème à $(N_\uparrow + 1, N_\downarrow)$ ou $(N_\uparrow, N_\downarrow + 1)$ fermions; dans ce dernier, il n'y a plus de séparabilité en coordonnées (R, Ω) comme dans l'équation (24), plus de spectre géométrique (25) donc au sens strict, plus de possibilité d'effet Efimov!

où la longueur d'onde thermique de de Broglie est prise à la masse de référence arbitraire $\bar{m}$, $\bar{\lambda} = (2\pi\hbar^2/\bar{m}k_B T)^{1/2}$ [19]. Le développement (32), dans la littérature récente, est souvent confondu avec celui du viriel, qui développe en fait en puissances des densités $\rho_\sigma \lambda_\sigma^3$ dans l'espace des phases ($\lambda_\sigma = (2\pi\hbar^2/m_\sigma k_B T)^{1/2}$).

Comment calculer les coefficients d'amas $b_{n_\uparrow,n_\downarrow}$? À la limite unitaire $a^{-1} = 0$, le plus simple est d'utiliser la méthode du régulateur harmonique de la référence [43], qui place d'abord le système dans les pièges harmoniques $U_\sigma(\mathbf{r})$ de l'équation (2) puis, tous calculs faits, les ouvre pour retrouver le cas homogène par approximation d'homogénéité locale (exacte dans la limite considérée $\omega \to 0^+$). En effet, le problème piégé est alors séparable en coordonnées hypersphériques comme dans la section 3.2 et, si l'on connaît les exposants d'échelle s dans l'espace libre à énergie nulle pour tous les $n_\uparrow \leq n_\uparrow^{\text{cible}}, n_\downarrow \leq n_\downarrow^{\text{cible}}$, on connaît aussi les niveaux d'énergie du système piégé comme dans l'équation (31), donc toutes les fonctions de partition canoniques $Z_{n_\uparrow,n_\downarrow}$ et en définitive le coefficient $b_{n_\uparrow^{\text{cible}},n_\downarrow^{\text{cible}}}$. Du coup, les coefficients d'amas doivent être des fonctionnelles des $\Lambda_{n_\uparrow,n_\downarrow}$ de l'équation (21). C'est bien ce que prédit la conjecture de la référence [44], selon laquelle, à la limite unitaire,

$$b_{n_\uparrow,n_\downarrow} = \frac{(n_\uparrow m_\uparrow + n_\downarrow m_\downarrow)^{3/2}}{\bar{m}^{3/2}} \left[\int_{-\infty}^{+\infty} \frac{\mathrm{d}S}{4\pi} S \frac{\mathrm{d}}{\mathrm{d}S} (\ln \Lambda_{n_\uparrow,n_\downarrow}(\mathrm{i}S)) + \mathrm{CorrStat}_{n_\uparrow,n_\downarrow} \right] \tag{33}$$

pour tout $(n_\uparrow, n_\downarrow) \in \mathbb{N}^{*2} \setminus \{1,1\}$ [20]. Ici, le préfacteur résulte du passage du cas piégé au cas homogène et la première contribution entre crochets est calquée sur le résultat de la référence [45] obtenu pour $N = 3$; la seconde contribution entre crochets est une éventuelle correction de statistique quantique de type gaz parfait provenant des sous-amas non monoatomiques indiscernables en lesquels se découplent les états propres internes du système piégé $(n_\uparrow, n_\downarrow)$ à haute énergie (le centre de masse du système reste dans son état fondamental).

Expliquons mieux cette histoire de découplage en sous-amas sur des exemples. Si $(n_\uparrow, n_\downarrow) = (1,1)$, les états propres prennent asymptotiquement — pour des valeurs arbitrairement grandes de l'énergie — la forme de deux fermions ↑ et ↓ non corrélés dans des niveaux oscillatoires de grandes amplitudes[21] ; les sous-amas étant monoatomiques, on a CorrStat = 0. Si $(n_\uparrow, n_\downarrow) = (2,1)$, un nouveau découplage est possible, à côté de celui en trois fermions décorrélés : les particules peuvent se séparer en un atome ↑ et un pairon ↑↓ de fermions fortement corrélés (le mouvement relatif au sein du pairon restant de faible amplitude), avec des niveaux oscillatoires très excités pour l'atome ↑ et pour le centre de masse du pairon ↑↓ ; le pairon étant seul dans sa catégorie, on a là encore CorrStat = 0. La conclusion reste la même pour $(n_\uparrow, n_\downarrow) = (3,1)$, si ce n'est qu'apparaît le triplon ↑↑↓ comme nouveau sous-amas découplé. En revanche, pour $(n_\uparrow, n_\downarrow) = (2,2)$, il y a découplage possible en deux pairons ↑↓ de très grande énergie relative, voir la figure 4 ; ils n'interagissent plus mais ils sont indiscernables et conduisent, comme les bosons identiques d'un gaz parfait, à une correction de statistique quantique ignorée par l'intégrale sur S dans l'équation (33) ; le calcul donne CorrStat = 1/32 [44].

La conjecture (33) est bien établie pour $N = 3$, par application inverse du théorème des résidus, qui convertit la somme sur les spectres (31) donc sur les racines s de $\Lambda_{n_\uparrow,n_\downarrow}$ en une intégrale [45]. Pour $N = 4$, les propriétés analytiques de la fonction $\Lambda_{n_\uparrow,n_\downarrow}$ dans le plan complexe

[19] La référence [42] utilise le choix $\bar{m}^{3/2} = (m_\uparrow^{3/2} + m_\downarrow^{3/2})/2$, naturel au sens où il conduit à un premier coefficient d'amas total $b_1 = (b_{1,0} + b_{0,1})/2$ égal à un.

[20] Le cas $(n_\uparrow = 1, n_\downarrow = 1)$ est différent et doit être exclu ; il correspond, au contraire de ce que nous avons supposé, à une résonance de diffusion à N corps avec $N = 2$ dans l'onde s : à la limite unitaire, il faut garder uniquement la solution en R^{-s}, $s = 1/2$, dans l'équation (22), comme si la bonne racine de Λ à garder était $-s$; en effet, la solution en R^s correspond à la partie régulière $\propto 1/a$ de l'état de diffusion à énergie nulle (voir la note 11 pour plus de précisions).

[21] Si le nombre d'onde relatif $k_{\text{rel}} \to +\infty$, l'amplitude de diffusion $f_{k_{\text{rel}}} \to 0$ dans l'équation (11) donc même à la limite unitaire, les interactions deviennent négligeables.

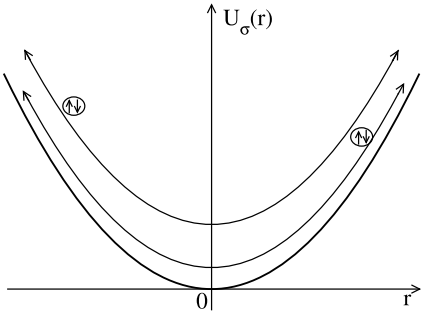

FIGURE 4. Un comportement asymptotique possible du problème unitaire à quatre fermions ($N_\uparrow = 2, N_\downarrow = 2$) dans les potentiels harmoniques $U_\sigma(\mathbf{r})$: deux pairons oscillent furieusement (avec des mouvements de grande amplitude) ; les fermions $\uparrow$ et $\downarrow$ dans chaque pairon ont une énergie relative $O(1)$ (en unités de $\hbar\omega$ si l'on veut respecter la dimension) et restent fortement corrélés ; les deux pairons ont une énergie relative $\to +\infty$ et sont découplés, ce qui autorise à les voir comme deux bosons identiques, dotés d'une structure interne (celle du mouvement relatif $\uparrow\downarrow$ au sein d'un pairon) mais n'interagissant pas entre eux. La correction de statistique quantique $\mathrm{CorrStat}_{2,2}$ est alors non nulle dans l'équation (33).

ne sont pas suffisamment connues pour qu'on puisse appliquer le théorème de Cauchy[22] ; dans le cas particulier $m_\uparrow/m_\downarrow = 1$, la conjecture a cependant été confirmée par un calcul très précis de Monte-Carlo quantique à petit nombre de corps [46] (en revanche, les valeurs expérimentales [47,48] ne sont pas confirmées, le problème semblant venir de l'impossibilité d'obtenir le bon polynôme de degré 4 en $z = \exp(\beta\mu)$ par ajustement de la pression P ou de la densité ρ mesurées sur l'intervalle de fugacité accessible expérimentalement [49])[23].

La démonstration de l'expression (33) dans le cas général reste donc ouverte. Une autre question intéressante porte sur le comportement des coefficients d'amas $b_{n_\uparrow,n_\downarrow}$ aux grands ordres $n_\sigma \to +\infty$, dont la connaissance est requise si l'on veut effectuer une sommation efficace de la série (32) après calcul de ses premiers termes, pour étendre son applicabilité au régime dégénéré $T \lesssim T_\mathrm{F}$ (par exemple, si le rayon de convergence est nul, on pourrait mettre en œuvre une resommation de type Borel conforme comme dans les références [50,51]).

4. Questions ouvertes dans un point de vue macroscopique

Dans cette section, le gaz de fermions en interaction, considéré dans la limite thermodynamique et à température non nulle mais arbitrairement basse, est décrit par une théorie hamiltonienne effective de basse énergie, l'hydrodynamique quantique de Landau et Khalatnikov [52][24].

[22] Il faut pouvoir rabattre sur l'axe imaginaire pur le chemin d'intégration entourant les racines et les pôles de $\Lambda_{n_\uparrow,n_\downarrow}$ sur l'axe réel sans croiser de singularité — pôle ou ligne de coupure — dans les demi-plans supérieur et inférieur.

[23] Les références [47,48] ont accès seulement au quatrième coefficient d'amas total $b_4 = (b_{4,0} + b_{3,1} + b_{2,2} + b_{1,3} + b_{0,4})/2$, ce qui interdit une comparaison avec la conjecture (33) secteur par secteur.

[24] L'appellation « hydrodynamique quantique », en physique non linéaire, est comprise par opposition à l'hydrodynamique des fluides classiques et fait référence à une équation d'Euler portant sur un champ de vitesse $\mathbf{v}(\mathbf{r})$ à valeurs réelles plutôt qu'opératorielles, mais contenant un terme de pression quantique $\propto \hbar^2$, ce qui lui permet de décrire le mouvement de tourbillons quantiques — à circulation quantifiée — dans le superfluide (comme l'équation de Gross–Pitayevski sur la fonction d'onde d'un condensat de bosons réécrite en termes de la densité et du gradient de la phase). Ici, l'appellation est à prendre au sens de la seconde quantification, le champ de vitesse étant désormais à valeur opérateur $\hat{\mathbf{v}}(\mathbf{r})$.

4.1. *Vue d'ensemble du régime superfluide considéré*

Le système tridimensionnel de fermions est ici spatialement homogène (dans un volume de quantification $[0,L]^3$ proche de la limite thermodynamique, cette limite étant prise à la fin des calculs), avec des particules de masses égales $m_\uparrow = m_\downarrow = m$ dans les deux états internes, non polarisé en spin (il y a le même nombre de particules dans les deux composantes, $N_\uparrow = N_\downarrow$, afin de permettre un appariement complet) et à l'équilibre thermique canonique dans une limite de basse température ($T \neq 0$ mais $T \to 0$).

Dans ces conditions, (i) les fermions s'assemblent en paires liées $\uparrow\downarrow$ dans l'onde s ; en présence des mers de Fermi dans les deux états internes, c'est ce à quoi conduit l'interaction attractive entre $\uparrow$ et $\downarrow$ de la section 3, au travers du célèbre mécanisme de Cooper ; ceci vaut donc même pour une longueur de diffusion a négative, où il n'y a pas d'état lié $\uparrow\downarrow$ dans l'espace libre, la taille d'une paire tendant toutefois vers $+\infty$ lorsque $a \to 0^-$ (dans le cas $a > 0$, il existe bien un état dimère et, sans surprise, c'est à lui que se réduit l'état de paire liée dans la limite de basse densité $\rho \to 0$)[25] ; (ii) ces paires liées, étant des sortes de bosons composites, forment un condensat dans le mode de vecteur d'onde $\mathbf{K}_{\text{paire}} = \mathbf{0}$ de leur centre de masse (de longueur de cohérence limitée par la taille de la boîte, infinie à la limite thermodynamique) et un superfluide.

Du coup, on s'attend à ce que le système admette, dans son état fondamental, une branche d'excitation acoustique (par ondes sonores) de départ linéaire en le nombre d'onde q avec une correction cubique,

$$\omega_{\mathbf{q}} \underset{q\to 0}{=} cq\left[1+\frac{\gamma}{8}\left(\frac{\hbar q}{mc}\right)^2+O(q^4\ln q)\right] \tag{34}$$

et que cette branche soit limitée supérieurement en énergie par le continuum de paire brisée, de bord inférieur l'énergie de liaison d'une paire E_{paire}, comme sur la figure 5a. Ici $\omega_{\mathbf{q}}$ est la pulsation propre au vecteur d'onde $\mathbf{q}$, c est la vitesse du son à température nulle et le paramètre de courbure γ est adimensionné de façon qu'il vaille un dans la limite $k_F a \to 0^+$ d'un gaz condensé de dimères en interaction faible (en accord avec la théorie de Bogolioubov)[26]. La branche en question est souvent dite de Goldstone [55], parce qu'on l'associe à la brisure de symétrie $U(1)$ dans la condensation de paires ; son pendant de Higgs est discuté dans la section 5.

Notre régime de basse température satisfait dans la suite aux deux conditions

$$0 < k_B T \ll mc^2 \quad \text{et} \quad 0 < k_B T \ll E_{\text{paire}} \tag{35}$$

la première assurant que soit peuplée thermiquement seulement la partie linéaire de la branche acoustique, la seconde qu'il y ait une densité négligeable de paires brisées (d'après la loi de Boltzmann, cette densité comporte un facteur d'activation $\exp(-E_{\text{paire}}/2k_B T)$, les fragments issus de la dissociation d'une paire liée — les quasi-particules fermioniques χ de la figure 5b — ayant individuellement une énergie minimale $E_{\text{paire}}/2$). Notre système se réduit alors à un gaz thermique de phonons, si l'on convient d'appeler comme tels les quanta de la branche acoustique (eu égard à son départ linéaire)[27].

[25] Il n'est pas complètement évident de voir que l'interaction de contact de Wigner–Bethe–Peierls est attractive. Une façon de faire est de l'obtenir comme la limite continue $b \to 0$ d'un modèle sur un réseau cubique $b\mathbb{Z}^3$ avec un couplage $\propto \hbar^2/mb^2$ entre sites voisins (pour représenter l'énergie cinétique) et une interaction sur site g_0/b^3 ; à longueur de diffusion $a \neq 0$ fixée, on trouve alors que $g_0 \approx -\hbar^2 b/m < 0$ lorsque $b \to 0$ (la constante de couplage nue g_0 est donc, dans le régime $b \ll |a|$ de la diffusion résonnante, fort différente de la constante de couplage effective $g = 4\pi\hbar^2 a/m$) [53].

[26] Notre convention de signe sur γ diffère de celle utilisée dans l'hélium 4 liquide, voir la référence [54].

[27] L'équation (34) ne vaut que pour une interaction $V(\mathbf{r}_{ij})$ à courte portée, décroissant assez vite lorsque $r_{ij} \to +\infty$. Dans le cas d'une interaction dipolaire, comme dans les gaz d'atomes froids magnétiques, la vitesse du son est anisotrope [58], voir aussi la contribution de Wilhelm Zwerger à ce dossier thématique [59] et le cours 2023-2024 de Jean Dalibard au Collège de France [60]. Dans le cas d'une interaction coulombienne, comme dans les gaz d'électrons supraconducteurs, la branche acoustique fait place à une branche de plasmons à bande interdite (la pulsation propre $\omega_{\mathbf{q}}$ a une limite > 0 en $q = 0$) [61]. Ici, nos atomes sont neutres et de moment dipolaire négligeable.

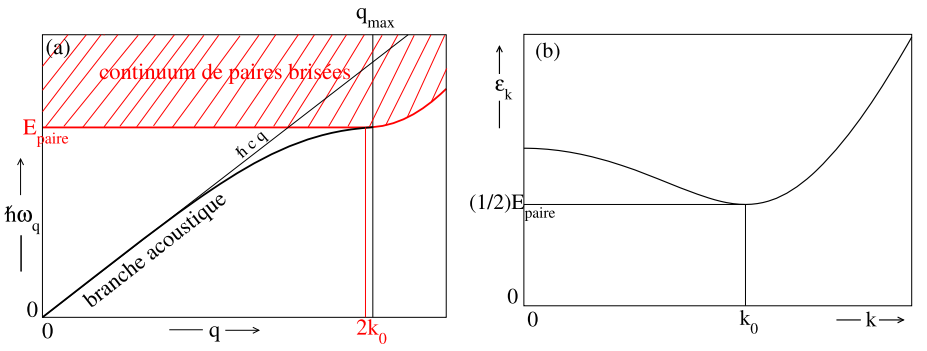

FIGURE 5. Énergie de différents types d'excitations d'un gaz homogène non polarisé de fermions à deux composantes à température nulle, en fonction de leur nombre d'onde q ou k. (a) Branche d'excitation acoustique $\hbar\omega_{\mathbf{q}}$ de départ linéaire $\hbar cq$ (c est la vitesse du son), limitée supérieurement par le continuum de paire brisée (zone hachurée) dont elle vient ici tangenter le bord inférieur en le point terminal de nombre d'onde $q_{\max}$. (b) Relation de dispersion $\varepsilon_{\mathbf{k}}$ d'une quasi-particule fermionique χ (voir texte). Sous l'effet d'une excitation percussionnelle de vecteur d'onde $\mathbf{q}$, une paire liée $\uparrow\downarrow$ du condensat de paires, initialement au repos, se dissocie en deux quasi-particules fermionique χ de spins opposés, de vecteurs d'onde $\mathbf{k}$ et $\mathbf{k}' = \mathbf{q} - \mathbf{k}$ et d'énergies $\varepsilon_{\mathbf{k}}$ et $\varepsilon_{\mathbf{k}'}$; comme le vecteur $\mathbf{k}$ n'est pas contraint (pas de conservation de l'énergie pour une excitation percussionnelle), il apparaît un continuum d'énergies finales $\{\varepsilon_{\mathbf{k}} + \varepsilon_{\mathbf{q}-\mathbf{k}}, \mathbf{k} \in \mathbb{R}^3\}$. Pour la force des interactions choisie sur la figure ($|\Delta|/\mu = 0{,}84$ soit $1/k_F a \simeq -0{,}16$ d'après la théorie BCS, avec μ le potentiel chimique du gaz et Δ le paramètre d'ordre complexe du condensat de paires), la branche acoustique est de départ concave ($\gamma < 0$ dans l'équation (34)) et la relation de dispersion $\varepsilon_{\mathbf{k}}$ présente un minimum $E_{\text{paire}}/2$ en $k = k_0 > 0$; le bord inférieur du continuum vaut donc exactement E_{paire}, du moins tant qu'on peut avoir $k = k' = k_0$ donc tant que $q = |\mathbf{k} + \mathbf{k}'| \leq 2k_0$. Les relations de dispersion représentées, approchées, sont celles de la théorie BCS pour $\varepsilon_{\mathbf{k}}$ et de la RPA d'Anderson pour $\hbar\omega_{\mathbf{q}}$. Selon la force des interactions, le domaine d'existence en q de la branche acoustique peut également être non compact, connexe $q \in]0, +\infty[$ ou pas $q \in]0, q_{\max}[\bigcup]q_{\min}, +\infty[$ ($q_{\min} > q_{\max}$) [56] ; la concavité de la branche est elle aussi variable [57] ; enfin, $k_0 = 0$ et $E_{\text{paire}} = 2(\mu^2 + |\Delta|^2)^{1/2}$ si $\mu < 0$, $k_0 = (2m\mu)^{1/2}/\hbar$ et $E_{\text{paire}} = 2|\Delta|$ sinon.

On peut alors se poser trois types de questions, partiellement ouvertes :

(1) nous allons le voir, les phonons (abrégés en ϕ) interagissent entre eux, le superfluide de fermions sous-jacent constituant un milieu non linéaire pour le son. Quels sont les effets de ces interactions sur les phonons de vecteur d'onde $\mathbf{q}$? On s'attend en particulier à ce qu'ils s'amortissent avec un taux $\Gamma_{\mathbf{q}}(T)$ et qu'ils subissent un déplacement de pulsation thermique $\Delta_{\mathbf{q}}(T)$ (on ne compte pas le déplacement à température nulle, qui donne naissance par définition au spectre (34) — le terme négligé en $q^5 \ln q$ provient précisément de l'effet croisé des interactions et des fluctuations quantiques du champ de phonons [62,63])[28].

[28] Dans le cas convexe $\gamma > 0$, il s'accompagne — toujours à $T = 0$ — d'une partie imaginaire non nulle $\approx q^5$, correspondant au mécanisme d'amortissement de Belyaev $\mathbf{q} \to \mathbf{k}, \mathbf{k}'$, voir plus loin.

(2) quelles sont les conséquences de la dynamique collisionnelle des phonons sur l'évolution d'une variable macroscopique du gaz particulièrement intéressante, l'opérateur phase $\hat{\phi}_0(t)$ du condensat de paires ?

(3) on enrichit le problème en considérant le cas partiellement polarisé $N_\uparrow \neq N_\downarrow$. Dans le cas faiblement polarisé, par exemple $N_\uparrow - N_\downarrow = O(1)$, les fermions non appariés (car surnuméraires) de la composante de spin majoritaire forment, dans le gaz en interaction, des quasi-particules fermioniques (abrégées en χ) d'une relation de dispersion $\varepsilon_{\mathbf{k}}$ différente de celles des fermions libres : elle présente notamment un minimum non nul, donc une bande d'énergie interdite, donné par la demi-énergie de liaison d'une paire $\uparrow\downarrow$, au voisinage duquel elle varie quadratiquement en nombre d'onde k (voir la figure 5b). Se pose alors la question de leurs interactions $\phi - \chi$ avec les phonons et $\chi - \chi$ entre elles ; en particulier, un désaccord persiste sur l'expression de l'amplitude de diffusion $\phi - \chi$ à basse énergie (les références [64] et [65] diffèrent)[29]. Dans le cas fortement polarisé, où $N_\uparrow - N_\downarrow$ est extensif comme N, on s'attend à ce que la condensation des paires liées à $T = 0$ puisse se faire dans une superposition d'ondes planes de leur centre de masse (plutôt que dans $\mathbf{K}_{\text{paire}} = \mathbf{0}$ comme supposé ici), voir les références [66,67], ce qui donne naissance à un superfluide modulé spatialement (un supersolide suivant la terminologie à la mode), sans que son domaine d'existence dans l'espace des paramètres $((N_\uparrow - N_\downarrow)/N, 1/k_F a, T/T_F)$ soit parfaitement bien connu théoriquement, le problème étant complexifié par sa grande sensibilité aux fluctuations thermiques [68] (il n'y a pas encore de résultats expérimentaux dans les gaz d'atomes froids tridimensionnels [69]).

Le cas le plus intéressant pour les points 1 et 2 est celui d'une branche acoustique de départ concave, $\gamma < 0$ dans l'équation (34), très différent du gaz de bosons en interaction faible assez bien connu (où $\gamma \simeq 1 > 0$ comme nous l'avons dit)[30]. En particulier, l'amortissement des phonons pour $\gamma < 0$ peut se produire seulement à $T \neq 0$, puisque la désintégration d'un phonon en un nombre quelconque $n > 1$ de phonons est interdite par la conservation de l'énergie-impulsion pour une branche acoustique concave ; à l'ordre dominant en température, il résulte pour la même raison, non pas comme pour $\gamma > 0$ de processus à trois phonons de type Belyaev $\phi \to \phi\phi$ ou Landau $\phi\phi \to \phi$ [70,71], mais des processus à quatre phonons $\phi\phi \to \phi\phi$ de Landau et Khalatnikov [52]. À notre connaissance, cet amortissement à quatre phonons n'a encore été observé expérimentalement dans aucun système. Il pourrait l'être dans un gaz d'atomes froids fermioniques dans une boîte de potentiel [72]. Il pourrait l'être aussi dans l'hélium 4 superfluide (un liquide de bosons) si l'on augmente suffisamment la pression pour rendre $\gamma < 0$ (le minimum de roton s'abaisse ce qui finit par rendre concave le départ de la branche acoustique) et si l'on abaisse suffisamment la température pour réduire la densité de rotons (au travers du facteur

[29] Ce problème intéresse également l'hélium 4 superfluide, dont la branche d'excitation admet elle aussi un minimum quadratique, le minimum de roton ; notre problème de diffusion $\phi - \chi$ est donc formellement équivalent à la diffusion roton–phonon étudiée déjà dans la référence [52], à la différence près que les rotons sont des bosons. Les prédictions de [52] sont cependant incomplètes et en désaccord avec [64,65].

[30] Qualitativement, ce cas $\gamma < 0$ s'obtient lorsque l'énergie de liaison E_{paire} est assez faible : si l'on réduit E_{paire}, le continuum de paire brisée sur la figure 5a s'abaisse, pousse sur la branche acoustique et finit par la faire se courber vers le bas. C'est certainement le cas dans la limite BCS $k_F a \to 0^-$ où $E_{\text{paire}}/mc^2 = O(\exp(-\pi/2k_F|a|))$ tend rapidement vers zéro ; ce n'est plus le cas dans la limite CBE $k_F a \to 0^+$ où $E_{\text{paire}} \sim E_{\text{dim}} = \hbar^2/ma^2 \gg mc^2$. On ne sait pas avec certitude de quel côté de la limite unitaire $1/k_F a = 0$ (c'est-à-dire pour quel signe de la longueur de diffusion a) se produit le changement de signe du paramètre de courbure γ, voir la section 5. Vu la forme du bord inférieur du continuum sur la figure 5a — et ceci indépendamment du signe de γ, l'effet de répulsion sur la branche acoustique est le plus fort à grand q mais le plus faible à petit q (là où la différence d'énergie entre le bord et la branche est le plus grand). On s'attend donc à avoir un intervalle de valeurs de $1/k_F a$ sur lequel la branche, convexe à faible q, est concave à grand q [57].

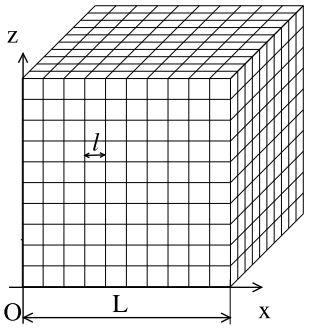

FIGURE 6. Découpage du gaz en portions cubiques mésoscopiques de côté ℓ, dans l'hydrodynamique quantique de Landau et Khalatnikov (cette théorie effective ne décrit pas les échelles de longueur $< \ell$). Voir texte pour le choix de ℓ.

d'activation $\exp(-E_{\rm roton}/k_{\rm B}T)$) et rendre négligeable l'amortissement parasite des phonons par les rotons [73][31].

4.2. *Quelle théorie macroscopique utiliser ?*

Une théorie effective de basse énergie renonce à décrire le système en dessous d'une certaine échelle de longueur ℓ ; on s'attend en revanche à ce que la théorie soit exacte aux grandes longueurs d'onde, ici à l'ordre dominant en température.

Dans ces conditions, il est légitime de découper le gaz en portions de taille ℓ, par exemple en boîtes cubiques de côté ℓ centrées sur le réseau cubique $\ell\mathbb{Z}^3$, voir la figure 6. Énonçons quelques contraintes sur le choix de ℓ :

(1) on doit avoir $\ell \gg \xi$ (ici $\xi = \hbar/mc$ est la longueur dite de relaxation ou de corrélation du superfluide) et $\rho\ell^3 \gg 1$ (il y a un grand nombre de fermions par site) de façon que (i) chaque portion cubique puisse être considérée comme mésoscopique et relever de la notion d'équation d'état liant de manière univoque la pression ou le potentiel chimique à la densité (comme c'est le cas à la limite thermodynamique), et (ii) le pas ℓ du réseau fournisse une coupure en nombre d'onde $\pi/\ell \ll mc/\hbar$ aux excitations phononiques du gaz, les restreignant ainsi à la partie quasi linéaire de la branche (34), partie universelle car décrite par deux paramètres, c et γ.

(2) on doit avoir $k_{\rm B}T \ll \hbar c\pi/\ell$ (c'est l'énergie du mode de phonons fondamental dans une portion) de façon qu'on puisse considérer que (i) chaque portion est à température nulle, et (ii) chaque portion est spatialement homogène à l'échelle de la longueur d'onde typique $q_{\rm th}^{-1} = \hbar c/k_{\rm B}T$ des ondes sonores thermiques.

(3) il faut aussi que $\ell \ll \ell_{\rm coh}$ où $\ell_{\rm coh}$ est la longueur de cohérence des paires de fermions, de façon que la notion de phase globale $\hat\phi$ ait un sens dans chaque portion (comme pour un condensat). Cette contrainte est inopérante ici puisque $\ell_{\rm coh} \approx L$ (les paires liées sont condensées à 3D).

On admet alors qu'on peut représenter le système par deux opérateurs de champ, le champ de densité $\hat\rho(\mathbf{r})$ et le champ de phase $\hat\phi(\mathbf{r}')$, avec $\mathbf{r},\mathbf{r}' \in \ell\mathbb{Z}^3$; ces variables sont canoniquement conjuguées au sens où

$$[\hat\rho(\mathbf{r})\ell^3, \hat\phi(\mathbf{r}')] = \mathrm{i}\,\delta_{\mathbf{r},\mathbf{r}'} \tag{36}$$

[31] Dans l'hélium 4 liquide, les processus de diffusion à quatre phonons entre des faisceaux de phonons produits intentionnellement (non thermiques) ont déjà fait l'objet d'études théoriques et expérimentales [74].

comme si $\hat\phi$ était un opérateur impulsion et $\hat\rho\ell^3$ un opérateur position en mécanique quantique ordinaire [52,75][32]. Le champ de phase donne accès au champ de vitesse par simple différentiation (il s'agit ici d'un gradient discret)[33] :

$$\hat{\mathbf{v}}(\mathbf{r}) = \frac{\hbar}{m}\mathbf{grad}\,\hat\phi(\mathbf{r}) \tag{37}$$

L' hamiltonien s'obtient en sommant l'énergie interne et l'énergie cinétique associée à la vitesse locale d'écoulement du fluide dans chaque portion :

$$H = \sum_{\mathbf{r}} \frac{1}{2} m\hat{\mathbf{v}}(\mathbf{r})\cdot\hat\rho(\mathbf{r})\ell^3\hat{\mathbf{v}}(\mathbf{r}) + \ell^3 e_0(\hat\rho(\mathbf{r})) \tag{38}$$

En effet, $e_0(\rho)$ est ici l'énergie volumique à température nulle du gaz homogène de fermions de densité ρ, et $m\hat\rho(\mathbf{r})\ell^3$ est la quantité de matière (la masse) dans la portion centrée en $\mathbf{r}$. Les équations du mouvement sur $\hat\rho$ et $\hat{\mathbf{v}}$ en point de vue de Heisenberg dérivant de l'hamiltonien H prennent la forme d'une équation de continuité et d'une équation d'Euler (sans terme de viscosité) à valeur opérateur[34], d'où le nom d'hydrodynamique quantique donné à la théorie (avec le risque de confusion signalé dans la note 24).

On l'aura compris, la grande force de cette théorie effective est qu'elle ne dépend pas de la nature des particules bosoniques ou fermioniques constituant le superfluide sous-jacent, ni de leurs interactions (fortes ou faibles, en phase liquide ou gazeuse) pourvu qu'elles restent à courte portée, si ce n'est au travers de l'équation d'état $e_0(\rho)$ et du paramètre de courbure γ à température nulle. Elle s'applique donc également bien aux gaz de bosons en interaction faible, aux gaz de fermions en interaction forte et à l'hélium 4 liquide (système pourtant extrêmement dense, défiant toute théorie microscopique).

Il ne faut cependant croire au formalisme que dans une limite de basse température, $T\to 0$, où les fluctuations spatiales de densité sont faibles et les gradients de phase aussi ; on doit donc développer l'équation (38) jusqu'à l'ordre pertinent (ici l'ordre quatre) en puissances de

$$\delta\hat\rho(\mathbf{r}) \equiv \hat\rho(\mathbf{r}) - \hat\rho_0 \quad\text{et}\quad \delta\hat\phi(\mathbf{r}) \equiv \hat\phi(\mathbf{r}) - \hat\phi_0 \tag{39}$$

où $\hat\rho_0$ et $\hat\phi_0$ sont les composantes de Fourier des champs $\hat\rho(\mathbf{r})$ et $\hat\phi(\mathbf{r})$ de vecteur d'onde nul (physiquement, $\hat\rho_0 = \hat N/L^3$ où $\hat N$ est l'opérateur nombre total de fermions, L^3 est le volume de la boîte de quantification $[0,L]^3$ et $\hat\phi_0$ est l'opérateur phase du condensat de paires liées [76]). L'hamiltonien développé s'écrit formellement

$$H = H_0 + H_2 + H_3 + H_4 + \cdots \tag{40}$$

où H_n est la contribution de degré total n en $\delta\hat\rho$ et $\delta\hat\phi$.

---

[32] Ces références historiques se placent pour simplifier dans un espace continu. La nécessité de discrétiser l'espace pour éviter les infinis et rendre la théorie renormalisable est souligné dans la publication [76]. Ici, nous mettons ces difficultés sous le tapis ; par exemple, nous ne distinguons pas dans (38) entre la notion d'équation d'état nue $e_{0,0}(\rho)$ — celle qui entre dans l'hamiltonien — et l'équation d'état vraie ou effective $e_0(\rho)$ — celle qu'on observe dans une expérience.

[33] Le fait que l'opérateur champ de vitesse soit un vecteur gradient ne signifie nullement que l'écoulement soit entièrement superfluide (ceci serait d'ailleurs physiquement faux même à l'équilibre thermique, à température non nulle). Expliquons-le en deux remarques. (i) On ne confondra pas l'opérateur $\hat{\mathbf{v}}(\mathbf{r})$ de l'hydrodynamique quantique (qui contient toutes les fluctuations quantiques et thermiques possibles) avec le champ de vitesse moyen $\mathbf{v}(\mathbf{r})$ de l'hydrodynamique ordinaire ; en particulier, le caractère superfluide ou pas de l'écoulement dépend du caractère irrotationnel ou pas de $\mathbf{v}(\mathbf{r})$ (sans chapeau). (ii) En général, on a $\mathbf{v}(\mathbf{r}) \neq \langle\hat{\mathbf{v}}(\mathbf{r})\rangle$ où la moyenne est prise dans l'état quantique du système, car $\mathbf{v}(\mathbf{r})$ est défini en termes de la densité moyenne de courant de matière, $\mathbf{v}(\mathbf{r}) = \langle\hat{\mathbf{j}}(\mathbf{r})\rangle/\langle\hat\rho(\mathbf{r})\rangle$ avec ici $\hat{\mathbf{j}}(\mathbf{r}) = [\hat\rho(\mathbf{r})\hat{\mathbf{v}}(\mathbf{r}) + \hat{\mathbf{v}}(\mathbf{r})\hat\rho(\mathbf{r})]/2$ (par définition, l'équation d'évolution de $\hat\rho$ en point de vue de Heisenberg s'écrit $\partial_t\hat\rho + \mathrm{div}\,\hat{\mathbf{j}} = 0$ et celle de la densité moyenne $\rho(\mathbf{r}) = \langle\hat\rho(\mathbf{r})\rangle$ s'écrit $\partial_t\rho + \mathrm{div}(\rho\mathbf{v}) = 0$) ; il serait donc faux de croire que $\mathbf{v}(\mathbf{r}) = (\hbar/m)\mathbf{grad}\langle[\hat\phi(\mathbf{r}) - \hat\phi(\mathbf{r}_0)]\rangle$ (où $\mathbf{r}_0$ est une position de référence arbitraire) et d'en déduire que $\mathbf{v}(\mathbf{r})$ est forcément un vecteur gradient.

[34] Voir la note 33 pour l'équation sur $\hat\rho(\mathbf{r})$. L'équation sur $\hat{\mathbf{v}}(\mathbf{r})$ s'obtient en prenant le gradient de celle sur $\hat\phi(\mathbf{r})$, $\hbar\partial_t\hat\phi = -\mu_0(\hat\rho) - m\hat{\mathbf{v}}^2/2$ où $\mu_0(\rho)$ est la fonction potentiel chimique à température nulle comme dans l'équation (43).

La contribution d'ordre 0 H_0 est une constante sans grand intérêt ; celle d'ordre 1 est exactement nulle (car $\sum_{\mathbf{r}} \ell^3 \delta\hat{\rho}(\mathbf{r}) = 0$ par construction) et a été directement omise dans l'équation (40). La contribution quadratique H_2 se diagonalise par transformation de Bogolioubov[35] :

$$H_2 = \text{cte} + \sum_{\mathbf{k}\neq\mathbf{0}} \hbar\omega_{\mathbf{k}} \hat{b}^\dagger_{\mathbf{k}} \hat{b}_{\mathbf{k}} \tag{41}$$

où les opérateurs de création $\hat{b}^\dagger_{\mathbf{k}}$ et d'annihilation $\hat{b}_{\mathbf{k}}$ d'une excitation élémentaire (un phonon) de vecteur d'onde $\mathbf{k}$ obéissent aux habituelles relations de commutation bosoniques

$$[\hat{b}_{\mathbf{k}}, \hat{b}_{\mathbf{k}'}] = 0 \quad \text{et} \quad [\hat{b}_{\mathbf{k}}, \hat{b}^\dagger_{\mathbf{k}'}] = \delta_{\mathbf{k},\mathbf{k}'} \tag{42}$$

Le spectre obtenu est ici exactement linéaire, $\omega_{\mathbf{k}} = ck$, avec la vitesse du son donnée par

$$mc^2 = \rho \frac{\mathrm{d}^2}{\mathrm{d}\rho^2} e_0(\rho) = \rho \frac{\mathrm{d}}{\mathrm{d}\rho} \mu_0(\rho) \tag{43}$$

où $\mu_0(\rho)$ est le potentiel chimique à température nulle du gaz de fermions de densité ρ. La relation (43) est exacte (c'est celle bien connue de l'hydrodynamique des superfluides [75]) mais l'absence systématique de courbure dans le spectre n'est pas réaliste physiquement : cette pathologie vient du fait que nous avons omis dans l'hamiltonien H des corrections dites de gradient [77] ; pour simplifier, comme l'ont fait d'illustres prédécesseurs [52], nous remplaçons ici $\omega_{\mathbf{k}}$ dans H_2 à la main par son approximation cubique (34), ce que justifie d'ailleurs la référence [78].

L'approximation H_2 correspond à un gaz parfait de phonons, et ne peut décrire l'atténuation du son. L'interaction entre phonons à l'origine de leur amortissement provient des contributions cubique H_3 et quartique H_4. Pour alléger, nous donnons ici seulement l'expression de la partie la plus utile de H_3, et encore en la simplifiant, pour bien faire comprendre la physique :

$$H_3|_{\text{simpl}} = \frac{\mathscr{A}}{2L^{3/2}} \sum_{\mathbf{k},\mathbf{k}',\mathbf{q}} (kk'q)^{1/2} \hat{b}^\dagger_{\mathbf{k}} \hat{b}^\dagger_{\mathbf{k}'} \hat{b}_{\mathbf{q}} \delta_{\mathbf{k}+\mathbf{k}',\mathbf{q}} + (k'kq)^{1/2} \hat{b}^\dagger_{\mathbf{k}'} \hat{b}_{\mathbf{k}} \hat{b}_{\mathbf{q}} \delta_{\mathbf{k}',\mathbf{k}+\mathbf{q}} + \cdots \tag{44}$$

avec l'amplitude constante (indépendante des nombres d'onde) mise en facteur,

$$\mathscr{A} = (\xi/2)^{3/2} \rho^{-1/2} \left[3mc^2 + \rho^2 \frac{\mathrm{d}^3}{\mathrm{d}\rho^3} e_0(\rho) \right] \tag{45}$$

et $\xi = \hbar/mc$ comme précédemment[36]. L'ellipse dans l'équation (44) contient des termes en $\hat{b}^\dagger\hat{b}^\dagger\hat{b}^\dagger$ et $\hat{b}\hat{b}\hat{b}$ sans grande importance car ils ne conservent pas l'énergie H_2. Les contributions en $\hat{b}^\dagger\hat{b}^\dagger\hat{b}$ et en $\hat{b}^\dagger\hat{b}\hat{b}$ sont en revanche centrales dans l'amortissement : elles correspondent respectivement aux processus de Belyaev (le phonon $\mathbf{q}$ se désintègre en deux phonons $\mathbf{k}$ et $\mathbf{k}'$) et de Landau (le phonon $\mathbf{q}$ fusionne avec un phonon $\mathbf{k}$ en un seul phonon $\mathbf{k}'$), dont on peut donner la représentation diagrammatique suivante en faisant jouer un rôle privilégié au phonon dont on étudie l'amortissement :

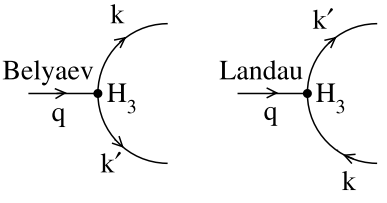

(46)

[35] Ladite transformation correspond aux développements modaux $\delta\hat{\rho}(\mathbf{r}) = L^{-3/2} \sum_{\mathbf{k}\neq\mathbf{0}} \rho_{\mathbf{k}} (\hat{b}_{\mathbf{k}} + \hat{b}^\dagger_{-\mathbf{k}}) \exp(\mathrm{i}\mathbf{k}\cdot\mathbf{r})$ et $\delta\hat{\phi}(\mathbf{r}) = L^{-3/2} \sum_{\mathbf{k}\neq\mathbf{0}} \phi_{\mathbf{k}} (\hat{b}_{\mathbf{k}} - \hat{b}^\dagger_{-\mathbf{k}}) \exp(\mathrm{i}\mathbf{k}\cdot\mathbf{r})$ où $\rho_{\mathbf{k}} = (\hbar\rho k/2mc)^{1/2}$ et $\phi_{\mathbf{k}} = (-\mathrm{i})(mc/2\hbar\rho k)^{1/2}$ sont les amplitudes des fluctuations quantiques de densité et de phase dans le mode de phonons de vecteur d'onde $\mathbf{k}$. On notera la relation $-\mathrm{i}\omega_{\mathbf{k}}\delta\rho_{\mathbf{k}} - \rho(\hbar/m)k^2\phi_{\mathbf{k}} = 0$ imposée par l'équation de continuité linéarisée.

[36] La véritable amplitude de couplage dépend des angles entre les trois vecteurs d'onde $\mathbf{k}_i$ mis en jeu ; comme l'amortissement est en réalité dominé à basse température par des processus aux petits angles entre les vecteurs d'onde, à cause de l'effet petit dénominateur décrit plus bas, nous l'avons écrite directement à angles nuls $\mathbf{k}_i \cdot \mathbf{k}_j / k_i k_j = 1$.

Comme H_3 est cubique, chaque sommet du diagramme représentant son action est le point de rencontre de trois lignes de phonons. On pourrait procéder de même avec H_4 (les sommets seraient alors à quatre lignes) mais nous ne le ferons pas car les processus quartiques jouent en général un rôle sous-dominant dans l'amortissement par rapport aux processus cubiques (par exemple, dans l'amortissement à quatre phonons $\phi\phi \to \phi\phi$ pour $\gamma < 0$, l'amplitude du processus direct $\mathbf{k},\mathbf{q} \to \mathbf{k}',\mathbf{k}''$ induit par H_4 au premier ordre de la théorie des perturbations est en pratique négligeable devant celle du processus indirect de même état initial et final $\mathbf{k},\mathbf{q} \to \mathbf{k}+\mathbf{q} \to \mathbf{k}',\mathbf{k}''$ induit par H_3 traité au second ordre, à cause de l'apparition dans cette dernière d'un dénominateur d'énergie très petit aux petits angles entre $\mathbf{k}$ et $\mathbf{q}$)[37].

4.3. *Comment calculer l'amortissement des phonons ?*

Imaginons qu'on applique sur le gaz, initialement à l'équilibre thermique, une brève excitation de type Bragg induisant un petit déplacement cohérent de Glauber d'amplitude $\alpha \in \mathbb{C}^*$ dans le mode de phonons de vecteur d'onde $\mathbf{q}$ sans toucher aux autres modes, ce qui correspond donc à l'opérateur d'évolution unitaire $U_{\rm exc} = \exp(\alpha \hat{b}^\dagger_{\mathbf{q}} - \alpha^* \hat{b}_{\mathbf{q}})$ [38]. On a alors, juste après l'excitation, une moyenne non nulle pour l'opérateur d'annihilation correspondant :

$$\langle \hat{b}_{\mathbf{q}}(0^+) \rangle = \alpha \neq 0 \tag{47}$$

Ceci conduit à une modulation observable de la densité moyenne du gaz aux vecteurs d'onde $\pm\mathbf{q}$ puisque $\langle \delta\hat{\rho}(\mathbf{r},0^+)\rangle$, combinaison linéaire des $\langle \hat{b}_{\mathbf{k}}(0^+)\rangle$ et des $\langle \hat{b}^\dagger_{\mathbf{k}}(0^+)\rangle$ comme dans la note 35, est alors $\neq 0$.

Dans la limite $\alpha \to 0$, c'est-à-dire dans le régime de réponse linéaire, le formalisme des fonctions de Green à N corps appliqué à la théorie effective de basse énergie, donc à l'hamiltonien de phonons (40) [plutôt qu'à une description microscopique du gaz de fermions avec potentiel d'interaction $V(\mathbf{r}_{ij})$ comme le font les références [75,80] par exemple], conduit à l'expression exacte

$$\langle \hat{b}_{\mathbf{q}}(t) \rangle \overset{t\geq 0}{=} \alpha \mathrm{e}^{-\mathrm{i}\omega_{\mathbf{q}} t} \int_{C_+} \frac{\mathrm{d}\zeta}{2\mathrm{i}\pi} \frac{\mathrm{e}^{-\mathrm{i}\zeta t/\hbar}}{\zeta - \Sigma_{\mathbf{q}}(\zeta)} \tag{48}$$

Dans cette expression, C_+ est le chemin d'intégration parallèle à l'axe réel dans le demi-plan complexe supérieur, décrit de droite à gauche (de $\mathrm{Re}\,\zeta = +\infty$ à $\mathrm{Re}\,\zeta = -\infty$), voir la figure 7, et $\Sigma_{\mathbf{q}}(\zeta)$ est la fonction énergie propre au vecteur d'onde $\mathbf{q}$ et à l'énergie complexe ζ [39], dont on ne connaît pas l'expression explicite mais qu'on définit par son développement perturbatif à tous

[37] Le dénominateur d'énergie en question $\hbar\omega_{\mathbf{q}} + \hbar\omega_{\mathbf{k}} - \hbar\omega_{\mathbf{k}+\mathbf{q}}$ serait même exactement nul à angle nul sans les termes de courbure dans la relation de dispersion (34), ce qui montre d'ailleurs toute la singularité d'une théorie à $\gamma = 0$ (ce sur quoi nous reviendrons dans la section 4.3).

[38] Dans une expérience d'atomes froids, l'excitation de Bragg est induite par la superposition de deux faisceaux laser loin de résonance de vecteurs d'onde $\mathbf{k}_1$ et $\mathbf{k}_2$ avec $\mathbf{k}_1 - \mathbf{k}_2 = \mathbf{q}$; même si les modes acoustiques $\pm\mathbf{q}$ sont initialement vides ($\hbar\omega_{\mathbf{q}} \gg k_{\rm B}T$) et peuvent seulement recevoir des phonons, les processus Raman (à deux photons) absorption d'un photon dans un faisceau laser-émission stimulée dans l'autre induisent les changements d'impulsion $\pm\hbar(\mathbf{k}_1 - \mathbf{k}_2) = \pm\hbar\mathbf{q}$ dans le gaz de fermions et excitent en général les deux modes en question ; on peut cependant jouer sur la durée de l'excitation de Bragg pour que le mode $-\mathbf{q}$ sorte intact de la procédure d'excitation [79].

[39] Par rapport à la variable énergie z habituelle (de la référence [80] par exemple), la variable énergie utilisée ici est translatée de l'énergie non perturbée du mode $\mathbf{q}$, $\zeta = z - \hbar\omega_{\mathbf{q}}$. Ceci explique pourquoi on a pu sortir le facteur de phase de l'évolution non perturbée dans (48) et pourquoi $\Sigma_{\mathbf{q}}(\zeta)$ est prise en $\zeta = \mathrm{i}0^+$ dans l'approximation (50) à venir (cela correspond effectivement à $z = \hbar\omega_{\mathbf{q}} + \mathrm{i}0^+$).

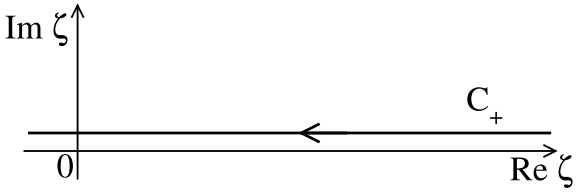

FIGURE 7. Chemin d'intégration dans le plan complexe suivi par l'équation (48).

les ordres en l'interaction phonon–phonon. Ici, nous nous limitons à l'interaction cubique H_3 (voir la section 4.2) et le développement prend la forme diagrammatique suivante

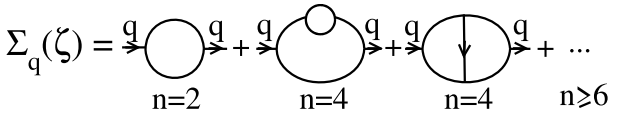

(49)

où l'entier n donne l'ordre en H_3 [63]. Nous n'indiquons que la topologie, il reste à sommer sur toutes les orientations possibles mais non redondantes des lignes internes, voir l'exemple de la portion de diagramme (46)[40] ; une valeur précise peut alors être attribuée à chaque diagramme, mettant en jeu une somme sur les vecteurs d'onde et les fréquences de Matsubara des lignes internes [80].

Afin d'obtenir des résultats explicites sur l'amortissement, on effectue traditionnellement les deux approximations suivantes[41] :

(1) l'approximation de Markov (le gaz de phonons vu par le mode **q** constitue un réservoir sans mémoire c'est-à-dire avec un temps de corrélation négligeable) : on ignore la dépendance en énergie de la fonction énergie propre comme suit (voir la note 39),

$$\Sigma_{\mathbf{q}}(\zeta) \simeq \Sigma_{\mathbf{q}}(\mathrm{i}0^+) \tag{50}$$

L'intégrale dans l'équation (48) se calcule alors par le théorème des résidus (en refermant le contour par un demi-cercle infini dans le demi-plan complexe inférieur),

$$\langle \hat{b}_{\mathbf{q}}(t)\rangle|_{\mathrm{Markov}} \overset{t\geqq 0}{=} \alpha \mathrm{e}^{-\mathrm{i}\omega_{\mathbf{q}}t}\mathrm{e}^{-\mathrm{i}\Sigma_{\mathbf{q}}(\mathrm{i}0^+)t/\hbar} \tag{51}$$

La décroissance du signal est dans ce cas exponentielle, avec un taux correspondant à la partie imaginaire de $\Sigma_{\mathbf{q}}(\mathrm{i}0^+)$ (la partie réelle donne le changement de pulsation propre du mode).

[40] Dans le premier diagramme de (49) (à une boucle), (i) orienter la ligne du haut vers la droite et la ligne du bas vers la gauche et (ii) orienter la ligne du haut vers la gauche et la ligne du bas vers la droite correspondent à la même contribution, par invariance du diagramme par rotation d'angle π autour de son axe horizontal. Il en va de même pour la boucle interne du deuxième diagramme de (49), par invariance par rotation locale de cette dernière. Pour la même raison d'invariance par rotation (cette fois globale) des diagrammes d'ordre $n = 4$, on décide, pour éviter un double comptage, de mettre la boucle interne dans la branche du haut et, dans le troisième diagramme de (49), d'orienter le pont vers le bas.

[41] Notre théorie effective étant exacte à l'ordre dominant en température, il vaut mieux ne l'utiliser que dans la limite $T \to 0$, qui plus est en fixant le rapport $\bar{q} = \hbar c q/k_{\mathrm{B}}T$ afin que le mode **q** soit lui aussi décrit exactement. On a alors $\omega_{\mathbf{q}}/\Gamma_{\mathrm{th}} \to +\infty$ où $\Gamma_{\mathrm{th}} = \Gamma_{q=k_{\mathrm{B}}T/\hbar c}$ est le taux de thermalisation du gaz de phonons et Γ_q est la fonction (52), puisque l'exposant ν introduit dans la figure 8 page 419 est toujours > 1, voir le tableau 1 page 420 : le taux de thermalisation Γ_{th} tend vers zéro plus vite que la pulsation propre $\omega_{\mathbf{q}}$ et le mode entre par définition dans le régime faiblement collisionnel. Dans le régime opposé $\omega_{\mathbf{q}} \ll \Gamma_{\mathrm{th}}$ dit hydrodynamique, le gaz de phonons a le temps d'atteindre un équilibre thermique local en chaque point d'oscillation de l'onde sonore **q** et l'amortissement se décrit au moyen de coefficients de type viscosité dans les équations hydrodynamiques classiques d'un modèle à deux fluides [81].

(2) l'approximation de Born : on calcule $\mathrm{Im}\,\Sigma_{\mathbf{q}}(\mathrm{i}0^+)$ perturbativement au premier ordre non nul n en H_3. Le taux d'amortissement des phonons $\mathbf{q}$ vaut alors[42,43]

$$\Gamma_{\mathbf{q}}|_{\text{Born–Markov}} = -\frac{2}{\hbar}\mathrm{Im}\,\Sigma^{(n)}_{\mathbf{q}}(\mathrm{i}0^+) \tag{52}$$

où l'exposant donne l'ordre en H_3. Dans le cas d'une branche acoustique convexe ($\gamma > 0$) à 3D, il suffit d'aller à l'ordre $n = 2$: c'est l'amortissement à trois phonons de Belyaev–Landau, très étudié théoriquement et observé dans l'hélium 4 liquide [83,84] et, dans une moindre mesure, dans les gaz d'atomes froids bosoniques, seul l'amortissement de Belyaev y ayant été vu [85]. Dans le cas concave ($\gamma < 0$), il faut aller à l'ordre $n = 4$ (la première contribution dans l'équation (49) est purement réelle pour $\zeta = \mathrm{i}0^+$ car ses dénominateurs d'énergie, de la forme $\hbar\omega_{\mathbf{q}} + \hbar\omega_{\mathbf{k}} - \hbar\omega_{\mathbf{k}+\mathbf{q}}$ et $\hbar\omega_{\mathbf{q}} - (\hbar\omega_{\mathbf{k}} + \hbar\omega_{\mathbf{q}-\mathbf{k}})$, ne peuvent s'annuler, mais les deux suivantes ne le sont pas dans les processus $\phi\phi \to \phi\phi$) ; ce cas a été peu étudié théoriquement (la référence [78] a d'ailleurs relevé et corrigé une erreur dans le calcul originel [52], et la référence [86] a obtenu une expression beaucoup plus explicite du résultat, le généralisant même à un potentiel chimique de phonons μ_ϕ non nul[44]) et n'a, à notre connaissance, jamais été observé expérimentalement (aucune mesure précise de $\Gamma^{\gamma<0}_{\mathbf{q}}$ n'a été faite dans aucun système).

Déterminons la validité de l'approximation de Born au moyen de l'estimation de l'ordre $n \in 2\mathbb{N}^*$ donnée dans la référence [63] :

$$\Sigma^{(n)}_{\mathbf{q}}(\mathrm{i}0^+) \approx \int\left(\prod_{i=1}^{n/2}\mathrm{d}^d k_i\right)\frac{\langle|L^{d/2}H_3|\rangle^n}{(\Delta E)^{n-1}} \approx |\gamma|T^3\left(\epsilon_{d\mathrm{D}} = \frac{T^{2d-4}}{|\gamma|^{(5-d)/2}}\right)^{n/2} \tag{53}$$

où $d \geq 2$ est la dimension de l'espace. L'écriture au second membre représente symboliquement le produit de n éléments de matrice de l'interaction cubique entre phonons au numérateur et le produit de $n-1$ dénominateurs d'énergie (associés à $n-1$ états intermédiaires) au dénominateur, et l'intégrale est prise sur les vecteurs d'onde de phonons indépendants $\mathbf{k}_i$. L'ordre de grandeur au troisième membre est obtenu comme dans la référence [63] en se limitant aux petits angles entre $\mathbf{k}_i$ et $\mathbf{q}$, en $O(|\gamma|^{1/2}T)$, ce qui est légitime lorsque $T \to 0$ [52] ; nous omettons ici la dépendance en la densité ρ, en $\xi = \hbar/mc$ et en la constante de couplage $\mathscr{A}$ de l'équation (45), au contraire de la référence [63], mais nous gardons celle en le paramètre de courbure γ, car nous

[42] Pour donner un autre éclairage à l'approximation (52), signalons pour $n = 2$ qu'on la retrouve exactement par la méthode de l'équation pilote bien connue en optique quantique (on obtient une équation d'évolution fermée sur l'opérateur densité $\hat\rho_S(t)$ d'un petit système S — ici le mode de phonons $\mathbf{q}$ — couplé à un gros réservoir R — ici les autres modes de phonons $\mathbf{k} \neq \mathbf{q}$, en recourant justement à l'approximation de Born–Markov) [36,82] ou, plus simplement, au moyen de la règle d'or de Fermi (on calcule $\mathrm{d}\langle\hat n_{\mathbf{q}}\rangle/\mathrm{d}t$ où $\langle\hat n_{\mathbf{q}}\rangle = \langle\hat b^\dagger_{\mathbf{q}}\hat b_{\mathbf{q}}\rangle$ est le nombre moyen de phonons dans le mode $\mathbf{q}$ hors d'équilibre, en sommant les flux entrants — processus de population $\mathbf{k},\mathbf{k}' \to \mathbf{q}$ et $\mathbf{k}' \to \mathbf{k},\mathbf{q}$ — et sortants — processus inverses de dépopulation $\mathbf{q} \to \mathbf{k},\mathbf{k}'$ et $\mathbf{q},\mathbf{k} \to \mathbf{k}'$ — puis en linéarisant en l'écart à l'équilibre thermique $\delta n_{\mathbf{q}}(t) \equiv \langle n_{\mathbf{q}}\rangle(t) - \bar n_{\mathbf{q}}$ juste après l'excitation de Bragg, sous la forme $(\mathrm{d}/\mathrm{d}t)\delta n_{\mathbf{q}}(t = 0^+) = -\Gamma_{\mathbf{q}}\delta n_{\mathbf{q}}(t = 0^+)$). Pour $n = 4$, on retrouve le même résultat (52) en étendant la règle d'or de Fermi aux ordres supérieurs [38].

[43] Il y a ici une petite subtilité mathématique : si le premier ordre non nul n est ≥ 4, l'approximation de Markov ne doit plus se contenter de remplacer $\Sigma_{\mathbf{q}}(\zeta)$ par $\Sigma_{\mathbf{q}}(\mathrm{i}0^+)$ mais doit l'approximer par un développement limité autour de $\zeta = \mathrm{i}0^+$. Par exemple, pour $n = 4$, on prend $\Sigma_{\mathbf{q}}(\zeta) \simeq \Sigma_{\mathbf{q}}(\mathrm{i}0^+) + \zeta(\mathrm{d}/\mathrm{d}\zeta)\Sigma_{\mathbf{q}}(\mathrm{i}0^+)$ si bien qu'à l'ordre 4 en H_3, $\zeta - \Sigma_{\mathbf{q}}(\zeta) \simeq [1 - (\mathrm{d}/\mathrm{d}\zeta)\Sigma_{\mathbf{q}}(\mathrm{i}0^+)][\zeta - \Sigma^{(2)}_{\mathbf{q}}(\mathrm{i}0^+) - \Sigma^{(4)\mathrm{eff}}_{\mathbf{q}}(\mathrm{i}0^+)]$ avec $\Sigma^{(4)\mathrm{eff}}_{\mathbf{q}}(\mathrm{i}0^+) = \Sigma^{(4)}_{\mathbf{q}}(\mathrm{i}0^+) + \Sigma^{(2)}_{\mathbf{q}}(\mathrm{i}0^+)(\mathrm{d}/\mathrm{d}\zeta)\Sigma^{(2)}_{\mathbf{q}}(\mathrm{i}0^+)$. Il faut alors remplacer $\Sigma^{(4)}_{\mathbf{q}}(\mathrm{i}0^+)$ par $\Sigma^{(4)\mathrm{eff}}_{\mathbf{q}}(\mathrm{i}0^+)$ dans l'expression (52) du taux d'amortissement. Dans le cas tridimensionnel concave, ceci ne change rien à $\Gamma_{\mathbf{q}}|_{\text{Born–Markov}}$ car $(\mathrm{d}/\mathrm{d}\zeta)\Sigma^{(2)}_{\mathbf{q}}(\mathrm{i}0^+)$ est une quantité réelle, tout comme $\Sigma^{(2)}_{\mathbf{q}}(\mathrm{i}0^+)$; dans le cas bidimensionnel concave, la conclusion est moins évidente mais reste la même, voir la note 48. En revanche, ce remplacement doit être effectué dans le calcul du déplacement de pulsation thermique $\Delta_{\mathbf{q}}$ du mode, $\hbar\Delta_{\mathbf{q}}|_{\text{Born–Markov}} = \mathrm{Re}\,[\Sigma^{(2)}_{\mathbf{q}}(\mathrm{i}0^+) + \Sigma^{(4)\mathrm{eff}}_{\mathbf{q}}(\mathrm{i}0^+)]$ – idem à $T = 0$.

[44] Si l'on se limite à l'ordre dominant en température aux processus collisionnels $\phi\phi \to \phi\phi$, le nombre de phonons devient une quantité conservée, ce qui autorise à prendre $\mu_\phi < 0$.

lierons bientôt γ et T. En résumé, le développement de Born est légitime en dimension $d=3$ si son petit paramètre tend vers zéro à basse température :

$$\epsilon_{3\mathrm{D}} = \frac{T^2}{|\gamma|} \underset{T\to 0}{\to} 0 \tag{54}$$

Pour discuter la validité de l'approximation de Markov, admettons que le comportement de la fonction énergie propre au voisinage de $\zeta = \mathrm{i}0^+$ soit caractérisé par deux exposants, ν et σ, celui donnant les valeurs typiques $\propto T^\nu$ de sa partie imaginaire et celui donnant son échelle de variation typique $\propto T^\sigma$, comme sur la figure 8 [45,46]. D'après l'équation (52), on a donc

$$\Gamma_{\mathbf{q}} \underset{T\to 0}{\approx} T^\nu \tag{55}$$

La fonction $\Sigma_{\mathbf{q}}(\zeta)$ admet alors une variation en énergie lente (négligeable) à l'échelle du taux d'amortissement (qui est bien l'inverse du temps caractéristique dans l'équation (48)) si elle est plus large que haute, ce qui impose

$$\nu > \sigma \tag{56}$$

L'exposant ν s'obtient par un calcul explicite du second membre de l'équation (52) dans la limite $T\to 0$, comme il a été fait dans la référence [78] pour le cas tridimensionnel[47] et dans la référence [63] pour le cas convexe bidimensionnel ; on peut aussi, plus simplement, utiliser l'estimation (53) avec $n=2$ si $\gamma>0$ et $d\in\{2,3\}$, $n=4$ si $\gamma<0$ et $d=3$ [48]. L'exposant σ s'obtient

[45] Les exposants introduits ici diffèrent d'une unité de ceux de la référence [63] par un choix de convention différent.

[46] Pour la clarté de l'exposition, nous avons supposé sur la figure 8 que la fonction représentée admet un maximum en l'origine. Ceci n'est pas nécessairement vrai (le cas bidimensionnel convexe de la référence [63] en fournit un contre-exemple, voir son équation (114)). La véritable définition des exposants ν et σ est que la fonction mise à l'échelle $\mathrm{Im}\,\Sigma_{\mathbf{q}}(\zeta=\tilde\zeta mc^2(k_{\mathrm{B}}T/mc^2)^\sigma)/[mc^2(k_{\mathrm{B}}T/mc^2)^\nu]$ admet une limite finie et non nulle lorsque $T\to 0$ à énergie complexe réduite $\tilde\zeta$ fixée ($\mathrm{Im}\,\tilde\zeta>0$).

[47] La référence historique [52] pour $\gamma<0$ fixé trouve elle aussi $\nu=7$ mais la dépendance en q de $\Gamma_{\mathbf{q}}$ est différente, par exemple $\Gamma_{\mathbf{q}}\approx qT^6$ dans [52] au lieu de q^3T^4 dans [78] lorsque $q\to 0$.

[48] Pour $\gamma<0$ fixé et $d=2$, Alice Sinatra a obtenu en 2021, dans la formulation des références [72,78], le résultat non publié que $\mathrm{Im}\,\Sigma^{(n=4)}_{\mathbf{q}}(\mathrm{i}0^+)=0$ à l'ordre T^3 (l'ordre dominant attendu en température). Pour le voir, il est en fait plus simple d'utiliser les expressions (84) et (85) de la référence [63] : (i) dans (84), on peut ignorer les processus $\phi\leftrightarrow\phi\phi\phi$ et se limiter au processus $\phi\phi\to\phi\phi$ (deuxième contribution), seul capable de conserver l'énergie-impulsion ; (ii) dans l'intégrande de (85), on a le droit de remplacer ζ par 0 au numérateur de la grande fraction pour la raison similaire que les processus $\phi\leftrightarrow\phi\phi$ ne conservent pas l'énergie-impulsion - ceci rend le numérateur réel ; (iii) on vérifie alors que, si l'écart d'énergie mis à l'échelle $\Delta E/[k_{\mathrm{B}}T(k_{\mathrm{B}}T/mc^2)^2]$ à côté de $\mathrm{i}0^+$ s'annule au dénominateur de la grande fraction, comme l'impose le Dirac $\delta(\Delta E)$ de la règle d'or de Fermi généralisée [38], le numérateur s'annule aussi (on le montre en remplaçant formellement γ au numérateur par son expression annulant ΔE, une fonction rationnelle des modules et des angles des vecteurs d'onde de phonons). En d'autres termes, la limite en $\zeta=0$ (mais aussi en $\zeta=-\Delta E$) de l'amplitude de transition au numérateur de la grande fraction, considérée comme une fraction rationnelle des angles, peut s'écrire $\Delta E\times P/Q$, où les polynômes ΔE, P et Q sont deux à deux premiers entre eux.

Ce raisonnement néglige cependant de possibles effets de bord dans l'intégrale sur les nombres d'onde de phonons, au sens de la référence [87], où l'un des nombres d'onde tend vers zéro, ce qui fait tendre vers zéro l'un des dénominateurs d'énergie des processus $\phi\leftrightarrow\phi\phi$. En incluant ces effets de bords, nous trouvons que les processus $\phi\to\phi\phi\phi$, $\phi\phi\to\phi\phi$ et $\phi\phi\phi\to\phi$, abrégés en $1\to 3$, $2\to 2$ et $3\to 1$ dans la référence [63], apportent chacun une contribution non nulle à $\mathrm{Im}\,\Sigma^{(n=4)}_{\mathbf{q}}(\mathrm{i}0^+)$ à l'ordre T^3, mais que la somme de ces contributions donne exactement zéro (la contribution du bord $q_1'+q_2'=q$ dans $2\to 2$, à savoir $C\int_0^{\bar q}\mathrm{d}\bar k\,(\bar n_k^{\mathrm{lin}}+\bar n_{q-k}^{\mathrm{lin}}+1)\bar k(\bar q-\bar k)/\bar q$, est compensée exactement par $1\to 3$, et celle des bords $q_1'=0$ et $q_2'=0$ dans leur ensemble, à savoir $2C\int_{\bar q}^{+\infty}\mathrm{d}\bar k\,(\bar n_{k-q}^{\mathrm{lin}}-\bar n_k^{\mathrm{lin}})\bar k(\bar k-\bar q)/\bar q$, est compensée exactement par $3\to 1$; ici, $\bar k=\hbar ck/k_{\mathrm{B}}T$, $\bar n_k^{\mathrm{lin}}=1/(\exp\bar k-1)$, $\Lambda=\rho^2((\mathrm{d}^3/\mathrm{d}\rho^3)e_0(\rho))/(3mc^2)$ et $C=k_{\mathrm{B}}T(k_{\mathrm{B}}T/mc^2)^2[9(1+\Lambda)^2/8\rho\xi^2]^2/[\pi(3\gamma)^2]$).

La conclusion n'est pas changée par la correction $\Sigma^{(2)}_{\mathbf{q}}(\mathrm{i}0^+)(\mathrm{d}/\mathrm{d}\zeta)\Sigma^{(2)}_{\mathbf{q}}(\mathrm{i}0^+)$ de notre note 43 car on trouve que les facteurs $\Sigma^{(2)}_{\mathbf{q}}(\mathrm{i}0^+)$ et $(\mathrm{d}/\mathrm{d}\zeta)\Sigma^{(2)}_{\mathbf{q}}(\mathrm{i}0^+)$ sont tous les deux réels. C'était évident pour le premier facteur (les effets de bord qu'il présente à 1D [87] sont supprimés à 2D par abaissement de la densité d'états des phonons à faible nombre d'onde). Ça ne l'était pas pour le second facteur : à cause des effets de bord dans l'intégration sur $\mathbf{k}$ (voir l'équation (39) de la référence [63]), les processus de Belyaev et de Landau donnent chacun une contribution non nulle à $\mathrm{Im}\,(\mathrm{d}/\mathrm{d}\zeta)\Sigma^{(2)}_{\mathbf{q}}(\mathrm{i}0^+)$ (elle vaut $2[9(1+\Lambda)^2/8\rho\xi^2]/[\bar q(3|\gamma|)^{3/2}]$ pour Landau à l'ordre dominant en température) mais ces contributions sont

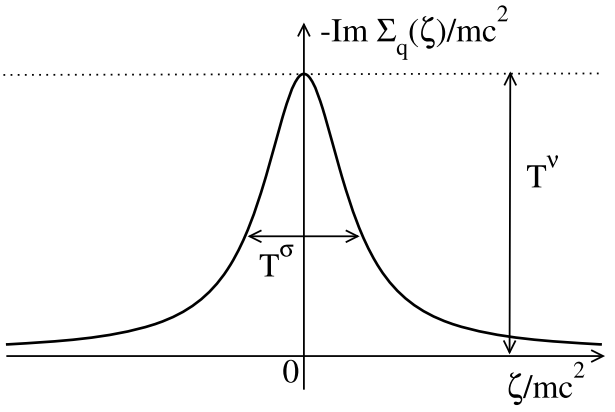

FIGURE 8. Dans la limite $T \to 0$, on admet que l'ordre de grandeur et la largeur typique de la fonction $\mathrm{Im}\,\Sigma_{\mathbf{q}}(\zeta)$ près de $\zeta = \mathrm{i}0^+$ sont caractérisés par deux lois de puissance en température, d'exposants ν et σ (en tenant compte d'une possible dépendance en température du paramètre de courbure γ).

en généralisant ladite estimation au cas $\zeta \neq 0$, c'est-à-dire en ajoutant ζ à ΔE dans (53) ; or, dans un développement aux petits angles entre $\mathbf{k}_i$ et $\mathbf{q}$, la partie de ΔE linéaire en les nombres d'onde s'annule et il ne reste que les contributions cubiques $\approx \gamma T^3$ si bien que, indépendamment de la dimensionnalité d,

$$\frac{1}{\zeta + \Delta E} \approx \frac{1}{\zeta + \gamma T^3} \quad \text{et donc} \quad T^\sigma \approx |\gamma| T^3 \tag{57}$$

en tenant compte de la dépendance en le paramètre γ, ce dernier — nous l'avons dit — pouvant varier en température. La condition de validité $T^\nu = o(\gamma T^3)$ qui en résulte dans (56) admet une interprétation simple : dans la limite $T \to 0$ prise avec la loi d'échelle $q \approx T$, il faut que le taux d'amortissement $\Gamma_{\mathbf{q}}$ tende vers zéro plus vite que le terme cubique en q dans $\omega_{\mathbf{q}}$,

$$\Gamma_q \overset{\hbar c q/k_{\mathrm{B}}T \text{ fixé}}{\underset{T\to 0}{=}} o(\omega_{\mathbf{q}}^{(3)}) \quad \text{avec} \quad \omega_{\mathbf{q}}^{(3)} = \gamma m c^2 (q\xi)^3/8\hbar \tag{58}$$

ce qui est donc la vraie marque de la nature markovienne de l'amortissement (plutôt que la condition perturbative irréfléchie $\Gamma_{\mathbf{q}} = o(\omega_{\mathbf{q}})$).

---

exactement opposées, en particulier parce que les dénominateurs d'énergie $\varepsilon_{\mathbf{q}} - (\varepsilon_{\mathbf{k}} + \varepsilon_{\mathbf{q}-\mathbf{k}})$ et $\varepsilon_{\mathbf{q}} + \varepsilon_{\mathbf{k}} - \varepsilon_{\mathbf{q}+\mathbf{k}}$ sont opposés $\sim \mp\hbar c k[1 - (v_q/c)\cos\theta]$ à l'ordre dominant en k ($v_q = \mathrm{d}\varepsilon_{\mathbf{q}}/\hbar \mathrm{d}q$ est la vitesse de groupe et θ est l'angle entre $\mathbf{k}$ et $\mathbf{q}$) et entrent dans la dérivée de la distribution de Dirac $\delta'(\varepsilon)$, qui est une fonction impaire de son argument.

Le cas bidimensionnel concave est donc spécial : la quantité $\mathrm{Im}\,\Sigma_{\mathbf{q}}^{(4)\mathrm{eff}}(\mathrm{i}0^+)$ de la note 43 — considérée à tous les ordres en température — ne donne pas la bonne loi d'échelle en température $\propto T^3$ de la fonction énergie propre d'ordre 4 en H_3 sur un voisinage en $O(T^3)$ de $\zeta = \mathrm{i}0^+$; elle ne donne pas non plus, d'ailleurs, le taux d'amortissement $\Gamma_{\mathbf{q}}$ puisqu'il y a échec des approximations de Born et de Markov comme dans le cas bidimensionnel convexe, voir la dernière ligne de notre tableau 1. Notons cependant, toujours pour $\gamma < 0$, que le cas limite $\rho\xi^2 \to +\infty$ d'une interaction très faible dans le superfluide sous-jacent doit être mis à part car on y dispose du petit paramètre supplémentaire $1/\rho\xi^2$ aidant à la validité de Markov (comme dans la section 3.2 de la référence [63]) et de Born (comme dans l'équation (17) de cette même référence) ; ce cas limite est inaccessible dans un gaz de fermions de spin 1/2 en interaction de contact — on y a $\rho\xi^2 = O(1)$ lorsque $\gamma < 0$ [88] — mais il l'est dans un gaz de bosons avec une interaction de portée $\gtrsim \xi$ comme l'envisage la référence [78].

Tableau 1. Dans l'étude de l'amortissement des phonons d'un superfluide, validité de l'approximation de Born–Markov dans la limite de basse température $T \to 0$ selon la dimension de l'espace d et le paramètre de courbure γ de la branche acoustique (plus précisément son signe et sa variation en température, la troisième ligne valant quel que soit le signe de γ).

	ν	σ	Markov	$\epsilon_{d\mathrm{D}}$	Born
$d=3, \gamma>0$ fixé	5	3	oui	$\approx T^2 \to 0$	oui
$d=3, \gamma<0$ fixé	7	3	oui	$\approx T^2 \to 0$	oui
$d=3, \gamma=O(T^2)$	5	5	non	$\approx T^0 \not\to 0$	non
$d=2, \gamma>0$ fixé	3	3	non	$\approx T^0 \not\to 0$	non

Les exposants ν et σ entrant dans la définition (56) du régime markovien sont ceux de la figure 8, et le petit paramètre du développement de Born $\epsilon_{d\mathrm{D}}$ est donné dans l'équation (53).

La situation est résumée sur le tableau 1 ci-dessus[49]. L'approximation de Born–Markov est donc utilisable en dimension 3, sauf sur un étroit intervalle de valeurs de γ, de largeur $\approx (k_\mathrm{B}T/mc^2)^2$ autour de $\gamma = 0$; en $\gamma = 0$, la relation de dispersion des phonons (34) a d'ailleurs un premier écart quintique à la loi linéaire cq, ce qui, on le sent bien, est un cas spécial.

Le calcul précis du taux d'amortissement $\Gamma_{\mathbf{q}}$ (ou ce qui en tient lieu pour une décroissance non exponentielle, comme l'inverse de la largeur de $|\langle \hat{b}_{\mathbf{q}}(t)\rangle|^2$ à la hauteur relative 1/e) pour ces faibles valeurs de la courbure constitue, à notre connaissance, une question ouverte; elle est d'une grande pertinence expérimentale, la force des interactions annulant γ étant semble-t-il proche de la limite unitaire (voir la référence [57] et notre section 5.1), point de prédilection des expériences sur les atomes froids car dans un régime de valeurs assez élevées de $T_\mathrm{c}/T_\mathrm{F}$ et de propriétés collisionnelles propices au refroidissement par évaporation [18].

Pour faire bonne mesure, nous avons aussi considéré le cas bidimensionnel convexe dans le tableau 1 : l'approximation de Born–Markov y échoue, et la référence [63] a dû faire appel à une approximation heuristique non perturbative sur la fonction énergie propre $\Sigma_{\mathbf{q}}(\zeta)$ pour arriver à un bon accord avec des simulations de champ classique (opérateurs $\hat{b}_{\mathbf{q}}, \hat{b}^\dagger_{\mathbf{q}}$ de l'hydrodynamique quantique remplacés par des nombres complexes $b_{\mathbf{q}}, b^*_{\mathbf{q}}$), ceci dans le régime d'interaction faible $\rho\xi^2 \gg 1$ du superfluide bosonique sous-jacent, où l'on pensait pourtant disposer d'un petit paramètre assurant le succès de la règle d'or de Fermi même dans la limite $k_\mathrm{B}T/mc^2 \to 0$ (cette attente raisonnable, confirmée dans la section 3.2 de la référence [63] à l'ordre deux en H_3, est infirmée dans la section 4.3 de cette même référence par un calcul à l'ordre quatre)[50].

[49] Dans la troisième ligne du tableau, on omet de possibles facteurs logarithmiques $\ln(1/T)$ pour simplifier. Ces facteurs proviennent du fait que, pour les lois d'échelle $\gamma \propto T^2$ et $q \propto T$, les termes en q^3 et en $q^5 \ln q$ sont du même ordre de grandeur dans la relation de dispersion (34) : dans ce régime de faible courbure, la contribution logarithmico-quintique à $\omega_{\mathbf{q}}$ n'est donc plus une petite correction et doit être gardée.

[50] Nous n'avons pas parlé ici du cas très particulier de la dimension $d = 1$, où deux vecteurs d'onde font un angle très petit (nul!) dès qu'ils sont de même sens. Disons simplement que le petit paramètre de Born reste donné par l'équation (53), obtenue pourtant sous l'hypothèse $d \geq 2$. En rétablissant la dépendance en densité comme dans [63], nous trouvons plus précisément $\epsilon_{1\mathrm{D}} = 1/[\gamma^2\rho\xi(k_\mathrm{B}T/mc^2)^2]$, le préfacteur dans (53) s'écrivant $\gamma(k_\mathrm{B}T)^3/(mc^2)^2$. Dans la limite de basse température $k_\mathrm{B}T/mc^2 \to 0$ à $\rho\xi$ fixé considérée ici, $\epsilon_{1\mathrm{D}} \to +\infty$ et il faut immédiatement faire appel à des approximations non perturbatives sur $\Sigma_{\mathbf{q}}(\zeta)$ et $\Gamma_{\mathbf{q}}$, comme le calcul autocohérent des références [89,90]. Dans la limite opposée d'interaction faible $\rho\xi \to +\infty$ à $k_\mathrm{B}T/mc^2$ fixé, $\epsilon_{1\mathrm{D}} \to 0$ et l'on peut utiliser la règle d'or de Fermi comme dans la référence [87]; plus précisément, on s'attend à ce que la condition de validité de la règle d'or s'écrive $\rho\xi(k_\mathrm{B}T/mc^2)^2 \gg \phi_{1\mathrm{D}}(\bar{q})$ où $\phi_{1\mathrm{D}}$ est une certaine fonction de $\bar{q} = \hbar cq/k_\mathrm{B}T$, en oubliant la dépendance en γ pour simplifier (à $\bar{q}$ fixé, l'approximation de Born impose cette condition, mais l'approximation de Markov est alors satisfaite aussi car on a $\hbar\Gamma_{\mathbf{q}}|^{\text{règle}}_{\text{d'or}} \approx \gamma[(k_\mathrm{B}T)^3/(mc^2)^2]\epsilon_{1\mathrm{D}} \approx k_\mathrm{B}T/(\gamma\rho\xi) \ll \Delta E \approx \gamma(k_\mathrm{B}T)^3/(mc^2)^2$ où ΔE, dénominateur d'énergie de Belyaev–Landau typique, donne la largeur en ζ de la fonction énergie propre comme dans l'équation (57)). À 2D, comme

4.4. *Diffusion de phase du condensat de paires*

Une question d'ordre à la fois pratique et fondamental porte sur le temps de cohérence du condensat de paires à l'équilibre thermique dans un gaz de fermions parfaitement isolé de son environnement.

Pour un système de fermions ↑ et ↓ infini non polarisé, le temps de cohérence est infini, comme l'affirme le phénomène de brisure de symétrie $U(1)$: dans l'ensemble grand canonique (terme $-\mu\hat{N}$ ajouté à l'hamiltonien du gaz de fermions où μ est le potentiel chimique et $\hat{N}$ l'opérateur nombre total de particules), le paramètre d'ordre complexe $\Delta(\mathbf{r},t)$ est uniforme et constant; dans l'ensemble canonique, il évolue donc avec le facteur de phase non amorti $\exp(-2\mathrm{i}\mu t/\hbar)$ [51], avançant à la pulsation immuable $2\mu/\hbar$; en tout cas, le temps de cohérence est infini.

Qu'en est-il dans un système de taille finie (boîte de quantification $[0,L]^3$, nombre total fixé N de fermions) ? Pour le savoir, suivons la référence [76] et écrivons l'équation d'évolution de l'opérateur phase du condensat, que nous notons $\hat{\phi}_0$ comme dans l'équation (39), dans le régime de l'hydrodynamique quantique[52] :

$$-\hbar\frac{\mathrm{d}}{\mathrm{d}t}\hat{\phi}_0 = \mu_0(\rho) + \sum_{\mathbf{q}\neq\mathbf{0}} \hat{b}^\dagger_{\mathbf{q}}\hat{b}_{\mathbf{q}}\frac{\mathrm{d}}{\mathrm{d}N}(\hbar\omega_{\mathbf{q}}) \equiv \hat{\mu} \tag{59}$$

Au second membre, $\mu_0(\rho) = \mathrm{d}E_0/\mathrm{d}N$ est le potentiel chimique des N fermions dans l'état fondamental d'énergie E_0 à la densité ρ et la somme sur $\mathbf{q}$ peut être interprétée comme la dérivée adiabatique (comprendre aux opérateurs nombres d'occupation $\hat{b}^\dagger_{\mathbf{q}}\hat{b}_{\mathbf{q}}$ des modes de phonons fixés) par rapport à N de la somme correspondante dans l'hamiltonien de phonons H_2 (41). Le second membre dans son ensemble est donc la dérivée isentropique de l'hamiltonien par rapport au nombre total de particules. En ce sens, il constitue un opérateur potentiel chimique des fermions, d'où la notation $\hat{\mu}$ au troisième membre, et l'équation (59) n'est autre qu'une version quantique de la fameuse seconde relation de Josephson, reliant la dérivée temporelle de la phase (classique) du paramètre d'ordre au potentiel chimique à l'équilibre μ.

Dans une réalisation donnée de l'expérience, que nous supposons correspondre à un état propre à N corps $|\psi_\lambda\rangle$ d'énergie E_λ échantillonnant l'ensemble canonique, les nombres d'occupation $\hat{b}^\dagger_{\mathbf{q}}\hat{b}_{\mathbf{q}}$ fluctuent et se décorrèlent sous l'effet des collisions incessantes entre phonons dues en particulier à H_3, voir l'équation (44). Aux temps assez longs pour qu'un grand nombre de collisions aient eu lieu, on s'attend donc à un étalement diffusif de la phase du condensat, avec un déphasage aléatoire de variance croissant linéairement en temps :

$$\mathrm{Var}_\lambda[\hat{\phi}_0(t) - \hat{\phi}_0(0)] \underset{\Gamma^\phi_{\mathrm{coll}}t\gg 1}{\sim} 2D_\lambda t \tag{60}$$

et un coefficient de diffusion D_λ sous-intensif, c'est-à-dire $\approx 1/N$ à la limite thermodynamique. Ici $\Gamma^\phi_{\mathrm{coll}} = \Gamma_{q=k_\mathrm{B}T/\hbar c}$ est le taux de collision typique entre phonons thermiques (la fonction Γ_q étant celle de l'équation (52)). L'étalement (60) induit une perte de cohérence temporelle

---

le montre la référence [63], le développement perturbatif en H_3 de la fonction énergie propre est soumis à une condition de validité similaire, $\rho\xi^2(k_\mathrm{B}T/mc^2)^2 \gg \phi_{2\mathrm{D}}(\tilde{q})$, voir son équation (96), mais qui, contrairement au cas 1D, ne s'obtient pas par simple comptage de puissances.

[51] Il y a un facteur 2 sous l'exponentielle car Δ est un paramètre d'ordre de paires alors que μ est le potentiel chimique des fermions. Il n'y a pas de facteur 2 dans l'équation (59) car l'opérateur phase $\hat{\phi}_0$ est conjugué à la densité de fermions.

[52] Pour obtenir cette équation, il a fallu éliminer par lissage temporel des termes en $\hat{b}_{\mathbf{q}}\hat{b}_{-\mathbf{q}}$ et $\hat{b}^\dagger_{\mathbf{q}}\hat{b}^\dagger_{-\mathbf{q}}$; c'est sans conséquence car ils oscillent avec une période $\approx \hbar/k_\mathrm{B}T$ bien plus courte que les échelles de temps collisionnelles qui nous intéressent ici (voir plus loin) et se moyennent donc automatiquement à zéro.

exponentielle de taux D_λ, en vertu de la relation de Wick (on s'attend à ce que la statistique du déphasage dans $|\psi_\lambda\rangle$ soit approximativement gaussienne [91]),

$$\begin{aligned}\left\langle \exp\{-\mathrm{i}[\hat\phi_0(t)-\hat\phi_0(0)]\}\right\rangle_\lambda &\simeq \exp[-\mathrm{i}\langle\hat\phi_0(t)-\hat\phi_0(0)\rangle_\lambda]\exp\{-\tfrac{1}{2}\mathrm{Var}_\lambda[\hat\phi_0(t)-\hat\phi_0(0)]\}\\ &\underset{\Gamma^\phi_{\rm coll}t\gg1}{\simeq} \exp[-\mathrm{i}\langle\hat\mu\rangle_\lambda t/\hbar]\exp(-D_\lambda t)\end{aligned} \tag{61}$$

ce que confirme d'ailleurs l'analyse par résolvante de la référence [76][53].

Dans le cas $\gamma > 0$ d'une branche acoustique convexe, la situation ressemble à celle des condensats de bosons en interaction faible bien étudiée dans la référence [95] : les collisions dominantes sont celles à trois phonons $\phi \leftrightarrow \phi\phi$ de Belyaev et de Landau, et D_λ a été calculé pour le condensat de paires de fermions à basse température dans la référence [86] ; nous en donnons ici l'expression simplifiée suivante, ne gardant que les lois d'échelle en N, T et γ (sous l'hypothèse $\gamma = O(1)$) :

$$D_\lambda^{\gamma>0} \approx N^{-1}T^4\gamma^0 \tag{62}$$

Il n'y a eu encore aucune vérification expérimentale dans les gaz d'atomes froids (seuls fluides quantiques suffisamment bien isolés pour que la perte de cohérence du condensat soit intrinsèque), même pour les bosons.

En revanche, dans le cas concave $\gamma < 0$, la question reste largement ouverte. La tentative de calcul de D_λ de la référence [86], tenant compte seulement des processus de collision Landau–Khalatnikov à quatre phonons $\phi\phi \to \phi\phi$ aux petits angles, de taux typique $\Gamma^\phi_{\rm coll} \propto (k_{\rm B}T/mc^2)^7 mc^2/\hbar|\gamma| \approx T^7$, a conduit à un coefficient de diffusion infini,

$$D_\lambda^{\gamma<0} = +\infty \tag{63}$$

plus précisément à une loi d'étalement superdiffusive (simplifiée comme dans (62))[54]

$$\mathrm{Var}_\lambda^{\gamma<0}[\hat\phi_0(t)-\hat\phi_0(0)] \approx N^{-1}T^{20/3}|\gamma|^{1/3}t^{5/3} \tag{64}$$

en particulier parce que les collisions $\phi\phi \to \phi\phi$ conservent le nombre total de phonons N_ϕ (au contraire de $\phi \leftrightarrow \phi\phi$)[55,56]. Aller au-delà et obtenir la vraie valeur (a priori finie) de D_λ reste une question ouverte : il faudrait tenir compte des processus sous-dominants à cinq phonons $\phi\phi \leftrightarrow \phi\phi\phi$ qui changent N_ϕ et se produisent à un taux $\approx T^9$ [96], de même ordre de grandeur que celui des processus $\phi\phi \to \phi\phi$ aux grands angles [52,78], ce qui n'est pas aisé[57].

---

[53] Si l'on admet que le gaz de phonons en interaction est un système quantique ergodique [92,93], la moyenne $\langle\hat\mu\rangle_\lambda$ dans l'état stationnaire $|\psi_\lambda\rangle$ ne dépend que des deux quantités conservées, l'énergie E et le nombre de particules N, et coïncide pour un grand système avec le potentiel chimique microcanonique $\mu_{\rm mc}(E=E_\lambda,N)$. Si l'énergie E fluctue d'une réalisation à l'autre de l'expérience autour de la moyenne $\bar E$, comme dans l'ensemble canonique, le facteur de phase au troisième membre de l'équation (61) fluctue et conduit à un brouillage gaussien en temps : la linéarisation de $\mu_{\rm mc}(E,N)$ autour de $\bar E$ donne $\mathrm{Var}[\hat\phi_0(t)-\hat\phi_0(0)] \sim [\partial_E\mu_{\rm mc}(\bar E,N)]^2(\mathrm{Var}\,E)t^2/\hbar^2$, effet parasite $\approx t^2/N$ masquant rapidement la diffusion de phase (60) $\approx t/N$ [94].

[54] Dans tous les cas, voir les équations (62) et (64), on trouve bien qu'il n'y a pas d'étalement de phase à la limite thermodynamique $N \to +\infty$: dans un gaz isolé, le temps de cohérence limité du condensat est un effet de taille finie.

[55] N_ϕ doit alors être ajouté à la liste des constantes du mouvement, à côté de E et N, dans la note 53.

[56] Le fait que, pour $\gamma < 0$, le taux d'amortissement des phonons $\Gamma_{\mathbf{q}}$ tende vers zéro comme q^3 (au lieu de q pour $\gamma > 0$) joue aussi un rôle ; cependant, sans la conservation de N_ϕ, il conduirait à une loi d'étalement en $t\ln t$ marginalement superdiffusive (voir l'équation (C.20) de la référence [86] et la moralité énoncée après son équation (72)).

[57] La publication [86], comprenant mal la référence [96], y avait vu un taux d'amortissement à cinq phonons en T^{11}. Erreur corrigée ici. En effet, la référence [96], considérant un quasi-équilibre thermique avec un petit potentiel chimique de phonons non nul $\mu_\phi \to 0^-$, obtient l'équation d'évolution $L^{-3}\mathrm{d}N_\phi/\mathrm{d}t = -\Gamma_\phi\mu_\phi$ sur le nombre moyen de phonons, où $\Gamma_\phi \approx T^{11}$ n'est pas le taux cherché malgré les apparences ; comme $L^{-3}\mathrm{d}N_\phi/\mathrm{d}t \approx T^2\mathrm{d}\mu_\phi/\mathrm{d}t$ pour la loi de Bose $\bar n_{\mathbf{q}} = 1/\{\exp[(\hbar cq-\mu_\phi)/k_{\rm B}T]-1\}$, on a en fait $-\mathrm{d}\mu_\phi/\mathrm{d}t \propto (\Gamma_\phi/T^2)\mu_\phi$, de taux $\approx T^9$.

5. Questions ouvertes requérant une théorie microscopique du problème à N corps

L'hydrodynamique quantique de la section 4 n'est qu'une théorie effective de basse énergie. Elle présente donc des limitations de deux types, que nous passons ici brièvement en revue, et qui empêchent de faire l'économie d'un calcul microscopique à N corps.

5.1. *Déterminer les ingrédients de l'hydrodynamique quantique*

L'hydrodynamique quantique fait intervenir deux quantités qui lui sont extérieures, l'équation d'état du gaz de fermions non polarisé à température nulle (au travers de l'énergie volumique $e_0(\rho)$ ou du potentiel chimique $\mu_0(\rho)$ — sa dérivée — à la densité ρ) et le paramètre de courbure γ de la branche acoustique (34).

Dans le présent cas de masses égales $m_\uparrow = m_\downarrow = m$, l'équation d'état a été mesurée expérimentalement [48,97] et différentes méthodes de calcul approchées donnent des résultats satisfaisants, comme le Monte-Carlo quantique diffusif à surface nodale fixée [98,99] ou l'approximation des fluctuations gaussiennes dans une formulation de champ par intégrale de chemin [100,101].

La situation est beaucoup plus ouverte pour le paramètre de courbure γ. L'approximation de la phase aléatoire d'Anderson (RPA) [61], équivalente pour ce problème au calcul des pulsations propres des équations BCS dépendant du temps linéarisées ou même à l'approximation des fluctuations gaussiennes pourtant plus performante [100,102][58], conduit à une expression analytique assez simple de γ en termes de $\mu/|\Delta|$ et $(\partial\mu/\partial|\Delta|)_a$, exacte $\gamma \to 1$ dans la limite $k_F a \to 0^+$ d'un condensat de dimères, raisonnable dans la limite BCS $k_F a \to 0^-$ ($\gamma \to -\infty$ exponentiellement en $1/k_F|a|$ sous l'effet de l'écrasement de la branche acoustique par le continuum de paire brisée) et présentant une annulation avec changement de signe pour $|\Delta|/\mu \simeq 0{,}87$, soit $1/k_F a \simeq -0{,}14$ pour l'équation d'état assez approximative de la théorie BCS, un changement de signe proche de la limite unitaire en tout cas [57].

En particulier, γ a même valeur positive à la limite unitaire dans ces trois approches (branche acoustique de départ convexe) :

$$\gamma^{\text{RPA}}_{a^{-1}=0} \simeq 0{,}084 \tag{65}$$

L'erreur commise est cependant non contrôlée, et l'on n'est même pas sûr du signe.

Une méthode complètement différente procède par extension du problème à une dimension spatiale d quelconque puis développement autour de la dimension quatre, en puissances donc du petit paramètre $\epsilon = 4 - d$. À la limite unitaire, elle conduit elle aussi à un départ convexe [104][59] :

$$\gamma^{\text{dimension}}_{a^{-1}=0} = \frac{1}{3}\left[1 - \frac{1}{4}\epsilon + O(\epsilon^2)\right] \underset{d=3}{\overset{\epsilon=1}{\simeq}} \frac{1}{4} > 0 \tag{66}$$

[58] Ces différentes approches conduisent exactement à la même équation implicite liant la pulsation propre $\omega_{\mathbf{q}}$, le potentiel chimique μ et le paramètre d'ordre Δ, et exactement à la même équation liant μ, Δ et la longueur de diffusion a dans l'onde s [57] ; elles diffèrent seulement par l'équation d'état $\mu = \mu_0(\rho)$ reliant μ à ρ dans l'état fondamental, celle des fluctuations gaussiennes étant la plus précise. Par exemple, à la limite unitaire $a^{-1} = 0$, les approches donnent toutes $mc^2/\mu = 2/3$ (c'est exact par invariance d'échelle, $\mu_0(\rho) \propto \rho^{2/3}$ dans l'équation (43)), $|\Delta|/\mu \simeq 1{,}16$ (proche de la valeur expérimentale $0{,}44E_F/0{,}376E_F \simeq 1{,}17$ sachant que $|\Delta| = E_{\text{paire}}/2$ dans ces théories et que $E_{\text{paire}}/2E_F \simeq 0{,}44$ dans l'expérience [103]) mais le rapport $\mu/E_F \simeq 0{,}376$ dans l'expérience [48], très mal reproduit $\simeq 0{,}59$ par la RPA et BCS, est bien meilleur $\simeq 0{,}40$ dans les fluctuations gaussiennes.

[59] Nous avons obtenu l'expression (66) en reportant directement l'équation (50) de la référence [104] dans la relation de dispersion (48) de cette même référence et en utilisant la propriété $mc^2 = 2\mu/3$ exacte par invariance d'échelle. En procédant différemment, c'est-à-dire en passant par son équation (52) et son résultat $c_2/c_1 = O(\epsilon^2) \simeq 0$ avec $d = 3$ dans son équation (48), on trouve la valeur assez proche $\gamma^{\text{dimension}}_{a^{-1}=0} = 8/45 \simeq 0{,}18$.

Expérimentalement, une mesure récente de la branche acoustique par excitation de Bragg dans un gaz d'atomes froids fermioniques conduit au contraire à un départ concave à la limite unitaire [105] :

$$\gamma^{\rm exp}_{a^{-1}=0} = \frac{8\mu}{3E_{\rm F}}\zeta \simeq \zeta \quad \text{avec } \zeta = -0{,}085(8) < 0 \tag{67}$$

sachant que le rapport $\mu/E_{\rm F}$ vaut $\simeq 3/8$ pour le gaz unitaire dans l'état fondamental [48] et que ζ est le paramètre de courbure de la branche acoustique pour l'adimensionnement de q par $k_{\rm F}$, $\omega_{\mathbf{q}} = cq(1+\zeta q^2/k_{\rm F}^2+\cdots)$. Mais le résultat (67) souffre de deux limitations [106] : (i) un ajustement cubique de la branche sur un intervalle de valeurs de q assez élevées, $q/k_{\rm F} \in [0{,}29\,;1{,}63]$, plutôt que sur un étroit voisinage de $q=0$ (pour la relation de dispersion de la RPA, par exemple, qui présente un point d'inflexion en $q \simeq 0{,}5k_{\rm F}$, un tel ajustement, mélangeant aveuglément des parties convexe et concave, ne donnerait pas le bon signe de $\gamma^{\rm RPA}_{a^{-1}=0}$), et (ii) une température relativement élevée, $T = 0{,}128(8)\,T_{\rm F} \simeq 0{,}8T_{\rm c}$: même si l'on part de la branche de la RPA de paramètre $\gamma > 0$ dans l'état fondamental, l'hydrodynamique quantique prédit un changement thermique $\delta\gamma_{\rm th}$ de la courbure (par interaction du mode $\mathbf{q}$ avec les phonons thermiques) assez négatif pour en changer le signe :

$$\delta\gamma_{\rm th} \sim -\frac{8\pi^2}{9(3\mu/E_{\rm F})^{1/2}}\left(\frac{T}{T_{\rm F}}\right)^2 \simeq -0{,}14 < -\gamma^{\rm RPA}_{a^{-1}=0} \tag{68}$$

La question du signe de γ à la limite unitaire, qui détermine crucialement la nature à trois phonons ($\gamma > 0$) ou à quatre phonons ($\gamma < 0$) des mécanismes d'amortissement du son dans le régime faiblement collisionnel à basse température, reste donc largement ouverte[60].

5.2. *Décrire les modes de haute fréquence*

L'hydrodynamique quantique, avec sa branche acoustique presque linéaire en le nombre d'onde q, ne peut décrire de manière fiable les ondes sonores de pulsation $\omega_{\mathbf{q}} > mc^2/\hbar$ du superfluide de fermions. Ignorante de la nature composite des paires liées $\uparrow\downarrow$, elle est totalement inapplicable aux pulsations $\omega \approx E_{\rm paire}/\hbar$, où $E_{\rm paire}$ est l'énergie de liaison d'une paire : à ces pulsations, les paires peuvent se briser en deux excitations fermioniques χ (la conservation de l'énergie ne l'interdit plus), voir la figure 5a.

Il faut alors avoir recours à une description microscopique du gaz de fermions. À température nulle, la principale méthode disponible est celle de la théorie variationnelle BCS dépendant du temps [108]. Sa spécialisation au régime de réponse linéaire donne l'équation aux valeurs propres suivante sur l'énergie z des modes de vecteur d'onde $\mathbf{q}$:

$$\det M(\mathbf{q},z) = 0 \quad \text{avec } M(\mathbf{q},z) = \begin{pmatrix} M_{|\Delta||\Delta|}(\mathbf{q},z) & M_{|\Delta|\theta}(\mathbf{q},z) \\ M_{\theta|\Delta|}(\mathbf{q},z) & M_{\theta\theta}(\mathbf{q},z) \end{pmatrix} \tag{69}$$

où les coefficients de la matrice 2×2 correspondent à une réponse en le module $|\Delta|$ ou en la phase θ du paramètre d'ordre complexe $\Delta(\mathbf{r},t)$. Dans la limite BCS d'interaction faible $k_{\rm F}a \to 0^-$, les éléments non diagonaux sont habituellement négligés (à juste titre) et la dynamique se découple en mode de module et mode de phase ; dans le cas général, cette distinction ne vaut plus.

[60] L'amortissement étudié expérimentalement dans la référence [107] est dans le régime hydrodynamique, au sens de la note 41. Cette référence ne permet donc pas de trancher.

L'exploration des solutions de l'équation (69) a commencé. À nombre d'onde q fixé, on trouve sous le bord $\varepsilon_{\mathbf{q}}^{\text{bord}}$ du continuum de paire brisée au plus une racine, celle $\hbar\omega_{\mathbf{q}}$ de la branche acoustique. Sur l'intervalle $z \in]\,\varepsilon_{\mathbf{q}}^{\text{bord}}, +\infty\,[$, la fonction $\det M(\mathbf{q},z)$ admet une ligne de coupure[61], il faut mettre un décalage infinitésimal $\mathrm{i}0^+$ dans z pour lui donner un sens ; elle acquiert alors une partie imaginaire, qu'on n'arrive pas à annuler simultanément avec la partie réelle, et l'équation (69) n'admet pas de solution. En revanche, on peut en trouver une, complexe $z_{\mathbf{q}}$ de partie imaginaire non infinitésimale < 0, en prolongeant analytiquement la fonction $z \mapsto \det M(\mathbf{q},z)$ du demi-plan complexe supérieur au demi-plan inférieur à travers sa ligne de coupure (ce qu'indique la flèche $\downarrow$ en indice) :

$$\det M_{\downarrow}(\mathbf{q}, z_{\mathbf{q}}) = 0 \quad \text{avec } \mathrm{Im}\, z_{\mathbf{q}} < 0 \tag{70}$$

Il existe donc un mode collectif dans le continuum, qui s'amortit exponentiellement en temps par émission de paires brisées. Le calcul a été fait d'abord dans la limite BCS $k_{\mathrm{F}}a \to 0^-$, aussi bien pour des fermions neutres que pour les électrons d'un supraconducteur, dans la référence [109]. Il a été ensuite généralisé aux gaz d'atomes froids fermioniques pour une valeur quelconque de $k_{\mathrm{F}}a$, sans qu'on puisse plus négliger les éléments non diagonaux $M_{|\Delta|\theta}$ et $M_{\theta|\Delta|}$ [110,111]. La branche d'Andrianov–Popov subsiste jusqu'à $1/k_{\mathrm{F}}a = 0{,}55$ (point d'annulation $\mu = 0$ du potentiel chimique dans la théorie BCS) et présente toujours un départ à $2|\Delta|$ quadratique en q avec un coefficient complexe :

$$z_{\mathbf{q}} \underset{q\to 0}{\overset{\mu>0}{=}} 2|\Delta| + \zeta \frac{\hbar^2 q^2}{4m_*} + O(q^3) \quad (\mathrm{Im}\,\zeta < 0) \tag{71}$$

où m_* est la masse effective d'une quasi-particule fermionique χ à l'endroit $k = k_0$ de son minimum d'énergie[62]. Nous avons écrit ici $2|\Delta|$ plutôt que E_{paire}, où Δ est le paramètre d'ordre à l'équilibre, même si la théorie BCS est incapable de distinguer (on a exactement $E_{\text{paire}} = 2|\Delta|$ pour tout $\mu > 0$ dans cette théorie), afin d'évoquer le mécanisme de Higgs [113] dont on pense que le mode collectif du continuum relève [114][63] ; d'ailleurs, dans la limite opposée $k_{\mathrm{F}}a \to 0^+$ d'un condensat de dimères bosoniques, où $2|\Delta| \ll E_{\text{paire}} \sim 2|\mu| \sim \hbar^2/ma^2$ (on a cette fois $\mu < 0$), on trouve bien une branche d'excitation collective commençant quadratiquement à $2|\Delta|$ et non pas à E_{paire} [111]. L'extension de l'équation (69) à température non nulle (au-delà d'une simple

[61] Les éléments de matrice de $M(\mathbf{q},z)$ comportent une intégrale sur le vecteur d'onde $\mathbf{k}$ d'un des fragments de dissociation d'une paire liée du condensat, avec dans l'intégrande le dénominateur d'énergie correspondant $z - (\varepsilon_{\mathbf{k}} + \varepsilon_{\mathbf{q}-\mathbf{k}})$; par définition, le dénominateur peut donc s'annuler quand z appartient au continuum de paire brisée, voir la légende de la figure 5.

[62] On l'aura compris, la masse effective est telle que $\varepsilon_{\mathbf{k}} - E_{\text{paire}}/2 \sim \hbar^2(k-k_0)^2/2m_*$ quand $k \to k_0$. La mise à l'échelle par m_* dans l'équation (71) assure que ζ a une limite finie et non nulle lorsque $k_{\mathrm{F}}a \to 0^-$ [109]. Dans ce même régime, la référence pourtant connue [112] prédit un comportement fantaisiste de $z_{\mathbf{q}}$ à faible q, avec une partie imaginaire tendant vers zéro linéairement en q, voir son équation (2.38). La quantité ζ n'a ici rien à voir avec celle de l'équation (67), il y a une coïncidence malheureuse de notations.

[63] Comme ce mécanisme résulte de la brisure de symétrie $U(1)$, ici par condensation des paires liées, il doit être caractérisé par l'échelle d'énergie associée au paramètre d'ordre, c'est-à-dire $|\Delta|$ à un facteur près ; c'est bien ce que trouve la référence [113], voir son équation (2b). En revanche, l'échelle d'énergie E_{paire} est reliée à la brisure de paires, pas à leur condensation, donc n'a a priori aucun rapport avec la branche de Higgs. Le fait d'avoir $E_{\text{paire}} = 2|\Delta|$ est source de confusion et empêche de découpler les deux phénomènes. Il serait par ailleurs intéressant de voir si la propriété $E_{\text{paire}} = 2|\Delta|$ reste rigoureusement vraie à température nulle dans une théorie plus élaborée que BCS ou dans les expériences.

généralisation de type BCS en champ moyen, peut-être insuffisante[64]) reste à notre connaissance une question ouverte.

D'un point de vue expérimental, dans les atomes froids ou les supraconducteurs, l'excitation à des pulsations $\omega > E_{\text{paire}}/\hbar$ a été effectuée seulement à nombre d'onde nul, où il n'y a d'après les théories à température nulle pas de mode collectif du continuum, le poids spectral du mode tendant vers 0 lorsque $q \to 0$ [110] ; on observe simplement aux temps longs des oscillations du paramètre d'ordre à la pulsation $E_{\text{paire}}/\hbar$ (c'est l'effet du bord non nul du continuum) qui s'amortissent en loi de puissance $t^{-\alpha}$ [117,118] par le même mécanisme que l'étalement du paquet d'ondes gaussien d'une particule libre en mécanique quantique ordinaire (l'excitation percussionnelle crée un « paquet d'ondes » de paires brisées $(\mathbf{k}, -\mathbf{k})$ dans le continuum, dont l'évolution gouvernée par la relation de dispersion $2\varepsilon_{\mathbf{k}}$ est de manière effective unidimensionnelle pour $k_0 > 0$ ($\mu > 0$), auquel cas $\alpha = 1/2$ [119], et tridimensionnelle pour $k_0 = 0$ ($\mu < 0$), auquel cas $\alpha = 3/2$ [120])[65]. L'observation du mode du continuum (à $q > 0$) et la mesure précise de sa relation de dispersion $z_{\mathbf{q}}$ restent donc à faire (des pistes sont données dans les références [110,121]).

Déclaration d'intérêts

Les auteurs ne travaillent pas, ne conseillent pas, ne possèdent pas de parts, ne reçoivent pas de fonds d'une organisation qui pourrait tirer profit de cet article, et n'ont déclaré aucune autre affiliation que leurs organismes de recherche.

English version (la version française commence à la page 394)

To obtain the English version, we translated the French version with ™DeepL Pro and a self-made glossary of technical terms. The result was improved with ™DeepL Write.

1. Introduction and general presentation

This text is essentially the transcript of our 90-minute talk at the prospective symposium "Open questions in the quantum many-body problem" held at the Institut Henri Poincaré in Paris, from

[64] Cette généralisation n'est pas une panacée, comme on le voit sur la partie imaginaire de la branche acoustique. Pour $\gamma > 0$ (mais pas pour $\gamma < 0$), ce reproche peut être fait à la RPA déjà à température nulle, puisqu'elle prédit à tort une pulsation propre $\omega_{\mathbf{q}}$ purement réelle. Cependant, ça ne semble pas être très grave car la partie imaginaire $(-1/2)\Gamma_{\mathbf{q}}(T=0) \approx q^5$ obtenue par l'hydrodynamique quantique (amortissement de Belyaev) vient se perdre dans les termes sous-sous-dominants négligés dans l'équation (34). Ce problème est plus visible à faible q à température non nulle, où $\Gamma_{\mathbf{q}}(T>0)$ commence linéairement en q avec un coefficient en T^4 (l'exposant ν vaut 5 dans le tableau 1 pour la loi d'échelle $q \propto T$ de la note 41), ce dont la théorie de type BCS en champ moyen ne peut rendre compte (elle prédit un coefficient en $O[-\exp(E_{\text{paire}}/2k_{\text{B}}T)]$ [115,116] puisque les seuls nombres d'occupation thermiques qu'elle fait apparaître sont ceux $\bar{n}_{\mathbf{k}} = 1/[\exp(\varepsilon_{\mathbf{k}}/k_{\text{B}}T)+1]$ des quasi-particules fermioniques χ). En d'autres termes, la linéarisation des équations BCS dépendant du temps ou, ce qui revient au même, l'approximation des fluctuations gaussiennes prend en considération le couplage $\phi - \chi$ mais pas le couplage $\phi - \phi$.

[65] Les observations de la référence [118] dans un gaz unitaire de fermions à $T \neq 0$ soulèvent cependant plusieurs questions : (i) l'exposant $\alpha \simeq 1 \pm 0{,}15$ mesuré est fort différent de la valeur prédite théoriquement ($\alpha = 1/2$ à la limite unitaire), (ii) il ne peut être exclu que la décroissance de l'amplitude des oscillations soit en réalité exponentielle, (iii) au contraire de l'amplitude, la pulsation des oscillations ne présente aucune réduction observable lorsque T se rapproche de la température de transition T_{c} (où il n'y a plus de brisure de symétrie $U(1)$ et $|\Delta|$ tend vers zéro) ce qui semble incompatible avec la qualification d'oscillations de Higgs utilisée dans cette référence (la pulsation mesurée n'est pas proportionnelle à $|\Delta|/\hbar$), mais suggère aussi une constance de E_{paire} en température assez troublante (la pulsation mesurée devrait être donnée par $E_{\text{paire}}/\hbar$ puisque l'excitation est faite à $q = 0$). Rappelons par ailleurs que la température n'est jamais très faible dans l'expérience, $T \gtrsim 0{,}1\,T_{\text{F}}$, voir notre section 2, ce qui rend la théorie à $T = 0$ stricto sensu inapplicable.

July 8 to 12, 2024, hence its style and level of precision differ from that of a usual research article. It is more complete than the presentation on Section 4 (treated briefly at the oral presentation) and on Section 5 (omitted at the oral presentation due to lack of time). Footnotes can be ignored on first reading. The presentation was recorded and is available online on the IHP Carmin channel (click here).

The system considered is inspired by experiments on cold atoms: it is a three-dimensional two-component Fermi gas (meaning two internal states $\uparrow$ and $\downarrow$) in an immaterial trap—made of light, at very low temperatures in the microkelvin range. This is the worthy descendant of laser-cooled atomic gases (in the famous "optical molasses", see the 1997 Nobel Prize in Physics awarded to Steven Chu, William Phillips and Claude Cohen-Tannoudji) and then of evaporation-cooled gaseous atomic Bose–Einstein condensates (see the 2001 Nobel Prize in Physics awarded to Eric Cornell, Carl Wieman and Wolfgang Ketterle).

Compared to their illustrious predecessors, cold fermionic atomic gases have the advantage (i) of being composed of fermions, thus covering both possible statistics (the gas can always be "bosonized" by forming strongly bound pairs $\uparrow\downarrow$) and making a direct link with the electron systems (fermions!) of solid-state physics, (ii) of remaining collisionally stable (weak three-body losses by recombination to deep molecular states) even in the strongly interacting regime as in the famous "unitary limit" described below (unlike, for the moment, bosonic cold-atom gases), and (iii) of constituting beautiful, simple and universal model systems in this regime, thanks to the negligible range of van der Waals interactions between $\uparrow$ and $\downarrow$ (more precisely, the associated van der Waals length is negligible); as we shall see, this allows the interaction to be replaced by contact conditions on the N-body wave function, depending solely on the s-wave scattering length a, which experimentalists can adjust at will by means of a Feshbach resonance, simply by applying a well-chosen uniform magnetic field.

Our system is not unrelated to those of other presentations at the symposium. The link is obvious with Tilman Enss's contribution on the viscosity of strongly interacting Fermi gases [1], which complements our own. If we place our fermions in an optical lattice, with about one particle per site (close to half-filling), we recover the problems of strongly correlated fermions and superconductivity at high critical temperature discussed by Antoine Georges. In a regime of strong on-site interaction $U_{\uparrow\downarrow}$ compared to tunnel coupling t between neighboring sites, $U_{\uparrow\downarrow} \gg t$, the system is described by a Heisenberg-type spin model Hamiltonian, with magnetic coupling $J \propto t^2/U_{\uparrow\downarrow}$, which links up with Sylvain Capponi's talk [2]. If we return to a uniform system (without lattice), but apply an artificial gauge field (a fictitious magnetic field) to our fermionic yet neutral cold atoms—which is what experimentalists know how to do, see Sylvain Nascimbène's talk [3]—we come across problems related to the talks by Thierry Jolicœur [4] (on the 2D fractional quantum Hall effect) and Carlos Sá de Melo [5] (spin–orbit coupling in one spatial dimension). All these bridges to solid-state physics are not so easy to build, however, because of non-conservative parasitic effects, finite sample sizes and difficulty in getting down to sufficiently low temperatures (in units of the Fermi temperature T_F or the magnetic coupling temperature J/k_B), see the presentations by Wolfgang Ketterle, Sylvain Nascimbène and Antoine Georges.

Let's finish with the outline of our contribution. In Section 2, we start from reality, outlining the progress of experiments on cold atoms since the 1980s and the situation reached in the case of fermions. In Section 3, we adopt a microscopic point of view, of interactions replaced by contact conditions, and review some open questions in the few-fermion problem. In Section 4, on the other hand, we adopt a macroscopic point of view, that of a low-energy effective theory (quantum hydrodynamics), and review some open questions related to the interaction between phonons (the quanta of sound waves) in the superfluid phase. Finally, in the short Section 5, we cross points of view and list some open questions that require a microscopic theoretical treatment of the full many-body problem.

2. A fairly recent physical system

Let's start by putting our Fermi gases into context, with a brief history of cold atoms.

The adventure began in the early 1980s with the laser cooling of alkalis. The low temperatures reached are spectacular when expressed in kelvins, $T \approx 1$ μK, but the spatial densities are unfortunately very low, $\rho \lesssim 10^{10}$ at/cm^3, so that the gases have very low quantum degeneracy, i.e. very low density in phase space, $\rho\lambda^3 \ll 1$, where λ is the thermal de Broglie wavelength of atoms with mass m:

$$\lambda = \left(\frac{2\pi\hbar^2}{m k_B T}\right)^{1/2} \tag{1}$$

The effects of quantum statistics (bosonic or fermionic) are imperceptible.

This all changed in 1995, when Eric Cornell and Carl Wieman at JILA [6], shortly followed by Wolfgang Ketterle at MIT [7], achieved Bose–Einstein condensation (BEC), obviously on bosonic isotopes, thanks to evaporative cooling in non-dissipative trapping potentials with harmonic bottoms[1]. Transition temperatures remain in the range of laser cooling, $T_c^{BEC} \simeq 0.1$ to 1 μK, but spatial densities are considerably higher, $\rho = 10^{12}$ to 10^{15} at/cm^3, enabling quantum degeneracy $\rho\lambda^3 \gtrsim 1$ to be achieved.

Finally, in 2004, evaporative cooling was successfully extended to fermionic isotopes down to the transition temperature [11,12]; gases with two internal states ↑ and ↓ no longer form Bose–Einstein condensates, but condense in ↑↓ pairs by the BCS mechanism [13]: the attractive van der Waals interactions between ↑ and ↓, in the presence of a Fermi sea in each internal state, lead to the formation of bound pairs, the famous Cooper pairs, "composite bosons", which can form a condensate at sufficiently low temperatures, $T < T_c^{BCS}$. The lowest experimentally accessible temperatures are of the order of $0.1\,T_F$, where the Fermi temperature T_F remains of the order of a microkelvin; this is nevertheless sufficient to go below T_c^{BCS} because the interactions between ↑ and ↓ are made very strong by means of a two-body scattering resonance (magnetic Feshbach resonance): the transition temperature T_c^{BCS} is then a fraction of T_F and we avoid the extreme situation of BCS superconductors, for which $T_c^{BCS} \lll T_F$ by several orders of magnitude.

Let's now describe our system of fermionic cold atoms in broad outline, in an attempt to idealize experimental reality. (i) The fermions have two internal states ↑ and ↓; as we are not considering here a Rabi coupling between ↑ and ↓, our considerations also apply to the case of a mixture of two formally spinless fermionic chemical species; for this reason, we do not assume that the masses m_σ of the particles are equal in the two internal states[2] and we consider the ratio $m_\uparrow/m_\downarrow$ as a free parameter. (ii) The fermions are trapped either in isotropic harmonic potentials of the same trapping angular frequency ω for the two components σ,

$$U_\sigma(\mathbf{r}) = \tfrac{1}{2} m_\sigma \omega^2 r^2 \tag{2}$$

where $\mathbf{r}$ is the 3D position vector, or in the cubic quantization box $[0,L]^3$ common to both components, with the usual periodic boundary conditions[3]. (iii) The van der Waals interaction between the two internal states ↑ and ↓, shown schematically in Figure 1a, is effectively made very strong (resonant) in s wave (relative orbital angular momentum $l = 0$) by application of

[1] Reference [8] later succeeded, using clever tricks, in obtaining a Bose–Einstein condensate without evaporation, by laser cooling alone (see also reference [9]); in particular, this involved (i) using a narrow atomic line with low saturation to keep the temperature limit of laser cooling [10] as low as possible, and (ii) preventing spontaneously emitted photons, which carry away part of the energy of atomic motion, from depositing it back into the gas by reabsorption.

[2] In the case where ↑ and ↓ are two spin states of the same chemical species, we naturally have $m_\uparrow = m_\downarrow$ in the experiment. However, by applying an optical lattice that couples differently to the two internal states (within a low filling factor limit), we could produce different effective masses m_σ. This remains to be done.

[3] Experimentally, flat-bottom potentials can be produced using Laguerre–Gauss or Bessel–Gauss beams and laser light sheets, after gravity compensation (levitation of atoms) by a magnetic field gradient [14–16].

a suitable magnetic field[4] so that the scattering length a between two atoms $\uparrow$ and $\downarrow$ (defined mathematically in Section 3.1) is sufficiently large in absolute value (it can be positive or negative) so that

$$\rho^{1/3}|a| \gtrsim 1 \tag{3}$$

We recall that the theory of weakly interacting Bose gases relies on the small parameter $(\rho a^3)^{1/2} \ll 1$, see Jan Solovej's contribution [17] to the symposium proceedings; condition (3) is therefore, on the contrary, the mark of a strongly interacting gas. The scattering length a is also much greater in absolute value than the interaction range b, defined in Figure 1a,

$$|a| \gg b \tag{4}$$

which is indeed the hallmark of a two-body scattering resonance. As b is of the order of a few nanometers in the experiments, we also have

$$b \ll \rho^{-1/3}, \lambda \tag{5}$$

which gives us the idea of constructing a model system, by taking the limit of a zero-range interaction $b \to 0$ at fixed a, characterized only by the algebraic length a. This idea will be implemented in Section 3.1. (iv) On the other hand, the interaction is not resonant in p wave (relative orbital angular momentum $l = 1$), so the $\uparrow\uparrow$ and $\downarrow\downarrow$ interactions, which occur predominantly in this wave at low energy (due to fermionic antisymmetry), are negligible.

As we shall see in Section 3, the existence of a well-defined model (of energy bounded from below when $b \to 0$) is a mathematically non-trivial problem. We can already propose a necessary condition, inspired by experimental reality. Since the van der Waals interaction supports (at least) a two-body bound state of size $\approx b$, as shown in Figure 1a, the gas phase considered so far and seen in experiments is only a metastable phase, temporarily escaping the solidification predicted by the laws of equilibrium physics, a solidification of which three-body losses are the precursors (see Figure 1b). These losses occur at a rate estimated as follows in reference [18] for equal masses:

$$\Gamma_{\text{losses}}^{\text{3-body}} \propto \frac{\hbar}{mb^2} \text{ Proba(3 fermions } \uparrow\uparrow\downarrow \text{ or } \downarrow\downarrow\uparrow \text{ in a same ball of radius } b) \tag{6}$$

The first factor represents the relevant energy scale of this recombination process: this is the binding energy of the strongly bound dimer formed, and the length scale $|a| \gg b$ cannot come into play. The second factor takes into account the fact that the three-fermion process cannot occur if one of the fermions is separated from the other two by a distance $\gg b$, by quasi-locality in position space: the interaction range and the size of the strongly bound dimer are both of the order of b. The proportionality factor in Equation (6) depends on the details of the microscopic physics. This leads to an experimental stability condition for the Fermi gas in the $b \to 0$ limit of a contact interaction:

$$\Gamma_{\text{losses}}^{\text{3-body}} \underset{b\to 0}{\to} 0 \tag{7}$$

[4] Without going into too much detail, it should be pointed out that, to understand this resonance, it is necessary to take into account the internal structure of the atoms and describe their binary interaction a minima by a two-channel model, with an open channel $V_o(r_{12})$ interaction potential and a closed channel $V_f(r_{12})$ interaction potential—think of the singlet and triplet interaction potentials of two spin-1/2 fermions. In a collision, atoms $\uparrow$ and $\downarrow$ enter through the open channel and, by conservation of energy, also exit through the open channel, as their relative incoming kinetic energy is less than the difference of dissociation limits $V_f(+\infty) - V_o(+\infty) > 0$. As there is a coupling between the two channels, however, the atoms virtually populate the closed channel during the collision. The applied magnetic field B induces a different Zeeman shift in the two channels. A clever choice of B is then all that's needed to ensure that the energy of a bound state in $V_f(r_{12})$—not the bare energy, but the energy shifted by the coupling—almost coincides with the dissociation limit $V_o(+\infty)$, inducing a two-body scattering (or collision) resonance in the open channel and making the scattering length a diverge.

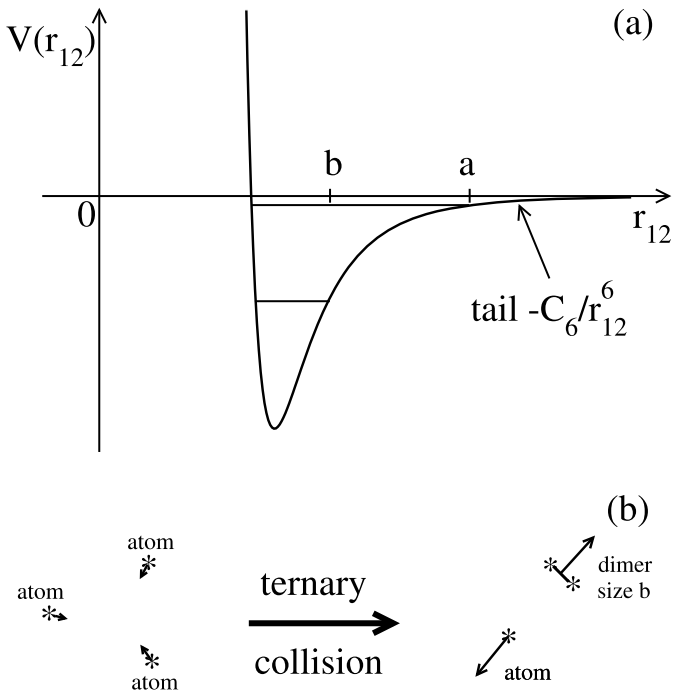

Figure 1. (a) Schematic representation of the resonant van der Waals (more precisely, Lennard-Jones) interaction ($|a| \gg b$) between $\uparrow$ and $\downarrow$ fermions as a function of their relative distance. The potential supports at least one strongly bound state of extension of the order of the van der Waals length $b \simeq (mC_6/\hbar^2)^{1/4}$ and therefore of binding energy $\approx \hbar^2/mb^2$ and, in the case of a scattering length $a > 0$ as in the figure, a last energy level of extension a (of binding energy $\hbar^2/ma^2$) on "the verge of disappearing" (here $m_\uparrow = m_\downarrow = m$ as in the experiments); if a were large but negative ($|a| \gg b, a < 0$), this weakly bound state would be on "the verge of appearing". (b) The strongly bound dimer state can be populated by three-body collisions, which causes particle losses in the Fermi gas, known as three-body losses (the collision products carry away the considerable binding energy $\approx \hbar^2/mb^2$ in the form of kinetic energy and leave the trap). The arrows represent the linear momenta before and after the collision.

The study of this system, though gaseous, is made non-trivial by the interaction strength. For example, since $k_F|a| \approx 1$, where $k_F = (3\pi^2\rho)^{1/3}$ is the Fermi wave number, the superfluid transition temperature is a priori of the order of the Fermi temperature $T_F = E_F/k_B$ (there is no other scale available than the Fermi energy $E_F = \hbar^2 k_F^2/2m$) and will be difficult to calculate accurately: BCS theory will be qualitative at best, and quantum Monte Carlo methods are difficult to apply to fermions; the challenge has, however, been met by reference [19], in the symmetric case of equal masses and chemical potentials in the two components, where Monte Carlo methods free of the famous "sign problem" exist.

3. Open questions from a microscopic point of view

In this section, fermion interactions are replaced in a zero-range limit by contact conditions on the N-body wave function, the Hamiltonian operator then reducing to that of the ideal gas (Wigner–Bethe–Peierls model [20,21]).

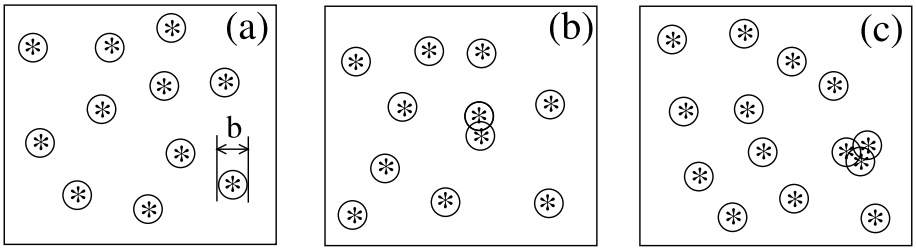

Figure 2. Photograph of the Fermi gas showing the positions (stars) of the N fermions, as would be obtained with a quantum gas microscope, in the limit of an interaction range $b \to 0$ (for illustrative purposes, we have surrounded each star with a circle of diameter b). (a) Typical case: the particles are separated by a distance $\gg b$ and do not interact. This sets the Hamiltonian operator (9) of the Wigner–Bethe–Peierls model. (b) Case where two particles $\uparrow$ and $\downarrow$, well separated from the others, undergo a binary collision. This sets the contact conditions (17) of the model. (c) Case of an isolated ternary collision. This raises the question of the need for three-body contact conditions.

3.1. *Defining the Wigner–Bethe–Peierls model*

To build the model, let's start from the simple perception that a photograph of the gas would give us, i.e. a measurement of the positions of the N fermions, as quantum gas microscopes have recently been able to do in the homogeneous case [22]. In the limit where the interaction range b tends to zero, the typical photograph looks like Figure 2a: the fermions are separated two by two by a distance $\gg b$ and the interaction potential $V(\mathbf{r}_i - \mathbf{r}_j)$ is negligible. The N-body wave function obeys in this case the stationary Schrödinger equation

$$E\psi = H_{\text{ideal gas}}\psi \tag{8}$$

with the Hamiltonian operator of the ideal gas, the sum of the kinetic energy $\mathbf{p}^2/2m_\sigma$ and trapping $U_\sigma(\mathbf{r})$ terms in each internal state σ:

$$H_{\text{ideal gas}} = \sum_{i=1}^{N_\uparrow} \left(\frac{\mathbf{p}_i^2}{2m_\uparrow} + U_\uparrow(\mathbf{r}_i) \right) + \sum_{j=N_\uparrow+1}^{N} \left(\frac{\mathbf{p}_j^2}{2m_\downarrow} + U_\downarrow(\mathbf{r}_j) \right) \tag{9}$$

It is convenient here to number the particles so that the first $N_\uparrow$ are in internal state $\uparrow$ and the last $N_\downarrow$ are in internal state $\downarrow$; the wave function $\psi(\mathbf{r}_1, \ldots, \mathbf{r}_N)$ is then an antisymmetric function of the first $N_\uparrow$ positions and an antisymmetric function of the last $N_\downarrow$ positions. Some pictures, however, will resemble Figure 2b: two fermions i and j, of different internal states, respectively $\uparrow$ and $\downarrow$, are separated from the others by a distance $\gg b$ but are separated from each other by a distance $\approx b$ and are therefore affected by the interaction potential $V(\mathbf{r}_i - \mathbf{r}_j)$. The correct way of looking at this is to say that i and j are undergoing isolated two-body scattering in the gas, which has two consequences, one qualitative, the other quantitative.

Qualitatively, we understand that in our very low density gas (in the sense of $\rho b^3 \ll 1$), it is better to characterize the interaction between $\uparrow$ and $\downarrow$ by its two-body scattering amplitude, more generally by a transmission operator known as the T matrix, than by the function $V(\mathbf{r})$ itself; as the interaction occurs in the s wave, the scattering amplitude f is isotropic and depends only on

the relative wave number $k_{\rm rel}$ of the two particles; in the limit $b \to 0$ at a fixed scattering length a, we then have the low-energy expansion[5]

$$f_{k_{\rm rel}} = \frac{-1}{a^{-1} + {\rm i}k_{\rm rel} - (1/2)k_{\rm rel}^2 r_{\rm e} + O(k_{\rm rel}^3 b^2)} \tag{10}$$

We assume in the following that the effective range $r_{\rm e}$ of the interaction is $O(b)$ and therefore becomes negligible as $b \to 0$ [6]. So the scattering amplitude reduces to the universal form for a contact interaction

$$f_{k_{\rm rel}}^{\rm contact} = \frac{-1}{a^{-1} + {\rm i}k_{\rm rel}} \tag{11}$$

Quantitatively, we expect the two nearby $\uparrow$ and $\downarrow$ fermions to decouple from the $N-2$ others in the N-body wave function, in the sense that

$$\psi(\mathbf{r}_1, \ldots, \mathbf{r}_N) \underset{r_{ij}=O(b)}{\simeq} \phi(\mathbf{r}_i - \mathbf{r}_j) A_{ij}(\mathbf{R}_{ij}; (\mathbf{r}_k)_{k\neq i,j}) \tag{12}$$

where $\mathbf{R}_{ij} = (m_\uparrow \mathbf{r}_i + m_\downarrow \mathbf{r}_j)/(m_\uparrow + m_\downarrow)$ is the center of mass position of the particles i and j, $\mathbf{r}_{ij} = \mathbf{r}_i - \mathbf{r}_j$ is their relative position, $(\mathbf{r}_k)_{k\neq i,j}$ is the $(N-2)$-uplet of the positions of the other particles, the function A_{ij} is generally not known, and $\phi(\mathbf{r})$ is a two-body scattering state, solution of Schrödinger equation

$$\varepsilon\phi(\mathbf{r}) = -\frac{\hbar^2}{2m_{\rm rel}}\Delta\phi(\mathbf{r}) + V(\mathbf{r})\phi(\mathbf{r}) \tag{13}$$

for the relative motion of mass $m_{\rm rel} = m_\uparrow m_\downarrow/(m_\uparrow + m_\downarrow)$ at an energy ε given in reference [24] (see its Equation (85)) but which we will retain only as $\approx \hbar^2 k_{\rm typ}^2/2m_{\rm rel}$, where the typical wave number $k_{\rm typ}$ in the gas is of the order of $k_{\rm F}$ for $T = O(T_{\rm F})$. In the limit $b \to 0$, it is in fact sufficient to analyze Equation (13) in the interval

$$b \ll r \ll k_{\rm typ}^{-1} \tag{14}$$

with the case $r \leq b$ providing only non-universal details of the interaction and the case $r > k_{\rm typ}^{-1}$ invalidating the factorization (12) (the pair ij is no longer well isolated as in the photo in Figure 2b). The first inequality in Equation (14) allows $V(\mathbf{r})$ to be set to zero in the right-hand side, and the second allows energy ε to be set to zero in the left-hand side of Equation (13), hence the simplified Schrödinger equation

$$0 = -\frac{\hbar^2}{2m_{\rm rel}}\Delta\phi(\mathbf{r}) \tag{15}$$

Its general solution in the s wave (rotationally symmetric) is a linear combination of the constant solution 1 (the incoming wave of zero energy) and the Coulomb solution (the scattered wave) with a relative amplitude fixed by $V(\mathbf{r})$ at short distances:

$$\phi(\mathbf{r}) = \mathcal{N}\left(1 - \frac{a}{r}\right) = \frac{1}{a} - \frac{1}{r} \tag{16}$$

By definition, see Jan Solovej's contribution [17], the quantity a is the scattering length of the potential. In the third expression, we have chosen the convenient normalization (factor $\mathcal{N}$ taken equal to $1/a$ in the second expression) to have a finite result at the $a^{-1} = 0$ scattering resonance.

[5] If $V(\mathbf{r})$ decays faster than $1/r^7$ at infinity, we can put an $O(k_{\rm rel}^4 b^3)$ in the denominator.

[6] Experimentally, however, there are so-called narrow magnetic Feshbach resonances, for which negative $r_{\rm e}$ is gigantic on the atomic scale and can be of the order of $1/k_{\rm F}$, due to an unusually weak coupling between the open and closed channels of our note 4, see reference [23]. These resonances are difficult to use, as they require very good control of the magnetic field. The existence of a non-zero effective range as $b \to 0$, however, has the advantage of stabilizing the gas in the unstable regime of Section 3.2 (the spectrum remains bounded from below and the three-body loss rate (6) tends to zero), and should enable the preparation and observation of long-lived Efimovian bound states, provided the mass ratio $m_\uparrow/m_\downarrow$ is large enough. The experiment remains to be done.

We thus arrive naturally at the definition of the Wigner–Bethe–Peierls model for our three-dimensional system of $(N_\uparrow, N_\downarrow)$ two-component fermions with zero-range interaction and s-wave scattering length $a \neq 0$:

(1) the Hamiltonian operator is the same as that of the ideal gas, as in Equations (8), (9)
(2) there is fermionic antisymmetry of the state vector ψ for the first $N_\uparrow$ and for the last $N_\downarrow$ positions
(3) the interaction is described not by a potential V but by the following contact conditions on ψ: for any index $i \in \{1, \ldots, N_\uparrow\}$ and any index $j \in \{N_\uparrow + 1, \ldots, N = N_\uparrow + N_\downarrow\}$, there exists a function A_{ij} such that[7]

$$\psi(\mathbf{r}_1, \ldots, \mathbf{r}_N) \underset{r_{ij}\to 0}{=} A_{ij}(\mathbf{R}_{ij}, (\mathbf{r}_k)_{k\neq i,j}) \left(\frac{1}{r_{ij}} - \frac{1}{a}\right) + O(r_{ij}) \tag{17}$$

where the distance r_{ij} between particles i and j tends to zero at fixed positions of their center of mass $\mathbf{R}_{ij}$ and other particles $\mathbf{r}_k$, with the constraints $\mathbf{R}_{ij} \neq \mathbf{r}_k \forall k \neq i, j$ and the $\mathbf{r}_k$ two-by-two distinct (as in Figure 2b).

Mathematically, point 3 means that the domain of the Hamiltonian operator is not the same as that of the ideal gas: in the absence of interaction ($a = 0$), we rightly eliminate solutions that diverge as $1/r_{ij}$, as stated in any good book on quantum mechanics. That's the only difference, but it's a big one[8]!

Figure 2c, which shows a trio of atoms in close proximity, well separated from the others and undergoing three-body scattering, raises a legitimate question: should we complete the model with three-body contact conditions? four-body? etc. Answer in the next section.

3.2. *Questions of existence*

It is not obvious that the Wigner–Bethe–Peierls model, as defined on page 433, leads to a self-adjoint Hamiltonian (without additional contact conditions) and, above all, to an energy spectrum bounded from below. In fact, we have boldly stretched an energy scale to $-\infty$, the $-\hbar^2/m_{\text{rel}}b^2$ scale associated with the interaction range, by taking the $b \to 0$ limit at a fixed scattering length a, i.e. without letting the interaction strength tend to zero, which could cause the system to collapse, as in the well-known Thomas effect in nuclear physics [26]!

The discussion becomes clearer in the special case $a^{-1} = 0$, known as the unitary limit (the scattering amplitude (11) of the model reaches the maximum modulus k_{rel}^{-1} allowed in the s wave by the unitarity of the scattering matrix S), as the contact conditions (17) become scale invariant (this is also the most interesting and open regime, because it corresponds to a maximally interacting gas phase). For simplicity's sake, let's restrict ourselves to $E = 0$ energy eigenstates in free space, with the center of mass of the N fermions at rest. As there is no external energy or potential to introduce a length scale, we expect the eigenstate ψ to be scale invariant, i.e. a

[7] The functions A_{ij} are not independent. Fermionic antisymmetry dictates that $A_{ij}(\mathbf{R}_{ij}, (\mathbf{r}_k)_{k\neq i,j}) = (-1)^{i-1}(-1)^{j-(N_\uparrow+1)} A_{1,N_\uparrow+1}(\mathbf{R}_{ij}, (\mathbf{r}_k)_{k\neq i,j})$ (to bring them to the first position in their respective internal states and thus reveal the function $A_{1,N_\uparrow+1}$, we had to pass $\mathbf{r}_i$ through $i-1$ position vectors of $\uparrow$ fermions and $\mathbf{r}_j$ through $j-(N_\uparrow+1)$ position vectors of $\downarrow$ fermions, hence the signs).

[8] A key point is that the scattering state $\phi(\mathbf{r}) = 1/r - 1/a$ is square-summable on a neighborhood of the origin, $\int_{r<r_{\max}} \mathrm{d}^3 r\, |\phi(\mathbf{r})|^2 < \infty$: there is therefore no cutoff to be put at short distance and a is the only length associated with the interaction. The situation is different in waves of angular momentum $l > 0$: $\phi(\mathbf{r}) = Y_l^{m_l}(\theta, \varphi)(r^l + a_{\text{gen}}^{2l+1}/r^{l+1})$ (where the parameter $a_{\text{gen}} \neq 0$ generalizing a is a length and $Y_l^{m_l}$ is a spherical harmonic) is then no longer square-summable, and a cutoff and thus a second length must be introduced to characterize the interaction [25].

homogeneous function of the coordinates (invariant up to a factor by the homothety $\mathbf{r}_i \to \lambda \mathbf{r}_i$ of ratio λ applied to the N positions), of the form [27,28]

$$\psi(\mathbf{r}_1,\ldots,\mathbf{r}_N) = R^{s-\frac{3N-5}{2}}\Phi(\Omega) \tag{18}$$

where (i) R is the internal hyperradius, the root-mean-square deviation of the mass-weighted positions of the N particles relative to their center of mass $\mathbf{C}$,

$$MR^2 = \sum_{i=1}^{N} m_i(\mathbf{r}_i-\mathbf{C})^2 \tag{19}$$

with $M=\sum_{i=1}^N m_i$ the total mass and $M\mathbf{C}=\sum_{i=1}^N m_i\mathbf{r}_i$; (ii) the scaling exponent (the degree of homogeneity) is conveniently defined by the quantity s after translation of $(3N-5)/2$—to reveal an $s\leftrightarrow -s$ symmetry; (iii) Φ is an unknown function of the $3N-4$ hyperangles completing R in the parameterization of $\mathbf{r}_i-\mathbf{C}$ in hyperspherical coordinates. Carrying over the ansatz (18) into the Schrödinger equation (8) (with $E=0$ and $U_\sigma\equiv 0$ as mentioned) gives an eigenvalue equation for Φ:

$$\left[-\Delta_\Omega + \left(\frac{3N-5}{2}\right)^2\right]\Phi(\Omega) = s^2\Phi(\Omega) \tag{20}$$

whose eigenvalues are precisely s^2! Since the Laplacian Δ_Ω is taken on a compact, the unit hypersphere S_{3N-4}, the possible values of s^2 form a discrete set, belonging to $\mathbb{R}$ if one assumes that the Hamiltonian is Hermitian; we generally don't know how to calculate them, because of the difficult contact conditions (17) on $\Phi(\Omega)$ [9].

In the following, we'll simply write formally that s is the root of an even transcendental function, the so-called Efimov function,

$$\Lambda_{N_\uparrow,N_\downarrow}(s) = 0 \tag{21}$$

without specifying this function (the most direct way to obtain it is to impose the contact conditions (17) on a Faddeev ansatz written in reciprocal space[10], which leads to a Skorniakov–Ter-Martirosian integral equation—here in the unitary limit at zero energy, in which we inject the Fourier equivalent of ansatz (18); the resulting transcendental equation (21) can be written explicitly for $N=3$ [29], and is written as the determinant of an operator for $N>3$, this operator being given explicitly for $N=4$ in sector $(3,1)$ by reference [30] and in sector $(2,2)$ by reference [31]). We must now distinguish between two cases.

First case: $s^2>0$**.** There are two possible values for the scaling exponent, one value >0 which we agree to call s, and the opposite value $-s<0$. By a phenomenon similar to that of Equation (16), ψ is in general a linear combination of two solutions, one containing a factor R^s, the other containing a factor R^{-s}, the relative amplitudes being univocally fixed by a length ℓ (the equivalent

[9] On the other hand, contact conditions (17) do not constrain the dependence of ψ on the hyperradius. This is because, if ψ obeys the contact conditions, $f(R)\psi$ also obeys them, provided that the factor $f(R)$ is a regular function of R. Indeed, in the limit $r_{ij}\to 0$ with $\mathbf{R}_{ij}$ and $(\mathbf{r}_k)_{k\neq i,j}$ fixed, we have $MR^2 = m_i(\mathbf{r}_i-\mathbf{C})^2 + m_j(\mathbf{r}_j-\mathbf{C})^2 + \text{const} = m_i\mathbf{r}_i^2 + m_j\mathbf{r}_j^2 + \text{const} = (m_i+m_j)\mathbf{R}_{ij}^2 + m_{\text{rel}}r_{ij}^2 + \text{const} = O(r_{ij}^2) + \text{const}$. Then $(1/r_{ij}-1/a)O(r_{ij}^2)$ is $O(r_{ij})$ and negligible.

[10] Let's briefly recall the construction of the ansatz. First, we write the Schrödinger equation for zero energy in the sense of distributions, $H_{\text{ideal gas}}\psi = \sum_{i=1}^{N_\uparrow}\sum_{j=N_\uparrow+1}^{N}(2\pi\hbar^2/m_{\text{rel}})\delta(\mathbf{r}_{ij})A_{ij}(\mathbf{R}_{ij},(\mathbf{r}_k)_{k\neq i,j})$ where Dirac distributions arise from the action of kinetic energy operators on singularities $1/r_{ij}$, by virtue of the Poisson equation $\Delta_{\mathbf{r}}(1/r) = -4\pi\delta(\mathbf{r})$, and m_{rel} is the reduced mass of two opposite-spin fermions as we said. We then take its Fourier transform ($\psi\to\tilde\psi$, $\Delta_{\mathbf{r}}\to -k^2$). Taking advantage of fermionic antisymmetry as in note 7 and of translational invariance (the center of mass is at rest), we reduce to $\tilde\psi(\mathbf{k}_1,\ldots,\mathbf{k}_N) = (\delta(\mathbf{k}_1+\cdots+\mathbf{k}_N)/\sum_{n=1}^N\hbar^2k_n^2/2m_n)\sum_{i=1}^{N_\uparrow}\sum_{j=N_\uparrow+1}^{N}(-1)^{i+j}D((\mathbf{k}_n)_{n\neq i,j})$ where D is the only unknown function (each A_{ij} is a function of the $(\mathbf{r}_k-\mathbf{R}_{ij})_{k\neq i,j}$ of which $D((\mathbf{k}_n)_{n\neq i,j})$ is the Fourier transform up to a factor).

of a in Equation (16)) determined by the microscopic details of the interaction at short distance $O(b)$ [11,12]:

$$\psi = \left[(R/\ell)^s - (R/\ell)^{-s}\right] R^{-\frac{3N-5}{2}} \Psi(\Omega) \tag{22}$$

However, in the absence of N-body scattering resonance, $\ell = O(b)$ is expected, so that $\ell \to 0$ when $b \to 0$: the solution R^{-s} becomes negligible, length ℓ disappears from the problem and we keep the following scale invariant N-body contact condition in the channel of scaling exponent s [32]:

$$\psi \underset{R\to 0}{\approx} R^{s-\frac{3N-5}{2}} \tag{23}$$

The wave function ψ, considered as a function of R, is nodeless so energy $E = 0$ corresponds to the ground state: there is no bound state (an eigenenergy $E < 0$ would tend to $-\infty$ when $b \to 0$)[13,14].

Second case: $s^2 < 0$. Here too, there are two possible values for the scaling exponent, one $s = \mathrm{i}|s|$ in $\mathrm{i}\mathbb{R}^+$, which we'll call s, and the other, its conjugate complex $-\mathrm{i}|s|$, or its opposite $-s$, in $\mathrm{i}\mathbb{R}^-$. As in the first case, we conclude that there is a length ℓ, a function of the microscopic details of the interaction, setting the relative amplitude of the two solutions:

$$\psi = \left[(R/\ell)^{\mathrm{i}|s|} - (R/\ell)^{-\mathrm{i}|s|}\right] R^{-\frac{3N-5}{2}} \Psi(\Omega) = 2\mathrm{i}\sin[|s|\ln(R/\ell)] R^{-\frac{3N-5}{2}} \Psi(\Omega) \tag{24}$$

This time, the two solutions have the same modulus, so we must keep them both (neither outweighs the other in the limit $b \to 0$)! The length ℓ does not disappear from the problem, but defines in the limit $b \to 0$ a N-body contact condition (24) which explicitly breaks the continuous scale invariance of the unitary limit. Since ψ has an infinite number of nodes at an arbitrarily large hyperdistance R—arbitrarily larger than the interaction range b—(see the third expression in Equation (24)), there is an infinite number of N-body bound states under the $E = 0$ energy solution; since the boundary condition (24) is invariant by changing ℓ into $\exp(\pm\pi/|s|)\ell$, we pass from one N-body bound state to the other by a homothety of ratio $\exp(\pi/|s|)$: the corresponding

[11] Scattering state (16) corresponds to the case $N = 2$; then $s = 1/2$ and $(3N-5)/2 = 1/2$, and ψ in Equation (22) is indeed a linear combination of R^0 and R^{-1}; in this case, $R \propto r_{12}$ and $\Phi(\Omega) = \text{const}$ in s wave. Explicit calculation of expression (22) for $N = 2$ gives $\psi \propto (r_{12}/\bar{\ell})^{s-1/2} - (r_{12}/\bar{\ell})^{-s-1/2}$ with $\bar{\ell} = (m_1 + m_2)\ell/(m_1 m_2)^{1/2}$, which must be proportional to the scattering state (16), hence the announced exponent value $s = 1/2$; the two-body parameter $\bar{\ell}$ is none other than the scattering length a.

[12] A minus sign has been placed between the two bracketed terms in Equation (22); a plus sign would also be possible, depending on the microscopic model.

[13] The special case of a $(N_\uparrow, N_\downarrow)$-body scattering resonance, where ℓ remains finite in the $b \to 0$ limit, is treated in detail in reference [33], which explains which N-body contact condition to use to correctly describe the resulting low-energy bound state. Indeed, condition (22) already proposed in [27] is only satisfactory for s small enough (for $s > 1$, we can see that state (22) is no longer square integrable near $R = 0$ and that a second length—a cutoff—must be introduced).

[14] On a narrow Feshbach resonance, see note 6, the effective range r_e is—for $1/a = 0$—the only relevant length scale when the true range b tends towards zero, so that the length ℓ is of the order of $|r_e| \gg b$. The wave function ψ in Equation (22) then admits a node far "outside" the interaction potential: the solution at $E = 0$ would not be of minimum energy, and the system would admit a bound state of $(N_\uparrow, N_\downarrow)$ fermions (with $N > 2$)! However, a specific study of the case $(N_\uparrow = 2, N_\downarrow = 1)$ shows that this is not true (as long as the mass ratio $m_\uparrow/m_\downarrow$ remains low enough for $s^2 \geq 0$ of course) [29,34]. Should we be surprised? Let's argue by contradiction. If there really were a bound state, it would lead to a relative wave number $k_{\text{rel}} \approx 1/|r_e|$ between the fermions, the effective range term would not be negligible in the denominator of the scattering amplitude (10) and we would lose scale invariance and therefore separability in hyperspherical coordinates. Equation (22) would be inapplicable and the prediction of a bound state would be invalid. More generally, in order to believe in (22)—this is a necessary condition, the hyperradius R must be much larger than any length scale appearing in any subsystem $(n_\uparrow, n_\downarrow)$ [with $n_\uparrow \leq N_\uparrow$, $n_\downarrow \leq N_\downarrow$ and $n_\uparrow + n_\downarrow < N_\uparrow + N_\downarrow = N$], in particular $R \gg b$ and $R \gg |r_e|$ for $(n_\uparrow = 1, n_\downarrow = 1)$. Needless to say, the $(N_\uparrow, N_\downarrow)$-body resonance of note 13 does not call into question (22) and the existence of a node at hyperdistance ℓ since the abnormally large $\ell \gg b$ length that appears does not pre-exist in any subsystem.

spectrum forms a geometric sequence of zero limit but it is not bounded below in the zero range limit[15],

$$E_n = -E_{\text{glob}} \mathrm{e}^{-2\pi n/|s|}, \quad n \in \mathbb{N}^*, \quad \text{with } E_{\text{glob}} \approx \hbar^2/Mb^2 \tag{25}$$

These N-body bound states, historically predicted by Efimov for $N = 3$, are said to be Efimovian. It would be very interesting to stabilize them in a cold atom experiment (we unfortunately verify that, if $s \in \mathrm{i}\mathbb{R}^{+*}$ in the problem with $(2,1)$ fermions, which occurs for $m_\uparrow/m_\downarrow > 13.6069\ldots$ as we shall see, the three-body loss rate of Equation (6) does not tend to zero when $b \to 0$, but rather to a quantity proportional to $\hbar k_{\text{F}}^2/m$ in the homogeneous gas at $T = 0$, which is considerable), for example using note 6.

But back to our mathematical problem: we conclude that the gas with $(N_\uparrow, N_\downarrow)$ fermions is stable for a zero-range $\uparrow\downarrow$ interaction, and that the Hamiltonian of the Wigner–Bethe–Peierls model is self-adjoint and bounded from below, if and only if the scaling exponents are all real:

$$s \in \mathbb{R}^* \quad \forall s \text{ solution of } \Lambda_{N_\uparrow,N_\downarrow}(s) = 0 \tag{26}$$

Of course, no gas subsystem $(n_\uparrow, n_\downarrow)$ must exhibit an Efimov effect either, otherwise (i) a $n_\uparrow + n_\downarrow < N_\uparrow + N_\downarrow$-body parameter would have to be introduced as in Equation (24) and the scale invariance at the origin of separability (18) and of result (26) would be broken—we would lose separability at all distances, and (ii) the subsystem could collapse in the $b \to 0$ limit of a zero range interaction and the energy would not be bounded below. Without saying so, we have done a proof by induction and the equivalent of the stability condition (26) must be satisfied for any number $n_\uparrow \le N_\uparrow$ and any number $n_\downarrow \le N_\downarrow$.

Remark 1. We could add $s = 0$ in the third case: this is in fact precisely the threshold for an Efimov effect. Expanding Equation (24) to first order in $|s|$, we find that

$$\psi \propto \ln(R/\ell) R^{-\frac{3N-5}{2}} \Phi(\Omega) \tag{27}$$

i.e. the length ℓ sets the relative amplitude of the solutions $R^{-(3N-5)/2}$ and $(\ln R)R^{-(3N-5)/2}$. This bears a striking resemblance to the definition of the scattering length of two particles in dimension two, see for example reference [36] and Jan Solovej's contribution [17]. However, in the $\ell = O(b)$ case where we are, the length ℓ tends towards zero when $b \to 0$, the first solution—with coefficient $\ln(1/\ell) \to +\infty$—wins out over the second and we keep the N-body contact condition in continuity with (23):

$$\psi \underset{R\to 0}{\approx} R^{-(3N-5)/2} \tag{28}$$

In the zero-range model, therefore, there is no breaking of scale invariance and no bound state at the Efimovian threshold[16,17].

[15] The precise expression of E_{glob} as a function of s and ℓ, and of the order of $\hbar^2/Mb^2$ for $\ell \approx b$, is given, for example, in reference [35]. In Equation (25) we take $n \ge 1$ (assuming $\exp(-2\pi/|s|) \ll 1$—otherwise the spectrum would not be entirely geometric [29]) because the Wigner–Bethe–Peierls model can only be applied to a bound state of size $\gg b$. We can however have $\ell \approx |r_{\text{e}}| \gg b$ and $E_{\text{glob}} \approx \hbar^2/Mr_{\text{e}}^2 \ll \hbar^2/Mb^2$ on a narrow Feshbach resonance, see our note 6; even if it is not obvious, the exclusion of $n = 0$ in (25) remains correct in this case [29,34]. This exclusion of $n = 0$ is consistent with the absence of a bound state when $s^2 \ge 0$, see our note 14: on the Efimovian side, the whole discrete spectrum must tend to zero when $|s| \to 0$ knowing that E_{glob} has a finite, non-zero limit.

[16] The considerations of note 14 apply at threshold. In particular, we must not believe in the bound state of energy $\propto -\hbar^2/M\ell^2$ that Equation (27) would lead us to predict: it would be of spatial extension ℓ and could not be described by our zero-range model when $\ell \approx b$; nor would it exist for $(N_\uparrow = 2, N_\downarrow = 1)$ in the—apparently favourable—case of a narrow Feshbach resonance where $\ell \approx |r_{\text{e}}| \gg b$, see note 14 and references [29,34].

[17] The fact that $\ln(1/\ell)$ tends slowly towards infinity when $b \to 0$ is not without practical consequences: if we want to compare with experiments, it is better to keep the contribution $\ln R$ in (27) [and the term $(R/\ell)^{-s}$ in (22) for $s > 0$ close enough to zero] to form the N-body contact condition. Thus, we find that the third cluster coefficient $b_{2,1}$ defined in Section 3.4 is actually a regular function of the mass ratio $m_\uparrow/m_\downarrow$ and therefore of s^2, whereas it has an infinite derivative at $s^2 = 0$ in the zero-range model [35,37], hence in Equation (33).

Remark 2. We've taken $a = \infty$ here for simplicity, but if the system is unstable for $a = \infty$, it will remain so for finite a (all else being equal): the Efimovian N-mers of the unitary gas of size $\ll |a|$ (there are as many as you like for $b \to 0$) make no difference between an infinite and a finite scattering length a.

Complement. In the unitary limit, the present analysis generalizes to nonzero energy E (still with the center of mass of the system at rest). Equation (18) becomes

$$\psi = F(R) R^{-\frac{3N-5}{2}} \Phi(\Omega) \tag{29}$$

(satisfying the Wigner–Bethe–Peierls contact conditions under note 9) with

$$EF(R) = -\frac{\hbar^2}{2M} \Delta_{2D} F(R) + \frac{\hbar^2 s^2}{2MR^2} F(R) \tag{30}$$

and Δ_{2D}, the 2D Laplacian for variable R, reduces here (in the absence of angular dependence) to $\mathrm{d}^2/\mathrm{d}R^2 + R^{-1}\mathrm{d}/\mathrm{d}R$. The Efimovian case $s^2 < 0$ therefore simply corresponds to the known "fall to the center" problem in an attractive $1/R^2$ potential [38]. Separability in hyperspherical coordinates (29) even extends to the trapped case [27,28], simply by adding the trapping term $(1/2)M\omega^2 R^2 F(R)$ to the right-hand side of Equation (30), and making the substitution $E \to E - E_{\mathrm{com}}$, the eigenvalue of the equation for $F(R)$ being the internal energy as opposed to that E_{com} of the center of mass. For $s^2 > 0$, this leads to the spectrum

$$E - E_{\mathrm{com}} = (s + 1 + 2q)\hbar\omega, \quad q \in \mathbb{N} \tag{31}$$

3.3. *What is known on the stability domain*

The problem of whether the stability condition (26) is satisfied can be tackled from two opposite ends.

The first involves solving the problem with $(N_\uparrow, N_\downarrow)$ fermions at $E = 0$ in the Wigner–Bethe–Peierls model and calculating the scaling exponents s (we proceed analytically as far as possible, but there is a final numerical step, at least for $N > 3$). To the best of our knowledge, this program has been completed in fermionic problem ($N_\uparrow > 1, N_\downarrow = 1$) up to $N_\uparrow = 4$, see Figure 3: in each case, an Efimov effect is found to appear above a critical mass ratio $m_\uparrow/m_\downarrow$ (impurity $\downarrow$ must be light enough), obviously a decreasing function of $N_\uparrow$ [18]. We note that the successive critical mass ratios get closer and closer together; mathematically, however, we don't know whether this sequence continues (is there an Efimov effect for (5,1) bodies? for (6,1) bodies? etc.). The ($N_\uparrow > 1, N_\downarrow = 2$) case has been studied for $N_\uparrow = 2$ by reference [31], which predicts stability as long as that the subsystems (2,1) and (1,2) are stable.

At the second extreme, the aim is to constrain (rather than calculate) critical mass ratios, by lower bounding the Hamiltonian spectrum. This is what reference [41] has done for the $(N_\uparrow, N_\downarrow = 1)$ fermion problem: it demonstrates the magnificent

Theorem. *There is a critical mass ratio $m_\uparrow/m_\downarrow = \alpha_c$ below which the fermionic system $(N_\uparrow, N_\downarrow = 1)$ is stable $\forall N_\uparrow$ for a contact interaction, and $\alpha_c > 1/0.36 = 2.77$.*

[18] Once we have an Efimov effect in the $(N_\uparrow, N_\downarrow)$ fermionic problem, as we said below Equation (26), we lose scale invariance and can no longer apply the reasoning behind Equations (18), (20) to the $(N_\uparrow + 1, N_\downarrow)$ or $(N_\uparrow, N_\downarrow + 1)$ fermionic problem; in the latter case, there is no separability in (R, Ω) coordinates as in Equation (24), no geometric spectrum (25) and, strictly speaking, no possible Efimov effect!

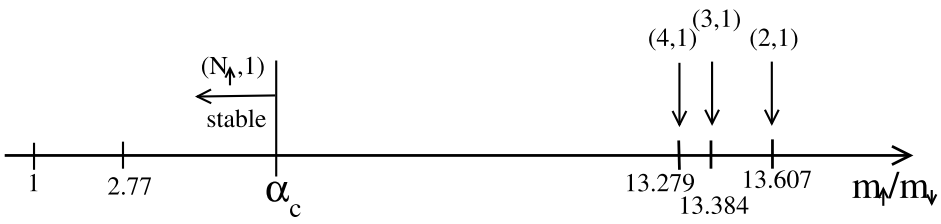

Figure 3. Known results on the stability of the $(N_\uparrow,1)$ system of $N_\uparrow$ spin $\uparrow$ fermions and one spin $\downarrow$ fermion, for a zero-range interaction, as a function of the $m_\uparrow/m_\downarrow$ mass ratio between a $\uparrow$ particle and the $\downarrow$ particle. Vertical arrows: critical values of $m_\uparrow/m_\downarrow$ (thresholds) for the $(N_\uparrow,1)$-body Efimov effect obtained by solving the corresponding problem, see references [39] for $N_\uparrow=2$, [30] for $N_\uparrow=3$, [40] for $N_\uparrow=4$; when $m_\uparrow/m_\downarrow$ exceeds these values, the energy of the system is no longer bounded below. Vertical bar with horizontal arrow: critical mass ratio α_c, whose existence is established by the Moser–Seiringer theorem [41], below which the system $(N_\uparrow,1)$ is stable $\forall N_\uparrow$; the theorem does not give the exact value of α_c but a more restrictive lower bound, $\alpha_c > 2.77$, than that, $m_\uparrow/m_\downarrow = 1$, of the cold-atom experiments (a superiority of the latter, however, is that the unitary Fermi gas appears to be stable, without collapse or significant three-body losses, for all values of $N_\uparrow$ and $N_\downarrow$).

3.4. *Cluster or virial expansion*

Some would argue that it is the macroscopic many-body problem that should ultimately be the focus of our attention, rather than the few-body system. To which we reply that the latter can say something about the former by means of cluster expansion, an expansion of the pressure P of the homogeneous gas at grand-canonical thermal equilibrium in powers of the fugacities of the components σ (the temperature $T = 1/k_B\beta$ is fixed and the chemical potentials μ_σ tend to $-\infty$, which corresponds to a quantum non-degenerate limit):

$$\frac{P\bar{\lambda}^3}{k_B T} = \sum_{(n_\uparrow,n_\downarrow)\in\mathbb{N}^{2*}} b_{n_\uparrow,n_\downarrow} e^{\beta\mu_\uparrow n_\uparrow} e^{\beta\mu_\downarrow n_\downarrow} \tag{32}$$

where the thermal de Broglie wavelength is taken at the arbitrary reference mass $\bar{m}$, $\bar{\lambda} = (2\pi\hbar^2/\bar{m}k_B T)^{1/2}$ [19]. The expansion (32), in recent literature, is often confused with the virial expansion, which expands in powers of the phase space densities $\rho_\sigma\lambda_\sigma^3$ ($\lambda_\sigma = (2\pi\hbar^2/m_\sigma k_B T)^{1/2}$).

How to calculate the cluster coefficients $b_{n_\uparrow,n_\downarrow}$? At the unitary limit $a^{-1}=0$, the simplest way is to use the harmonic regulator method of reference [43], which first places the system in the harmonic traps $U_\sigma(\mathbf{r})$ of Equation (2) and then, all calculations done, opens the traps to obtain the homogeneous case from the local density approximation (exact in the limit $\omega\to 0^+$). The trapped problem is then separable in hyperspherical coordinates as in Section 3.2 and, if we know the zero-energy free space scaling exponents s for all $n_\uparrow \le n_\uparrow^{\text{target}}, n_\downarrow \le n_\downarrow^{\text{target}}$, we also know the energy levels of the trapped system as in Equation (31), hence all the canonical partition functions $Z_{n_\uparrow,n_\downarrow}$ and ultimately the coefficient $b_{n_\uparrow^{\text{target}},n_\downarrow^{\text{target}}}$. As a result, the cluster coefficients must be functionals of the $\Lambda_{n_\uparrow,n_\downarrow}$ of Equation (21). This is indeed what is predicted by the conjecture in reference [44], claiming that, at the unitary limit,

$$b_{n_\uparrow,n_\downarrow} = \frac{(n_\uparrow m_\uparrow + n_\downarrow m_\downarrow)^{3/2}}{\bar{m}^{3/2}} \left[\int_{-\infty}^{+\infty} \frac{dS}{4\pi} S \frac{d}{dS}(\ln\Lambda_{n_\uparrow,n_\downarrow}(iS)) + \text{CorrStat}_{n_\uparrow,n_\downarrow}\right] \tag{33}$$

[19] Reference [42] uses the natural choice $\bar{m}^{3/2} = (m_\uparrow^{3/2} + m_\downarrow^{3/2})/2$ leading to a first total cluster coefficient $b_1 = (b_{1,0} + b_{0,1})/2$ equal to one.

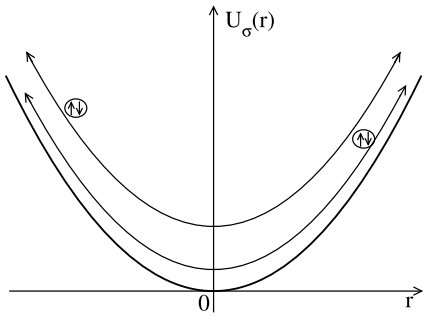

Figure 4. A possible asymptotic behavior of the unitary four-fermion problem ($N_\uparrow = 2, N_\downarrow = 2$) in harmonic potentials $U_\sigma(\mathbf{r})$: two pairons oscillate furiously (with large-amplitude motions); fermions $\uparrow$ and $\downarrow$ in each pairon have relative energy $O(1)$ (in $\hbar\omega$ units if dimension is to be respected) and remain strongly correlated; the two pairons have relative energy $\to +\infty$ and are decoupled, so they can be seen as two identical bosons that have an internal structure (that of relative motion $\uparrow\downarrow$ within a pairon) and do not interact. The quantum statistical correction $\mathrm{CorrStat}_{2,2}$ is then non-zero in Equation (33).

for any $(n_\uparrow, n_\downarrow) \in \mathbb{N}^{*2} \setminus \{1,1\}$ [20]. Here, the prefactor relates the homogeneous case to the trapped case, and the first contribution in square brackets is modelled on the $N = 3$ result of reference [45]; the second contribution in square brackets is an ideal-gas quantum statistical correction originating from the indistinguishable non-monoatomic subclusters into which the internal eigenstates of the trapped system $(n_\uparrow, n_\downarrow)$ decouple at high energy (the center of mass of the system remains in its ground state).

Let's explain this subcluster decoupling story a little better with some examples. If $(n_\uparrow, n_\downarrow) = (1,1)$, the eigenstates asymptotically (for arbitrarily large energy values) take the form of two uncorrelated fermions $\uparrow$ and $\downarrow$ in large-amplitude oscillatory levels[21]; the subclusters being monoatomic, we have CorrStat = 0. If $(n_\uparrow, n_\downarrow) = (2,1)$, a new decoupling is possible, alongside that into three decorrelated fermions: the particles can separate into an atom $\uparrow$ and a "pairon" $\uparrow\downarrow$ of strongly correlated fermions (the relative motion within the pairon remaining of low amplitude), with highly excited oscillatory levels for the atom $\uparrow$ and for the center of mass of the pairon $\uparrow\downarrow$; the pairon is alone in its category, and we again have CorrStat = 0. The conclusion remains the same for $(n_\uparrow, n_\downarrow) = (3,1)$, except that the triplon $\uparrow\uparrow\downarrow$ appears as a new decoupled subcluster. On the other hand, for $(n_\uparrow, n_\downarrow) = (2,2)$, there is possible decoupling into two $\uparrow\downarrow$ pairons of very high relative energy, see Figure 4; they no longer interact but are indistinguishable and lead, like identical bosons in an ideal gas, to a quantum statistical correction ignored by the integral over S in Equation (33); the calculation gives CorrStat = 1/32 [44].

Conjecture (33) is well established for $N = 3$, by inverse application of the residue theorem, which converts the sum over the spectra (31), i.e. over the roots s of $\Lambda_{n_\uparrow,n_\downarrow}$, into an integral [45]. For $N = 4$, the analytical properties of function $\Lambda_{n_\uparrow,n_\downarrow}$ in the complex plane are not sufficiently known to apply Cauchy's theorem[22]; for the special case $m_\uparrow/m_\downarrow = 1$, however, the conjecture

[20] Case $(n_\uparrow = 1, n_\downarrow = 1)$ is different and must be excluded; it corresponds, contrary to what we have assumed, to a N-body scattering resonance with $N = 2$ in s wave: in the unitary limit, we must keep only the solution $R^{-s}, s = 1/2$, in Equation (22), as if the right root of Λ to keep was $-s$; in fact, the solution R^s corresponds to the regular part $\propto 1/a$ of the zero-energy scattering state (see note 11 for further details).

[21] If the relative wavenumber $k_{\mathrm{rel}} \to +\infty$, the scattering amplitude $f_{k_{\mathrm{rel}}} \to 0$ in Equation (11) so even at the unitary limit, interactions become negligible.

[22] It must be possible to unfold the integration path surrounding the roots and poles of $\Lambda_{n_\uparrow,n_\downarrow}$ on the real axis onto the imaginary axis without crossing any singularity—pole or branch cut—in the upper and lower half-planes.

has been confirmed by a very accurate few-body quantum Monte Carlo calculation [46] (on the other hand, the experimental values [47,48] are not confirmed, the problem arising from the impossibility of obtaining the correct polynomial of degree 4 in $z = \exp(\beta\mu)$ by fitting the pressure P or density ρ measured on the experimentally accessible fugacity interval [49])[23]. The proof of expression (33) in the general case therefore remains open. Another interesting question concerns the behavior of the cluster coefficients $b_{n_\uparrow,n_\downarrow}$ at large orders $n_\sigma \to +\infty$, which is required to perform an efficient summation of the series (32) after calculation of its first terms, in order to extend its applicability to the degenerate regime $T \lesssim T_F$ (for example, if the radius of convergence is zero, one could implement a conformal Borel-type resummation as in references [50,51]).

4. Open questions from a macroscopic point of view

In this section, the interacting Fermi gas, considered in the thermodynamic limit and at non-zero but arbitrarily low temperature, is described by an effective low-energy Hamiltonian theory, Landau and Khalatnikov quantum hydrodynamics [52][24].

4.1. *Overview of the considered superfluid regime*

The three-dimensional system of fermions is here spatially homogeneous (in a quantization volume $[0,L]^3$ close to the thermodynamic limit, which is taken at the end of the calculations), with particles of equal mass $m_\uparrow = m_\downarrow = m$ in both internal states, spin-unpolarized (there are the same number of particles in both components, $N_\uparrow = N_\downarrow$, to allow complete pairing) and at canonical thermal equilibrium in a low-temperature limit ($T \neq 0$ but $T \to 0$).

Under these conditions, (i) fermions assemble into bound pairs $\uparrow\downarrow$ in the s wave; in the presence of Fermi seas in both internal states, this is what the attractive interaction between $\uparrow$ and $\downarrow$ in Section 3 leads to, via the famous Cooper mechanism; this is true even for a negative scattering length a, where there is no $\uparrow\downarrow$ bound state in free space, although the size of a pair tends to $+\infty$ as $a \to 0^-$ (in the $a > 0$ case, a dimer state does exist and, not surprisingly, this is what the bound pair state reduces to in the low-density limit $\rho \to 0$)[25]; (ii) these bound pairs, being composite bosons of sorts, form a condensate in the mode of wave vector $\mathbf{K}_{\text{pair}} = \mathbf{0}$ of their center of mass (of coherence length limited by the size of the box, infinite at the thermodynamic limit) and a superfluid.

As a result, we expect the system to have, in its ground state, a branch of acoustic excitation (by sound waves) that starts out linear in wavenumber q with a cubic correction,

$$\omega_{\mathbf{q}} \underset{q\to 0}{=} cq\left[1 + \frac{\gamma}{8}\left(\frac{\hbar q}{mc}\right)^2 + O(q^4 \ln q)\right] \tag{34}$$

[23] References [47,48] have access only to the fourth total cluster coefficient $b_4 = (b_{4,0} + b_{3,1} + b_{2,2} + b_{1,3} + b_{0,4})/2$, which prohibits a comparison with the conjecture (33) sector by sector.

[24] The term "quantum hydrodynamics", in non-linear physics, is understood in contrast to classical fluid hydrodynamics and refers to an Euler equation for a real-valued rather than operator-valued velocity field $\mathbf{v}(\mathbf{r})$ with a $\propto \hbar^2$ quantum pressure term, which allows to describe the motion of quantum vortices—with quantized circulation—in the superfluid (like the Gross–Pitaevskii equation for the wave function of a Bose condensate written in terms of density and phase gradient). Here, the name is to be taken in the sense of the second quantization, the velocity field now being operator-valued $\hat{\mathbf{v}}(\mathbf{r})$.

[25] It is not entirely obvious that the Wigner–Bethe–Peierls contact interaction is attractive. To see this, we obtain it as the continuous limit $b \to 0$ of a model on a cubic lattice $b\mathbb{Z}^3$ with a coupling $\propto \hbar^2/mb^2$ between neighboring sites (to represent the kinetic energy) and an on-site interaction g_0/b^3; at a fixed scattering length $a \neq 0$, we find that $g_0 \approx -\hbar^2 b/m < 0$ as $b \to 0$ (the bare coupling constant g_0 is therefore, in the resonant scattering regime $b \ll |a|$, quite different from the effective coupling constant $g = 4\pi\hbar^2 a/m$) [53].

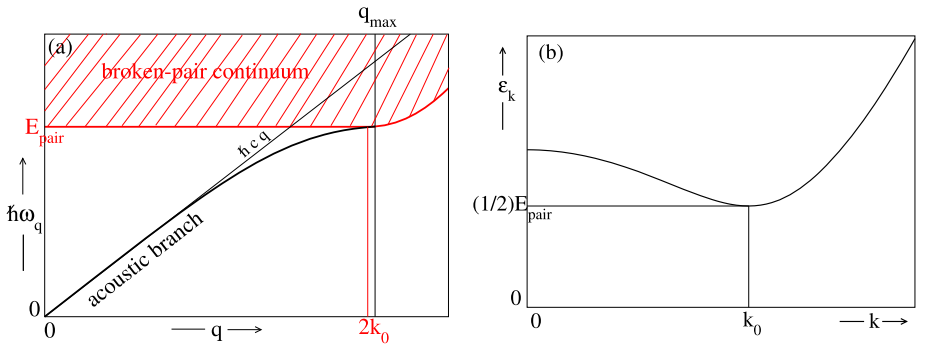

Figure 5. Energy of different types of excitations of an unpolarized homogeneous two-component Fermi gas at zero temperature, as a function of their wave number q or k. (a) Acoustic excitation branch $\hbar\omega_{\mathbf{q}}$ of linear departure $\hbar cq$ (c is the speed of sound), bounded at the top by the broken-pair continuum (hatched area). Here, the branch tangentially reaches the lower edge of the continuum at the terminal point of wave number $q_{\max}$. (b) Dispersion relation $\varepsilon_{\mathbf{k}}$ of a fermionic quasiparticle χ (see text). Under the effect of a percussive excitation of wave vector $\mathbf{q}$, a bound pair $\uparrow\downarrow$ of the pair condensate, initially at rest, dissociates into two fermionic quasiparticles χ of opposite spins, wave vectors $\mathbf{k}$ and $\mathbf{k}' = \mathbf{q} - \mathbf{k}$ and energies $\varepsilon_{\mathbf{k}}$ and $\varepsilon_{\mathbf{k}'}$; as vector $\mathbf{k}$ is not constrained (no conservation of energy for a percussive excitation), a continuum of final energies $\{\varepsilon_{\mathbf{k}} + \varepsilon_{\mathbf{q}-\mathbf{k}}, \mathbf{k} \in \mathbb{R}^3\}$ appears. For the interaction strength chosen in the figure ($|\Delta|/\mu = 0.84$ or $1/k_F a \simeq -0.16$ according to BCS theory, with μ the chemical potential of the gas and Δ the complex order parameter of the pair condensate), the acoustic branch is concave at low q ($\gamma < 0$ in Equation (34)) and the dispersion relation $\varepsilon_{\mathbf{k}}$ has a minimum $E_{\text{pair}}/2$ at $k = k_0 > 0$; the lower edge of the continuum is therefore exactly E_{pair}, at least as long as one can have $k = k' = k_0$, i.e. as long as $q = |\mathbf{k} + \mathbf{k}'| \leq 2k_0$. The approximate dispersion relations shown are derived from BCS theory for $\varepsilon_{\mathbf{k}}$ and Anderson's RPA for $\hbar\omega_{\mathbf{q}}$. Depending on the interaction strength, the domain of existence in q of the acoustic branch may also be non-compact, connected $q \in]0, +\infty[$ or not $q \in]0, q_{\max}[\cup]q_{\min}, +\infty[$ ($q_{\min} > q_{\max}$) [56]; the concavity of the branch is also variable [57]; finally, $k_0 = 0$ and $E_{\text{pair}} = 2(\mu^2 + |\Delta|^2)^{1/2}$ if $\mu < 0$, $k_0 = (2m\mu)^{1/2}/\hbar$ and $E_{\text{pair}} = 2|\Delta|$ otherwise.

and this branch to be energy-limited at the top by the broken-pair continuum, with a lower edge of the continuum given by the pair binding energy E_{pair}, as in Figure 5a. Here $\omega_{\mathbf{q}}$ is the angular eigenfrequency at wave vector $\mathbf{q}$, c is the speed of sound at zero temperature and the curvature parameter γ is scaled so that it tends to one in the limit $k_F a \to 0^+$ of a weakly interacting condensed gas of dimers (in agreement with Bogolioubov theory)[26]. The acoustic branch is often referred to as Goldstone [55], because it is associated with $U(1)$ symmetry breaking in pair condensation; its Higgs counterpart is discussed in Section 5.

In the following, our low-temperature regime satisfies two conditions:

$$0 < k_B T \ll mc^2 \quad \text{and} \quad 0 < k_B T \ll E_{\text{pair}} \tag{35}$$

The first ensures that only the linear part of the acoustic branch is thermally populated, the second that there is a negligible density of broken pairs (according to Boltzmann's law, this density has an activation factor $\exp(-E_{\text{pair}}/2k_B T)$, the fragments resulting from the dissociation of a bound pair—the χ fermionic quasiparticles in Figure 5b—individually having a minimum

[26] Our sign convention on γ differs from that used in liquid helium-4, see reference [54].

energy $E_{\rm pair}/2$). Our system then reduces to a thermal gas of phonons, if we agree to call the quanta of the acoustic branch as such (in view of its linear departure)[27].

This raises three types of partially open questions:

(1) as we shall see, phonons (abbreviated to ϕ) interact, the underlying Fermi superfluid constituting a nonlinear medium for sound. What are the effects of these interactions on phonons of wave vector **q**? In particular, they are expected to damp with a rate $\Gamma_{\mathbf{q}}(T)$ and to undergo a thermal angular frequency shift $\Delta_{\mathbf{q}}(T)$ (we don't count the shift at zero temperature, which by definition gives rise to the spectrum (34)—the neglected term $q^5 \ln q$ arises precisely from the cross-effect of interactions and quantum fluctuations in the phonon field [62,63])[28].

(2) what are the consequences of phonon collisional dynamics on the evolution of a particularly interesting macroscopic gas variable, the phase operator $\hat{\phi}_0(t)$ of the pair condensate?

(3) we enrich the problem by considering the partially polarized case $N_\uparrow \neq N_\downarrow$. In the weakly polarized case, e.g. $N_\uparrow - N_\downarrow = O(1)$, the unpaired supernumerary fermions of the majority spin component form, in the interacting gas, fermionic quasiparticles (abbreviated to χ) with a dispersion relation $\varepsilon_{\mathbf{k}}$ different from those of the free fermions: it has a non-zero minimum, i.e. a gap, given by half the binding energy of a pair $\uparrow\downarrow$, where it varies quadratically with the wave number k (see Figure 5b). The question then arises of the $\phi-\chi$ and of the $\chi-\chi$ interactions; in particular, disagreement persists over the expression of the low-energy $\phi-\chi$ scattering amplitude (references [64] and [65] differ)[29]. In the highly polarized case, where $N_\uparrow - N_\downarrow$ is extensive like N, it is expected that $T = 0$ pair condensation may take place in a plane-wave superposition of their center of mass (rather than in $\mathbf{K}_{\rm pair} = \mathbf{0}$ as assumed here), see references [66,67], giving rise to a spatially modulated superfluid (a supersolid following the fashionable terminology), with an imperfectly known domain of existence in parameter space $((N_\uparrow - N_\downarrow)/N, 1/k_{\rm F}a, T/T_{\rm F})$, the problem being complicated by its high sensitivity to thermal fluctuations [68] (there are as yet no experimental results in three-dimensional cold atom gases [69]).

The most interesting case for points 1 and 2 is that of a concave acoustic branch, $\gamma < 0$ in Equation (34), very different from the fairly well-known weakly interacting Bose gas (where $\gamma \simeq 1 > 0$ as we said)[30]. In particular, phonon damping for $\gamma < 0$ can only occur at $T \neq 0$, since

[27] Equation (34) holds only for a short-range interaction $V(\mathbf{r}_{ij})$, decreasing fast enough when $r_{ij} \to +\infty$. In the case of a dipolar interaction, as in gases of cold magnetic atoms, the speed of sound is anisotropic [58], see also Wilhelm Zwerger's contribution to this special issue [59] and Jean Dalibard's 2023-2024 lecture at the Collège de France [60]. In the case of a Coulomb interaction, as in superconducting electron gases, the acoustic branch gives way to a gapped plasmon branch ($\omega_{\mathbf{q}}$ has a positive limit at $q = 0$) [61]. Here, our atoms are neutral and of negligible dipole moment.

[28] In the convex case $\gamma > 0$, it is accompanied—still at $T = 0$—by a non-zero imaginary part $\approx q^5$, corresponding to the Beliaev damping mechanism $\mathbf{q} \to \mathbf{k}, \mathbf{k}'$, see below.

[29] This problem is relevant for superfluid helium-4, whose excitation branch also has a quadratic minimum, the roton minimum; our $\phi-\chi$ scattering problem is therefore formally equivalent to the roton–phonon scattering already studied in reference [52], with the difference that rotons are bosons. The predictions of [52] are, however, incomplete and at odds with [64,65].

[30] Qualitatively, the case $\gamma < 0$ is obtained when the binding energy $E_{\rm pair}$ is low enough: if we reduce $E_{\rm pair}$, the broken pair continuum in Figure 5a lowers, pushes on the acoustic branch and eventually bends it downwards. This is what happens in the BCS limit $k_{\rm F}a \to 0^-$ where $E_{\rm pair}/mc^2 = O(\exp(-\pi/2k_{\rm F}|a|))$ tends rapidly to zero; it no longer happens in the BEC limit $k_{\rm F}a \to 0^+$ where $E_{\rm pair} \sim E_{\rm dim} = \hbar^2/ma^2 \gg mc^2$. It is not clear on which side of the unitary limit $1/k_{\rm F}a = 0$ (i.e. for which sign of the scattering length a) the curvature parameter γ changes sign, see Section 5. Given the shape of the lower continuum edge in Figure 5a—regardless of the sign of γ, the repulsion effect on the acoustic branch is strongest at large q and weakest at small q (where the energy difference between the continuum edge and the branch is greatest). We therefore expect to have an interval of values of $1/k_{\rm F}a$ over which the branch is convex at small q and concave at large q [57].

the decay of a phonon into any number $n > 1$ of phonons is forbidden by energy–momentum conservation for a concave acoustic branch; at the leading order in temperature, it results for the same reason from the $\phi\phi \to \phi\phi$ four-phonon processes of Landau and Khalatnikov [52] (for $\gamma > 0$ it results from the Beliaev $\phi \to \phi\phi$ or Landau $\phi\phi \to \phi$ three-phonon processes [70,71]). To our knowledge, this four-phonon damping has not yet been observed experimentally in any system. It could be observed in a Fermi gas of cold atoms in a box trap [72]. It could also be observed in superfluid helium-4 (a liquid of bosons) if the pressure is increased sufficiently to make $\gamma < 0$ (the roton minimum is lowered, which ends up making the acoustic branch concave at low q) and if the temperature is lowered sufficiently to reduce the density of rotons (through the activation factor $\exp(-E_{\rm roton}/k_{\rm B}T)$) and make the parasitic damping of phonons by rotons negligible [73][31].

4.2. *Which macroscopic theory to use?*

An effective low-energy theory gives up describing the system below a certain length scale ℓ; on the other hand, the theory is expected to be accurate at long wavelengths, in this case at leading order in temperature. Under these conditions, it is legitimate to cut the gas into portions of size ℓ, for example into cubic boxes of side ℓ centered on the cubic lattice $\ell\mathbb{Z}^3$, see Figure 6. Let's set out some constraints on the choice of ℓ:

(1) we must have $\ell \gg \xi$ (here $\xi = \hbar/mc$ is the so-called healing or correlation length of the superfluid) and $\rho\ell^3 \gg 1$ (there are a large number of fermions per site) so that (i) each cubic portion can be considered mesoscopic with a well-defined equation of state linking pressure or chemical potential to density (as is the case in the thermodynamic limit), and (ii) the lattice spacing ℓ provides a wave number cutoff $\pi/\ell \ll mc/\hbar$ to the phononic excitations of the gas, restricting them to the quasi-linear part of the branch (34), which is universal because it is described by two parameters, c and γ.

(2) we must have $k_{\rm B}T \ll \hbar c\pi/\ell$ (this is the energy of the ground phonon mode in a portion) so that we can consider that (i) each portion is at zero temperature, and (ii) each portion is spatially homogeneous on the scale of the typical wavelength $q_{\rm th}^{-1} = \hbar c/k_{\rm B}T$ of thermal sound waves.

(3) it is also necessary that $\ell \ll \ell_{\rm coh}$ where $\ell_{\rm coh}$ is the coherence length of the fermion pairs, so that the notion of global phase $\hat\phi$ makes sense in each portion (as for a condensate). This constraint is inoperative here since $\ell_{\rm coh} \approx L$ (bound pairs are condensed in 3D).

We can then represent the system by two field operators, the density field $\hat\rho(\mathbf{r})$ and the phase field $\hat\phi(\mathbf{r}')$, with $\mathbf{r}, \mathbf{r}' \in \ell\mathbb{Z}^3$; these are canonically conjugate variables,

$$[\hat\rho(\mathbf{r})\ell^3, \hat\phi(\mathbf{r}')] = \mathrm{i}\,\delta_{\mathbf{r},\mathbf{r}'} \tag{36}$$

as if $\hat\phi$ were a momentum operator and $\hat\rho\ell^3$ a position operator in ordinary quantum mechanics [52,75][32]. The phase field gives access to the velocity field by simple differentiation (this is a

[31] In liquid helium-4, four-phonon scattering processes between intentionally produced (non-thermal) phonon beams have already been the subject of theoretical and experimental studies [74].

[32] These historical references use a continuous space description for simplicity. The need to discretize the space to avoid infinities and make the theory renormalizable is emphasized in publication [76]. Here, we sweep these difficulties under the carpet; for example, we do not distinguish in (38) between the notion of bare equation of state $e_{0,0}(\rho)$—which enters the Hamiltonian—and true or effective equation of state $e_0(\rho)$—which is observed in an experiment.

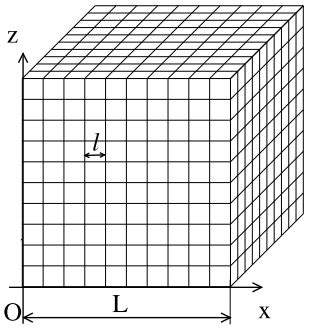

Figure 6. Cutting the gas into mesoscopic cubic portions of side ℓ, in the quantum hydrodynamics of Landau and Khalatnikov (this effective theory does not describe length scales $< \ell$). See text for choice of ℓ.

discrete gradient)[33]:

$$\hat{\mathbf{v}}(\mathbf{r}) = \frac{\hbar}{m}\mathbf{grad}\,\hat{\phi}(\mathbf{r}) \tag{37}$$

The Hamiltonian is obtained by summing the internal energy and the kinetic energy associated with the local fluid velocity in each portion:

$$H = \sum_{\mathbf{r}} \frac{1}{2} m\hat{\mathbf{v}}(\mathbf{r}) \cdot \hat{\rho}(\mathbf{r})\ell^3\hat{\mathbf{v}}(\mathbf{r}) + \ell^3 e_0(\hat{\rho}(\mathbf{r})) \tag{38}$$

Here, $e_0(\rho)$ is the zero-temperature energy density of the homogeneous Fermi gas with density ρ, and $m\hat{\rho}(\mathbf{r})\ell^3$ is the amount of matter (the mass) in the portion centered at $\mathbf{r}$. The equations of motion for $\hat{\rho}$ and $\hat{\mathbf{v}}$ in the Heisenberg picture, derived from the Hamiltonian H, take the form of a continuity equation and an operator-valued Euler equation (without viscosity term)[34], hence the name quantum hydrodynamics given to the theory (with the risk of confusion pointed out in note 24).

As you will have gathered, the great strength of this effective theory is that it does not depend on the nature of the bosonic or fermionic particles constituting the underlying superfluid, nor on their interactions (strong or weak, in liquid or gas phase) as long as they remain short-range, except through the equation of state $e_0(\rho)$ and the curvature parameter γ at zero temperature. It therefore applies equally well to weakly interacting Bose gases, strongly interacting Fermi gases and liquid helium-4 (an extremely dense system that defies microscopic theory).

However, the formalism can only be trusted in a low-temperature limit, $T \to 0$, where spatial density fluctuations and phase gradients are small; Equation (38) must therefore be expanded to the relevant order (here, fourth order) in powers of

$$\delta\hat{\rho}(\mathbf{r}) \equiv \hat{\rho}(\mathbf{r}) - \hat{\rho}_0 \quad \text{and} \quad \delta\hat{\phi}(\mathbf{r}) \equiv \hat{\phi}(\mathbf{r}) - \hat{\phi}_0 \tag{39}$$

[33] The fact that the velocity field operator is a gradient vector in no way implies that the flow is entirely superfluid (this would be physically false even at thermal equilibrium, at non-zero temperature). Let's explain this in two points. (i) Don't confuse the $\hat{\mathbf{v}}(\mathbf{r})$ operator of quantum hydrodynamics (which contains all possible quantum and thermal fluctuations) with the $\mathbf{v}(\mathbf{r})$ mean velocity field of ordinary hydrodynamics; in particular, whether or not the flow is superfluid depends on whether or not $\mathbf{v}(\mathbf{r})$ (without hat) is irrotational. (ii) In general, we have $\mathbf{v}(\mathbf{r}) \neq \langle\hat{\mathbf{v}}(\mathbf{r})\rangle$ where the expectation value is taken in the quantum state of the system, since $\mathbf{v}(\mathbf{r})$ is defined in terms of the mean matter current density, $\mathbf{v}(\mathbf{r}) = \langle\hat{\mathbf{j}}(\mathbf{r})\rangle / \langle\hat{\rho}(\mathbf{r})\rangle$ with here $\hat{\mathbf{j}}(\mathbf{r}) = [\hat{\rho}(\mathbf{r})\hat{\mathbf{v}}(\mathbf{r}) + \hat{\mathbf{v}}(\mathbf{r})\hat{\rho}(\mathbf{r})]/2$ (by definition, the evolution equation of $\hat{\rho}$ in the Heisenberg picture is written $\partial_t\hat{\rho} + \mathrm{div}\,\hat{\mathbf{j}} = 0$ and that for the mean density $\rho(\mathbf{r}) = \langle\hat{\rho}(\mathbf{r})\rangle$ is written $\partial_t\rho + \mathrm{div}(\rho\mathbf{v}) = 0$); it would therefore be wrong to believe that $\mathbf{v}(\mathbf{r}) = (\hbar/m)\mathbf{grad}\langle[\hat{\phi}(\mathbf{r}) - \hat{\phi}(\mathbf{r}_0)]\rangle$ (where $\mathbf{r}_0$ is an arbitrary reference position) and deduce that $\mathbf{v}(\mathbf{r})$ is necessarily a gradient vector.

[34] See note 33 for the equation for $\hat{\rho}(\mathbf{r})$. The equation for $\hat{\mathbf{v}}(\mathbf{r})$ is obtained by taking the gradient of that for $\hat{\phi}(\mathbf{r})$, $\hbar\partial_t\hat{\phi} = -\mu_0(\hat{\rho}) - m\hat{\mathbf{v}}^2/2$, where $\mu_0(\rho)$ is the zero-temperature chemical potential function, as in Equation (43).

where $\hat\rho_0$ and $\hat\phi_0$ are the zero-wave-vector Fourier components of the fields $\hat\rho(\mathbf{r})$ and $\hat\phi(\mathbf{r})$ (physically, $\hat\rho_0 = \hat N/L^3$, where $\hat N$ is the total number of fermions operator, L^3 is the volume of the quantization box $[0,L]^3$ and $\hat\phi_0$ is the phase operator of the pair condensate [76]). The expanded Hamiltonian is formally written as

$$H = H_0 + H_2 + H_3 + H_4 + \cdots \tag{40}$$

where H_n is the contribution of total degree n in $\delta\hat\rho$ and $\delta\hat\phi$.

The 0-order contribution H_0 is a constant of little interest; the 1-order contribution is exactly zero (because $\sum_{\mathbf{r}} \ell^3 \delta\hat\rho(\mathbf{r}) = 0$ by construction) and has been omitted directly from Equation (40). The quadratic contribution H_2 is diagonalized by a Bogolioubov transformation[35]:

$$H_2 = \text{const} + \sum_{\mathbf{k}\neq\mathbf{0}} \hbar\omega_{\mathbf{k}} \hat b^\dagger_{\mathbf{k}} \hat b_{\mathbf{k}} \tag{41}$$

where the creation $\hat b^\dagger_{\mathbf{k}}$ and annihilation $\hat b_{\mathbf{k}}$ operators of an elementary excitation (a phonon) of wave vector $\mathbf{k}$ obey the usual bosonic commutation relations

$$[\hat b_{\mathbf{k}}, \hat b_{\mathbf{k}'}] = 0 \quad \text{and} \quad [\hat b_{\mathbf{k}}, \hat b^\dagger_{\mathbf{k}'}] = \delta_{\mathbf{k},\mathbf{k}'} \tag{42}$$

The spectrum obtained here is exactly linear, $\omega_{\mathbf{k}} = ck$, with the speed of sound given by

$$mc^2 = \rho \frac{\mathrm{d}^2}{\mathrm{d}\rho^2} e_0(\rho) = \rho \frac{\mathrm{d}}{\mathrm{d}\rho} \mu_0(\rho) \tag{43}$$

where $\mu_0(\rho)$ is the zero-temperature chemical potential of the Fermi gas with density ρ. The relation (43) is exact (it's well known from superfluid hydrodynamics [75]), but the systematic absence of curvature in the spectrum is not physically realistic: this pathology stems from the fact that we have omitted so-called gradient corrections [77] from Hamiltonian H; to simplify, as illustrious predecessors [52] have done, we replace $\omega_{\mathbf{k}}$ in H_2 by hand with its cubic approximation (34), which is justified by reference [78].

The approximation H_2 corresponds to an ideal gas of phonons, and cannot describe sound attenuation. The interaction between phonons that causes their damping comes from the cubic contribution H_3 and the quartic contribution H_4. For the sake of simplicity, we give here only the expression of the most useful part of H_3, simplified to make the physics clear:

$$H_3|_{\text{simpl}} = \frac{\mathscr{A}}{2L^{3/2}} \sum_{\mathbf{k},\mathbf{k}',\mathbf{q}} (kk'q)^{1/2} \hat b^\dagger_{\mathbf{k}} \hat b^\dagger_{\mathbf{k}'} \hat b_{\mathbf{q}} \delta_{\mathbf{k}+\mathbf{k}',\mathbf{q}} + (k'kq)^{1/2} \hat b^\dagger_{\mathbf{k}'} \hat b_{\mathbf{k}} \hat b_{\mathbf{q}} \delta_{\mathbf{k}',\mathbf{k}+\mathbf{q}} + \cdots \tag{44}$$

with the constant amplitude (independent of the wave numbers) as a factor,

$$\mathscr{A} = (\xi/2)^{3/2} \rho^{-1/2} \left[3mc^2 + \rho^2 \frac{\mathrm{d}^3}{\mathrm{d}\rho^3} e_0(\rho) \right] \tag{45}$$

and $\xi = \hbar/mc$ as before[36]. The ellipse in Equation (44) contains terms $\hat b^\dagger \hat b^\dagger \hat b^\dagger$ and $\hat b \hat b \hat b$ of no great importance, as they do not conserve the energy H_2. The terms $\hat b^\dagger \hat b^\dagger \hat b$ and $\hat b^\dagger \hat b \hat b$, on the other hand, are central to damping: they correspond respectively to the Beliaev process (phonon $\mathbf{q}$ decays into two phonons $\mathbf{k}$ and $\mathbf{k}'$) and to the Landau process (phonon $\mathbf{q}$ merges with a phonon

[35] This transformation corresponds to the modal expansions $\delta\hat\rho(\mathbf{r}) = L^{-3/2} \sum_{\mathbf{k}\neq\mathbf{0}} \rho_{\mathbf{k}} (\hat b_{\mathbf{k}} + \hat b^\dagger_{-\mathbf{k}}) \exp(\mathrm{i}\mathbf{k}\cdot\mathbf{r})$ and $\delta\hat\phi(\mathbf{r}) = L^{-3/2} \sum_{\mathbf{k}\neq\mathbf{0}} \phi_{\mathbf{k}} (\hat b_{\mathbf{k}} - \hat b^\dagger_{-\mathbf{k}}) \exp(\mathrm{i}\mathbf{k}\cdot\mathbf{r})$ where $\rho_{\mathbf{k}} = (\hbar\rho k/2mc)^{1/2}$ and $\phi_{\mathbf{k}} = (-\mathrm{i})(mc/2\hbar\rho k)^{1/2}$ are the amplitudes of the quantum fluctuations of density and phase in the phonon mode of wave vector $\mathbf{k}$. Note the relation $-\mathrm{i}\omega_{\mathbf{k}}\delta\rho_{\mathbf{k}} - \rho(\hbar/m)k^2\phi_{\mathbf{k}} = 0$ imposed by the linearized continuity equation.

[36] The true coupling amplitude depends on the angles between the three wave vectors $\mathbf{k}_i$ involved; as damping is actually dominated at low temperatures by processes at small angles between wave vectors, due to the small denominator effect described below, we have written the amplitude directly at zero angles $\mathbf{k}_i \cdot \mathbf{k}_j / k_i k_j = 1$.

k to form a single phonon **k**′), which can be represented diagrammatically as follows, where the phonon whose damping we are studying plays a privileged role:

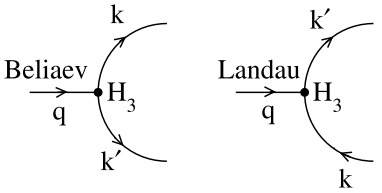

(46)

As H_3 is cubic, each vertex of the diagram representing its action is the meeting point of three phonon lines. We could proceed in the same way with H_4 (the vertices would be four lines), but we won't do so, as quartic processes generally play a sub-dominant role in damping compared with cubic processes (for example, in the four-phonon damping $\phi\phi \to \phi\phi$ for $\gamma < 0$, the amplitude of the direct process $\mathbf{k},\mathbf{q} \to \mathbf{k}',\mathbf{k}''$ induced by H_4 in first-order perturbation theory is in practice negligible compared to that of the indirect process of the same initial and final state $\mathbf{k},\mathbf{q} \to \mathbf{k}+\mathbf{q} \to \mathbf{k}',\mathbf{k}''$ induced by H_3 treated in second-order, due to the appearance in the latter of a very small energy denominator at small angles between **k** and **q**)[37].

4.3. *How to calculate phonon damping?*

Let's imagine that we apply a short pulse of Bragg excitation to the gas, initially at thermal equilibrium, inducing a small coherent Glauber displacement of amplitude $\alpha \in \mathbb{C}^*$ in the phonon mode of wave vector **q** without affecting the other modes, which corresponds to the unitary evolution operator $U_{\rm exc} = \exp(\alpha \hat{b}^\dagger_{\mathbf{q}} - \alpha^* \hat{b}_{\mathbf{q}})$ [38]. Immediately after excitation, we have a non-zero mean for the corresponding annihilation operator:

$$\langle \hat{b}_{\mathbf{q}}(0^+) \rangle = \alpha \neq 0 \tag{47}$$

This leads to an observable modulation of the mean gas density at wave vectors $\pm\mathbf{q}$ since $\langle \delta\hat{\rho}(\mathbf{r},0^+)\rangle$, a linear combination of $\langle \hat{b}_{\mathbf{k}}(0^+)\rangle$ and $\langle \hat{b}^\dagger_{\mathbf{k}}(0^+)\rangle$ as in note 35, is then $\neq 0$.

In the limit $\alpha \to 0$, i.e. in the linear response regime, the many-body Green's function formalism applied to the effective low-energy theory, hence to the phonon Hamiltonian (40) (rather than to a microscopic description of the Fermi gas with interaction potential $V(\mathbf{r}_{ij})$ as references [75,80] for example do), leads to the exact expression

$$\langle \hat{b}_{\mathbf{q}}(t) \rangle \overset{t\geq 0}{=} \alpha \mathrm{e}^{-\mathrm{i}\omega_{\mathbf{q}} t} \int_{C_+} \frac{\mathrm{d}\zeta}{2\mathrm{i}\pi} \frac{\mathrm{e}^{-\mathrm{i}\zeta t/\hbar}}{\zeta - \Sigma_{\mathbf{q}}(\zeta)} \tag{48}$$

In this expression, C_+ is the integration path parallel to the real axis in the upper complex half-plane, followed from right to left (from $\mathrm{Re}\,\zeta = +\infty$ to $\mathrm{Re}\,\zeta = -\infty$), see Figure 7, and $\Sigma_{\mathbf{q}}(\zeta)$ is the self-energy at wave vector **q** and complex energy ζ [39], which is not known explictly but is defined by its perturbative expansion to all orders in the phonon–phonon interaction. Here, we restrict

[37] This energy denominator $\hbar\omega_{\mathbf{q}} + \hbar\omega_{\mathbf{k}} - \hbar\omega_{\mathbf{k}+\mathbf{q}}$ would be exactly zero at zero angle without the curvature terms in the dispersion relation (34), which incidentally shows the singularity of a $\gamma = 0$ theory (to which we'll return in Section 4.3).

[38] In a cold atom experiment, Bragg excitation is induced by the superposition of two far off-resonance laser beams of wave vectors $\mathbf{k}_1$ and $\mathbf{k}_2$ with $\mathbf{k}_1 - \mathbf{k}_2 = \mathbf{q}$; even if the $\pm\mathbf{q}$ acoustic modes are initially empty ($\hbar\omega_{\mathbf{q}} \gg k_{\rm B}T$) and can only receive phonons, Raman (two-photon) processes—absorption of a photon in one laser beam, stimulated emission in the other—induce $\pm\hbar(\mathbf{k}_1 - \mathbf{k}_2) = \pm\hbar\mathbf{q}$ momentum changes in the Fermi gas and generally excite the two modes; however, the duration of the Bragg excitation can be adjusted so that the $-\mathbf{q}$ mode emerges intact from the excitation procedure [79].

[39] In comparison with the usual energy variable z (of reference [80], for example), the energy variable used here is shifted by the unperturbed energy of mode **q**, $\zeta = z - \hbar\omega_{\mathbf{q}}$. This explains why we were able to take out the unperturbed phase factor in (48) and why $\Sigma_{\mathbf{q}}(\zeta)$ is taken at $\zeta = \mathrm{i}0^+$ in the approximation (50) to come (it actually corresponds to $z = \hbar\omega_{\mathbf{q}} + \mathrm{i}0^+$).

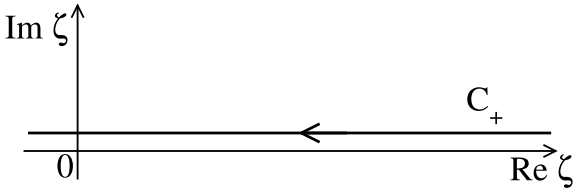

Figure 7. Integration path in the complex plane followed by Equation (48).

ourselves to the cubic interaction H_3 (see Section 4.2) and the expansion takes the following diagrammatic form

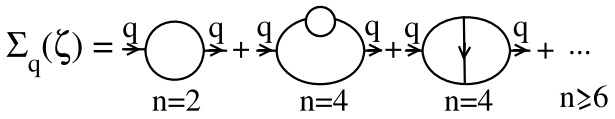

(49)

where the integer n gives the order in H_3 [63]. We only indicate the topology; it remains to sum over all possible non-redundant orientations of the internal lines, see example of diagram section (46)[40]; a precise value can then be assigned to each diagram, involving a sum over the wave vectors and Matsubara frequencies of the internal lines [80].

In order to obtain explicit results for the damping, we traditionally perform the following two approximations[41]:

(1) the Markov approximation (the phonon gas seen by mode $\mathbf{q}$ constitutes a reservoir with no memory, i.e. with negligible correlation time): we ignore the energy dependence of the self-energy as follows (see note 39),

$$\Sigma_{\mathbf{q}}(\zeta) \simeq \Sigma_{\mathbf{q}}(\mathrm{i}0^+) \tag{50}$$

The integral in Equation (48) is then calculated by the residue theorem (one closes the contour with an infinite semicircle in the lower complex half-plane),

$$\langle \hat{b}_{\mathbf{q}}(t)\rangle|_{\mathrm{Markov}} \overset{t\geqq 0}{=} \alpha \mathrm{e}^{-\mathrm{i}\omega_{\mathbf{q}}t}\mathrm{e}^{-\mathrm{i}\Sigma_{\mathbf{q}}(\mathrm{i}0^+)t/\hbar} \tag{51}$$

The signal decay in this case is exponential, with a rate corresponding to the imaginary part of $\Sigma_{\mathbf{q}}(\mathrm{i}0^+)$ (the real part gives the change in the mode angular frequency).

[40] In the first diagram of (49) (with one loop), (i) orienting the top line to the right and the bottom line to the left and (ii) orienting the top line to the left and the bottom line to the right correspond to the same contribution, by invariance of the diagram by angle π rotation around its horizontal axis. The same applies to the inner loop of the second diagram in (49), which is locally rotationally symmetric. For the same reason of rotational symmetry (this time global) of the diagrams of order $n = 4$, we decide, in order to avoid double counting, to put the inner loop in the upper branch and, in the third diagram of (49), to orient the bridge downwards.

[41] Our effective theory being exact to the leading order in temperature, we use it only in the $T \to 0$ limit, fixing the ratio $\tilde{q} = \hbar c q/k_{\mathrm{B}}T$ so that the mode $\mathbf{q}$ is also described exactly. We then have $\omega_{\mathbf{q}}/\Gamma_{\mathrm{th}} \to +\infty$ where $\Gamma_{\mathrm{th}} = \Gamma_{q=k_{\mathrm{B}}T/\hbar c}$ is the thermalization rate of the phonon gas and Γ_q is the function (52), since the exponent ν introduced in Figure 8 on page 450 is always > 1, see Table 1 on page 451: the thermalization rate Γ_{th} tends towards zero faster than the angular eigenfrequency $\omega_{\mathbf{q}}$ and the mode by definition enters the collisionless regime. In the opposite, hydrodynamic regime $\omega_{\mathbf{q}} \ll \Gamma_{\mathrm{th}}$, the phonon gas has time to reach local thermal equilibrium at each oscillation point of the sound wave $\mathbf{q}$, and damping is described by viscosity-type coefficients in the classical hydrodynamic equations of a two-fluid model [81].

(2) Born approximation: $\mathrm{Im}\,\Sigma_{\mathbf{q}}(\mathrm{i}0^+)$ is calculated perturbatively to leading order n in H_3. The damping rate of phonon $\mathbf{q}$ is then[42,43]

$$\Gamma_{\mathbf{q}}|_{\text{Born–Markov}} = -\frac{2}{\hbar}\mathrm{Im}\,\Sigma^{(n)}_{\mathbf{q}}(\mathrm{i}0^+) \tag{52}$$

where the exponent gives the order in H_3. In the case of a convex acoustic branch ($\gamma > 0$) in 3D, it's sufficient to go to order $n = 2$: this is the three-phonon Beliaev–Landau damping, much studied theoretically and observed in liquid helium-4 [83,84] and, to a lesser extent, in bosonic cold-atom gases, only Beliaev damping having been seen there [85]. In the concave case ($\gamma < 0$), we need to go to order $n = 4$ (the first contribution in Equation (49) is purely real for $\zeta = \mathrm{i}0^+$ because its energy denominators, of the form $\hbar\omega_{\mathbf{q}} + \hbar\omega_{\mathbf{k}} - \hbar\omega_{\mathbf{k}+\mathbf{q}}$ and $\hbar\omega_{\mathbf{q}} - (\hbar\omega_{\mathbf{k}} + \hbar\omega_{\mathbf{q}-\mathbf{k}})$, cannot vanish, but the next two are not in $\phi\phi \to \phi\phi$ processes); this case has been little studied theoretically (reference [78] noted and corrected an error in the original calculation [52], and reference [86] obtained a much more explicit expression of the result, even generalizing it to a non-zero phonon chemical potential μ_ϕ)[44] and it has, to our knowledge, never been observed experimentally (no precise measurement of $\Gamma_{\mathbf{q}}^{\gamma<0}$ has been made in any system).

Let's determine the validity of the Born approximation by means of the estimate of order $n \in 2\mathbb{N}^*$ given in reference [63]:

$$\Sigma^{(n)}_{\mathbf{q}}(\mathrm{i}0^+) \approx \int \left(\prod_{i=1}^{n/2} \mathrm{d}^d k_i\right) \frac{\langle\ |L^{d/2} H_3|\ \rangle^n}{(\Delta E)^{n-1}} \approx |\gamma| T^3 \left(\epsilon_{d\mathrm{D}} = \frac{T^{2d-4}}{|\gamma|^{(5-d)/2}}\right)^{n/2} \tag{53}$$

where $d \geq 2$ is the dimension of space. The writing in the second expression symbolically represents the product of n matrix elements of the cubic phonon interaction in the numerator and the product of $n-1$ energy denominators (associated with $n-1$ intermediate states) in the denominator, and the integral is taken over the independent phonon wave vectors $\mathbf{k}_i$. The order of magnitude in the third expression is obtained as in reference [63] by restricting to the small $O(|\gamma|^{1/2}T)$ angles between $\mathbf{k}_i$ and $\mathbf{q}$, which is legitimate when $T \to 0$ [52]; we omit here the dependence in the density ρ, in $\xi = \hbar/mc$ and in the coupling constant $\mathscr{A}$ of Equation (45), unlike reference [63], but we keep that in the curvature parameter γ, as we will soon link γ and T.

---

[42] To shed further light on the approximation (52), let's point out for $n = 2$ that it can be obtained by the quantum master equation method well known in quantum optics (we obtain a closed evolution equation for the density operator $\hat{\rho}_S(t)$ of a small system S—here the phonon mode $\mathbf{q}$—coupled to a large reservoir R—here the other phonon modes $\mathbf{k} \neq \mathbf{q}$, by resorting to the Born–Markov approximation) [36,82] or, more simply, using Fermi's golden rule (we calculate $\mathrm{d}\langle\hat{n}_{\mathbf{q}}\rangle/\mathrm{d}t$, where $\langle\hat{n}_{\mathbf{q}}\rangle = \langle\hat{b}^\dagger_{\mathbf{q}}\hat{b}_{\mathbf{q}}\rangle$ is the mean number of phonons in the non-equilibrium mode $\mathbf{q}$, by summing the incoming fluxes—population processes $\mathbf{k},\mathbf{k}' \to \mathbf{q}$ and $\mathbf{k}' \to \mathbf{k},\mathbf{q}$—and outgoing fluxes—inverse depopulation processes $\mathbf{q} \to \mathbf{k},\mathbf{k}'$ and $\mathbf{q},\mathbf{k} \to \mathbf{k}'$—and linearizing just after the Bragg excitation, as $(\mathrm{d}/\mathrm{d}t)\delta n_{\mathbf{q}}(t = 0^+) = -\Gamma_{\mathbf{q}}\delta n_{\mathbf{q}}(t = 0^+)$, where $\delta n_{\mathbf{q}}(t) \equiv \langle n_{\mathbf{q}}\rangle(t) - \bar{n}_{\mathbf{q}}$ is the deviation from thermal equilibrium). For $n = 4$, we find the same result (52) by extending Fermi's golden rule to higher orders [38].

[43] There's a little mathematical subtlety here: if the leading order n is ≥ 4, the Markov approximation must no longer simply replace $\Sigma_{\mathbf{q}}(\zeta)$ with $\Sigma_{\mathbf{q}}(\mathrm{i}0^+)$ but must approximate it by a Taylor expansion around $\zeta = \mathrm{i}0^+$. For example, for $n = 4$, we take $\Sigma_{\mathbf{q}}(\zeta) \simeq \Sigma_{\mathbf{q}}(\mathrm{i}0^+) + \zeta(\mathrm{d}/\mathrm{d}\zeta)\Sigma_{\mathbf{q}}(\mathrm{i}0^+)$ so that at order 4 in H_3, $\zeta - \Sigma_{\mathbf{q}}(\zeta) \simeq [1 - (\mathrm{d}/\mathrm{d}\zeta)\Sigma_{\mathbf{q}}(\mathrm{i}0^+)][\zeta - \Sigma^{(2)}_{\mathbf{q}}(\mathrm{i}0^+) - \Sigma^{(4)\mathrm{eff}}_{\mathbf{q}}(\mathrm{i}0^+)]$ with $\Sigma^{(4)\mathrm{eff}}_{\mathbf{q}}(\mathrm{i}0^+) = \Sigma^{(4)}_{\mathbf{q}}(\mathrm{i}0^+) + \Sigma^{(2)}_{\mathbf{q}}(\mathrm{i}0^+)(\mathrm{d}/\mathrm{d}\zeta)\Sigma^{(2)}_{\mathbf{q}}(\mathrm{i}0^+)$. Then replace $\Sigma^{(4)}_{\mathbf{q}}(\mathrm{i}0^+)$ with $\Sigma^{(4)\mathrm{eff}}_{\mathbf{q}}(\mathrm{i}0^+)$ in the damping rate expression (52). In the three-dimensional concave case, this makes no difference to $\Gamma_{\mathbf{q}}|_{\text{Born–Markov}}$, since $(\mathrm{d}/\mathrm{d}\zeta)\Sigma^{(2)}_{\mathbf{q}}(\mathrm{i}0^+)$ is a real quantity, as is $\Sigma^{(2)}_{\mathbf{q}}(\mathrm{i}0^+)$; in the two-dimensional concave case, the conclusion is less obvious but remains the same, see note 48. On the other hand, this substitution must be made in the calculation of the thermal angular frequency shift $\Delta_{\mathbf{q}}$ of the mode, $\hbar\Delta_{\mathbf{q}}|_{\text{Born–Markov}} = \mathrm{Re}\,[\Sigma^{(2)}_{\mathbf{q}}(\mathrm{i}0^+) + \Sigma^{(4)\mathrm{eff}}_{\mathbf{q}}(\mathrm{i}0^+)] - \text{idem at } T = 0$.

[44] If we restrict ourselves at low temperature to the leading collisional processes $\phi\phi \to \phi\phi$, the phonon number becomes a conserved quantity, allowing us to take $\mu_\phi < 0$.

In short, the Born expansion is legitimate in dimension $d = 3$ if its small parameter tends to zero at low temperature:

$$\epsilon_{3\mathrm{D}} = \frac{T^2}{|\gamma|} \underset{T\to 0}{\to} 0. \tag{54}$$

To discuss the validity of the Markov approximation, we assume that the behavior of the self-energy in the vicinity of $\zeta = \mathrm{i}0^+$ is characterized by two exponents, ν and σ, the one giving the typical values $\propto T^\nu$ of its imaginary part and the one giving its typical scale of variation $\propto T^\sigma$, as in Figure 8 [45,46]. From Equation (52), we therefore have

$$\Gamma_{\mathbf{q}} \underset{T\to 0}{\approx} T^\nu \tag{55}$$

The function $\Sigma_{\mathbf{q}}(\zeta)$ then has a slow (negligible) energy variation on the scale of the damping rate (which is indeed the inverse of the characteristic time in Equation (48)) if it is wider than high, which imposes

$$\nu > \sigma \tag{56}$$

The exponent ν is obtained by an explicit calculation of the right-hand side of Equation (52) in the limit $T \to 0$, as was done in reference [78] for the three-dimensional case[47] and in reference [63] for the two-dimensional convex case; more simply, we can use the estimate (53) with $n = 2$ if $\gamma > 0$ and $d \in \{2,3\}$, $n = 4$ if $\gamma < 0$ and $d = 3$ [48]. The exponent σ is obtained by generalizing the previous

[45] The exponents introduced here differ by one unit from those in reference [63] due to a different choice of convention.

[46] For the sake of clarity, we have assumed in Figure 8 that the function shown has a maximum at the origin. This is not necessarily true (the two-dimensional convex case of reference [63] provides a counter-example, see its Equation (114)). The true definition of exponents ν and σ is that the scaled function $\mathrm{Im}\,\Sigma_{\mathbf{q}}(\zeta = \bar{\zeta} mc^2 (k_{\mathrm{B}}T/mc^2)^\sigma)/[mc^2(k_{\mathrm{B}}T/mc^2)^\nu]$ has a finite, non-zero limit as $T \to 0$ with fixed reduced complex energy $\bar{\zeta}$ ($\mathrm{Im}\,\bar{\zeta} > 0$).

[47] The historical reference [52] for fixed $\gamma < 0$ also finds $\nu = 7$ but the q dependence of $\Gamma_{\mathbf{q}}$ is different, e.g. $\Gamma_{\mathbf{q}} \approx qT^6$ in [52] instead of q^3T^4 in [78] as $q \to 0$.

[48] For fixed $\gamma < 0$ and $d = 2$, Alice Sinatra obtained in 2021, in the formulation of references [72,78], the unpublished result that $\mathrm{Im}\,\Sigma_{\mathbf{q}}^{(n=4)}(\mathrm{i}0^+) = 0$ at order T^3 (the expected leading order in temperature). To see this, it is actually simpler to use expressions (84) and (85) in reference [63]: (i) in (84), we can ignore processes $\phi \leftrightarrow \phi\phi\phi$ and restrict ourselves to process $\phi\phi \to \phi\phi$ (second contribution), the only one conserving energy–momentum; (ii) in the integrand of (85), we are entitled to replace ζ by 0 in the numerator of the large fraction for the similar reason that processes $\phi \leftrightarrow \phi\phi$ do not conserve energy–momentum—this makes the numerator real; (iii) we then check that, if the scaled energy difference $\Delta E/[k_{\mathrm{B}}T(k_{\mathrm{B}}T/mc^2)^2]$ next to $\mathrm{i}0^+$ vanishes in the denominator of the large fraction, as required by the Dirac distribution $\delta(\Delta E)$ of the generalized Fermi golden rule [38], the numerator also vanishes (we show this by formally replacing γ in the numerator by its ΔE-cancelling expression, a rational function of the moduli and angles of the phonon wavevectors). In other words, the limit at $\zeta = 0$ (but also at $\zeta = -\Delta E$) of the transition amplitude in the numerator of the large fraction, considered as a rational fraction of the angles, can be written $\Delta E \times P/Q$, where the polynomials ΔE, P and Q are two by two coprime.

However, this reasoning neglects possible edge effects in the integral on phonon wave numbers, in the sense of reference [87], where one of the wave numbers tends to zero, which makes one of the energy denominators of the $\phi \leftrightarrow \phi\phi$ processes tend to zero. Including these edge effects, we find that the processes $\phi \to \phi\phi\phi$, $\phi\phi \to \phi\phi$ and $\phi\phi\phi \to \phi$, abbreviated as $1 \to 3$, $2 \to 2$ and $3 \to 1$ in reference [63], each make a non-zero contribution to $\mathrm{Im}\,\Sigma_{\mathbf{q}}^{(n=4)}(\mathrm{i}0^+)$ at order T^3, but the sum of these contributions is exactly zero (the contribution of the edge $q_1' + q_2' = q$ in $2 \to 2$, i.e. $C\int_0^{\bar{q}} \mathrm{d}\bar{k}\,(\bar{n}_{\bar{k}}^{\mathrm{lin}} + \bar{n}_{q-k}^{\mathrm{lin}} + 1)\bar{k}(\bar{q} - \bar{k})/\bar{q}$, is exactly offset by $1 \to 3$, and that of the edges $q_1' = 0$ and $q_2' = 0$ as a whole, i.e. $2C\int_{\bar{q}}^{+\infty} \mathrm{d}\bar{k}\,(\bar{n}_{k-q}^{\mathrm{lin}} - \bar{n}_{\bar{k}}^{\mathrm{lin}})\bar{k}(\bar{k} - \bar{q})/\bar{q}$, is exactly offset by $3 \to 1$; here, $\bar{k} = \hbar ck/k_{\mathrm{B}}T$, $\bar{n}_{\bar{k}}^{\mathrm{lin}} = 1/(\exp\bar{k} - 1)$, $\Lambda = \rho^2((\mathrm{d}^3/\mathrm{d}\rho^3)e_0(\rho))/(3mc^2)$ and $C = k_{\mathrm{B}}T(k_{\mathrm{B}}T/mc^2)^2[9(1+\Lambda)^2/8\rho\xi^2]^2/[\pi(3\gamma)^2]$).

The conclusion is not changed by the correction $\Sigma_{\mathbf{q}}^{(2)}(\mathrm{i}0^+)(\mathrm{d}/\mathrm{d}\zeta)\Sigma_{\mathbf{q}}^{(2)}(\mathrm{i}0^+)$ of our note 43, as we find that factors $\Sigma_{\mathbf{q}}^{(2)}(\mathrm{i}0^+)$ and $(\mathrm{d}/\mathrm{d}\zeta)\Sigma_{\mathbf{q}}^{(2)}(\mathrm{i}0^+)$ are both real. This was obvious for the first factor (the edge effects it presents in 1D [87] are suppressed in 2D by a lowering of the phonon density of states at low wavenumber). This was not the case for the second factor: because of edge effects in the integration over $\mathbf{k}$ (see Equation (39) in reference [63]), the Beliaev and Landau processes each give a non-zero contribution to $\mathrm{Im}\,(\mathrm{d}/\mathrm{d}\zeta)\Sigma_{\mathbf{q}}^{(2)}(\mathrm{i}0^+)$ (it is $2[9(1+\Lambda)^2/8\rho\xi^2]/[\bar{q}(3|\gamma|)^{3/2}]$ for Landau at temperature leading order) but these contributions are exactly opposite, in particular because the energy denominators $\varepsilon_{\mathbf{q}} - (\varepsilon_{\mathbf{k}} + \varepsilon_{\mathbf{q}-\mathbf{k}})$ and $\varepsilon_{\mathbf{q}} + \varepsilon_{\mathbf{k}} - \varepsilon_{\mathbf{q}+\mathbf{k}}$ are opposite $\sim \mp\hbar ck[1 - (v_q/c)\cos\theta]$ at leading order in k ($v_q = \mathrm{d}\varepsilon_{\mathbf{q}}/\hbar\mathrm{d}q$ is the group velocity and θ

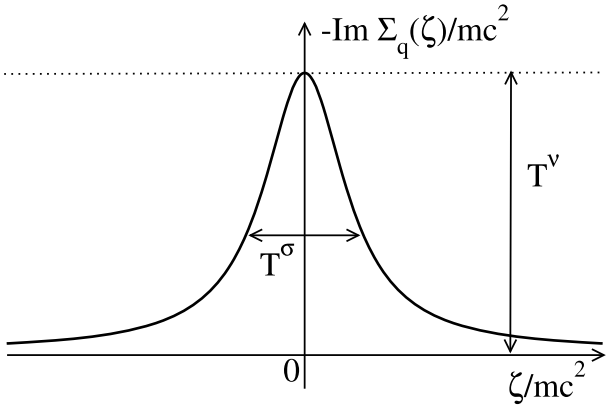

Figure 8. In the limit $T \to 0$, the order of magnitude and typical width of function $\mathrm{Im}\,\Sigma_{\mathbf{q}}(\zeta)$ near $\zeta = \mathrm{i}0^+$ are assumed to be characterized by two power laws in temperature, with exponents ν and σ (taking into account a possible temperature dependence of the curvature parameter γ).

estimate to the case $\zeta \neq 0$, i.e. by adding ζ to ΔE in (53); however, in an expansion at small angles between $\mathbf{k}_i$ and $\mathbf{q}$, the part of ΔE linear in the wave numbers vanishes, leaving only the cubic contributions $\approx \gamma T^3$, so that, independently of the dimension of space d,

$$\frac{1}{\zeta + \Delta E} \approx \frac{1}{\zeta + \gamma T^3} \quad \text{and therefore } T^\sigma \approx |\gamma| T^3 \tag{57}$$

taking into account the dependence on the parameter γ, which—as we said—may vary with temperature. The resulting validity condition $T^\nu = o(\gamma T^3)$ in (56) can be given a simple interpretation: in the limit $T \to 0$ taken with the scaling law $q \approx T$, the damping rate $\Gamma_{\mathbf{q}}$ must tend to zero faster than the q^3 term in $\omega_{\mathbf{q}}$,

$$\Gamma_q \underset{T\to 0}{\overset{\hbar c q/k_{\mathrm{B}}T \text{ fixed}}{=}} o(\omega_{\mathbf{q}}^{(3)}) \quad \text{with } \omega_{\mathbf{q}}^{(3)} = \gamma m c^2 (q\xi)^3/8\hbar \tag{58}$$

which is the true mark of the Markovian nature of damping (rather than the naive perturbative condition $\Gamma_{\mathbf{q}} = o(\omega_{\mathbf{q}})$).

The situation is summarized in Table 1 below[49]. The Born–Markov approximation is therefore usable in dimension 3, except over a narrow interval of values of γ, of width $\approx (k_{\mathrm{B}}T/mc^2)^2$ around $\gamma = 0$; for $\gamma = 0$, the phonon dispersion relation (34) deviates quintically from the linear law cq, which is obviously a special case.

---

is the angle between $\mathbf{k}$ and $\mathbf{q}$) and enter the derivative of the Dirac distribution $\delta'(\varepsilon)$, which is an odd function of its argument.

The two-dimensional concave case is therefore special: the quantity $\mathrm{Im}\,\Sigma_{\mathbf{q}}^{(4)\mathrm{eff}}(\mathrm{i}0^+)$ of note 43—considered at all temperature orders—does not give the correct temperature scaling law $\propto T^3$ of the self-energy at fourth order in H_3 on a $O(T^3)$ neighborhood of $\zeta = \mathrm{i}0^+$; nor does it give the damping rate $\Gamma_{\mathbf{q}}$, since the Born and Markov approximations fail, as in the two-dimensional convex case (see the last line of our Table 1). Note, however, still for $\gamma < 0$, that the limiting case $\rho\xi^2 \to +\infty$ of a very weakly interacting underlying superfluid must be set apart as there we have the additional small parameter $1/\rho\xi^2$ helping validity of Markov (as in Section 3.2 of reference [63]) and Born (as in Equation (17) of the same reference); this limiting case is inaccessible in a gas of spin-1/2 fermions with contact interaction—we have $\rho\xi^2 = O(1)$ when $\gamma < 0$ [88]—but it is in a Bose gas with an interaction range $\gtrsim \xi$ as considered in reference [78].

[49] In the third row of the table, possible logarithmic factors $\ln(1/T)$ are omitted for simplicity. These factors arise from the fact that, for scaling laws $\gamma \propto T^2$ and $q \propto T$, the terms q^3 and $q^5 \ln q$ are of the same order of magnitude in the dispersion relation (34): in this low curvature regime, the logarithmico-quintic contribution to $\omega_{\mathbf{q}}$ is no longer a small correction and must be kept.

Table 1. In the study of phonon damping in a superfluid, validity of the Born–Markov approximation in the low-temperature limit $T \to 0$ depending on the dimension of space d and the curvature parameter γ of the acoustic branch (more precisely, its sign and its temperature dependence, the third line holding regardless of the sign of γ).

	ν	σ	Markov	$\epsilon_{d\mathrm{D}}$	Born
$d=3, \gamma>0$ fixed	5	3	yes	$\approx T^2 \to 0$	yes
$d=3, \gamma<0$ fixed	7	3	yes	$\approx T^2 \to 0$	yes
$d=3, \gamma=O(T^2)$	5	5	no	$\approx T^0 \not\to 0$	no
$d=2, \gamma>0$ fixed	3	3	no	$\approx T^0 \not\to 0$	no

The exponents ν and σ used in the definition (56) of the Markovian regime are shown in Figure 8, and the small parameter of the Born expansion $\epsilon_{d\mathrm{D}}$ is given in Equation (53).

The precise calculation of the damping rate $\Gamma_{\mathbf{q}}$ (or what takes its place for non-exponential decay, such as the inverse of the width of $|\langle \hat{b}_{\mathbf{q}}(t)\rangle|^2$ at relative height $1/\mathrm{e}$) for these small values of curvature is, to our knowledge, an open question; it is of great experimental relevance, as the interaction strength leading to $\gamma = 0$ seems to be close to the unitary limit (see reference [57] and our Section 5.1), the preferred point for cold atom experiments in a regime of fairly high values of $T_\mathrm{c}/T_\mathrm{F}$ and collisional properties conducive to evaporative cooling [18].

For good measure, we have also considered the two-dimensional convex case in Table 1: the Born–Markov approximation fails here, and reference [63] had to resort to a non-perturbative heuristic approximation on the self-energy $\Sigma_{\mathbf{q}}(\zeta)$ to reach good agreement with classical field simulations (quantum hydrodynamics operators $\hat{b}_{\mathbf{q}}, \hat{b}^\dagger_{\mathbf{q}}$ replaced by complex numbers $b_{\mathbf{q}}, b^*_{\mathbf{q}}$) in the weakly interacting regime $\rho\xi^2 \gg 1$ of the underlying bosonic superfluid, where a small parameter was thought to be available and to ensure the success of Fermi's golden rule even in the $k_\mathrm{B}T/mc^2 \to 0$ limit (this reasonable expectation, confirmed in Section 3.2 of reference [63] to order two in H_3, is invalidated in Section 4.3 of the same reference by a calculation to order four)[50].

4.4. *Phase diffusion of the pair condensate*

A fundamental and practical question concerns the coherence time of the pair condensate at thermal equilibrium in a Fermi gas perfectly isolated from its environment.

For an infinite unpolarized system of $\uparrow$ and $\downarrow$ fermions, the coherence time is infinite, as asserted by the $U(1)$ symmetry-breaking phenomenon: in the grand canonical ensemble (term $-\mu\hat{N}$ added to the Hamiltonian of the Fermi gas where μ is the chemical potential and $\hat{N}$ the total

[50] We haven't even mentioned the very special case of dimension $d = 1$, where two wave vectors make a very small angle (zero!) as soon as they are in the same direction. Let's just say that the Born small parameter is still given by Equation (53), even though this equation was obtained under the assumption $d \geq 2$. Restoring the density dependence as in [63], we find more precisely $\epsilon_{1\mathrm{D}} = 1/[\gamma^2\rho\xi(k_\mathrm{B}T/mc^2)^2]$, the prefactor in (53) being written $\gamma(k_\mathrm{B}T)^3/(mc^2)^2$. In the low-temperature limit $k_\mathrm{B}T/mc^2 \to 0$ at $\rho\xi$ fixed considered here, $\epsilon_{1\mathrm{D}} \to +\infty$ and we must immediately resort to non-perturbative approximations on $\Sigma_{\mathbf{q}}(\zeta)$ and $\Gamma_{\mathbf{q}}$, such as the self-consistent calculation of references [89,90]. In the opposite weakly-interacting limit $\rho\xi \to +\infty$ at $k_\mathrm{B}T/mc^2$ fixed, $\epsilon_{1\mathrm{D}} \to 0$ and we can use Fermi's golden rule as in reference [87]; more precisely, we expect the validity condition of the golden rule to be written as $\rho\xi(k_\mathrm{B}T/mc^2)^2 \gg \phi_{1\mathrm{D}}(\bar{q})$ where $\phi_{1\mathrm{D}}$ is some function of $\bar{q} = \hbar cq/k_\mathrm{B}T$, forgetting the γ dependence for simplicity (at a fixed $\bar{q}$, the Born approximation imposes this condition, but the Markov approximation is then also satisfied because we have $\hbar\Gamma_{\mathbf{q}}|^{\mathrm{golden}}_{\mathrm{rule}} \approx \gamma[(k_\mathrm{B}T)^3/(mc^2)^2]\epsilon_{1\mathrm{D}} \approx k_\mathrm{B}T/(\gamma\rho\xi) \ll \Delta E \approx \gamma(k_\mathrm{B}T)^3/(mc^2)^2$ where ΔE, the typical Beliaev–Landau energy denominator, gives the width in ζ of the self-energy as in Equation (57)). In 2D, as shown in reference [63], the perturbative H_3-expansion of the self-energy is subject to a similar validity condition, $\rho\xi^2(k_\mathrm{B}T/mc^2)^2 \gg \phi_{2\mathrm{D}}(\bar{q})$, see its Equation (96), which, unlike the 1D case, is not obtained by simple power counting.

number of particles operator), the complex order parameter $\Delta(\mathbf{r},t)$ is uniform and constant; in the canonical ensemble, it therefore evolves with the undamped phase factor $\exp(-2\mathrm{i}\mu t/\hbar)$ [51], advancing at the immutable angular frequency $2\mu/\hbar$; in any case, the coherence time is infinite.

What about a finite size system (quantization box $[0,L]^3$, fixed total number of fermions N)? To find out, let's follow reference [76] and write the evolution equation for the condensate phase operator, which we denote $\hat{\phi}_0$ as in Equation (39), in the quantum hydrodynamics regime[52]:

$$-\hbar\frac{\mathrm{d}}{\mathrm{d}t}\hat{\phi}_0 = \mu_0(\rho) + \sum_{\mathbf{q}\neq\mathbf{0}} \hat{b}^\dagger_{\mathbf{q}}\hat{b}_{\mathbf{q}}\frac{\mathrm{d}}{\mathrm{d}N}(\hbar\omega_{\mathbf{q}}) \equiv \hat{\mu} \tag{59}$$

In the second expression, $\mu_0(\rho) = \mathrm{d}E_0/\mathrm{d}N$ is the chemical potential of the N fermions in the ground state of energy E_0 at density ρ, and the sum over $\mathbf{q}$ can be interpreted as the adiabatic derivative (meaning at fixed number operators $\hat{b}^\dagger_{\mathbf{q}}\hat{b}_{\mathbf{q}}$ of the phonon modes) with respect to N of the corresponding sum in the phonon Hamiltonian H_2 (41). The second expression as a whole is therefore the isentropic derivative of the Hamiltonian with respect to the total number of particles. In this sense, it is a chemical potential operator for the fermions, hence the notation $\hat{\mu}$ in the third expression, and Equation (59) is a quantum version of the famous second Josephson relation, linking the time derivative of the (classical) phase of the order parameter to the equilibrium chemical potential μ.

In a given realization of the experiment, which we assume to correspond to a N-body eigenstate $|\psi_\lambda\rangle$ of energy E_λ sampling the canonical ensemble, the occupation numbers $\hat{b}^\dagger_{\mathbf{q}}\hat{b}_{\mathbf{q}}$ fluctuate and decorrelate under the effect of incessant collisions between phonons due in particular to H_3, see Equation (44). At times long enough for a large number of collisions to have taken place, we therefore expect a diffusive spreading of the condensate phase, the variance of the random phase shift increasing linearly with time:

$$\mathrm{Var}_\lambda[\hat{\phi}_0(t)-\hat{\phi}_0(0)] \underset{\Gamma^\phi_{\mathrm{coll}}t\gg1}{\sim} 2D_\lambda t \tag{60}$$

with a subintensive diffusion coefficient D_λ, i.e. $\approx 1/N$ in the thermodynamic limit. Here $\Gamma^\phi_{\mathrm{coll}} = \Gamma_{q=k_\mathrm{B}T/\hbar c}$ is the typical collision rate between thermal phonons (the function Γ_q is that of Equation (52)). The spreading (60) induces an exponential loss of temporal coherence of rate D_λ, by virtue of Wick's relation (the phase shift statistic in $|\psi_\lambda\rangle$ is expected to be approximately Gaussian [91]),

$$\begin{aligned}\left\langle \exp\{-\mathrm{i}[\hat{\phi}_0(t)-\hat{\phi}_0(0)]\}\right\rangle_\lambda &\simeq \exp[-\mathrm{i}\langle\hat{\phi}_0(t)-\hat{\phi}_0(0)\rangle_\lambda]\exp\{-\tfrac{1}{2}\mathrm{Var}_\lambda[\hat{\phi}_0(t)-\hat{\phi}_0(0)]\}\\ &\underset{\Gamma^\phi_{\mathrm{coll}}t\gg1}{\simeq} \exp[-\mathrm{i}\langle\hat{\mu}\rangle_\lambda t/\hbar]\exp(-D_\lambda t)\end{aligned} \tag{61}$$

which is confirmed by the resolvent analysis of reference [76][53].

In the case $\gamma > 0$ of a convex acoustic branch, the situation resembles that of weakly interacting Bose condensates well studied in reference [95]: the dominant collisions are the three-phonon Beliaev–Landau ones $\phi \leftrightarrow \phi\phi$, and D_λ has been calculated for the low-temperature Fermi pair

[51] There is a factor of 2 under the exponential because Δ is a pair-order parameter whereas μ is the chemical potential of the fermions. There is no factor of 2 in Equation (59) because the phase operator $\hat{\phi}_0$ is conjugate to the fermion density.

[52] To obtain this equation, we had to eliminate $\hat{b}_{\mathbf{q}}\hat{b}_{-\mathbf{q}}$ and $\hat{b}^\dagger_{\mathbf{q}}\hat{b}^\dagger_{-\mathbf{q}}$ terms by temporal smoothing; this is of no consequence, as they oscillate with a period $\approx \hbar/k_\mathrm{B}T$ much shorter than the collisional timescales of interest here (see below) and automatically average to zero.

[53] If we assume that the interacting phonon gas is an ergodic quantum system [92,93], the mean $\langle\hat{\mu}\rangle_\lambda$ in the steady state $|\psi_\lambda\rangle$ depends only on the two conserved quantities, the energy E and the number of particles N, and coincides for a large system with the microcanonical chemical potential $\mu_{\mathrm{mc}}(E=E_\lambda,N)$. If the energy E fluctuates from one realization of the experiment to the next around the mean value $\bar{E}$, as in the canonical ensemble, the phase factor in the third expression of Equation (61) fluctuates and leads to a Gaussian-in-time loss of coherence: linearization of $\mu_{\mathrm{mc}}(E,N)$ around $\bar{E}$ gives $\mathrm{Var}[\hat{\phi}_0(t)-\hat{\phi}_0(0)] \sim [\partial_E\mu_{\mathrm{mc}}(\bar{E},N)]^2(\mathrm{Var}\,E)t^2/\hbar^2$, a parasitic effect $\approx t^2/N$ rapidly masking the phase diffusion (60) $\approx t/N$ [94].

condensate in reference [86]; we give here a simplified expression, keeping only the scaling laws in N, T and γ (under the assumption $\gamma = O(1)$):

$$D_\lambda^{\gamma>0} \approx N^{-1} T^4 \gamma^0. \tag{62}$$

There has been no experimental verification yet in cold atomic gases (the only quantum fluids sufficiently well isolated for the condensate loss of coherence to be intrinsic), even for bosons.

In the concave case $\gamma < 0$, on the other hand, the question remains largely open. An attempt to calculate D_λ in reference [86], taking into account only the Landau–Khalatnikov four-phonon collision processes $\phi\phi \to \phi\phi$ at small angles, of typical rate $\Gamma^\phi_{\rm coll} \propto (k_{\rm B}T/mc^2)^7 mc^2/\hbar|\gamma| \approx T^7$, led to an infinite diffusion coefficient,

$$D_\lambda^{\gamma<0} = +\infty \tag{63}$$

more precisely to a superdiffusive spreading law (simplified as in (62))[54]

$$\mathrm{Var}_\lambda^{\gamma<0}[\hat\phi_0(t) - \hat\phi_0(0)] \approx N^{-1} T^{20/3} |\gamma|^{1/3} t^{5/3} \tag{64}$$

in particular because collisions $\phi\phi \to \phi\phi$ preserve the total number N_ϕ of phonons (unlike $\phi \leftrightarrow \phi\phi$)[55,56]. To go beyond this and obtain the true (a priori finite) value of D_λ remains an open question: one would have to take into account the subdominant five-phonon processes $\phi\phi \leftrightarrow \phi\phi\phi$ which change N_ϕ and occur at a rate $\approx T^9$ [96], of the same order of magnitude as that of large-angle $\phi\phi \to \phi\phi$ processes [52,78], which is not easy[57].

5. Open questions requiring a microscopic theory of the many-body problem

The quantum hydrodynamics of Section 4 is only a low-energy effective theory. It therefore has limitations of two kinds, which we briefly review here, and which make it impossible to dispense with a many-body microscopic calculation.

5.1. *Determining the ingredients of quantum hydrodynamics*

Quantum hydrodynamics involves two quantities that are external to it, the equation of state of the unpolarized Fermi gas at zero temperature (through the energy density $e_0(\rho)$ or the chemical potential $\mu_0(\rho)$—its derivative—at density ρ) and the curvature parameter γ of the acoustic branch (34).

In the present case of equal mass $m_\uparrow = m_\downarrow = m$, the equation of state has been measured experimentally [48,97] and various approximate calculation methods give satisfactory results, such as fixed-node diffusive quantum Monte Carlo [98,99] or the Gaussian fluctuations approximation in a path integral formulation [100,101].

The situation is much more open for the curvature parameter γ. The Anderson random phase approximation (RPA) [61], equivalent for this problem to the eigenfrequency calculation of linearized time-dependent BCS equations or even to the more powerful Gaussian fluctuations

[54] In all cases, see Equations (62) and (64), we find that there is no phase spreading at the thermodynamic limit $N \to +\infty$: in an isolated gas, the limited coherence time of the condensate is a finite-size effect.

[55] N_ϕ should then be added to the list of constants of motion, alongside E and N, in note 53.

[56] The fact that, for $\gamma < 0$, the phonon damping rate $\Gamma_{\mathbf{q}}$ tends towards zero as q^3 (instead of q for $\gamma > 0$) also plays a role; however, without the conservation of N_ϕ, it would lead to a marginally superdiffusive $t \ln t$ spreading law (see Equation (C.20) of reference [86] and the morality stated below its Equation (72)).

[57] Publication [86], misunderstanding reference [96], had seen there a five-phonon damping rate scaling as T^{11}. The error has been corrected here. Indeed, reference [96], considering a quasi-thermal equilibrium with a small non-zero phonon chemical potential $\mu_\phi \to 0^-$, obtains the evolution equation $L^{-3}\mathrm{d}N_\phi/\mathrm{d}t = -\Gamma_\phi \mu_\phi$ for the average phonon number, where $\Gamma_\phi \approx T^{11}$ is not the rate sought despite appearances; as $L^{-3}\mathrm{d}N_\phi/\mathrm{d}t \approx T^2 \mathrm{d}\mu_\phi/\mathrm{d}t$ for Bose's law $\tilde n_{\mathbf{q}} = 1/\{\exp[(\hbar cq - \mu_\phi)/k_{\rm B}T] - 1\}$, we actually have $-\mathrm{d}\mu_\phi/\mathrm{d}t \propto (\Gamma_\phi/T^2)\mu_\phi$, of rate $\approx T^9$.

approximation [100,102][58], leads to a fairly simple analytical expression of γ in terms of $\mu/|\Delta|$ and $(\partial\mu/\partial|\Delta|)_a$, exact in the limit $k_F a \to 0^+$ of a condensate of dimers ($\gamma \to 1$), reasonable in the BCS limit $k_F a \to 0^-$ ($\gamma \to -\infty$ exponentially with $1/k_F|a|$ since the acoustic branch is crushed by the broken-pair continuum) and changing sign for $|\Delta|/\mu \simeq 0.87$, i.e. $1/k_F a \simeq -0.14$ for the rather approximate BCS equation of state, not far from the unitary limit in any case [57].

In particular, γ has the same positive value at the unitary limit in all three approaches (convex acoustic branch at low q):

$$\gamma^{\rm RPA}_{a^{-1}=0} \simeq 0.084 \tag{65}$$

The error, however, is uncontrolled, and we're not even sure of the sign.

A completely different method proceeds by extending the problem to an arbitrary spatial dimension d and expanding around dimension four, in powers of the small parameter $\epsilon = 4-d$. At the unitary limit, it too predicts a convex branch at low q [104][59]:

$$\gamma^{\rm dimension}_{a^{-1}=0} = \frac{1}{3}\left[1 - \frac{1}{4}\epsilon + O(\epsilon^2)\right] \underset{d=3}{\overset{\epsilon=1}{\simeq}} \frac{1}{4} > 0 \tag{66}$$

Experimentally, a recent measurement of the acoustic branch by Bragg excitation in a cold-atom Fermi gas leads, on the contrary, to a concave branch at the unitary limit [105]:

$$\gamma^{\rm exp}_{a^{-1}=0} = \frac{8\mu}{3E_F}\zeta \simeq \zeta \quad \text{with } \zeta = -0.085(8) < 0 \tag{67}$$

where the ratio μ/E_F is $\simeq 3/8$ for the ground-state unitary gas [48] and ζ is the acoustic-branch curvature parameter for a rescaling of q by k_F, $\omega_{\mathbf{q}} = cq(1+\zeta q^2/k_F^2+\cdots)$. The result (67) suffers from two limitations [106]: (i) a cubic fit of the branch over an interval of rather high q values, $q/k_F \in [0.29, 1.63]$, rather than over a narrow neighborhood of $q=0$ (for the RPA dispersion relation, for example, which has an inflection point at $q \simeq 0.5 k_F$, such a fit, blindly mixing convex and concave parts, would not give the right sign of $\gamma^{\rm RPA}_{a^{-1}=0}$), and (ii) a relatively high temperature, $T = 0.128(8)\,T_F \simeq 0.8 T_c$: even if we start from the RPA branch of parameter $\gamma > 0$ in the ground state, quantum hydrodynamics predicts a thermal change $\delta\gamma_{\rm th}$ in curvature (by interaction of the mode $\mathbf{q}$ with thermal phonons) negative enough to change its sign:

$$\delta\gamma_{\rm th} \sim -\frac{8\pi^2}{9(3\mu/E_F)^{1/2}}\left(\frac{T}{T_F}\right)^2 \simeq -0.14 < -\gamma^{\rm RPA}_{a^{-1}=0} \tag{68}$$

The question of the sign of γ at the unitary limit, which crucially determines the three-phonon ($\gamma > 0$) or four-phonon ($\gamma < 0$) nature of sound damping in the low-temperature collisionless regime, therefore remains largely open[60].

[58] These different approaches lead to exactly the same implicit equation linking angular eigenfrequency $\omega_{\mathbf{q}}$, chemical potential μ and order parameter Δ, and exactly the same equation linking μ, Δ and s-wave scattering length a [57]; they differ only in the equation of state $\mu = \mu_0(\rho)$ linking μ to ρ in the ground state, the one of Gaussian fluctuations being the most accurate. For example, at the unitary limit $a^{-1} = 0$, the approaches all give $mc^2/\mu = 2/3$ (this is exact by scale invariance, $\mu_0(\rho) \propto \rho^{2/3}$ in Equation (43)), $|\Delta|/\mu \simeq 1.16$ (close to the experimental value $0.44E_F/0.376E_F \simeq 1.17$ knowing that $|\Delta| = E_{\rm pair}/2$ in these theories and that $E_{\rm pair}/2E_F \simeq 0.44$ in the experiment [103]) but the ratio $\mu/E_F \simeq 0.376$ in the experiment [48], very poorly reproduced $\simeq 0.59$ by RPA and BCS, is much better $\simeq 0.40$ in Gaussian fluctuations.

[59] We obtained expression (66) by directly inserting Equation (50) of reference [104] into the dispersion relation (48) of the same reference and using the exact property $mc^2 = 2\mu/3$ due to scale invariance. Proceeding differently, i.e. via its Equation (52) and its result $c_2/c_1 = O(\epsilon^2) \simeq 0$ with $d=3$ in its Equation (48), we find the fairly close value $\gamma^{\rm dimension}_{a^{-1}=0} = 8/45 \simeq 0.18$.

[60] The damping studied experimentally in reference [107] is in the hydrodynamic regime, in the sense of note 41. This reference therefore does not allow us to resolve the problem.

5.2. *Describing high-frequency modes*

Quantum hydrodynamics, with its almost linear acoustic branch, cannot reliably describe the sound waves of angular frequency $\omega_{\mathbf{q}} > mc^2/\hbar$ in the Fermi superfluid. Ignoring the composite nature of bound pairs $\uparrow\downarrow$, it is totally inapplicable to angular frequencies $\omega \approx E_{\text{pair}}/\hbar$, where E_{pair} is the binding energy of a pair: at these frequencies, pairs can break into two fermionic excitations χ (conservation of energy no longer prohibits this), see Figure 5a.

A microscopic description of the Fermi gas is then required. At zero temperature, the main method available is that of the time-dependent BCS variational theory [108]. Its specialization to the linear response regime yields the following eigenvalue equation for the energy z of the modes of wave vector $\mathbf{q}$:

$$\det M(\mathbf{q},z)=0 \quad \text{with } M(\mathbf{q},z)=\begin{pmatrix} M_{|\Delta||\Delta|}(\mathbf{q},z) & M_{|\Delta|\theta}(\mathbf{q},z) \\ M_{\theta|\Delta|}(\mathbf{q},z) & M_{\theta\theta}(\mathbf{q},z)\end{pmatrix} \tag{69}$$

where the coefficients of the 2×2 matrix correspond to a response in the modulus $|\Delta|$ or in the phase θ of the complex order parameter $\Delta(\mathbf{r},t)$. In the weakly-interacting BCS limit $k_{\text{F}}a \to 0^-$, off-diagonal elements are usually (rightly) neglected and the dynamics decouples into modulus and phase modes; in the general case, this distinction no longer applies.

The exploration of solutions to Equation (69) has begun. At a fixed wavenumber q, we find at most one root under the edge $\varepsilon_{\mathbf{q}}^{\text{bord}}$ of the broken-pair continuum, the root $\hbar\omega_{\mathbf{q}}$ of the acoustic branch. On the interval $z\in\,]\,\varepsilon_{\mathbf{q}}^{\text{bord}},+\infty\,[$, the function $\det M(\mathbf{q},z)$ has a branch cut[61], it is necessary to add an infinitesimal shift $\mathrm{i}0^+$ to z to make sense of it; the function then acquires an imaginary part, which cannot vanish simultaneously with the real part, and Equation (69) has no solution. On the other hand, a complex $z_{\mathbf{q}}$ with a non-infinitesimal < 0 imaginary part can be found, by performing an analytic continuation of function $z\mapsto \det M(\mathbf{q},z)$ from the upper half-plane to the lower half-plane through its branch cut (indicated by arrow $\downarrow$ in the subscript):

$$\det M_{\downarrow}(\mathbf{q},z_{\mathbf{q}})=0 \quad \text{with } \operatorname{Im} z_{\mathbf{q}}<0 \tag{70}$$

There is therefore a collective mode in the continuum, which decays exponentially in time through the emission of broken pairs. The calculation was first performed in the BCS limit $k_{\text{F}}a\to 0^-$, both for neutral fermions and for electrons in a superconductor, in reference [109]. It was then generalized to fermionic cold-atom gases for arbitrary values of $k_{\text{F}}a$, no longer neglecting the off-diagonal elements $M_{|\Delta|\theta}$ and $M_{\theta|\Delta|}$ [110,111]. The Andrianov–Popov branch persists up to $1/k_{\text{F}}a = 0.55$ (point of zero chemical potential $\mu = 0$ in BCS theory) and always starts at $2|\Delta|$ quadratically in q with a complex coefficient:

$$z_{\mathbf{q}} \underset{q\to 0}{\overset{\mu>0}{=}} 2|\Delta| + \zeta\frac{\hbar^2 q^2}{4m_*} + O(q^3) \quad (\operatorname{Im}\zeta<0) \tag{71}$$

where m_* is the effective mass of a fermionic quasiparticle χ at the location $k = k_0$ of its energy minimum[62]. We have written $2|\Delta|$ here rather than E_{pair}, where Δ is the equilibrium order parameter, even though BCS theory is unable to distinguish (we have exactly $E_{\text{pair}} = 2|\Delta|$ for all $\mu > 0$ in this theory), in order to evoke the Higgs mechanism [113] which we think

[61] The matrix elements of $M(\mathbf{q},z)$ involve an integral over the wave vector $\mathbf{k}$ of one of the dissociation fragments of a bound pair of the condensate, and the integrand contains the corresponding energy denominator $z-(\varepsilon_{\mathbf{k}}+\varepsilon_{\mathbf{q}-\mathbf{k}})$; by definition, the denominator vanishes when z belongs to the broken-pair continuum, see the legend to Figure 5.

[62] The effective mass is such that $\varepsilon_{\mathbf{k}}-E_{\text{pair}}/2 \sim \hbar^2(k-k_0)^2/2m_*$ as $k\to k_0$. Scaling by m_* in Equation (71) ensures that ζ has a finite, non-zero limit when $k_{\text{F}}a\to 0^-$ [109]. In this regime, the well-known reference [112] predicts an incorrect behavior for $z_{\mathbf{q}}$ at low q, with an imaginary part tending linearly to zero $\propto q$, see its Equation (2.38). The quantity ζ here has nothing to do with that in Equation (67), there is an unfortunate coincidence of notations.

the collective mode of the continuum comes under [114][63]; moreover, in the opposite limit $k_F a \to 0^+$ of a bosonic dimer condensate, where $2|\Delta| \ll E_{\text{pair}} \sim 2|\mu| \sim \hbar^2/ma^2$ (this time we have $\mu < 0$), we do indeed find a collective excitation branch starting quadratically at $2|\Delta|$ and not at E_{pair} [111]. The extension of Equation (69) to non-zero temperature (beyond a simple BCS-type mean-field generalization, perhaps insufficient[64]) remains to our knowledge an open question.

From an experimental point of view, in cold atoms or superconductors, excitation at angular frequencies $\omega > E_{\text{pair}}/\hbar$ has only been carried out at zero wavenumber, where there is, according to zero temperature theories, no collective mode in the continuum, the spectral weight of the mode tending to 0 as $q \to 0$ [110]; at long times, we simply observe oscillations of the order parameter at angular frequency $E_{\text{pair}}/\hbar$ (this is the effect of the non-zero edge of the continuum), which attenuate with a power law $t^{-\alpha}$ [117,118] by the same mechanism as the spreading of the Gaussian wave packet of a free particle in ordinary quantum mechanics (percussive excitation creates a "wave packet" of broken pairs $(\mathbf{k}, -\mathbf{k})$ in the continuum, whose evolution governed by the dispersion relation $2\varepsilon_{\mathbf{k}}$ is effectively one-dimensional for $k_0 > 0$ ($\mu > 0$), in which case $\alpha = 1/2$ [119], and three-dimensional for $k_0 = 0$ ($\mu < 0$), in which case $\alpha = 3/2$ [120])[65]. The observation of the continuum mode (at $q > 0$) and the precise measurement of its dispersion relation $z_{\mathbf{q}}$ therefore remain to be done (hints are given in references [110,121]).

Declaration of interests

The authors do not work for, advise, own shares in, or receive funds from any organization that could benefit from this article, and have declared no affiliations other than their research organizations.

Références

[1] T. Enss, « Quantum transport in strongly correlated Fermi gases », *C. R. Phys.* **26** (2025), p. 217-224.

[63] As this mechanism results from $U(1)$ symmetry breaking, here by condensation of bound pairs, it must be characterized by the energy scale associated with the order parameter, i.e. $|\Delta|$ up to a factor; this is indeed what reference [113] finds, see its Equation (2b). On the other hand, the energy scale E_{pair} is related to pair breaking, not pair condensation, and therefore has no a priori connection with the Higgs branch. Having $E_{\text{pair}} = 2|\Delta|$ is a source of confusion and prevents the two phenomena from being decoupled. It would also be interesting to see whether property $E_{\text{pair}} = 2|\Delta|$ remains rigorously true at zero temperature in a theory more elaborate than BCS or in experiments.

[64] This generalization is not a panacea, as can be seen on the imaginary part of the acoustic branch. For $\gamma > 0$ (but not for $\gamma < 0$), this criticism can be leveled at RPA already at zero temperature, since it wrongly predicts a purely real angular eigenfrequency $\omega_{\mathbf{q}}$. However, this doesn't seem too serious, since the imaginary part $(-1/2)\Gamma_{\mathbf{q}}(T = 0) \approx q^5$ obtained by quantum hydrodynamics (Beliaev damping) gets lost in the neglected sub-subdominant terms in Equation (34). This problem is most visible at low q at non-zero temperature, where $\Gamma_{\mathbf{q}}(T > 0)$ starts linearly in q with a coefficient $\propto T^4$ (exponent ν is 5 in Table 1 for the scaling law $q \propto T$ of note 41), which the BCS-type mean-field theory cannot account for (it predicts a coefficient $O[-\exp(E_{\text{pair}}/2k_B T)]$ [115,116] since the only thermal occupation numbers it brings out are those $\bar{n}_{\mathbf{k}} = 1/[\exp(\varepsilon_{\mathbf{k}}/k_B T) + 1]$ of fermionic quasiparticles χ). In other words, the linearization of the time-dependent BCS equations or, what amounts to the same thing, the Gaussian fluctuations approximation takes into account the $\phi - \chi$ coupling but not the $\phi - \phi$ coupling.

[65] The observations of reference [118] in a unitary Fermi gas at $T \neq 0$ raise several questions: (i) the measured exponent $\alpha \simeq 1 \pm 0.15$ is very different from the theoretically predicted value ($\alpha = 1/2$ at the unitary limit), (ii) it cannot be ruled out that the decay of the oscillation amplitude is in fact exponential, (iii) in contrast to the amplitude, the angular frequency of the oscillations shows no observable reduction as T approaches the transition temperature T_c (where there is no more $U(1)$ symmetry breaking and $|\Delta|$ tends to zero), which seems incompatible with the qualification of Higgs oscillations used in this reference (the measured angular frequency is not proportional to $|\Delta|/\hbar$), but also suggests a rather troubling lack of dependence of E_{pair} with temperature (the measured angular frequency should be given by $E_{\text{pair}}/\hbar$ since the excitation is done at $q = 0$). Incidentally, the temperature is never very low in the experiment, $T \gtrsim 0.1 T_F$, see our Section 2, which makes the theory at $T = 0$ stricto sensu inapplicable.

[2] S. Capponi, « Classical and quantum spin liquids », *C. R. Phys.* **26** (2025), p. 91-111.

[3] S. Nascimbene, « Simulating quantum Hall physics in ultracold atomic gases : prospects and challenges », *C. R. Phys.* **26** (2025), p. 317-338.

[4] T. Jolicœur, « Interlayer phase coherence and composite fermions », *C. R. Phys.* **26** (2025), p. 113-124.

[5] X. Zhang et C. A. R. Sá de Melo, « Effects of spin–orbit coupling and Rabi fields in Tomonaga–Luttinger liquids : current status and open questions », *C. R. Phys.* **26** (2025). (à paraître).

[6] M. H. Anderson, J. R. Ensher, M. R. Matthews, C. E. Wieman et E. A. Cornell, « Observation of Bose–Einstein condensation in a dilute atomic vapor », *Science* **269** (1995), p. 198-201.

[7] K. B. Davis, M.-O. Mewes, M. R. Andrews, N. J. van Druten, D. S. Durfee, D. M. Kurn et W. Ketterle, « Bose–Einstein condensation in a gas of sodium atoms », *Phys. Rev. Lett.* **75** (1995), p. 3969-3973.

[8] S. Stellmer, B. Pasquiou, R. Grimm et F. Schreck, « Laser cooling to quantum degeneracy », *Phys. Rev. Lett.* **110** (2013), article no. 263003.

[9] A. Urvoy, Z. Vendeiro, J. Ramette, A. Adiyatullin et V. Vuletić, « Direct laser cooling to Bose–Einstein condensation in a dipole trap », *Phys. Rev. Lett.* **122** (2019), article no. 203202.

[10] Y. Castin, H. Wallis et J. Dalibard, « Limit of Doppler cooling », *J. Opt. Soc. Am. B* **6** (1989), p. 2046-2057.

[11] C. A. Regal, M. Greiner et D. S. Jin, « Observation of resonance condensation of Fermionic atom pairs », *Phys. Rev. Lett.* **92** (2004), article no. 040403.

[12] M. W. Zwierlein, C. A. Stan, C. H. Schunck, S. M. F. Raupach, A. J. Kerman et W. Ketterle, « Condensation of pairs of fermionic atoms near a Feshbach resonance », *Phys. Rev. Lett.* **92** (2004), article no. 120403.

[13] S. Giorgini, L. P. Pitaevskii et S. Stringari, « Theory of ultracold atomic Fermi gases », *Rev. Mod. Phys.* **80** (2008), p. 1215-1274.

[14] A. L. Gaunt, T. F. Schmidutz, I. Gotlibovych, R. P. Smith et Z. Hadzibabic, « Bose–Einstein condensation of atoms in a uniform potential », *Phys. Rev. Lett.* **110** (2013), article no. 200406.

[15] B. Mukherjee, Z. Yan, P. B. Patel, Z. Hadzibabic, T. Yefsah, J. Struck et M. W. Zwierlein, « Homogeneous atomic Fermi gases », *Phys. Rev. Lett.* **118** (2017), article no. 123401.

[16] N. Navon, R. P. Smith et Z. Hadzibabic, « Quantum gases in optical boxes », *Nat. Phys.* **17** (2021), p. 1334-1341.

[17] J. P. Solovej, « Mathematical physics of dilute Bose gases », *C. R. Phys.* **26** (2025), p. 339-348.

[18] D. S. Petrov, C. Salomon et G. V. Shlyapnikov, « Weakly bound dimers of Fermionic atoms », *Phys. Rev. Lett.* **93** (2004), article no. 090404.

[19] E. Burovski, N. Prokof'ev, B. Svistunov et M. Troyer, « Critical temperature and thermodynamics of attractive fermions at unitarity », *Phys. Rev. Lett.* **96** (2006), article no. 160402.

[20] E. Wigner, « Über die Streuung von Neutronen an Protonen », *Z. Phys.* **83** (1933), p. 253-258.

[21] H. Bethe et R. Peierls, « Quantum theory of the diplon », *Proc. R. Soc. Lond. Ser. A* **148** (1935), p. 146-156.

[22] J. Verstraten, K. Dai, M. Dixmerias, B. Peaudecerf, T. de Jongh et T. Yefsah, « *In situ* imaging of a single-atom wave packet in continuous space », *Phys. Rev. Lett.* **134** (2025), article no. 083403.

[23] V. Gurarie et L. Radzihovsky, « Resonantly paired fermionic superfluids », *Ann. Phys.* **322** (2007), p. 2-119.

[24] F. Werner et Y. Castin, « General relations for quantum gases in two and three dimensions : two-component fermions », *Phys. Rev. A* **86** (2012), article no. 013626.

[25] L. Pricoupenko, « Pseudopotential in resonant regimes », *Phys. Rev. A* **73** (2006), article no. 012701.

[26] L. H. Thomas, « The interaction between a neutron and a proton and the structure of H^3 », *Phys. Rev.* **47** (1935), p. 903-909.

[27] F. Werner et Y. Castin, « Unitary gas in an isotropic harmonic trap : symmetry properties and applications », *Phys. Rev. A* **74** (2006), article no. 053604.

[28] Y. Castin et F. Werner, « The unitary gas and its symmetry properties », in *The BCS-BEC Crossover and the Unitary Fermi Gas* (W. Zwerger, ed.), Lecture Notes in Physics, vol. 836, Springer: Berlin, 2011. Online at https://hal.science/hal-00576619.

[29] Y. Castin et E. Tignone, « Trimers in the resonant (2+1)-fermion problem on a narrow Feshbach resonance : crossover from Efimovian to hydrogenoid spectrum », *Phys. Rev. A* **84** (2011), article no. 062704.

[30] Y. Castin, C. Mora et L. Pricoupenko, « Four-Body Efimov effect for three fermions and a lighter particle », *Phys. Rev. Lett.* **105** (2010), article no. 223201. Online at https://hal.science/hal-00494915v2. [version française : « Effet Efimov à quatre corps pour trois fermions identiques et une particule légère »].

[31] S. Endo et Y. Castin, « Absence of a four-body Efimov effect in the 2+2 fermionic problem », *Phys. Rev. A* **92** (2015), article no. 053624. Online at https://hal.science/hal-01178707v3. [version française : « Absence d'effet Efimov à quatre corps dans le problème à 2+2 fermions »].

[32] F. Werner, *Atomes froids piégés en interaction résonnante : gaz unitaire et problème à trois corps*, Thèse de doctorat en physique quantique, Université Paris VI: Paris, 2008. Online at https://theses.hal.science/tel-00285587.

[33] L. Pricoupenko, « Universality of isolated N-body resonances at large scattering length », *Phys. Rev. A* **108** (2023), article no. 013315.

[34] S. Endo et Y. Castin, « Unitary boson–boson and boson–fermion mixtures : third virial coefficient and three-body parameter on a narrow Feshbach resonance », *Eur. Phys. J. D* **70** (2016), article no. 238. Online at https://hal.science/hal-01350476v3. [version française : « Mélanges unitaires boson–boson et boson–fermion : troisième coefficient du viriel et paramètre à trois corps sur une résonance de Feshbach étroite »].

[35] C. Gao, S. Endo et Y. Castin, « The third virial coefficient of a two-component unitary Fermi gas across an Efimov-effect threshold », *Europhys. Lett.* **109** (2015), article no. 16003. Online at https://hal.science/hal-01078973v4. [version française : « Le troisième coefficient du viriel d'un gaz unitaire de fermions à deux composantes à travers un seuil de l'effet Efimov »].

[36] Y. Castin, *Mécanique quantique : seconde quantification et résolvante*, cours du Master 2 Concepts fondamentaux de la physique, École normale supérieure: Paris, 2011. Online at https://hal.science/hal-04943729.

[37] K. M. Daily et D. Blume, « Thermodynamics of the two-component Fermi gas with unequal masses at unitarity », *Phys. Rev. A* **85** (2012), article no. 013609.

[38] L. Landau et E. Lifchitz, *Mécanique quantique - Théorie non relativiste*, cours de physique théorique tome 3, Mir: Moscou, 1970. Online at https://archive.org/details/landau-lifchitz-physique-theorique-vol-03-mechanique-quantique-theorie-non-relativiste-mir-1970.

[39] V. Efimov, « Energy levels of three resonantly interacting particles », *Nucl. Phys.* **A210** (1973), p. 157-188.

[40] B. Bazak et D. S. Petrov, « Five-body Efimov effect and universal pentamer in fermionic mixtures », *Phys. Rev. Lett.* **118** (2017), article no. 083002.

[41] T. Moser et R. Seiringer, « Stability of a Fermionic $N+1$ particle system with point interactions », *Commun. Math. Phys.* **356** (2017), p. 329-355.

[42] S. Endo et Y. Castin, « Quatrièmes coefficients d'amas et du viriel d'un gaz unitaire de fermions pour un rapport de masse quelconque/Fourth cluster and virial coefficients of a unitary Fermi gas for an arbitrary mass ratio », *C. R. Phys.* **23** (2022), p. 41-110.

[43] A. Comtet, Y. Georgelin et S. Ouvry, « Statistical aspects of the anyon model », *J. Phys. A : Math. Gen.* **22** (1989), p. 3917-3925.

[44] S. Endo et Y. Castin, « The interaction-sensitive states of a trapped two-component ideal Fermi gas and application to the virial expansion of the unitary Fermi gas », *J. Phys. A : Math. Theor.* **49** (2016), article no. 265301. Online at https://hal.science/hal-01246611v6. [version française : « Les états sensibles aux interactions d'un gaz parfait piégé de fermions à deux composantes et application au développement du viriel du gaz unitaire de fermions »].

[45] Y. Castin et F. Werner, « Le troisième coefficient du viriel du gaz de Bose unitaire », *Rev. Can. Phys.* **91** (2013), p. 382-389. Online at https://hal.science/hal-00768515v2. [accès libre : hal-00768677] [version anglaise : « Third virial coefficient of the unitary Bose gas »].

[46] Y. Hou et J. E. Drut, « Fourth- and fifth-order virial coefficients from weak coupling to unitarity », *Phys. Rev. Lett.* **125** (2020), article no. 050403.

[47] S. Nascimbene, N. Navon, K. Jiang, F. Chevy et C. Salomon, « Exploring the thermodynamics of a universal Fermi gas », *Nature (London)* **463** (2010), p. 1057-1060.

[48] M. J. H. Ku, A. T. Sommer, L. W. Cheuk et M. W. Zwierlein, « Revealing the superfluid Lambda transition in the Universal thermodynamics of a unitary Fermi gas », *Science* **335** (2012), p. 563-567.

[49] S. Endo et Y. Castin, *The interaction-sensitive states of a trapped two-component ideal Fermi gas and application to the virial expansion of the unitary Fermi gas*. Online at https://hal.archives-ouvertes.fr/hal-01246611. version augmentée hal-01246611 v5 (2021) [version française : « Les états sensibles aux interactions d'un gaz parfait piégé de fermions à deux composantes et application au développement du viriel du gaz unitaire de fermions », hal-01246611 v6 (2024)].

[50] R. Rossi, T. Ohgoe, K. Van Houcke et F. Werner, « Resummation of diagrammatic series with zero convergence radius for strongly correlated fermions », *Phys. Rev. Lett.* **121** (2018), article no. 130405.

[51] J. Zinn-Justin, *Analyse complexe et méthodes numériques*, EDP Sciences/CNRS Éditions: Les Ulis/Paris, 2025.

[52] L. Landau et I. Khalatnikov, « Teoriya vyazkosti Geliya-II », *Zh. Eksp. Teor. Fiz.* **19** (1949), p. 637-650. [traduit en anglais dans *Collected papers of L.D. Landau*, chapitre 69, pp. 494–510, édité par D. ter Haar (Pergamon, New York, 1965)].

[53] Y. Castin, « Basic tools for degenerate Fermi gases », in *Proceedings of the 2006 Varenna Enrico Fermi School on Fermi Gases* (M. Inguscio, W. Ketterle et C. Salomon, eds.), SIF: Bologne, 2007, p. 289-349. Online at https://hal.science/hal-00122049v2.

[54] H. J. Maris et W. E. Massey, « Phonon dispersion and the propagation of sound in liquid helium-4 below 0.6 °K », *Phys. Rev. Lett.* **25** (1970), p. 220-222.

[55] J. Goldstone, « Field theories with « Superconductor »solutions », *Nuovo Cimento* **19** (1961), p. 154-164.

[56] R. Combescot, M. Y. Kagan et S. Stringari, « Collective mode of homogeneous superfluid Fermi gases in the BEC-BCS crossover », *Phys. Rev. A* **74** (2006), article no. 042717.

[57] H. Kurkjian, Y. Castin et A. Sinatra, « Concavity of the collective excitation branch of a Fermi gas in the BEC-BCS crossover », *Phys. Rev. A* **93** (2016), article no. 013623. Online at https://hal.science/hal-01228798v2. [version française : « Concavité de la branche d'excitation collective d'un gaz de fermions dans la zone de raccordement CBE-BCS »].

[58] A. R. P. Lima et A. Pelster, « Beyond mean-field low-lying excitations of dipolar Bose gases », *Phys. Rev. A* **86** (2012), article no. 063609.

[59] W. Zwerger, « Reflections on dipolar quantum fluids », *C. R. Phys.* **25** (2024), p. 389-413.

[60] J. Dalibard, *Interactions magnétiques entre atomes froids : gouttelettes quantiques et états supersolides*, cours 2023–2024 du Collège de France, chaire *Atomes et rayonnement*, 2024. Online at https://pro.college-de-france.fr/jean.dalibard/ (accessed on oct. 18, 2024).

[61] P. W. Anderson, « Random-phase approximation in the theory of superconductivity », *Phys. Rev.* **112** (1958), p. 1900-1916.

[62] M. A. Escobedo et C. Manuel, « Effective field theory and dispersion law of the phonons of a nonrelativistic superfluid », *Phys. Rev. A* **82** (2010), article no. 023614.

[63] Y. Castin, A. Serafin et A. Sinatra, « Amortissement des phonons dans un superfluide 2D : insuffisance de la règle d'or de Fermi à basse température », *C. R. Phys.* **24** (2023), p. 187-239. Online at https://hal.science/hal-04168815v2. [version anglaise : « Phonon damping in a 2D superfluid : insufficiency of Fermi's golden rule at low temperature »].

[64] Y. Castin, « Marche au hasard d'une quasi-particule massive dans le gaz de phonons d'un superfluide à très basse température », *C. R. Phys.* **21** (2020), p. 571-618. Online at https://hal.science/hal-02895083v2. [version anglaise : « Random walk of a massive quasiparticle in the phonon gas of an ultralow temperature superfluid »].

[65] A. Nicolis et R. Penco, « Mutual interactions of phonons, rotons and gravity », *Phys. Rev. B* **97** (2018), article no. 134516.

[66] P. Fulde et R. A. Ferrell, « Superconductivity in a strong spin-exchange field », *Phys. Rev.* **135** (1964), A550-A563.

[67] A. I. Larkin et Y. N. Ovchinnikov, « Non uniform state of superconductors », *Zh. Eksp. Teor. Fiz.* **47** (1964), p. 1136-1146. [version anglaise : « Non uniform state of superconductors », Sov. Phys. J. Exp. Theor. Phys. **20** (1965) pp. 762–770].

[68] L. Radzihovsky et A. Vishwanath, « Quantum liquid crystals in an imbalanced Fermi gas : fluctuations and fractional vortices in Larkin–Ovchinnikov states », *Phys. Rev. Lett.* **103** (2009), article no. 010404.

[69] Y.-a. Liao, A. S. C. Rittner, T. Paprotta, W. Li, G. B. Partridge, R. G. Hulet, S. K. Baur et E. J. Mueller, « Spin-imbalance in a one-dimensional Fermi gas », *Nature* **467** (2010), p. 567-569.

[70] S. T. Beliaev, « Energy-spectrum of a non-ideal Bose gas », *Zh. Eksp. Teor. Fiz.* **34** (1958), p. 433-446. [version anglaise : « Energy-spectrum of a non-ideal Bose gas », Sov. Phys. J. Exp. Theor. Phys. **34** (1958) pp. 299–307].

[71] P. C. Hohenberg et P. C. Martin, « Microscopic theory of superfluid helium », *Ann. Phys.* **34** (1965), p. 291-359.

[72] H. Kurkjian, Y. Castin et A. Sinatra, « Landau–Khalatnikov phonon damping in strongly interacting Fermi gases », *Europhys. Lett.* **116** (2016), article no. 40002.

[73] Y. Castin, A. Sinatra et H. Kurkjian, « Landau phonon-roton theory revisited for superfluid ^{4}He and Fermi gases », *Phys. Rev. Lett.* **119** (2017), article no. 260402. Online at https://hal.science/hal-01570314v3. [version française : « Le couplage de Landau phonon-roton revisité pour l'hélium 4 liquide et étendu aux gaz de fermions superfluides »].

[74] I. N. Adamenko, Y. A. Kitsenko, K. E. Nemchenko et A. F. G. Wyatt, « Theory of scattering between two phonon beams in superfluid helium », *Phys. Rev. B* **80** (2009), article no. 014509.

[75] E. Lifchitz et L. Pitayevski, *Physique statistique, deuxième partie*, cours de physique théorique de L. Landau et E. Lifchitz, Éditions Mir: Moscou, 1990. Online at https://archive.org/details/landau-lifchitz-physique-theorique-vol-09-physique-statistique-deuxieme-parte-mir-1990.

[76] H. Kurkjian, Y. Castin et A. Sinatra, « Brouillage thermique d'un gaz cohérent de fermions », *C. R. Phys.* **17** (2016), p. 789-801. Online at https://hal.science/hal-01118346v4. [version anglaise : « Thermal blurring of a coherent Fermi gas »].

[77] D. T. Son et M. Wingate, « General coordinate invariance and conformal invariance in nonrelativistic physics : unitary Fermi gas », *Ann. Phys.* **321** (2006), p. 197-224.

[78] H. Kurkjian, Y. Castin et A. Sinatra, « Three-phonon and four-phonon interaction processes in a pair-condensed Fermi gas », *Annalen der Physik* **529** (2017), article no. 1600352. Online at https://hal.science/hal-01392846v3. [accès libre : hal-01392846] [version française : « Processus d'interaction à trois et quatre phonons dans un gaz de fermions condensé par paires »].

[79] A. Sinatra, C. Lobo et Y. Castin, « The truncated Wigner method for Bose condensed gases : limits of validity and applications », *J. Phys. B* **35** (2002), p. 3599-3631.

[80] A. L. Fetter et J. D. Walecka, *Quantum Theory of Many-Particle Systems*, Dover: Mineola, 2003.

[81] I. M. Khalatnikov, *An Introduction to The Theory Of Superfluidity*, CRC Press: Boca Raton, 2018.

[82] C. Cohen-Tannoudji, J. Dupont-Roc et G. Grynberg, *Processus d'interaction entre photons et atomes*, EDP Sciences/CNRS Éditions: Paris, 1988.
[83] P. R. Roach, J. B. Ketterson et M. Kuchnir, « Ultrasonic attenuation in liquid ^{4}He under pressure », *Phys. Rev. A* **5** (1972), p. 2205-2214.
[84] R. A. Sherlock, N. G. Mills et A. F. G. Wyatt, « The angular spreading of phonon beams in liquid ^{4}He : upward phonon dispersion », *J. Phys. C : Solid State Phys.* **8** (1975), p. 2575-2590.
[85] N. Katz, J. Steinhauer, R. Ozeri et N. Davidson, « Beliaev damping of quasiparticles in a Bose–Einstein condensate », *Phys. Rev. Lett.* **89** (2002), article no. 220401.
[86] Y. Castin, « Étalement de la phase et cohérence temporelle d'un gaz de fermions condensé par paires à basse température », *C. R. Phys.* **20** (2019), p. 540-568. Online at https://hal.science/hal-01849311v2. [version anglaise : « Phase spreading and temporal coherence of a pair-condensed Fermi gas at low temperature »].
[87] A. Micheli et S. Robertson, « Phonon decay in one-dimensional atomic Bose quasicondensates via Beliaev–Landau damping », *Phys. Rev. B* **106** (2022), article no. 214528.
[88] S. Van Loon et C. A. R. Sá de Melo, « Effects of quantum fluctuations on the low-energy collective modes of two-dimensional superfluid Fermi gases from the BCS to the Bose limit », *Phys. Rev. Lett.* **131** (2023), article no. 113001.
[89] A. F. Andreev, « The hydrodynamics of two- and one-dimensional liquids », *Zh. Eksp. Teor. Fiz.* **78** (1980), p. 2064-2072. Online at http://jetp.ras.ru/cgi-bin/e/index/r/78/5/p2064?a=list. [version anglaise : « The hydrodynamics of two- and one-dimensional liquids », Sov. Phys. J. Exp. Theor. Phys. **51** (1980) pp. 1038–1042].
[90] M. Punk et W. Zwerger, « Collective mode damping and viscosity in a 1D unitary Fermi gas », *New J. Phys.* **8** (2006), article no. 168.
[91] A. Sinatra et Y. Castin, « Genuine phase diffusion of a Bose–Einstein condensate in the microcanonical ensemble : a classical field study », *Phys. Rev. A* **78** (2008), article no. 053615.
[92] J. M. Deutsch, « Quantum statistical mechanics in a closed system », *Phys. Rev. A* **43** (1991), p. 2046-2049.
[93] M. Srednicki, « Chaos and quantum thermalization », *Phys. Rev. E* **50** (1994), p. 888-901.
[94] A. Sinatra, Y. Castin et E. Witkowska, « Nondiffusive phase spreading of a Bose–Einstein condensate at finite temperature », *Phys. Rev. A* **75** (2007), article no. 033616.
[95] A. Sinatra, Y. Castin et E. Witkowska, « Coherence time of a Bose–Einstein condensate », *Phys. Rev. A* **80** (2009), article no. 033614.
[96] I. M. Khalatnikov, « Pogloshcheniye zvuka v gelii II », *Zh. Eksp. Teor. Fiz.* **20** (1950), p. 243-266.
[97] N. Navon, S. Nascimbène, F. Chevy et C. Salomon, « The equation of state of a low-temperature Fermi gas with tunable interactions », *Science* **328** (2010), p. 729-732.
[98] G. E. Astrakharchik, J. Boronat, J. Casulleras et S. Giorgini, « Equation of state of a Fermi gas in the BEC-BCS crossover : a quantum Monte Carlo study », *Phys. Rev. Lett.* **93** (2004), article no. 200404.
[99] M. M. Forbes, S. Gandolfi et A. Gezerlis, « Resonantly interacting fermions in a box », *Phys. Rev. Lett.* **106** (2011), article no. 235303.
[100] R. B. Diener, R. Sensarma et M. Randeria, « Quantum fluctuations in the superfluid state of the BCS-BEC crossover », *Phys. Rev. A* **77** (2008), article no. 023626.
[101] H. Hu, X. Liu et P. Drummond, « Equation of state of a superfluid Fermi gas in the BCS-BEC crossover », *Europhys. Lett.* **74** (2006), p. 574-577.
[102] M. Marini, F. Pistolesi et G. C. Strinati, « Evolution from BCS superconductivity to Bose condensation : analytic results for the crossover in three dimensions », *Eur. Phys. J. B* **1** (1998), p. 151-159.
[103] A. Schirotzek, Y. I. Shin, C. H. Schunck et W. Ketterle, « Determination of the superfluid gap in atomic Fermi gases by quasiparticle spectroscopy », *Phys. Rev. Lett.* **101** (2008), article no. 140403.
[104] G. Rupak et T. Schäfer, « Density functional theory for non-relativistic fermions in the unitarity limit », *Nucl. Phys. A* **816** (2009), p. 52-64.
[105] H. Biss, L. Sobirey, N. Luick, M. Bohlen, J. J. Kinnunen, G. M. Bruun, T. Lompe et H. Moritz, « Excitation spectrum and superfluid gap of an ultracold Fermi gas », *Phys. Rev. Lett.* **128** (2022), article no. 100401.
[106] Y. Castin, « Comment on "Excitation spectrum and superfluid gap of an ultracold Fermi gas" », *Phys. Rev. Lett.* **133** (2024), article no. 109301. Online at https://hal.science/hal-04336110v2. [version française : « Commentaire sur "Excitation spectrum and superfluid gap of an ultracold Fermi gas" »,]
[107] P. B. Patel, Z. Yan, B. Mukherjee, R. J. Fletcher, J. Struck et M. W. Zwierlein, « Universal sound diffusion in a strongly interacting Fermi gas », *Science* **370** (2020), p. 1222-1226.
[108] J.-P. Blaizot et G. Ripka, *Quantum Theory of Finite Systems*, The MIT Press: Cambridge, MA, 1986.
[109] V. A. Andrianov et V. N. Popov, « Gidrodinamičeskoe dejstvie i Boze-spektr sverhtekučih Fermi-sistem », *Teoreticheskaya i Matematicheskaya Fizika* **28** (1976), p. 340-351. Online at https : / / www . mathnet . ru / links / 85ad2cf909603fa6ff8041064c52d0bf/tmf4269.pdf. [version anglaise : « Hydrodynamic action and Bose spectrum of superfluid Fermi systems », Theoretical and Mathematical Physics **28** (1976) pp. 829–837].

[110] H. Kurkjian, S. N. Klimin, J. Tempere et Y. Castin, « Pair-breaking collective branch in BCS superconductors and superfluid Fermi gases », *Phys. Rev. Lett.* **122** (2019), article no. 093403. Online at https://hal.science/hal-01782342v2. [version française : « Branche d'excitation collective du continuum dans les supraconducteurs BCS et les gaz de fermions superfluides »].

[111] Y. Castin et H. Kurkjian, « Branche d'excitation collective du continuum dans les gaz de fermions condensés par paires : étude analytique et lois d'échelle », *C. R. Phys.* **21** (2020), p. 253-310. Online at https://hal.science/hal-02196152v2. [version anglaise : « Collective excitation branch in the continuum of pair-condensed Fermi gases : analytical study and scaling laws »].

[112] P. B. Littlewood et C. M. Varma, « Amplitude collective modes in superconductors and their coupling to charge-density waves », *Phys. Rev. B* **26** (1982), p. 4883-4893.

[113] P. W. Higgs, « Broken symmetries and the masses of gauge bosons », *Phys. Rev. Lett.* **13** (1964), p. 508-509.

[114] D. Pekker et C. M. Varma, « Amplitude/higgs modes in condensed matter physics », *Annu. Rev. Conden. Matter Phys.* **6** (2015), p. 269-297.

[115] I. O. Kulik, O. Entin-Wohlman et R. Orbach, « Pair susceptibility and mode propagation in superconductors : a microscopic approach », *J. Low Temp. Phys.* **43** (1981), p. 591-620.

[116] S. N. Klimin, J. Tempere et H. Kurkjian, « Phononic collective excitations in superfluid Fermi gases at nonzero temperatures », *Phys. Rev. A* **100** (2019), article no. 063634.

[117] R. Matsunaga, Y. I. Hamada, K. Makise, Y. Uzawa, H. Terai, Z. Wang et R. Shimano, « Higgs amplitude mode in the BCS superconductors $Nb_{1-x}Ti_xN$ Induced by terahertz pulse excitation », *Phys. Rev. Lett.* **111** (2013), article no. 057002.

[118] P. Dyke, S. Musolino, H. Kurkjian et al., « Higgs oscillations in a unitary Fermi superfluid », *Phys. Rev. Lett.* **132** (2024), article no. 223402.

[119] A. F. Volkov et S. M. Kogan, « Collisionless relaxation of the energy gap in superconductors », *Zh. Eksp. Teor. Fiz.* **65** (1973), p. 2038-2046. Online at http://jetp.ras.ru/cgi-bin/e/index/r/65/5/p2038?a=list. [version anglaise : « Collisionless relaxation of the energy gap in superconductors », Sov. Phys. J. Exp. Theor. Phys. **38** (1974) pp. 1018–1021].

[120] V. Gurarie, « Nonequilibrium dynamics of weakly and strongly paired superconductors », *Phys. Rev. Lett.* **103** (2009), article no. 075301.

[121] Y. Castin, « Spectroscopie de Bragg et mode du continuum de paire brisée dans un gaz de fermions superfluide », *C. R. Phys.* **21** (2020), p. 203-219. Online at https://hal.science/hal-02377014v2. [version anglaise : « Bragg spectroscopy and pair-breaking-continuum mode in a superfluid Fermi gas »].

ACADÉMIE DES SCIENCES
INSTITUT DE FRANCE

Comptes Rendus. Physique
2025, Vol. 26, p. 217-224
https://doi.org/10.5802/crphys.237

Intervention in a conference / *Intervention en colloque*

Quantum transport in strongly correlated Fermi gases

Transport quantique dans des gaz de fermions fortement corrélés

Tilman Enss [a]

[a] Institute for Theoretical Physics, University of Heidelberg, Germany
E-mail: enss@thphys.uni-heidelberg.de

Abstract. Transport in strongly correlated fermions cannot be understood by fermionic quasiparticles alone. We present a theoretical framework for quantum transport that incorporates strong local correlations of fermion pairs. These contact correlations add essential contributions to viscous, thermal and sound transport coefficients. The bulk viscosity, in particular, receives its dominant contribution from pair excitations. Moreover, it can be measured elegantly by observing the response to a time-dependent scattering length even when the fluid is not moving. Rapid changes of the scattering length drive the system far out of local equilibrium, and we show how it relaxes back to equilibrium following a hydrodynamic attractor before a Navier–Stokes description becomes valid. This paper summarizes a talk given at the Symposium "Open questions in the quantum many-body problem" at the Institut Henry Poincaré, Paris, in July 2024.

Résumé. Le transport dans les fermions fortement corrélés ne peut être compris par les seules quasiparticules fermioniques. Nous présentons un cadre théorique pour le transport quantique qui incorpore les fortes corrélations locales des paires de fermions. Ces corrélations de contact ajoutent des contributions essentielles aux coefficients de transport visqueux, thermique et sonore. La viscosité de volume, en particulier, reçoit sa contribution dominante des excitations de paires. En outre, elle peut être mesurée de manière élégante en observant la réponse à une longueur de diffusion dépendant du temps, même lorsque le fluide n'est pas en mouvement. Des changements rapides de la longueur de diffusion éloignent le système de l'équilibre local, et nous montrons comment il retourne à l'équilibre en suivant un attracteur hydrodynamique avant qu'une description de Navier–Stokes ne devienne correcte. Cet article résume un exposé donné au symposium « Open questions in the quantum many-body problem » à l'Institut Henri Poincaré, Paris, en juillet 2024.

Keywords. Strongly correlated fermions, Quantum transport, Bulk viscosity, Hydrodynamics, Attractors.

Mots-clés. Fermions fortement corrélés, Transport quantique, Viscosité de volume, Hydrodynamique, Attracteur.

Funding. Deutsche Forschungsgemeinschaft (DFG) (Project-ID 273811115) (SFB 1225 ISOQUANT) and Germany's Excellence Strategy EXC 2181/1-390900948 (Heidelberg STRUCTURES Excellence Cluster).

Manuscript received 18 November 2024, revised 23 January 2025, accepted 24 January 2025.

1. Introduction

Resonantly interacting fermions are characterized by strong short-range correlations between ↑ and ↓ fermions (see Yvan Castin's presentation in this volume). These correlations give rise to remarkable transport properties that have been observed in experiments with ultracold Fermi

gases in recent years. Noteworthy examples include (i) dilute clouds of opposite spin bounce off one another and create shock waves before they eventually merge diffusively [1]; (ii) the unitary Fermi gas exhibits extremely low friction, given by the ratio of shear viscosity to entropy density $\eta/s \gtrsim 0.5\hbar/k_B$, and thereby constitutes a nearly perfect fluid [2–4]; (iii) a quantum lower bound on diffusivity $D \gtrsim \hbar/m$ is observed for spin diffusion (i) [1, 5–9] and momentum diffusion (ii) but also for thermal and sound diffusion [10–17]; (iv) several transport relaxation rates $\tau^{-1} \sim k_B T/\hbar$ scale proportional to temperature in the normal state above the superfluid critical temperature T_c, reminiscent of quantum critical scaling [9, 13, 18, 19].

Important questions include how this collective behavior arises from the microscopic Hamiltonian and how to derive an effective description at large scales. Near equilibrium, hydrodynamics works well as an effective description in the strongly correlated regime that is dominated by frequent collisions. However, dissipative hydrodynamics requires the equation of state and the transport cofficients as input, and their computation from first principles remains a challenging task. Explicit computations have shown quantum limited diffusion in many instances, but a universal many-body mechanism for different microscopic models has not yet emerged. Beyond hydrodynamics, the short-time behavior and the approach to equilibrium can exhibit relaxation phenomena on different scales, for instance attractor behavior beyond a Navier–Stokes description [20, 21].

2. Boltzmann kinetic theory

The dilute two-component Fermi gas is described by the Hamiltonian [22]

$$\hat{H} = \int \mathrm{d}^d x \sum_{\sigma=\uparrow,\downarrow} \psi_\sigma^\dagger(\boldsymbol{x}) \left(-\frac{\hbar^2\nabla^2}{2m} - \mu_\sigma \right) \psi_\sigma(\boldsymbol{x}) + g_0 \int \mathrm{d}^d x\, \psi_\uparrow^\dagger(\boldsymbol{x}) \psi_\downarrow^\dagger(\boldsymbol{x}) \psi_\downarrow(\boldsymbol{x}) \psi_\uparrow(\boldsymbol{x}) \tag{1}$$

for nonrelativistic fermions of mass m with an attractive short-range (contact) interaction. The bare coupling strength $g_0 = [(4\pi\hbar^2 a/m)^{-1} - m\Lambda/(2\pi^2\hbar^2)]^{-1}$ in three dimensions is given in terms of the low-energy s-wave scattering length a and a large-wavenumber cutoff Λ. In the following we set $\hbar = 1$.

The first approach to transport in a Fermi gas is by Boltzmann kinetic theory [23]. The single-particle distribution function $f(\boldsymbol{r}, \boldsymbol{p}, t)$ evolves according to the Boltzmann equation

$$\frac{\partial f}{\partial t} + \boldsymbol{v}_{\boldsymbol{p}} \cdot \nabla_{\boldsymbol{r}} f + \boldsymbol{F} \cdot \nabla_{\boldsymbol{p}} f = \left(\frac{\partial f}{\partial t} \right)_{\mathrm{coll}}, \tag{2}$$

where the left-hand side is the streaming term that includes mean-field interactions, while the right-hand side denotes the collision integral

$$\left(\frac{\partial f_1}{\partial t} \right)_{\mathrm{coll}} \simeq -\int \mathrm{d}\boldsymbol{p}_2\, \mathrm{d}\Omega\, \frac{\mathrm{d}\sigma}{\mathrm{d}\Omega} |\boldsymbol{v}_1 - \boldsymbol{v}_2| [f_1 f_2 (1-f_{1'})(1-f_{2'}) - (1-f_1)(1-f_2) f_{1'} f_{2'}]. \tag{3}$$

The collision integral describes how scattering between two particles 1, 2 into new states $1'$, $2'$ leads to a loss (first term) or gain (second term) of particles in state 1. At high temperatures above the Fermi temperature ($T \gg T_F$) the resonant cross section $\mathrm{d}\sigma/\mathrm{d}\Omega = 4\hbar^2/|\boldsymbol{p}_1 - \boldsymbol{p}_2|^2$ is so simple that the collision integral can be computed analytically. In the degenerate Fermi gas ($T \lesssim T_F$) Pauli blocking of final states reduces the Fermi distribution factors in the collision integral. At the same time, however, Pauli blocking of the intermediate virtual states between scatterings enhances the cross section $\mathrm{d}\sigma/\mathrm{d}\Omega$ [19, 24]. Near the scattering resonance, remarkably these two competing effects cancel almost perfectly and the resulting collision rate τ^{-1} follows nearly classical scaling [13, 25]. The relaxation time τ is then combined with thermodynamics (in the case of shear viscosity, the pressure p) to yield the frequency dependent transport coefficient, for instance the complex shear viscosity $\eta(\omega) = p\tau_\eta/(1 - \mathrm{i}\omega\tau_\eta)$ as follows from the memory

function formalism [13, 26]. The Boltzmann prediction for sound attenuation is found to agree with experimental data [11] for the degenerate unitary gas down to $T \simeq 2T_c$, which constitutes a remarkable success of kinetic theory in the strongly correlated regime. While finite-range corrections to transport are subleading for s-wave interactions, they can give rise to prominent effects such as quasi-bound states for p-wave interactions [27].

In the collision integral (3) the two-particle distribution function has been factorized into the product of two separate distribution functions for particles 1 and 2. This factorization is based on the assumption of molecular chaos and does not capture the strong local pair correlations $g^{(2)}_{\uparrow\downarrow}(r) \sim \mathscr{C}/r^2 + \mathscr{O}(1/r)$ at short distance, where $\mathscr{C}$ denotes the expectation value of the contact operator (see below). In the following we will see how these short-range correlations affect transport.

3. Kubo formula and bulk viscosity

A more general approach to transport, which makes no quasiparticle assumption, is derived in linear response theory. The transport coefficients are related by Kubo formulas to equilibrium expectation values; for instance the frequency dependent shear viscosity is given in terms of the transverse stress response function [4, 28],

$$\eta(\omega) = \int \mathrm{d}^d x\, \mathrm{d}t\, \frac{\mathrm{e}^{\mathrm{i}(\omega+\mathrm{i}0)t}-1}{\mathrm{i}(\omega+\mathrm{i}0)}\, \mathrm{i}\theta(t)\langle[\hat{\Pi}_{xy}(\boldsymbol{x},t),\hat{\Pi}_{xy}(0,0)]\rangle. \tag{4}$$

The microscopic expression for the shear stress operator is $\hat{\Pi}_{xy}(\boldsymbol{x}) = (1/2m)\sum_\sigma [\partial_x\hat{\psi}^\dagger_\sigma(\boldsymbol{x})\partial_y\hat{\psi}_\sigma(\boldsymbol{x}) + \partial_y\hat{\psi}^\dagger_\sigma(\boldsymbol{x})\partial_x\hat{\psi}_\sigma(\boldsymbol{x})] - \int \mathrm{d}^3 r\, (r_x r_y/r)\,((\partial v(r))/\partial r)\hat{\psi}^\dagger_\uparrow(\boldsymbol{x}+\boldsymbol{r}/2)\hat{\psi}^\dagger_\downarrow(\boldsymbol{x}-\boldsymbol{r}/2)\hat{\psi}_\downarrow(\boldsymbol{x}-\boldsymbol{r}/2)\hat{\psi}_\uparrow(\boldsymbol{x}+\boldsymbol{r}/2)$ for short-range potential $v(r)$ [29]. It has two contributions: the first, quadratic term gives the main contribution for gases, while the second, quartic term dominates in fluids [4]. Furthermore, the bulk viscosity ζ characterizes friction during isotropic expansion and contributes to sound attenuation. In constrast to the shear viscosity, however, the bulk viscosity is constrained by symmetry and vanishes identically for a scale invariant gas such as the ideal gas but also for the unitary Fermi gas [30, 31]. It can be computed by the Kubo formula [32]

$$\zeta(\omega) = \int \mathrm{d}^d x\, \mathrm{d}t\, \frac{\mathrm{e}^{\mathrm{i}(\omega+\mathrm{i}0)t}-1}{\mathrm{i}(\omega+\mathrm{i}0)}\, \mathrm{i}\theta(t)\langle[\delta\hat{p}(\boldsymbol{x},t),\delta\hat{p}(0,0)]\rangle \tag{5}$$

in terms of the operator $\delta\hat{p}$ that measures pressure fluctuations. The pressure $p = -\partial E/\partial V$ is obtained by performing a scale transformation, and specifically for the dilute gas in three dimensions one obtains the pressure operator

$$\hat{p} = \frac{2}{3}\hat{\mathscr{H}} + \frac{\hat{\mathscr{C}}}{12\pi m a}, \tag{6}$$

where $\hat{\mathscr{H}}$ denotes the Hamiltonian density and a the scattering length. The last term involves on the contact operator

$$\hat{\mathscr{C}} = m^2 g_0^2 \hat{n}_\uparrow(\boldsymbol{x})\hat{n}_\downarrow(\boldsymbol{x}) = \hat{\Delta}^\dagger(\boldsymbol{x})\hat{\Delta}(\boldsymbol{x}), \tag{7}$$

which is the continuum version of the doublon or pair density regularized by the bare coupling $g_0 \sim -r_0$ such that its zero-range limit $r_0 \to 0$ is well defined [33]. Equivalently, the contact operator can be expressed in terms of the local pair operator $\hat{\Delta} = m g_0 \hat{\psi}_\downarrow\hat{\psi}_\uparrow$, such that the contact measures the density of local pairs. At the scattering resonance $1/a = 0$ the scale invariant pressure relation $p = (2/3)\mathscr{E}$ is recovered, while the contact term quantifies the deviation from scale invariance due to pairing fluctuations. The pressure fluctuations are now given as the component of the pressure orthogonal to density and energy fluctuations [32],

$$\delta\hat{p} = \hat{p} - (\partial p/\partial n)_{\mathscr{E}}\hat{n} - (\partial p/\partial\mathscr{E})_n\hat{\mathscr{H}}. \tag{8}$$

Because conserved quantities do not contribute to dissipation, in the dynamical response the dissipation at $\omega > 0$ can only arise from the response function of the contact operator, $\delta\hat{p} = \hat{\mathscr{C}}/(12\pi ma)$, which is not conserved. One thus finds that the bulk viscosity at nonzero frequency is given by [32, 34–36]

$$\zeta(\omega > 0) = \frac{1}{(12\pi ma)^2} \int \mathrm{d}^d x \, \mathrm{d}t \, \frac{\mathrm{e}^{\mathrm{i}(\omega+\mathrm{i}0)t} - 1}{\mathrm{i}(\omega + \mathrm{i}0)} \, \mathrm{i}\theta(t) \langle [\hat{\mathscr{C}}(\boldsymbol{x}, t), \hat{\mathscr{C}}(0,0)] \rangle . \tag{9}$$

Hence, bulk viscosity is a pure interaction effect that arises from fluctuations of the pair density, not of single fermions. These contributions are not easy to capture in a fermionic kinetic theory, even if the interaction functional is included [37]. Instead, the bulk viscosity can be computed using self-consistent conserving approaches (Luttinger–Ward), which are formulated in terms of coupled fermion and pair degrees of freedom [4, 5, 35, 38]. Explicit microscopic computations for the contact correlations and bulk viscosity in the degenerate, strongly correlated gas [35] show a low-frequency Drude peak in the complex bulk viscosity $\zeta(\omega) \simeq \chi\tau_\zeta/(1 - \mathrm{i}\omega\tau_\zeta)$ followed by an anomalous contact tail $\zeta(\omega \to \infty) \sim C/\omega^{3/2}$ at large frequency. Remarkably, in the unitary gas the bulk scattering rate $\tau_\zeta^{-1} \propto T$ exhibits a T-linear scaling in a wide temperature range from slightly above T_c to high temperatures above T_F, in distinction to other transport relaxation rates that decay at high temperatures. This unusual scaling arises from scattering between pairs, not individual fermions, and is specific to the bulk viscosity.

Open questions concern the response in the low-temperature, superfluid state, where a superfluid of fermion pairs can behave differently from a bosonic superfluid due to the additional pair-breaking excitations [39, 40]. In particular for the bulk viscosity, but also for the other transport coefficients it is desirable to derive a kinetic theory that captures the strong fermion correlations. A kinetic formulation in terms of coupled fermions and pairs has been derived in the high-temperature virial expansion [41]: the fermionic contribution to the total bulk viscosity agrees with previous Boltzmann calculations [37], but the pair contribution is found to be much larger near unitarity. Efforts are underway to extend this to the quantum degenerate regime.

3.1. *Measurement of the bulk viscosity*

Often transport measurements observe the damping of fluid motion: elliptic flow or quadrupole motion for shear viscosity, and isotropic flow or radial breathing for the bulk viscosity. The measurement of sound attenuation [11, 12, 14–17, 42] gives access to a combination of several transport coefficients, as sound decays by both momentum and thermal relaxation processes. For the bulk viscosity, however, there is another way of measurement in a dilute gas that works even if the fluid is homogeneous and at rest [43]. In linear response the contact correlation, and thereby the bulk viscosity, is given by the response of the contact to an earlier change of scattering length [35],

$$\mathrm{i}\theta(t - t') \langle [\hat{\mathscr{C}}(\boldsymbol{x}, t), \hat{\mathscr{C}}(0, t')] \rangle = -4\pi m \left. \frac{\partial \langle \hat{\mathscr{C}}(\boldsymbol{x}, t) \rangle}{\partial a^{-1}(0, t')} \right|_{S,N} \tag{10}$$

at fixed entropy and particle number. Experimentally the spatially integrated contact has been measured with a high temporal resolution [6, 8], and one can modulate the scattering length in time via the applied magnetic field to measure the response. In this way, the frequency dependence of the bulk viscosity can be mapped out.

4. Attractors to hydrodynamics

When a system is brought far from equilibrium, one might expect that the approach to equilibrium at long times is governed by hydrodynamics (Navier–Stokes equation). In heavy-ion

collisions, however, fluid behavior is found already at short times after a collision, earlier than hydrodynamics is expected to be valid, in a so-called hydrodynamic attractor [44]. In general, one can ask which equations describe the approach to hydrodynamics and whether they are universal. Furthermore, if hydrodynamics is viewed as a "derivative expansion" in powers of $\omega\tau$, what determines the higher orders? Some answers may be provided by experiments with ultracold quantum gases, where the time-resolved evolution toward equilibrium can be observed starting from defined initial conditions or subject to a particular driving.

Hydrodynamic attractors can arise in many forms of fluid motion, but there is a particularly simple case where it can be studied in a uniform ultracold atomic gas at rest, with no moving parts, when the scattering length $a(t)$ is ramped at time $t > 0$ to bring the system out of local equilibrium [20, 43]. The relaxation back to equilibrium can be observed in the equation of state, most directly in the contact density expectation value, which is given in linear response as

$$\mathscr{C}(t) = \mathscr{C}_{\mathrm{eq}} + \int_0^\infty \mathrm{d}t' \, \frac{\partial \mathscr{C}(t)}{\partial a^{-1}(t')} \delta a^{-1}(t'). \tag{11}$$

Using Equation (10) this can be expressed in terms of the contact correlation, and one finds that the approach to equilibrium occurs via local dissipation, with the dissipation rate set by the bulk viscosity [43]. The Drude peak of the bulk viscosity [35] $\zeta(\omega) \simeq \chi\tau_\zeta/(1 - \mathrm{i}\omega\tau_\zeta)$ (see above) corresponds in the time domain to an exponential decay of the contact response within the bulk relaxation time τ_ζ:

$$\frac{\partial \mathscr{C}(t)}{\partial a^{-1}(t')} \simeq \theta(t - t') \left(\frac{\partial \mathscr{C}}{\partial a^{-1}} \right)_{S,N} \frac{\exp[-(t - t')/\tau_\zeta]}{\tau_\zeta}. \tag{12}$$

By inserting this form into Equation (11) one can predict the time evolution of the contact following arbitrary drives $\delta a^{-1}(t)$ as long as the drive amplitude is small enough to remain in the linear response regime. But does this time evolution agree with the prediction of Navier–Stokes hydrodynamics? When the scattering length is varied, the local pressure also changes in time, and the nonequilibrium component of the pressure is quantified by the dissipative bulk pressure

$$\pi(t) = \frac{\mathscr{C}(t) - \mathscr{C}_{\mathrm{eq}}[a(t)]}{12\pi m a(t)}, \tag{13}$$

which for a dilute gas is given in terms of the difference of the instantaneous contact and the equilibrium contact for the instantaneous scattering length [43]. In Navier–Stokes hydrodynamics the bulk pressure $\pi = -\zeta V_a$ is driven by the local expansion of the fluid, $V_a = \nabla \cdot \boldsymbol{v}$, times the bulk viscosity ζ. On the other hand, when the scattering length is changed, the local scale variation arises equally from the rate of change of the scattering length, $V_a(t) = -3\dot{a}(t)/a(t)$. Therefore, both expansion and variations of the scattering length are equivalent ways to probe local bulk dissipation. In contrast to Navier–Stokes hydrodynamics, we obtain the equation of motion for $\pi(t)$ from the time derivative of Equation (12), which we have derived microscopically [20]:

$$\tau\dot{\pi}(t) + \pi(t) = -\zeta[a(t)] V_a(t). \tag{14}$$

This differs from Navier–Stokes by the relaxation term on the left-hand side, which has the same form as in a Müller–Israel–Stewart formulation. For a given external drive $a(t)$ the bulk pressure is obtained by integrating this differential equation, and the result can be compared to the Navier–Stokes prediction $\pi_{\mathrm{NS}}(t) = -\zeta[a(t)] V_a(t)$. For slow drive frequencies $\omega\tau_\zeta \ll 1$ the dissipative term $\tau\dot{\pi}$ has little effect and the bulk pressure follows the drive almost instantaneously. For fast drives $\omega\tau_\zeta \gtrsim 1$, instead, $\pi(t)$ follows the drive with a time delay and a deviation from Navier–Stokes hydrodynamics is predicted. This is exemplified by a power-law drive $a^{-1}(t > t_{\mathrm{ini}}) \equiv a_{\mathrm{ini}}^{-1}(t/t_{\mathrm{ini}})^{-\alpha}$, which starts at a finite scattering length and sweeps at first fast, then slower toward unitarity $a^{-1} = 0$. In this case the bulk pressure is found analytically as [20]

$$\pi(t) = \pi_{\mathrm{ini}} \, \mathrm{e}^{-(t - t_{\mathrm{ini}})/\tau_\zeta} + \pi_{\mathrm{att}}(t), \quad \pi_{\mathrm{att}}(t) = c_\alpha \chi \, \mathrm{e}^{-t/\tau_\zeta} \Gamma(-2\alpha, -t/\tau_\zeta) \tag{15}$$

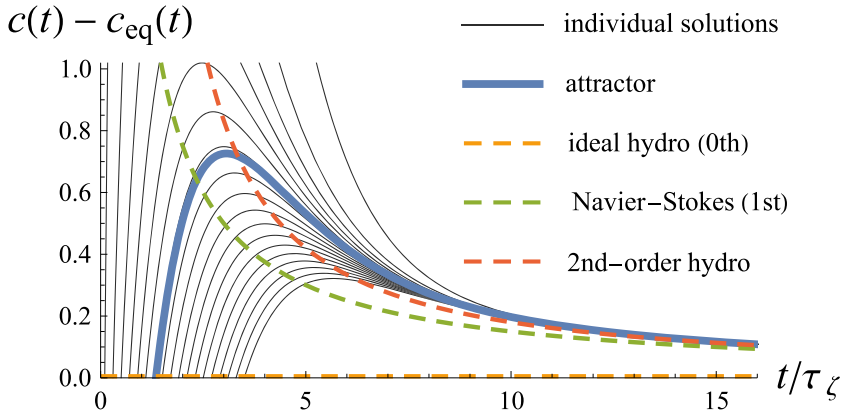

Figure 1. Hydrodynamic attractor. The normalized bulk pressure $c(t) - c_{\mathrm{eq}}(t) = \pi(t)/\chi$ exhibits different time evolutions for different initial conditions (thin lines), which quickly converge toward the attractor solution (thick blue line) and only later approach Navier–Stokes hydrodynamics (green dashed line). Adapted from [20].

in terms of the sum rule $\chi = \zeta/\tau_\zeta$ and the incomplete Gamma function $\Gamma(s,z)$. The first term describes the exponential decay of initial conditions on time scale τ_ζ, while the so-called hydrodynamic attractor solution $\pi_{\mathrm{att}}(t)$ is the same for different initial conditions and depends only on the transport properties ζ, τ_ζ as well as the drive parameter α. For different initial conditions the bulk pressure is found to first converge toward the attractor solution π_{att} before the attractor itself approaches the Navier–Stokes prediction at longer times, cf. Figure 1.

Standard hydrodynamics is recovered in the solution $\pi(t)$ in the long-time limit. When expanding in "temporal gradients" $\tau_\zeta/t \ll 1$, the leading order reproduces $\pi_{\mathrm{NS}}(t)$, but the subsequent orders have factorially growing coefficients $a_n \sim (n+2\alpha)!$ and form an asymptotic series. The initial condition, furthermore, is nonperturbative in τ_ζ/t and is therefore a nonhydrodynamic mode. Even though the gradient expansion does not converge, the solution obtained from the equation of motion is physical and accessible with current experiments [20].

5. Conclusion

The short-time attractor behavior in a driven system is an example of a microscopically motivated extension of hydrodynamics beyond Navier–Stokes. Cold atom experiments can observe these attractors in real time by measuring the response of the contact to variations in the scattering length, thus probing isotropic expansion and local dissipation by an external drive with no moving parts. A remarkable prediction of quantum transport theory is that the bulk relaxation rate $\tau_\zeta^{-1} \propto T$ scales approximately linearly in temperature but is largely independent of density [35]; this is because pressure fluctuations couple predominantly to pairs rather than individual fermions. The computation of frequency dependent transport coefficients remains a challenge, also in the superfluid state. Recently, the accurate computation of fermion and pair spectra was achieved by solving the self-consistent Luttinger–Ward equations directly in real frequency [45–47], which match recent experiments [48]. It will be interesting to extend these methods and compute dynamical response functions in real frequency, such as Equations (4) and (5), which determine the transport coefficients near equilibrium. Interesting questions arise also in the far-from-equilibrium response, which is strongly affected by conformal symmetry [49] and which can generically be computed using the Keldysh formulation [50].

Declaration of interests

The authors do not work for, advise, own shares in, or receive funds from any organization that could benefit from this article, and have declared no affiliations other than their research organizations.

Funding

This work is supported by the Deutsche Forschungsgemeinschaft (DFG) via Project-ID 273811115 (SFB 1225 ISOQUANT) and under Germany's Excellence Strategy EXC 2181/1-390900948 (the Heidelberg STRUCTURES Excellence Cluster).

References

[1] A. Sommer, M. Ku, G. Roati and M. W. Zwierlein, "Universal spin transport in a strongly interacting Fermi gas", *Nature (London)* **472** (2011), pp. 201–204.

[2] T. Schäfer and D. Teaney, "Nearly perfect fluidity: from cold atomic gases to hot quark gluon plasmas", *Rep. Prog. Phys.* **72** (2009), article no. 126001.

[3] C. Cao, E. Elliott, J. Joseph, H. Wu, J. Petricka, T. Schäfer and J. E. Thomas, "Observation of universal temperature scaling in the quantum viscosity of a unitary Fermi gas", *Science* **331** (2011), pp. 58–61.

[4] T. Enss, R. Haussmann and W. Zwerger, "Viscosity and scale invariance in the unitary Fermi gas", *Ann. Phys. (NY)* **326** (2011), pp. 770–796.

[5] T. Enss and R. Haussmann, "Quantum mechanical limitations to spin transport in the unitary Fermi gas", *Phys. Rev. Lett.* **109** (2012), article no. 195303.

[6] A. B. Bardon, S. Beattie, C. Luciuk, et al., "Transverse demagnetization dynamics of a unitary Fermi gas", *Science* **344** (2014), pp. 722–724.

[7] S. Trotzky, S. Beattie, C. Luciuk, et al., "Observation of the Leggett–Rice effect in a unitary Fermi gas", *Phys. Rev. Lett.* **114** (2015), article no. 015301.

[8] C. Luciuk, S. Smale, F. Böttcher, H. Sharum, B. A. Olsen, S. Trotzky, T. Enss and J. H. Thywissen, "Observation of quantum-limited spin transport in strongly interacting two-dimensional Fermi gases", *Phys. Rev. Lett.* **118** (2017), article no. 130405.

[9] T. Enss and J. H. Thywissen, "Universal spin transport and quantum bounds for unitary fermions", *Annu. Rev. Condens. Matter Phys.* **10** (2019), pp. 85–106.

[10] M. Braby, J. Chao and T. Schäfer, "Thermal conductivity and sound attenuation in dilute atomic Fermi gases", *Phys. Rev. A* **82** (2010), article no. 033619.

[11] P. B. Patel, Z. Yan, B. Mukherjee, R. J. Fletcher, J. Struck and M. W. Zwierlein, "Universal sound diffusion in a strongly interacting Fermi gas", *Science* **370** (2020), no. 6521, pp. 1222–1226.

[12] M. Bohlen, L. Sobirey, N. Luick, H. Biss, T. Enss, T. Lompe and H. Moritz, "Sound propagation and quantum-limited damping in a two-dimensional Fermi gas", *Phys. Rev. Lett.* **124** (2020), no. 24, article no. 240403.

[13] B. Frank, W. Zwerger and T. Enss, "Quantum critical thermal transport in the unitary Fermi gas", *Phys. Rev. Res.* **2** (2020), no. 2, article no. 023301.

[14] X. Li, X. Luo, S. Wang, et al., "Second sound attenuation near quantum criticality", *Science* **375** (2022), no. 6580, pp. 528–533.

[15] X. Wang, X. Li, I. Arakelyan and J. E. Thomas, "Hydrodynamic relaxation in a strongly interacting Fermi gas", *Phys. Rev. Lett.* **128** (2022), no. 9, article no. 090402.

[16] Z. Yan, P. B. Patel, B. Mukherjee, C. J. Vale, R. J. Fletcher and M. W. Zwierlein, "Thermography of the superfluid transition in a strongly interacting Fermi gas", *Science* **383** (2024), no. 6683, pp. 629–633.

[17] X. Li, J. Huang and J. E. Thomas, "Universal density shift coefficients for the thermal conductivity and shear viscosity of a unitary Fermi gas", *Phys. Rev. Res.* **6** (2024), no. 4, article no. L042021.

[18] P. Nikolić and S. Sachdev, "Renormalization-group fixed points, universal phase diagram, and $1/N$ expansion for quantum liquids with interactions near the unitarity limit", *Phys. Rev. A* **75** (2007), article no. 033608.

[19] T. Enss, "Quantum critical transport in the unitary Fermi gas", *Phys. Rev. A* **86** (2012), article no. 013616.

[20] K. Fujii and T. Enss, "Hydrodynamic attractor in ultracold atoms", *Phys. Rev. Lett.* **133** (2024), no. 17, article no. 173402.

[21] A. Mazeliauskas, T. Enss, et al., *Hydrodynamic attractor in periodically driven ultracold quantum gases*, preprint, 2025, 2501.19240.

[22] *The BCS–BEC Crossover and the Unitary Fermi Gas*, (W. Zwerger, ed.), Lecture Notes in Physics 836, Springer: Berlin, 2012.
[23] H. Smith and H. H. Jensen, *Transport Phenomena*, Oxford University Press: Oxford, 1989.
[24] G. M. Bruun and H. Smith, "Viscosity and thermal relaxation for a resonantly interacting Fermi gas", *Phys. Rev. A* **72** (2005), article no. 043605.
[25] G. M. Bruun, "Feshbach resonances and medium effects in ultracold atomic gases", *Few-Body Systems* **45** (2009), pp. 227–232.
[26] I. Mandal and H. Freire, "Transport properties in non-Fermi liquid phases of nodal-point semimetals", *J. Phys.: Condens. Matter* **36** (2024), article no. 443002.
[27] J. Maki and T. Enss, "Transport in p-wave-interacting Fermi gases", *Phys. Rev. A* **107** (2023), article no. 023317.
[28] E. Taylor and M. Randeria, "Viscosity of strongly interacting quantum fluids: spectral functions and sum rules", *Phys. Rev. A* **81** (2010), article no. 053610.
[29] P. C. Martin and J. Schwinger, "Theory of many-particle systems. I", *Phys. Rev.* **115** (1959), pp. 1342–1373.
[30] F. Werner and Y. Castin, "Unitary gas in an isotropic harmonic trap: Symmetry properties and applications", *Phys. Rev. A* **74** (2006), article no. 053604.
[31] D. T. Son, "Vanishing bulk viscosities and conformal invariance of the unitary Fermi gas", *Phys. Rev. Lett.* **98** (2007), article no. 020604.
[32] K. Fujii and Y. Nishida, "Bulk viscosity of resonating fermions revisited: Kubo formula, sum rule, and the dimer and high-temperature limits", *Phys. Rev. A* **102** (2020), article no. 023310.
[33] F. Werner and Y. Castin, "General relations for quantum gases in two and three dimensions. Two-component fermions", *Phys. Rev. A* **86** (2012), article no. 013626.
[34] Y. Nishida, "Viscosity spectral functions of resonating fermions in the quantum virial expansion", *Ann. Phys. (NY)* **410** (2019), article no. 167949.
[35] T. Enss, "Bulk viscosity and contact correlations in attractive Fermi gases", *Phys. Rev. Lett.* **123** (2019), article no. 205301.
[36] J. Hofmann, "High-temperature expansion of the viscosity in interacting quantum gases", *Phys. Rev. A* **101** (2020), article no. 013620.
[37] K. Dusling and T. Schäfer, "Bulk viscosity and conformal symmetry breaking in the dilute Fermi gas near unitarity", *Phys. Rev. Lett.* **111** (2013), article no. 120603.
[38] R. Haussmann, W. Rantner, S. Cerrito and W. Zwerger, "Thermodynamics of the BCS-BEC crossover", *Phys. Rev. A* **75** (2007), article no. 023610.
[39] D. Einzel, "Spin-independent transport parameters for superfluid 3 He-B", *J. Low Temp. Phys.* **54** (1984), pp. 427–474.
[40] H. Kurkjian, S. N. Klimin, J. Tempere and Y. Castin, "Pair-breaking collective branch in BCS superconductors and superfluid Fermi gases", *Phys. Rev. Lett.* **122** (2019), no. 9, article no. 093403.
[41] K. Fujii and T. Enss, "Bulk viscosity of resonantly interacting fermions in the quantum virial expansion", *Ann. Phys.* **453** (2023), article no. 169296.
[42] S. Huang, Y. Ji, T. Repplinger, et al., *Emergence of sound in a tunable Fermi fluid*, preprint, 2024, 2407.13769.
[43] K. Fujii and Y. Nishida, "Hydrodynamics with spacetime-dependent scattering length", *Phys. Rev. A* **98** (2018), article no. 063634.
[44] M. P. Heller and M. Spaliński, "Hydrodynamics beyond the gradient expansion: resurgence and resummation", *Phys. Rev. Lett.* **115** (2015), no. 7, article no. 072501.
[45] C. H. Johansen, B. Frank and J. Lang, "Spectral functions of the strongly interacting three-dimensional Fermi gas", *Phys. Rev. A* **109** (2024), article no. 023324.
[46] T. Enss, "Particle and pair spectra for strongly correlated Fermi gases: A real-frequency solver", *Phys. Rev. A* **109** (2024), no. 2, article no. 023325.
[47] E. Dizer, J. Horak and J. M. Pawlowski, "Spectral properties and observables in ultracold Fermi gases", *Phys. Rev. A* **109** (2024), no. 6, article no. 063311.
[48] X. Li, S. Wang, X. Luo, et al., "Observation and quantification of pseudogap in unitary Fermi gases", *Nature* **626** (2024), pp. 288–293.
[49] J. Maki, S. Zhang and F. Zhou, "Dynamics of strongly interacting Fermi gases with time-dependent interactions: Consequence of conformal symmetry", *Phys. Rev. Lett.* **128** (2022), no. 4, article no. 040401.
[50] M. Bonitz, *Quantum Kinetic Theory*, Springer: Cham, 2016.

ACADÉMIE DES SCIENCES
INSTITUT DE FRANCE

Comptes Rendus. Physique
2025, Vol. 26, p. 91-111
https://doi.org/10.5802/crphys.228

Intervention in a conference / *Intervention en colloque*

Classical and quantum spin liquids

Liquides de spins classiques et quantiques

Sylvain Capponi [a]

[a] Laboratoire de Physique Théorique, Université de Toulouse, CNRS, UPS, Toulouse, France

E-mail: sylvain.capponi@univ-tlse3.fr

Abstract. When considering magnetic systems in the thermodynamic limit and at low enough temperature, one finds typically magnetically ordered phases. In contrast, in the high-temperature regime, the interactions between the spin degrees of freedom become less relevant and the system loses its order: this is a paramagnet. This phenomenon of phase transition has been well understood using statistical mechanics and simple modelling.

In this short lecture notes, we will review the possibility that a many-body magnetic system may remain magnetically disordered down to zero-temperature, both for classical or quantum spins. These exotic phases of matter are known, respectively, as classical and quantum spin liquids.

We will address in particular the question of classification of these classical or quantum disordered phases. Indeed, while they have no local order parameter by definition, they can still possess different qualitative features related e.g. to the nature of their correlations or elementary excitations, which could be probed experimentally.

Résumé. Lorsque l'on considère des systèmes magnétiques dans la limite thermodynamique et à suffisamment basse température, on trouve des phases généralement ordonnées sur le plan magnétique. Au contraire, à haute température, les interactions entre les degrés de liberté de spin deviennent moins pertinentes et le système perd son ordre : c'est une phase paramagnétique. Ce phénomène de transition de phase a été bien compris grâce à la mécanique statistique et à des modèles simples.

Dans ces brèves note de cours, nous examinerons la possibilité qu'un système magnétique puisse rester désordonné magnétiquement jusqu'à la température nulle, à la fois pour des spins classiques ou quantiques. Ces phases exotiques de la matière sont connues respectivement sous le nom de liquides de spin classiques et quantiques.

Nous aborderons en particulier la question de la classification de ces phases désordonnées classiques ou quantiques. En effet, bien qu'elles n'aient pas de paramètre d'ordre local par définition, elles peuvent néanmoins posséder différentes caractéristiques qualitatives liées par exemple à la nature de leurs corrélations ou de leurs excitations élémentaires, qui peuvent être sondées expérimentalement.

Keywords. Magnetism, Spin liquids, Condensed matter.

Mots-clés. Magnétisme, Liquides de spins, Matière condensée.

Manuscript received 17 October 2024, revised 13 December 2024, accepted 18 December 2024.

1. Introduction

Magnetism is a collective phenomenon that has been known and studied for extremely long time. Usual magnets are a direct evidence that a collection of microscopic elementary spin degrees of freedom tend to order along the same direction at low-enough temperature, while they are in random directions at higher temperature: this is the famous ferromagnetic transition. This phenomenon of phase transitions is well understood and can only occur in the thermodynamic limit,

hence we will consider infinite systems. For simplicity, we will focus on localized spins and will not consider itinerant magnetism, where charge degrees of freedom of the carriers also play a role. Quite interestingly, simple models based on two-body interactions are enough to generate various properties, as is well-known in many-body physics. As was emphasized by Anderson, "more is different" [1], which means that, within our simple framework, many-body physics can lead to various emergent properties: magnetic order, quasi-particles, gauge structure etc. which cannot be understood at the single-particle level.

This review will focus on so-called "spin liquids", dubbed by analogy with the liquid phase of matter that does not have any magnetic order or does not break any symmetry. Still, we will see that this is a much richer concept since some spin liquids can nevertheless possess some structure giving rise e.g. to algebraic spin correlations or fractionalization of elementary excitations. In a modern formulation that we will explain, spin liquids can be viewed as fractionalized phases described by matter (*spinons*) coupled to emergent gauge fields.

In a broader perspective, some features are linked to field theory, quantum many-body physics, quantum information, as well as experimental studies on several materials. We will point out some of these connections and refer to complementary reviews on these topics. For instance, an experimental definition of spin liquid is usually made by measuring the ordering temperature T_c and computing the frustration parameter [2] $f = |\theta_{CW}|/T_c$ where θ_{CW} is the Curie–Weiss temperature (proportional to the spin exchange energy scale). Clearly a large ratio f (typically >10) indicates that the ordering occurs at a much lower temperature than expected, pointing to a physical mechanism that prevents magnetic ordering. This usually occurs in frustrated materials with competing interactions, which is a very active area of research [3, 4].

In order to set up the stage, we will consider spin degrees of freedom, that can be discrete (Ising) or continuous (Heisenberg), localized on various regular lattices (square, honeycomb, triangular, kagome, pyrochlore etc.) in dimensions $d = 1$, 2 or 3, see e.g. Figure 1. We will also tackle constrained dimer models which are useful effective descriptions of some frustrated models at low-energy.

As a disclaimer, we will not consider disorder, although it plays a crucial role in many situations, and will not discuss localization or spin glass behaviors.

In Sections 2 and 3, we will treat respectively classical and quantum spin liquids. In both cases, we will try to define spin liquids, discuss possible classifications and argue that they do exist in some simple models. Although exact solutions are rare, they pave the way for investigating exotic phases of matter in a more realistic microscopic model as well as in real materials, which gives a support for the realization of classical and quantum spin liquids in nature.

2. Classical spin liquids

A major success of statistical physics in the last century was to characterize the existence of a phase transition in the two-dimensional (2d) Ising model and related ones, showing that spins can order at low-temperature into a ferromagnet or antiferromagnet.

Then in 1950, Wannier considered classical Ising spins on the frustrated triangular lattice [5] and showed that there are an extensive number of groundstate configurations, contradicting the Nernst's principle of thermodynamics: this was the birth of classical spin liquids (CSL).

By definition, a CSL has an extensive degeneracy for its groundstates, which allows cooperative fluctuations and the absence of order. Of course such a situation is fragile and often unstable to fluctuations: this is the famous order-by-disorder mechanism [6]. Both thermal or quantum fluctuations will generally select an ordered state. Nevertheless, we do consider CSL since there can exist a large parameter regime where a cooperative paramagnet is the correct picture and the system remains magnetically disordered [7].

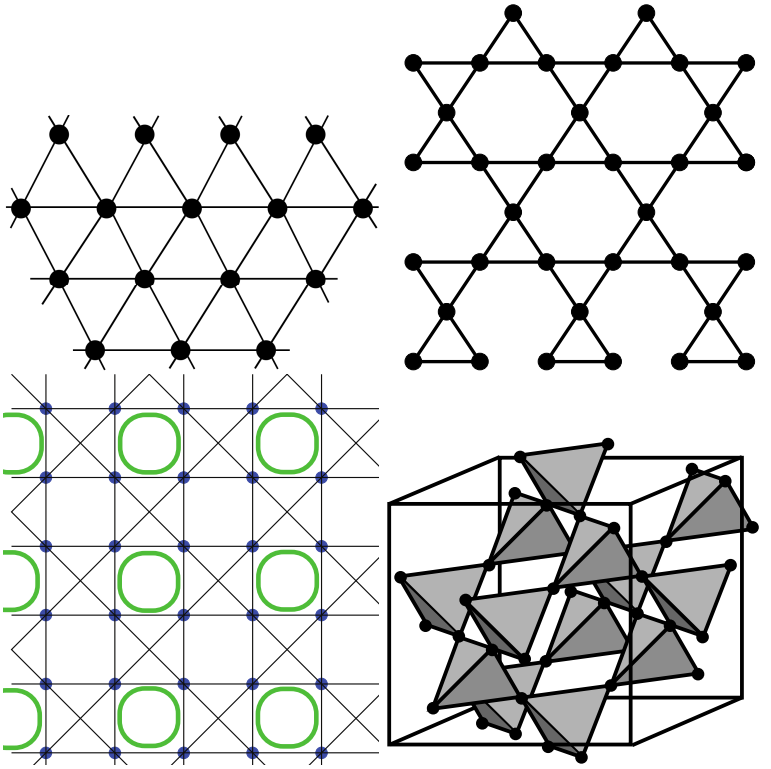

Figure 1. Structures of some lattices. From top left to bottom right: two-dimensional (2d) triangular, kagome, checkerboard and three-dimensional (3d) pyrochlore. For the checkerboard lattice, we have highlighted in green one plaquette phase groundstate in the quantum $S = 1/2$ case.

We will now review some simple classical models where CSL can be stabilized. The classical variables can be either discrete (Ising spins) or continuous O(3) variables (Heisenberg spins) or even dimer configurations. For a more extensive review on this topic, we refer for instance to [8].

2.1. *Ising model*

The Ising model is one of the most famous statistical mechanics problem [9]. The energy of a configuration is simply given by

$$E(\{\sigma\}) = J \sum_{\langle ij \rangle} \sigma_i \sigma_j \tag{1}$$

where the sum runs over all nearest neighbor bonds of a lattice and $\sigma_i = \pm 1$ is the Ising spin variable at each site.

This model has been very fruitful in the modern understanding of phase transitions: in one-dimension (1d), there is no transition; in 2d, there is the famous exact Onsager's solution; in 3d, the transition has been shown to be continuous but it is not yet proven whether it is conformally invariant.

We have chosen the antiferromagnetic (AF) case ($J > 0$) where frustration can lead to a large number of groundstates. Frustration means that no configuration can satisfy all constraints of having antiparallel spins on every bond. This has been analyzed by Wannier in 1950 on

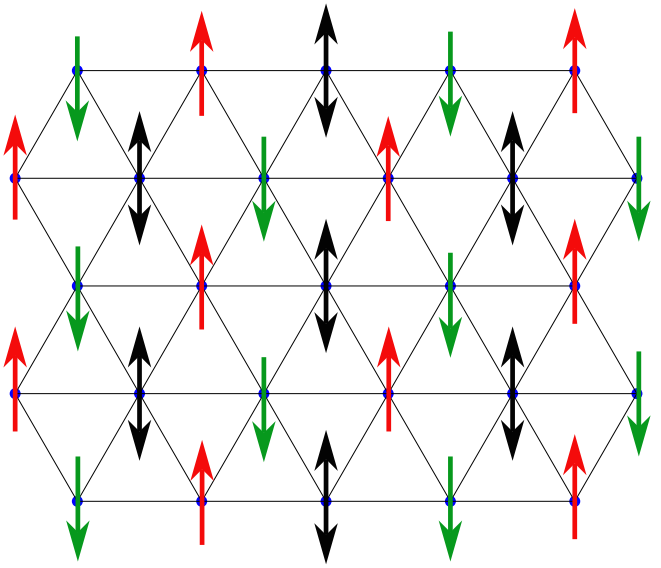

Figure 2. Triangular Ising antiferromagnet. Starting from a perfect Néel order on some honeycomb lattice (spins in red and green), the additional spins can be in any $\sigma = \pm 1$ state, leading to an extensive degeneracy.

the triangular lattice [5], see Figure 2. Using a mapping to a dimer counting problem on the honeycomb lattice, it is possible to show that the residual entropy at zero temperature is $S_0/N \simeq 0.323 k_B$, which implies that the number of groundstate configurations is extensive.

It is quite easy to get a rigorous bound by considering a perfect Néel AF on the non-frustrated bipartite honeycomb lattice with N sites, see Figure 2. Then the additional sites of the triangular lattice can be in any $\sigma = \pm 1$ state, so that there are at least $2^{N/3}$ degenerate groundstates, i.e. the residual entropy per spin is larger than $k_B \log(2)/3 \simeq 0.231 k_B$.

Such a $T = 0$ residual entropy violates the Nernst's third principle of thermodynamics and is common to many classical models. This Nernst's principle is more robust and obeyed in quantum mechanics although there are subextensive cases with fractons [10] and even extensive degeneracy e.g. in the SYK model [11].

Coming back to the triangular lattice case, there is no order at any finite temperature and correlations are algebraic [8], which appears quite peculiar a priori. This can be understood using e.g. mapping to constrained model as explained in the next section.

Quite interestingly, there are still several open questions when considering additional further neighbor interactions, e.g. on the kagome lattice. There is no more any exact solution and the standard Monte-Carlo numerical simulations suffer from slowing down due to the large number of low-energy states. However, since the partition function can be written as a tensor network contraction, recent tensor algorithms have allowed to get a numerical solution [12].

2.2. *Constrained models*

2.2.1. *Vertex models*

One can also consider situations where the "spin" variables live on edges of the lattice, as done in lattice gauge theory, while interactions are on the vertices. In this framework, constraints can be introduced. For instance, on the square lattice, one can impose the so-called ice rule with a

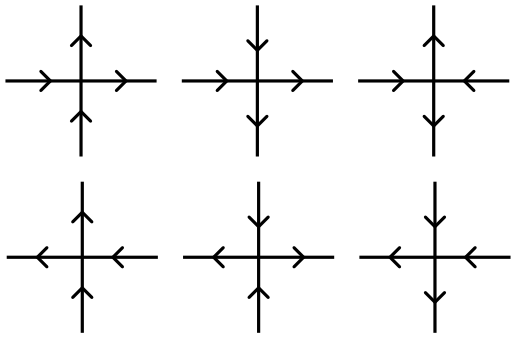

Figure 3. The six allowed configurations on the square lattice such that at each vertex, there are exactly 2 incoming and 2 outgoing arrows (ice rule).

constraint of having 2-in/2-out arrows at each vertex, see Figure 3. This is the famous six-vertex model solved by Baxter [13].

A simple estimate of the number of configurations for N sites can be found using Pauling's estimate [14]: since there are only 6 valid configurations around each vertex, instead of $2^4 = 16$, if one neglects correlations, there are approximately $2^{2N}(6/16)^N$ states, which leads to a residual entropy per site

$$S_0/N = k_B \log(3/2) \simeq 0.405 k_B \tag{2}$$

in good agreement with the exact solution by Lieb [15]: $S_0/N = 3/2\log(4/3)k_B \simeq 0.431 k_B$. Note that a similar counting can be done on a three-dimensional (3d) pyrochlore lattice which has the same coordination number, see Figure 1.

Such systems are called "ice" because there is a similar constraint for H atoms in water–ice and this residual entropy has indeed been measured experimentally long time ago [16].

Quite interestingly, this local constraint leads to an effective gauge theory, similarly to Gauss' law in electromagnetism: charge conservation is expressed with $\mathrm{div}\mathbf{E} = 0$. As a result, using this analogy with electromagnetism, it can be shown [8] that the system has critical (power-law) dipolar correlations, leading to specific signatures, known as pinch points, in the structure factors: this is called a *Coulomb phase*.

In magnetism, these properties can be found in so-called spin ice materials, which have been quite popular recently as examples of cooperative paramagnets having a Coulomb phase [17] and in which defects can be viewed as magnetic monopoles [18].

2.2.2. *Dimer models*

It is also possible to consider constrained models by putting hardcore dimers on all bonds of a lattice so that each site belongs to one and only one dimer (fully packed dimer configurations). This situation is very analogous to the previous vertex models, which can be seen as a constrained model with exactly two dimers per site. The number of configurations was solved in general on planar graphs [19, 20]. On bipartite lattices, it is generally possible to write down an effective field theory in terms of an height field, from which one can deduce that dimer correlations are dipolar. Such a phase is again a *Coulomb phase* [8].

2.3. *Continuous spins: Heisenberg*

In some cases, a more appropriate description is provided by considering spins as classical n-component vectors of fixed length S. The simplest antiferromagnetic Heisenberg model

is given by:

$$\mathcal{H} = J \sum_{\langle ij \rangle} \mathbf{S}_i \cdot \mathbf{S}_j \tag{3}$$

where $J > 0$ is the AF exchange energy and the sum runs over nearest neighbors of the lattice.

On a Bravais lattice, by going to Fourier space, one finds that groundstate configurations correspond to the minimum of the Fourier transform $J(\mathbf{q})$. For instance, on a triangular lattice, one finds a unique groundstate (up to symmetries) with a 120-degree spiral order.

When considering other non-Bravais frustrated lattices, the situation becomes more involved since in Fourier space $J(\mathbf{q})$ is an $m \times m$ matrix, where m is the number of spins per unit cell. In principle, one should find the smallest eigenvalue, keeping in mind that each spin has a fixed length: $\forall i\, |\mathbf{S}_i|^2 = S^2$ (strong constraint). Since this cannot be done easily, the Luttinger–Tisza method [21] consists in assuming a *weak constraint*: $\sum_i |\mathbf{S}_i|^2 = NS$ which can provide a solution but not always.

On some lattices such as 2d kagome or checkerboard, or 3d pyrochlore, see Figure 1, made of corner-sharing triangles or tetrahedra respectively, the classical Heisenberg model takes a simpler form:

$$\mathcal{H} = \frac{J}{2} \sum_p \mathcal{S}_p^2, \tag{4}$$

up to a constant, where $\mathcal{S}_p$ is the total spin on a plaquette p and the sum runs over all plaquettes. From this expression, it is clear that if a configuration can satisfy $\mathcal{S}_p = \mathbf{0}$ for all plaquettes, then it is a groundstate. Hence, one can look for solutions using so-called Maxwellian counting originally applied in mechanics of rigid bodies [22]. Following Chalker's presentation [8], we have $F = N(n-1)$ degrees of freedom for n-component spins. Let N_p be the number of corner sharing units (plaquettes), each made of q spins, hence $N = qN_p/2$. In order to have a zero-energy configuration, one has to satisfy one constraint per cluster (total spin $\mathcal{S}_p = \mathbf{0}$), i.e. $K = nN_p$ scalar constraints. Assuming that they can be satisfied and are linearly independent (which is obviously not true in general), one ends up with an effective number of degrees of freedom:

$$\boxed{D = F - K = \left(\frac{q}{2}(n-1) - n\right) N_p}$$

For instance, when considering Heisenberg spins ($n = 3$) on 3d pyrochlore or 2d checkerboard lattices (both having $q = 4$), one finds that $D = N_p$ is extensive, leading to a macroscopic degeneracy and CSL behavior [23]. Quite remarkably for instance, on 3d pyrochlore, the system remains disordered at all temperature [24].

Note that this argument does not provide any information for the kagome lattice, for which the constraints are indeed not independent. A proper treatment leads to $D = N/9$ zero modes in this case and the order-by-disorder mechanism selects coplanar spin configurations [25]. Finally, let us mention that frustration can also occur from competing interaction, e.g. next-nearest-neighbor coupling J_2 on the square lattice: this is the famous J_1–J_2 Heisenberg model on the square lattice, which also has a very large degeneracy when $J_2 = J_1/2$.

2.4. *Classification*

Inspired by the Luttinger–Tisza model, a classification can be made depending on the structure of the flat bands in the spectrum. Indeed, for the particular case (4), the Hamiltonian can be brought in this form:

$$\mathcal{H} = \frac{J}{2} \sum_{\ell,m} \sum_q (L_q^\ell L_{-q}^m) S_q^\ell \cdot S_{-q}^m \tag{5}$$

defining an n-component vector $\mathbf{L}(q)$, from which the number of dispersive modes can be obtained [26, 27].

Quite interestingly, the analysis of $\mathbf{L}(q)$ allows to get higher-rank tensor, e.g. Gauss' law with tensors with fracton excitations, with quadratic or quartic dispersion relations etc. Analysing the band structure, the gap closing points, the number of pinch points and their nature allow to classify different CSL [26, 27].

Closing this section on CSL, it is very exciting to see the ongoing classification as well as novel exotic CSL (algebraic, fracton etc.) which could potentially be relevant in real materials. It would be interesting to go beyond the specific case (4) for a complete classification of CSL.

Last but not least, CSL are parent states when quantum fluctuations start playing a role and natural starting point to realize exotic quantum states.

3. Quantum spin liquids

3.1. *General features*

There are different ways to add quantum fluctuations in a classical model, for instance adding a transverse magnetic field or XY exchange to an Ising model, or simply promoting the spins into quantum operators in the Heisenberg model. Based on the order-by-disorder mechanism, one expects on general grounds that quantum fluctuations will select some ordered phase. In this part, we will focus on groundstate properties at zero temperature in quantum models and review the possibility to get unconventional phases of matter, in particular quantum spin liquids (QSL) that we will define.

Note that the definition is often negative, in the sense that such a QSL phase does not break any symmetry, but recent advances have shown the role of several observables: quantum entanglement, topology as well as spectroscopic features [28], which could help to characterize and distinguish various QSL.

The story of QSL goes back to Anderson's idea of a resonating valence-bond (RVB) groundstate, that is a coherent superposition of valence-bond configurations (made of 2-site singlets of spin 1/2) [29], see Figure 4. By definition, such a state does not break any spin or lattice symmetries, as expected for a spin liquid. From a variational point of view, a nearest-neighbor RVB state (made only of nearest-neighbor singlet) has a variational energy per site of $(-3/8)J$ which is already lower than the one of a classical Néel state $(-(1/4)J)$ on a spin-1/2 Heisenberg chain. Hence it was proposed to be a good candidate for $S = 1/2$ Heisenberg model on the triangular lattice, which turned out to be wrong since this model is now believed to be ordered magnetically. But it has been a fruitful idea ever since and we will discuss some exotic properties of this wavefunction as well as its relevance for some simple microscopic models.

On the one hand, there exist some simple groundstates that obviously do not break spin or lattice symmetries, such as a trivial singlet product state on the Shastry–Sutherland lattice, see Figure 5. Such a product-state is featureless and does not possess any exotic property [30].

On the other hand, we know that in condensed matter systems, some gapped phases can be nontrivial in the sense of having topological order, e.g. the famous fractional quantum Hall effect (FQHE). Topological phases of matter are gapped quantum phases containing nontrivial features which are not due to spontaneous symmetry breaking. While such systems have exponentially decaying correlation and look quite simple from a classical point of view, they do exhibit nontrivial properties. For example, the groundstate degeneracy can depend on the topology of the closed manifold (torus versus sphere), or there can exist protected gapless edge excitations if the system has a boundary, or bulk excitations can possess nontrivial statistics etc. Generally also, there are nontrivial features in the bipartite entanglement spectrum [31]. Clearly, QSL are much richer than their classical analogue, and the role of quantum order was pointed out by Wen [32].

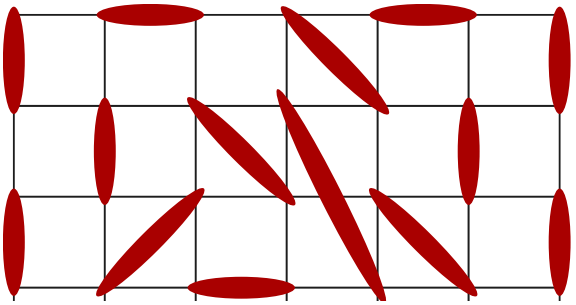

Figure 4. Example of a valence-bond configuration on the square lattice. Each dimer corresponds to a singlet state made of two spins-1/2. An equal weight superposition of all coverings is known as the RVB wavefunction.

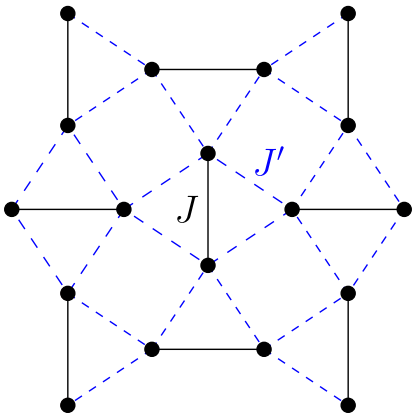

Figure 5. Shastry–Sutherland lattice for which the product of singlets on the J bonds is an exact eigenstate and the unique groundstate for small enough J'/J.

Since QSL cannot be classified according to symmetry breaking, one possible classification was proposed based on the nature of the elementary excitations (gapped or gapless spinons) as well as the emergent gauge field (U(1), SU(2), $Z_2 \ldots$) which mediate their interactions [33]. More recently, entanglement properties were also shown to be relevant for this classification: quantum spin liquids are by definition quantum states that are not connected adiabatically to trivial product states [28]. There are two classes: (i) long-range entangled (LRE) if it cannot be adiabatically connected to a product state under any local unitary transformation (e.g. FQHE, Z2 QSL, chiral spin liquid etc.); (ii) short-range entangled (SRE) if it cannot be adiabatically connected to a product state while respecting some symmetries: symmetry protected topological (SPT) state, e.g. Haldane $S = 1$ chain, topological insulator etc.

There are intimate relations between these definitions since topological order is probably needed to realize fractionalization in dimension $d \geq 2$ [34].

Building on RVB idea, Kalmeyer and Laughlin have proposed a chiral spin liquid phase to be realized on the triangular lattice [35]. This phase is analogous to the FQHE on a lattice: existence of chiral edge modes, quantized thermal transport, bulk excitations are anyons etc. We will see later microscopic models where it is possibly realized.

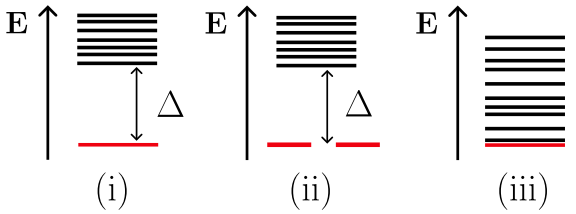

Figure 6. Three different possibilities for the many-body spectrum: (i) a unique groundstate and a finite gap Δ; (ii) degenerate groundstates and a finite gap Δ; (iii) gapless.

3.2. *Classification based on many-body spectrum*

We will now consider the low-energy features of the many-body spectrum of a generic model Hamiltonian $\mathscr{H}$. Note that sometimes we only have a wavefunction (e.g. RVB), but it is possible to consider a parent Hamiltonian for which this is the groundstate, see later. For the sake of simplicity, we will assume $\mathscr{H}$ to be short-ranged and local, most of the time with some U(1) or SU(2) spin symmetry. A typical example is the Heisenberg model

$$\mathscr{H} = J \sum_{\langle ij \rangle} \hat{S}_i \cdot \hat{S}_j + \cdots \tag{6}$$

where $J > 0$ is the AF coupling constant, $\hat{S}$ are quantum spin operators ($S = 1/2, 1, \ldots$) and additional interactions could be needed to stabilize a QSL groundstate.

Focusing on low-energy, we can distinguish three qualitative different spectra, see Figure 6: (i) a unique groundstate and a finite gap Δ; (ii) degenerate groundstates and a finite gap; (iii) gapless. We will see in the following some examples, as well as some refinements regarding case (ii) since the degeneracy can result either from symmetry breaking or from the topological nature.

We will make use of exact and rigorous results, when available. Indeed, even if some models are fine-tuned or artificial, they have the merit of showing the existence of exotic quantum phases. For realistic and generic models, I will refer to several numerical studies, with the caveat that finite-size effects cannot be fully controlled. Indeed, it has been shown that deciding whether a 2d translation-invariant Hamiltonian has a gap or not in the thermodynamic limit is undecidable [36] ...

When discussing the low-energy spectrum, a seminal result was provided by Lieb, Schultz and Mattis (LSM) [37] in 1d, which was later extended to arbitrary dimension d [38, 39]. Basically, LSM forbids having case (i) spectrum for an odd number of half-integer spins per unit cell.

Note that a similar result can also be obtained in finite magnetic field [38], since LSM relies on interplay of U(1) symmetry and translations, constraining whether some magnetization plateaux phases can be featureless or not[1]. In any dimensions, a featureless magnetization plateau is possible iff $nS(1-m) =$ integer, where n is the number of spins per unit cell, S the spin value and m the total magnetization normalized by its maximal value.

Let us mention some recent extensions that have been obtained when considering symmetries beyond translations (nonsymmorphic or point-group) or by matching UV/IR anomalies in field theory. Namely, the groundstate of a $S = 1/2$ Hamiltonian *cannot* be featureless (case (i)) [40]:

- on the diamond lattice [41];
- if there is an even-order rotation symmetry [42];
- on the pyrochlore lattice (4 spins per unit cell) [43].

[1] A quantum groundstate is said to be featureless when it can be adiabatically connected to a trivial product state.

Note that when LSM-like argument does not apply, a featureless groundstate, depicted as case (i), is possible but it is not always straightforward to construct one. There are explicit constructions e.g. for 1/3-magnetization plateau on the kagome lattice [44] or a featureless spin-1/2 wavefunction on the honeycomb lattice [45, 46].

3.3. *Classification based on slave particle representations*

In order to make some analytic progress, it can be convenient to use exact fermionic or bosonic representations of spin operators, known as slave particles due to some constraints [47].

For instance, one can introduce Abrikosov fermions

$$\hat{S}^z = \tfrac{1}{2}(c_\uparrow^\dagger c_\uparrow - c_\downarrow^\dagger c_\downarrow) \quad S^+ = c_\uparrow^\dagger c_\downarrow \quad S^- = c_\downarrow^\dagger c_\uparrow \tag{7}$$

which is a faithful representation of a spin-1/2 at each site provided a single occupancy constraint is added. In this language, the spin–spin interaction is quartic so that a natural mean-field approximation can be performed, leading to

$$\mathscr{H}_{\rm MF} = \sum_{\langle ij\rangle} \chi_{ij}(c_{i\uparrow}^\dagger c_{j\uparrow} + c_{i\downarrow}^\dagger c_{j\downarrow}) + \eta_{ij}(c_{i\uparrow}c_{j\downarrow} - c_{i\downarrow}c_{j\uparrow}) + \text{h.c.} \tag{8}$$

which is quadratic and can be solved. Of course, this mean-field solution may or may not be stable when considering fluctuations, in particular the gauge field enforcing the one fermion per site constraint. This is thus amenable to analytic studies or numerical ones when performing an exact Gutzwiller projection [48] to enforce the constraint.

Similarly, a slave-boson description can be obtained from Schwinger bosons:

$$\hat{\mathbf{S}} = \tfrac{1}{2} b_\alpha^\dagger \sigma_{\alpha\beta} b_\beta \tag{9}$$

imposing a constraint $\sum_\alpha b_\alpha^\dagger b_\alpha = 2S$ at each site. This also allows to perform mean-field decoupling. Note that from a numerical point of view, one needs to work with permanent rather than determinant for the projection, which is very costly.

In all theses approaches, known as parton constructions, there is some redundancy of the mean-field descriptions, revealing the gauge nature of these theories. This has been used to classify possible solutions (Ansatz) using a projective symmetry group (PSG) approach [32]. In particular, different spin liquids that do not break any symmetry can have different PSG. Even though this is obtained from a mean-field approach, it should be a property of the phase itself.

Such a PSG classification is still being worked on in the community, for bosonic or fermionic spinons on all lattices. For instance, when time-reversal symmetry is broken (as in chiral spin liquid), an additional classification is needed [49, 50].

Depending on the nature of the gauge fields and the spinon spectrum, several QSL could be realized [47], e.g.:

- for a Z_2 gauge field and gapped spinons, a gapped Z_2 QSL phase emerges, which is stable in 2d and 3d;
- for a U(1) gauge field and gapped spinons, a genuine QSL is unstable in 2d [51] towards a valence-bond crystal (VBC) phase that break some lattice symmetries;
- for a U(1) gauge field and gapless Dirac spinons, the situation is not fully settled and an algebraic Dirac spin liquid could be stabilized in (2 + 1)d [52].

What is even more dizzying is that there could exist several different QSL within the same gauge symmetry class, dubbed symmetry-enriched topological (SET) order, which can be analyzed using topological quantum field theory [53]. As an example, there are about 2^{21} different gapped Z_2 QSL on the 2d square lattice [54]!

This parton construction approach has been very fruitful to provide various QSL Ansatz and is still ongoing effort to classify QSL in 3d on various lattices, see e.g. [40, 55].

3.4. *Unique groundstate and finite gap*

3.4.1. *Trivial phase*

Of course, in some situations a featureless paramagnetic groundstate is possible, with a finite gap to all excitations. It can be adiabatically connected to a trivial product state. For instance, this is the case for Heisenberg spin ladder or bilayers, including some exact results for fine-tuned frustrated models [3]. Quite interestingly, there is also the famous example of Shastry–Sutherland lattice [30], see Figure 5, on which the groundstate is a product state of singlets for small enough J'/J.

In such trivial phase, correlations are short-range and there is no topological entanglement entropy (a subdominant contribution to the area law). Note that it can still lead to rich physics when adding e.g. a finite magnetic field with the appearance of nontrivial magnetization plateaux as well as superfluid or supersolid phases [3].

3.4.2. *One-dimensional SPT phase*

A famous example of 1d SPT phase is provided by the Haldane phase of a $S = 1$ Heisenberg chain [56], which can be understood from the exact groundstate of a slightly deformed Hamiltonian known as AKLT model [57]:

$$\mathscr{H}_{\mathrm{AKLT}} = J \sum_i \left(\hat{S}_i \cdot \hat{S}_{i+1} + \tfrac{1}{3} (\hat{S}_i \cdot \hat{S}_{i+1})^2 \right). \tag{10}$$

While the groundstate is unique on a chain with periodic boundary conditions (PBC), it becomes 4-fold degenerate in the presence of open boundary conditions (OBC) due to the emergence of $S = 1/2$ edge states. Thus, it has some topological properties, which are also revealed in the bipartite entanglement spectrum. It has been understood that these phases are not adiabatically connected to trivial ones, provided some symmetries are present [58], hence their name: symmetry-protected topological (SPT) phases.

3.4.3. *Two-dimensional SPT phase*

It turns out that AKLT construction [57] can also be performed in higher dimension, e.g. $S = 3/2$ on the honeycomb lattice or $S = 2$ on the square lattice. For these models, it can be shown that the groundstate is unique and all correlations decay exponentially. While there is no rigorous proof of a finite-spin gap, all numerical studies point to a finite value, see e.g. [59].

Such states are also known as valence-bond solids (VBS) since they can be understood from valence-bond configurations and they do not break any spin or lattice symmetries.

Similarly to the 1d case, the properties depend on having periodic versus open boundary conditions, which signals some topological properties: these states are called 2d SPT phases [60].

3.5. *Gapped spectrum with groundstate degeneracy*

3.5.1. *Spontaneous symmetry breaking*

The most well-known example of a gapped spectrum with groundstate degeneracy occurs when there is a spontaneous symmetry breaking (SSB) of a *discrete* lattice symmetry. This is known to occur e.g. in the 1d Majumdar–Ghosh $S = 1/2$ model [61]:

$$\mathscr{H}_{\mathrm{MG}} = J \sum_i \left(\hat{S}_i \cdot \hat{S}_{i+1} + \tfrac{1}{2} \hat{S}_i \cdot \hat{S}_{i+2} \right), \tag{11}$$

where a spontaneous dimerization occurs, or in various 2d spin models with columnar or plaquette orders, e.g. J_1–J_2–J_3 $S = 1/2$ on the honeycomb lattice [62] or $S = 1/2$ on the checkerboard lattice [63] (see Figure 1 where one plaquette phase is sketched with green symbols) and so on.

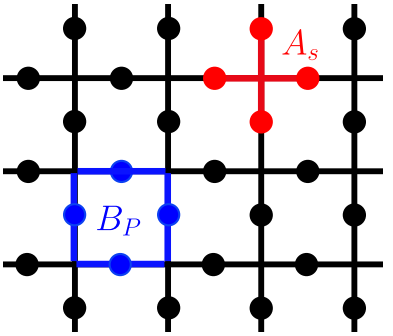

Figure 7. Illustration of Kitaev's toric code model on the square lattice.

Quite interestingly, a similar mechanism can also occur in the presence of magnetic field giving rise to magnetization plateaux with SSB, e.g. exact magnon states close to saturation in frustrated lattices [64] or similar mechanism at other magnetization values [65].

These situations are well understood and magnetic excitations are conventional, e.g. gapped $S = 1$ magnons in 2d.

3.5.2. *Topological phase*

Quite generally, gapped topological phases can also be characterized by the fact that elementary excitations are gapped anyons, which statistics can be nontrivial, e.g. nonabelian, which could be useful for topological quantum computation. The groundstate degeneracy depends on the genus of the manifold, which is quite different from the usual spontaneous symmetry breaking. Remarkably, the fractionalization of excitations is strongly tied to the topological properties [34, 66] and could be detected in broad continuum-like excitations in the spin dynamical structure factors $S(\mathbf{q},\omega)$.

At a more fundamental level, a gapped topological phase in $(2+1)$d can be probed using the topological entanglement entropy [67, 68], which is a subleading constant term to the usual area law.

3.5.3. *Some specific models*

In this endeavour to discover QSL in realistic models or materials, the quest for exact solution or controlled approximation is crucial. Indeed, this allows to show that some of these phases are possible, sometimes stable, and hence relevant to more generic situations.

3.5.3.1. Kitaev's toric code. In 2003, Kitaev has introduced the toric code as an exact model for which the groundstate is a gapped Z_2 topological phase [69] in $(2+1)$d. As in a gauge theory, the Ising spins live on the links of a square lattice and the Hamiltonian is given by

$$\mathcal{H}_{\text{toric}} = -\sum_s A_s - \sum_P B_P \tag{12}$$

where the first (respectively second) sum runs over all sites (respectively plaquettes) of a 2d square lattice, A_s is the product of σ_x on all links around a site s while B_P is the product of all σ_z on all bonds of a plaquette P, see Figure 7.

Since all A_s and B_P commute together, an exact solution can be provided. The groundstate is featureless and there are four types of excitations (all with quantum dimensions $d_i = 1$): trivial, e, m, $f = e - m$ pair. e and m have π-shift mutual statistics, hence they are anyons (abelian) and f-excitations behave as fermions.

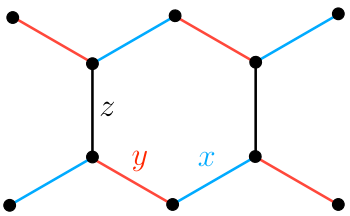

Figure 8. Illustration of Kitaev's honeycomb model.

This solution was a breakthrough since it has shown the existence of a topological phase, analogous to the famous $\nu = 1/3$ FQHE, in a simple spin model. However, it is very fine-tuned since the quasiparticles have no dispersion and the correlation length is zero.

3.5.3.2. Kitaev's honeycomb model. Later, Kitaev has found an even more interesting exact solution on the honeycomb lattice [70]. The model is defined in terms of spin-1/2 variables on the sites of a 2d honeycomb lattice:

$$\mathscr{H}_{\text{honeycomb}} = -J_x \sum_x \sigma_j^x \sigma_k^x - J_y \sum_y \sigma_j^y \sigma_k^y - J_z \sum_z \sigma_j^z \sigma_k^z \tag{13}$$

where each term acts on the three different kind of bonds, see Figure 8.

Using a faithful Majorana representation of the spin operators, the exact solution provides a gapped or gapless phase depending on the parameters. The gapped phase is similar to the previous toric code case, while the gapless phase is more intriguing: in the presence of a magnetic field, a gapped phase with nonabelian anyons can be stabilized, similar to a topological superconductor.

Following this seminal work, a generalization by Levin and Wen has given access to a huge zoo of topological phases in so-called string-net models [71].

3.5.3.3. Quantum dimer models. In the context of QSL, quantum dimer models (QDM) have been very inspiring examples and we refer to the review by Moessner and Raman in Ref. [3] for an extensive discussion. The Hilbert space consists in fully-packed dimer configurations (i.e. as in classical dimer models) and quantum fluctuations arise from a simple model introduced by Rokhsar and Kivelson (RK) [72], e.g. on the square lattice:

$$H_{\text{QDM}} = \sum \Big[-t \left(|\square\rangle\langle\square| + \text{h.c.} \right) + v \left(|\square\rangle\langle\square| + |\square\rangle\langle\square| \right) \Big], \tag{14}$$

(in terms of hard core dimer objects $\square$) where t and v are the amplitudes of kinetic and potential terms, and the sum runs over all elementary square plaquettes. Graphically, these processes are represented in Figure 9. As in the classical case, the local constraint provides a natural gauge structure and conserved quantities: winding number and U(1) symmetry on bipartite lattices (e.g. square), or topological sectors and Z_2 symmetry on non-bipartite ones (e.g. triangular).

Precisely when $v = t$, so-called RK point, the groundstate can be obtained as an equal weight superposition of all configurations. On most bipartite lattices, it is part of a Coulomb phase (with algebraic correlations) but unstable towards crystalline phases that break lattice symmetries, see Figure 10. On nonbipartite lattices, the RK point belongs generically to an extended gapped Z_2 RVB topological phase [73].

The instability of U(1) QDM is linked to a famous result by Polyakov about gauge theories [51]. However, Z_2 gauge theories can be deconfined in (2+1)d in (3+1)d as well as U(1) ones in (3+1)d.

As a conclusion, QDM models can exhibit various nonmagnetic phases including valence bond crystals (VBC), Coulomb phase or gapped Z_2 RVB topological phase.

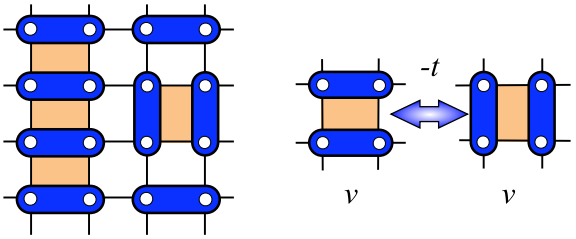

Figure 9. Left: A dimer configuration on the square lattice. Flippable plaquettes are shaded. Right: Flippable plaquettes contribute a diagonal term v to the Hamiltonian and can be flipped with amplitude $-t$ ($t>0$).

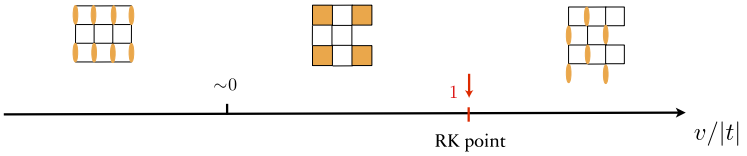

Figure 10. Schematic phase diagram of the QDM on the square lattice as a function of v/t: the critical groundstate at the RK point is unstable to crystalline phases such as columnar, plaquette or staggered.

3.5.3.4. Anisotropic spin models. Following the success of QDM to describe unconventional phases, a natural roadmap was to engineer spin models with strong anisotropies (in spin space), such that QDM emerge as en effective description.

For instance, let us mention a model introduced on the kagome lattice (see Figure 1) by Balents, Fisher and Girvin [74]:

$$\mathscr{H}_{\rm BFG} = J_z \sum_{\hexagon} (S^z_{\hexagon})^2 - J_\perp \sum_{\hexagon} \{(S^x_{\hexagon})^2 + (S^y_{\hexagon})^2\} \tag{15}$$

where J_z is the dominant energy scale that constrains the total S_z to vanish on each hexagonal plaquette, i.e. there are exactly 3 up and 3 down spins per hexagon. As a result, the model maps at low-energy onto an effective QDM-like model on the dual triangular lattice, where there are exactly three dimers per site. Subsequent large-scale numerical studies have shown that this model does exhibit fractionalization and realizes a gapped Z_2 topological phase [75], which is adiabatically connected to the RK point of this QDM-like model.

Quite interestingly other spin models are amenable to large-scale unbiased quantum Monte-Carlo (QMC) simulations, e.g. an SO(N)-symmetric spin model on the kagome lattice which groundstate is a gapped Z_2 QSL [76].

3.5.3.5. SU(2)-symmetric spin models. In order to get closer to realistic spin models, similar physical properties were investigated in SU(2)-symmetric spin models, e.g. using decorated lattices to reproduce QDM physics [77]. As a result, it was possible to construct groundstate having gapped Z_2 or gapless U(1) properties in 2d and 3d spin models.

Later, Cano and Fendley have proposed SU(2) spin-1/2 models with local interactions that can stabilize RVB groundstates, similar to the RK points of the corresponding QDM model [78]. As discussed previously, depending on the lattice, it can be a quantum critical point or a genuine gapped spin liquid phase. Quite interestingly, by adapting this construction, it is also possible to engineer a spin model having similar properties as the QDM one for any interaction v/t parameter [79].

3.5.3.6. Chiral QSL. We have already mentioned the original proposal by Kalmeyer and Laughlin [35] to realize in a spin system a quantum phase analogous to the $\nu = 1/2$ bosonic FQHE phase. This is a gapped phase, with 2-fold degeneracy on a torus. With open boundaries, a rich edge physics emerges with gapless chiral modes described by an $SU(2)_1$ conformal field theory (CFT).

Regarding microscopic models, several large-scale numerical studies have shown that a chiral QSL groundstate can be stabilized on various spin-1/2 models with local interactions on the kagome or triangular lattice with explicit time-reversal symmetry breaking [80–84] or without [85]. It is also possible to construct parent Hamiltonians having an exact chiral QSL as groundstate, but they are generally long-ranged [86, 87].

Quite interestingly, it is also possible to realize more exotic FQHE phases with higher spin models, e.g. Moore–Read phase with nonabelian $SU(2)_2$ anyons using spin-1 models [88, 89] or Read–Rezayi state with nonabelian $SU(2)_3$ using $S = 3/2$ model [90], or even with higher $SU(N)$ symmetry [91]. Let us also mention that gapped chiral QSL with nonabelian anyons are also found for the Kitaev model (13) in magnetic field [92] or as exact groundstate of a Kitaev model on a decorated triangle-honeycomb lattice [93].

3.6. *Gapless spectrum*

3.6.1. *Magnetic long-range order*

Although we are interested in disordered phase, for completeness we will review basic properties of magnetically ordered phases.

When there is a long-range magnetic order due to spontaneous symmetry breaking of the *continuous* spin SU(2) symmetry, there are necesseraly gapless spinwave excitations, corresponding to the Nambu–Goldstone low-energy modes.

It is also possible to get more involved symmetry breaking, e.g. nematic (or quadrupolar) order. A simple example can be provided in a spin-1 system where the groundstate prefers $S^z = \pm 1$ and not 0 state locally, i.e. no net magnetization but a preferred direction, hence the name nematic as in liquid crystals, see e.g. a review in [3].

3.6.2. *Dirac spin liquid*

Using the parton construction described above, it is possible in some cases to assume a static gauge pattern such that the fermionic tight-binding model spectrum exhibits a Dirac spectrum. Then, by enforcing the single-particle occupation constraint, one can construct a spin wavefunction with exotic properties since several physical correlations are algebraic at $T = 0$: this state is known as the algebraic Dirac spin liquid (DSL). Its stability in $(2+1)$d is an active field of research since DSL is unstable towards many competing phases [52] such as magnetic order, chiral QSL or VBC.

Recent numerical studies have argued that DSL could be realized in several microscopic models such as an extended $S = 1/2$ triangular Heisenberg model [94, 95]. Notably, there are specific signatures of low-energy excitations [96] that could be probed numerically [97] or experimentally.

In $(3+1)$d, DSL is a stable phase of matter that could describe quantum spin ice [4, 98] with sharp spectroscopic signatures.

3.6.3. *Gapless Z_2 QSL*

Going back to Kitaev's model on the honeycomb lattice described in Section 3.5.3.2, it also contains a gapless Z_2 phase when all couplings are similar in magnitudes.

In the field theory language, it can be seen as an instability of the DSL by adding a pairing field in the spinon quadratic Hamiltonian so that the gauge field symmetry reduces from U(1) to Z_2. This could be stabilized on the frustrated $S = 1/2$ square lattice [99] or on the Shastry–Sutherland lattice [100, 101].

Of course, the parton construction is very versatile and many other QSL are possible. For instance, if there is no spinon Fermi surface but only a quadratic band touching, a quadratic gapless Z_2 QSL could be stabilized [102].

3.6.4. *Spinon Fermi sea*

A natural route to engineer a critical spin wavefunction is to perform a Gutzwiller projection on a filled Fermi sea, using the parton construction.

In 1d, this critical wavefunction is the exact groundstate of the famous Haldane–Shastry spin-1/2 chain with $1/r^2$ interaction [56, 103] and has a very good variational energy for the usual Heisenberg chain.

In 2d, this wavefunction was proposed as a *spin Bose metal* [104]. Such a spinon Fermi surface would contain gapless excitations at all momenta in $S(\mathbf{q},\omega)$ and violate area law in the entanglement entropy scaling (as in a Fermi liquid).

3.6.5. *RVB*

Even when considering only nearest-neighbor valence bonds in Figure 4, such an RVB wavefunction is nontrivial: clearly, spin correlations are short-range but dimer–dimer correlations decay algebraically [105, 106] on a 2d bipartite square lattice, qualitatively similar to the QDM case at its RK point. We have already discussed its parent Hamiltonian [78] and the fact that in 2d, this can only exist as a critical point.

The situation is more interesting in 3d where a U(1) QSL phase can be stable on bipartite lattices. For instance, starting from the RK point of a QDM on a bipartite diamond lattice, it is possible to engineer an XXZ model on the dual pyrochlore lattice which could stabilize a U(1) QSL phase [107] or SU(2) models on decorated lattices with similar properties [77].

4. Conclusion

We have described several classical and quantum spin liquids, which by definition do not break any symmetry (neither in spin space or real space). Despite this negative definition, we have seen that they can be classified in various categories.

In the classical case, this classification is rather recent and in progress [26, 27], including the well-known U(1) Coulomb phase (e.g. in classical spin ice materials) but also higher-rank Coulomb phases with fracton-like excitations [108]. At the moment, the classification mostly relies on the specific form of some models as in Equation (4) and it would be valuable in the future to go beyond and see if a full description of all possible CSL can be obtained. For instance, there are weird CSL analogous to Z_2 QSL [109] that deserve further studies.

In the quantum case, there is already a simple distinction depending on the many-body spectrum, see Figure 6, which leads to various qualitative behaviors in some observables, that can be probed experimentally. Moreover, since the seminal work by Wen [32], much progress has been made to classify the different QSL according to the nature of the gauge group and the spinon spectrum. In order to go beyond the PSG classification, braided tensor categories in $(2+1)$d have allowed further progress [53] as well as group cohomology [40]. As a result, there is a really huge number of distinct QSL and the focus should be now to understand on which microscopic models

they can be realized. It would be crucial to understand if this classification is valid beyond mean-field, and in particular connect the solutions that can be found using a bosonic versus fermionic slave-particle description.

Thanks to some famous exact solutions that we have partly reviewed, various gapped or gapless QSL are known to be stable in 2d or 3d, which pave the way for their realization using realistic microscopic models or existing quantum materials. We have discussed in details some famous examples of QSL such as gapped Z_2, gapless U(1), chiral spin liquid, Dirac spin liquid, spin Bose metal...Among these QSL, a lot has still to be understood particularly on the Dirac spin liquid in $(2+1)$d which may or may not be stable as a phase.

Besides the achievements of analytical tools, there is a large activity in numerical simulations with the developments of novel algorithms (e.g. tensor networks, neural networks etc.). While we focused on zero-temperature, it is crucial to further improve these methods to tackle finite-temperature (for thermodynamics) as well as finite-time evolution (for dynamics). These numerical tools are called for since there are very few exact results and one would like to investigate realistic models for classical or quantum spin liquids.

While we have focused on describing some exotic phases of matter, it is also very important to understand whether there can exist unconventional phase transitions between them, which description is beyond the standard Landau–Ginzburg paradigm. This can occur for instance between a magnetically ordered phase and a valence-bond crystal one, so-called deconfined quantum criticality [110] or weakly first-order behavior [111], or even more exotic Stiefel liquids which have no Lagrangian descriptions [112] that could describe quantum critical spin liquids.

Declaration of interests

The authors do not work for, advise, own shares in, or receive funds from any organization that could benefit from this article, and have declared no affiliations other than their research organizations.

Acknowledgments

I would like to thank Yvan Castin and Carlos Sá de Melo for the organisation of the symposium "Open questions in the quantum many-body problem" at Institut Henri Poincaré (IHP, Paris) where this lecture was presented.

References

[1] P. W. Anderson, "More is different", *Science* **177** (1972), no. 4047, pp. 393–396.
[2] A. P. Ramirez, "Strongly geometrically frustrated magnets", *Annu. Rev. Mater. Res.* **24** (1994), no. 24, pp. 453–480.
[3] C. Lacroix, F. Mila and P. Mendels, *Introduction to Frustrated Magnetism: Materials, Experiments, Theory*, Springer Series in Solid-State Sciences, 164, Springer: Berlin, 2011.
[4] Y. Zhou, K. Kanoda and T.-K. Ng, "Quantum spin liquid states", *Rev. Mod. Phys.* **89** (2017), article no. 025003.
[5] G. H. Wannier, "Antiferromagnetism. The triangular Ising net", *Phys. Rev.* **79** (1950), pp. 357–364.
[6] J. Villain, R. Bidaux, J.-P. Carton and R. Conte, "Order as an effect of disorder", *J. Phys. France* **41** (1980), no. 11, pp. 1263–1272.
[7] J. Villain, "Insulating spin glasses", *Z. Phys. B: Condens. Matter.* **33** (1979), no. 1, pp. 31–42.
[8] J. T. Chalker, "Spin liquids and frustrated magnetism", in *Topological Aspects of Condensed Matter Physics: Lecture Notes of the Les Houches Summer School: Volume 103, August 2014*, Oxford University Press, 2017.
[9] H. Duminil-Copin, *100 years of the (critical) Ising model on the hypercubic lattice*, preprint, 2022, 2208.00864.
[10] W. Shirley, K. Slagle, Z. Wang and X. Chen, "Fracton models on general three-dimensional manifolds", *Phys. Rev. X* **8** (2018), article no. 031051.

[11] D. Chowdhury, A. Georges, O. Parcollet and S. Sachdev, "Sachdev–Ye–Kitaev models and beyond: Window into non-Fermi liquids", *Rev. Mod. Phys.* **94** (2022), article no. 035004.

[12] J. Colbois, B. Vanhecke, L. Vanderstraeten, A. Smerald, F. Verstraete and F. Mila, "Partial lifting of degeneracy in the J_1–J_2–J_3 Ising antiferromagnet on the kagome lattice", *Phys. Rev. B* **106** (2022), article no. 174403.

[13] R. J. Baxter, *Exactly Solved Models in Statistical Mechanics*, Academic: London, 1982. Dover, New York, 2007.

[14] L. Pauling, "The structure and entropy of ice and of other crystals with some randomness of atomic arrangement", *J. Am. Chem. Soc.* **57** (1935), no. 12, pp. 2680–2684.

[15] E. H. Lieb, "Residual entropy of square ice", *Phys. Rev.* **162** (1967), pp. 162–172.

[16] W. F. Giauque and J. W. Stout, "The entropy of water and the third law of thermodynamics. The heat capacity of ice from 15 to 273 K", *J. Am. Chem. Soc.* **58** (1936), no. 7, pp. 1144–1150.

[17] S. T. Bramwell and M. J. Harris, "The history of spin ice", *J. Phys.: Condens. Matter.* **32** (2020), no. 37, article no. 374010.

[18] C. Castelnovo, R. Moessner and S. L. Sondhi, "Magnetic monopoles in spin ice", *Nature* **451** (2008), no. 7174, pp. 42–45.

[19] P. W. Kasteleyn, "The statistics of dimers on a lattice: I. The number of dimer arrangements on a quadratic lattice", *Physica* **27** (1961), no. 12, pp. 1209–1225.

[20] H. N. V. Temperley and M. E. Fisher, "Dimer problem in statistical mechanics-an exact result", *Philos. Mag.* **6** (1961), no. 68, pp. 1061–1063.

[21] J. M. Luttinger and L. Tisza, "Theory of dipole interaction in crystals", *Phys. Rev.* **70** (1946), pp. 954–964.

[22] J. C. Maxwell, "XLV. On reciprocal figures and diagrams of forces", *Lond. Edinb. Dublin Philos. Mag. J. Sci.* **27** (1864), no. 182, pp. 250–261.

[23] R. Moessner and J. T. Chalker, "Low-temperature properties of classical geometrically frustrated antiferromagnets", *Phys. Rev. B* **58** (1998), pp. 12049–12062.

[24] R. Moessner and J. T. Chalker, "Properties of a classical spin liquid: The Heisenberg pyrochlore antiferromagnet", *Phys. Rev. Lett.* **80** (1998), pp. 2929–2932.

[25] J. T. Chalker, P. C. W. Holdsworth and E. F. Shender, "Hidden order in a frustrated system: Properties of the Heisenberg Kagomé antiferromagnet", *Phys. Rev. Lett.* **68** (1992), pp. 855–858.

[26] N. Davier, F. A. Gómez Albarracín, H. D. Rosales and P. Pujol, "Combined approach to analyze and classify families of classical spin liquids", *Phys. Rev. B* **108** (2023), article no. 054408.

[27] H. Yan, O. Benton, R. Moessner and A. H. Nevidomskyy, "Classification of classical spin liquids: Typology and resulting landscape", *Phys. Rev. B* **110** (2024), article no. L020402.

[28] L. Savary and L. Balents, "Quantum spin liquids: a review", *Rep. Prog. Phys.* **80** (2016), no. 1, article no. 016502.

[29] P. W. Anderson, "Resonating valence bonds: A new kind of insulator?", *Mater. Res. Bull.* **8** (1973), no. 2, pp. 153–160.

[30] B. S. Shastry and B. Sutherland, "Excitation spectrum of a dimerized next-neighbor antiferromagnetic chain", *Phys. Rev. Lett.* **47** (1981), pp. 964–967.

[31] H. Li and F. D. M. Haldane, "Entanglement spectrum as a generalization of entanglement entropy: Identification of topological order in non-Abelian fractional quantum Hall effect states", *Phys. Rev. Lett.* **101** (2008), article no. 010504.

[32] X.-G. Wen, "Quantum orders and symmetric spin liquids", *Phys. Rev. B* **65** (2002), article no. 165113.

[33] X.-G. Wen, *Quantum Field Theory of Many-body Systems*, South Asia edition, Oxford University Press: New Delhi, 2004. Includes bibliographical references and index.

[34] M. Oshikawa and T. Senthil, "Fractionalization, topological order, and quasiparticle statistics", *Phys. Rev. Lett.* **96** (2006), article no. 060601.

[35] V. Kalmeyer and R. B. Laughlin, "Equivalence of the resonating-valence-bond and fractional quantum Hall states", *Phys. Rev. Lett.* **59** (1987), pp. 2095–2098.

[36] T. S. Cubitt, D. Perez-Garcia and M. M. Wolf, "Undecidability of the spectral gap", *Nature* **528** (2015), no. 7581, pp. 207–211.

[37] E. Lieb, T. Schultz and D. Mattis, "Two soluble models of an antiferromagnetic chain", *Ann. Phys.* **16** (1961), no. 3, pp. 407–466.

[38] M. Oshikawa, "Commensurability, excitation gap, and topology in quantum many-particle systems on a periodic lattice", *Phys. Rev. Lett.* **84** (2000), pp. 1535–1538.

[39] M. B. Hastings, "Lieb–Schultz–Mattis in higher dimensions", *Phys. Rev. B* **69** (2004), no. 10, article no. 104431.

[40] C. Liu and W. Ye, *Crystallography, group cohomology, and Lieb–Schultz–Mattis constraints*, preprint, 2024, 2410.03607.

[41] S. A. Parameswaran, A. M. Turner, D. P. Arovas and A. Vishwanath, "Topological order and absence of band insulators at integer filling in non-symmorphic crystals", *Nat. Phys.* **9** (2013), no. 5, pp. 299–303.

[42] H. C. Po, H. Watanabe, C.-M. Jian and M. P. Zaletel, "Lattice homotopy constraints on phases of quantum magnets", *Phys. Rev. Lett.* **119** (2017), article no. 127202.

[43] W. Ye, M. Guo, Y.-C. He, C. Wang and L. Zou, "Topological characterization of Lieb–Schultz–Mattis constraints and applications to symmetry-enriched quantum criticality", *SciPost Phys.* **13** (2022), article no. 066.
[44] S. A. Parameswaran, I. Kimchi, A. M. Turner, D. M. Stamper-Kurn and A. Vishwanath, "Wannier permanent wave functions for featureless bosonic Mott insulators on the 1/3-filled Kagome lattice", *Phys. Rev. Lett.* **110** (2013), article no. 125301.
[45] I. Kimchi, S. A. Parameswaran, A. M. Turner, F. Wang and A. Vishwanath, "Featureless and nonfractionalized Mott insulators on the honeycomb lattice at 1/2 site filling", *Proc. Natl. Acad. Sci. USA* **110** (2013), no. 41, pp. 16378–16383.
[46] P. Kim, H. Lee, S. Jiang, B. Ware, C.-M. Jian, M. Zaletel, J. H. Han and Y. Ran, "Featureless quantum insulator on the honeycomb lattice", *Phys. Rev. B* **94** (2016), article no. 064432.
[47] P. A. Lee, N. Nagaosa and X.-G. Wen, "Doping a Mott insulator: Physics of high-temperature superconductivity", *Rev. Mod. Phys.* **78** (2006), pp. 17–85.
[48] M. C. Gutzwiller, "Effect of correlation on the ferromagnetism of transition metals", *Phys. Rev. Lett.* **10** (1963), pp. 159–162.
[49] L. Messio, C. Lhuillier and G. Misguich, "Time reversal symmetry breaking chiral spin liquids: Projective symmetry group approach of bosonic mean-field theories", *Phys. Rev. B* **87** (2013), article no. 125127.
[50] S. Bieri, C. Lhuillier and L. Messio, "Projective symmetry group classification of chiral spin liquids", *Phys. Rev. B* **93** (2016), article no. 094437.
[51] A. M. Polyakov, "Quark confinement and topology of gauge theories", *Nuclear Phys. B* **120** (1977), no. 3, pp. 429–458.
[52] M. Hermele, T. Senthil, M. P. A. Fisher, P. A. Lee, N. Nagaosa and X.-G. Wen, "Stability of $U(1)$ spin liquids in two dimensions", *Phys. Rev. B* **70** (2004), article no. 214437.
[53] M. Barkeshli, P. Bonderson, M. Cheng and Z. Wang, "Symmetry fractionalization, defects, and gauging of topological phases", *Phys. Rev. B* **100** (2019), article no. 115147.
[54] A. M. Essin and M. Hermele, "Classifying fractionalization: Symmetry classification of gapped $\mathbb{Z}_2$ spin liquids in two dimensions", *Phys. Rev. B* **87** (2013), article no. 104406.
[55] A. Chauhan, A. Maity, C. Liu, J. Sonnenschein, F. Ferrari and Y. Iqbal, "Quantum spin liquids on the diamond lattice", *Phys. Rev. B* **108** (2023), article no. 134424.
[56] F. D. M. Haldane, "Exact Jastrow-Gutzwiller resonating-valence-bond ground state of the spin-$\frac{1}{2}$ antiferromagnetic Heisenberg chain with $1/r^2$ exchange", *Phys. Rev. Lett.* **60** (1988), pp. 635–638.
[57] I. Affleck, T. Kennedy, E. H. Lieb and H. Tasaki, "Rigorous results on valence-bond ground states in antiferromagnets", *Phys. Rev. Lett.* **59** (1987), no. 7, pp. 799–802.
[58] F. Pollmann, E. Berg, A. M. Turner and M. Oshikawa, "Symmetry protection of topological phases in one-dimensional quantum spin systems", *Phys. Rev. B* **85** (2012), article no. 075125.
[59] M. Lemm, A. W. Sandvik and L. Wang, "Existence of a spectral gap in the Affleck–Kennedy–Lieb–Tasaki model on the hexagonal lattice", *Phys. Rev. Lett.* **124** (2020), article no. 177204.
[60] X. Chen, Z.-X. Liu and X.-G. Wen, "Two-dimensional symmetry-protected topological orders and their protected gapless edge excitations", *Phys. Rev. B* **84** (2011), article no. 235141.
[61] C. K. Majumdar and D. K. Ghosh, "On next-nearest-neighbor interaction in linear chain. I", *J. Math. Phys.* **10** (1969), no. 8, pp. 1388–1398.
[62] J. B. Fouet, P. Sindzingre and C. Lhuillier, "An investigation of the quantum J_1–J_2–J_3 model on the honeycomb lattice", *Eur. Phys. J. B* **20** (2001), pp. 241–254.
[63] J.-B. Fouet, M. Mambrini, P. Sindzingre and C. Lhuillier, "Planar pyrochlore: A valence-bond crystal", *Phys. Rev. B* **67** (2003), article no. 054411.
[64] J. Schulenburg, A. Honecker, J. Schnack, J. Richter and H.-J. Schmidt, "Macroscopic magnetization jumps due to independent magnons in frustrated quantum spin lattices", *Phys. Rev. Lett.* **88** (2002), article no. 167207.
[65] S. Capponi, O. Derzhko, A. Honecker, A. M. Läuchli and J. Richter, "Numerical study of magnetization plateaus in the spin-$\frac{1}{2}$ kagome Heisenberg antiferromagnet", *Phys. Rev. B* **88** (2013), article no. 144416.
[66] X. G. Wen, "Mean-field theory of spin-liquid states with finite energy gap and topological orders", *Phys. Rev. B* **44** (1991), pp. 2664–2672.
[67] M. Levin and X.-G. Wen, "Detecting topological order in a ground state wave function", *Phys. Rev. Lett.* **96** (2006), article no. 110405.
[68] A. Kitaev and J. Preskill, "Topological entanglement entropy", *Phys. Rev. Lett.* **96** (2006), article no. 110404.
[69] A. Y. Kitaev, "Fault-tolerant quantum computation by anyons", *Ann. Phys.* **303** (2003), no. 1, pp. 2–30.
[70] A. Kitaev, "Anyons in an exactly solved model and beyond", *Ann. Phys.* **321** (2006), no. 1, pp. 2–111.
[71] M. A. Levin and X.-G. Wen, "String-net condensation: A physical mechanism for topological phases", *Phys. Rev. B* **71** (2005), article no. 045110.
[72] D. S. Rokhsar and S. A. Kivelson, "Superconductivity and the quantum hard-core dimer gas", *Phys. Rev. Lett.* **61** (1988), pp. 2376–2379.

[73] R. Moessner and S. L. Sondhi, "Resonating valence bond phase in the triangular lattice quantum dimer model", *Phys. Rev. Lett.* **86** (2001), pp. 1881–1884.

[74] L. Balents, M. P. A. Fisher and S. M. Girvin, "Fractionalization in an easy-axis Kagome antiferromagnet", *Phys. Rev. B* **65** (2002), article no. 224412.

[75] D. N. Sheng and L. Balents, "Numerical evidences of fractionalization in an easy-axis two-spin Heisenberg antiferromagnet", *Phys. Rev. Lett.* **94** (2005), article no. 146805.

[76] M. S. Block, J. D'Emidio and R. K. Kaul, "Kagome model for a $\mathbb{Z}_2$ quantum spin liquid", *Phys. Rev. B* **101** (2020), article no. 020402.

[77] K. S. Raman, R. Moessner and S. L. Sondhi, "SU(2)-invariant spin-$\frac{1}{2}$ Hamiltonians with resonating and other valence bond phases", *Phys. Rev. B* **72** (2005), article no. 064413.

[78] J. Cano and P. Fendley, "Spin Hamiltonians with resonating-valence-bond ground states", *Phys. Rev. Lett.* **105** (2010), article no. 067205.

[79] M. Mambrini, S. Capponi and F. Alet, "Engineering SU(2) invariant spin models to mimic quantum dimer physics on the square lattice", *Phys. Rev. B* **92** (2015), article no. 134413.

[80] B. Bauer, L. Cincio, B. P. Keller, M. Dolfi, G. Vidal, S. Trebst and A. W. W. Ludwig, "Chiral spin liquid and emergent anyons in a Kagome lattice Mott insulator", *Nat. Commun.* **5** (2014), no. 1, article no. 5137.

[81] S.-S. Gong, W. Zhu and D. N. Sheng, "Emergent chiral spin liquid: Fractional quantum Hall effect in a Kagome Heisenberg model", *Sci. Rep.* **4** (2014), no. 1, article no. 6317.

[82] Y.-C. He, D. N. Sheng and Y. Chen, "Chiral spin liquid in a frustrated anisotropic Kagome Heisenberg model", *Phys. Rev. Lett.* **112** (2014), article no. 137202.

[83] S.-S. Gong, W. Zhu, L. Balents and D. N. Sheng, "Global phase diagram of competing ordered and quantum spin-liquid phases on the kagome lattice", *Phys. Rev. B* **91** (2015), article no. 075112.

[84] A. Wietek and A. M. Läuchli, "Chiral spin liquid and quantum criticality in extended $S = \frac{1}{2}$ Heisenberg models on the triangular lattice", *Phys. Rev. B* **95** (2017), article no. 035141.

[85] A. Szasz, J. Motruk, M. P. Zaletel and J. E. Moore, "Chiral spin liquid phase of the triangular lattice Hubbard model: A density matrix renormalization group study", *Phys. Rev. X* **10** (2020), article no. 021042.

[86] D. F. Schroeter, E. Kapit, R. Thomale and M. Greiter, "Spin Hamiltonian for which the chiral spin liquid is the exact ground state", *Phys. Rev. Lett.* **99** (2007), article no. 097202.

[87] A. E. B. Nielsen, G. Sierra and J. I. Cirac, "Local models of fractional quantum Hall states in lattices and physical implementation", *Nat. Commun.* **4** (2013), no. 1, article no. 2864.

[88] J.-Y. Chen, L. Vanderstraeten, S. Capponi and D. Poilblanc, "Non-Abelian chiral spin liquid in a quantum antiferromagnet revealed by an iPEPS study", *Phys. Rev. B* **98** (2018), article no. 184409.

[89] Z.-X. Liu, H.-H. Tu, Y.-H. Wu, R.-Q. He, X.-J. Liu, Y. Zhou and T.-K. Ng, "Non-Abelian $S = 1$ chiral spin liquid on the kagome lattice", *Phys. Rev. B* **97** (2018), article no. 195158.

[90] W.-W. Luo, Y. Huang, D. N. Sheng and W. Zhu, "Global quantum phase diagram and non-Abelian chiral spin liquid in a spin-$\frac{3}{2}$ square-lattice antiferromagnet", *Phys. Rev. B* **108** (2023), article no. 035130.

[91] J.-Y. Chen, J.-W. Li, P. Nataf, et al., "Abelian SU$(N)_1$ chiral spin liquids on the square lattice", *Phys. Rev. B* **104** (2021), article no. 235104.

[92] Z. Zhu, I. Kimchi, D. N. Sheng and L. Fu, "Robust non-Abelian spin liquid and a possible intermediate phase in the antiferromagnetic Kitaev model with magnetic field", *Phys. Rev. B* **97** (2018), article no. 241110.

[93] H. Yao and S. A. Kivelson, "Exact chiral spin liquid with non-Abelian anyons", *Phys. Rev. Lett.* **99** (2007), article no. 247203.

[94] Y. Iqbal, W.-J. Hu, R. Thomale, D. Poilblanc and F. Becca, "Spin liquid nature in the Heisenberg J_1–J_2 triangular antiferromagnet", *Phys. Rev. B* **93** (2016), article no. 144411.

[95] S. Hu, W. Zhu, S. Eggert and Y.-C. He, "Dirac spin liquid on the spin-1/2 triangular Heisenberg antiferromagnet", *Phys. Rev. Lett.* **123** (2019), article no. 207203.

[96] X.-Y. Song, Y.-C. He, A. Vishwanath and C. Wang, "From spinon band topology to the symmetry quantum numbers of monopoles in dirac spin liquids", *Phys. Rev. X* **10** (2020), article no. 011033.

[97] A. Wietek, S. Capponi and A. M. Läuchli, "Quantum electrodynamics in 2 + 1 dimensions as the organizing principle of a triangular lattice antiferromagnet", *Phys. Rev. X* **14** (2024), article no. 021010.

[98] M. J. P. Gingras and P. A. McClarty, "Quantum spin ice: a search for gapless quantum spin liquids in pyrochlore magnets", *Rep. Prog. Phys.* **77** (2014), no. 5, article no. 056501.

[99] W.-J. Hu, F. Becca, A. Parola and S. Sorella, "Direct evidence for a gapless Z_2 spin liquid by frustrating Néel antiferromagnetism", *Phys. Rev. B* **88** (2013), article no. 060402.

[100] J. Yang, A. W. Sandvik and L. Wang, "Quantum criticality and spin liquid phase in the Shastry–Sutherland model", *Phys. Rev. B* **105** (2022), article no. L060409.

[101] L. L. Viteritti, R. Rende, A. Parola, S. Goldt and F. Becca, *Transformer wave function for the Shastry–Sutherland model: emergence of a spin-liquid phase*, preprint, 2024, 2311.16889.

[102] R. V. Mishmash, J. R. Garrison, S. Bieri and C. Xu, "Theory of a competitive spin liquid state for weak Mott insulators on the triangular lattice", *Phys. Rev. Lett.* **111** (2013), article no. 157203.

[103] B. S. Shastry, "Exact solution of an $S = 1/2$ Heisenberg antiferromagnetic chain with long-ranged interactions", *Phys. Rev. Lett.* **60** (1988), pp. 639–642.

[104] O. I. Motrunich, "Variational study of triangular lattice spin-1/2 model with ring exchanges and spin liquid state in κ–$(ET)_2Cu_2(CN)_3$", *Phys. Rev. B* **72** (2005), article no. 045105.

[105] A. F. Albuquerque and F. Alet, "Critical correlations for short-range valence-bond wave functions on the square lattice", *Phys. Rev. B* **82** (2010), article no. 180408.

[106] Y. Tang, A. W. Sandvik and C. L. Henley, "Properties of resonating-valence-bond spin liquids and critical dimer models", *Phys. Rev. B* **84** (2011), article no. 174427.

[107] M. Hermele, M. P. A. Fisher and L. Balents, "Pyrochlore photons: The U(1) spin liquid in a $S = (1/2)$ three-dimensional frustrated magnet", *Phys. Rev. B* **69** (2004), no. 6, article no. 064404.

[108] N. Seiberg and S.-H. Shao, "Exotic $\mathbb{Z}_N$ symmetries, duality, and fractons in 3 + 1-dimensional quantum field theory", *SciPost Phys.* **10** (2021), article no. 003.

[109] J. Rehn, A. Sen and R. Moessner, "Fractionalized $\mathbb{Z}_2$ classical Heisenberg spin liquids", *Phys. Rev. Lett.* **118** (2017), article no. 047201.

[110] T. Senthil, "Deconfined quantum critical points: a review", in *50 Years of the Renormalization Group, Dedicated to the Memory of Michael E. Fisher*, World Scientific: Singapore, 2024.

[111] J. Takahashi, H. Shao, B. Zhao, W. Guo and A. W. Sandvik, *SO(5) multicriticality in two-dimensional quantum magnets*, preprint, 2024, 2405.06607.

[112] L. Zou, Y.-C. He and C. Wang, "Stiefel liquids: Possible non-Lagrangian quantum criticality from intertwined orders", *Phys. Rev. X* **11** (2021), article no. 031043.

ACADÉMIE DES SCIENCES
INSTITUT DE FRANCE

Comptes Rendus. Physique
2025, Vol. 26, p. 483-514
https://doi.org/10.5802/crphys.254

Intervention in a conference / *Intervention en colloque*

Effects of spin–orbit coupling and Rabi fields in Tomonaga–Luttinger liquids: current status and open questions

Effets du couplage spin-orbite et des champs de Rabi dans les liquides de Tomonaga-Luttinger : état de l'art et questions ouvertes

Xiaoyong Zhang [*,a] **and Carlos A. R. Sá de Melo** [a]

[a] School of Physics, Georgia Institute of Technology, Atlanta, GA 30332, USA

E-mails: xzhang840@gatech.edu (X. Zhang), carlos.sademelo@physics.gatech.edu (C. A. R. Sá de Melo)

Abstract. We discuss the effects of spin–orbit coupling and Rabi fields in Tomonaga–Luttinger liquids for SU(2) and SU(3) Fermi systems. In the SU(2) case, we show that spin–orbit coupling and Rabi fields mix separated spin and charge excitations producing helical massless bosons, which we call Weyl bosons in analogy to their cousins, the Weyl fermions. We discuss the phase diagram and the velocities of bosonic modes, showing where different flavors of Weyl bosons emerge. We suggest that the dispersion and helicity of Weyl bosons can be detected through measurements of the the dynamical structure factor tensor. In the SU(3) case, we preliminarily discuss the effects of spin–orbit coupling and Rabi fields, and conjecture that the emergent collective modes have a scalar (charge), vector (spin) and tensor (quadrupolar) components, suggesting that these modes are more complex than Weyl bosons. To describe spin–orbit coupling, we use the terminology color-orbit coupling, where the three internal states are labeled as colors Red, Green and Blue. We discuss the phase diagram and velocities of boson modes in the non-interacting regime and ponder over several open questions that need to be addressed for SU(3) systems. Lastly, we make some concluding remarks and suggest potential experimental candidates, with two and three internal states, where spin–orbit or color-orbit coupling and Rabi fields could be used to investigate the emergence of unusual collective modes with scalar, vector and tensor properties.

Résumé. Nous étudions les effets du couplage spin-orbite et des champs de Rabi dans les liquides de Tomonaga-Luttinger pour les systèmes de fermions de symétrie SU(2) ou SU(3). Dans le cas d'une symétrie SU(2), nous montrons que le couplage spin-orbite et les champs de Rabi mélangent les excitations de spin et de charge — autrement séparées — en produisant des bosons hélicoïdaux sans masse, que nous appelons bosons de Weyl par analogie avec leurs cousins, les fermions de Weyl. Nous déterminons le diagramme de phase et les vitesses des modes bosoniques, en précisant dans quels secteurs émergent les différents types de bosons de Weyl. Nous proposons d'extraire la relation de dispersion et l'hélicité des bosons de Weyl de mesures du facteur de structure dynamique tensoriel. Dans le cas d'une symétrie SU(3), nous effectuons une première analyse des effets du couplage spin-orbite et des champs de Rabi, et conjecturons que les modes collectifs émergents ont une composante scalaire (charge), vectorielle (spin) et tensorielle (quadripolaire), ce qui suggère que ces modes sont plus complexes que les bosons de Weyl. Pour décrire le couplage spin-orbite, nous utilisons la notion de couplage couleur-orbite, où les trois états internes sont repérés par les couleurs rouge, verte et bleue. Nous discutons du diagramme de phase et des vitesses des modes de bosons

* Corresponding author

dans le régime sans interaction et réfléchissons à plusieurs questions ouvertes restant à traiter dans les systèmes de symétrie SU(3). Enfin, nous formulons quelques remarques finales et identifions des systèmes expérimentaux, à deux ou à trois états internes, dans lesquels le couplage spin-orbite ou couleur-orbite et les champs de Rabi pourraient être utilisés pour étudier l'émergence de modes collectifs inhabituels avec des propriétés scalaires, vectorielles et tensorielles.

Keywords. Spin–orbit coupling, Color-orbit coupling, Rabi fields, Tomonaga–Luttinger liquids, Weyl bosons, Interacting fermions, One dimension.

Mots-clés. Couplage spin-orbite, Couplage couleur-orbite, Champs de Rabi, Liquides de Tomonaga-Luttinger, Bosons de Weyl, Fermions en interaction, Systèmes unidimensionnels.

Manuscript received 11 January 2025, revised 2 June 2025, accepted 16 June 2025.

1. Introduction

While spin and charge are intrinsic properties of elementary particles, in one dimension (1D), interactions are responsible for the separation of spin and charge leading to spin-density (SDW) and charge-density (CDW) waves that propagate with different velocities. Spin–charge separation is theoretically described by the Tomonaga–Luttinger liquid model [1–6] in condensed matter physics (CMP), but is regarded as a general phenomenon of a large variety of quantum fields: non-Abelian Yang–Mills theory describing knotted strings as stable solitons [7–9], supersymmetric gauge theory characterizing magnetic superconductors [10], and quark-lepton unification theory suggesting the similarity between spinons and neutrinos [11]. A few experiments in condensed matter have claimed observing spin–charge separation: angle-resolved photoemission in $SrCuO_2$ [12,13] and tunneling spectroscopy in GaAs/AlGaAs heterostructures [14,15] at low temperatures. Very recently, spin–charge separation was also observed in ultracold gases (^{6}Li) as a function of interactions and temperature [16,17]. A major experimental advantage of ultracold gases over condensed matter and high energy systems is the tunability of interactions, temperature, density and external fields, permitting for a thorough exploration of spin–charge separation and mixing [16,17]. This tunability potentially allows for investigations of the interplay between spin and charge degrees of freedom in unprecedented ways like, for instance, as a function of synthetic spin–orbit coupling, Rabi (spin-flip) fields, density or chemical potential.

In CMP, spin–orbit coupling (SOC) is a relativistic quantum mechanical effect that entangles the spin of a particle to its spatial degrees of freedom. SOC plays an important role in spin-Hall systems [18,19], topological insulators [20,21] and superconductors [22–24]. However, tunability of SOC, spin-flip fields, density or chemical potential is limited. There are two common types of SOC: the Rashba [25] and the Dresselhaus [26] terms, that have been discussed in the context of semiconductors [27–32]. In ultracold atoms, SOC is synthetically created using two-photon Raman transitions instead of originating from relativistic effects [33,34]. This makes SOC tunable in bosonic [35–37] and fermionic [38–40] quantum gases, where equal mixtures of Rashba and Dresselhaus (ERD) terms have been created [35], as well as, Rashba-only (RO) [41–43]. Furthermore, Dresselhaus-only (DO) and arbitrary mixtures of Rashba and Dresselhaus terms have also been suggested [44].

In particle physics, all known elementary particles obey Pauli's spin-statistics theorem, that is, particles are either fermions with half-integer spins or bosons with integer spins [45]. The Standard Model is the theory that unifies electromagnetic, weak and strong interactions, by invoking the existence of one scalar boson (Higgs), four vector bosons (gluon, photon, Z and W), and twelve elementary fermions (six leptons and six quarks) [46,47]. All the currently known elementary fermions have spin $s = 1/2$ and can be of three types at most: Dirac, Majorana or Weyl fermions. The first type are Dirac fermions, which are massive and charged, reflecting

the existence of particles and anti-particles, like the electron and the positron [48]. The second type are Majorana fermions, which are also massive but neutral, such that the particle is also its own antiparticle [49]. The third type are Weyl fermions, which are massless Dirac fermions that become helical, as found by Weyl [50]. None of elementary Fermi particles described in the Standard Model are Weyl fermions.

In condensed matter physics, observations of Majorana fermions have been retracted [51], but there are reports that quasiparticles behave as Dirac or Weyl fermions in solid state materials. Dirac fermions emerge in cuprate superconductors [52,53], iron-based superconductors [54–56] and graphene [57]. Weyl fermions arise in the electronic structure of TaAs crystals [58,59] which do not have inversion centers and are detected as noninteracting quasiparticles via angular-resolved photoemission spectroscopy.

In solid-state condensed matter systems, one often relies on chance to discover materials with unusual properties. In ultracold atoms, however, it is common to simulate Hamiltonians found in condensed matter and particle physics, but it is also possible to design Hamiltonians possessing collective excitations or quasiparticles that go beyond those existing in standard models of condensed matter on in the Standard Model of particle physics. For example, it is possible to prepare bosonic atoms with two internal spin states creating pseudo-spin-1/2 bosons [35,37] or fermionic atoms with three internal spin states, producing pseudo-spin-1 fermions [60,61]. It is also possible to adjust the interactions of these atoms from weak (or zero) to strong using Feshbach resonances [62].

In this article, we discuss the emergence of collective modes in interacting Fermi systems that we call Weyl bosons: massless pseudospin-1/2 helical particles like Weyl fermions that arise in relativistic field theories of spin-1/2 fermions. From a more general perspective, these new types of excitations are potentially interesting, because they provide unconventional extensions of ideas that exist in the Standard Model of particle physics. In principle, Weyl bosons emerge in Fermi systems in one (1D), two (2D) and three (3D) dimensions, as a result of the existence of spin–orbit coupling, synthetic or real, and Rabi or Zeeman fields. However, we confine ourselves to the 1D case, where exact calculations can be performed in the long-wavelength-low-energy regime using the bosonization method. We discuss the creation of Weyl bosons for SU(2) (two internal states) when SOC and Rabi fields are active and conjecture the emergence of more exotic bosons, with a tensor structure, in SU(3) (three internal states) interacting Fermi systems, when color-orbit coupling and color-flip fields are present.

To explore the effects of SOC and Rabi fields on spin and charge density modes and their evolution into spin–charge-mixed helical collective modes (Weyl bosons) for SU(2) Fermi systems, as well as to investigate more exotic bosonic collective modes in SU(3) Fermi systems, we organize the remainder of this paper as follows. In Section 2, we discuss conventional spin–orbit coupling in condensed matter and synthetic spin–orbit coupling in ultracold atoms. In Section 3, we review briefly some aspects of spin–charge separation, in 1D for spin-1/2 Fermi systems, within the Tomonaga–Luttinger description, discuss bosonization in the condensed matter context, and mention some open questions that remain in this area. In Section 4, we describe SU(2) fermions with two internal states. We explore how spin and charge recombine in the presence of SOC and Rabi fields producing Weyl bosons with a maximum of two flavors, highlight experimental challenges in detecting such exotic modes in ^{6}Li, ^{40}K and ^{173}Yb via charge–charge, spin–charge and spin–spin dynamical structure factors [16,17,63,64] and discuss some open questions. In Section 5, we describe SU(3) fermions with three internal states (colors). We analyze the collective modes and their quadrupolar tensor structure in the presence of color-orbit coupling and color Rabi fields. We discuss open questions regarding the effects of SU(3) interactions, and possible experimental signatures of the emergent tensor boson modes in ^{173}Yb and ^{87}Sr. In Section 6, we present some conclusions and discuss possible theoretical and experimental outlooks.

We warn the reader that technical details, tedious derivations, and lengthy expressions are not shown in this article. We rather just outline how results are obtained and illustrate their consequences through figures. Furthermore, we set $\hbar = 1$ throughout the manuscript.

2. Synthetic spin–orbit coupling in quantum gases

Synthetic spin–orbit coupling (SOC) in quantum gases is a rapidly advancing field that merges the precise controllability of ultracold atomic systems with phenomena traditionally associated with condensed matter physics. Standard spin–orbit coupling, due to relativistic effects, plays a pivotal role in various quantum phenomena, including topological insulators, quantum spin-Hall materials, and spintronic systems [18]. In ultracold atomic gases, synthetic SOC refers to the coupling between the spin (pseudo-spin or internal state) of a particle and its center-of-mass motion, usually created via counter-propagating Raman beams. Given that SOC in cold atoms is artificially created [35,65], its highly tunable environment potentially allows for the exploration of complex quantum phases and topological states.

2.1. *Typical Hamiltonian*

For a particle of mass m and two internal states (spin 1/2), the Hamiltonian is

$$\hat{H}_1 = \frac{\hat{\mathbf{k}}^2}{2m} I + \hat{H}_{\rm SOC}, \tag{1}$$

where $\hat{\mathbf{k}}$ is the momentum operator, I is the identity matrix, and $H_{\rm SOC}$ is the spin–orbit coupling. An external potential $V_{\rm ext}(\mathbf{r})$ can also be present due to the underlying lattice structure for condensed matter systems or due to harmonic, box or optical lattice confinement for ultracold atoms. However, since we focus on the effects of spin–orbit coupling, for the reminder of our discussion, we describe only the continuum regime, where the external potential is not considered.

In the context of cold atoms, there are two types of SOC that are of general interest: the Rashba and the Dresselhaus terms. Both types of coupling were first studied in solid state materials that lack inversion symmetry and were realized synthetically in ultracold atomic systems.

In solid state materials, the Rashba SOC originates from structural inversion asymmetry, which refers to the lack of inversion symmetry due to the external constraint on the material rather than its intrinsic crystal lattice. The constraint is typically a surface or interface. At these locations, the structural asymmetry creates an effective electric field $\mathbf{E} = \mathrm{E}\mathbf{e_z}$, perpendicular to the surface/interface, which causes inversion symmetry to be broken along the z-axis (normal to the surface/interface). Due to relativistic effects, this electric field generates an effective magnetic field $\mathbf{B} = -\mathbf{k} \times \mathbf{E}/mc^2$, in SI units, at the rest frame of electrons. The $\mathbf{B}$ field couples with the spin of electrons through the Zeeman coupling $-\boldsymbol{\mu} \cdot \mathbf{B}$, where $\boldsymbol{\mu}$ is the magnetic moment, and results in the Rashba SOC Hamiltonian

$$\hat{H}_{\rm R} = \alpha_{\rm R}(\hat{\mathbf{k}} \times \mathbf{e}_z) \cdot \boldsymbol{\sigma} = \alpha_{\rm R}(\hat{k}_y \sigma_x - \hat{k}_x \sigma_y), \tag{2}$$

where $\alpha_{\rm R}$ is the Rashba coupling constant, and the electron momentum $\mathbf{k}$ in $\mathbf{B}$ is promoted to the operator $\hat{\mathbf{k}}$. As seen in Equation (2), the linear coupling between momentum and spin of electrons lifts the momentum degeneracy when $\hat{\mathbf{k}} \to -\hat{\mathbf{k}}$ in the Hamiltonian of Equation (1) using $\hat{H}_{\rm SOC} = \hat{H}_{\rm R}$.

In contrast, for solid state materials, the Dresselhaus SOC arises from bulk inversion asymmetry inherent in certain crystal lattices, particularly those lacking a center of inversion, such as zinc-blende structures (e.g., GaAs, InAs). In these materials, the SOC Hamiltonian is constrained

by the T_d (achiral tetrahedral) symmetry of the crystal, such that, close to the Γ point of the Brillouin zone, $\hat{H}_{\rm SOC}$ takes the following form

$$\hat{H}_{\rm D} = \gamma[\hat{k}_x(\hat{k}_y^2 - \hat{k}_z^2)\sigma_x + \hat{k}_y(\hat{k}_z^2 - \hat{k}_x^2)\sigma_y + \hat{k}_z(\hat{k}_x^2 - \hat{k}_y^2)\sigma_z], \tag{3}$$

where γ is the Dresselhaus coupling constant, which is determined by the material's band structure. For a two-dimensional electron gas in the xy plane, where $\langle \hat{k}_z \rangle = 0$ and $\langle \hat{k}_z^2 \rangle \neq 0$, the Dresselhaus Hamiltonian can be separated into a linear term

$$\hat{H}_{\rm D}^{(1)} = \beta_{\rm D}(\hat{k}_x\sigma_x - \hat{k}_y\sigma_y), \tag{4}$$

where $\beta_{\rm D} = -\gamma\langle \hat{k}_z^2 \rangle$ is the effective Dresselhaus coupling constant, and a cubic term

$$\hat{H}_{\rm D}^{(3)} = \gamma(\hat{k}_x\hat{k}_y^2\sigma_x - \hat{k}_y\hat{k}_x^2\sigma_y). \tag{5}$$

In the low-momentum regime, only the linear term is generally considered, because it is typically orders of magnitude larger than the cubic term. In the remainder of this article, the linear Dresselhaus Hamiltonian $\hat{H}_{\rm D}^{(1)}$ is referred to as $\hat{H}_{\rm D}$ without the cubic contribution.

A more general case in solid state materials includes both Rashba and Dresselhaus SOC leading to

$$\hat{H}_{\rm SOC} = \alpha_{\rm R}(\sigma_x\hat{k}_y - \sigma_y\hat{k}_x) + \beta_{\rm D}(\hat{k}_x\sigma_x - \hat{k}_y\sigma_y). \tag{6}$$

The special case of equal Rashba and Dresselhaus (ERD) SOC, that is, $\alpha_{\rm R} = \beta_{\rm D} = \alpha$, leads to

$$\hat{H}_{\rm ERD} = \alpha(\hat{k}_x + \hat{k}_y)(\sigma_x - \sigma_y). \tag{7}$$

A global unitary SU(2) rotation $U = I/\sqrt{2} + {\rm i}(\sigma_x + \sigma_y)/2$, where I is the identity matrix, brings the Hamiltonian to $\hat{H}_{\rm ERD} = -2\alpha\hat{k}_+\sigma_z$, where $\hat{k}_+ = (\hat{k}_x + \hat{k}_y)/\sqrt{2}$. In 1D systems, $\hat{k}_+ = \hat{k}_x/\sqrt{2}$, giving

$$\hat{H}_{\rm ERD} = -\sqrt{2}\alpha\hat{k}_x\sigma_z. \tag{8}$$

The ERD Hamiltonian has been synthesized in ultracold atomic systems [35,65], and are briefly reviewed next.

2.2. *Synthetic SOC via Raman coupling*

Using pairs of Raman beams, spin–orbit coupling has been realized in ^{87}Rb Bose–Einstein condensates [35], as well as, in fermionic systems like ^{6}Li [38] and ^{40}K [66]. Heating effects can be substantial in ^{6}Li, but may be manageable in ^{40}K. While most experiments utilize two internal states of the atoms to create an SU(2) SOC, it is also possible to create SOC for atoms with N internal states and SU(N) symmetric interactions like in ^{173}Yb [67,68] and ^{87}Sr [69]. Next, we discuss the experimental realization of SOC in ultracold atoms with two or three internal states, which is relevant for the posterior discussion of systems with SU(2) and SU(3) invariant interactions.

We consider a cloud of ultracold atoms with two internal states labeled as $|\uparrow\rangle$, $|\downarrow\rangle$ and a higher energy excited state $|e\rangle$. Two laser beams with frequencies ω_1, ω_2 and wavevectors $\mathbf{k}_1$, $\mathbf{k}_2$ can couple to the atoms, driving Raman transitions between the pseudo-spin-1/2 states via the excited state $|e\rangle$, as shown in Figure 1(a). The Hamiltonian describing the Raman coupling is

$$\hat{H}_{\rm RC} = -\tfrac{1}{2}[\Omega_1 {\rm e}^{{\rm i}(\mathbf{k}_1\cdot\mathbf{r}-\omega_1 t)}|e\rangle\langle\uparrow| + \Omega_2 {\rm e}^{{\rm i}(\mathbf{k}_2\cdot\mathbf{r}-\omega_2 t)}|e\rangle\langle\downarrow| + {\rm H.c.}], \tag{9}$$

where use the convention $|\uparrow\rangle$ is state $|1\rangle$ (low energy), and $|\downarrow\rangle$ is state $|2\rangle$ (high energy) for the matrix notation of $\hat{H}_{\rm RC}$. Here, Ω_1 and Ω_2 are the Rabi frequencies, taken to be real, $\mathbf{r}$ is the position of the atom, and H.c. denotes Hermitian conjugation. In the experimental setup, the one-photon detuning $|\Delta|$ (the difference between the laser frequencies and the excited state's energy) is large

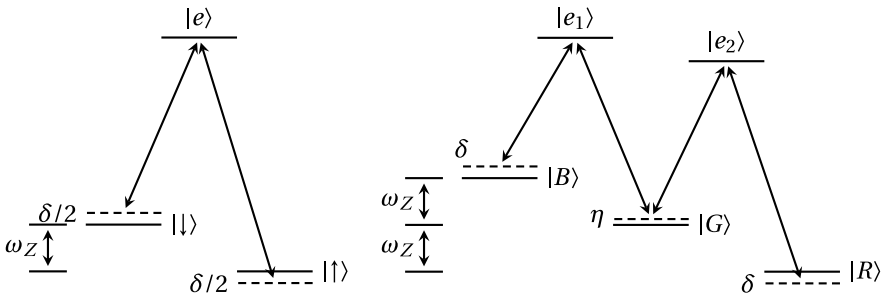

(a) Two levels **(b)** Three levels

Figure 1. Energy level diagrams showing the Raman processes used to synthesize spin–orbit coupling for (a) two-level ($|\uparrow\rangle, |\downarrow\rangle$) and (b) three-level ($|R\rangle, |G\rangle, |B\rangle$) systems. The frequencies ω_Z are Zeeman shifts, δ is the detuning and η is a reference energy, while $|e\rangle, |e_1\rangle$ and $|e_2\rangle$ are intermediate higher-energy states used by the Raman beams.

compared to $|\Omega_1|$ and $|\Omega_2|$, allowing for the the excited state $|e\rangle$ to be adiabatically eliminated [70]. Then, the effective Hamiltonian in the rotating-frame becomes

$$\hat{H}_{\rm RC}^{\rm eff} = \frac{1}{2}\begin{pmatrix} -\delta & \Omega e^{-i2\mathbf{k}_T\cdot\mathbf{r}} \\ \Omega e^{i2\mathbf{k}_T\cdot\mathbf{r}} & \delta \end{pmatrix}, \tag{10}$$

where $\Omega = \Omega_1\Omega_2/2\Delta$ is the effective two-photon Rabi frequency, $\mathbf{k}_T = (\mathbf{k}_1 - \mathbf{k}_2)/2$ is a measure of the momentum transferred to the atoms, $\delta = \omega_Z - \omega$ is the detuning from the Raman transition, ω_Z is the splitting between the two internal states and $\omega = \omega_1 - \omega_2$ is the two-photon detuning.

Using the kinetic energy operator $\hat{H}_{\rm K} = (\hat{\mathbf{k}}^2/2m)I$, where I is the identity matrix, and performing a suitable global SU(2) transformation, leads to the standard Hamiltonian matrix with kinetic, SOC and Rabi/Zeeman terms [35]

$$\hat{H}_{\rm KS} = \frac{(\hat{\mathbf{k}}I - \mathbf{k}_T\sigma_z)^2}{2m} - \frac{\delta}{2}\sigma_z + \frac{\Omega}{2}\sigma_x = \left(\frac{\hat{\mathbf{k}}^2 + \mathbf{k}_T^2}{2m}\right)I - \left(\frac{\mathbf{k}_T}{m}\right)\cdot\hat{\mathbf{k}}\sigma_z - \frac{\delta}{2}\sigma_z + \frac{\Omega}{2}\sigma_x, \tag{11}$$

where $\mathbf{k}_T$ and $-\mathbf{k}_T$ are the momentum transferred to the $|\uparrow\rangle$ and $|\downarrow\rangle$, respectively, and $\{\sigma_x, \sigma_y, \sigma_z\}$ are the Pauli matrices. The second term in Equation (11) explicitly shows the coupling between the momentum operator $\hat{\mathbf{k}}$ and spin matrix σ_z, which corresponds to the ERD SOC introduced in Section 2.1.

Spin–orbit coupling for three internal states can also be created experimentally using a pair of counter-propagating Raman beams, as in ^{87}Rb at the $F = 1$ manifold of a Bose–Einstein condensate (BEC) [71]. A pair of counterpropagating Raman beams along the x-axis with frequencies ω_L and $\omega_L + \delta\omega_L$ are used to create the SOC. These beams couple atomic states $|m_{\rm F}, k_x\rangle$ that differ by one unit of internal angular momentum ($\hbar = 1$). The Zeeman field B_0 is applied along the y-direction to produce the Zeeman shift $\omega_Z = g\mu_B B_0 \approx \delta\omega_L$. Then, the Hamiltonian matrix with kinetic, SOC and Rabi/Zeeman terms is [60,61,70,71]

$$\hat{H}_{\rm KS} = \begin{pmatrix} \frac{(\hat{k}_x - k_T)^2}{2m} + \frac{\hat{\mathbf{k}}_\perp^2}{2m} - \delta & \frac{\Omega_{\rm R}}{2} & 0 \\ \frac{\Omega_{\rm R}}{2} & \frac{\hat{k}_x^2}{2m} + \frac{\hat{\mathbf{k}}_\perp^2}{2m} + \eta & \frac{\Omega_{\rm R}}{2} \\ 0 & \frac{\Omega_{\rm R}}{2} & \frac{(\hat{k}_x + k_T)^2}{2m} + \frac{\hat{\mathbf{k}}_\perp^2}{2m} + \delta \end{pmatrix}, \tag{12}$$

where $\hat{\mathbf{k}}_\perp = (\hat{k}_y, \hat{k}_z)$ is the transverse momentum (yz plane) of the atom, $\Omega_{\rm R}$ is the resonant Rabi frequency, $\delta = \omega_Z - \delta\omega_L$ is the detuning from the Raman resonance, and η is a quadratic Zeeman shift, and $k_T = 2k_{\rm R}$, where $k_{\rm R}$ is the wavenumber (momentum) of each Raman beam, is the

magnitude of the momentum transferred to the lowest and highest energy state. In Figure 1(b), we show the corresponding level diagram.

A similar three-internal-state Hamiltonian with SOC and Rabi fields was used to investigate Fermi liquid properties for pseudo-spin-1 fermions [60] and exotic topological color superfluidity for fermions with SU(3) attractive interactions [61] in three dimensions. However, in this manuscript, we concentrate on the effects of SOC in one dimensional systems for two reasons. First, because we are interested in the emergence of bosonic helical modes (Weyl bosons) for SU(2) Fermi systems with two internal states, where spin and charge are initially separated, and analytical results can be obtained via bosonization. Second, because we are fascinated by the potential realization of tensor bosons for SU(3) Fermi systems with three internal states, where exact results may also obtained, via the bosonization technique, in the low-frequency and long-wavelength regimes. For pedagogical reasons, we discuss first the interacting Fermi gas with two internal spin states in 1D, without SOC and Rabi fields, to introduce the bosonization technique that is later applied to the same system in the presence of SOC and Rabi fields.

3. Spin–charge separation in 1D interacting fermions

In conventional higher-dimensional (2D and 3D) systems, electrons are elementary particles that carry both spin and charge densities that propagate with the same velocity. However, in 1D systems, electron–electron interactions may lead to the decoupling of spin and charge degrees of freedom under certain conditions. This decoupling results in the emergence of separate collective excitations describing charge density and spin density waves that propagate at different velocities. The physics of interacting 1D Fermi gases was explored early on by Tomonaga and Luttinger [1,2], and later developed into the Tomonaga–Luttinger liquid theory, via the development of bosonization techniques [3,72], which became a powerful tool for the discovery of spin–charge separation in 1D Fermi systems. There have been claims of experimental observations of spin–charge separation in semiconductor nanowires and quasi-1D organic conductors [12,73]. More recently, claims of spin–charge separation have also been made in 1D ultracold atomic gases [16]. In this section, we review the basics of the bosonization method, that leads to spin–charge separation in 1D continuum Fermi gases with sufficiently long-ranged interactions.

3.1. *Bosonization and spin–charge separation*

For a comprehensive introduction to bosonization and spin–charge separation in 1D systems, we refer the reader to standard textbooks [4,5]. Consider a 1D Fermi gas with mass m, two spin states and kinetic energy operator

$$\hat{H}_{\rm kin} = \sum_{ks} \frac{k^2}{2m} c_s^\dagger(k) c_s(k), \tag{13}$$

where k is the one-dimensional momentum and s is the spin label. The Fermi surface for a degenerate gas of fermions in 1D consists of points. For sufficient low energies, we linearize the kinetic energy operator around the Fermi points ($\pm k_{\rm F}$) leading to

$$\hat{H}_{\rm kin} = \sum_{ksr} \{E_{\rm F} + {\rm sgn}(r)\, v_{\rm F}[k - {\rm sgn}(r)\, k_{\rm F}]\} c_{sr}^\dagger(k) c_{sr}(k), \tag{14}$$

where $r = \{L, R\}$ represents the linearized band on the left near $-k_{\rm F}$ or on the right near $+k_{\rm F}$, $E_{\rm F} = k_{\rm F}^2/2m$ is the Fermi energy, and $v_{\rm F} = k_{\rm F}/m$ is the Fermi velocity. The function ${\rm sgn}(r)$ gives the sign of the slope and of the corresponding Fermi momentum: ${\rm sgn}(L) = -1$, ${\rm sgn}(R) = +1$. The reference Hamiltonian $\hat{H}_0 = \sum_{ksr} E_{\rm F} c_{sr}^\dagger(k) c_{sr}(k)$, corresponding to the energy $E_0 = N E_{\rm F}$, where N is the total number of fermions, is set to zero without loss of generality. Thus, we drop this reference term from the kinetic energy operator $\hat{H}_{\rm kin}$ from now on.

A typical interaction between the fermions can be modeled as

$$\hat{H}_{\rm int} = \frac{1}{2L_b} \sum_{kk'qss'} V_{ss'}(q) c_s^\dagger(k-q) c_{s'}^\dagger(k'+q) c_{s'}(k') c_s(k), \tag{15}$$

where $V_{ss'}(q)$ is the interaction with real (momentum) space range R_0 ($q_0 = 2\pi/R_0$) and dimensions of energy times length, and L_b is the length of the system. The interaction may have different origins depending on the physics manifested in the system: for example, it can be Coulomb interactions, involving direct and exchange contributions for charged fermions, effective interactions with finite range for charged or neutral fermions, or SU(2) invariant interactions for neutral fermions. In the analysis below the interactions are not too strong, that is, $|V_{s,s'}(q)|/L_b \ll NE_{\rm F}$ for all q. Furthermore, when the range R_0 is sufficiently large, only small momentum transfers q contribute significantly to the interaction Hamiltonian, that is, the terms with $qR_0 \ll 1$ are dominant. Furthermore,large momentum transfers are found to be irrelevant in renormalization group approaches [4,5,74]. Thus, for spin-independent interactions $V_{ss'}(q) = V(q)$, the interaction Hamiltonian acquires, in the long wavelength limits ($q \approx 0$), a density–density form [4,5]

$$\hat{H}_{\rm int} = \frac{1}{2L_b} \sum_{qss'r} \left[g_4 \hat{\rho}_{sr}(q) \hat{\rho}_{s'r}(-q) + g_2 \hat{\rho}_{sr}(q) \hat{\rho}_{s'\bar{r}}(-q) \right], \tag{16}$$

where $\hat{\rho}_{sr}(q) = \sum_k c_{sr}^\dagger(k) c_{sr}(k+q)$ is the Fourier transform of the real-space spin-dependent density operator in branch r. For spin-dependent interactions $V_{ss'}(q)$, the terms $g_2 \to g_{2ss'}(q)$ and $g_4 \to g_{4ss'}(q)$ carry s and s' subscripts and are proportional to $V_{ss'}(q)/2$. Here, g_2 and g_4 have dimensions of energy times length. In Equation (16), the term with coefficient g_4 couples fermions on the same side of the Fermi surface, while the term with coefficient g_2 couples fermions from one side of the Fermi surface with fermions on the other side. Both g_2 and g_4 are small-momentum-transfer ($q \approx 0$) scattering processes. We do not consider large-momentum-transfer ($q \approx 2k_{\rm F}$) terms, called g_1, because the finite-ranged interaction produces $g_1 \ll \min\{g_2, g_4\}$, which also becomes irrelevant from the renormalization group point of view [4,5,74]. In passing, we note that for the Coulomb interaction $g_2 = g_4$ and both terms depend logarithmically in $|q|$ [75], however for a more generic effective finite-ranged interactions $g_2 \to g_2(q \approx 0)$ and $g_4 \to g_4(q \approx 0)$, g_2 also may be different from g_4, a condition used in the discussion below.

To obtain the spin and charge modes, we use the bosonization technique. Boson operators are constructed as [4,5]

$$b_s^\dagger(q) = \sqrt{\frac{2\pi}{|q|L_b}} \Theta(-{\rm sgn}(r)q) \hat{\rho}_{sr}(q), \tag{17}$$

satisfying standard bosonic commutation relations. Here, $\Theta(x)$ is the Heaviside step function. Using these boson operators and defining the momentum $q = k - {\rm sgn}(r)k_{\rm F}$, the kinetic part of the Hamiltonian becomes

$$\hat{H}'_{\rm kin} = \sum_{qs} v_{\rm F}|q| b_s^\dagger(q) b_s(q). \tag{18}$$

This is not exactly the original kinetic energy operator, but is a valid representation of it in the low-momentum limit, due to the commutation relation

$$[\hat{H}_{\rm kin}, b_s(q)] = [\hat{H}'_{\rm kin}, b_s(q)] = -v_{\rm F}|q| b_s(q), \tag{19}$$

that secures the equivalency between $\hat{H}_{\rm kin}$ in the fermionic representation and $\hat{H}'_{\rm kin}$ in the bosonic one. Thus, we use the equivalence between $\hat{H}'_{\rm kin}$ and $\hat{H}_{\rm kin}$, to write the full Hamiltonian $\hat{H} = \hat{H}_{\rm kin} + \hat{H}_{\rm int}$ as a quadratic form of the bosonic operators:

$$\hat{H} = \sum_q \left\{ v_{\rm F}|q| \sum_s b_s^\dagger(q) b_s(q) + |q| \sum_{ss'} \left[\frac{g_4}{4\pi} b_s^\dagger(q) b_{s'}(q) + \frac{g_2}{4\pi} b_s^\dagger(q) b_{s'}^\dagger(-q) + {\rm H.c.} \right] \right\}. \tag{20}$$

Next, we define boson operators in the charge and spin sectors

$$b_\rho^\dagger(q) = \frac{1}{\sqrt{2}}(b_\uparrow^\dagger(q) + b_\downarrow^\dagger(q)) \quad \text{and} \quad b_\sigma^\dagger(q) = \frac{1}{\sqrt{2}}(b_\uparrow^\dagger(q) - b_\downarrow^\dagger(q)), \tag{21}$$

where $b_\rho^\dagger(q)$ creates an excitation in the charge density sector and $b_\sigma^\dagger(q)$ creates an excitation in the spin density sector. In this basis, the Hamiltonian becomes block diagonal in the charge and spin degrees of freedom, that is,

$$\hat{H} = \sum_q \left\{ v_F|q| b_\rho^\dagger(q) b_\rho(q) + |q| \left[\frac{g_4}{2\pi} b_\rho^\dagger(q) b_\rho(q) + \frac{g_2}{2\pi} b_\rho^\dagger(q) b_\rho^\dagger(-q) + \text{H.c.} \right] \right\} + \sum_q v_F|q| b_\sigma^\dagger(q) b_\sigma(q), \tag{22}$$

indicating that spin and charge excitations are already separated. A simple Bogoliubov transformation in the charge sector leads to

$$\hat{H} = \sum_q [v_\rho|q| d_\rho^\dagger(q) d_\rho(q) + v_\sigma|q| d_\sigma^\dagger(q) d_\sigma(q)], \tag{23}$$

where two different velocities arise for the final charge density $d_\rho^\dagger(q)$ and spin density $d_\sigma^\dagger(q)$ excitations:

$$v_\rho = \sqrt{\left(v_F + \frac{g_4}{\pi}\right)^2 - \left(\frac{g_2}{\pi}\right)^2} \quad \text{and} \quad v_\sigma = v_F, \tag{24}$$

with v_ρ (v_σ) being the velocity for charge (spin) excitations. This is the standard result found in textbooks [4,5]. The low-energy Hamiltonian $\hat{H}$, shown in Equation (23), is fully separated into spin and charge excitations that have different propagation speeds. The spin excitation, often called spin density wave (SDW), carries spin current but no charge, while the charge excitation, often called charge density wave (CDW), carries charge current but no spin. This phenomenon is highly non-trivial since the two quantum numbers spin and charge that are both carried by one kind of elementary particle are fully dissociated into two independent excitation (spin and charge) modes. The separation between spin and charge is a peculiarity of one-dimensional systems in the absence of spin–orbit coupling and Zeeman fields, but in the presence of interactions. When the interactions are zero $g_4 = g_2 = 0$, the velocities $v_\rho = v_\sigma = v_F$, that is, spin and charge excitations both travel at the Fermi velocity v_F and thus are not separated. The role played by interactions is crucial in separating charge and spin, that is, in creating $v_\rho \neq v_\sigma$. Although spin–charge separation in 1D is a very old topic, there are still several open questions, which are discussed next.

3.2. *Open questions for spin–charge separation*

Spin–charge separation is a fundamental phenomenon in condensed matter physics, which emerges for one-dimensional systems in the low-energy and long-wavelength regime, when spin–orbit coupling and Zeeman fields are absent. So far, to our knowledge, there is no rigorous proof that spin–charge separation occurs at all energies and wavelengths for arbitrary interaction potentials in 1D. This seems to be the case both for continuum and lattice systems. Furthermore, we are not aware of Bethe-Ansatz-type solutions that prove spin–charge separation for an arbitrary interaction, for either continuum or lattice models in 1D. Therefore, the question "Does spin–charge separation exist for 1D fermions at all energies, wavelengths and arbitrary interaction potentials either in the continuum or in the lattice?" does not seem to have yet a rigorous answer, and thus appears to be an open question[1].

[1] This statement was triggered by a question that Yvan Castin asked, regarding C. A. R. Sá de Melo's presentation at the Institut Henri Poincaré, wondering if spin–charge separation in 1D is only a low-frequency-long-wavelength result or a more general property.

However, based on the Bethe Ansatz, it seems that a rigorous answer to the less general question "Is there spin–charge separation for a zero-ranged potential in the 1D continuum?" is now known theoretically [76]. While, Bethe-Ansatz solutions for the ground state energy for contact (delta function) potential were explored by Yang [77] and Gaudin [78] long ago, it was not until very recently that the charge and spin excitation spectra of such model system were obtained [76]. Not long after these recent theoretical results, experiments claiming the observation of spin–charge separation in ^{6}Li emerged [16], but with some additional harmonic confinement. It would be quite interesting to have experimental measurements of dynamical structure factors in 1D box potentials to further verify the existence of spin and charge density modes propagating with different velocities.

The related question "Is there spin–charge separation for the Hubbard model in the 1D lattice?" appears to be still open. In the Tomonaga–Luttinger regime of the 1D Hubbard model, spin–charge separation is well established [4], and in the limit of $U \to \infty$, a Bethe Ansatz analysis suggests that spin–charge separation remains [79]. However, to our knowledge, there is no Bethe-Ansatz solution that provides the answer to this question for arbitrary U. Nevertheless, there seems to be recent experimental evidence that spin–charge separation occurs in strongly correlated 1D conductors [80], which should stimulate the search for Bethe-Ansatz solutions for arbritary values of $U > 0$ in the 1D Hubbard model.

In the absence of very general results, the separation between spin and charge in 1D was discussed above in the low-energy and long-wavelength regime, for finite ranged interactions, but without spin–orbit coupling and Rabi fields. However, an arbitrary small amount of SOC and Rabi fields couple charge and spin excitations in SU(2) (spin-1/2) and produce more exotic collective modes that we call Weyl bosons, as we discuss next.

4. SU(2) fermions with SOC and Rabi fields

Fermions with two internal states, attractive interactions, SOC and Rabi fields have been studied theoretically in 3D [81–86], as well as in 2D [87,88] both at zero and finite temperatures, where the focus was on superfluid properties. On the experimental side, a few ultracold Fermi systems with SOC were preliminarily explored such as ^{6}Li [38], ^{40}K [89] and ^{173}Yb [39,68]. Here, we discuss fermions with two internal states, repulsive interactions, SOC and Rabi fields in 1D, and make direct connections to spin–charge separation in the absence of spin–orbit and Rabi couplings and to the special mixing of spin and charge when SOC and Rabi fields are present.

Our discussion about spin-1/2 fermions with SOC and Rabi fields in 1D begins from the experimentally realized Hamiltonian matrix in momentum space with kinetic, SOC and Rabi/Zeeman terms discussed in Equation (11) by setting the detuning δ to zero:

$$\hat{H}_{\rm KS} = \epsilon_k I - h_x \sigma_x - h_z(k)\sigma_z. \tag{25}$$

Here, k is the momentum along the real space x direction, $\epsilon_k = (k^2 + k_T^2)/2m$ is the shifted kinetic energy, k_T is the magnitude of the momentum transferred, h_x is the Rabi field, and $h_z(k) = kk_T/m$ is the momentum-dependent Zeeman field representing the SOC. Notice that, for our 1D system, the SOC is the equal Rashba and Dresselhaus (ERD) type discussed in Section 2.1 and shown in Equation (8). In our 1D analysis, we converted the notation used in Equation (11) via the following prescription: $\mathbf{k} \to k\mathbf{e_x}$, $\delta \to 0$, $\Omega/2 \to h_x$, and $\mathbf{k_T}\cdot\mathbf{k}/m \to kk_T/m = h_z(k)$. This notation highlights the role played by h_x and $h_z(k)$ as a uniform Zeeman field along the spin-space x direction and a momentum-dependent Zeeman field along spin-space z direction, respectively.

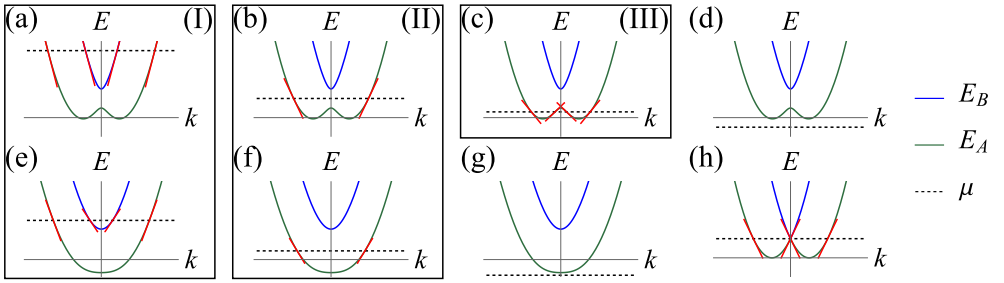

Figure 2. Schematic plots of $E_A(k)$ (green solid line) and $E_B(k)$ (blue solid line) showing effects of SOC (k_T) and Rabi fields (h_x). The red solid lines are linearizations around Fermi points, and the horizontal black dashed lines indicate the chemical potential μ. In panels (a), (b), (c) and (d), $E_A(k)$ has double minima, since $|h_x|/E_T < 2$. In panels (e), (f), and (g), $E_A(k)$ has a single minimum, since $|h_x|/E_T \geq 2$. In panel (h), $h_x = 0$, and the system is equivalent to no SOC due to the spin-gauge symmetry. We show relevant linearizations inside the boxes. Case (I), with four Fermi points, is displayed in panels (a) and (e). Case (II), with two Fermi points, is displayed in panels (b) and (f). Case (III), with four Fermi points, is displayed in panel (c). The Roman numeral in the top-right corner of each box indicates the associated linearization.

We diagonalize the Hamiltonian matrix $\hat{H}_{\rm KS}$ via the momentum-dependent SU(2) rotation matrix

$$U(k,k_T,h_x)=\begin{pmatrix}\cos[\theta(k,k_T,h_x)/2] & -\sin[\theta(k,k_T,h_x)/2]\\ \sin[\theta(k,k_T,h_x)/2] & \cos[\theta(k,k_T,h_x)/2]\end{pmatrix}, \tag{26}$$

where the SU(2) rotation angle

$$\theta(k,k_T,h_x)=2\arctan\left[\frac{h_z(k)-h_{\rm eff}(k)}{h_x}\right]=\arctan\left[-\frac{h_x}{h_z(k)}\right] \tag{27}$$

depends on momentum k, the SOC parameter k_T via $h_z(k)$, and the Rabi field h_x. The resulting dispersions of the energy eigenvalues are

$$E_A(k)=\epsilon_k-h_{\rm eff}(k) \quad \text{and} \quad E_B(k)=\epsilon_k+h_{\rm eff}(k), \tag{28}$$

where $h_{\rm eff}(k)=\sqrt{h_x^2+h_z^2(k)}$ plays the role of a momentum-dependent Zeeman field. The creation operators in the energy eigenbasis are

$$\left(a_A^\dagger(k)\ a_B^\dagger(k)\right)=\left(c_\uparrow^\dagger(k)\ c_\downarrow^\dagger(k)\right)U^\dagger(k), \tag{29}$$

where $c_s^\dagger(k)$ are the creation operators with momentum k and spin $s=\{\uparrow,\downarrow\}$. The operators $a_\alpha^\dagger(k)$ create helical fermions, because the matrix $U(k)$ has an SU(2) momentum-dependent rotation angle $\theta(k,k_T,h_x)$ induced by SOC when both k_T and h_x are non-zero. Thus, the diagonalized kinetic energy operator in second quantization is

$$\hat{H}_{\rm kin}=\sum_{k\alpha}E_\alpha(k)a_\alpha^\dagger(k)a_\alpha(k). \tag{30}$$

In Figure 2, we show $E_A(k)$ and $E_B(k)$ in various situations [90]. When $h_x\neq 0$, the eigenvalues $E_A(k)$ and $E_B(k)$ are non-degenerate with $E_A(k)$ having either double minima ($|h_x|<2E_T$), revealed in Figure 2(a,b,c,d), or a single minimum ($|h_x|\geq 2E_T$) displayed in Figure 2(e,f,g), where $E_T=k_T^2/2m$. When $h_x=0$, we have $h_{\rm eff}(k)=|h_z(k)|$ and the two bands intersect at $k=0$, as shown in Figure 2(h).

A natural question that arises is: How is the SOC-induced helicity of the fermions transferred to the low-energy excitations of the interacting problem? To answer this question, we need to investigate the effects of SOC on the interaction part of the Hamiltonian.

Since, in this section, we are interested in spin-1/2 cold atom systems, we model interactions for two-internal-state ^{6}Li, ^{40}K or ^{173}Yb as

$$\hat{H}_{\rm int} = V_0 \int_0^{L_b} {\rm d}x' \int_0^{L_b} {\rm d}x \hat{n}_\uparrow(x)\hat{n}_\downarrow(x') f(|x-x'|), \tag{31}$$

where L_b is the length of system, $\hat{n}_s(x) = \psi_s^\dagger(x)\psi_s(x)$ is the local density operator with spin label $s = \{\uparrow,\downarrow\}$. The interaction in Equation (31) is SU(2) invariant and spin-dependent like the general case mentioned in Equation (15) of Section 3. The dimensionless function $f(|x-x'|)$ controls the range R_0, and the parameter V_0, possessing energy dimensions, controls the strength of interactions. A transformation to momentum space yields

$$\hat{H}_{\rm int} = \frac{V_0}{L_b}\sum_q \hat{\rho}_\uparrow(q)\hat{\rho}_\downarrow(-q)\tilde{f}(q), \tag{32}$$

where $\hat{\rho}_s(q) = \sum_k c_s^\dagger(k)c_s(k+q)$ is the Fourier transform of the local density operator $\hat{n}_s(x)$, and $\tilde{f}(q) = \int {\rm d}y {\rm e}^{-{\rm i}qy} f(|y|)$, with dimensions of length, is the Fourier transform of the dimensionless function $f(|y|)$. Since any finite-ranged real space interaction leads to the same low-energy and long-wavelength effective interaction, we choose the dimensionless function to be the Gaussian $f(|y|) = 1/\sqrt{2\pi}\exp -y^2/2R_0^2$. The Fourier transform of $f(|y|)$, shown in Equation (32), is $\tilde{f}(q) = R_0 \exp -q^2R_0^2/2$, having dimensions of length. The application of this approach to specific ultracold fermions (^{6}Li,^{40}K,^{173}Yb) is discussed later.

When $h_x = 0$, the spin-gauge transformation $\psi_\uparrow(x) \to {\rm e}^{{\rm i}k_T x}\psi_\uparrow(x)$, $\psi_\downarrow(x) \to {\rm e}^{-{\rm i}k_T x}\psi_\downarrow(x)$ gauges away k_T in the kinetic energy without changing the interaction $\hat{V}$ (spin-gauge symmetry). However, when both $k_T \neq 0$ and $h_x \neq 0$, the interaction written in the basis of eigenstates of the kinetic energy operator with SOC and Rabi fields acquires a much more complex structure controlled by the unitary transformation $U(k)$ that connects $\left(a_A^\dagger(k)\ a_B^\dagger(k)\right)$ and $\left(c_\uparrow^\dagger(k)\ c_\downarrow^\dagger(k)\right)$. The bosonization procedure must be performed in the eigenbasis $\left(a_A^\dagger(k)\ a_B^\dagger(k)\right)$ of the kinetic energy operator $\hat{H}_{\rm int}$ and not in the starting basis $\left(c_\uparrow^\dagger(k)\ c_\downarrow^\dagger(k)\right)$, as discussed next.

4.1. *Bosonization with SOC and Rabi fields*

To describe low-energy excitations of the total Hamiltonian $\hat{H} = \hat{H}_{\rm kin} + \hat{H}_{\rm int}$, we use the bosonization technique presented in Section 3.1 and linearize the kinetic energy operator $\hat{H}_{\rm kin}$ in Equation (30) around the chemical potential μ for each energy dispersion $E_A(k)$ and $E_B(k)$, given in Equation (28). Linearization is only possible when $\mu > \min\{E_A(k), E_B(k)\}$. However, the linear-spectrum approximation is strictly valid only in the low-energy regime near the Fermi points where curvature effects are negligible. When the Fermi velocities are non-zero, the curvature of the dispersions are a second-order effect. A treatment of nonlinear (band-curvature) corrections, without spin–orbit coupling and Rabi fields, can be found in the literature [91]. For $h_x \neq 0$ and arbitrary k_T, there are three typical linearization cases shown in Figure 2: (I) μ intersects twice $E_A(k)$ and twice $E_B(k)$, see Figures 2(a,e); (II) μ intersects only $E_A(k)$ twice, see Figures 2(b,f); (III) μ intersects $E_A(k)$ four times, see Figure 2(c). When $\mu < \min\{E_A(k), E_B(k)\}$, μ does not intersect either $E_A(k)$ or $E_B(k)$, thus no linearization is possible, see Figure 2(d,g). The special situation of $h_x = 0$ and arbitrary k_T is shown in Figure 2(h). Intersections of μ to either $E_A(k)$ or $E_B(k)$ allows for linearization of dispersions, shown as red lines in Figure 2.

We label fermions via indices $\{r,\alpha\}$, where r describes left (L) or right (R) moving particles and α labels the band indices A or B indicating linearization of $E_A(k)$ or $E_B(k)$. In the special case of Figure 2(c), we set $\alpha = A^{(1)}$ for the outer red lines and $\alpha = A^{(2)}$ for the inner red lines, since only $E_A(k)$ is crossed by μ. The linearized kinetic energy operator is

$$\hat{H}_{\rm kin} = \sum_{k\alpha r}\{\mu + {\rm sgn}(r)u_\alpha[k - {\rm sgn}(r)k_{\mu\alpha}]\}a_{\alpha r}^\dagger(k)a_{\alpha r}(k), \tag{33}$$

where u_α is the Fermi velocity $\mathrm{d}E_\alpha(k)/\mathrm{d}k$ at $k = k_{\mu\alpha}$, with $k_{\mu\alpha}$ being the positive momentum where μ intersects the band labeled by α. The operator $a^\dagger_{\alpha r}(k)$ creates a fermion with momentum k in band α and branch r. Both u_α and $k_{\mu\alpha}$ depend on k_T, h_x and μ. The function $\mathrm{sgn}(r)$ refers to the sign of r, where $\mathrm{sgn}(R) = +1$ and $\mathrm{sgn}(L) = -1$. The reference Hamiltonian $\hat{H}_0 = \sum_{k\alpha r} \mu a^\dagger_{\alpha r}(k) a_{\alpha r}(k)$, corresponding to the energy $E_0 = N\mu$, where N is the total number of fermions, is set to zero without loss of generality. Thus, we drop this reference term from the kinetic energy operator $\hat{H}_{\rm kin}$ from now on.

We bosonize $\hat{H}_{\rm kin}$ in Equation (33) using the transformation

$$b^\dagger_\alpha(q) = \sqrt{\frac{2\pi}{|q|L_b}} \sum_r \Theta(-\mathrm{sgn}(r)q)\hat{\rho}_{\alpha r}(q), \tag{34}$$

where $\hat{\rho}_{\alpha r}(q) = \sum_k a^\dagger_{\alpha r}(q) a_{\alpha r}(k+q)$ is the fermion density operator for an r-moving particle in band α, and $\Theta(x)$ is the Heaviside step function. This leads to

$$\hat{H}_{\rm kin} = \sum_{q\alpha} |q u_\alpha| b^\dagger_\alpha(q) b_\alpha(q) + K_\Omega \tag{35}$$

for the kinetic energy in bosonized form, where $K_\Omega = \sum_{q>0,\alpha} |q u_\alpha|$. Here, the bosonization of the interaction is more complex because it requires four sets of momentum-dependent unitary transformations, when writing the interaction Hamiltonian in terms of the creation $a^\dagger_A, a^\dagger_B$ and annihilation a_A, a_B operators. Using the appropriate momentum labels, the interaction in Equation (32) is bosonized as

$$\hat{H}_{\rm int} = \sum_{q>0} q\mathbf{\Phi}^\dagger(q) g \mathbf{\Phi}(q) = \frac{1}{2}\sum_q |q| \mathbf{\Phi}^\dagger(q) g \mathbf{\Phi}(q) + V_\Omega, \tag{36}$$

where $\mathbf{\Phi}(q)$ is either a two-component vector or a four-component vector, g is either a 2×2 or a 4×4 matrix representing the interaction strength of different scattering processes shown in Figure 3, and $V_\Omega = \sum_{qij} |q| g_{ij}/2$, with g_{ij} being the elements of the matrix g. In case (I), where μ intersects bands A and B, there are four Fermi points, and

$$\mathbf{\Phi}^T(q) = \left(b^\dagger_A(q)\ b^\dagger_B(q)\ b_A(-q)\ b_B(-q)\right).$$

In case (II), where μ intersects only band A, there are two Fermi points, and $\mathbf{\Phi}^T(q) = \left(b^\dagger_A(q)\ b_A(-q)\right)$. In case (III), where μ intersects only band A, there are four Fermi points, and

$$\mathbf{\Phi}^T(q) = \left(b^\dagger_{A^{(1)}}(q)\ b^\dagger_{A^{(2)}}(q)\ b_{A^{(1)}}(-q)\ b_{A^{(2)}}(-q)\right).$$

The elements of the g matrix are $g_{ij} = \eta_{ij}\tilde{f}(q\to 0)$, having dimensions of energy times length, while η_{ij} has dimension of energy and depends on k_T, h_x and μ via SU(2) rotation angles $\theta(k, k_T, h_x)$ and $\theta(k+q, k_T, h_x)$.

For case (I), the g matrix is 4×4 and depends on the angles θ_A and θ_B, where $\theta_\alpha = \theta(k_{\mu\alpha}, k_T, h_x)$ is the SU(2) angle defined in Equation (27) with $k = k_{\mu\alpha}$. For case (II), the g matrix is 2×2 and depends only on θ_A as

$$g = \frac{\tilde{f}(0)V_0}{4\pi}\begin{pmatrix} \sin^2\theta_A & (1+\cos^2\theta_A) \\ (1+\cos^2\theta_A) & \sin^2\theta_A \end{pmatrix}. \tag{37}$$

For case (III), the g matrix is 4×4 and depends on the SU(2) angles $\theta_{A^{(1)}}$ and $\theta_{A^{(2)}}$. The g matrix in cases (I) and (III) can also be obtained analytically [92], but for simplicity and brevity, we discuss in detail only case (II) as an example [92]. In general, $g_{4\alpha\beta}$ ($g_{2\alpha\beta}$) shown in Figure 3 are the diagonal (off-diagonal) terms of each 2×2 block of the g matrix, where the blocks are labeled by α, β. For instance, in case (II), $g_{4AA} = (\tilde{f}(0)V_0/4\pi)\sin^2\theta_A$ are the diagonal and $g_{2AA} = (\tilde{f}(0)V_0/4\pi)(1+\cos^2\theta_A)$ are the off-diagonal elements of matrix g in Equation (37).

Only small momentum-transfer interactions ($q\to 0$) are retained, since larger momentum-transfer contributions $q = 2k_{\mu\alpha}$ are suppressed due to the finite range R_0 of the interaction,

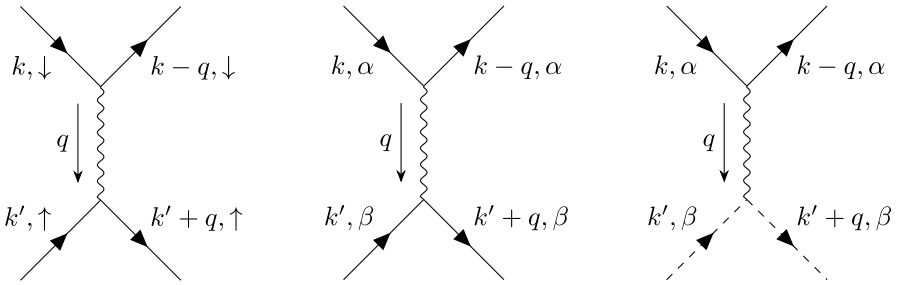

Figure 3. Schematics of scattering processes. In panel (a), we show the scattering process in the spin basis $\{\uparrow,\downarrow\}$. In panels (b) and (c), we show the low-momentum-transfer scattering processes in the $\{\alpha,\beta\}$ basis after linearization, where $\{\alpha,\beta\}=\{A,B\}$ for case (I), $\{\alpha,\beta\}=\{A\}$ for case (II), and $\{\alpha,\beta\}=\{A^{(1)},A^{(2)}\}$ for case (III). The solid (dashed) lines represent right (left) moving fermions, and the wiggly lines represent the interactions.

and even when these terms are included they are irrelevant under the renormalization group flow [4,6,92]. This is an important point in our discussion, because we use a finite-ranged interaction. As an example, for the Gaussian-ranged interaction, $\tilde{f}(0)=R_0$. The limit of zero interaction range is discussed later, when connections to ultracold atoms are directly made. The bosonized Hamiltonian is now ready for diagonalization, as discussed next.

4.2. *Diagonalization of bosonized Hamiltonian*

To obtain the excitation spectrum of the bosonized Hamiltonian

$$\hat{H}=\hat{H}_{\rm kin}+\hat{H}_{\rm int},$$

it is necessary to diagonalize it via a Bogoliubov transformation $\mathscr{B}$ connecting $\mathbf{\Phi}(q)$ in Equation (36) to $\mathbf{\Psi}(q)=\mathscr{B}\mathbf{\Phi}(q)$, leading to boson operators

$$\mathbf{\Psi}^T(q)=\left(d_1^\dagger(q)\ d_2^\dagger(q)\ d_1(-q)\ d_2(-q)\right)$$

for cases (I) and (III), where the number of collective modes is $N_{\rm C}=2$ and to $\mathbf{\Psi}^T(q)=\left(d_1^\dagger(q)\ d_1(-q)\right)$ for case (II), where $N_{\rm C}=1$. Barring any instabilities, $N_{\rm C}=N_{\rm F}/2$, where $N_{\rm F}$ is the number of Fermi points at μ. The Bogoliubov matrices $\mathscr{B}$ are 4×4 in cases (I) and (III) and 2×2 in case (II). This is a very standard procedure, so we do not dwell on the details. After implementing the Bogoliubov transformations, the diagonalized Hamiltonian becomes

$$\hat{H}=\sum_{q\ell}|q|v_\ell d_\ell^\dagger(q)d_\ell(q)+\omega_\Omega, \tag{38}$$

where $v_\ell\geq0$ is the velocity of collective mode ℓ that depends on $\{k_T,h_x,\mu\}$ for given V_0. The ground state energy is $\omega_\Omega=\sum_{q>0,\ell}|qv_\ell|$. Defining $\mathscr{L}$ to be the set of collective modes, such that $\ell\in\mathscr{L}$, we have two modes for cases (I) and (III) with $\mathscr{L}=\{1,2\}$, and we have one mode for case (II) with $\mathscr{L}=\{1\}$. The mode with $\ell=1$ has larger velocity and energy, while the mode with $\ell=2$ has smaller velocity and energy. The velocities v_ℓ can be obtained analytically, but have complicated expressions in cases (I) and (III) [92]. For simplicity and brevity, we give analytical results only for case (II), see Figures 2(b) and (f), where there is only one mode with velocity

$$v_1=\sqrt{u_A+\frac{\tilde{f}(0)V_0}{2\pi}}\sqrt{u_A-\frac{\tilde{f}(0)V_0}{2\pi}\cos^2\theta_A}. \tag{39}$$

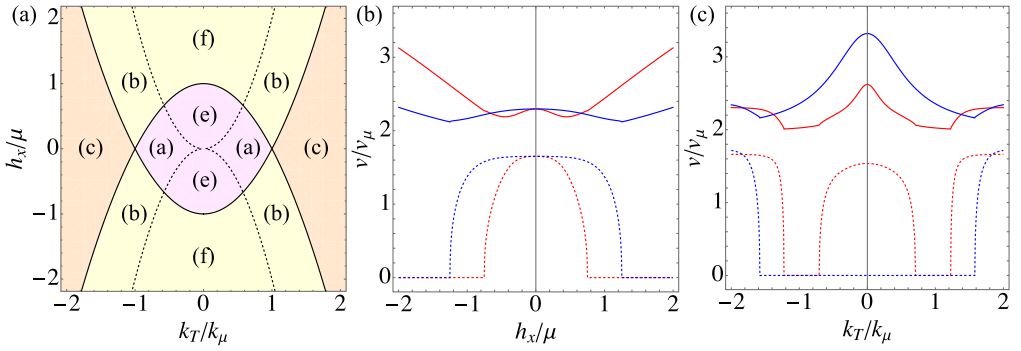

Figure 4. Phase diagram and velocities of collective modes. In panel (a), we show the phase diagram of h_x/μ versus k_T/k_μ, for chemical potential $\mu > 0$ and $k_\mu = \sqrt{2m\mu}$. The interaction parameter is chosen to be $\tilde{f}(0)V_0/v_\mu = 2$, where $v_\mu = k_\mu/m$. The pink, yellow and orange regions represent phases with four (two), two (one), and four (two) Fermi points (collective modes). These phases are separated by black solid lines, where topological quantum phase (Lifshitz) transitions occur. The labels (a) and (e) in the pink region, (b) and (f) in the yellow region, and (c) in the orange region refer to the cases illustrated in the panels of Figure 2. The black dashed lines at $|h_x| = 2E_T$ separate regions where $E_A(k)$ has a single minimum ($|h_x|/E_T > 2$) from regions where $E_A(k)$ has double minima ($|h_x|/E_T < 2$). In panel (b), we show the velocities v_1/v_μ (solid lines) and v_2/v_μ (dashed lines) as functions of h_x/μ for fixed values of k_T/k_μ. The red curves correspond to $k_T/k_\mu = 0.5$, and the blue curves to $k_T/k_\mu = 1.5$. In panel (c), we show the velocities v_1/v_μ (solid lines) and v_2/v_μ (dashed lines) as functions of k_T/k_μ for fixed values of h_x/μ. The red curves correspond to $h_x/\mu = 0.5$, and the blue curves to $h_x/\mu = 1.5$.

In the expression above, for $h_x \neq 0$ and $k_T \neq 0$, the Fermi velocity is

$$u_A = \left(1 - \frac{2E_T}{h_{\rm eff}(k_{\mu A})}\right)\frac{k_{\mu A}}{m}, \tag{40}$$

where $E_T = k_T^2/2m$ is the momentum-transfer energy, $h_{\rm eff}(k_{\mu A}) = \sqrt{h_x^2 + h_z^2(k_{\mu A})}$ is the effective Zeeman field at $k_{\mu A}$ with $h_z(k_{\mu A}) = k_{\mu A}k_T/m$ being the momentum-dependent Zeeman field, and with

$$k_{\mu A} = \sqrt{2m(\mu + E_T + \sqrt{4\mu E_T + h_x^2})} \tag{41}$$

being the Fermi momentum for band A.

In Figure 4, we illustrate properties of our system in the plane h_x/μ versus k_T/k_μ, with $\mu > 0$ and $k_\mu = \sqrt{2m\mu}$. Panel (a) shows a partial phase diagram for $\mu > 0$. Panel (b) displays the velocities v_ℓ/v_μ of collective modes with $\ell = 1,2$ as a function of h_x/μ at fixed k_T/k_μ. Panel (c) reveals the velocity v_ℓ/v_μ of collective modes with $\ell = 1,2$ as a function of k_T/k_μ at fixed h_x/μ. We fix the chemical potential μ and, for simplicity, show only the case of $\mu > 0$, instead of fixing the density n as was discussed in the literature [90].

In Figure 4(a), we show the phase diagram of h_x/μ versus k_T/k_μ, for $\mu > 0$, with $k_\mu = \sqrt{2m\mu}$, and $\tilde{f}(0)V_0/v_\mu = 1$, where $v_\mu = k_\mu/m$. Case (I), where μ intersects bands A and B as shown in Figure 2(a,e), is represented by the pink region, with the number of Fermi points $N_{\rm F} = 4$ and the number of collective modes $N_{\rm C} = 2$. Case (II), where μ intersects only band A twice, as seen in Figure 2(b,f), is represented by the yellow region with $N_{\rm F} = 2$ and $N_{\rm C} = 1$. Case (III), where μ intersects only band A four times as shown in Figure 2(c), is represented by the orange region with $N_{\rm F} = 4$ and $N_{\rm C} = 2$. For the vertex separating the pink, yellow and orange regions ($h_x/\mu = 0$

and $k_T/k_\mu = 1$), $N_F = 4$ as in Figure 2(h) and $N_C = 2$; at this location there is perfect spin–charge separation. In fact, along the line $h_x/\mu = 0$, there is spin–charge separation also in the pink and orange regions, due to the spin-gauge symmetry.

Furthermore, in Figure 4(a), the lines or points separating different phases indicate topological quantum phase transitions of the Lifshitz-type [93–95], where the Fermi *surfaces* change from four to two to zero points, depending on h_x/μ and k_T/k_μ. The black dashed lines (parabolas) at $h_x = \pm 2E_T$ separate regions where the lower band $E_A(k)$ has two minima ($|h_x| < 2E_T$) from regions where the lower band $E_A(k)$ has one minimum ($|h_x| > 2E_T$) and the line at $h_x/\mu = 0$ represents the locus of spin–charge separation.

In Figure 4, we also show the collective mode velocities v_1/v_μ and v_2/v_μ, where $v_\mu = k_\mu/m$, as a function of h_x/μ and fixed k_T/k_μ in panel (b) or as a function of k_T/k_μ for fixed h_x/μ in panel (c). Solid and dotted curves represent v_1/v_μ and v_2/v_μ, respectively. In panel (b), the red curves correspond to $k_T/k_\mu = 0.5$, and the blue curves to $k_T/k_\mu = 1.5$; in panel (c), the red curves correspond to $h_x/\mu = 0.5$, and the blue curves to $h_x/\mu = 1.5$. Both v_1/v_μ and v_2/v_μ vary continuously but exhibit nonanalytic behavior at phase boundaries (black solid lines in panel (a)). This nonanalyticity reflects a topological (Lifshitz) quantum phase transition, characterized by a change in the number of Fermi points from $N_F = 4$ to $N_F = 2$. Additionally, at the phase boundaries, the velocity of the second mode vanishes. This results from the linearization, where the slope at a local maximum or minimum becomes zero. To obtain the next order correction to the collective mode dispersion, it is necessary to include curvature effects as described in Ref. [91]. However, we do not address the additional correction in this paper.

We notice that, in the limit $h_x/\mu \to 0$ for fixed nonzero k_T/k_μ, the velocities approach their theoretical values at $h_x/\mu = 0$ due to spin-gauge symmetry, thereby restoring spin–charge separation. When spin–charge separation happens at $h_x = 0$, the higher-velocity mode (v_1) is associated with charge and the lower-velocity mode (v_2) is associated with spin. In the absence of SOC ($k_T = 0$) with $h_x \neq 0$, the collective modes are generally a mix of charge and spin density waves, but are nonhelical. However, when both $k_T \neq 0$ and $h_x \neq 0$, the collective modes are a mix of charge and spin density waves with a helical structure, which is carried over by the momentum-dependent rotation angles $\theta(k, k_T, h_x)$ of the SU(2) rotation matrices $U(k)$ defined in Equation (26).

To visualize helical modulations in the collective modes, we decompose

$$d^\dagger_\ell(q) = \sum_r \left[A_{\ell r}(q)\hat{\rho}_r(q) + \mathbf{B}_{\ell r}(q)\cdot\hat{\mathbf{s}}_r(q)\right] \tag{42}$$

in terms of the Fourier transforms $\hat{\rho}_r(q)$ and $\hat{\mathbf{s}}_r(q)$ of the charge-density $\hat{n}_r(x) = \sum_s \psi^\dagger_{sr}(x)\psi_{sr}(x)$ and spin-density $\hat{\mathbf{S}}_r(x) = \frac{1}{2}\sum_{ss'}\psi^\dagger_{sr}(x)(\boldsymbol{\sigma})_{ss'}\psi_{s'r}(x)$ operators, respectively. Here, the factor of $1/2$ in $\hat{\mathbf{S}}_r(x)$ represents the angular momentum $\hbar/2$ with $\hbar = 1$, r labels right (R) or left (L) going fermions, and $\psi^\dagger_{sr}(x)$ is the creation operator for r-going fermions with spin projection s at position x. The collective mode operators in real space are

$$\mathscr{D}^\dagger_\ell(x) = \sum_r \int \mathrm{d}x' \left[a_{\ell r}(x-x')\hat{n}_r(x') + \mathbf{b}_{\ell r}(x-x')\cdot\hat{\mathbf{S}}_r(x')\right], \tag{43}$$

where the spatial modulation and helicity of the vector fields $\mathbf{b}_{\ell r}(x-x')$ are controlled by k_T and h_x [90,92]. When k_T and h_x are both non-zero, all the modes present are helical, with $q > 0$ ($q < 0$) modes having positive (negative) helicity. The global helicity of the Hamiltonian in Equation (38) is zero, such that $q > 0$ and $q < 0$ bosons for each mode are helical pairs. Given that these bosons are massless and helical, we name them Weyl bosons in analogy to Weyl fermions [50], which are massless and helical spin-1/2 particles. The helicity of Weyl bosons is like that of circularly polarized photons, however unlike photons, in SU(2) Fermi systems, Weyl bosons can have up to two flavors of right or left helicities. We emphasize that our flavored Weyl bosons

are collective modes of interacting and spin–orbit-Rabi-coupled spin-1/2 fermions. They are intrinsically *pseudo-relativistic* (*relativistic*) bosons due the presence of synthetic (real) Zeeman fields and synthetic (real) spin–orbit coupling that provides *relativistic* corrections. They also appear in 2D and 3D, but in 1D, analytical results are easily obtained via the bosonization method. We also notice that the emergence of Weyl bosons in the context of particle physics corresponds to an effect Beyond the Standard Model (BSM), thus the analysis above offers some hope for those interested in simulating BSM effects with ultracold atoms.

The theoretical results described above need serious experimental testing, thus we discuss next potential experimental systems that may reveal the existence of Weyl bosons.

4.3. *Connection to ultracold Fermi atoms*

For ultracold fermions such as ^{6}Li, ^{40}K and ^{173}Yb, with two internal states selected and SU(2) invariant interactions, the zero-range approximation is typically used. Thus, the effective zero-ranged interaction is replaced by the scattering length. To take the limit of zero range ($R_0 \to 0$), we use the explicit Gaussian form $f(|y|) = 1/\sqrt{2\pi}\exp -y^2/2R_0^2$, discussed right after Equation (32) and connect it to the delta sequence $\delta_n(y) = (n/\sqrt{2\pi})\exp(-n^2y^2/2)$. With this connection, we write the 1D interaction

$$V(x-x') = V_0 f(|x-x'|), \tag{44}$$

with range R_0, in the limit of $R_0 \to 0$, as the contact potential

$$V(x-x') \approx \widetilde{V}_0 \delta(x-x'), \tag{45}$$

where $\widetilde{V}_0 = R_0 V_0$, with dimensions of energy times length, is held constant as $R_0 \to 0$. Notice that $\widetilde{V}_0$ is also equivalent to $\tilde{f}(0)V_0$ discussed in the previous sections, where $\tilde{f}(0) = R_0$. The corresponding 1D scattering length a_{1D} is defined by the relation $\widetilde{V}_0 = -2\hbar^2/ma_{1D} > 0$ (with $\hbar$ restored to make units clear) [96]. The relationship between a_{1D} and the 3D scattering length a_{3D} is [16,96]

$$a_{1D} = -\frac{a_\perp}{a_{3D}}\left[1 - C\frac{a_{3D}}{a_\perp}\right], \tag{46}$$

where $C = |\zeta(1/2)|/\sqrt{2}$ is a constant with $\zeta(1/2)$ being the Riemann zeta function $\zeta(z)$ evaluated at $z = 1/2$, and $a_\perp = \sqrt{\hbar/m\omega_r}$ is the transverse confinement length with ω_r being the frequency of the transverse harmonic potential [96].

Given that ^{6}Li experiences substantial heating due to the Raman beams [38] that produce SOC and Rabi fields, the effects proposed above are more likely realizable in ^{40}K or ^{173}Yb. So, we choose to give numbers compatible with ^{40}K as an illustration, since typical SOC and Rabi fields are known [89]. We envision using optical boxes in 1D with dimensions ranging from 10 μm to 100 μm [97], and number of atoms varying from a few [98] to thousands [99]. As an example, we consider a 1D optical box with length $L_b = 25$ μm, a tight transverse confinement frequency $\omega_r = 2\pi \times 227.5$ kHz, similar to confinements achieved in ^{6}Li [16], number of atoms $N = 400$, interaction parameter $\widetilde{V}_0 = R_0 V_0 = v_\mu$ in the zero-range limit $R_0 \to 0$. For ^{40}K, the momentum transfer chosen is $k_T = 2\pi \times (768.86\ \text{nm})^{-1}$ [89], the density is $n = 400/25\ \mu\text{m} = 1.6 \times 10^5/\text{cm}$, and the 3D scattering length from Equation (46) is $a_{3D} \approx 134 a_0$, where a_0 is the Bohr radius. Other examples can be found in the literature [90].

Keeping in mind this connection to ultracold atoms, we discuss next the dynamical structure factor tensor, which can potentially be measured using Bragg scattering techniques to detect the dispersion, spectral weight and helicity of the collective modes that we call Weyl bosons.

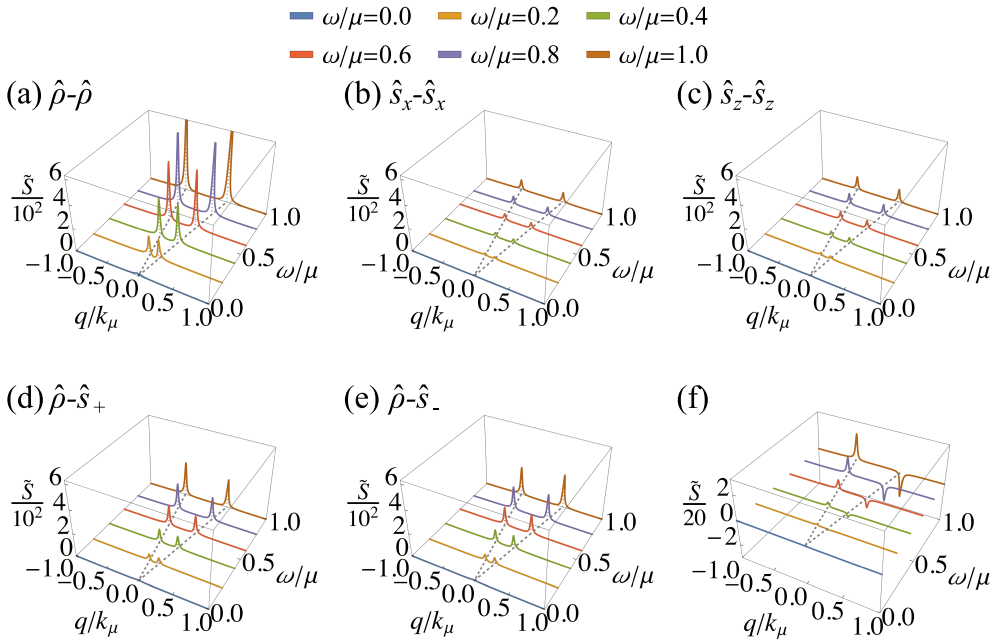

Figure 5. Dimensionless dynamical structure factor (DSF) tensor $\widetilde{S}_{ij}(q,\omega) = S_{ij}(q,\omega)\mu/k_\mu^2$, with energy broadening $\delta/\mu = 0.05$. The parameters used are $h_x/\mu = 1.5$ for the Rabi field, $k_T/k_\mu = 0.5$ ($E_T/\mu = 0.25$) for the SOC, $\widetilde{V}_0/v_\mu = \tilde{f}(0)V_0/v_\mu = 2$ ($a_{3D} \approx 134a_0$) for the interaction and $k_\mu L_b = 408.60$. These are typical values for ^{40}K, at density $n = 1.6\times10^5/\text{cm}$, in a 1D box potential of length $L_b = 25$ μm. These parameters correspond to a point in the yellow region of the phase diagram of Figure 4(a) leading to a single collective mode (Weyl boson). Panels (a), (b) and (c) show the charge–charge and spin–spin responses $\hat{\rho}$-$\hat{\rho}$, $\hat{s}_x$-$\hat{s}_x$ and $\hat{s}_z$-$\hat{s}_z$, respectively. Panels (d) and (e) display the charge–spin $\hat{\rho}$-$\hat{s}_+$ and $\hat{\rho}$-$\hat{s}_-$ responses, respectively, and (f) shows the difference of (d) and (e). The gray dashed lines show the dispersing helical collective mode (Weyl boson).

4.4. *Dynamical structure factor tensor*

Bragg scattering techniques have been used to measure velocities of charge and spin density collective modes [63,64], as well as to identify spin–charge separation [16,17] in ^{6}Li. These experiments traditionally measure either charge or spin dynamical structure factors (DSF). Here, we investigate not only spin–spin and charge–charge, but also spin–charge responses at $T = 0$ via the DSF tensor

$$S_{ij}(q,\omega) = 2\pi\sum_{p\ell}\langle\Omega|\hat{\mathcal{O}}_i(q)|p,\ell\rangle\langle p,\ell|\hat{\mathcal{O}}_j(-q)|\Omega\rangle\,\delta(\omega-\varepsilon_{p\ell}+\omega_\Omega), \tag{47}$$

for the ground state $|\Omega\rangle$, in the Källén–Lehmann spectral representation [100,101]. The operators $\hat{\mathcal{O}}_i(q)$, with $i = \{c,x,y,z\}$, are the charge $\hat{\mathcal{O}}_c(q) = \hat{\rho}(q)$ and spin $\hat{\mathcal{O}}_a(q) = \hat{s}_a(q)$ operators, where $a = \{x,y,z\}$. The eigenstates of the bosonized Hamiltonian $\hat{H}$ given in Equation (38) are $|p,\ell\rangle$ with corresponding eigenenergies $\varepsilon_{p\ell} = |p|v_\ell$, while ω_Ω is the ground state energy discussed following Equation (38). We emphasize that, in our units ($\hbar = 1$), both $\hat{\rho}(q)$ and $\hat{s}_a(q)$ have dimensions of inverse length and $S_{ij}(q,\omega)$ has dimensions of mass; these properties are used in the plots of Figure 5.

To calculate $S_{ij}(q,\omega)$, we use the decomposition $\hat{\mathcal{O}}_i(q) = \hat{\mathcal{O}}_{iR}(q) + \hat{\mathcal{O}}_{iL}(q)$ in Equation (47), and implement the Moore–Penrose inverse [102,103] of Equation (42) to write the operators $\hat{\mathcal{O}}_{ir}(q)$ as a linear combination of the boson creation $d^\dagger_\ell(q)$ and annihilation $d_\ell(-q)$ operators. When $q > 0$, we obtain

$$\hat{\mathcal{O}}_{ir}(q) = \sqrt{\frac{|q|L}{2\pi}} \sum_\ell (F_{ir\ell}(q) d^\dagger_\ell(q) + G_{ir\ell}(q) d_\ell(-q)), \tag{48}$$

where the expression relating $q > 0$ and $q < 0$ is $\hat{\mathcal{O}}_{ir}(-q) = \hat{\mathcal{O}}^\dagger_{ir}(q)$. Currently, there is no simple analytical form of the tensors $F_{ir\ell}(q)$ and $G_{ir\ell}(q)$, so we do not show their complicated structure here, but rather we perform the Moore–Penrose inverse numerically to obtain the matrix elements $\langle \Omega|\hat{\mathcal{O}}_i(q)|p,\ell\rangle$ and $\langle p,\ell|\hat{\mathcal{O}}_j(-q)|\Omega\rangle$. Summation over p in Equation (47) (only the terms with $p = q$ survive) leads to

$$S_{ij}(q,\omega) = \sum_\ell \mathscr{A}_{ij\ell}(q)\delta(\omega - \varepsilon_{q\ell} + \omega_\Omega), \tag{49}$$

where $\mathscr{A}_{ij\ell}(q)$ plays the role of the spectral weight tensor with dimensions of squared-density (squared-length in 1D), $\varepsilon_{q\ell} = |q|v_\ell$ is the collective mode energy, and we set the ground state energy $\omega_\Omega = 0$ as our energy reference in Figure 5. The spectral weight tensor is

$$\mathscr{A}_{ij\ell}(q) = \mathscr{A}_{ij\ell+}(q)\Theta(q) + \mathscr{A}_{ij\ell-}(q)\Theta(-q). \tag{50}$$

where $\mathscr{A}_{ij\ell+}(q) = |q|L\sum_{rr'} G_{ir\ell}(q)G^*_{jr'\ell}(q)$ is the spectral weight for $q > 0$, $\mathscr{A}_{ij\ell-}(q) = |q|L\sum_{rr'} F^*_{ir\ell}(-q)F_{jr'\ell}(-q)$ is the spectral weight for $q < 0$ and $\Theta(q)$ is the Heaviside step function. The spectral weight tensor is even in q obeying the relation $\mathscr{A}_{ij\ell}(-q) = \mathscr{A}_{ij\ell}(q)$, implying that $\mathscr{A}_{ij\ell+}(-q) = \mathscr{A}_{ij\ell-}(q)$.

The symmetry properties obeyed by $\mathscr{A}_{ij\ell}(q)$ are important in establishing the general Onsager reciprocal relation [104,105] satisfied by the DSF tensor

$$S_{ij}(q,\omega,k_T,h_x) = \epsilon_i\epsilon_j S_{ji}(-q,\omega,-k_T,-h_x), \tag{51}$$

where ϵ_i is the parity of operators $\hat{\mathcal{O}}_i(x,t)$ under time-reversal. For $i = c$ (charge density), $\epsilon_i = +1$, and for $i = \{x,y,z\}$ (spin density), $\epsilon_i = -1$. We verified analytically and numerically this fundamental symmetry relation regarding the dynamical structure factor tensor.

In Figure 5, we show matrix elements of the dimensionless DSF tensor $\widetilde{S}_{ij}(q,\omega) = S_{ij}(q,\omega)\mu/k^2_\mu = S_{ij}(q,\omega)/2m$ with energy broadening $\delta/\mu = 0.05$. The parameters used are $h_x/\mu = 1.5$ for the Rabi field, $k_T/k_\mu = 0.5$ ($E_T/\mu = 0.25$) for the SOC, $\widetilde{V}_0/v_\mu = \tilde{f}(0)V_0/v_\mu = 2$ ($a_{3D} \approx 134a_0$) for the interaction, and $k_\mu L_b = 408.60$ corresponding to typical values for ^{40}K with density $n = 400/25\ \mu\text{m} = 1.6\times10^5/\text{cm}$, in a 1D box of length $L_b = 25\ \mu$m. These values represent a point in the yellow region of Figure 4(a), where there is only one collective mode (Weyl boson).

In all panels of Figure 5, the gray dashed lines represent the dispersing helical mode (Weyl boson). We emphasize that both $\hat{\rho}(q)$ and $\hat{s}_a(q)$ have dimensions of inverse length in our units ($\hbar = 1$). We use either the standard index $a = \{x,y,z\}$ for the spin components or $a = \{+,-,z\}$, with + (−) labeling the spin raising (lowering) operator $\hat{s}_+$ ($\hat{s}_-$).

In panel (a), we illustrate the charge–charge response $\hat{\rho}$-$\hat{\rho}$, while in panels (b) and (c) we show the spin–spin response $\hat{s}_x$-$\hat{s}_x$ and $\hat{s}_z$-$\hat{s}_z$. In panels (d) and (e), we display the charge–spin $\hat{\rho}$-$\hat{s}_+$ and $\hat{\rho}$-$\hat{s}_-$ responses, respectively. To reveal the helicity of the modes, we show the difference of $\hat{\rho}$-$\hat{s}_+$ and $\hat{\rho}$-$\hat{s}_-$ in panel (f). Since the difference of $\hat{\rho}$-$\hat{s}_+$ and $\hat{\rho}$-$\hat{s}_-$ is small, we use a different scale to help visualization in (f). We verified that for $h_x \neq 0$ and $k_T = 0$, the modes are non-helical, and that the only non-zero responses are $\hat{\rho}$-$\hat{\rho}$, $\hat{s}_x$-$\hat{s}_x$ and $\hat{\rho}$-$\hat{s}_x$. Furthermore, for $h_x = 0$ and any k_T, there is spin–charge separation, and the only non-zero responses are $\hat{\rho}$-$\hat{\rho}$, and $\hat{s}_z$-$\hat{s}_z$. The Weyl bosons with $q > 0$ and $q < 0$ are helical pairs representing special spin-charged mixed states introduced by SOC and Rabi fields.

Apart from Weyl modes with one flavor illustrated in Figure 5, there are also examples of Weyl modes with two flavors, existing in the pink region of Figure 4(a), which can be found in the literature [90]. Having completed our analysis of what is known about SU(2) fermions with spin–orbit coupling and Rabi fields in 1D, we discuss next a few open questions.

4.5. *Open questions for SU(2) fermions*

Before listing a few open questions for SU(2) fermions in the presence of spin–orbit coupling and Rabi fields, we summarize briefly the main results discussed above. We analyzed the phase diagram and collective modes of interacting one-dimensional SU(2) Fermi systems with spin–orbit and Rabi coupling. We have shown that Lifshitz-type topological quantum phase transitions occur in the plane of spin–orbit versus Rabi coupling, where there are quantum phases with two, one or zero helical collective modes (Weyl bosons) depending on the topology of the Fermi *surface*. We demonstrated that the velocities of the collective modes are continuous, but nonanalytical as topological phase boundaries are crossed. We also identified the locus of spin–charge separation, and demonstrated that, when spin–orbit and Rabi couplings are both non-zero, the collective modes are helical with mixed spin and charge density components. Lastly, we obtained the dynamical structure factor tensor for charge–charge, spin–charge and spin–spin responses, revealing the dispersions, spectral weights and helicities of collective modes (Weyl bosons). These results pave the way for their experimental detection in systems like ^{6}Li, ^{40}K and ^{173}Yb, but there are a few open questions that we present below.

The discussion above highlights exciting predictions about the creation of Weyl bosons and their possible detection in SU(2) Fermi systems not only in solid state materials and ultracold fermions such as ^{6}Li, ^{40}K and ^{173}Yb in one dimensional, but also in two- and three-dimensional systems. The one-dimensional case is quite appealing because analytical results for the collective mode dispersion and velocity are obtained via the bosonization method in the long-wavelength regime. However, as far as we know, there are currently no experiments either in condensed matter with real spin–orbit and Rabi (Zeeman) fields or in ultracold atoms with synthetic spin–orbit and Rabi (Zeeman) fields that probe the effects proposed. So, there are not only open theoretical questions, but also experimental ones, both in the context of condensed matter and ultracold atoms.

In condensed matter, one important open experimental question is: are there solid state materials in one, two or three dimensions, where real spin–orbit coupling and Rabi (Zeeman fields) can be manipulated to probe the expected theoretical phase diagram and the emergence of Weyl bosons with one or two flavors? Can measurements of the charge–charge (density–density) dynamical structure factor be achieved, using for instance, inelastic neutron scattering or inelastic X-ray scattering? Can the spin–spin dynamical structure factor be measured for solid state systems with spin–orbit and Zeeman coupling using techniques such as inelastic neutron scattering, resonant inelastic X-ray scattering, muon spin resonance, and spin-polarized neutron scattering? Are there any techniques that can probe the charge–spin or spin–charge dynamical structure factors to extract the helicity of the collective modes?

In ultracold atoms, there are several open experimental questions. Can spin–orbit and Rabi coupling be realized and studied experimentally in interacting Fermi systems of ^{6}Li, ^{40}K and ^{173}Yb in one, two and three dimensions? Would box trapping potentials help in realizing such systems? If experimental realization is possible, would the tunability of spin–orbit and Rabi fields be sufficient to probe the theoretical phase diagrams and the topological phases transitions predicted? Would Bragg spectroscopy be sufficient for measuring charge–charge (density–density) and spin–spin structure factors and identify Weyl bosons? Is there a technique that can measure

the charge–spin (density–spin) and spin–charge (spin–density) structure factors to elucidate the helicity of the collective modes (Weyl bosons)?

On the theoretical front, we also list a few open questions for interacting SU(2) fermions with spin–orbit and Rabi (Zeeman) coupling. Are there qualitative differences between the collective modes (Weyl bosons) in one, two and three dimensions? What is the interplay between the continuum of excitations and Weyl bosons? What are the lifetimes of Weyl bosons? Are there stable higher-energy helical collective modes in one, two and three dimensions? Are there any fractionalization effects in the charge (density) and spin sectors that arise from spin–orbit and Rabi (Zeeman) coupling beyond the long-wavelength regime?

Although there are many open questions for SU(2) fermions, an inquisitive mind may also wonder about additional generalizations. An intriguing possibility is the investigation of SU(N) fermions such ^{173}Yb and ^{87}Sr in the presence of SOC and Rabi fields, where Fermi liquid properties [60] and color superfluidity were investigated [61] in 3D for SU(3) fermions. Thus, driven by curiosity, we discuss next the effects of SOC and Rabi fields on SU(3) fermions with three internal states, focusing again on one dimensional systems.

5. SU(3) fermions with SOC and Rabi fields

Ultracold atomic physics has emerged as a versatile platform for simulating complex quantum systems due to the high degree of control over atomic interactions and internal degrees of freedom. Particularly, fermionic atoms with multiple internal states can emulate and break higher symmetries beyond the conventional SU(2) spin symmetry as discussed in Section 4. In this context, SU(3) fermions, with three internal states, have garnered significant interest for their potential to simulate exotic quantum phases [60,61] and for applications in quantum information processing [106].

In systems with full SU(3) symmetry, both the kinetic energy and interactions are invariant under global transformations belonging to the SU(3) group. This symmetry arises naturally in ultracold gases of alkaline-earth-like atoms, such as ^{173}Yb or ^{87}Sr, where the nuclear spin degrees of freedom are decoupled from the electronic states due to the zero electronic angular momentum in the ground state. Consequently, atoms can occupy multiple hyperfine states that interact identically, realizing an SU(N) symmetry with N up to the number of accessible hyperfine states.

In this article, we are particularly interested in 1D interacting Fermi systems and on the effects of spin–orbit coupling and Rabi fields. For fermions with three internal states, we introduce spin–orbit coupling and Rabi fields similarly to the spin-1 case discussed in Section 2. However, we use the terminology of color-orbit coupling to describe how the center of mass momentum couples with internal states (colors). Thus, we call the internal states Red, Green and Blue (R,G,B) as in SU(3) quark systems, and write a general momentum-space Hamiltonian matrix as

$$\hat{H}_{\rm KS}(k)=\begin{pmatrix}\varepsilon_R(k) & \Omega_{RG} & \Omega_{RB}\\ \Omega^*_{RG} & \varepsilon_G(k) & \Omega_{GB}\\ \Omega^*_{RB} & \Omega^*_{GB} & \varepsilon_B(k)\end{pmatrix}, \tag{52}$$

where $\varepsilon_c(k)=(k-k_c)^2/2m+\eta_c$, with color $c=\{R,G,B\}$. This is a particular example of the 3D case discussed in the literature [60,61]. Considering the experimentally realizable Hamiltonian described in Equation (12) of Section 2, we simplify the general Hamiltonian in Equation (52) by letting $\Omega_{RB}=0$, $\Omega_{RG}=\Omega^*_{RG}=\Omega_{GB}=\Omega^*_{GB}=\Omega$, $k_R=k_T$, $k_G=0$, $k_B=-k_T$, and we set the reference

energies η_c to $\eta_R = -\delta$, $\eta_G = \eta$, $\eta_B = \delta$. This choice sets the independent-particle Hamiltonian matrix to

$$\hat{H}_{\rm KS}(k) = \begin{pmatrix} \varepsilon_R(k) & \Omega & 0 \\ \Omega & \varepsilon_G(k) & \Omega \\ 0 & \Omega & \varepsilon_B(k) \end{pmatrix}, \tag{53}$$

where $\varepsilon_R = (k - k_T)^2/2m - \delta$, $\varepsilon_G = k^2/2m + \eta$, $\varepsilon_B = (k + k_T)^2/2m + \delta$ are the dispersions of the Red, Green and Blue states. Here, k_T is the momentum transfer, and $E_T = k_T^2/2m$ is the associated transfer energy. The notation used here is similar to that described in the spin-1 matrix of Equation (12) and in the illustration shown in Figure 1(b): Ω describes a Rabi coupling, δ represents the detuning, and η is a reference energy. In our 1D analysis, we converted the 3D notation used in Equation (12) via the following mapping: $k_x \to k$, $\mathbf{k}_\perp \to \mathbf{0}$, and $k_T \to k_T$ for momenta, as well as $\delta \to \delta$, $\eta \to \eta$ and $\Omega_R/2 \to \Omega$ for energies.

Using a compact notation, we rewrite

$$\hat{H}_{\rm KS}(k) = \varepsilon(k) I - h_x J_x - h_z J_z + b_z J_z^2, \tag{54}$$

where I is the identity matrix and J_ℓ are spin-1 angular momentum matrices

$$J_x = \frac{1}{\sqrt{2}} \begin{pmatrix} 0 & 1 & 0 \\ 1 & 0 & 1 \\ 0 & 1 & 0 \end{pmatrix}, \quad J_y = \frac{1}{\sqrt{2}\mathrm{i}} \begin{pmatrix} 0 & 1 & 0 \\ -1 & 0 & 1 \\ 0 & -1 & 0 \end{pmatrix}, \quad J_z = \begin{pmatrix} 1 & 0 & 0 \\ 0 & 0 & 0 \\ 0 & 0 & -1 \end{pmatrix}.$$

The coefficients that multiply the matrices are $\varepsilon(k) = k^2/2m + \eta$ corresponding to a shifted kinetic energy, $h_x = -\sqrt{2}\Omega$ describing a color-flip (Rabi) field, $h_z(k) = 2kk_T/2m + \delta$ reflecting the color-orbit coupling, and $b_z = k_T^2/2m - \eta$ representing the quadrupolar field. Notice that the quadrupolar term $b_z J_z^2$ lies beyond the realm of the angular momentum SO(3) Lie Group for the spin-1 representation (the 3-representation of SU(2), also called the ajoint representation), requiring the larger SU(3) Lie Group to cover the Hilbert space of the Hamiltonian. As discussed later, we do not use directly the eight Gell-Mann matrices to cover SU(3), but rather use three angular momentum matrices J_ℓ and five quadrupolar tensor matrices $J_\ell J_{\ell'}$ (from the set of nine) to cover the SU(3) space, where $\{\ell, \ell'\} \in \{x, y, z\}$.

We write the independent particle Hamiltonian in second-quantized notation as

$$\hat{H}_{\rm kin} = \sum_k \mathbf{F}^\dagger(k) \hat{H}_{\rm KS}(k) \mathbf{F}(k), \tag{55}$$

where the spinor operator $\mathbf{F}^\dagger(k) = \left(f_R^\dagger(k) \; f_G^\dagger(k) \; f_B^\dagger(k) \right)$ creates fermions with colors $\{R, G, B\}$ and momentum k. The SU(3)-invariant interaction Hamiltonian has the structure

$$\hat{H}_{\rm int} = V_0 \sum_{c \neq c'} \int_0^{L_b} \mathrm{d}x' \int_0^{L_b} \mathrm{d}x \hat{n}_c(x) \hat{n}_{c'}(x') g(|x - x'|), \tag{56}$$

where L_b is the length of system, $\hat{n}_c(x) = \psi_c^\dagger(x)\psi_c(x)$ is the local color density operator with color label $c = \{R, G, B\}$, V_0 is the interaction strength with dimensions of energy, and $g(|x - x'|)$ is a dimensionless function that controls the interaction range R_0.

As we shall see next, color-orbit coupling and color-flip fields change dramatically the eigenvalues and eigenstates of the Hamiltonian in Equation (55).

5.1. *Color-orbit-mixed energy dispersions*

The independent-particle Hamiltonian in Equation (55) is diagonalized via a change of basis implemented by a unitary matrix $R(k)$ satisfying $R(k)R^\dagger(k) = I$. Defining the new basis state by the labels $\{\Uparrow, 0, \Downarrow\}$, then the new creation operators are

$$\mathbf{\Phi}^\dagger(k) = \left(\phi_\Uparrow^\dagger(k) \; \phi_0^\dagger(k) \; \phi_\Downarrow^\dagger(k) \right) = \left(f_R^\dagger(k) \; f_G^\dagger(k) \; f_B^\dagger(k) \right) R^\dagger(k),$$

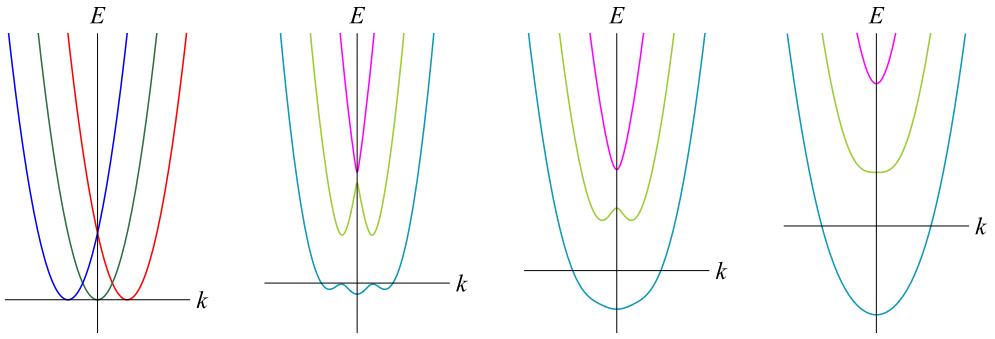

(a) $h_x/E_T = 0$ **(b)** $h_x/E_T = 0.35$ **(c)** $h_x/E_T = 1$ **(d)** $h_x/E_T = 2.1$

Figure 6. Schematic plots of the dispersion relations $\mathscr{E}_\alpha(k)$, with $\alpha \in \{\Uparrow, 0, \Downarrow\}$, for various h_x/E_T, where $E_T = k_T^2/2m$. The unit of momentum is k_T and the unit of energy is E_T. The values of h_x/E_T are indicated in each panel. In (a), the eigenmodes are the same as the internal states $\{R, G, B\}$, and are color-coded as red, green and blue solid lines correspondingly. In (b), (c) and (d), the eigenmodes are labeled by $\{\Uparrow, 0, \Downarrow\}$, and are color-coded as blue-green, yellow-green, and magenta solid lines respectively.

where $R(k)$ written in matrix form is

$$R(k) = \begin{pmatrix} R_{\Uparrow R}(k) & R_{\Uparrow G}(k) & R_{\Uparrow B}(k) \\ R_{0R}(k) & R_{0G}(k) & R_{0B}(k) \\ R_{\Downarrow R}(k) & R_{\Downarrow G}(k) & R_{\Downarrow B}(k) \end{pmatrix}. \tag{57}$$

Due to the presence of the quadratic term $b_z J_z^2$ in the Hamiltonian, $R(k)$ is a general SU(3) matrix and cannot be expressed as a linear combinations of angular momentum operators. The diagonalized independent-particle Hamiltonian matrix is

$$\hat{H}_{\rm MC}(k) = R(k)\hat{H}_{\rm KS}(k)R^\dagger(k) = \begin{pmatrix} \mathscr{E}_\Uparrow(k) & 0 & 0 \\ 0 & \mathscr{E}_0(k) & 0 \\ 0 & 0 & \mathscr{E}_\Downarrow(k) \end{pmatrix}, \tag{58}$$

where $\mathscr{E}_\alpha(k)$ are the eigenenergies with $\alpha \in \{\Uparrow, 0, \Downarrow\}$. These results are analogous to the 3D case [60,61]. In the mixed-color basis, the second-quantized kinetic energy Hamiltonian becomes

$$\hat{H}_{\rm kin} = \sum_k \mathbf{\Phi}^\dagger(k)\hat{H}_{\rm MC}(k)\mathbf{\Phi}(k) = \sum_k \mathscr{E}_\alpha(k)\phi_\alpha^\dagger(k)\phi_\alpha(k). \tag{59}$$

In Figure 6, we show schematically the eigenvalues (dispersion relations) $\mathscr{E}_\alpha(k)$, using $E_T = k_T^2/2m$ as the unit of energy and k_T as the unit of momentum, for various h_x/E_T. There are four qualitative different cases illustrated in panels (a), (b), (c) and (d).

In Figure 6(a), there is no Rabi field $h_x/E_T = 0$, but the momentum transfer is for $+k_T$ for the R band, zero (0) for the G band, and $-k_T$ for the B band. In this case, the system is equivalent to the situation where there is no SOC and the $\{R, G, B\}$ bands are triply degenerate due to a color-gauge symmetry, where the momentum shifts $+k_T$ and $-k_T$ can be gauged away in analogy with the lattice case [107,108].

In Figure 6(b), the dispersions of the $\{\Uparrow, 0, \Downarrow\}$ bands are shown for $h_x/E_T = 0.35$, where the Rabi field is relatively weak in comparison to E_T. In this case, the lowest band ($\Uparrow$) has triple minima and double maxima (blue-green solid line), the middle band (0) has double minima and single maximum (yellow-green solid line), and the highest band ($\Downarrow$) has a single minimum (magenta solid line). For the lowest band ($\Uparrow$), the energy at $k = 0$ is always lower than the local energy minima at $k = \pm k_{\rm min}$, provided that $|h_x|/E_T < 0.544$.

In Figure 6(c), the color-flip (Rabi) field h_x is comparable to the momentum transfer energy E_T, that is, $h_x/E_T = 1$, such that the lowest band ($\Uparrow$) has a single minimum, the middle band (0) has double minima and a single maximum, while the highest band ($\Downarrow$) has a single minimum. This behavior occurs in the range $0.544 < |h_x|/E_T < 2.000$.

In Figure 6(d), the color-flip (Rabi) field h_x is sufficiently strong in comparison to E_T, that is, $|h_x|/E_T > 2.000$, such that all three bands $\{\Uparrow, 0, \Downarrow\}$ have single minima.

In summary, when the color-flip (Rabi) field h_x is zero, the system has spin-gauge symmetry and is equivalent to the situation without SOC. However, when the color-flip field h_x exists there are qualitative changes in the eigenenergies. The highest band ($\Downarrow$) has always a single minimum as shown in panels (b), (c) and (d) of Figure 6. The middle band (0) has double minima and a single maximum when $|h_x|/E_T < 2.000$, as shown in panels (b) and (c) of Figure 6, and has a single minimum when $|h_x|/E_T > 2.000$, as shown in panel (d) of Figure 6. The lowest band ($\Uparrow$) has triple minima and double maxima when $|h_x|/E_T < 0.544$, as illustrated in panel (b) of Figure 6, and has a single minimum when $|h_x|/E_T > 0.544$, as seen in panels (c) and (d) of Figure 6. Now that we have identified the regimes where the eigenvalues $\mathscr{E}_{\Uparrow}(k)$, $\mathscr{E}_0(k)$ and $\mathscr{E}_{\Downarrow}(k)$ change qualitatively, we discuss next the phase diagram and the velocities of the collective (boson) modes.

5.2. *Phase diagram and velocities of boson modes*

In our analysis of the phase diagram for SU(3) fermions, we use $E_T = k_T^2/2m$ and k_T as our energy and momentum scales, respectively, and discuss initially the case of no interactions. For our Fermi system with three internal states, the phase diagram of chemical potential μ/E_T versus Rabi field h_x/E_T is obtained by monitoring the topology of the Fermi surfaces associated with the energy eigenvalues $\mathscr{E}_{\Uparrow}(k)$, $\mathscr{E}_0(k)$ and $\mathscr{E}_{\Downarrow}(k)$. Similarly to the SU(2) case, as the chemical potential varies, the change in the number of Fermi points N_F determines the number of collective modes $N_C = N_F/2$ and defines topological quantum phase transitions of the Lifshitz-type [93–95].

In Figure 7(a), we show the phase diagram of μ/E_T versus h_x/E_T, which is obtained similarly to the SU(2) case, that is, by tracking the topology of the Fermi surfaces and the number of Fermi points N_F. The black solid lines separate phases where the number of collective modes $N_C = N_F/2$ is different, the gray dashed lines describe the locations where the number of minima for the two lowest-energy bands changes, as seen in Figure 6, and the red solid line represents a fixed density curve for $n = 1.2k_T$, where n is the total density in 1D. Long-wavelength and low-energy properties of the collective modes arise from the linearization around the Fermi points and the bosonization process discussed next.

When three degenerate bands are involved, that is, in the absence of color-orbit coupling and color-flip (Rabi) fields where SU(3) is fully preserved, it is natural to seek for analogous effects to spin–charge separation found in SU(2) invariant Tomonaga–Luttinger liquids. Furthermore, when SU(3) symmetry is explicitly broken, due to color-orbit coupling and color-flip fields (see Figure 6), the Fermi system becomes a non-degenerate three-, two- or one-band Tomonaga–Luttinger liquid, depending on the location of the chemical potential. The properties of this three-band Fermi system is explored via a generalized bosonization technique that allows for an analysis of its collective modes. Similar to the standard bosonization technique [4,5], as well as the SU(2) case discussed in Section 4.1 and found in the literature [90], we linearize $\hat{H}_{\rm kin}$ in Equation (59) around the chemical potential giving

$$\hat{H}_{\rm kin} = \sum_{k\alpha r} \{\mu + {\rm sgn}(r)\, v_\alpha [k - {\rm sgn}(r)\, k_{\mu\alpha}]\} \phi^\dagger_{\alpha r}(k) \phi_{\alpha r}(k). \tag{60}$$

Here, $r \in \{L, R\}$ represents left-going or right-going fermions with ${\rm sgn}(L) = -1$ and ${\rm sgn}(R) = 1$, v_α is the velocity at the positive momenta $k_{\mu\alpha}$ where the chemical potential μ intersects band α, that is, $v_{\mu\alpha} = {\rm d}\mathscr{E}_\alpha(k)/{\rm d}k$, and the operator $\phi^\dagger_{\alpha r}(k)$ creates a fermion with momentum k in

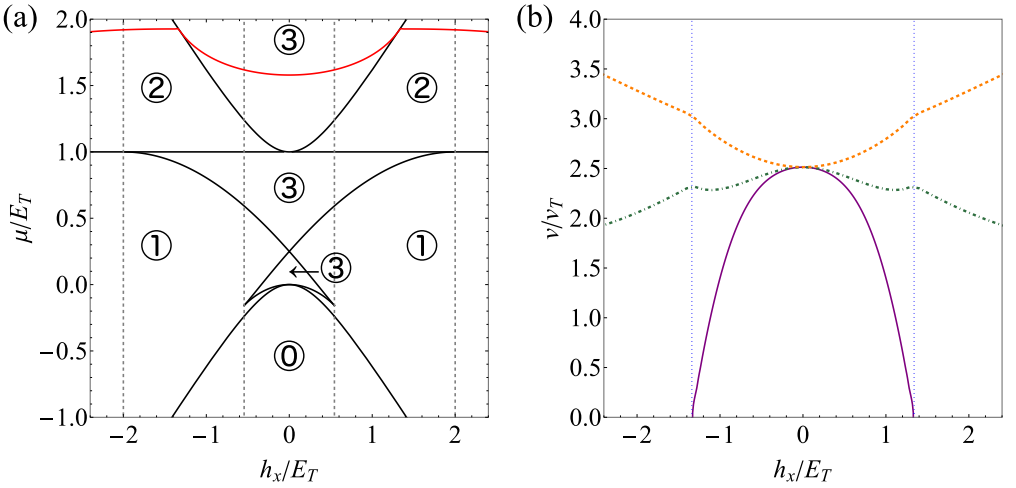

Figure 7. Phase diagram and velocities of collective modes. In panel (a), we show the phase diagram in the plane of μ/E_T versus h_x/E_T. The black solid lines separate phases with different number of collective modes N_C. The values of N_C are indicated by the circled numbers. The gray dashed lines show the location where the number of minima of the two lowest-energy bands changes: the lines at $|h_x|/E_T = \pm 2.000$ separate double minima and single maximum ($|h_x|/E_T < 2.000$) from a single minimum ($|h_x|/E_T < 2.000$) for the middle band (0), and the lines at $|h_x|/E_T = \pm 0.544$ separate triple minima and double maxima ($|h_x|/E_T < 0.544$) from a single minimum ($|h_x|/E_T > 0.544$) for the lowest band ($\Uparrow$). The red solid line represents a constant density curve with $n = 1.2k_T$, where n is the total density in 1D. In panel (b), we show the collective mode velocities $v_\Uparrow$, v_0 and $v_\Downarrow$ along the red curve, shown in panel (a), for non-interacting fermions with energy bands labeled by $\{\Uparrow, 0, \Downarrow\}$. The orange dashed line indicates $v_\Uparrow$, the green dot-dashed line describes v_0, and the purple solid line represents $v_\Downarrow$. In panel (b), the blue dotted lines show the locations where the red solid and the black solid lines intersect in panel (a), revealing a phase change. The number of collective modes changes from $N_C = 2$ to $N_C = 3$ at $h_x/E_T = -1.340$ and from from $N_C = 3$ to $N_C = 2$ at $h_x/E_T = +1.340$.

band α and branch r. Both v_α and $k_{\mu\alpha}$ depend on k_T, h_x and μ. The reference Hamiltonian $\hat{H}_0 = \sum_{k\alpha r} \mu \phi^\dagger_{\alpha r}(k)\phi_{\alpha r}(k)$, corresponding to the energy $E_0 = N\mu$, where N is the total number of fermions, is set to zero without loss of generality. Thus, like in the SU(2) case, we drop this reference term from the kinetic energy operator $\hat{H}_{\rm kin}$ from now on.

To bosonize $\hat{H}_{\rm kin}$, we first define the standard density operator in the momentum space

$$\hat{\rho}_{\alpha r}(q) = \sum_k \phi^\dagger_{\alpha r}(k)\phi_{\alpha r}(k+q), \tag{61}$$

where $\alpha \in \{\Uparrow, 0, \Downarrow\}$ and use the commutation relation

$$[\hat{H}_{\rm kin}, \hat{\rho}_{\alpha r}(q)] = -{\rm sgn}(r)\, v_\alpha q \hat{\rho}_{\alpha r}(q). \tag{62}$$

Combining the last two expressions gives

$$\hat{H}_{\rm kin} = \frac{2\pi}{L_b} \sum_{q>0,\alpha r} v_\alpha \hat{\rho}_{\alpha r}(-q)\hat{\rho}_{\alpha r}(q) \tag{63}$$

in terms of density operators defined in Equation (61), where L_b is the length of the system. The kinetic energy operator is bosonized via the relation

$$b^\dagger_\alpha(q) = \sqrt{\frac{2\pi}{|q|L_b}} \sum_r \Theta\big(-\mathrm{sgn}(r)q\big)\hat{\rho}_{\alpha r}(q), \tag{64}$$

where $\Theta(z)$ is the Heaviside step function, leading to

$$\hat{H}_{\rm kin} = \sum_{q\alpha} v_\alpha |q| b^\dagger_\alpha(q) b_\alpha(q) + K_\Omega, \tag{65}$$

where v_α represents the velocity of the collective mode, labeled by the band index α, in the absence of interactions, and $K_\Omega = \sum_{q>0,\alpha} |q\, v_\alpha|$. As expected, without interactions, the collective mode velocities are just the Fermi velocities v_α at $k = k_{\mu\alpha}$, but they are functions of the color-flip (Rabi) fields h_x, color-orbit coupling parameter k_T and chemical potential μ or density n.

In Figure 7(b), we show the velocities of the collective modes as a function of h_x, at a fixed density $n = 1.2k_T$, corresponding to the red solid curve in Figure 7(a). The orange dashed line, the green dot-dashed line and the purple solid line indicate the collective mode velocities $v_\Uparrow$, v_0, and $v_\Downarrow$, respectively. The blue dotted lines show that the number of collective modes changes from $N_{\rm C} = 2$ to $N_{\rm C} = 3$ at $h_x/E_T = -1.340$ and from $N_{\rm C} = 3$ to $N_{\rm C} = 2$ at $h_x/E_T = +1.340$.

Having discussed the bosonization procedure for non-interacting SU(3) fermions in the presence of color-orbit coupling and color-flipping (Rabi) fields, it is clear that among the open questions is the effect of SU(3) symmetric interactions in changing the collective mode velocities, spectral weight and internal properties (quantum numbers), as discussed next.

5.3. *Open questions for SU(3) fermions*

Without SU(3) symmetric interactions, the emergent boson modes $b^\dagger_\alpha(q)$ and $b_\alpha(q)$ are simply related to the density operators $\hat{\rho}^\dagger_{\alpha r}(q)$ and $\hat{\rho}_{\alpha r}(q)$, as seen in Equation (64). However, SU(3) symmetric interactions $\hat{H}_{\rm int}$, given in Equation (56), are expected to introduce additional bilinears involving $\hat{\rho}^\dagger_{\alpha r}(q)$ and $\hat{\rho}_{\alpha r}(q)$ that require a generalized Bogoliubov transformation to diagonalize the total Hamiltonian $\hat{H} = \hat{H}_{\rm kin} + \hat{H}_{\rm int}$. In analogy to the SU(2) case, we identify the eigenmodes of $\hat{H}$ with the final bosonic operators $d^\dagger_\ell(q)$ and $d_\ell(q)$, but now ℓ can have a maximum of three flavors, that is, $\ell = \{1,2,3\}$.

As discussed in Section 4.2, for fermions with two internal states, the boson operators $d^\dagger_\ell(q)$ and $d_\ell(q)$ covered the SU(2) space and were decomposed into charge (scalar) and spin (vector) sectors. When Rabi fields and SOC are zero, the degenerate Fermi bands and the SU(2) invariant interaction lead to the standard spin–charge separation, and when Rabi field and SOC are nonzero, the bosonic modes become Weyl bosons, with a helical structure expressed in terms of a mixture of charge- and spin-density operators. The coverage of the SU(2) Lie group leads to a singlet sector that transforms like the identity (charge density), and a triplet sector that transforms like angular momentum (spin density).

In the SU(3) case, it is natural to conjecture that the final bosonic operators $d^\dagger_\ell(q)$ and $d_\ell(q)$ are decomposed into singlet (charge density), triplet (spin density) and quintet (quadrupolar density) sectors. Hence, the set of operators $\{\hat{\rho}, \hat{\mathbf{J}}, \hat{\mathbf{K}}\}$, where $\hat{\rho}$ is the density, $\hat{\mathbf{J}}$ is the angular momentum, and $\hat{\mathbf{K}}$ is the symmetric quadrupolar tensor quintet

$$\hat{\mathbf{K}} = \big(\tfrac{1}{2}\{\hat{J}_x, \hat{J}_y\}, \tfrac{1}{2}\{\hat{J}_y, \hat{J}_z\}, \tfrac{1}{2}\{\hat{J}_z, \hat{J}_x\}, \hat{J}^2_x - \tfrac{1}{3}\hat{\rho}, \hat{J}^2_y - \tfrac{1}{3}\hat{\rho}\big)^T, \tag{66}$$

provide a physically transparent coverage of SU(3), which is preferable, instead of using the Gell-Mann matrices used for quark SU(3) physics. Here, $\{\hat{A}, \hat{B}\}$ represents the anti-commutator of operators $\hat{A}$ and $\hat{B}$. Hence, the final boson operators may be decomposed as

$$d^\dagger_\ell(q) = \sum_r \big[A_{\ell r}(q)\hat{\rho}_r(q) + \mathbf{B}_{\ell r}(q)\cdot\hat{\mathbf{J}}_r(q) + \mathbf{C}_{\ell r}(q)\cdot\hat{\mathbf{K}}_r(q)\big], \tag{67}$$

where $\hat{\rho}(q)$, $\hat{\mathbf{J}}(q)$, and $\hat{\mathbf{K}}(q)$ are second-quantized momentum-space fermionic representations of $\{\hat{\rho}, \hat{\mathbf{J}}, \hat{\mathbf{K}}\}$, respectively, and the label r represents either left (L) or right (R) going fermions.

If the conjectured decomposition above holds for bosonic eigenmodes of SU(3) Fermi systems, several open questions arise both with and without color-orbit coupling and color-flip (Rabi) fields: If no color-orbit or color-flip fields are present, is there spin–charge–quadrupole separation when interactions are included? Is there an expanded analogy to spin–charge separation found for SU(2)? Are there separated charge, spin and quadrupolar density modes? Furthermore, if color-orbit coupling, color-flip fields, and interactions are present, what are the extensions of Weyl bosons to the SU(3) case? Do helical or nematic modes arise due to the spin or quadrupolar sectors?

Since there the quadrupolar operator has a tensorial structure, what experimentally measurable response functions can reveal this feature? Is there an extension of the dynamical structure factor tensor $S_{ij}(q,\omega)$, found for SU(2) systems, that can be measured for the SU(3) case? Selection rules involving quadrupolar operators are different from those involving angular momentum operators: can they be used to detect the tensorial nature of the bosonic modes?[2]

Given the expected tensorial, vector and scalar components of the SU(3) bosonic modes $d_\ell(q)$ is there a closer connection to spin-squeezing [109], magnetization [110], and topology [111] of condensed spin-1 bosons?

Experimental studies of SU(3) fermions with color-orbit and color-flip (Rabi) fields remain challenging. However, recent advances have realized SU(3) color-orbit coupling in a laser-trapped ultracold gas of ^{87}Sr [112]. Moreover, the development of box potentials offers promising prospects for trapping fermions with three internal states [97]. These developments suggest that similar investigations using other atomic species, such as ^{173}Yb, may become feasible in the near future.

Having discussed several open questions for SU(3) fermions in the presence or absence of color-orbit coupling and color-flip (Rabi) fields, we present, next, our conclusions and general outlook.

6. Conclusions and general outlook

We have discussed the current research status and open questions regarding the effects of spin–orbit coupling and Rabi fields for SU(2) Tomonaga–Luttinger liquids and color-orbit coupling and color-flip fields for SU(3) Tomonaga–Luttinger liquids. In this article, we focused on one dimensional systems realized in ultracold fermions, but some of the current status results and open questions when spin–orbit (color-orbit) and Rabi (color-flip) fields are present are also applicable to standard condensed matter and to two-dimensional and three-dimensional systems. We concentrated on one-dimensional systems, because several intermediate and advanced analytical results can be obtained using the bosonization method.

For SU(2) systems, the emergence of Weyl bosons, that is, helical, massless pseudo-spin 1/2 bosons, is not a phenomenon only restricted to one dimension, but also arises in two and three dimensions. The helicity induced by the spin–orbit and Rabi fields created by Raman processes and affecting fermionic states is transferred to the charge and spin density sectors creating helical collective excitations. The analysis in one dimension is more beautiful, because we can start from charge and spin separated systems, and create Weyl bosons by coupling these two channels via spin–orbit and Rabi fields. However, we expect that in two and three dimensions, where charge and spin densities are not separated, Weyl bosons will also emerge due to spin–orbit coupling and

[2] This question was inspired by a related question that Wolfgang Ketterle asked, regarding C. A. R. Sá de Melo's presentation at the Institut Henri Poincaré, covering the atomic processes and the selection rules that are needed to detect experimentally SU(3) tensorial modes.

Rabi fields and could be detected by measuring the components of the dynamical structure factor tensor, just like in one dimension. Currently, in any dimension, the experimental exploration of this phenomenon for ^{6}Li, ^{40}K, ^{173}Yb and ^{87}Sr is very difficult, because of difficulties associated with specific atomic properties or technicalities that prevent the creation of simultaneous spin–orbit coupling and Rabi fields at sufficiently low temperatures.

For SU(3) systems, the ideal candidates are ^{173}Yb and ^{87}Sr, where the interactions are naturally SU(N) symmetric, with $N \leq 6$ in the former and $N \leq 10$ in the latter. When $N = 3$, both candidates are SU(3) symmetric without color-orbit and color-flip (Rabi) fields. The existence of up to three collective modes with scalar (singlet), vector (triplet) and tensorial (quintuplet) components are expected when expressed in terms of the charge, spin and quadrupolar densities. Thus, the collective bosonic modes are anticipated to be much more exotic that the Weyl bosons found in the SU(2) case. Although one dimensional systems allow for several analytical results and transparent symmetry considerations arising directly from bosonization, similar results are also envisaged in two and three dimensions. However, experimental investigations of color-orbit and color-flip (Rabi) fields of interacting SU(3) fermions, in any dimension, have not yet been performed due to technical difficulties.

Due to the absence of experiments exploring interacting SU(2) or SU(3) fermions in the presence of spin–orbit and Rabi fields or color-orbit and color-flip fields, the entire presentation above is currently only of theoretical interest. However, as an outlook, it is important to emphasize that SU(2) or SU(3) symmetric interactions are not necessary for the emergence of Weyl bosons or tensorial collective bosonic modes in one, two or three dimensions. This means that for any interacting ultracold Fermi system with two or three internal states, it is sufficient to create spin–orbit and Rabi couplings or color-orbit and color-flip couplings to produce the exotic collective modes discussed above. Furthermore, in the context of standard condensed matter systems, it is also sufficient to find a material, with either two or three bands, and essentially any kind of spin–orbit coupling and Zeeman fields to produce similar types of collective modes.

On the one hand, the experimental outlook for ultracold fermions is to find a way to overcome the difficulties in standard systems such as ^{6}Li, ^{40}K, ^{173}Yb and ^{87}Sr or to explore novel systems such as ^{171}Dy or ^{173}Dy; on the other hand, the experimental outlook for standard condensed matter, is to find solid state materials that meet the appropriate theoretical requirements. In the mean time, while we await experimental progress, there are plenty of open theoretical questions that need to be addressed.

Declaration of interests

The authors do not work for, advise, own shares in, or receive funds from any organization that could benefit from this article, and have declared no affiliations other than their research organizations.

Acknowledgements

CARSM would like to acknowledge the Institut Henri Poincaré for its hospitality, the Mercator Fellowship from the German Research Foundation (DFG) for support, and Yvan Castin, Wolfgang Ketterle, and Thierry Giamarchi for discussions.

References

[1] S.-I. Tomonaga, "Remarks on Bloch's method of sound waves applied to many-fermion problems", *Prog. Theor. Phys.* **5** (1950), no. 4, pp. 544–569.

[2] J. M. Luttinger, "An exactly soluble model of a manyfermion system", *J. Math. Phys.* **4** (1963), no. 9, pp. 1154–1162.

[3] F. D. M. Haldane, "'Luttinger liquid theory' of one-dimensional quantum fluids. I. Properties of the Luttinger model and their extension to the general 1D interacting spinless Fermi gas", *J. Phys. C: Solid State Phys.* **14** (1981), no. 19, pp. 2585–2609.

[4] T. Giamarchi, *Quantum Physics in One Dimension*, Oxford University Press: Oxford, 2003.

[5] A. Altland and B. Simons, *Condensed Matter Field Theory*, 3rd edition, Cambridge University Press: Cambridge, 2023.

[6] A. Imambekov, T. L. Schmidt and L. I. Glazman, "One-dimensional quantum liquids: beyond the Luttinger liquid paradigm", *Rev. Mod. Phys.* **84** (2012), pp. 1253–1306.

[7] A. J. Niemi and N. R. Walet, "Splitting the gluon?", *Phys. Rev. D* **72** (2005), article no. 054007.

[8] L. Faddeev and A. J. Niemi, "Spin-charge separation, conformal covariance and the SU(2) Yang–Mills theory", *Nucl. Phys. B* **776** (2007), no. 1, pp. 38–65.

[9] M. N. Chernodub and A. J. Niemi, "Spin-charge separation and the Pauli electron", *JETP Lett.* **85** (2007), no. 8, pp. 353–357.

[10] G. A. Diamandis, B. C. Georgalas and N. E. Mavromatos, "N=1 supersymmetric spin-charge separation in effective gauge theories of planar magnetic superconductors", *Mod. Phys. Lett. A* **13** (1998), no. 05, pp. 387–404.

[11] C. Xiong, "From the fourth color to spin-charge separation: Neutrinos and spinons", *Mod. Phys. Lett. A* **30** (2015), no. 25, article no. 1530021.

[12] C. Kim, A. Y. Matsuura, Z.-X. Shen, N. Motoyama, H. Eisaki, S. Uchida, T. Tohyama and S. Maekawa, "Observation of spin-charge separation in one-dimensional $SrCuO_2$", *Phys. Rev. Lett.* **77** (1996), pp. 4054–4057.

[13] B. J. Kim et al., "Distinct spinon and holon dispersions in photoemission spectral functions from one-dimensional SrCuO2", *Nat. Phys.* **2** (2006), no. 6, pp. 397–401.

[14] O. M. Auslaender, A. Yacoby, R. de Picciotto, K. W. Baldwin, L. N. Pfeiffer and K. W. West, "Tunneling spectroscopy of the elementary excitations in a one-dimensional wire", *Science* **295** (2002), no. 5556, pp. 825–828.

[15] O. M. Auslaender, H. Steinberg, A. Yacoby, Y. Tserkovnyak, B. I. Halperin, K. W. Baldwin, L. N. Pfeiffer and K. W. West, "Spin-charge separation and localization in one dimension", *Science* **308** (2005), no. 5718, pp. 88–92.

[16] R. Senaratne et al., "Spin-charge separation in a one-dimensional Fermi gas with tunable interactions", *Science* **376** (2022), no. 6599, pp. 1305–1308.

[17] D. Cavazos-Cavazos, R. Senaratne, A. Kafle and R. G. Hulet, "Thermal disruption of a Luttinger liquid", *Nat. Commun.* **14** (2023), no. 1, article no. 3154.

[18] J. Sinova, S. O. Valenzuela, J. Wunderlich, C. H. Back and T. Jungwirth, "Spin Hall effects", *Rev. Mod. Phys.* **87** (2015), pp. 1213–1260.

[19] T. Kawada, M. Kawaguchi, T. Funato, H. Kohno and M. Hayashi, "Acoustic spin Hall effect in strong spin–orbit metals", *Sci. Adv.* **7** (2021), no. 2, article no. eabd9697.

[20] M. Z. Hasan and C. L. Kane, "Colloquium: topological insulators", *Rev. Mod. Phys.* **82** (2010), pp. 3045–3067.

[21] X.-L. Qi and S.-C. Zhang, "Topological insulators and superconductors", *Rev. Mod. Phys.* **83** (2011), pp. 1057–1110.

[22] M. Sato and Y. Ando, "Topological superconductors: a review", *Rep. Prog. Phys.* **80** (2017), no. 7, article no. 076501.

[23] H. D. Scammell, J. Ingham, M. Geier and T. Li, "Intrinsic first- and higher-order topological superconductivity in a doped topological insulator", *Phys. Rev. B* **105** (2022), article no. 195149.

[24] M. Zeng, D.-H. Xu, Z.-M. Wang and L.-H. Hu, "Spin-orbit coupled superconductivity with spin-singlet nonunitary pairing", *Phys. Rev. B* **107** (2023), article no. 094507.

[25] E. Rashba and V. Sheka, "Combined resonance in electron InSb", *Sov. Phys., Solid State* **3** (1961), no. 6, pp. 1357–1362.

[26] G. Dresselhaus, "Spin-orbit coupling effects in zinc blende structures", *Phys. Rev.* **100** (1955), pp. 580–586.

[27] Y. A. Bychkov and É. I. Rashba, "Properties of a 2D electron gas with lifted spectral degeneracy", *JETP Lett.* **39** (1984), no. 2, pp. 78–81.

[28] J. Sinova and A. H. MacDonald, "Theory of spin–orbit effects in semiconductors", *Semicond. Semimetals* **82** (2008), pp. 45–87.

[29] S. Schott et al., "Tuning the effective spin–orbit coupling in molecular semiconductors", *Nat. Commun.* **8** (2017), no. 1, article no. 15200.

[30] J. Chen, K. Wu, W. Hu and J. Yang, "Spin–orbit coupling in 2D semiconductors: a theoretical perspective", *J. Phys. Chem. Lett.* **12** (2021), no. 51, pp. 12256–12268.

[31] E. Marcellina, A. R. Hamilton, R. Winkler and D. Culcer, "Spin-orbit interactions in inversion-asymmetric two-dimensional hole systems: a variational analysis", *Phys. Rev. B* **95** (2017), article no. 075305.

[32] D. Shcherbakov et al., "Layer- and gate-tunable spin–orbit coupling in a high-mobility few-layer semiconductor", *Sci. Adv.* **7** (2021), no. 5, article no. eabe2892.

[33] D. L. Campbell, G. Juzeliūnas and I. B. Spielman, "Realistic Rashba and Dresselhaus spin–orbit coupling for neutral atoms", *Phys. Rev. A* **84** (2011), article no. 025602.
[34] V. Galitski and I. B. Spielman, "Spin–orbit coupling in quantum gases", *Nature* **494** (2013), no. 7435, pp. 49–54.
[35] Y.-J. Lin, K. Jiménez-García and I. B. Spielman, "Spin–orbit-coupled Bose–Einstein condensates", *Nature* **471** (2011), no. 7336, pp. 83–86.
[36] M. Atala, M. Aidelsburger, M. Lohse, J. T. Barreiro, B. Paredes and I. Bloch, "Observation of chiral currents with ultracold atoms in bosonic ladders", *Nat. Phys.* **10** (2014), no. 8, pp. 588–593.
[37] A. Frölian, C. S. Chisholm, E. Neri, C. R. Cabrera, R. Ramos, A. Celi and L. Tarruell, "Realizing a 1D topological gauge theory in an optically dressed BEC", *Nature* **608** (2022), no. 7922, pp. 293–297.
[38] L. W. Cheuk, A. T. Sommer, Z. Hadzibabic, T. Yefsah, W. S. Bakr and M. W. Zwierlein, "Spin-injection spectroscopy of a spin-orbit coupled Fermi gas", *Phys. Rev. Lett.* **109** (2012), article no. 095302.
[39] M. Mancini et al., "Observation of chiral edge states with neutral fermions in synthetic Hall ribbons", *Science* **349** (2015), no. 6255, pp. 1510–1513.
[40] S. Kolkowitz et al., "Spin–orbit-coupled fermions in an optical lattice clock", *Nature* **542** (2017), no. 7639, pp. 66–70.
[41] D. L. Campbell and I. B. Spielman, "Rashba realization: Raman with RF", *New J. Phys.* **18** (2016), no. 3, article no. 033035.
[42] L. Huang et al., "Experimental realization of two-dimensional synthetic spin–orbit coupling in ultracold Fermi gases", *Nat. Phys.* **12** (2016), no. 6, pp. 540–544.
[43] A. Valdés-Curiel, D. Trypogeorgos, Q.-Y. Liang, R. P. Anderson and I. B. Spielman, "Topological features without a lattice in Rashba spin–orbit coupled atoms", *Nat. Commun.* **12** (2021), no. 1, article no. 593.
[44] K. Seo, L. Han and C. A. R. Sá de Melo, "Topological phase transitions in ultracold Fermi superfluids: the evolution from Bardeen-Cooper-Schrieffer to Bose-Einstein-condensate superfluids under artificial spin–orbit fields", *Phys. Rev. A* **85** (2012), article no. 033601.
[45] W. Pauli, "The connection between spin and statistics", *Phys. Rev.* **58** (1940), pp. 716–722.
[46] M. K. Gaillard, P. D. Grannis and F. J. Sciulli, "The standard model of particle physics", *Rev. Mod. Phys.* **71** (1999), S96–S111.
[47] S. Weinberg, "The making of the standard model", *Eur. Phys. J. C* **34** (2004), no. 1, pp. 5–13.
[48] P. A. M. Dirac, "The quantum theory of the electron", *Proc. R. Soc. Lond. A* **117** (1928), no. 778, pp. 610–624.
[49] E. Majorana, "Teoria simmetrica dell'elettrone e del positrone", *Nuovo Cimento* **14** (1937), no. 4, pp. 171–184.
[50] H. Weyl, "Elektron und gravitation. I", *Z. Phys.* **56** (1929), no. 5, pp. 330–352.
[51] D. Castelvecchi, "Evidence of elusive Majorana particle dies — but computing hope lives on", *Nature* **591** (2021), no. 7850, pp. 354–355.
[52] O. Vafek and A. Vishwanath, "Dirac fermions in solids: from high-T_c cuprates and graphene to topological insulators and weyl semimetals", *Annu. Rev. Condens. Matter Phys.* **5** (2014), pp. 83–112.
[53] M. Horio et al., "Two-dimensional type-II Dirac fermions in layered oxides", *Nat. Commun.* **9** (2018), no. 1, article no. 3252.
[54] Y. Ran, F. Wang, H. Zhai, A. Vishwanath and D.-H. Lee, "Nodal spin density wave and band topology of the FeAs-based materials", *Phys. Rev. B* **79** (2009), article no. 014505.
[55] P. Richard et al., "Observation of Dirac cone electronic dispersion in $BaFe_2As_2$", *Phys. Rev. Lett.* **104** (2010), article no. 137001.
[56] S. Y. Tan et al., "Observation of Dirac cone band dispersions in FeSe thin films by photoemission spectroscopy", *Phys. Rev. B* **93** (2016), article no. 104513.
[57] K. S. Novoselov, A. K. Geim, S. V. Morozov, D. Jiang, M. I. Katsnelson, I. V. Grigorieva, S. V. Dubonos and A. A. Firsov, "Two-dimensional gas of massless Dirac fermions in graphene", *Nature* **438** (2005), no. 7065, pp. 197–200.
[58] S.-Y. Xu et al., "Discovery of a Weyl fermion semimetal and topological Fermi arcs", *Science* **349** (2015), no. 6248, pp. 613–617.
[59] B. Q. Lv et al., "Experimental discovery of weyl semimetal TaAs", *Phys. Rev. X* **5** (2015), article no. 031013.
[60] D. M. Kurkcuoglu and C. A. R. Sá de Melo, "Creating spin-one fermions in the presence of artificial spin–orbit fields: emergent spinor physics and spectroscopic properties", *J. Low-Temp. Phys.* **191** (2018), no. 3, pp. 174–183.
[61] D. M. Kurkcuoglu and C. A. R. Sá de Melo, "Color superfluidity of neutral ultracold fermions in the presence of color-flip and color-orbit fields", *Phys. Rev. A* **97** (2018), article no. 023632.
[62] C. Chin, R. Grimm, P. Julienne and E. Tiesinga, "Feshbach resonances in ultracold gases", *Rev. Mod. Phys.* **82** (2010), pp. 1225–1286.
[63] H. Biss, L. Sobirey, N. Luick, M. Bohlen, J. J. Kinnunen, G. M. Bruun, T. Lompe and H. Moritz, "Excitation spectrum and superfluid gap of an ultracold Fermi gas", *Phys. Rev. Lett.* **128** (2022), article no. 100401.
[64] L. Sobirey, H. Biss, N. Luick, M. Bohlen, H. Moritz and T. Lompe, "Observing the influence of reduced dimensionality on fermionic superfluids", *Phys. Rev. Lett.* **129** (2022), article no. 083601.

[65] M. Chapman and C. A. R. Sá de Melo, "Atoms playing dress-up", *Nature* **471** (2011), no. 7336, pp. 41–42.
[66] P. Wang, Z.-Q. Yu, Z. Fu, J. Miao, L. Huang, S. Chai, H. Zhai and J. Zhang, "Spin-orbit coupled degenerate Fermi gases", *Phys. Rev. Lett.* **109** (2012), article no. 095301.
[67] T. Fukuhara, Y. Takasu, M. Kumakura and Y. Takahashi, "Degenerate Fermi gases of ytterbium", *Phys. Rev. Lett.* **98** (2007), article no. 030401.
[68] Y. Takasu, Y. Fukushima, Y. Nakamura and Y. Takahashi, "Magnetoassociation of a Feshbach molecule and spin–orbit interaction between the ground and electronically excited states", *Phys. Rev. A* **96** (2017), article no. 023602.
[69] B. J. DeSalvo, M. Yan, P. G. Mickelson, Y. N. Martinez de Escobar and T. C. Killian, "Degenerate Fermi gas of ^{87}Sr", *Phys. Rev. Lett.* **105** (2010), article no. 030402.
[70] I. B. Spielman, "Raman processes and effective gauge potentials", *Phys. Rev. A* **79** (2009), article no. 063613.
[71] Y.-J. Lin, R. L. Compton, A. R. Perry, W. D. Phillips, J. V. Porto and I. B. Spielman, "Bose-Einstein condensate in a uniform light-induced vector potential", *Phys. Rev. Lett.* **102** (2009), article no. 130401.
[72] D. C. Mattis and E. H. Lieb, "Exact solution of a manyfermion system and its associated boson field", *J. Math. Phys.* **6** (1965), no. 2, pp. 304–312.
[73] M. Dressel, "Spin-charge separation in quasi one-dimensional organic conductors", *Naturwissenschaften* **90** (2003), no. 8, pp. 337–344.
[74] J. Sólyom, "The Fermi gas model of one-dimensional conductors", *Adv. Phys.* **28** (1979), no. 2, pp. 201–303.
[75] D.-W. Wang, A. J. Millis and S. D. Sarma, "Coulomb Luttinger liquid", *Phys. Rev. B* **64** (2001), no. 19, article no. 193307.
[76] F. He, Y.-Z. Jiang, H.-Q. Lin, R. G. Hulet, H. Pu and X.-W. Guan, "Emergence and disruption of spin-charge separation in one-dimensional repulsive fermions", *Phys. Rev. Lett.* **125** (2020), article no. 190401.
[77] C. N. Yang, "Some exact results for the many-body problem in one dimension with repulsive delta-function interaction", *Phys. Rev. Lett.* **19** (1967), pp. 1312–1315.
[78] M. Gaudin, "Un système à une dimension de fermions en interaction", *Phys. Lett. A* **24** (1967), no. 1, pp. 55–56.
[79] O. Tsyplyatyev, "Splitting of the Fermi point of strongly interacting electrons in one dimension: a nonlinear effect of spin-charge separation", *Phys. Rev. B* **105** (2022), article no. L121112.
[80] P. M. T. Vianez et al., "Observing separate spin and charge Fermi seas in a strongly correlated one-dimensional conductor", *Sci. Adv.* **8** (2022), no. 24, article no. eabm2781.
[81] L. Han and C. A. R. Sá de Melo, "Evolution from BCS to BEC superfluidity in the presence of spin–orbit coupling", *Phys. Rev. A* **85** (2012), article no. 011606.
[82] K. Seo, L. Han and C. A. R. Sá de Melo, "Emergence of Majorana and Dirac particles in ultracold fermions via tunable interactions, spin-orbit effects, and Zeeman fields", *Phys. Rev. Lett.* **109** (2012), article no. 105303.
[83] P. D. Powell, G. Baym and C. A. R. Sá de Melo, "Superfluid transition temperature and fluctuation theory of spin–orbit- and Rabi-coupled fermions with tunable interactions", *Phys. Rev. A* **105** (2022), article no. 063304.
[84] M. Gong, S. Tewari and C. Zhang, "BCS-BEC crossover and topological phase transition in 3D spin-orbit coupled degenerate Fermi gases", *Phys. Rev. Lett.* **107** (2011), article no. 195303.
[85] H. Hu, L. Jiang, X.-J. Liu and H. Pu, "Probing anisotropic superfluidity in atomic Fermi gases with Rashba spin-orbit coupling", *Phys. Rev. Lett.* **107** (2011), article no. 195304.
[86] Z.-Q. Yu and H. Zhai, "Spin-orbit coupled Fermi gases across a Feshbach resonance", *Phys. Rev. Lett.* **107** (2011), article no. 195305.
[87] J. P. A. Devreese, J. Tempere and C. A. R. Sá de Melo, "Effects of spin-orbit coupling on the Berezinskii-Kosterlitz-Thouless transition and the vortex-antivortex structure in two-dimensional Fermi gases", *Phys. Rev. Lett.* **113** (2014), article no. 165304.
[88] J. P. A. Devreese, J. Tempere and C. A. R. Sá de Melo, "Topological phases and collective modes in U(1) and SU(2) sectors of spin–orbit-coupled two-dimensional superfluid Fermi gases", *Phys. Rev. A* **105** (2022), article no. 033304.
[89] R. A. Williams, M. C. Beeler, L. J. LeBlanc, K. Jiménez-García and I. B. Spielman, "Raman-induced interactions in a single-component Fermi gas near an *s*-wave Feshbach resonance", *Phys. Rev. Lett.* **111** (2013), article no. 095301.
[90] X. Zhang and C. A. R. Sá de Melo, "Beyond spin-charge separation: helical modes and topological quantum phase transitions in one-dimensional Fermi gases with spin–orbit and Rabi couplings", preprint, 2024, 2405.20255.
[91] A. Imambekov and L. I. Glazman, "Universal theory of nonlinear Luttinger liquids", *Science* **323** (2009), no. 5911, pp. 228–231.
[92] X. Zhang, *Effects of spin–orbit coupling and Rabi fields in SU(2) and SU(3) symmetric Tomonaga–Luttinger liquids*, PhD thesis, Georgia Institute of Technology, 2025.
[93] I. M. Lifshitz, "Anomalies of electron characteristics of a metal in the high pressure region", *Sov. Phys. JETP* **11** (1960), no. 5, pp. 1130–1135.

[94] R. D. Duncan and C. A. R. Sá de Melo, "Thermodynamic properties in the evolution from BCS to Bose-Einstein condensation for a d-wave superconductor at low temperatures", *Phys. Rev. B* **62** (2000), pp. 9675–9687.
[95] S. S. Botelho and C. A. R. Sá de Melo, "Lifshitz transition in *d*-wave superconductors", *Phys. Rev. B* **71** (2005), article no. 134507.
[96] M. Olshanii, "Atomic scattering in the presence of an external confinement and a gas of impenetrable bosons", *Phys. Rev. Lett.* **81** (1998), pp. 938–941.
[97] N. Navon, R. P. Smith and Z. Hadzibabic, "Quantum gases in optical boxes", *Nat. Phys.* **17** (2021), no. 12, pp. 1334–1341.
[98] K.-N. Schymik, S. Pancaldi, F. Nogrette, D. Barredo, J. Paris, A. Browaeys and T. Lahaye, "Single atoms with 6000-second trapping lifetimes in optical-tweezer arrays at cryogenic temperatures", *Phys. Rev. Appl.* **16** (2021), article no. 034013.
[99] T. F. Schmidutz, I. Gotlibovych, A. L. Gaunt, R. P. Smith, N. Navon and Z. Hadzibabic, "Quantum Joule-Thomson effect in a saturated homogeneous Bose gas", *Phys. Rev. Lett.* **112** (2014), article no. 040403.
[100] G. Källén, "On the definition of the renormalization constants in quantum electrodynamics", *Helv. Phys. Acta* **25** (1952), no. IV, pp. 417–434.
[101] H. Lehmann, "Über Eigenschaften von Ausbreitungsfunktionen und Renormierungskonstanten quantisierter Felder", *Nuovo Cimento* **11** (1954), no. 4, pp. 342–357.
[102] E. H. Moore, "On the reciprocal of the general algebraic matrix", *Bull. Am. Math. Soc.* **26** (1920), pp. 394–395.
[103] R. Penrose, "A generalized inverse for matrices", *Math. Proc. Camb. Philos. Soc.* **51** (1955), no. 3, pp. 406–413.
[104] L. Onsager, "Reciprocal relations in irreversible processes. I", *Phys. Rev.* **37** (1931), pp. 405–426.
[105] L. Onsager, "Reciprocal relations in irreversible processes. II", *Phys. Rev.* **38** (1931), pp. 2265–2279.
[106] F. Scazza, C. Hofrichter, M. Höfer, P. C. De Groot, I. Bloch and S. Fölling, "Observation of two-orbital spin-exchange interactions with ultracold SU(N)-symmetric fermions", *Nat. Phys.* **10** (2014), no. 10, pp. 779–784.
[107] M. H. Yau and C. A. R. Sá de Melo, "SU(3) vs. SU(2) fermions in optical lattices: Color-Hall vs. spin-Hall topological insulators", *EPL* **135** (2021), no. 1, article no. 16001.
[108] M. H. Yau and C. A. R. Sá de Melo, "Eigenspectrum, Chern numbers and phase diagrams of ultracold color-orbit-coupled SU(3) fermions in optical lattices", *Phys. Rev. A* **103** (2021), article no. 043302.
[109] C. D. Hamley, C. S. Gerving, T. M. Hoang, E. M. Bookjans and M. S. Chapman, "Spin-nematic squeezed vacuum in a quantum gas", *Nat. Phys.* **8** (2012), no. 4, pp. 305–308.
[110] H. M. Bharath, M. S. Chapman and C. A. R. Sá de Melo, "Staircase in magnetization and entanglement entropy of spinor condensates", *Phys. Rev. A* **98** (2018), article no. 031601.
[111] B. H. M., M. Boguslawski, M. Barrios, L. Xin and M. S. Chapman, "Exploring non-abelian geometric phases in spin-1 ultracold atoms", *Phys. Rev. Lett.* **123** (2019), article no. 173202.
[112] C. S. Madasu et al., "Experimental realization of a SU(3) color-orbit coupling in an ultracold gas", preprint, 2025, 2502.04714.

ACADÉMIE DES SCIENCES
INSTITUT DE FRANCE

Comptes Rendus. Physique
2025, Vol. 26, p. 317-338
https://doi.org/10.5802/crphys.243

Intervention in a conference / *Intervention en colloque*

Simulating quantum Hall physics in ultracold atomic gases: prospects and challenges

Simuler l'effet Hall quantique dans les gaz d'atomes ultrafroids : perspectives et défis

Sylvain Nascimbene [a]

[a] Laboratoire Kastler Brossel, Collège de France, CNRS, ENS-PSL University, Sorbonne Université, 11 Place Marcelin Berthelot, 75005 Paris, France

E-mail: sylvain.nascimbene@lkb.ens.fr

Abstract. This proceedings presents recent advancements in the realization of topological states of matter using ultracold atomic gases. We focus on the simulation of the quantum Hall effect, originally discovered in two-dimensional electron gases subjected to a magnetic field. Given that ultracold atoms are neutral, simulating the effect of a magnetic field requires an ad-hoc technique. We review various methods developed for this purpose, highlighting their respective advantages and limitations. Furthermore, we explore the extension of these techniques to interacting quantum gases within topological bands, aiming to create analogs of fractional quantum Hall states. These many-body states are distinguished by their topological order, which is characterized by long-range entanglement among particles and the emergence of low-lying excitations exhibiting fractional quantum statistics. The discussion will encompass the current state of research and potential future directions in the field.

Résumé. Cet acte de congrès présente les avancées récentes dans la réalisation d'états topologiques de la matière à l'aide de gaz atomiques ultrafroids. Nous nous concentrons sur la simulation de l'effet Hall quantique, découvert dans des gaz d'électrons bidimensionnels soumis à un champ magnétique. Étant donné que les atomes ultrafroids sont neutres, la simulation de l'effet d'un champ magnétique nécessite une technique ad hoc. Nous passons en revue diverses méthodes développées à cette fin, en soulignant leurs avantages et leurs limites respectifs. En outre, nous explorons l'extension de ces techniques aux gaz quantiques en interaction dans des bandes topologiques, dans le but de créer des analogues d'états de Hall fractionnaires. Ces états à N corps se distinguent par leur ordre topologique, qui se caractérise par une intrication à longue portée entre les particules et l'émergence d'excitations de basse énergie présentant des statistiques quantiques fractionnaires. La discussion portera sur l'état actuel de la recherche et sur les orientations futures potentielles dans ce domaine.

Keywords. Topological phase, Quantum simulation, Quantum gases.

Mots-clés. Phase topologique, Simulation quantique, Gaz quantiques.

Funding. European Union (grant TOPODY 756722 from the European Research Council), Institut Universitaire de France.

Manuscript received 17 September 2024, revised 12 February 2025, accepted 24 February 2025.

The quantum Hall effect was discovered in 1980 by von Klitzing [1] by studying the properties of condensed-matter systems in which the electron gas is constrained to evolve in a

two-dimensional (2D) plane xy. At low temperature and in the presence of a strong magnetic field $\mathbf{B} = B\mathbf{e}_z$, he observed a quantization of the Hall conductance according to

$$I_y = \sigma_{xy} V_x, \quad \sigma_{xy} = n\sigma_0,$$

where n is an integer, $\sigma_0 = e^2/h$ is the quantum of conductance, with e representing the electron charge and h the Planck constant. This discovery was pivotal in the field of quantum many-body physics and laid the groundwork for the exploration of topological states of matter. We will discuss here the current state of research in ultracold atomic gases towards the simulation of the quantum Hall effect and the realization of various topological states of matter associated with it.

1. Topological bands and the integer quantum Hall effect

1.1. *Landau levels*

The integer quantum Hall effect can be understood in terms of a special topological structure of single-particle quantum eigenstates of motion. Before delving into more complex systems, we examine the idealized model of a charged particle evolving in 2D and subjected solely to a perpendicular magnetic field [2]. Its dynamics is determined by the Hamiltonian

$$H = \frac{(\mathbf{p} - q\mathbf{A})^2}{2M},$$

where q is the particle charge ($-e$ for an electron, but in the subsequent discussion we will assume $q > 0$) and M is its mass. The selection of the gauge influences the inherent symmetries of the system. In our discussion, we will primarily utilize the symmetric gauge, defined as

$$\mathbf{A} = \frac{1}{2}\mathbf{B} \times \mathbf{r} = \frac{Br}{2}\mathbf{e}_\phi.$$

While this choice explicitly breaks translational invariance, it preserves rotational symmetry around the origin.

The Hamiltonian can be expanded as

$$H = H_0 - \frac{\omega_c}{2} L_z, \tag{1}$$

$$H_0 = \frac{p_x^2 + p_y^2}{2M} + \frac{1}{8} M\omega_c^2 (x^2 + y^2), \tag{2}$$

where we introduce the cyclotron frequency $\omega_c = qB/M$ and the angular momentum projection $L_z = xp_y - yp_x$. The Hamiltonian H_0 corresponds to an isotropic harmonic oscillator in 2D, of frequency $\omega_c/2$. We can exhibit an eigenbasis $|n_0, m\rangle$ of H_0 in common with the angular momentum L_z, corresponding to the energy spectrum $E^0_{n_0,m} = (n_0 + 1)(\hbar\omega_c/2)$ where $n_0 \in \mathbb{N}$ and $m \in \{-n_0, -n_0 + 2, \ldots, n_0 - 2, n_0\}$ (see Figure 1(a)).

Together with the term $(-\omega_c/2)L_z$, we get the energy spectrum of a charged particle in a magnetic field $E_{n_0,m} = E^0_{n_0,m} - m(\hbar\omega_c/2)$, which can be written as

$$E_{n,m} = (n + \tfrac{1}{2})\hbar\omega_c,$$

with $n = (n_0 - m)/2 \in \mathbb{N}$ and $m \geq -n$. The energy spectrum consists of infinitely degenerate flat bands known as Landau levels, as illustrated in Figure 1(b).

In the following we will focus on properties of the ground band, the lowest Landau level (LLL). Its eigenstates are described by the wavefunctions

$$\psi_m(x, y) \propto r^m e^{im\phi} e^{-r^2/4\ell^2},$$

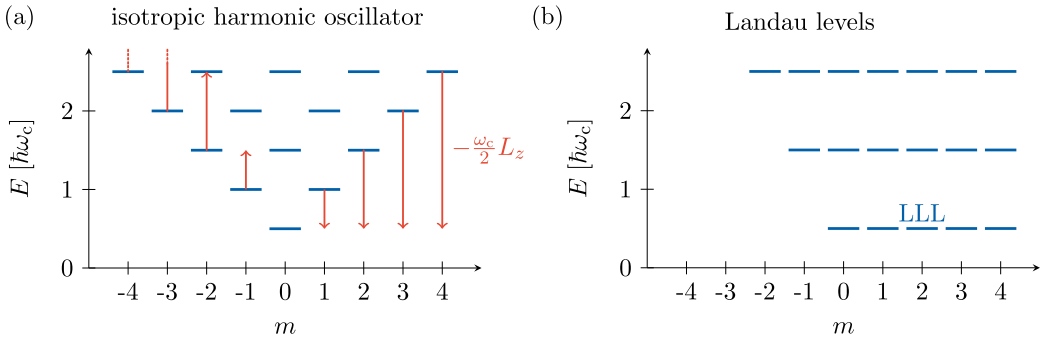

Figure 1. (a) Spectrum of the isotropic quantum harmonic oscillator in two dimensions. Offseting the states by $-(\omega_c/2)L_z$ (red arrows) yields the spectrum of a charged particle subjected to a magnetic field, corresponding to Landau levels shown in (b).

where $m \geq 0$. Here, we introduced the polar coordinates (r,ϕ) and the cyclotron length $\ell = \sqrt{\hbar/qB}$. The density probability of ψ_m is concentrated in a ring of radius $r_m \simeq \sqrt{2m}\ell$, of width $\Delta r \simeq \ell$ independent of m. The area enclosed by this ring is thread by a magnetic flux

$$\Phi_m = B\pi r_m^2 \simeq m\Phi_0,$$

where $\Phi_0 = h/q$ is the magnetic flux quantum.

In the following, we will consider a finite geometry, assuming that the motion is restricted to a disk $r \leq R$ by a circular hard wall. This restriction only weakly affects the so-called bulk states ψ_m with $r_m \leq R$ (i.e. $m \leq m_{\max} = R^2/2\ell^2$) for which the density probability is almost fully contained within the disk. For $m \geq m_{\max}$, the eigenstates become squeezed by the confinement hard wall close to $r = R$, leading to an increase of (kinetic) energy (see Figure 2(a)). As a result, these states acquire a non-zero azimuthal velocity $\langle v_\phi \rangle$, in contrast with the dispersionless bulk modes. More precisely, we write the azimuthal velocity component as

$$\begin{aligned} v_\phi &= \frac{1}{M}\left(\frac{\hbar}{\mathrm{i}r}\partial_\phi - qA_\phi\right) \\ &= \frac{1}{M}\left(\frac{\hbar m}{r} - \frac{qB}{2}r\right) \\ &= \omega_c \frac{r_m^2 - r^2}{r}. \end{aligned}$$

For bulk states, the azimuthal velocity almost vanishes since $r \simeq r_m$. Conversely, for edge modes the density is localized around $r = R$, hence $v_\phi \propto (r_m^2 - R^2) \propto (m - m_{\max})$, corresponding to a chiral dispersive mode [3] (see Figure 2(b)).

Introducing the complex coordinate $z = re^{\mathrm{i}\phi} = x + \mathrm{i}y$, a generic bulk state of the Landau level can be expanded over the ψ_m basis as

$$\psi(z) = \sum_{m\geq 0}^{m_{\max}} c_m z^m e^{-r^2/4\ell^2},$$

which is the product of a gaussian factor in r and a complex polynomial $P(z)$. This polynomial is fully characterized by its roots z_k, as

$$P(z) \propto \prod_{k=1}^{m_{\max}} (z - z_k).$$

One checks that the complex phase of $P(z)$ winds once around every non-degenerate root z_k, corresponding to a unit-charge quantum vortex.

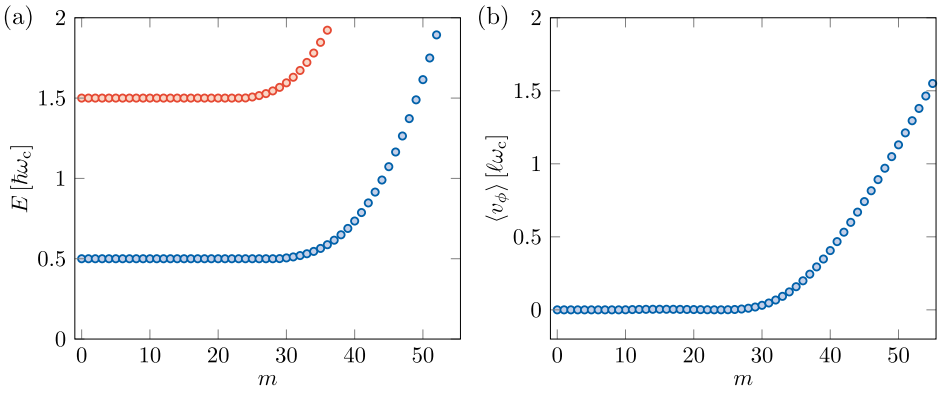

Figure 2. (a) Spectrum of a quantum Hall system restricted to a disk for radius $R = 10\ell$. (b) Mean azimuthal velocity for the quantum states of the ground energy band.

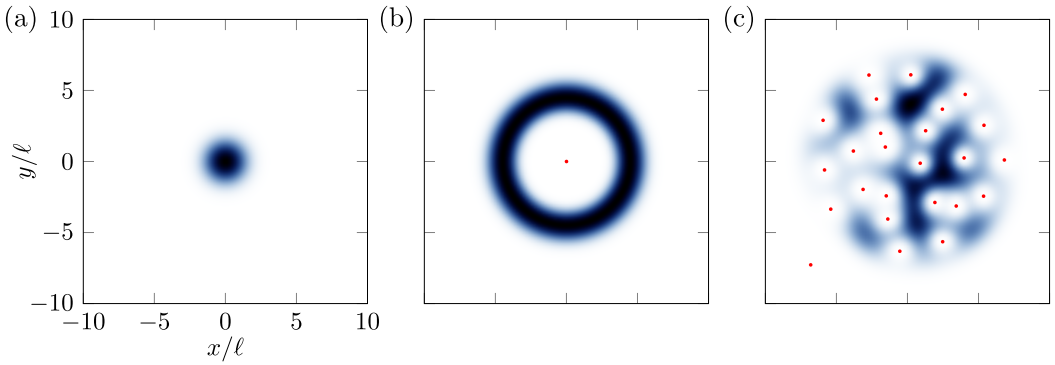

Figure 3. Probability density distribution of a few states of the LLL: the state $\psi_{m=0}$ (a), the state $\psi_{m=10}$ (b), and a state defined by a random complex polynomial of degree 25 (c). Vortex point defects are shown as red dots.

We show in Figure 3 the density probability of a few typical states of the LLL, namely $\psi_{m=0}$, $\psi_{m=10}$, and a state defined by a random complex polynomial of degree 25, which could be realized using a thermal Bose gas restricted to the LLL [4]. We also show for each of them the position of the quantum vortices as red dots.

1.2. *Quantization of the Hall conductance*

The first explanation of the Hall conductance quantization was given by Laughlin based on a particle pumping argument [5]. For this, we consider a slightly modified geometry, coined Corbino disk $r_{\min} \le r \le r_{\max}$ [3,6] (see Figure 4(a)). In a fermionic band insulator, the states with

$$m_{\min} = \frac{r_{\min}^2}{2\ell^2} \le m \le m_{\max} = \frac{r_{\max}^2}{2\ell^2}$$

are occupied with one particle. We consider a solenoid, placed within the inner radius, which can introduce an additional magnetic flux Φ. By slowly increasing this flux by one unit of flux quantum Φ_0, the adiabatic eigenstates undergo a spectral flow in which the state ψ_m (which originally encloses a magnetic flux $m\Phi_0$) is transferred to the next state ψ_{m+1} (enclosing a

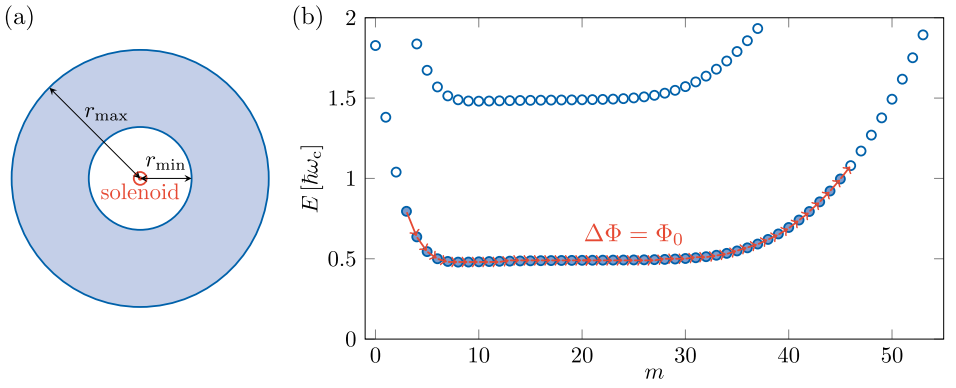

Figure 4. (a) Scheme of the Corbino disk used for Laughlin's pump experiment. (b) Single-particle spectrum of a Corbino disk defined by the radii $r_{\min} = 2\ell$ and $r_{\max} = 10\ell$. Starting in a fermionic insulator with a Fermi level $E_F = \hbar\omega_c$, the adiabatic increase of the solenoid flux $\Delta\Phi = \Phi_0$ transfers each state m to $m+1$ (red arrows), or equivalently a state from one edge to the other.

magnetic flux $(m+1)\Phi_0$). Globally, such a pump cycle transfers one particle from the inner edge (state $m_{\min}$) to the outer edge (state $m_{\max}$), as shown in Figure 4(b).

This pump process can be interpreted in terms of a quantized Hall conductance. Indeed, the flux variation $\dot{\Phi}$ gives rise to an "induced voltage" $V_\phi = -\dot{\Phi}$ along any circular path within the Corbino disk, while the transfer of particles from the inner to outer edges can be interpreted as a radial current

$$I_r = q\frac{\dot{\Phi}}{\Phi_0} = -\frac{q^2}{h}V_\phi.$$

This relationship aligns with the quantization of the Hall conductance.

1.3. *Topological bands in lattice systems*

The quantization of Hall conductance is not limited to ideal Landau levels; it can also be extended to Bloch bands in lattice systems.

We begin by examining the natural extension of Landau levels to a discrete square lattice, known as the Hofstadter model [7,8]. This model features a square lattice with nearest-neighbor hopping, where the positions of the lattice sites are defined as $\mathbf{r}_{i,j} = i\,a\mathbf{e}_x + j\,a\mathbf{e}_y$, where a is the lattice spacing and i, j are integers. In this framework, the magnetic field is incorporated through the Peierls substitution, which introduces complex phases into the hopping amplitudes. These phases correspond to the Aharonov–Bohm phase acquired along the path connecting neighboring sites. To simplify the description, we adopt the Landau gauge, where $A_x = -By$. In this gauge, the hopping terms along the y-direction remain real, while the hopping terms along the x-direction acquire a Peierls phase given by

$$\phi_{(i,j)\to(i+1,j)} = \frac{q}{\hbar}\int_{\mathbf{r}_{i,j}}^{\mathbf{r}_{i+1,j}} \mathrm{d}\mathbf{r}\, A_x(\mathbf{r}) = -2\pi\frac{\Phi}{\Phi_0}j, \tag{3}$$

where $\Phi = Ba^2$ is the magnetic flux through a unit cell.

In the general case, the position-dependent Peierls phases disrupt translational symmetry along the y-direction, making it impossible to define y-momentum. However, when the ratio Φ/Φ_0 takes on rational values p/q, discrete translation invariance by the distance qa along y is recovered (in addition to the discrete invariance along x by the distance a). As a result, one

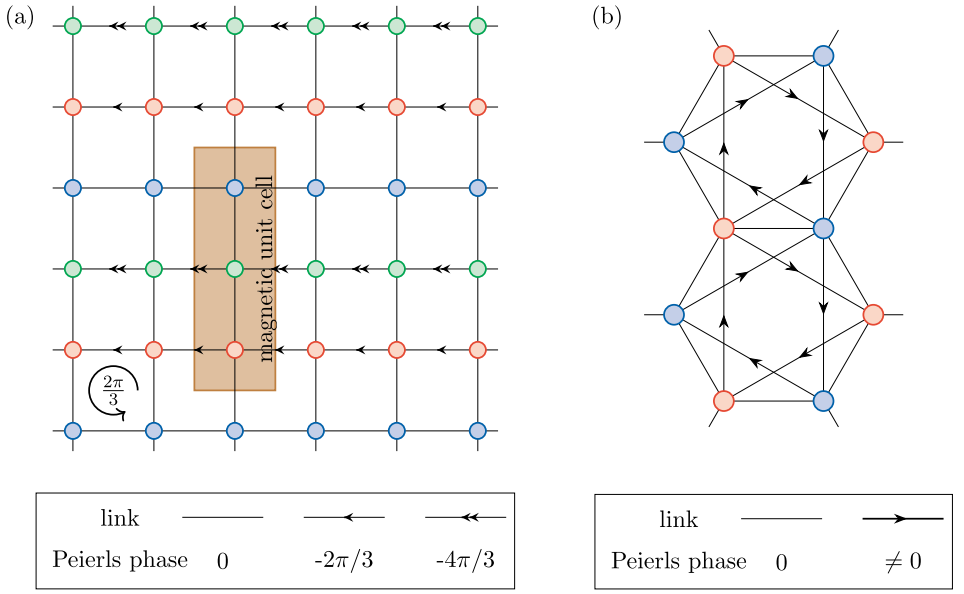

Figure 5. (a) Scheme of the Hofstadter model, a square lattice model with complex-valued hopping matrix elements as defined in Equation (3). For a ratio $p/q = 1/3$, the lattice exhibits three inequivalent sites and a magnetic Brillouin zone defined by three square unit cells. (b) Scheme of the Haldane model, a hexagonal lattice model with real-valued nearest-neighbour hoppings and complex-valued next-nearest neighbour hoppings.

can introduce a conserved quasi-momentum (q_x, q_y) defined over a magnetic Brillouin zone $(0, 2\pi/a) \times (0, 2\pi/qa)$ (see the case $p/q = 1/3$ in Figure 5(a)).

As a result of the magnetic translation symmetries discussed above, quantum levels are organized into a set of q magnetic Bloch bands. A given band, provided it is separated in energy from other bands, gives rise to a quantized Hall effect. Each band, when sufficiently separated in energy from others, can give rise to a quantized Hall effect. Specifically, the transverse linear response of a band insulator manifests as a quantized Hall conductance expressed by $\sigma_{xy} = \mathscr{C}\sigma_0$, where $\mathscr{C}$ is an integer known as the Chern number. This integer characterizes the topological properties of the Bloch band, analogous to the genus of a closed surface in geometry. For instance, in the case where $p = 1$, the lowest Bloch band consistently exhibits a Chern number of $\mathscr{C} = 1$, resembling the behavior of a Landau level. We do not discuss here the concept of Chern number in more detail, since it is very well explained in several review articles (see for example [9] for a review in a context of ultracold quantum gases).

The concept of the Chern number is not confined to lattice models that can be viewed as discretized versions of continuous systems with uniform magnetic fields. It can be defined for any isolated Bloch band within a given lattice model. A Chern insulator emerges when fermionic insulators fill Bloch bands that possess a non-zero Chern number, which requires that the configuration of Peierls phases breaks time-reversal symmetry. A notable example of a Chern insulator is the Haldane model [10], illustrated in Figure 5(b).

2. Realizing quantum Hall systems with ultracold atoms

Since magnetic fields do not exert mechanical effects on neutral particles, simulating quantum Hall physics relies on analogies. In this section, we will review some of these analogies, discuss

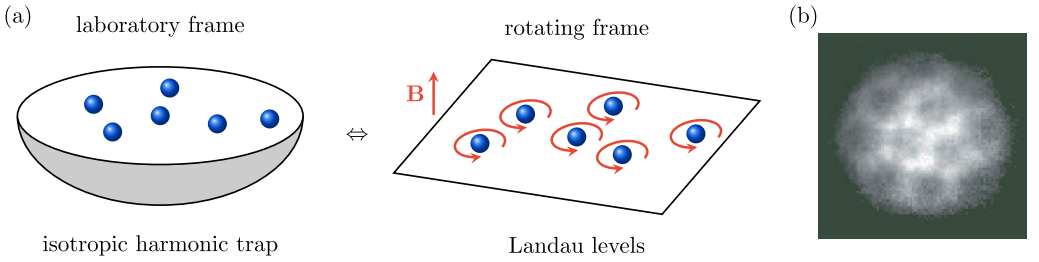

Figure 6. (a) Schematics of the analogy between an atom held in an isotropic harmonic trap in a rotating frame and a charged particle subjected to a magnetic field. (b) Image of an atomic Bose–Einstein condensate set in rotation, which exhibits a triangular lattice of quantized vortices (from [12]).

their current limitations, and explore potential strategies to overcome these challenges in the future.

2.1. *Rotating gases*

2.1.1. *Landau levels in rotating gases*

Historically, the first protocol to create an effective magnetic field involves rotating gases [11]. Consider an atom evolving in two dimensions under an isotropic harmonic trap, described by the Hamiltonian

$$H = \frac{p_x^2}{2M} + \frac{p_y^2}{2M} + \frac{1}{2}M\omega^2(x^2+y^2).$$

In a reference frame that rotates around the center of the harmonic trap at a frequency Ω, the Hamiltonian transforms to

$$H' = \frac{\mathbf{p}'^2}{2M} + \frac{1}{2}M\omega^2\mathbf{r}'^2 - \Omega L_z',$$

where $L_z' = x'p_y' - y'p_x'$ is the angular momentum and (x', y') are the rotated coordinates. When the rotation frequency Ω matches the confinement frequency ω, we recover the Landau Hamiltonian given in Equation (1), corresponding to a particle of charge $q = 1$ and a cyclotron frequency $\omega_c = 2\omega$ (see Figure 6(a)).

2.1.2. *Abrikosov vortex lattices in Bose–Einstein condensates*

Most experiments with rotating gases have focused on Bose–Einstein condensates containing a large number of atoms N. These systems can be effectively described by a classical field $\psi(x, y)$ representing the macroscopic wavefunction shared by all atoms. As previously discussed, a generic wavefunction in the LLL is characterized by its zeros, which correspond to unit-charged quantum vortices.

In the absence of interactions, any configuration of vortices can be expected due to the flat-band nature of the LLL. However, interactions lead to a well-defined many-body ground state. In dilute gases, atoms primarily interact at short range, resulting in a ground state that minimizes the interaction energy [13]

$$E_{\text{int}} = g\frac{N(N-1)}{2}\int \mathrm{d}r^2\,|\psi(r)|^4,$$

where g is the interaction coupling constant. Without a magnetic field, such as in a free Bose gas within a box potential of area $\mathscr{A}$, the energy is minimized with a uniform density $n = |\psi|^2 = N/\mathscr{A}$ (ignoring boundary effects). When a magnetic field is applied, distributing the density over

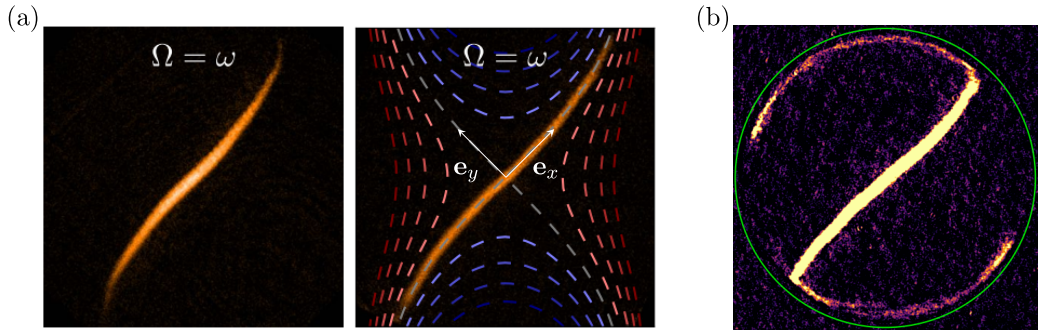

Figure 7. (a) In situ image of an atomic gas in the momentum state $p_x = 0$ of the LLL (from [18]). The right panel indicates as dashed lines the equipotential lines of the rotating saddle potential. (b) In situ image of the atomic gas in the presence of a sharp circular box potential (green circle). The atoms populate a chiral edge mode propagating along the boundary (from [19]).

the area $\mathscr{A}$ necessitates the insertion of $N_\Phi = B\mathscr{A}/\Phi_0$ quantum vortices. As shown in [14], the interaction energy is minimized with a regular arrangement of vortices in a triangular lattice.

Vortex lattices have been realized and extensively studied in the early years of atomic BECs, although most cases did not restrict to the LLL (see Figure 6(b)) [11,15–17]. However, exploring quantum Hall physics through rotating gases presents significant challenges, as these systems are highly sensitive to any static defect potential in the lab frame, which induces time-dependent perturbations in the rotating frame.

2.1.3. *Recent experiments in the LLL*

Recent experiments conducted by the group of Zwierlein have rekindled interest in rotating gases [18]. Compared to experiments from the 2000s, these new studies benefit from advanced techniques such as high-resolution in situ imaging and potential imprinting. This allows fine potential defect diagnosis, as well as the capability to project a hard-wall potential, enabling the investigation of uniform gases in a circular box. The rotation was induced by a rotating quadrupolar potential given by $V(x,y) = -Qxy$ with $Q > 0$, as illustrated in Figure 7(a) (we will omit the prime notation in the following discussion).

The dynamics induced by the saddle potential can initially be understood through classical orbits. In the lowest Landau level, the slow motion of atoms—characterized by the drift of guiding centers of cyclotron orbits—is governed by the equation of motion

$$\mathbf{v} = \frac{1}{q}\frac{\nabla V \times \mathbf{B}}{B^2},$$

which simplifies here to

$$\mathbf{v} = \frac{Q}{2M\omega}(x\mathbf{e}_x - y\mathbf{e}_y).$$

Starting from a rotationally symmetric Gaussian distribution, we expect the gas to contract along the y-direction while elongating along the x-direction. Eventually, the extent along y saturates at the cyclotron length ℓ, beyond which classical dynamics ceases to apply.

This dynamics accounts for the formation of a highly elongated gas in the MIT experiments, as illustrated in Figure 7(a). This state can be interpreted as the occupation of a well-defined wavefunction from the LLL, specifically a momentum state expressed in the Landau gauge $\mathbf{A} = -By\mathbf{e}_x$.

In this gauge, rotational symmetry is broken, and the system exhibits continuous translation symmetry along the x-direction. The Hamiltonian is given by

$$H = \frac{(p_x + qBy)^2}{2M} + \frac{p_y^2}{2M},$$

where the momentum p_x acts as a fixed parameter, resulting in a one-dimensional harmonic oscillator along y. The LLL, parameterized by p_x, corresponds to the ground state:

$$\psi_{p_x}(x,y) = \mathrm{e}^{\mathrm{i}p_x x/\hbar} \exp\left[-\frac{(y - p_x \ell^2/\hbar)^2}{2\ell^2}\right].$$

Returning to the MIT experiments, the elongated gas is very close to the state $p_x = 0$[1].

The control of rotating gases at the level of a single LLL wavefunction laid the groundwork for subsequent experiments, where the population of chiral edge modes localized near the boundary of a sharp box potential was observed (see Figure 7(b)) [19]. Additionally, the effects of interactions in the flat-band limit were investigated, revealing a redistribution of momentum within the LLL due to interactions, which led to vortex crystallization as a precursor to the formation of an Abrikosov lattice [20].

2.2. *Lattice systems*

2.2.1. *Peierls phase engineering*

Atomic gases in optical lattices provide a versatile platform for simulating a wide range of discrete lattice models [21]. Here, we focus on the realization of lattices with non-trivial topological bands, which require complex-valued hopping amplitudes. In a standard optical lattice created by the dipole trapping of an off-resonant standing wave, atoms hop through spontaneous tunneling events characterized by real-valued transition amplitudes. The proposal by Jaksch and Zoller [22] established the framework for simulating Peierls phases.

We present a simplified version of this scheme that aligns more closely with actual experimental implementations. By introducing a linear potential, we create an energy offset $\hbar\Delta$ between neighboring wells along the x-direction, effectively suppressing tunneling (see Figure 8(a)). The x-dynamics can be restored by employing a pair of laser beams to induce a two-photon optical transition.

The hopping amplitude inherits the electric field amplitudes $E_1 E_2^* \propto \mathrm{e}^{\mathrm{i}\delta\mathbf{k}\cdot\mathbf{r}}$, where $\delta\mathbf{k}$ represents the relative light momentum. The complex phases of these amplitudes function as the Peierls phases associated with a magnetic field, yielding a flux per plaquette given by

$$\Phi = \Phi_0 \frac{\delta k_y a}{2\pi}.$$

Since the lattice spacing a is comparable to the laser wavelength, the flux is typically on the order of 1 and can be adjusted by modifying the lattice geometry or the angle between the two driving beams. This scheme, along with similar protocols, has been successfully implemented to simulate both the Hofstadter and Haldane models discussed in Section 1.3 [23,25,26].

2.2.2. *Probing the band topology*

Various protocols have been developed to probe band topology (see [9] for a review). Here, we focus on one such method that examines the transverse linear response of an atomic gas evolving under the Hofstadter model with a flux $p/q = 1/4$ [24]. Instead of filling the lowest energy band with a fermionic band insulator, a thermal Bose gas samples the ground band uniformly and

[1] The momentum state $p_x = 0$ is the only momentum state unaffected by the saddle potential.

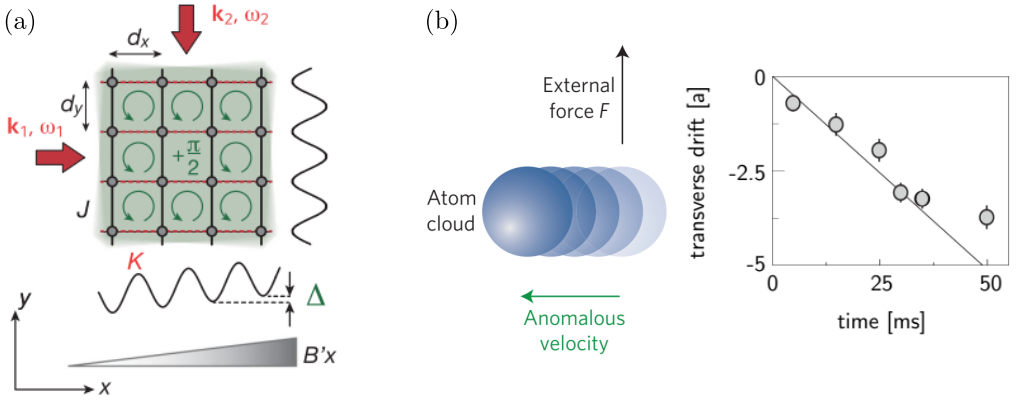

Figure 8. (a) Scheme of the lattice configuration and shaking protocol used to engineer the Hofstadter model with a magnetic flux $p/q = 1/4$ (from [23]). A linear potential induced by a magnetic field gradient suppresses tunneling along the x-direction. A pair of Bragg laser beams induces resonant tunneling along x, imprinting the complex phase profile of the Bragg process onto the hopping matrix elements. (b) Scheme of the transverse Hall response measurements and measured Hall drift as a function of time (adapted from [24]). The solid line represents the quantized drift expected for a Chern number $\mathscr{C} = 1$.

incoherently. Applying a force F_x along the x-direction induces a transverse drift along the y-direction of the center of mass (see Figure 8(b)), as described by

$$y(t) = \frac{4a^2 F_x}{\hbar} \mathscr{C}\, t,$$

where $\mathscr{C}$ is the Chern number of the occupied band. This technique has provided the first experimental evidence of a quantized Chern number in ultracold atomic gases.

2.2.3. *The issue of Floquet heating*

Experiments utilizing shaken optical lattices face a common challenge: the limited duration of coherence due to Floquet heating. This phenomenon arises because the laser-assisted hopping involves a time-dependent potential $V(x,t) \propto \cos(\delta\mathbf{k}\cdot\mathbf{r} - \Delta t)$, where the angular frequency Δ is determined by the energy difference $\hbar\Delta$ between neighbouring wells. While this time modulation prevents the definition of stationary states, the Floquet formalism allows for the characterization of time-periodic eigenstates–eigenstates of the unitary evolution over one modulation period. These states are defined by a quasi-energy that is considered modulo $\hbar\Delta$ (analogous to the quasi-momentum of Bloch states) [27,28].

In the Floquet picture, the notion of ground band no longer makes sense. However, an effective ground band can still be identified when the modulation frequency significantly exceeds the typical tunneling rates and band gaps to higher bands. Despite this, the effective ground band remains coupled to higher bands, which can be brought into resonance by the absorption of quanta of energy $\hbar\Delta$ (see Figure 9(a) and (b)). These detrimental couplings can be mitigated by appropriately selecting the modulation frequency [29]. An additional source of heating arises when considering interacting atoms, which can absorb quanta of the modulation energy during two-body collisional processes [30–33].

These heating processes have not hindered the success of remarkable experiments, including the realization of various types of topological bands and initial studies of strongly interacting systems, as discussed later. However, Floquet heating remains a significant challenge for the

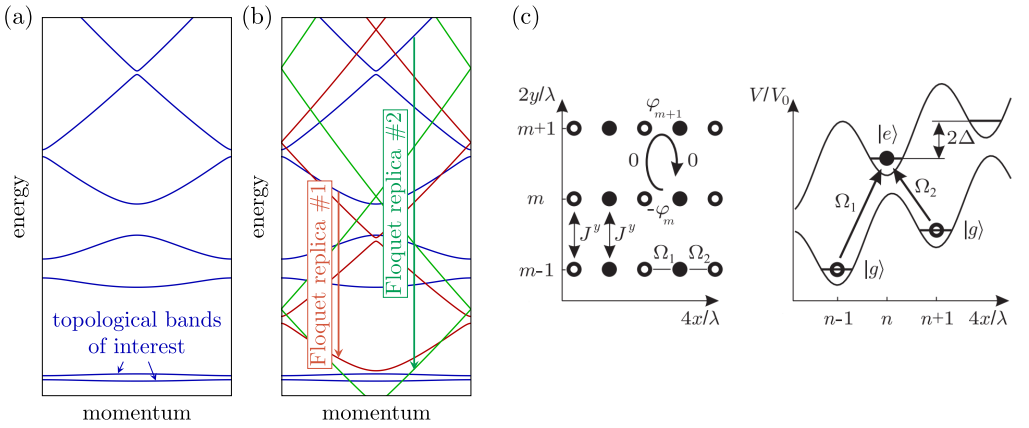

Figure 9. (a) Scheme of a typical bandstructure, with low-energy bands of interest separated in energy with respect to higher dispersive bands. (b) When targeting the bandstructure (a) using time-modulated optical lattices, the modulation frequency Δ gives rise, in a Floquet picture, to an infinite number of replicas separated in energy by integer multiples of the energy quantum $\hbar\Delta$ (two of them are shown in red and green). The bands of interest may become resonantly coupled with higher bands, leading to heating of the system. (c) Reproduction of the scheme of the protocol of Jaksch and Zoller [22], which involves spin flips upon hopping between lattice sites. Such a scheme involves a much higher modulation frequency, which could solve the issue of Floquet heating.

future realization of complex topological states, which require extended experimental timescales for their generation.

Future experiments could address the issue of Floquet heating by employing more complex protocols that utilize an internal degree of freedom of the atom, as originally proposed by Jaksch and Zoller [22] (see also [34]). By ensuring that the laser-assisted tunneling is accompanied by a transition between two internal states (see Figure 9(c)), the modulation frequency $\hbar\Delta$ would become a hyperfine or electronic resonant frequency, which is several orders of magnitude larger than the typical energy scale of motion. In this scenario, an effective static Hamiltonian can be accurately defined, and Floquet heating is not expected to occur.

We also note that an off-resonant laser field coupled to an internal degree of freedom can be utilized to simulate a magnetic field in the continuum. In this scenario, the laser-dressed states become position-dependent due to the spatial variation of the laser electric field. An atom that adiabatically follows a given dressed state experiences a geometrical Berry phase, similar to the Aharonov–Bohm phase experienced by a charged particle in a magnetic field. The group led by Spielman demonstrated the nucleation of quantized vortices in a Bose–Einstein condensate using this technique [35].

2.3. *Synthetic dimensions*

The last technique we discuss involves the concept of synthetic dimensions [36]. In this framework, a quantum Hall system is defined where the xy plane is replaced by a synthetic plane composed of one spatial dimension x and one synthetic dimension [37–39]. The spatial coordinate y is substituted with another degree of freedom, which can be a momentum state or an internal degree of freedom [40,41]. In a well-developed scheme, the discrete projection m of an internal

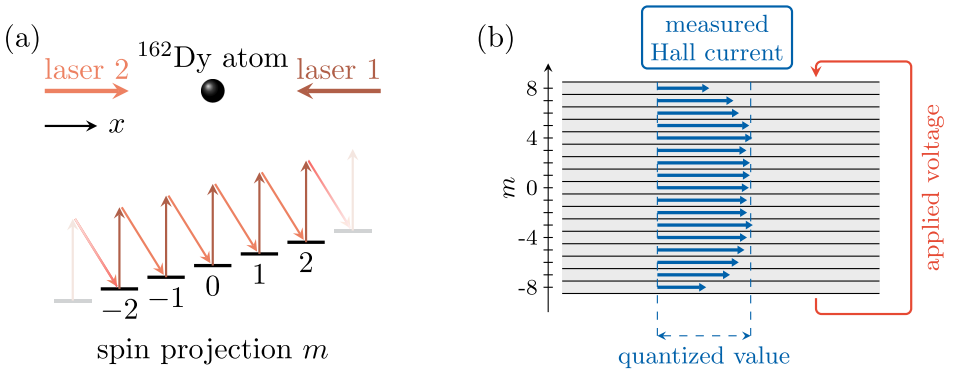

Figure 10. (a) Scheme of the laser configuration used to simulate a magnetic field in a hybrid system involving a spatial dimension x and a synthetic dimension encoded in the spin projection m. The dynamics along m is induced by resonant two-photon optical transitions. An effective magnetic field arises from the velocity kicks that occur along xx during spin transitions. (b) Measured Hall response resolved in magnetic projection m, which is consistent with a quantized value in the bulk of the synthetic dimension.

spin J (with $-J \leq m \leq J$) is utilized [38,39,42]. The dynamics along m is induced by two-photon Raman transitions involving a pair of lasers counter-propagating along x (see Figure 10(a)).

The occurrence of an effective magnetic field arises from the correlated dynamics in the spin projection m and velocity v_x. Specifically, a spin transition $m \to m+1$ is accompanied by a velocity kick $v_x \to v_x - 2\hbar k_{\text{laser}}/M$ due to the momentum exchange with light. This relationship leads to the equation of motion

$$M\dot{v}_x = -2\hbar k_{\text{laser}}\dot{m},$$

which can be interpreted as the dynamics of a charged particle under the influence of a magnetic field

$$M\dot{v}_x = qB\dot{y},$$

where $q = 1$ and $\mathbf{B} = -2\hbar k_{\text{laser}}\mathbf{e}_z$. This effective magnetic field results in a quantum Hall effect, which is evidenced by a quantized transverse response in the bulk of the synthetic dimension [42] (see Figure 10(b)). Synthetic dimensions are particularly advantageous for revealing the occurrence of topological edge modes due to their finite nature [38,39]. They also facilitate the engineering of complex geometries, such as cylinders [43–47] or systems in dimensions greater than three [48,49].

Synthetic dimensions also come with some peculiarities and limitations. First, synthetic dimensions can be limited in size, particularly when encoding them in the internal spin of an atom. Exploring topological effects in the thermodynamic limit then requires using large-spin lanthanide atoms [42]. Alternatively, synthetic dimensions can be encoded in momentum states of an atom [50] or rotational states of a molecule [51], with no fundamental limitation in size.

So far, synthetic dimensions have primarily been employed to engineer various types of topological bands, typically studied in the absence of significant interaction effects. Notable exceptions include two works that reported the observation of non-linear effects in a momentum-state lattice [52] and a universal Hall response in a ladder geometry [53]. More generally, interactions in systems with synthetic dimensions are expected to exhibit a peculiar structure. Since atoms on different synthetic sites can interact, the interactions are anticipated to be of infinite range along

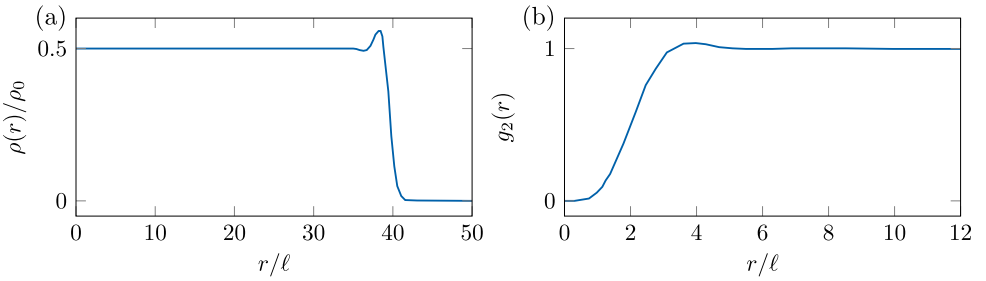

Figure 11. Density profile $\rho(r)$ (a) and correlation function $g_2(r)$ (b) of a bosonic Laughlin state with 400 particles, computed from a Monte Carlo simulation [66].

synthetic dimensions. This characteristic may significantly alter the phenomenology of strongly-interacting topological systems [40,54–59], and the conditions for the occurrence of genuine two-dimensional fractional Hall states in systems with synthetic dimensions remain to be elucidated.

3. Towards fractional quantum Hall states

In the context of a Bose–Einstein condensate, we have primarily considered the many-body ground state where each LLL orbital is filled with a large number of atoms, resulting in a high filling factor $\nu = N_{\rm at}/N_{\rm orb} \gg 1$. In the regime of lower fillings, the many-body system can no longer be described by a macroscopic wavefunction, leading to the emergence of more complex correlations among the particles.

The strongly-correlated regime poses significant challenges for numerical modeling. Even in bosonic systems, the presence of gauge fields results in complex-valued many-body wavefunctions, which introduces a sign problem in Monte Carlo simulations. In many cases, exact diagonalization remains the only viable approach, although it is constrained by the size of the systems that can be studied. Recently, advancements in computational techniques have allowed for the simulation of larger system sizes using methods such as DMRG [60–62] or other tensor network computations [63]. Variational projected entangled-pair states have also been developed to study the bosonic Harper–Hofstadter model in the thermodynamic limit [64].

3.1. *The bosonic Laughlin state*

We focus our discussion on the bosonic Laughlin state at filling factor $\nu = 1/2$, a prominent example of a fractional quantum Hall state [65]. For an ensemble of N particles, the many-body wavefunction is given by

$$\psi_L(z_1, z_2, \ldots, z_N) = \prod_{1\le i<j\le N} (z_i - z_j)^2 \prod_{i=1}^{N} \mathrm{e}^{-|z_i|^2/4\ell^2}.$$

This wavefunction being expressed as a symmetric polynomial of the complex coordinates z_i (aside from a Gaussian factor that we will disregard for simplicity), it belongs to the LLL introduced in Section 1.1. A notable feature of this wavefunction is that it forbids two particles from occupying the same point, as evidenced by the second-order correlation function $g_2(r)$ plotted in Figure 11(b)). This property leads to the remarkable conclusion that the Laughlin state is the exact many-body ground state for zero-range repulsive interactions, a scenario particularly relevant for rotating atomic Bose gases.

Any wavefunction derived by multiplying the Laughlin wavefunction by another symmetric polynomial also exhibits a zero interaction energy. Among this family of degenerate ground

states, the Laughlin state uniquely minimizes the angular momentum projection $m_{\rm tot} = N(N-1)$, effectively leading to a minimal spatial extent centered around $\mathbf{r} = \mathbf{0}$. The maximum (single-particle) angular momentum $m = 2(N-1)$ occupied in the Laughlin state corresponds to a radius $R \simeq 2\sqrt{N}\ell$, which results in an area of $\mathscr{A} = \pi R^2 = 2\times(2\pi\ell)^2 N$. The proportionality $\mathscr{A} \propto N$ reflects the behavior of an incompressible liquid. The bulk density of the Laughlin state is expressed as

$$\bar{\rho} = \rho_0/2, \tag{4}$$

where $\rho_0 = 1/(2\pi\ell^2)$ is the density expected when each orbital is filled with a single particle, akin to a fermionic Hall insulator. In practice, the density is nearly uniform throughout most of the disk $r < R$, with a slight ripple around $r = R$ [66], see Figure 11(a).

Since $\rho_0 \propto B$, the uniform density given in Equation (4) is proportional to the magnetic field strength. According to the Středa formula $\sigma_{xy} = \partial\bar{\rho}/\partial B$, which relates the Hall conductance to the variation of density with respect to the magnetic field [67], we have

$$\sigma_{xy} = \frac{1}{2}\frac{1}{h},$$

i.e. a half-quantized value (we recall our convention of a unit charge $q = 1$). Furthermore, the excitation of density modulations is suppressed in the bulk by a finite energy gap (roughly given by the interaction energy experienced by a pair of atoms in the state $\psi_{m=0}$ [68]).

3.2. *State-of-the art: Laughlin state with 2 particles*

A recent experiment conducted by the group of Greiner has successfully demonstrated the realization of a Laughlin state with just two atoms [69]. In this experiment, the researchers utilized an optical lattice to simulate the Hofstadter model with a flux of $p/q = 1/3$ per plaquette. They confined the dynamics to a 4×4 lattice, resulting in a total flux through the 9 plaquettes amounting to $3\Phi_0$. This configuration corresponds to $N_{\rm orb} = 3$ orbitals in the ground band, which is precisely the number needed to define the Laughlin state.

The interacting two-body ground state was adiabatically prepared by slowly ramping local potential tilts. The resulting state exhibited the expected anti-bunching between the atoms (see Figure 12(a)). Furthermore, by measuring the change in density in response to variations in the artificial magnetic field, they were able to determine a Hall response conductance of $0.6(2)/h$ via the Středa formula. This result is consistent with a half-quantized Hall response (see Figure 12(b)).

A recent preprint from the group of Jochim also reported the realization of a 2-atom Laughlin state composed of a pair of rapidly rotating fermionic atoms [70]. Notably, other platforms have successfully produced two-photon Laughlin states [71,72].

3.3. *Towards larger Laughlin states*

While robust quantization of the Hall conductance only occurs for large enough systems, increasing the number of atoms in a Laughlin droplet remains a significant hurdle. Several approaches can be taken to address this

- Starting with independent one-dimensional chains of atoms, ramping up inter-chain couplings in an adiabatic manner [73].
- A patchwork construction [74], which involves preparing multiple 4×4 plaquettes, each containing 2 atoms in a Laughlin state, and then adiabatically coupling these plaquettes together.

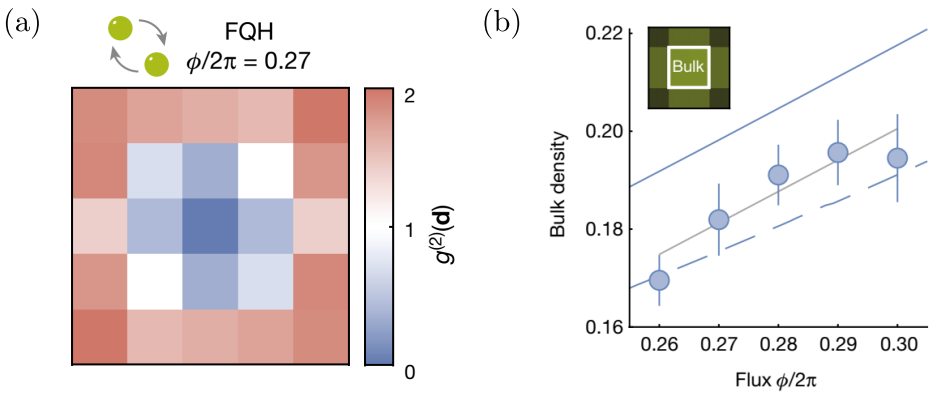

Figure 12. Correlation function $g_2(\mathrm{d})$ measured for a 2-particle Laughlin state in [69] (b) Variation of the density with magnetic flux measured in the same system, consistent with a half-quantized Hall conductance.

- By adjusting a parameter that controls a phase transition from a non-topological to a topological band, similar to methods using local energy offsets [24], one can transition from a trivial phase (like a Bose superfluid) to a Laughlin state [62].

In these methods, maintaining an adiabatic process is crucial for achieving a low-entropy Laughlin state. The importance of the adiabatic path was highlighted in earlier proposals for creating small Laughlin states in rotating systems [75]. However, as the number of atoms increases, it becomes increasingly difficult to maintain adiabatic conditions.

Another potential approach is to create a more complex system with a central region hosting a Laughlin droplet surrounded by a large reservoir in a gapless non-topological phase [76]. By tuning the energy of the reservoir, it may be possible to transfer entropy from the central region to the reservoir, resulting in a low-entropy Laughlin droplet. This technique has been successfully used in lattice Fermi gases to produce antiferromagnets with long-range magnetic order [77].

Finally, we mention proposals for preparing topological many-body states using dissipative dynamics [78,79], for instance fractional Hall states by pumping interacting bosons into the lowest Chern band of a topological lattice [80].

3.4. *Probing long-range entanglement*

In contrast to an integer quantum Hall phase, a fractional Hall state exhibits long-ranged entanglement associated with what is known as topological order [81]. This topological order is characterized by the existence of degenerate many-body ground states in a toroidal geometry that cannot be distinguished using local observables. However, this property poses challenges for experiments, as implementing periodic boundary conditions can be difficult.

Topological order can be more easily revealed by analyzing long-range entanglement through the entanglement entropy $S_A = -\mathrm{Tr}(\rho_A \log \rho_A)$ upon spatial partition of the system between two subregions A and B (where ρ_A is the reduced density matrix obtained by tracing out the B subregion). For a partition with a perimeter L, systems with short-range entanglement follow the area law, scaling linearly with L according to $S_A(L) = \alpha L + o(1)$ [82], whereas systems with topological order are expected to modify this law to $S_A(L) = \alpha L - \gamma + o(1)$. The subleading term γ, known as the topological shift, quantifies a global entanglement feature that persists over long distances [83].

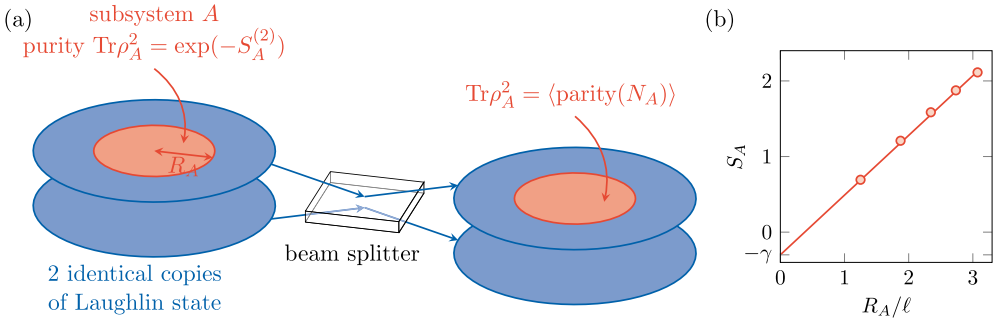

Figure 13. (a) Scheme of the method for measuring the (Renyi) entanglement entropy of a subregion A within a many-body system. The process involves interfering two identical copies of the system using a 50/50 beam splitter. The purity of the reduced density matrix ρ_A can then be determined from the mean parity of the atom count in region A [84,85]. (b) Expected variation of the (von Neumann) entanglement entropy S_A as a function of the radius R_A of subregion A. The y-intercept of the linear fit represents the entanglement entropy γ (from [88]).

The group led by Greiner has successfully measured the Renyi entanglement entropy defined as $S_A^{(2)} = -\log \mathrm{Tr}(\rho_A^2)$, using a protocol based on many-body interference between two copies of a many-body system [84,85] (see Figure 13(a)). In this approach, two copies 1 and 2 of a bosonic many-body state undergo a local beam-splitter operation $|1\rangle \to (|1\rangle + |2\rangle)/\sqrt{2}$ and $|2\rangle \to (|1\rangle - |2\rangle)/\sqrt{2}$. The purity of the system reduced to subregion A is linked to the mean parity of the number of particles $N_A^{(1)}$ found in region A of system 1 after the splitting as

$$\mathrm{Tr}(\rho_A^2) = \langle \mathrm{Parity}(N_A^{(1)})\rangle.$$

If the original many-body state is pure, an even number of atoms is expected in system 1, similar to the Hanbury Brown and Twiss effect. As the size of A increases from zero, the mean parity should quiclky drop to zero on a lengthscale ℓ. Taking the logarithm gives the Renyi entropy, whose scaling with L can reveal the topological shift γ. Numerical simulations on small Laughlin droplets confirm this scenario [86–88] (see Figure 13(b)).

3.5. *Anyonic quasi-hole excitations*

A key feature of fractional quantum Hall states is the unique nature of their elementary excitations. We recall that a wavefunction $\psi(z_1, z_2, \ldots, z_N) = P(z_1, z_2, \ldots, z_N)\psi_L(z_1, z_2, \ldots, z_N)$, where P is a symmetric polynomial, exhibits zero interaction energy and is therefore degenerate with the Laughlin ground state. A polynomial P with a degree less than the number of particles corresponds to edge excitations of the Laughlin droplet. Here, we focus on a bulk excitation, known as a quasi-hole excitation, represented by

$$\psi_\eta(z_1, z_2, \ldots, z_N) = \prod_{i=1}^{N}(z_i - \eta)\psi_L(z_1, z_2, \ldots, z_N).$$

It exhibits a density hole at $z = \eta$, corresponding to a deficit of 1/2 particle (see Figure 14(b)). This can be understood by considering two quasi-holes at the same point, leading to the wavefunction

$$\psi_{\eta,\eta}(z_1, z_2, \ldots, z_N) = \prod_{i=1}^{N}(z_i - \eta)^2\psi_L(z_1, z_2, \ldots, z_N).$$

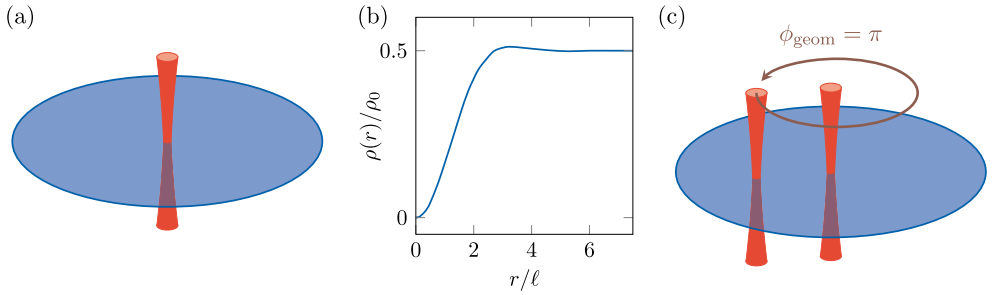

Figure 14. (a) Scheme of the protocol used to nucleate a quasi-hole excitation by focusing a laser beam producing a repulsive potential. (b) Density profile of a Laughlin state with a quasi-hole excitation at $r = 0$ (from [89]). The atom number deficit corresponds to a fractional charge of $1/2$ atom, and the r.m.s. size of the hole is linked with the quasi-hole spin $S = 1/4$. (c) Scheme of the braiding operation by moving adiabatically one quasi-hole around another, which gives rise to a geometrical phase $\phi_{\rm geom} = 2S(2\pi) = \pi$.

It can be identified with the state obtained by removing from a Laughlin wavefunction of $(N+1)$ particles a single atom at $z_{N+1} = \eta$.

In practice, a quasi-hole state can be generated by applying a repulsive laser beam focused at $z = \eta$ [90] (see Figure 14(a)). This technique is already well-established for injecting and controlling quantum vortices in Bose–Einstein condensates [91,92].

Beyond the fractional charge, the quasi-hole density profile provides further insights [93]. The relationship between the mean square radius and angular momentum [94] indicates that the size of the quasi-hole is linked to its angular momentum, according to

$$\delta L_z = \int \mathrm{d}^2 z \left(\frac{|z-\eta|^2}{2\ell^2} - 1 \right) (\rho_\eta(z) - \bar{\rho}).$$

This excess angular momentum can be interpreted as the internal spin $S = \delta L_z$ of the quasi-hole [89]. For the bosonic Laughlin state, numerical studies suggest $S = 1/4$. This fractional spin challenges the conventional understanding of half-integer and integer spins for fermions and bosons, respectively. According to the spin-statistics theorem, this hints at the existence of a fractional statistical phase, leading to the term anyons for such quasi-particles [95]. Real-space probes of quasi-hole excitations can also be generalized to Chern insulators in lattice systems [96].

3.6. *Braiding of anyonic excitations*

The fractional statistical phase is defined as the geometrical phase acquired by the system upon an exchange of two particles. To probe this statistical phase, two key requirements must be met (i) the ability to create and spatially manipulate quasiholes, which can be achieved using focused laser beams (see Figure 14(c)). When a quasihole encircles another, the many-body system acquires a statistical phase given by $\phi_{\rm geom} = 2S(2\pi) = \pi$. (ii) an interferometric protocol to reveal the value of this phase. We do not discuss this point here and refer to the first proposal for a statistical phase interferometer in the context of cold atomic gases, by Paredes et al. [97].

Successful measurement of the statistical phase hinges on minimizing various imperfections. First, the geometrical phase should not be significantly affected by a dynamical phase that may arise during the adiabatic braiding process. This dynamical phase can occur if there is cross-talk between the quasiholes when they are too close together or if they are positioned near

the confining edge potential. To keep dynamical phases small, uncontrolled energy offsets must be maintained well below the bulk excitation gap. Second, the Laughlin droplet must be prepared with very low residual entropy to ensure that the average number of thermal quasiholes remains negligible over the area encircled by the quasiholes during the braiding operation. These stringent requirements impose significant constraints on the control over the system, making the measurement quite challenging.

3.7. *Extension to other fractional quantum Hall states*

So far, our discussion has focused on the bosonic Laughlin state at filling $\nu = 1/2$. This focus is motivated by the fact that the Laughlin state emerges as the exact many-body ground state for short-range binary interactions, making it the most experimentally accessible fractional quantum Hall state in quantum gas systems. Other fractional quantum Hall states could also be realized using more sophisticated experimental protocols. While each fractional Hall state is characterized by a unique topological order, certain key properties—such as topological entropy or the existence of fractionalized quasi-particles—can be probed using protocols similar to those developed for the Laughlin state.

Among the various fractional Hall states, the bosonic Moore-Read/Pfaffian state, which occurs at filling $\nu = 1$, is particularly noteworthy due to its exotic properties. This state involves the pairing of bosonic particles and is characterized by three-body antibunching. As a result, it could be stabilized in the presence of three-body repulsive interactions [98], although engineering such interactions remains a significant experimental challenge. Alternatively, it has been proposed that the Pfaffian state could be stabilized through strong three-body dissipation [99] or by carefully tuning two-body interactions [100]. The Pfaffian state is especially intriguing because its elementary excitations exhibit non-Abelian exchange statistics [101]. Demonstrating non-Abelian braiding of these excitations—a critical step toward realizing topological quantum computing [102]—remains one of the most ambitious challenges in experimental physics across platforms.

4. Conclusion

In this proceedings, we have discussed the current status of simulating quantum Hall physics using ultracold atomic gases. Various techniques have been explored to replicate the effects of a magnetic field on charged particles, including rotating gases, lattice systems, and synthetic dimensions. While the realization of topological bands is well-established at the single-particle level, achieving strongly-interacting topological systems remains a significant challenge. Recent advancements, leveraging a high degree of control over local potentials and individual particles, have shown promising progress toward realizing fractional quantum Hall systems in ultracold atomic gases.

While our focus has been primarily on the quantum Hall effect, the field of ultracold atomic gases has also seen the emergence of diverse topological systems, such as 1D SSH chains [103], spin-orbit coupled systems [104] and 3D Weyl semi-metals [105]. The exploration of interacting gases within these topological band structures opens up exciting possibilities for discovering a wide range of intriguing strongly-correlated systems.

Declaration of interests

The authors do not work for, advise, own shares in, or receive funds from any organization that could benefit from this article, and have declared no affiliations other than their research organizations.

Acknowledgements

The author acknowledges fruitful discussions with Jean Dalibard while preparing the talk at the Institut Henri Poincaré. The author also acknowledges support from European Union (grant TOPODY 756722 from the European Research Council) and Institut Universitaire de France.

References

[1] K. v. Klitzing, G. Dorda and M. Pepper, "New method for high-accuracy determination of the fine-structure constant based on quantized Hall resistance", *Phys. Rev. Lett.* **45** (1980), pp. 494–497.

[2] L. D. Landau and E. M. Lifshitz, *Course of Theoretical Physics Vol 3 Quantum Mechanics*, Pergamon Press: London, 1958.

[3] B. I. Halperin, "Quantized Hall conductance, current-carrying edge states, and the existence of extended states in a two-dimensional disordered potential", *Phys. Rev. B* **25** (1982), pp. 2185–2190.

[4] Y. Castin, Z. Hadzibabic, S. Stock, J. Dalibard and S. Stringari, "Quantized vortices in the ideal Bose gas: a physical realization of random polynomials", *Phys. Rev. Lett.* **96** (2006), article no. 040405.

[5] R. B. Laughlin, "Quantized Hall conductivity in two dimensions", *Phys. Rev. B* **23** (1981), pp. 5632–5633.

[6] O. M. Corbino, "Azioni Elettromagnetiche Doyute Agli Ioni dei Metalli Deviati Dalla Traiettoria Normale per Effetto di un Campo", *Nuovo Cimento* **1** (1911), pp. 397–420.

[7] P. G. Harper, "Single band motion of conduction electrons in a uniform magnetic field", *Proc. Phys. Soc. A* **68** (1955), pp. 874–878.

[8] D. R. Hofstadter, "Energy levels and wave functions of Bloch electrons in rational and irrational magnetic fields", *Phys. Rev. B* **14** (1976), pp. 2239–2249.

[9] N. R. Cooper, J. Dalibard and I. B. Spielman, "Topological bands for ultracold atoms", *Rev. Mod. Phys.* **91** (2019), article no. 015005.

[10] F. D. M. Haldane, "Model for a quantum Hall effect without Landau levels: condensed-matter realization of the "Parity Anomaly"", *Phys. Rev. Lett.* **61** (1988), pp. 2015–2018.

[11] K. W. Madison, F. Chevy, W. Wohlleben and J. Dalibard, "Vortex formation in a stirred Bose–Einstein condensate", *Phys. Rev. Lett.* **84** (2000), pp. 806–809.

[12] K. W. Madison, F. Chevy, W. Wohlleben and J. Dalibard, "Vortices in a stirred Bose–Einstein condensate", *J. Mod. Opt.* **47** (2000), pp. 2715–2723.

[13] A. A. Abrikosov, "On the magnetic properties of superconductors of the second group", *Sov. Phys. - JETP* **5** (1957), pp. 1174–1182.

[14] W. H. Kleiner, L. M. Roth and S. H. Autler, "Bulk solution of Ginzburg–Landau equations for type II superconductors: upper critical field region", *Phys. Rev.* **133** (1964), A1226–A1227.

[15] J. R. Abo-Shaeer, C. Raman, J. M. Vogels and W. Ketterle, "Observation of vortex lattices in Bose–Einstein condensates", *Science* **292** (2001), pp. 476–479.

[16] V. Bretin, S. Stock, Y. Seurin and J. Dalibard, "Fast rotation of a Bose–Einstein condensate", *Phys. Rev. Lett.* **92** (2004), article no. 050403.

[17] V. Schweikhard, I. Coddington, P. Engels, V. P. Mogendorff and E. A. Cornell, "Rapidly rotating Bose–Einstein condensates in and near the lowest Landau level", *Phys. Rev. Lett.* **92** (2004), article no. 040404.

[18] R. J. Fletcher, A. Shaffer, C. C. Wilson, P. B. Patel, Z. Yan, V. Crépel, B. Mukherjee and M. W. Zwierlein, "Geometric squeezing into the lowest Landau level", *Science* **372** (2021), pp. 1318–1322.

[19] R. Yao, S. Chi, B. Mukherjee, A. Shaffer, M. Zwierlein and R. J. Fletcher, "Observation of chiral edge transport in a rapidly-Rotating quantum gas", *Nat. Phys.* **20** (2024), pp. 1726–1731.

[20] B. Mukherjee, A. Shaffer, P. B. Patel, Z. Yan, C. C. Wilson, V. Crépel, R. J. Fletcher and M. Zwierlein, "Crystallization of bosonic quantum Hall states in a rotating quantum gas", *Nature* **601** (2022), pp. 58–62.

[21] C. Gross and I. Bloch, "Quantum simulations with ultracold atoms in optical lattices", *Science* **357** (2017), pp. 995–1001.

[22] D. Jaksch and P. Zoller, "Creation of effective magnetic fields in optical lattices: the Hofstadter butterfly for cold neutral atoms", *New J. Phys.* **5** (2003), article no. 56.

[23] M. Aidelsburger, M. Atala, M. Lohse, J. T. Barreiro, B. Paredes and I. Bloch, "Realization of the Hofstadter Hamiltonian with ultracold atoms in optical lattices", *Phys. Rev. Lett.* **111** (2013), article no. 185301.

[24] M. Aidelsburger, M. Lohse, C. Schweizer, et al., "Measuring the Chern number of Hofstadter bands with ultracold bosonic atoms", *Nat. Phys.* **11** (2015), pp. 162–166.

[25] H. Miyake, G. A. Siviloglou, C. J. Kennedy, W. C. Burton and W. Ketterle, "Realizing the Harper Hamiltonian with laser-assisted tunneling in optical lattices", *Phys. Rev. Lett.* **111** (2013), article no. 185302.

[26] G. Jotzu, M. Messer, R. Desbuquois, M. Lebrat, T. Uehlinger, D. Greif and T. Esslinger, "Experimental realization of the topological Haldane model with ultracold fermions", *Nature* **515** (2014), pp. 237–240.
[27] M. Holthaus, "Floquet engineering with quasienergy bands of periodically driven optical lattices", *J. Phys. B: At. Mol. Opt. Phys.* **49** (2015), article no. 013001.
[28] A. Eckardt, "Colloquium: atomic quantum gases in periodically driven optical lattices", *Rev. Mod. Phys.* **89** (2017), article no. 011004.
[29] M. Weinberg, C. Ölschläger, C. Sträter, S. Prelle, A. Eckardt, K. Sengstock and J. Simonet, "Multiphoton interband excitations of quantum gases in driven optical lattices", *Phys. Rev. A* **92** (2015), article no. 043621.
[30] M. Reitter, J. Näger, K. Wintersperger, C. Sträter, I. Bloch, A. Eckardt and U. Schneider, "Interaction dependent heating and atom loss in a periodically driven optical lattice", *Phys. Rev. Lett.* **119** (2017), article no. 200402.
[31] T. Boulier, J. Maslek, M. Bukov, et al., "Parametric heating in a 2D periodically driven bosonic system: beyond the weakly interacting regime", *Phys. Rev. X* **9** (2019), article no. 011047.
[32] K. Wintersperger, M. Bukov, J. Näger, et al., "Parametric instabilities of interacting bosons in periodically driven 1D optical lattices", *Phys. Rev. X* **10** (2020), article no. 011030.
[33] K. Viebahn, J. Minguzzi, K. Sandholzer, A.-S. Walter, M. Sajnani, F. Görg and T. Esslinger, "Suppressing dissipation in a Floquet–Hubbard system", *Phys. Rev. X* **11** (2021), article no. 011057.
[34] F. Gerbier and J. Dalibard, "Gauge fields for ultracold atoms in optical superlattices", *New J. Phys.* **12** (2010), article no. 033007.
[35] Y.-J. Lin, R. L. Compton, K. Jiménez-García, J. V. Porto and I. B. Spielman, "Synthetic magnetic fields for ultracold neutral atoms", *Nature* **462** (2009), pp. 628–632.
[36] O. Boada, A. Celi, J. I. Latorre and M. Lewenstein, "Quantum simulation of an extra dimension", *Phys. Rev. Lett.* **108** (2012), article no. 133001.
[37] A. Celi, P. Massignan, J. Ruseckas, N. Goldman, I. B. Spielman, G. Juzeliūnas and M. Lewenstein, "Synthetic gauge fields in synthetic dimensions", *Phys. Rev. Lett.* **112** (2014), article no. 043001.
[38] M. Mancini, G. Pagano, G. Cappellini, et al., "Observation of Chiral edge states with neutral fermions in synthetic hall ribbons", *Science* **349** (2015), pp. 1510–1513.
[39] B. K. Stuhl, H.-I. Lu, L. M. Aycock, D. Genkina and I. B. Spielman, "Visualizing edge states with an atomic Bose gas in the quantum Hall regime", *Science* **349** (2015), pp. 1514–1518.
[40] T. Ozawa and H. M. Price, "Topological quantum matter in synthetic dimensions", *Nat. Rev. Phys.* **1** (2019), pp. 349–357.
[41] A. Fabre and S. Nascimbene, "Atomic topological quantum matter using synthetic dimensions", *Europhys. Lett.* **145** (2024), article no. 65001.
[42] T. Chalopin, T. Satoor, A. Evrard, V. Makhalov, J. Dalibard, R. Lopes and S. Nascimbene, "Probing Chiral edge dynamics and bulk topology of a synthetic Hall system", *Nat. Phys.* **16** (2020), pp. 1017–1021.
[43] J. H. Han, J. H. Kang and Y. Shin, "Band gap closing in a synthetic Hall tube of neutral fermions", *Phys. Rev. Lett.* **122** (2019), article no. 065303.
[44] Y. Yan, S.-L. Zhang, S. Choudhury and Q. Zhou, "Emergent periodic and quasiperiodic lattices on surfaces of synthetic Hall tori and synthetic Hall cylinders", *Phys. Rev. Lett.* **123** (2019), article no. 260405.
[45] X.-W. Luo, J. Zhang and C. Zhang, "Tunable flux through a synthetic Hall tube of neutral fermions", *Phys. Rev. A* **102** (2020), article no. 063327.
[46] Q.-Y. Liang, D. Trypogeorgos, A. Valdés-Curiel, J. Tao, M. Zhao and I. B. Spielman, "Coherence and decoherence in the Harper–Hofstadter model", *Phys. Rev. Res.* **3** (2021), article no. 023058.
[47] A. Fabre, J.-B. Bouhiron, T. Satoor, R. Lopes and S. Nascimbene, "Laughlin's topological charge pump in an atomic Hall cylinder", *Phys. Rev. Lett.* **128** (2022), article no. 173202.
[48] M. Lohse, C. Schweizer, H. M. Price, O. Zilberberg and I. Bloch, "Exploring 4D quantum Hall physics with a 2D topological charge pump", *Nature* **553** (2018), pp. 55–58.
[49] J.-B. Bouhiron, A. Fabre, Q. Liu, Q. Redon, N. Mittal, T. Satoor, R. Lopes and S. Nascimbene, "Realization of an atomic quantum Hall system in four dimensions", *Science* **384** (2024), pp. 223–227.
[50] F. A. An, E. J. Meier, J. Ang'ong'a and B. Gadway, "Correlated dynamics in a synthetic lattice of momentum states", *Phys. Rev. Lett.* **120** (2018), article no. 040407.
[51] B. Sundar, B. Gadway and K. R. A. Hazzard, "Synthetic dimensions in ultracold polar molecules", *Sci. Rep.* **8** (2018), article no. 3422.
[52] F. A. An, B. Sundar, J. Hou, X.-W. Luo, E. J. Meier, C. Zhang, K. R. A. Hazzard and B. Gadway, "Nonlinear dynamics in a synthetic momentum-state lattice", *Phys. Rev. Lett.* **127** (2021), article no. 130401.
[53] T.-W. Zhou, G. Cappellini, D. Tusi, et al., "Observation of universal Hall response in strongly interacting fermions", *Science* **381** (2023), pp. 427–430.
[54] S. Barbarino, L. Taddia, D. Rossini, L. Mazza and R. Fazio, "Magnetic crystals and helical liquids in alkaline-earth fermionic gases", *Nat. Commun.* **6** (2015), pp. 1–9.

[55] E. Cornfeld and E. Sela, "Chiral currents in one-dimensional fractional quantum Hall states", *Phys. Rev. B* **92** (2015), article no. 115446.
[56] M. Łącki, H. Pichler, A. Sterdyniak, A. Lyras, V. E. Lembessis, O. Al-Dossary, J. C. Budich and P. Zoller, "Quantum Hall physics with cold atoms in cylindrical optical lattices", *Phys. Rev. A* **93** (2016), article no. 013604.
[57] S. Barbarino, L. Taddia, D. Rossini, L. Mazza and R. Fazio, "Synthetic gauge fields in synthetic dimensions: interactions and chiral edge modes", *New J. Phys.* **18** (2016), article no. 035010.
[58] T. Bilitewski and N. R. Cooper, "Synthetic dimensions in the strong-coupling limit: supersolids and pair superfluids", *Phys. Rev. A* **94** (2016), article no. 023630.
[59] J. Jünemann, A. Piga, S.-J. Ran, M. Lewenstein, M. Rizzi and A. Bermudez, "Exploring interacting topological insulators with ultracold atoms: the synthetic Creutz–Hubbard model", *Phys. Rev. X* **7** (2017), article no. 031057.
[60] M. P. Zaletel, R. S. K. Mong and F. Pollmann, "Topological characterization of fractional quantum Hall ground states from microscopic Hamiltonians", *Phys. Rev. Lett.* **110** (2013), article no. 236801.
[61] J. Motruk, M. P. Zaletel, R. S. K. Mong and F. Pollmann, "Density matrix renormalization group on a cylinder in mixed real and momentum space", *Phys. Rev. B* **93** (2016), article no. 155139.
[62] J. Motruk and F. Pollmann, "Phase transitions and adiabatic preparation of a fractional Chern insulator in a Boson cold-atom model", *Phys. Rev. B* **96** (2017), article no. 165107.
[63] M. Gerster, M. Rizzi, P. Silvi, M. Dalmonte and S. Montangero, "Fractional quantum Hall effect in the interacting hofstadter model via tensor networks", *Phys. Rev. B* **96** (2017), article no. 195123.
[64] E. L. Weerda and M. Rizzi, "Fractional quantum Hall states with variational projected entangled-pair states: a study of the bosonic Harper–Hofstadter model", *Phys. Rev. B* **109** (2024), article no. L241117.
[65] R. B. Laughlin, "Anomalous quantum Hall effect: an incompressible quantum fluid with fractionally charged excitations", *Phys. Rev. Lett.* **50** (1983), pp. 1395–1398.
[66] O. Ciftja, "Monte Carlo study of Bose Laughlin wave function for filling factors 1/2, 1/4 and 1/6", *Europhys. Lett.* **74** (2006), p. 486.
[67] P. Streda, "Theory of quantised Hall conductivity in two dimensions", *J. Phys. C: Solid State Phys.* **15** (1982), p. L717.
[68] N. Regnault and T. Jolicoeur, "Quantum Hall fractions in rotating Bose–Einstein condensates", *Phys. Rev. Lett.* **91** (2003), article no. 030402.
[69] J. Léonard, S. Kim, J. Kwan, P. Segura, F. Grusdt, C. Repellin, N. Goldman and M. Greiner, "Realization of a fractional quantum Hall state with ultracold atoms", *Nature* **619** (2023), pp. 495–499.
[70] P. Lunt, P. Hill, J. Reiter, P. M. Preiss, M. Gaka and S. Jochim, "Realization of a Laughlin state of two rapidly rotating fermions", *Phys. Rev. Lett.* **133** (2024), article no. 253401.
[71] L. W. Clark, N. Schine, C. Baum, N. Jia and J. Simon, "Observation of Laughlin states made of light", *Nature* **582** (2020), pp. 41–45.
[72] C. Wang, F.-M. Liu, M.-C. Chen, et al., "Realization of fractional quantum Hall state with interacting photons", *Science* **384** (2024), pp. 579–584.
[73] Y.-C. He, F. Grusdt, A. Kaufman, M. Greiner and A. Vishwanath, "Realizing and adiabatically preparing bosonic integer and fractional quantum Hall states in optical lattices", *Phys. Rev. B* **96** (2017), article no. 201103.
[74] F. A. Palm, J. Kwan, B. Bakkali-Hassani, M. Greiner, U. Schollwöck, N. Goldman and F. Grusdt, "Growing extended Laughlin states in a quantum gas microscope: a patchwork construction", *Phys. Rev. Res.* **6** (2024), article no. 013198.
[75] M. Popp, B. Paredes and J. I. Cirac, "Adiabatic path to fractional quantum Hall states of a few bosonic atoms", *Phys. Rev. A* **70** (2004), article no. 053612.
[76] B. Wang, M. Aidelsburger, J. Dalibard, A. Eckardt and N. Goldman, "Cold-atom elevator: from edge-state injection to the preparation of fractional Chern insulators", *Phys. Rev. Lett.* **132** (2024), article no. 163402.
[77] A. Mazurenko, C. S. Chiu, G. Ji, et al., "A cold-atom Fermi–Hubbard antiferromagnet", *Nature* **545** (2017), pp. 462–466.
[78] S. Diehl, E. Rico, M. A. Baranov and P. Zoller, "Topology by dissipation in atomic quantum wires", *Nat. Phys.* **7** (2011), pp. 971–977.
[79] J. C. Budich, P. Zoller and S. Diehl, "Dissipative preparation of Chern insulators", *Phys. Rev. A* **91** (2015), article no. 042117.
[80] Z. Liu, E. J. Bergholtz and J. C. Budich, "Dissipative preparation of fractional Chern insulators", *Phys. Rev. Res.* **3** (2021), article no. 043119.
[81] X. G. Wen, "Topological orders in rigid states", *Int. J. Mod. Phys. B* **04** (1990), pp. 239–271.
[82] J. Eisert, M. Cramer and M. B. Plenio, "*Colloquium*: area laws for the entanglement entropy", *Rev. Mod. Phys.* **82** (2010), pp. 277–306.
[83] A. Kitaev and J. Preskill, "Topological entanglement entropy", *Phys. Rev. Lett.* **96** (2006), article no. 110404.
[84] A. J. Daley, H. Pichler, J. Schachenmayer and P. Zoller, "Measuring entanglement growth in quench dynamics of bosons in an optical lattice", *Phys. Rev. Lett.* **109** (2012), article no. 020505.

[85] R. Islam, R. Ma, P. M. Preiss, M. Eric Tai, A. Lukin, M. Rispoli and M. Greiner, "Measuring entanglement entropy in a quantum many-body system", *Nature* **528** (2015), pp. 77–83.
[86] O. S. Zozulya, M. Haque, K. Schoutens and E. H. Rezayi, "Bipartite entanglement entropy in fractional quantum Hall states", *Phys. Rev. B* **76** (2007), article no. 125310.
[87] M. Haque, O. Zozulya and K. Schoutens, "Entanglement entropy in fermionic Laughlin states", *Phys. Rev. Lett.* **98** (2007), article no. 060401.
[88] A. G. Morris and D. L. Feder, "Topological entropy of quantum Hall states in rotating Bose gases", *Phys. Rev. A* **79** (2009), article no. 013619.
[89] T. Comparin, A. Opler, E. Macaluso, A. Biella, A. P. Polychronakos and L. Mazza, "Measurable fractional spin for quantum Hall quasiparticles on the disk", *Phys. Rev. B* **105** (2022), article no. 085125.
[90] B. Wang, X. Dong and A. Eckardt, "Measurable signatures of bosonic fractional Chern insulator states and their fractional excitations in a quantum-gas microscope", *SciPost Phys.* **12** (2022), article no. 095.
[91] E. C. Samson, K. E. Wilson, Z. L. Newman and B. P. Anderson, "Deterministic creation, pinning, and manipulation of quantized vortices in a Bose–Einstein condensate", *Phys. Rev. A* **93** (2016), article no. 023603.
[92] W. J. Kwon, G. Del Pace, K. Xhani, L. Galantucci, A. Muzi Falconi, M. Inguscio, F. Scazza and G. Roati, "Sound emission and annihilations in a programmable quantum vortex collider", *Nature* **600** (2021), pp. 64–69.
[93] E. Macaluso, T. Comparin, L. Mazza and I. Carusotto, "Fusion channels of non-Abelian anyons from angular-momentum and density-profile measurements", *Phys. Rev. Lett.* **123** (2019), article no. 266801.
[94] T.-L. Ho and E. J. Mueller, "Rotating spin-1 Bose clusters", *Phys. Rev. Lett.* **89** (2002), article no. 050401.
[95] F. Wilczek, "Quantum mechanics of fractional-spin particles", *Phys. Rev. Lett.* **49** (1982), pp. 957–959.
[96] R. O. Umucalılar, "Real-space probe for lattice quasiholes", *Phys. Rev. A* **98** (2018), article no. 063629.
[97] B. Paredes, P. Fedichev, J. I. Cirac and P. Zoller, "1/2-anyons in small atomic Bose–Einstein condensates", *Phys. Rev. Lett.* **87** (2001), article no. 010402.
[98] M. Greiter, X.-G. Wen and F. Wilczek, "Paired Hall state at half filling", *Phys. Rev. Lett.* **66** (1991), pp. 3205–3208.
[99] M. Roncaglia, M. Rizzi and J. I. Cirac, "Pfaffian state generation by strong three-body dissipation", *Phys. Rev. Lett.* **104** (2010), article no. 096803.
[100] F. A. Palm, M. Buser, J. Léonard, M. Aidelsburger, U. Schollwöck and F. Grusdt, "Bosonic Pfaffian state in the Hofstadter–Bose–Hubbard model", *Phys. Rev. B* **103** (2021), article no. L161101.
[101] G. Moore and N. Read, "Nonabelions in the fractional quantum Hall effect", *Nucl. Phys. B* **360** (1991), pp. 362–396.
[102] C. Nayak, S. H. Simon, A. Stern, M. Freedman and S. Das Sarma, "Non-Abelian anyons and topological quantum computation", *Rev. Mod. Phys.* **80** (2008), pp. 1083–1159.
[103] M. Atala, M. Aidelsburger, J. T. Barreiro, D. Abanin, T. Kitagawa, E. Demler and I. Bloch, "Direct measurement of the Zak phase in topological bloch bands", *Nat. Phys.* **9** (2013), pp. 795–800.
[104] Y.-J. Lin, K. Jiménez-García and I. B. Spielman, "Spin–orbit-coupled Bose–Einstein condensates", *Nature* **471** (2011), pp. 83–86.
[105] Z.-Y. Wang, X.-C. Cheng, B.-Z. Wang, et al., "Realization of an ideal Weyl semimetal band in a quantum gas with 3D spin–orbit coupling", *Science* **372** (2021), pp. 271–276.

Comptes Rendus
Physique

Objectif de la revue

Les *Comptes Rendus Physique* sont une revue électronique évaluée par les pairs de niveau international, qui couvre l'ensemble des domaines de la physique et de l'astrophysique.

Ils publient des numéros thématiques, des articles originaux de recherche, des articles de synthèse, des mises en perspective historiques, des textes à visée pédagogique, ou encore des actes de colloque, en anglais ou en français, sans limite de longueur et dans un format aussi souple que possible (figures, données associées, etc.).

Depuis 2020, les *Comptes Rendus Physique* sont publiés avec le centre Mersenne pour l'édition scientifique ouverte, selon une politique vertueuse de libre accès diamant, gratuit pour les auteurs (pas de frais de publication) comme pour les lecteurs (accès libre, immédiat et pérenne).

À propos de la revue

Les *Comptes Rendus Physique* sont exclusivement publiés au format électronique.

Toutes les informations sur la revue, ainsi que le texte intégral de l'ensemble des articles, sont disponibles sur son site internet, à l'adresse https://comptes-rendus.academie-sciences.fr/physique.

Informations à l'attention des auteurs

Pour toute question relative à la soumission d'un manuscrit, merci de consulter le site internet de la revue : https://comptes-rendus.academie-sciences.fr/physique.

Contact

Académie des sciences
23 quai de Conti
75006 Paris (France)
cr-physique@academie-sciences.fr

Comptes Rendus
de l'Académie des sciences
Physique

Special issue / Numéro spécial
Open questions in the quantum many-body problem / *Questions ouvertes dans le problème quantique à N corps*

Guest editors / Rédacteurs en chef invités
Yvan Castin (LKB-ENS, Paris, France), Carlos Sá de Melo (Georgia Tech, Atlanta, USA)

Cover illustration / Illustration de couverture
Le colloque s'est tenu à Paris à l'Institut Henri Poincaré (IHP), dont on admire ici la porte d'entrée caractéristique. Les feux d'artifice sur les côtés symbolisent à la fois le problème quantique à N corps et l'explosion d'idées pendant la rencontre. Crédits photographiques : Antoine Taveneaux — Travail personnel, CC BY-SA 3.0, recadrée, https://commons.wikimedia.org/w/index.php?curid=24436674 (Institut Poincaré) et Carlos Sá de Melo (feux d'artifice).

Contents / *Sommaire*

1878-1535 (electronic)

Académie des sciences - Paris

COMPTES RENDUS
DE L'ACADÉMIE DES SCIENCES

Physique